



HAL
open science

Commande et observation non linéaires de systèmes aéronautiques et spatiaux

Laurent Burlion

► **To cite this version:**

Laurent Burlion. Commande et observation non linéaires de systèmes aéronautiques et spatiaux. Automatique / Robotique. Institut National Polytechnique de Toulouse (INP Toulouse), 2019. tel-02908400

HAL Id: tel-02908400

<https://hal.science/tel-02908400>

Submitted on 29 Jul 2020

HAL is a multi-disciplinary open access archive for the deposit and dissemination of scientific research documents, whether they are published or not. The documents may come from teaching and research institutions in France or abroad, or from public or private research centers.

L'archive ouverte pluridisciplinaire **HAL**, est destinée au dépôt et à la diffusion de documents scientifiques de niveau recherche, publiés ou non, émanant des établissements d'enseignement et de recherche français ou étrangers, des laboratoires publics ou privés.

Institut National Polytechnique de TOULOUSE

HABILITATION A DIRIGER DES RECHERCHES

par

Laurent Burlion

Assistant Professor, Rutgers, the State University of New Jersey, USA

Docteur de l'Université de Paris Saclay

Ingénieur Principal des Etudes et Techniques de l'Armement

**Commande et observation
non linéaires
de systèmes aéronautiques et spatiaux**

Jury :

Tarek Ahmed-Ali (Examineur)
Jean-Marc Biannic (Examineur)
Stéphane Caux (Examineur)
Franck Cazaurang (Rapporteur)
Benoît Clément (Rapporteur)
Isabelle Fantoni (Rapporteur)
Andres Marcos (Examineur)

9 Décembre 2019

Remerciements

Cette Habilitation à Diriger des Recherches représente à peu de choses près dix ans de ma carrière, et, plus globalement, de ma vie. Dix années riches et bien remplies que j'ai passées en grande partie à Toulouse, une ville très agréable sur tous les plans.

Je remercie du fond du coeur le jury, mes anciens collègues de l'Onera, les étudiants que j'ai eu le plaisir de co-encadrer ainsi que les nombreux chercheurs avec qui j'ai eu l'honneur de travailler au cours de ces dernières années. Enfin, je remercie ma famille et amis qui m'ont toujours encouragés à poursuivre cette carrière professionnelle.

"Non, la vie d'un individu n'a rien de linéaire, et pourtant son histoire est plus facile à raconter dans une apparente linéarité, dans un enchaînement qui se veut logique."

Gregory Benford

"If you don't understand linear dynamics systems, you certainly can't understand nonlinear dynamical systems."
Stephen Boyd

à Mathilde

Table des matières

I	Présentation générale	8
1	Introduction	9
1.1	Avant propos	9
1.2	Organisation du mémoire	10
2	Curriculum Vitae	12
2.1	Etat civil	12
2.2	Formation	12
2.3	Travaux de thèse	13
2.4	Stages de recherche à l'étranger	13
2.5	Expérience professionnelle	14
2.6	Activités d'enseignement	15
2.7	Publications et animations scientifiques	15
2.8	Co-encadrement d'un PostDoc	16
2.9	Co-encadrements de six thèses	16
2.10	Encadrements de Master	18
2.11	Encadrements de projets d'élèves	19
2.12	Participations à des jurys de thèses	19
2.13	Sélection de projets	19
3	Résumés des thèses encadrées	21
3.1	Thèse de Guillaume Sabiron	21
3.2	Thèse d'Elodie Duraffourg	22
3.3	Thèse de Victor Gibert	23
3.4	Thèse d'Emmanuel Chambon	23
3.5	Thèse de Torbjørn Cunis	24
3.6	Thèse d'Anthony Bourdelle	26
4	Publications	27
4.1	Articles parus dans des revues indexées	27
4.2	Articles soumis	29

4.3	Chapitres de livre	30
4.4	Articles parus dans une revue électronique	30
4.5	Brevet	31
4.6	Communications avec actes et comité de sélection	31
4.7	Communications soumises	37
4.8	Communications diverses	37
5	Coordination du projet VISIOLAND	38
5.1	Résumé du projet	38
5.2	Activités réalisées	39
5.3	Bilan du projet	41
II	Synthèse d'une sélection de travaux	43
6	Commande sous contrainte de sortie pour la sécurisation des systèmes aérospatiaux	44
6.1	Introduction	45
6.2	Positionnement de nos travaux	45
6.2.1	Contraintes fréquentielles et temporelles	45
6.2.2	Etat de l'art sur les contraintes temporelles	46
6.3	Présentation de la méthode OIST	48
6.3.1	L'idée clef	48
6.3.2	Généralisation	49
6.4	Nos contributions	50
7	Analyse, synthèse ou observation non linéaires pour l'atterrissage basé vision de systèmes aérospatiaux	106
7.1	Introduction	108
7.2	Contexte et positionnement de nos travaux	108
7.2.1	Utilisation de la vision dans l'industrie aéronautique	108
7.2.2	Asservissements visuels "classiques" puis "saturés"	109
7.3	Problématique	111
7.4	Nos contributions	113
7.4.1	Estimation de la profondeur	113
7.4.2	Analyse et commande de la dynamique longitudinale	113
8	Commande et observation de systèmes aérospatiaux à dynamique non linéaire	143
8.1	Introduction	144
8.2	La commande par Backstepping	145

8.2.1	Principe de la méthode	145
8.2.2	Positionnement de nos travaux	145
8.3	Nos contributions	146
8.3.1	Backstepping et commande échantillonnée	146
8.3.2	Backstepping et modes souples	146
8.3.3	Backstepping borné et atterrissage basé vision	147
III	Conclusions et perspectives	191
8.4	Direction générale de nos travaux	192
8.5	Quelques travaux en cours et à venir	193
8.6	Nouvelles applications	194
8.7	Création d'un Laboratoire drone	195
	Bibliographie	197

Première partie
Présentation générale

Chapitre 1

Introduction

1.1 Avant propos

Ce sont principalement la commande et l'observation des systèmes non linéaires qui ont motivé nos recherches depuis une quinzaine d'années. Nous avons aussi travaillé sur l'analyse de ces systèmes mais de façon plus sporadique. En 2003, nous avons commencé une thèse, au laboratoire des signaux et systèmes de SUPELEC, sur la commande non linéaire des systèmes échantillonnées. Cette thèse nous a permis de prendre goût à l'analyse et à la commande des systèmes à dynamique non linéaire. Nous y avons étendu l'algorithme du Backstepping au cas des systèmes à entrées échantillonnées en synthétisant une commande d'ordre quelconque. Nous avons prouvé que l'augmentation de l'ordre de la commande implique une amélioration de la précision et de la rapidité. Nous avons développé aussi un nouvel algorithme de commande adaptative basé sur l'approximation des séries de Taylor lorsque les paramètres du modèles sont incertains. Par la suite, nos encadrants ont continué à travailler sur ce thème des systèmes échantillonnés en dimension finie puis infinie et nous avons régulièrement collaboré avec eux sur des problèmes d'estimation lorsque les sorties mesurées sont échantillonnées ou retardées.

Entre 2003 et 2010, nous avons en parallèle de notre thèse occupé un poste d'ingénieur expert à la Direction Générale pour l'Armement et avons travaillé sur des applications de la commande non linéaire : cette expérience a été enrichissante et nous a notamment permis d'expertiser des méthodes avancées de guidage-pilotage utilisées alors dans l'industrie de la défense.

En 2010, nous avons rejoint l'Office National d'Etudes et de Recherches en Aérospatiale (ONERA) : cela a été un réel changement ! Nous n'étions alors plus l'un des rares ingénieurs à travailler sur l'automatique dans notre service

mais étions désormais au sein d'une équipe spécialisée dans l'identification et la commande des systèmes aéronautiques et spatiaux. Cette atmosphère stimulante nous a permis de réaliser combien la recherche en automatique linéaire était encore riche et source d'inspiration pour les chercheurs en automatique non linéaire. Nous avons notamment commencé par travailler sur un problème à mi-chemin entre ces deux communautés : celui de la commande saturée des systèmes linéaires. C'est alors que nous avons découvert puis effectué des travaux de recherche sur la synthèse de boucles dites d'anti-windup permettant d'obtenir un bon compromis entre la taille du domaine d'emploi et la performance d'une commande linéaire saturée. En même temps, nous avons commencé à cotoyer l'industrie aéronautique (Dassault Aviation puis Airbus) et avons pas à pas été initié à de nouvelles problématiques qui ont inspiré nos travaux de recherche en commande et observation non linéaires.

1.2 Organisation du mémoire

Ce mémoire est organisé en trois parties. Tout d'abord, nous retraçons notre parcours et donnons les grandes lignes de nos activités de recherche, d'encadrement ou contractuelles. Nous présentons dans la seconde partie de ce mémoire trois thématiques de recherche en lien avec nos activités réalisées à l'ONERA entre les années 2010 et 2018 :

- la commande sous contrainte de sortie : nous avons notamment proposé une nouvelle méthode, dénommée OIST (Output to Input Saturation Transformation), permettant de contraindre une sortie d'un système sans avoir à déterminer l'évolution future de ce dernier. Cette méthode peut se combiner avec la synthèse H_∞ structurée. Elle permet aussi d'étendre la synthèse anti-windup au cas où la saturation ne porte plus sur la commande mais sur une sortie du système.
- la synthèse d'observateurs et/ou de boucles d'anti-windup pour le guidage basé vision. Ces travaux ont été motivés par l'atterrissage automatique d'un avion de ligne en utilisant des capteurs inertiels et une simple caméra monoculaire. Il s'agissait notamment de restaurer la stabilité de la boucle de guidage basé vision alors que la profondeur de champ de la caméra n'est pas connue et que les entrées de cette boucle de guidage sont saturées.
- la commande de systèmes à dynamique non linéaire. Nous avons principalement travaillé sur des systèmes triangulaires (strict-feedback) et avons étudié plusieurs extensions du backstepping en présence de paramètres incertains (constants ou temps variant) et de sorties (ou commande) échantillonnées ou retardées.

Enfin, nous concluons ce manuscrit en présentant les perspectives de nos travaux de recherche.

Chapitre 2

Curriculum Vitae

2.1 Etat civil



Laurent Burlion est né a Brest le 6 Avril 1979. Il est marié et a trois enfants. Il vit actuellement dans le New Jersey aux USA et est professeur assistant à l'université de Rutgers.

2.2 Formation

- 2003-2006 : Préparation d'un Doctorat à l'Université de Paris Sud - Orsay au "Laboratoire des Signaux et Systèmes" de SUPELEC
Contribution à l'analyse et à la commande des systèmes non linéaires à commande échantillonnée
Thèse soutenue le 9 Février 2007 (mention Très Honorable)
- 2003 : Diplôme d'Ingénieur de l'ENSIETA et DEA de l'école Centrale Nantes (mention Bien)
- 1999-2000 : Année de formation humaine et militaire (marine)
- 1999-2003 : Formation d'ingénieur militaire à l'ENSIETA
- 1997-1999 : Math-Sup & Spé (option MP*)
- 1997 : Baccalauréat S (mention Bien)

2.3 Travaux de thèse

Titre : Contribution à l'analyse et à la commande de systèmes non linéaires à commande échantillonnée

Jury : Mme. F. Lamnabhi-Lagarrigue (directrice de thèse) et M.M. T. Ahmed-Ali (co-directeur de thèse), A. Astofi (Rapporteur), J. Daafouz (président), C. Moog (Rapporteur) et C. Prieur (examineur).

Résumé : A la frontière des systèmes non linéaires continus et discrets, la classe des systèmes non linéaires à commande échantillonnée est une classe de systèmes à part entière qui a stimulé et stimule toujours de nombreuses recherches. Le sujet est d'autant plus important qu'il a été trop souvent sous-estimé au profit de la recherche sur les commandes continues alors que paradoxalement les commandes sont principalement implémentées numériquement sur les applications industrielles actuelles. S'appuyant sur les dernières recherches du domaine, cette thèse se veut à la fois une contribution à l'étude et à la synthèse de lois de commande échantillonnées pour certaines classes de systèmes non linéaires.

Publications associées : [a1], [a2], [a3], [c2], [c3], [c4], [c5], [c6], [c7].

2.4 Stages de recherche à l'étranger

Nos différents séjours à l'étranger nous ont beaucoup marqués et expliquent en grande partie notre décision d'avoir récemment rejoint l'université de Rutgers aux USA.

- 09/2017-08/2018 : séjour d'études et de recherches exploratoires à l'université du Michigan - Département d'Aérospatial (sous la direction du Prof. Ilya Kolmanovsky)
Méthodes avancées de guidage/pilotage sous contraintes pour la sécurisation du vol de drones
- été 2004 : stage de recherche à l'Université de Florence
Département de Mathématiques (sous la direction du Prof. Gianna Stefani)
Commande optimale de systèmes dynamiques hybrides
- été 2002 : ingénieur stagiaire à l'Université de Cambridge
Département d'ingénierie (sous la direction du Prof. John Lygeros)
Simulation d'un système dynamique hybride pour le contrôle du trafic aérien

2.5 Expérience professionnelle

- Depuis Janvier 2019 : Assistant Professor à l'université de Rutgers,
New Jersey, USA :
- Responsable d'un laboratoire de recherche
 - Responsable d'un cours par semestre
- 04/2010 - 12/2018 : Ingénieur de recherche a l'ONERA
 Activités contractuelles et recherches amont sur les
 méthodologies d'analyse et de synthèse de lois de
 commande ou d'observateurs pour le guidage et le
 pilotage d'engins aérospatiaux :
- Commande non linéaire adaptative ou robuste
 - Asservissements visuels
 - Prise en compte des saturations d'actionneurs
 - Prise en compte de contraintes d'état
- Responsable du projet ANR Visioland
 Responsable des activités *Commande et
 Identification* vis à vis de la direction scientifique
- 09/2003 - 03/2010 : Ingénieur des Etudes et Techniques de l'Armement
 au Laboratoire de Recherches Balistiques et
 Aérodynamiques Aérodynamiques de la DGA
- expertise en performances des systèmes de
missiles tactiques et stratégiques
 - expertise en guidage-pilotage de missiles
tactiques et stratégiques
 - réalisation de simulations numériques de
systèmes complexes
 - réalisation d'une thèse en commande non
linéaire (2003-2006)
 - référent technique en charge du développement
de la compétence guidage-pilotage
 - suivi des propositions de sujets de thèses
DGA-CNRS
 - encadrement de stagiaires

2.6 Activités d'enseignement

- **Responsable de cours (niveau équivalent à Bac+3 et Bac+4) à l'université de Rutgers (USA) :**
 - « Vehicle Dynamics », cours magistraux (environ 30h), Automne 2019.
 - « Aircraft Flight Dynamics », cours magistraux (environ 30h), Printemps 2019.
- **Vacations dans l'enseignement supérieur (environ 200h au total) :**
 - « Kalman filtering » (Automnes 2013, 2014, 2015 et 2016) INP ENSEEIHT, cours de 3^{ème} année.
 - « Introduction to linear control systems » (Automnes 2014, 2015 et 2016) Isae SUPAERO, cours de 2^{ème} année (M1).
 - « Linear filtering and signal processing » (Automnes 2014, 2015 et 2016) Isae SUPAERO, cours de 2^{ème} année (M1).
 - « Introduction to flight dynamics » (Printemps 2014 et 2015) Isae SUPAERO, cours de 2^{ème} année (M1).
 - « Analyse » (Printemps 2012, Automne 2012) Université Paul Sabatier, Toulouse, cours de 1^{ère} année (L1).

2.7 Publications et animations scientifiques

- 25 articles parus dans des revues à comité de lecture,
- 2 articles soumis dans des revues à comité de lecture,
- 4 chapitres de livre,
- 1 brevet,
- 53 communications dans des congrès avec comité de sélection,
- Membre du comité technique IFAC TC 7.3 (Aerospace) (depuis 2014),
- Membre du comité technique IEEE CSS TCAC (Aerospace Control) (depuis 2019),
- Co-Organisateur d'une session "open invited track" portant sur l'atterrissage basé vision à l'IFAC World Congress 2017,
- Co-Organisateur d'une session "open invited track" portant sur l'utilisation de senseurs visuels à bord des avions à l'IFAC World Congress 2020,
- Activité régulière de "Review" pour les principaux journaux et conférences d'Automatique.

2.8 Co-encadrement d'un PostDoc

□ Corentin Chauffaut

- **Titre** : Conception et implémentation de lois de commande pour l'exploration de bâtiment avec un micro-drone, dans le cadre du projet "Explo-Drone".
- **Durée** : 1 an (02/2015 à 02/2016)
- **Co-encadrement** : Francois Defaÿ et Henry de Plinval
- **Financement** : Université de Toulouse
- **Publications associées** : [c34], [c37].
- **Devenir du candidat** : ingénieur, Isae SUPAERO.

2.9 Co-encadrements de six thèses

(Ces thèses sont resumées dans le chapitre suivant)

□ Guillaume Sabiron

- **Titre** : Synthèse d'une Solution GNC basée sur des Capteurs de Flux Optique Bio-inspirés adaptés à la mesure des basses vitesses pour un Atterrissage Lunaire Autonome en Douceur.
- Thèse soutenue le 18/11/2014
- **Co-encadrement** : Philippe Mouyon (équivalence HDR)
- **Jury** : Mme. I. Fantoni (rapporteuse) et M.M. F. Chaumette (président), L. Burlion (encadrant), N. Marchand (rapporteur), F. Ruffier (encadrant), T. Raharijaona (encadrant), et P. Morin (examinateur).
- **Prix de thèse 2015 de la Fondation ISAE-SUPAERO**
- **Financement** ESA et Airbus Defense and Space
- **Publications associées** : [a4], [ch1], [c12], [c20], [c23], [c24], [ac4].
- **Devenir du candidat** : ingénieur de recherche, IFP Energies Nouvelles.

□ Elodie Duraffourg

- **Titre** : Commande non linéaire en présence de modes souples - Applications aérospatiales
- Thèse soutenue le 11/12/2014
- **Co-encadrement** : Tarek Ahmed-Ali (HDR)
- **Jury** : Mme. F. Lamnabhi-Lagarrigue (présidente) et M.M. L. Burlion (encadrant), N. Christov (rapporteur), S. Laghrouche (exa-

minateur) et R. Outbib (rapporteur).

- Financement ONERA
- Publications associées : [a10], [c14], [c15], [c16], [c17], [c18].
- **Devenir du candidat** : ingénieur d'études pilotage, Airbus Defense and Space.

□ **Victor Gibert**

- **Titre** : Analyse d'observabilité et synthèse d'observateurs robustes pour l'atterrissage basé vision d'avions de ligne sur des pistes inconnues
- Thèse soutenue le 13/07/2016
- Co-encadrement : Frank Plestan (HDR)
- **Jury** : M. P. Rives (président), M. L. Burlion (encadrant), Mme. I. Fantoni (rapporteur), MM. J. Gangloff (rapporteur), J. Boada-Bauxell (examineur), A. Chriette (encadrant).
- **Prix de la meilleure présentation "My thesis in 3 minutes" et du meilleur poster**, Airbus PhD days, Toulouse, 2015.
- **Prix de la meilleure présentation**, Journée des Doctorants de l'Ecole Doctorale STIM, Angers, 2015.
- Financement AIRBUS.
- Publications associées : [a16], [ch3], [p1], [c27], [c28], [c32], [c42].
- **Devenir du candidat** : ingénieur d'études amont, Airbus.

□ **Emmanuel Chambon**

- **Titre** : Commande de systèmes linéaires sous contraintes fréquentielles et temporelles – Application au lanceur flexible
- Thèse soutenue le 29/11/2016
- Co-encadrement : Pierre Apkarian (HDR)
- **Jury** : Mme. M. Ganet (examinatrice) et M.M. L. Zaccarian (président), L. Burlion (encadrant), M. Turner (Rapporteur), M. Zasadzinski (rapporteur), et M. A. Zolghadri (examineur).
- **Prix de thèse 2017 de la Fondation ISAE-SUPAERO**
- Financement ONERA
- Publications associées : [a7], [a11], [a12], [ch4], [c25], [c29], [c33], [ac1].
- **Devenir du candidat** : ingénieur Pilotage Lanceur, ArianeGroup.

□ **Torbjørn Cunis**

- **Titre** : Modélisation, analyse et commande pour la récupération d'un aéronef en situation de décrochage : de la théorie des systèmes au pilote automatique

- Thèse soutenue le 27/09/2019
 - Co-encadrement : Jean-Philippe Condomines
 - **Jury** : Mme. S. Tarbouriech (présidente) et M.M. M. Alamir (rapporteur), L. Burlion (directeur de thèse), M. Lowenberg (examinateur), P. Seiler (rapporteur) et L. Goerig (membre invité).
 - Financement ONERA
 - Publications associées : [a17], [a22], [a25], [s2], [c36], [c41], [c52], [ac5].
 - **Devenir du candidat** : Post Doctorant, Université du Michigan.
- **Anthony Bourdelle**
- **Titre** : Contributions méthodologiques à la modélisation et à la compensation des ballottements d'ergol pour le contrôle en attitude des véhicules spatiaux
 - Soutenance de thèse prévue au Printemps 2020
 - Co-encadrement : Jean-Marc Biannic (HDR)
 - **Jury** : Mme. C. Pittet (examinatrice) et M.M. L. Burlion (encadrant), F. Cazaurang (président), B. Clément (rapporteur), A. Falcoz (examinateur), A. Marcos (rapporteur) et J.S. Schotté (examinateur).
 - **Best Student Paper Award** dans la catégorie Flight Dynamics/GNC and Avionics de la conférence EUCASS 2019
 - Financement CNES
 - Publications associées : [c48], [c49], [c50], [c51].
 - **Devenir du candidat** : ingénieur d'études amont, SIREHNA.

2.10 Encadrements de Master

- **Nicolas Jacob**(*Supélec*)
- **Titre** : Commande non linéaire prédictive d'un missile
 - Période : Avril-Août 2007
- **Mathieu Archen**(*Ensica*)
- **Titre** : Commande non linéaire de systèmes flexibles
 - Période : Avril-Août 2011
- **David Hernandez**(*Ecole Centrale Nantes*)
- **Titre** : Transport d'une charge par un duo de drones hélicoptères
 - Période : Avril-Août 2012
- **Emmanuel Chambon**(*Mines de Paris*)
- **Titre** : Atterrissage automatique d'un drone à voilure fixe basé

- sur une approche énergétique
- Période : Avril-Août 2013
- **Baptiste Espivent** (*Supélec*)
 - **Titre** : Modélisation avancée et commande d'un drone multi-rotor
 - Période : Avril-Août 2014

2.11 Encadrements de projets d'élèves

- **Simon Duverger et Clara Issanchou** (*Insa Toulouse*)
 - **Titre** : Modélisation et commande non linéaire d'un Kite automatisé
 - Co-encadrement : Clément Toussaint
 - Période : Hiver 2014
- **Anouar El-Mourabit et Bartolomé Pontin** (*Isae Supaero*)
 - **Titre** : Virtual Constraints for Kite-Based Systems Control
 - Co-encadrement : Clément Toussaint
 - Période : Printemps 2014

2.12 Participations à des jurys de thèses

- **Contribution à la commande non linéaire d'un système électropneumatique pour une utilisation aéronautique : application sur un benchmark dédié**
 - Thèse soutenue par A. Girin le 04/12/2007
 - Participation au jury en tant que membre invité
- **Contribution à la synthèse d'observateurs non linéaires pour les systèmes commandés en réseaux**
 - Thèse soutenue par C. Hann le 11/02/2014
 - Participation au jury en tant qu'examinateur

2.13 Sélection de projets

La situation privilégiée de l'ONERA comme acteur central de la recherche aéronautique et spatiale en France nous a permis de collaborer à la fois avec des partenaires académiques et industriels sur plusieurs projets de recherche. Nous citons ici les principaux projets auxquels nous avons participé et qui ont bien souvent inspirés nos travaux de recherche – rattachés au thème général de la commande non linéaire des systèmes dynamiques –

et ainsi alimentés par les besoins que génèrent les applications aéronautiques et spatiales.

- DROPTER (Drone reconfiguration in the event of unforeseeable situations). Financé par l'Onera. Période : 09/2017-12/2018.
- COSOR (Orbital robotic systems control). Financé par le Cnes et l'Onera. Période : 09/2016-12/2018.
- VISIOLAND (VISION based LANDING solutions). Financé par l'ANR. Collaboration avec Airbus, l'Ircyn, l'Inria et Spikenet Technology. Période : 11/2013-11/2017.
- R&T CNES : "Adaptive control of a flexible satellite". Financé par le CNES. Collaboration avec l'UMR-CNRS Greyc. Période : 01/2014-12/2014.
- SMAC (Systems Modeling Analysis Control) Financé par l'Onera. Période : 01/2012-12/2015.
- NPI ESA "Soft Lunar Landing". Co-Financé par Airbus Defense and Space et l'agence Spatiale Europeenne (ESA). Collaboration avec l'ISM et Airbus Defense and Space. Période : 09/2011-11/2014.
- CLEANSKY "Smart Fixed Wing Aircraft". Financé par la commission Européenne. Collaboration avec Airbus (Load control department). Période : 01/2011-12/2013.
- NICE (Nonlinear Innovative Control designs and Evaluations). Financé par l'Agence Européenne de la Défense (EDA). Collaboration avec Dassault Aviation, le LAAS-CNRS et l'Université de Tor Vergata. Période : 04/2010-09/2012.

Ces différents projets ont fait l'objet de rapports d'avancements et finaux. Nous avons fait le choix de ne pas les répertorier dans le présent manuscrit.

Chapitre 3

Résumés des thèses encadrées

3.1 Thèse de Guillaume Sabiron

"Synthèse d'une Solution GNC basée sur des Capteurs de Flux Optique Bio-inspirés adaptés à la mesure des basses vitesses pour un Atterrissage Lunaire Autonome en Douceur".(2011-2014)

Dans cette thèse, nous nous intéressons au problème de l'atterrissage lunaire autonome et nous proposons une méthode innovante amenant une alternative à l'utilisation de capteurs classiques qui peuvent se révéler encombrants, énergivores et très onéreux. La première partie est consacrée au développement et à la construction de capteurs de mouvement inspirés de la vision des insectes volants et mesurant le flux optique. Le flux optique correspond à la vitesse angulaire relative de l'environnement mesurée par la rétine d'un agent. Dans un environnement fixe, les mouvements d'un robot génèrent un flux optique contenant des informations essentielles sur le mouvement de ce dernier. En utilisant le principe du "temps de passage", nous présentons les résultats expérimentaux obtenus en extérieur avec deux versions de ces capteurs. Premièrement, un capteur mesurant le flux optique dans les deux directions opposées est développé et testé en laboratoire. Deuxièmement un capteur adapté à la mesure des faibles flux optiques similaires à ceux pouvant être mesurés lors d'un alunissage est développé, caractérisé et enfin testé sur un drone hélicoptère en conditions extérieures. Dans la seconde partie, une méthode permettant de réaliser le guidage, la navigation et la commande (GNC pour Guidance Navigation and Control) du système est proposée. L'innovation réside dans le fait que l'atterrissage en douceur est uniquement assuré par les capteurs de flux optique. L'utilisation des capteurs inertiels est réduite au maximum. Plusieurs capteurs orientés

dans différentes directions de visée, et fixés à la structure de l'atterrisseur permettent d'atteindre les conditions finales définies par les partenaires industriels. Les nombreuses informations décrivant la position et l'attitude du système contenues dans le flux optique sont exploitées grâce aux algorithmes de navigation qui permettent d'estimer les flux optiques ventraux et d'expansion ainsi que le tangage. Nous avons également montré qu'il est possible de contrôler l'atterrisseur planétaire en faisant suivre aux flux optiques estimés une consigne optimale au sens de la consommation d'énergie. Les simulations réalisées durant la thèse ont permis de valider le fonctionnement et le potentiel de la solution GNC proposée en intégrant le code du capteur ainsi que des images simulées du sol de la lune.

3.2 Thèse d'Elodie Duraffourg

"Commande non linéaire en présence de modes souples. Applications aérospatiales". (2011-2014)

En aérospatial, les contraintes de masse ont conduit à utiliser des structures plus légères et par conséquent plus souples, induisant de nouveaux objectifs de commande, comme la réduction des efforts structuraux. Pour satisfaire ces objectifs, les modes de flexion doivent être considérés dès la synthèse de la loi de commande, ce qui entraîne certaines contraintes comme les non linéarités, le sous actionnement et l'altération des mesures par les modes souples. En considérant ces contraintes, cette thèse traite de la synthèse d'une méthode de commande non linéaire pour les systèmes aérospatiaux souples. Nous nous intéressons particulièrement au problème d'atténuation des oscillations provoquées par les modes souples. Pour cela, nous définissons une classe de système non linéaire, sous actionnée et à minimum de phase, représentative des systèmes aérospatiaux souples. Pour cette classe de système, nous proposons une loi de commande non linéaire synthétisée par retour d'état en utilisant des changements de variables et la technique du backstepping. La synthèse est effectuée de façon à améliorer le régime transitoire des modes souples. Les états souples n'étant pas mesurés, le problème du retour de sortie est également traité par l'intermédiaire d'observateurs adaptatifs (à temps fini et asymptotique). Des incertitudes sur la pulsation et l'amortissement des modes souples sont en particulier considérées. La méthode proposée est illustrée par des simulations numériques réalisées sur un lanceur et un avion hypersonique.

3.3 Thèse de Victor Gibert

"Analyse d'observabilité et synthèse d'observateurs robustes pour l'atterrissage basé vision d'avions de ligne sur des pistes inconnues". (2013-2016)

Dans le cadre de la génération des avions de transport du futur, Les constructeurs souhaitent développer une capacité d'atterrissage automatique permanente et ce, sur tout type de piste (voire sur des pistes inconnues). Dans ce but, la commande basée sur des capteurs visuels, appelée asservissement visuel, est envisagée afin de s'affranchir du besoin d'informations issues de systèmes extérieurs (ILS, GNSS). La vision, en fournissant une vue du monde extérieur, permet d'estimer la position relative de l'avion par rapport à la piste. La particularité de cette étude repose sur la méconnaissance des caractéristiques de la piste, ce qui réduit les possibilités d'utilisation de la vision. Des solutions d'estimation de position relative, basées sur des informations visuelles génériques à toute piste (points et droites de bord de piste), sont proposées. Le principe d'estimation repose sur l'utilisation de la dynamique des informations visuelles par rapport à la dynamique connue de l'avion grâce aux centrales inertielles. La validation de cette nouvelle approche est réalisée sur un simulateur complet incluant la chaîne de traitement d'image, utilisant des images synthétiques.

3.4 Thèse d'Emmanuel Chambon

"Commande de systèmes linéaires sous contraintes fréquentielles et temporelles. Application au lanceur flexible". (2013-2016)

Dans la plupart des problèmes de synthèse actuels, la loi de commande obtenue doit répondre simultanément à des critères fréquentiels et temporels en vue de satisfaire un cahier des charges précis. Les derniers développements des techniques de synthèse H_∞ de contrôleurs structurés permettent d'obtenir des lois de commande satisfaisant des critères fréquentiels multiples appliqués à plusieurs modèles de synthèse. Dans ce mémoire, cette approche est appliquée à la synthèse de loi de commande robuste en utilisant une structure de contrôleur basé observateur. En revanche, la synthèse de loi de commande satisfaisant une contrainte temporelle sur une sortie ou un état du système considéré est plus complexe car la formulation d'un équivalent fréquentiel est illusoire dans la plupart des cas. Dans ce travail de thèse, la technique additionnelle OIST est considérée pour ce type de contraintes. Elle consiste à

saturer la sortie du contrôleur dès que la contrainte n'est plus vérifiée afin de restreindre l'ensemble des sorties admissibles. Des résultats satisfaisants sont obtenus dans le cas des systèmes à minimum de phase. Initialement formulée pour les systèmes linéaires connus dont l'état est mesuré, la technique OIST peut être généralisée pour permettre de considérer des systèmes incertains dont seulement une partie de l'état est connue. C'est l'extension OISTeR qui est proposée dans ce travail. Elle utilise les données d'un observateur par intervalles pour borner de manière garantie le vecteur d'état. La théorie des observateurs par intervalles a récemment fait l'objet de nombreux travaux. La méthode la plus rapide pour obtenir un observateur par intervalles d'un système donné est de considérer un système intermédiaire coopératif dans de nouvelles coordonnées. Le passage dans ces nouvelles coordonnées s'effectue au moyen d'une matrice de transformation. Les méthodes de détermination actuelles de cette transformation sont faciles à mettre en oeuvre mais sont assez peu polyvalentes notamment dans le cas où des contraintes de précision sont spécifiées sur l'observateur par intervalles. Une nouvelle technique de détermination de la transformation, intitulée SCorpIO est proposée dans ce mémoire. Elle repose sur la reformulation du problème mathématique sous-jacent en problème de synthèse de loi de commande structurée. L'ensemble des techniques présentées est appliqué au contrôle d'un lanceur flexible durant son vol atmosphérique, en présence de rafales de vent. La difficulté de ce problème repose sur le critère temporel spécifié sur l'angle d'incidence qui doit rester borné afin de minimiser la charge aérodynamique sur les structures. Dans ce mémoire, des solutions sont proposées et illustrées sur un modèle simplifié du lanceur. Des pistes pour la prise en compte de modèles plus complexes sont données.

3.5 Thèse de Torbjørn Cunis

"Modélisation, analyse et commande pour la récupération d'un aéronef en situation de décrochage : de la théorie des systèmes au pilote automatique". (2016-2019)

Le travail effectué au cours de cette thèse tente d'apporter des solutions algorithmiques à la problématique de reprise au décrochage d'un aéronef. A travers de nombreux exemples d'application sur des modèles aérodynamiques, le lecteur pourra appréhender les concepts abstraits présentés dans cette thèse. Alors que la capacité pour un aéronef à revenir à une situation nominale après une sortie du domaine de vol est un élément clé pour les systèmes de transport aérien du futur, les recherches menées dans ce cadre sont

encore peu nombreuses. Pourtant, un tel dépassement conduit généralement à une perte de contrôle (dénommée LOC-I), que l'Association du Transport Aérien International (IATA) a classé dans la catégorie des « risques les plus élevés pour l'aviation ».

Dans un premier temps, nous avons montré que les modèles polynomiaux habituellement utilisés en théorie des systèmes ne représentent pas fidèlement l'aérodynamique d'un modèle d'avion sur l'ensemble de son enveloppe de vol. Nous avons donc tout d'abord montré qu'un modèle polynomial par morceaux représente avec exactitude les coefficients aérodynamiques pour les angles d'attaque faibles et élevés. Nous avons alors pu étendre à cette classe de systèmes, des méthodes récentes d'étude de bifurcation et d'analyse de stabilité qui utilisent des techniques de programmation semi-définie basées sur la positivité de polynômes (SOS) ; nous avons notamment appliqué ces résultats au modèle d'avion de transport générique dénommé GTM. Dans le même esprit, nous avons développé un modèle pour un petit aéronef à voilure fixe basé sur des simulations numériques en mécanique des fluides (CFD). Les coefficients dynamiques n'étant pas déterminés en CFD, nous avons identifié le coefficient d'amortissement du tangage en comparant l'analyse de bifurcation et les données de vol, ce qui nous a permis d'étudier à la fois la dynamique et la stabilité du vol en cas de fort décrochage.

Des résultats antérieurs ont montré que les techniques SOS étaient prometteuses pour la certification des lois de commande pour des systèmes non-linéaires, cependant sans avoir été appliqués à l'ingénierie aéronautique. En adaptant ces techniques aux modèles polynomiaux par morceaux, nous avons montré qu'il est désormais possible de les utiliser d'une manière précise mais réalisable sur le plan calculatoire. Ensuite, nous avons synthétisé des lois de commandes linéaires et polynomiales pour la récupération d'un fort décrochage. En outre, nous sommes désormais en mesure d'estimer des régions d'attraction pour des modèles polynomiaux par morceaux ; pour cela, nous avons proposé un algorithme amélioré pour l'analyse de stabilité locale des systèmes à commutation, tels que ceux qui sont définis par des splines, rendant ainsi notre travail disponible pour l'analyse et la certification futures de modèles d'avion très fidèles.

La commande prédictive basée modèle (MPC) s'est avérée être une approche très efficace lorsque la dynamique du système est fortement non linéaire et soumise à des contraintes d'état qui rendent difficile la récupération après le décrochage. Cependant, pour des systèmes réalistes, il est nécessaire de prendre des précautions afin de prouver rigoureusement la stabilité en boucle fermée. En utilisant la technique SOS, nous avons ainsi montré la stabilité d'une stratégie de récupération d'un fort décrochage visant à minimiser la perte d'altitude. Nous avons aussi montré qu'une telle stratégie de commande

permet la récupération d'une spirale infernale en utilisant le simulateur GTM. Les résultats de cette thèse sont donc prometteurs et fournissent de nouvelles approches théoriques pour la modélisation, l'analyse de stabilité et le contrôle de la dynamique des futurs aéronefs ainsi que pour le développement et la certification de systèmes de commande de vol visant à prévenir les accidents dus à la perte de contrôle.

3.6 Thèse d'Anthony Bourdelle

"Contributions méthodologiques à la modélisation et à la compensation des ballottements d'ergol pour le contrôle en attitude des véhicules spatiaux". (2016-2019)

La conception de missions spatiales, toujours plus ambitieuses, exige un haut de niveau de performances en précision et en stabilité de pointage en dépit des perturbations. En particulier, le ballottement des ergols est un phénomène complexe qui résulte du mouvement du fluide dans les réservoirs lors des manœuvres du satellite, dégradant les performances du contrôle d'attitude et pouvant conduire à l'instabilité. Les ballottements sont habituellement pris en compte dans la synthèse de lois de commande via des modèles mécaniques équivalents, qui sont valides seulement dans le cadre d'hypothèses très contraignantes pour les satellites. Nous développons alors une modélisation innovante du ballottement sous forme de système LPV incertain dont l'identification repose sur des données de Mécanique des Fluides Numériques. En s'appuyant sur ce modèle nous proposons une stratégie de compensation basée sur un observateur LPV robuste dont la synthèse est effectuée via des techniques de synthèse H_∞ multi-modèles. L'intérêt principal de cette stratégie est qu'elle est mise en œuvre indépendamment d'un contrôleur d'attitude pré-existant, satisfaisant hors ballottement. Enfin, le respect des capacités des actionneurs est assuré par une approche Reference Governor qui modifie la référence à suivre par le système. L'ensemble de la stratégie est rigoureusement testée et analysée sur un modèle de test. Les résultats suggèrent alors qu'une telle amélioration du système de contrôle d'attitude avec une atténuation efficace des effets du ballottement pourrait contribuer à réduire la complexité et la masse des réservoirs, et améliorer ainsi la disponibilité des missions.

Chapitre 4

Publications

4.1 Articles parus dans des revues indexées

- [a25] T. Cunis, J-P. Condomines and L. Burlion, *Local stability analysis for large polynomial spline systems*,, accepted to Automatica.
- [a24] L. Burlion, M. Malisoff and F. Mazenc, *Stabilization and robustness analysis of saturating integrators arising in vision based landing of aircraft with sampling*, accepted to Systems & Control Letters.
- [a23] M. Nicotra, D. Liao-McPherson, L. Burlion and I. Kolmanovsky, *Spacecraft Attitude Control with Nonconvex Constraints : An Explicit Reference Governor Approach*, accepted to IEEE Trans. on Automatic Control.
- [a22] T. Cunis, J-P. Condomines, L. Burlion and A. la Cour-Harbo, *Dynamic stability analysis of aircraft flight in deep stall*, to appear in AIAA Journal of Aircraft.
- [a21] T. Ahmed-Ali, E. Fridman, F. Giri, M. Kahelras, F. Lamnabhi-Lagarrigue and L. Burlion, *Observer design for a class of parabolic systems with large delays and sampled measurements*, to appear in IEEE Trans. on Automatic Control, 2020.
- [a20] L. Burlion, L. Zaccarian, H. de Plinval and S. Tarbouriech, *Discontinuous model recovery anti-windup for image based visual servoing*, Automatica, vol.104, pp.41-47, 2019.
- [a19] F. Mazenc, L. Burlion and M. Malisoff, *Backstepping design for output feedback stabilization for a class of uncertain systems*, Systems & Control Letters, vol.123, pp.134-143, 2019.

- [a18] F. Mazenc, L. Burlion and M. Malisoff, *Stabilization and robustness analysis for a chain of saturating integrators with imprecise measurements*, IEEE Control Systems Letters, vol.3(2), 2019.
- [a17] T. Cunis, L. Burlion and J-P. Condomines, *On Piece-wise Polynomial Modeling for Control and Analysis of Aircraft Dynamics beyond Stall*, AIAA Journal of Guidance, Control and Dynamics, vol.42(4), pp.949-957, 2019.
- [a16] V. Gibert, F. Plestan, L. Burlion, J. Boada and A. Chriette, *New scheme for visual estimation of deviations based on sliding mode and high gain approaches : application to the landing of a civil aircraft*, Control Engineering Practice, vol.75, pp.17-25, 2018.
- [a15] F. Mazenc, M. Malisoff, L. Burlion and J. Weston, *Bounded Backstepping Control and Robustness Analysis for Time-Varying Systems under Converging-Input-Converging-State Conditions*, European Journal of Control, vol.42, pp.15-24, 2018.
- [a14] L. Burlion, J-M. Biannic and T. Ahmed-Ali, *Attitude tracking of a flexible spacecraft under angular velocity constraints*, International Journal of Control, published online 12-2017.
- [a13] T. Ahmed-Ali, F. Giri, M. Krstic, L. Burlion and F. Lamnabhi-Lagarrigue, *Adaptive Observers design in presence of heat PDE sensor*, Automatica, vol.82, pp. 93-100, 2017.
- [a12] E. Chambon, L. Burlion and P. Apkarian, *Time-response shaping using Output to Input Saturation Transformation*, International Journal of Control, vol. 91(3), pp.534-553, 2018.
- [a11] E. Chambon, L. Burlion and P. Apkarian, *Détermination de matrice semblable Metzler par optimisation non lisse*, JESA, European Journal of Automation, vol.50, pp.75-94, 2017.
- [a10] E. Duraffourg, L. Burlion and T. Ahmed-Ali, *Finite-time observer based Backstepping control of a flexible launch vehicle*, Journal of Vibration and Control, vol. 24(2), pp. 1535-1550, 2018.
- [a9] T. Ahmed-Ali, F. Giri, M. Krstic, L. Burlion and F. Lamnabhi-Lagarrigue, *Adaptive Boundary Observer for Parabolic PDEs subject to Domain and Boundary Parameter Uncertainties*, Automatica, vol.72, pp 115-122, 2016.
- [a8] T. Ahmed-Ali, E. Fridman, F. Giri, L. Burlion and F. Lamnabhi-Lagarrigue, *Using exponential time-varying gains for sampled-data*

stabilization and estimation, Automatica, vol.67, pp 244-251, 2016.

- [a7] E. Chambon, L. Burlion and P. Apkarian, *A Nonsmooth Optimization-based Approach to Interval Observers Design*, in IET Control Theory & Applications, vol. 10, no. 11, pp. 1258-1268, 2016.
- [a6] T. Folin, T. Ahmed-Ali, F. Giri, L. Burlion and F. Lamnabhi-Lagarri-gue, *Sampled-Data Adaptive Observer for a Class of State-Affine Out-put-Injection Nonlinear Systems*, in IEEE Trans. on Automatic Control, vol. 61(2), pp.462-467, 2016.
- [a5] T Ahmed-Ali, F. Giri, M. Krstic, F. Lamnabhi-Lagarri-gue and L. Burlion, *Adaptive observer for a class of parabolic PDEs*, in IEEE Trans. on Automatic Control, vol.61(10), pp.3083-3090, 2016.
- [a4] G. Sabiron, T. Raharijaona, L. Burlion, E. Kervendal, E. Bornschlegl and F. Ruffier, *Sub-optimal Lunar Landing GNC using Non-Gimbaled Optic Flow Sensors*, in IEEE Trans. on Aerospace and Electronic Sys-tems, vol. 51 (4), pp.2525-2545, 2015.
- [a3] R. Postoyan, T. Ahmed-Ali, L. Burlion, F. Lamnabhi-Lagarri-gue, *On the Lyapunov-based adaptive control redesign for a class of non-linear sampled-data systems*, Automatica, vol.44(8), pp 2099-2107, 2008.
- [a2] L. Burlion, T. Ahmed-Ali and F. Lamnabhi-Lagarri-gue, *On the sta-bility of a class of nonlinear hybrid systems*, Nonlinear Analysis : Theory, Methods and Applications, vol.65(12), 2236-2247, 2006.
- [a1] L. Burlion, T. Ahmed-Ali and F. Lamnabhi-Lagarri-gue, *On the sta-bilization of sampled-data nonlinear systems by using backstepping on the higher order approximate models*, International Journal of Control, vol.79(9), 1087-1095, 2006.

4.2 Articles soumis

- [s2] T. Cunis, J.P. Condomines, L. Burlion, *Stability and control synthe-sis for deep-stall recovery using sum-of-squares*, submitted to AIAA Journal of Guidance, Control and Dynamics.
- [s1] L. Burlion, V. Gibert, M. Malisoff and F. Mazenc, *Stabilization and robustness analysis of a nonlinear system arising in vision based lan-ding of airliners*, submitted to International Journal of Robust and Nonlinear Control.

4.3 Chapitres de livre

Ouvrage : *Advances in Aerospace Guidance Navigation and Control : selected papers of the 3rd CEAS Specialist Conference on Guidance, Navigation and Control* Springer , Edited by J. Bordeneuve-Guibé, A. Drouin and C. Roos, 2015.

- [ch4] E. Chambon, P. Apkarian and L. Burlion, *Flexible launch vehicle control using robust observer-based controller obtained through structured H_∞ synthesis*, Part I, Guidance and Control, pp.23-38.
- [ch3] V. Gibert, L. Burlion, A. Chriette, J. Boada and F. Plestan, *A new observer for range identification in perspective vision systems*, Part II, Estimation and Navigation, pp.401-414.
- [ch2] H. de Plinval and L. Burlion, *Nonlinear visual servoing control for VTOL UAVs with field of view constraint"*, Part III, Atmospheric Applications, pp.531-548.

Ouvrage : *Advances in Aerospace Guidance Navigation and Control : selected papers of the 2nd CEAS Specialist Conference on Guidance, Navigation and Control* Springer , Edited by Q. Chu, B. Mulder, D. Choukroun, E.-J. van Kampen, C. de Visser, G. Looye, 2013.

- [ch1] G. Sabiron, P. Chavent, L. Burlion, E. Kervendal, P. Fabiani, T. Raharijaona and F. Ruffier, *Toward an autonomous lunar landing based on low-speed optic flow sensors*, pp.681-699.

4.4 Articles parus dans une revue électronique

- [ae2] P. Bidaud, L. Burlion, H. de Plinval, T. Loquen, J. Marzat and C. Pralet, *Dealing with complexity through advanced control techniques*, in a special issue celebrating the 70th birthday of ONERA, Vol.12(13), AL12-13 (the electronic Journal of Onera, on-line accessible), 2016.
- [ae1] J.M. Biannic, L. Burlion and H. de Plinval, *Robust control design over large flight envelopes : a promising approach for aerial robotics*, in a special issue of the Aerospace Lab Journal on Aerial Robotics, Vol.8(1), AL8-01 (the electronic Journal of Onera, on-line accessible), 2014.

4.5 Brevet

- [p1] US Patent 20,160,026,189, *Method and system for automatic autonomous landing of an aircraft*, J. Boada-Bauxell, V. Gibert, L. Burlion, A. Chriette and F. Plestan, April 2018.

4.6 Communications avec actes et comité de sélection

- [c53] L. Burlion, M. Malisoff and M. Mazenc, *Stabilization and robustness analysis for a chain of saturating integrators arising in the visual landing of aircraft*, accepted to the 58th IEEE Conference on Decision and Control, (CDC 2019).
- [c52] T. Cunis, D. Liao-MacPherson, J-P Condomines, L Burlion, I. Kolmanovsky, *Economic Model Predictive Control Strategies for Aircraft Deep-stall Recovery with Stability Guarantees*, accepted to the 58th IEEE Conference on Decision and Control, (CDC 2019).
- [c51] J.-M. Biannic, A. Bourdelle, H. Evain, S. Moreno and L. Burlion, *On robust LPV-based observation of fuel slosh dynamics for attitude control design*, in Proc. of the 3rd IFAC Workshop on Linear Parameter Varying Systems, (LPVS'19), 2019.
- [c50] A. Bourdelle, J-M. Biannic, S. Moreno, C. Pittet and L. Burlion, *Propellant sloshing torque H_∞ -based observer design for enhanced attitude control*, in Proc. of IFAC ACA, 2019.
- [c49] A. Bourdelle, J-M. Biannic, H. Evain, C. Pittet, S. Moreno and L. Burlion, *Modeling and control of propellant slosh dynamics in observation spacecraft*, in Proc. of the 8th European Conference for Aeronautics and Space Sciences, (EUCASS 2019), Madrid, Spain. **Best student paper award** dans la catégorie Flight Dynamics, GNC and Avionics.
- [c48] A. Bourdelle, L. Burlion, J-M. Biannic, H. Evain, S. Moreno, C. Pittet, A. Dalmon, S. Tanguy and T. Ahmed-Ali *Towards new control design oriented models for fuel sloshing in observation spacecraft*, AIAA SciTech 2019 Forum, San Diego, CA, 2019.
- [c47] L. Burlion, M. Nicotra and I. Kolmanovsky, *A fast reference governor for the constrained control of linear discrete-time systems with parametric uncertainties*, in Proc. of the 57th IEEE Conference on

- Decision and Control, (CDC 2018), pp. 6289-6294, 2018.
- [c46] F. Mazenc, L. Burlion and V. Gibert, *Stabilization of a nonlinear system that arises in the context of vision based landing of an airliner*, in Proc. of the 57th IEEE Conference on Decision and Control, (CDC 2018), pp. 5313-5318, 2018.
- [c45] T. Ahmed-Ali, E. Fridman, F. Giri, M. Kahelras, F. Lamnabhi-Lagarrigue and L. Burlion, *Observer design for a class of parabolic systems with arbitrarily delayed measurements*, in Proc. of the 57th IEEE Conference on Decision and Control, (CDC 2018), pp. 2199-2204, 2018.
- [c44] J-M. Biannic, L. Burlion and S. Tarbouriech, *Finite time LPV analysis of vision based landing system with Anti-Windup augmentation*, in Proc. of the 2nd IFAC Workshop on Linear Parameter Varying Systems, (LPVS'18), vol. 51(26), pp.37-42, 2018.
- [c43] F. Mazenc, L. Burlion and M. Malisoff, *Backstepping design for output feedback stabilization for uncertain systems using dynamic extension*, in Proc. of the 2nd IFAC Conference on Modelling, Identification and Control of Nonlinear Systems, (MICNON 2018), pp.260-265, 2018.
- [c42] F. Mazenc, L. Burlion and V. Gibert, *Stabilization of a system that arises in the context of vision based landing of a civil aircraft*, in Proc. of the annual American Control Conference, (ACC 2018), pp. 2978-2983, 2018.
- [c41] T. Cunis, L. Burlion and J-P. Condomines, *Piece-wise Identification and Analysis of the Aerodynamic Coefficients, Trim Conditions, and Safe Sets of the Generic Transport Model*, AIAA SciTech 2018 Forum, Kissimmee, FL, January 2018.
- [c40] F. Mazenc, M. Malisoff and L. Burlion, *Bounded backstepping through a dynamic extension with delay*, in Proc. of the 56th IEEE Conference on Decision and Control, (CDC 2017), pp.4351-4356, 2017.
- [c39] J-M. Biannic and L. Burlion, *Performance analysis of saturated parameter-varying systems with application to vision-based landing assessment*, in Proc of the 20th IFAC World Congress, pp.10513-10517, 2017.
- [c38] L. Burlion and H. de Plinval, *Vision based anti-windup design with application to the landing of an airliner*, in Proc of the 20th IFAC

World Congress, pp.10482-10487, 2017.

- [c37] C. Chauffaut, L. Burlion, F. Defay and H. de Plinval, *Collision Avoidance of multiple MAVs using a multiple Outputs to Input Saturation Technique*, in Proc of the International Micro Air Vehicle Conference and Competition, (IMAV 2017), pp.190-195, 2017.
- [c36] T. Cunis, J-P. Condomines and L. Burlion, *Six-degrees-of-freedom trim analysis of unmanned aerial systems based on piecewise polynomial aerodynamic coefficients*, in Proc. of the 2017 Workshop on Research, Education and Development of Unmanned Aerial Systems, (RedUAS 2017), pp. 108-113, 2017.
- [c35] L. Burlion and H. de Plinval, *Toward vision based landing of a fixed-wing UAV on an unknown runway under some FoV constraints*, in Proc of the 2017 International Conference on Unmanned Aircraft Systems, (ICUAS 2017), Miami, Florida, pp. 1824-1832, 2017.
- [c34] C. Chauffaut, F Defay, L Burlion and H de Plinval, *UAV obstacle avoidance scheme using an Output to Input Saturation Transformation technique*, in Proc of the International Conference on Unmanned Aircraft Systems, (ICUAS 2016), pp. 227-234, 2016.
- [c33] E. Chambon, L. Burlion and P. Apkarian, *Output to Input Saturation Transformation : Demonstration and Application to Disturbed Linear Systems*, in Proc of the 54th IEEE Conference on Decision and Control, pp.7566-7571, 2015.
- [c32] V. Gibert, L. Burlion, A. Chriette, J. Boada and F. Plestan, *New pose estimation scheme in perspective vision system during civil aircraft landings*, in Proc of the 11th IFAC Symposium on Robot Control, SYROCO 2015, vol.48(19), pp.238-243, 2015.
- [c31] L. Burlion and H. de Plinval, *Visual landing insensitive to the depth with variable constraints : a twisting based solution*, in Proc. of the 23rd Mediterranean Conference on Control and Automation, MED 2015, pp.603-610, 2015.
- [c30] T. Ahmed-Ali, E. Fridman, F. Giri, L. Burlion and F. Lamnabhi-Lagarrigue, *A new approach to enlarging sampling intervals for some sampled-data systems and observers*, in Proc of the 12th IFAC workshop on Time Delay Systems, IFAC TDS 2015, vol.48(12), pp.440-445, 2015.
- [c29] E. Chambon, P. Apkarian and L. Burlion, *Metzler matrix transform determination using a non-smooth optimization technique with*

- application to interval observers*, in Proc. of the SIAM conference on Control and Its Applications, SIAM CT 15, pp. 205-211, 2015.
- [c28] V. Gibert, L. Burlion, A. Chriette, J. Boada and F. Plestan, *Non-linear observers in vision system : application to civil aircraft vision based landing*, in Proc. of the European Control Conference, ECC 2015, pp. 1812-1817, 2015.
- [c27] V. Gibert, L. Burlion, A. Chriette, J. Boada and F. Plestan, *Vision based automatic landing of a civil aircraft by using nonlinear pose estimation*, in Proc of the 6th European Conference for Aeronautics and Space Sciences, (EUCASS 2015), Krakow, Poland, 2015.
- [c26] T. Ahmed-Ali, F. Giri, M. Krstic, L. Burlion and F. Lamnabhi-Lagarrigue, *Adaptive observers for parabolic PDEs with uncertain parameter in the boundary condition*, in Proc. of the European Control Conference, ECC 2015, pp. 1337-1342, 2015.
- [c25] E. Chambon, L. Burlion, and P. Apkarian, *Robust output interval constraint using O/I saturation transformation with application to uncertain linear launch vehicle*, in Proc. of the European Control Conference, ECC 2015, pp. 1796-1801, 2015.
- [c24] G. Sabiron, L. Burlion, E. Kervendal, E. Bornschlegl, T. Raharijaona and F. Ruffier, *Autonomous Lunar Landing Based on Bio-inspired Visual Motion sensors tested in flight*, in Proc of 9th International ESA Conference on Guidance, Navigation & Control Systems, ESA GNC 2014.
- [c23] G. Sabiron, L. Burlion, T. Raharijaona and F. Ruffier, *Optic flow-based nonlinear control and optimal guidance for lunar landing*, in proc of IEEE International Conference on Robotics and Biomimetics, ROBIO 2014, pp. 1241-1247, 2014.
- [c22] T. Ahmed-Ali, L. Burlion, F. Lamnabhi-Lagarrigue and C. Hann, *A sampled-data observer with time-varying gain for a class of nonlinear systems with sampled-measurements*, in Proc of the 53rd Conference on Decision and Control, Los Angeles, pp.316-321, 2014.
- [c21] L. Burlion, H. de Plinval and P. Mouyon, *Backstepping based Visual Servoing for Transport Aircraft Automatic Landing*, in Proc. of IEEE Multi conference on Systems and Control, MSC 2014, pp. 1461-1466, 2014.
- [c20] G. Sabiron, L. Burlion, G. Jonniaux, E. Kervendal, E. Bornschlegl, T. Raharijaona, and F. Ruffier, *Backup State Observer Based on Optic*

- Flow Applied to Lunar Landing*, in Proc of international conference on Intelligent ROBot and Systems, IROS 2014, pp. 2325-2332, 2014.
- [c19] L. Burlion, C. Poussot-Vassal, P. Vuillemin, M. Leitner and T. Kier, *Longitudinal manoeuvre load control of a flexible large-scale aircraft*, in Proc of the 19th IFAC World Congress, pp. 3413-3418, 2014.
- [c18] E. Duraffourg, L. Burlion, T. Ahmed-Ali and F. Lamnabhi-Lagarri-gue, *Finite time adaptive observer of a flexible nonlinear model of a launcher*, in Proc of the 19th IFAC World Congress, pp. 546-551, 2014.
- [c17] L. Burlion, E. Duraffourg, T. Ahmed-Ali and F. Lamnabhi-Lagarri-gue, *Global asymptotic stabilization for some nonlinear models of flexible aerospace vehicles*, in Proc of the 52nd Conference on Decision and Control, Florence, pp.4230-4235, 2013.
- [c16] E. Duraffourg, L. Burlion and T. Ahmed-Ali, *Longitudinal Modeling and Preliminary Control of a Non-linear Flexible Launch Vehicle*, in Proc. of the 11th IFAC International Workshop on Adaptation and Learning in Control and Signal Processing, Caen, pp.209-214, 2013.
- [c15] E. Duraffourg, L. Burlion, T. Ahmed-Ali and F. Lamnabhi-Lagarri-gue, *Nonlinear full-state control of a flexible hypersonic vehicle*, in Proc. of the IEEE conference on Electronics, Control, Measurement, Signals and their application to Mechatronics, 2013.
- [c14] E. Duraffourg, L. Burlion, T. Ahmed-Ali and F. Lamnabhi-Lagarri-gue, *Nonlinear control of the longitudinal rotational dynamics of a flexible aircraft*, in Proc. of the European Control Conference, pp.335-340, 2013.
- [c13] L. Burlion and H. de Plinval, *Keeping a ground point in the camera field of view of a landing UAV*, in Proc of the IEEE International Conference on Robotics and Automation, pp.5763-5768, 2013.
- [c12] G. Sabiron, P. Chavent, L. Burlion, E. Kervendal, P. Fabiani, T. Raharijaona and F. Ruffier, *Toward an autonomous lunar landing based on low-speed optic flow sensors*, in Proc of Euro GNC 2013, pp.993-1011, 2013.
- [c11] L. Burlion and H. de Plinval, *Automatic UAV landing with ground target maintained in the field of view*, in Proc of Euro GNC 2013, pp.1546-1562, 2013.
- [c10] J-M. Biannic, L. Burlion, S. Tarbouriech and G. Garcia, *On dynamic inversion with rate limitations*, American Control Conference,

pp. 191-196, 2012.

- [c9] L. Burlion, *A new Saturation function to convert an output constraint into an input constraint*, 20th Mediterranean Conference on Control and Automation, (MED 2012), pp.1217-1222, 2012.
- [c8] L. Burlion, T. Ahmed-Ali and F. Lamnabhi-Lagarrigue, *Updating the gain of global finite-time high gain observers*, in Proc. of the 50th IEEE Conference on Decision and Control and European Control Conference, pp. 8145-8150, 2011.
- [c7] L. Burlion, T. Ahmed-Ali, R. Postoyan and F. Lamnabhi-Lagarrigue, *Adaptive control redesign for some nonlinear sampled-data systems*, in proc. of the IFAC Symposium on Nonlinear Control, (NOLCOS'07), pp.754-759, 2007.
- [c6] L. Burlion, T. Ahmed-Ali and F. Lamnabhi-Lagarrigue, *On the adaptive control of nonlinear sample-data systems*, in Proc. of the European Control Conference, (ECC'07), 2007.
- [c5] T. Ahmed-Ali, L. Burlion and F. Lamnabhi-Lagarrigue, *On the stabilization of sampled-data systems by using higher order approximations of the exact discretized systems*, in Proc. of IMACS World Congress, 2005.
- [c4] L. Burlion, T. Ahmed-Ali and F. Lamnabhi-Lagarrigue, *On the design of Lyapunov functions for state-dependent impulsive dynamical systems*, in Proc. of the IFAC World Congress, pp. 379-384, 2005.
- [c3] L. Burlion, T. Ahmed-Ali and F. Lamnabhi-Lagarrigue, *Stabilization of switching systems : a viability approach*, in Proc. of the 16th International Symposium on Mathematical Theory of Networked Systems, (MTNS 2004), 2004.
- [c2] L. Burlion, T. Ahmed-Ali and F. Lamnabhi-Lagarrigue, *On the stability of a class of nonlinear hybrid systems*, in Proc. of the 6th IFAC-Symposium on Nonlinear Control Systems (NOLCOS 2004), 2004.
- [c1] L. Burlion, T. Ahmed-Ali and N. Seube, *Glider's roll control based on Backstepping*, in Proc. of the IFAC Conference on Control Applications in Marine Systems (CAMS 2004), 2004.

4.7 Communications soumises

- [cs1] L. Burlion and I. Kolmanovsky, *Aircraft vision-based landing using robust Extended Command Governors*, submitted to the 21st IFAC World Congress, July 2020.

4.8 Communications diverses

- [ac1] E. Chambon, P. Apkarian and L. Burlion, *Détermination d'une matrice semblable Metzler par optimisation non lisse*, 6èmes Journées Doctorales & Journées Nationales du GDR MACS, JN/JDMACS 2015, Juin 2015
- [ac2] C. Chauffaut, F. Defay, L. Burlion and H. de Plinval, *Toward in-door obstacles avoidance on a Micro Air Vehicle*, in Proc. of the 15th ONERA-DLR Aerospace Symposium, ODAS 2015, May, 2015
- [ac3] L. Burlion and H. de Plinval, *Automatic vision-based landing for aircraft with unknown depth and constrained velocity*, in Proc. of the 15th ONERA-DLR Aerospace Symposium, ODAS 2015, May, 2015
- [ac4] G. Sabiron, L. Burlion, T. Raharijaona and F. Ruffier, *Optic flow based observer in case of IMU Loss of a lunar lander*, in Proc. of the 15th ONERA-DLR Aerospace Symposium, ODAS 2015, May, 2015
- [ac5] T. Cunis, L. Burlion, J-P. Philippe Condomines, *Non-linear Analysis and Control Proposal for In-flight Loss-of-control*, open invited track extended abstract, IFAC World Congress 2017

Chapitre 5

Coordination du projet VISIOLAND

Nous avons monté et coordonné le projet ANR VISIOLAND (VISION-based aircraft LANDing techniques). Ce projet a occupé 60% de notre temps entre Décembre 2013 et Décembre 2017 : ainsi, il nous semble important de rappeler ici les grandes lignes de ce projet qui a orienté en partie nos travaux de recherche sur cette période. Ces travaux de recherche sont d'ailleurs détaillés dans la seconde partie de ce manuscrit.

5.1 Résumé du projet

La phase d'atterrissage est, pour un avion de transport civil, une des phases les plus critiques du vol. Elle requiert de la part du pilote une habileté certaine et reste très exposée aux risques d'incidents et d'accidents. Le développement d'une capacité d'atterrissage automatique a permis d'accroître la robustesse des opérations d'atterrissage tout en allégeant la tâche du pilote dans cette phase décisive. Bien que cette capacité soit désormais disponible sur tous les porteurs de plus de 100 places (AIRBUS et BOEING), son utilisation reste toutefois limitée. Un des principaux facteurs limitant vient aujourd'hui de la dépendance à des moyens de positionnement extérieurs à l'avion, dont la disponibilité géographique (taux de couverture) comme temporelle (taux de panne) n'est pas totale. En effet, le moyen le plus répandu, l'ILS (Instrument Landing System) qui envoie à l'avion un signal permettant d'en déduire des déviations par rapport à l'axe d'atterrissage, nécessite des infrastructures aéroport que seuls les grandes plateformes occidentales peuvent s'offrir. En outre, même dans le cas où les aéroports en sont équipés, la probabilité de panne de l'équipement n'est pas négligeable. En terme de

localisation, il existe aujourd’hui un moyen qui offre une couverture mondiale : le GPS. Néanmoins, sa précision et son intégrité, dans le monde civil, ne sont pas suffisants pour de l’atterrissage automatique. Il faut pour cela disposer d’un moyen complémentaire permettant de faire un recalage local du GPS (GPS différentiel). Ce recalage peut être soit fourni par une station sol propre à l’aéroport (GBAS), soit par un réseau satellite complémentaire (SBAS) qui offre un recalage régional (WAAS, EGNOS, ...). Si ces réseaux permettent d’envisager, à l’horizon 2025, une couverture géographique mondiale, leur disponibilité reste aujourd’hui relativement limitée.

La tendance générale dans le transport aérien est d’aller vers une augmentation du niveau global d’automatisation de la tâche de pilotage lors de l’atterrissage des avions. Cette évolution doit permettre de répondre à plusieurs besoins. Le premier est celui d’une recherche constante de l’amélioration du niveau de robustesse des opérations lors des phases d’atterrissage (réduction des atterrissages durs et des remises de gaz). Le second est une évolution de la tâche du pilote et un transfert des tâches de pilotage court terme de l’attitude avion vers une gestion accrue de la mission et de l’interaction avec le trafic aérien environnant. Pour les raisons exposées précédemment, l’atterrissage automatique tel qu’il est conçu aujourd’hui n’offre pas une disponibilité géographique et temporelle suffisante pour répondre seul à ce besoin. En revanche, l’utilisation d’une caméra embarquée est une des solutions possibles pour augmenter la capacité « sensorielle » de l’avion et répondre au manque d’information de positionnement lorsque les systèmes extérieurs sont pris en défaut.

Nous avons, à travers le projet VISIOLAND, étudié comment la camera pouvait répondre au besoin d’automatisation, partielle ou totale, de la tâche pilote en vue de l’atterrissage de l’aéronef.

5.2 Activités réalisées

Le consortium regroupait cinq partenaires académiques et industriels avec des compétences reconnues et complémentaires :

- AIRBUS, un des leaders mondiaux de la production d’avions de ligne, a contribué par son expérience et sa maîtrise du contexte opérationnel et industriel mis au service du consortium. Il a ainsi défini les scénarios d’emploi d’un atterrissage basé vision et montré comment intégrer ce nouveau concept dans les architectures existantes d’atterrissage automatique de manière à pouvoir in fine le certifier Il a mis et adapté

- à disposition du projet un simulateur d'avion de ligne avec lequel le pilote et les nouveaux algorithmes ont pu interagir.
- SPIKENET TECHNOLOGY, PME Toulousaine, qui développe et commercialise une technologie basée sur les neurosciences pour le traitement d'informations visuelles a adapté la technologie disruptive SN-vision aux besoins du projet. Ainsi, SPIKENET a développé un système logiciel permettant la détection de pistes d'atterrissage à partir d'un capteur visuel installé dans le cockpit d'un avion, et également étudié la possibilité d'utiliser une caméra DVS ; cette détection a été réalisée par une méthode neuronale extrêmement rapide couplée avec l'algorithme de suivi de piste (INRIA)
 - l'INRIA (LAGADIC) dont l'axe de recherche est l'application de la vision à la robotique, a mis au point des algorithmes de suivi et de localisation à partir de séquences d'images. Plus précisément, l'INRIA a proposé deux approches complémentaires de suivi de la piste dans l'image : la première basée modèle (MBT), la seconde qualifiée de dense (DVBT).
 - l'IRCCyN (devenu le LS2N en Janvier 2017) dont l'expertise en automatique théorique est reconnue, a développé sur cette base des méthodes utilisant les informations visuelles dans la boucle de guidage via la synthèse d'observateurs. Ces méthodes ont été développées en coopération avec AIRBUS et l'ONERA.
 - l'ONERA (DTIS) est le partenaire privilégié d'AIRBUS dans le développement de ses méthodes et outils de pilotage, guidage et d'aide à la décision, outils qu'il a adaptés au contexte du projet. Notamment, il a proposé de nouvelles techniques de commande basées vision ainsi que des outils d'analyse correspondant afin d'utiliser des informations visuelles tout en prenant en compte les limitations physiques d'un avion ou d'un drone. Des outils de diagnostic d'intégrité des informations visuelles ont aussi été mis au point.

Les innovations techniques et scientifiques ainsi réalisées ont été évaluées de la façon suivante :

- un aéronef à voilure fixe conçu par la société l'Avion Jaune et automatisé à l'ONERA ainsi qu'un AIRBUS d'essai ont acquis des séquences d'images afin de tester les algorithmes de perception développés dans le projet.
- un simulateur d'AIRBUS certifié très représentatif d'un avion de ligne a été couplé à un générateur d'images (synthétiques ou réelles) : celui-ci a permis de tester en partie les logiciels développés dans le projet.

5.3 Bilan du projet

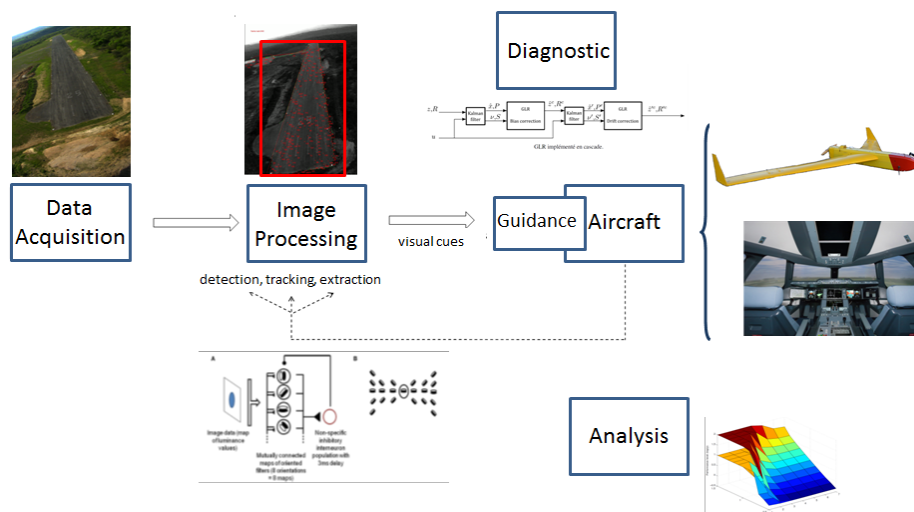


FIGURE 5.1 – Résumé en images des activités réalisées au sein du projet VISIOLAND : le consortium couvrait l'ensemble des compétences requises depuis l'acquisition et le traitement d'images jusqu'à l'implémentation en temps réel des asservissements visuels sur un drone ou simulateur certifié d'un Airbus.

VISIOLAND a fait l'objet d'un brevet et d'une quinzaine de publications ou communications internationales à comité de lecture. Le but étant de réduire la tâche du pilote lorsque celui est aujourd'hui en pilotage « à vue », le projet VISIOLAND s'est restreint à l'utilisation d'une caméra dans le domaine visible. On pourrait certainement chercher dans un second temps, en prolongement du projet, à utiliser des capteurs couvrant d'autres gammes de fréquence afin d'offrir également une augmentation du domaine opérationnel de l'avion.

Le projet VISIOLAND a répondu aux objectifs ambitieux que les partenaires s'étaient donné à savoir le développement de logiciels permettant de réaliser un atterrissage basé vision. Il a aussi donné de bons résultats en termes de brevets et de publications/communications. Le consortium aurait certainement souhaité aller plus loin dans l'intégration de ses logiciels sur le simulateur certifié d'AIRBUS et sur le drone Avion Jaune de l'ONERA. A la suite du projet VISIOLAND, AIRBUS a intensifié ses travaux sur les asservissements visuels et a notamment lancé les projets EAGLE (Eye for Autonomous Guidance and Landing Extension) et ATTOL (Autonomous Taxi, Take-Off and

Landing).

Deuxième partie

Synthèse d'une sélection de
travaux

Chapitre 6

Commande sous contrainte de sortie pour la sécurisation des systèmes aérospatiaux

Résumé du chapitre : l'utilisation d'une boucle d'anti-windup est une pratique courante lorsque l'on souhaite élargir le domaine d'emploi d'une commande en présence de saturations au niveau des actionneurs. Nous présentons dans ce chapitre une approche originale qui nous a permis d'étendre la synthèse anti-windup au cas où la saturation porte cette fois sur une sortie ; cette saturation est alors qualifiée de contrainte de sortie. L'idée principale de notre approche est de transformer la contrainte de sortie en une saturation en entrée et qui porte donc directement sur la loi de commande. Les bornes de cette saturation sont alors temps variant et nous verrons qu'elles dépendent de nos sorties mesurées.

6.1 Introduction

Nos travaux sur les saturations de lois de commande ont commencé à notre arrivée à l'Onera en 2010. Le projet EDA NICE nous a initié aux techniques d'anti-windup qui permettent d'élargir le domaine d'emploi d'une loi de commande saturée. À partir de 2011, le projet Europeen Cleansky (2011-2013) nous a conduit à nous interroger sur la possibilité d'utiliser des techniques anti-windup [58, 108] lorsque nous avons cette fois des contraintes de sorties en lieu et place des saturations de lois de commande. C'est alors qu'a germé l'idée de transformer des contraintes de sorties en saturations de lois de commande. Nous avons pour but de proposer une solution simple et élégante permettant de contraindre une sortie sur un modèle d'avion de très grande dimension sans utiliser de prédiction (ce que fait la commande prédictive) et tout en utilisant une commande H_∞ structurée [6, 15] dans le cas "nominal" où la sortie à contraindre est "suffisamment" loin de ses contraintes. La thèse d'Emmanuel Chambon (2013-2016) nous a ensuite permis de formaliser davantage cette approche en proposant un certain nombre de résultats théoriques. Le Post Doctorat de Corentin Chauffaut (2015) a permis d'implémenter cette technique sur des drones.

6.2 Positionnement de nos travaux

6.2.1 Contraintes fréquentielles et temporelles

La complexité croissante des systèmes aérospatiaux a conduit l'industrie à développer des algorithmes de contrôle fiables et efficaces tout au long des phases de vie de ces systèmes. Par exemple, la phase atmosphérique du vol d'un lanceur est particulièrement critique : sa structure est soumise à des forces aérodynamiques très importantes et potentiellement destructives si la loi de commande n'en tient pas compte. Le même problème se pose pour un avion soumis à de fortes turbulences. Une stratégie de commande efficace repose alors sur une modélisation fidèle des phénomènes physiques à l'œuvre ainsi que sur une formulation d'un cahier des charges précis de contraintes à satisfaire. En pratique, ces contraintes sont de deux ordres :

- soit il s'agit de contraintes fréquentielles de sorte que le comportement fréquentiel du système en boucle fermée est adapté. Elles concernent principalement la stabilité en boucle fermée mais également l'atténuation des modes souples présents à basse fréquence et qui ne doivent pas être excités par la loi de commande obtenue
- soit il s'agit de contraintes temporelles qui concernent les signaux

temporels du système au cours de son évolution dynamique. Pour le lanceur, une contrainte temporelle porte sur l'angle d'incidence α qui doit rester dans un intervalle spécifié. En limitant cet angle, les forces aérodynamiques en jeu sont réduites et la destruction du lanceur est évitée. Pour l'avion, des contraintes s'appliquent aux moments de torsion et de flexion appliqués à la voilure qui doivent rester en dessous d'un certain seuil.

Un défi essentiel de la commande des systèmes aéronautiques et spatiaux est ainsi de pouvoir considérer à la fois des contraintes fréquentielles et temporelles. Les contraintes fréquentielles sont généralement traitées par une synthèse H_∞ lorsque le modèle est linéaire. Reste cependant à prendre en compte des contraintes temporelles qui représentent des contraintes de sécurité à respecter ; de telles contraintes se marient difficilement avec les contraintes fréquentielles et en pratique l'industriel ajoutera une surcouche souvent dénommée "loi de protection" et souvent synthétisée de manière "heuristique". Il utilisera alors des simulations Monte Carlo pour valider la synthèse globale.

Les travaux que nous avons menés sur ces doubles contraintes fréquentielles et temporelles ont été initiés grâce aux deux projets suivants :

- le projet CLEANSKY (plus précisément le package "SFWA", Smart Fixed Wing Aircraft). Notre but était de proposer une méthode pour limiter les moments de flexion au niveau de l'emplanture des ailes d'un avion lorsque ce dernier traverse une zone de turbulence, cette méthode pouvant être habilement combinée avec une loi de commande H_∞ structurée [26].
- le Projet d'Intérêt Commun sur les lanceurs (PIC lanceur) entre l'ONERA et le CNES. Nous n'y avons pas directement travaillé mais avons co-encadré la thèse d'Emmanuel Chambon avec Pierre Apkarian, qui était impliqué dans ce PIC. Le but de la thèse d'Emmanuel était de proposer une solution permettant de limiter l'angle d'incidence du lanceur alors que le modèle du lanceur était incertain et que l'incidence n'était pas mesurée [31].

6.2.2 Etat de l'art sur les contraintes temporelles

Les techniques de commande sous contraintes temporelles sur les sorties sont nombreuses et variées de part l'importance de ces contraintes. En effet, elles sont destinées à assurer la bonne marche des systèmes en définissant les zones de fonctionnements nominal et dégradé. Dans les ressources documentaires [66, 101, 67], ces stratégies de commande sont divisées en trois familles :

- les méthodes dites prudentes qui consistent à faire en sorte que les signaux de sortie n'atteignent jamais les contraintes (et donc ne les violent pas). Ces méthodes sont souvent considérées comme peu performantes car les signaux de sortie sont forcés de ne jamais stationner sur les contraintes, ce qui est obtenu en utilisant une commande conservatrice qui sous-estime le domaine admissible ; nous pouvons citer par exemple les travaux basés sur des fonctions de Lyapunov barrières [109] ou les méthodes dites à faible gain [83] ;
- les approches dites évolutionnaires qui reposent sur une loi de commande nominale existante qui est modifiée par un signal supplémentaire seulement lorsque les contraintes temporelles sont violées. Un exemple d'approche évolutionnaire est l'utilisation d'un compensateur anti-windup qui ne modifie la dynamique de la boucle fermée que lorsqu'une saturation s'active sur la commande [58, 108] ; Un autre exemple est la technique des "reference governors" [64, 79, 59] qui modifie la référence à suivre lorsqu'on s'approche des contraintes.
- Les méthodes dites tactiques qui prennent en compte les contraintes temporelles au sein d'un problème de contrôle optimal. Outre les méthodes qualifiées de Model Predictive Control (MPC) (voir par exemple [86]), nous pouvons aussi citer par exemple [68, 60, 7]. Notons que [7] cherche en effet à prendre en compte des contraintes fréquentielles et temporelles ; cependant, les contraintes temporelles nécessitent de réaliser des simulations temporelles.

Remarquons aussi qu'un certain nombre de méthodes cherchent à synthétiser des lois qui ne permettent pas d'éviter de violer des contraintes mais freinent le système de manière à ce qu'il ne les viole que "légèrement" [80, 111].

A l'époque où nous avons commencé à développer la méthode qui fait l'objet de ce chapitre, c'est donc l'approche "reference governors" qui permettait de ne pas modifier la loi de commande nominale. Ceci étant cette méthode devenait rapidement gourmande en ressources calculatoires lorsque des paramètres étaient incertains [29] et nous avons alors choisi de développer une méthode sans prédiction. Aujourd'hui, et comme décrit dans nos perspectives, nous travaillons aussi sur les "reference governors" lorsque les paramètres sont incertains [24, 25].

6.3 Présentation de la méthode OIST

Par souci de simplicité, nous considérons ici la classe des systèmes LTI (Linéaires Temps Invariant) de la forme suivante :

$$\begin{cases} \dot{x} &= Ax + Bu \\ z &= C_z x + D_z u \end{cases} \quad (6.1)$$

où z est une sortie à maintenir dans l'intervalle $[z_{\min}, z_{\max}]$ et u est la commande.

Rappelons alors que le **degré relatif** de la sortie z par rapport à l'entrée de commande u quantifie l'ordre de la dérivée de z qui fait apparaître pour la première fois l'entrée de commande u . Puisque la dérivée k -ième de z par rapport au temps s'écrit :

$$z^{(k)}(t) = C_z A^k x(t) + C_z A^{k-1} B u(t) + D_z u^{(k)}(t) \quad (6.2)$$

Il est aisé de voir que ce degré relatif vaut 0 si $D_z \neq 0$ et que sinon il s'agit du plus petit entier $k \geq 1$ tel que $C_z A^{k-1} B \neq 0$.

Lorsque le degré relatif vaut 0, imposer à z de rester dans l'intervalle $[z_{\min}, z_{\max}]$ revient simplement à imposer à u la contrainte suivante :

$$z_{\min} - C_z x \leq D_z u \leq z_{\max} - C_z x \quad (6.3)$$

La contrainte sur z est ainsi transformée en une contrainte sur la commande u . La question est alors de savoir si on peut généraliser cette idée aux degrés relatifs strictement supérieurs à 0.

6.3.1 L'idée clef

Etant donnée une grandeur scalaire et temps variant $z(t)$, celle-ci restera toujours dans l'intervalle $[z_{\min}, z_{\max}]$ ssi :

- elle est dans cet intervalle à l'état initial i.e $z(0) \in [z_{\min}, z_{\max}]$
- et sa dérivée temporelle vérifie $\forall t \geq 0$

$$\begin{cases} \dot{z}(t) \leq 0 & \text{si } z(t) = z_{\max} \\ \dot{z}(t) \geq 0 & \text{si } z(t) = z_{\min} \end{cases} \quad (6.4)$$

Imposer de telles contraintes à la dérivée de $z(t)$ n'est pas aisé à utiliser dans une synthèse de loi de commande puisque nous avons alors affaire à un système hybride ; aussi, nous avons proposé de relaxer le résultat précédent ainsi :

Etant donnée une grandeur scalaire et temps variant $z(t)$, celle-ci restera toujours dans l'intervalle $[z_{\min}, z_{\max}]$ si :

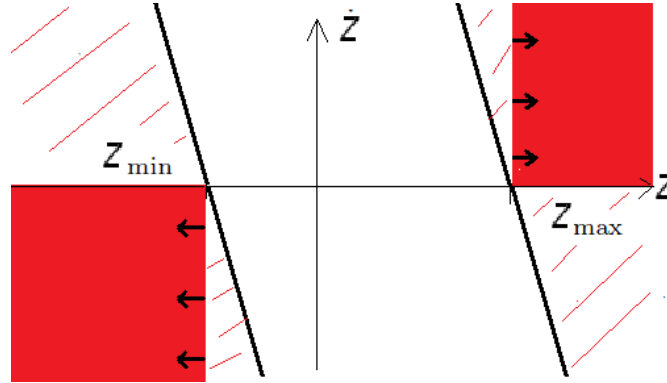


FIGURE 6.1 – Illustration de la méthode pour un degré relatif égal à 1

- elle est dans cet intervalle à l'état initial i.e $z(0) \in [z_{\min}, z_{\max}]$
- et sa dérivée temporelle vérifie $\forall t \geq 0$

$$\begin{cases} \dot{z}(t) \leq -K(z(t) - z_{\max}) \\ \dot{z}(t) \geq -K(z(t) - z_{\min}) \end{cases} \quad (6.5)$$

où $K \in \mathbb{R}^{>0}$.

S'ensuit alors l'application suivante pour la synthèse d'une loi de commande : lorsque le degré relatif de z par rapport à u vaut 1, alors z vérifie $\dot{z} = C_z Ax + C_z Bu$ où $C_z B \neq 0$. Imposer à la commande u la contrainte (temps variant) suivante :

$$-C_z Ax - K(z - z_{\min}) \leq C_z Bu \leq -C_z Ax - K(z - z_{\max}) \quad (6.6)$$

permet alors de maintenir $z(t)$ dans l'intervalle $[z_{\min}, z_{\max}]$ si toutefois $z(0)$ appartient bien à cet intervalle. La contrainte sur la variable z se retrouve ainsi transformée en une contrainte sur la commande u d'où le nom de la méthode **OIST (Output to Input Saturation Transformation)**.

L'idée clef est ainsi illustrée par la figure 6.1 :

- il est interdit à (z, \dot{z}) de rentrer dans les carrés remplis de rouge
- l'approximation consiste à maintenir (z, \dot{z}) entre deux droites de pente $-K$.

6.3.2 Généralisation

Notons r le degré relatif de z par rapport à u . Afin de traiter le cas du degré relatif r strictement supérieur à 1, nous avons commencé par généraliser "l'idée clef" au cas où $z_{\min}(t)$ et $z_{\max}(t)$ sont temps variant. En effet,

être capable de traiter des contraintes temps variant permet alors d'itérer plusieurs fois l'opération de transformation des contraintes :

- les contraintes sur z sont comme précédemment transformées en contraintes temps variant sur \dot{z}
- la nouvelle variable à contraindre est ainsi \dot{z} et cette contrainte est transformée en une contrainte sur $\ddot{z} = z^{(2)}$ toujours en utilisant la transformation OIST
- la contrainte est ainsi reportée sur les dérivées successives de z jusqu'à l'obtention d'une contrainte sur $z^{(r)}$ qui dépend de la commande u .

La procédure que nous venons de décrire est résumée par le lemme suivant :

Lemme des bornes propagées [30]

Soient $K_1, \dots, K_r \in \mathbb{R}^{>0}$. Notons $z_{\min}^{(0)} = z_{\min}$, $z_{\max}^{(0)} = z_{\max}$ ainsi que pour $i \in \{1, \dots, r\}$

$$\begin{cases} z_{\max}^{(i)} &= z^{(i)} - \left[\prod_{j=1}^i \left(\frac{d}{dt} + K_j \right) \right] (z - z_{\max}) \\ z_{\min}^{(i)} &= z^{(i)} - \left[\prod_{j=1}^i \left(\frac{d}{dt} + K_j \right) \right] (z - z_{\min}) \end{cases} \quad (6.7)$$

Si, pour tout $i \in \{0, \dots, r-1\}$

$$z^{(i)}(0) \in [z_{\min}^{(i)}(0), z_{\max}^{(i)}(0)] \quad (6.8)$$

et $\forall t \in \mathbb{R}^{\geq 0}$

$$z^{(r)}(t) \in [z_{\min}^{(r)}(t), z_{\max}^{(r)}(t)] \quad (6.9)$$

alors $\forall t \in \mathbb{R}^{\geq 0}$

$$z(t) \in [z_{\min}(t), z_{\max}(t)] \quad (6.10)$$

Ce lemme, dont la preuve est donnée dans [30], montre ainsi qu'en satisfaisant une contrainte temporelle (donnée par les bornes propagées) sur la dérivée k -ième de la sortie contrainte z alors la contrainte temporelle sur z est satisfaite. Ce Lemme peut alors être appliqué à un système linéaire pré-stabilisé dont il faut contraindre une sortie z de degré relatif r par rapport à l'entrée de commande u : il conduit ainsi à appliquer une saturation à bornes temps variant sur l'entrée de commande. Le lemme peut aussi être généralisé et appliqué à des systèmes non linéaires pré-stabilisés [17]. Cependant, dans tous les cas de figure, il reste à prouver que le système obtenu n'est pas déstabilisé en appliquant la transformation OIST.

6.4 Nos contributions

Outre le fait que nous avons eu l'idée de cette transformation originale dénommée OIST, nous avons ensuite proposé plusieurs extensions :

- Dans [33], nous nous sommes intéressés aux systèmes LTI où z est de degré relatif r par rapport à l'entrée de commande. Nous avons considéré une entrée inconnue mais bornée. Nous nous sommes demandés ce qui se passait si la perturbation était non matching, c'est à dire, si la perturbation apparaissait dans l'expression de $z^{(i)}$ où $i < r$. Cela nous a conduit notamment à modifier le lemme des bornes propagées de manière à ce que les bornes temps variant de la saturation OIST ne se chevauchent jamais. Nous avons aussi proposé une preuve de stabilité lorsqu'on applique OIST à une sortie minimum de phase d'un système LTI préstabilisé par un correcteur dynamique.
- Dans [20], nous avons étendu l'approche OIST à un modèle non linéaire de satellite souple avec mesures partielles de l'état. Cette contribution repose sur l'utilisation d'observateurs par intervalles obtenus par un changement de coordonnées temps variant [87]. La solution d'évitement de chevauchement des saturations est étendue à ce cas plus complexe; de plus, nous avons montré que la méthode OIST pouvait être plus performante qu'une solution utilisant une fonction de Lyapunov "barrière" lorsque l'attitude d'un satellite doit suivre une trajectoire tout ayant une vitesse angulaire contrainte.
- Fort du constat qu'OIST nécessitait des observateurs par intervalles lorsqu'on ne mesure pas tout l'état du système, nous avons aussi effectué des recherches sur les observateurs par intervalles. Notamment, dans [32], nous avons proposé une nouvelle méthode de construction d'un observateur par intervalles avec changement de coordonnées à temps invariant. Cette méthode repose sur la formulation du problème mathématique d'origine en problème de stabilisation d'un système linéaire dit fictif (puisque ne modélisant pas la dynamique d'un système réel) et présente la caractéristique d'utiliser les algorithmes de la synthèse H_∞ structurée.
- Nous avons commencé à appliquer OIST à des problématiques drones en regardant notamment des problèmes de contraintes sur le champ de vision d'une caméra [21, 44] où d'évitement d'obstacles [34]. Ces travaux applicatifs préliminaires demandent encore de développer des outils d'analyse permettant d'étudier finement les propriétés des systèmes bouclés.

Enfin, les principaux détails techniques sont donnés dans les articles [26, 33, 20, 34] qui sont rassemblés ci-après. Le premier article [26] ne propose pas de preuve théorique mais a le mérite de montrer comment on a combiné la synthèse H_∞ structurée à OIST pour contrôler un système de très grande dimension dont une sortie était contrainte.

AUTHOR'S PERSONAL COPY

Longitudinal Manoeuvre Load Control of a Flexible Large-Scale Aircraft

L. Burlion* C. Poussot-Vassal* P. Vuillemin* M. Leitner**
T. Kier**

* *Onera - The French Aerospace Lab, F-31055 Toulouse, France.*

** *DLR, Institute of Robotics and Mechatronics, 82234, Weßling, Germany.*

Abstract: This paper discusses the design and validation of an integrated long range flexible aircraft load controller, at a single flight/mass configuration. The contributions of the paper are in twofold: (i) first, a very recent frequency-limited model approximation technique is used to reduce the dimension of the large-scale aeroservoelastic aircraft model over a finite frequency support while guaranteeing optimal mismatch error, secondly, (ii) a structured controller is designed using an \mathcal{H}_∞ -objective and coupled with an output saturation strategy to achieve flight performance and load clearance, *i.e.* wing root bending moment saturation. The entire procedure - approximation and control - is finally assessed on the high fidelity large-scale aircraft model, illustrating the effectiveness of the procedure on a high fidelity model, used in the industrial context in the load control validation process.

Keywords: Aircraft modelling, Model approximation, Load control, Output saturation

1. INTRODUCTION

1.1 Motivations and aircraft load control framework

The many different objectives flexible aircraft should fulfill (*e.g.* flight performances, load protection, noise reduction, etc.) render the controller design and tuning tasks very complex. Traditionally, these objectives are - reasonably - dissociated to each others, allowing to treat each flexible (modal) contribution separately¹, *e.g.* flight dynamics, then loads, then vibrations (see *e.g.* Gardonio (2002)). However, following efforts from structure and material engineers in lightning the aircraft mass in order to reduce the overall fuel consumption and gas emissions (*e.g.* fuselage and wing), the modal behaviour of each flexible modes and aerodynamical delays is likely to blend each other. More specifically, in the *load control* context, the first aeroelastic load mode might appears in low frequencies and interfere with the aircraft flight (rigid) dynamics.

As a matter of consequence, a control approach consists to design the flight and load controllers in a unified step, to both guarantee (i) good flight performances in *normal cruise situations* and (ii) load preservation when *strong manoeuvre or gust disturbance occur* to guarantee that load upper and lower limitations are never reached. The load control is a critical step in the aircraft validation since aircraft manufacturer must guarantee the authorities that critical loads are monitored in all situations, whatever the manoeuvre is (see also Gaulocher et al. (2007); Haghghat et al. (2012)).

Moreover, it is worth mentioning that the aeroservoelastic models involved in the design and validation procedures of such a controller take into account the flight physics,

¹ Even if in practice iterative re-tuning is required.

the aeroelastic phenomenon (structural loads, unsteady aerodynamic loads and delays) and the flight control system behaviour. Consequently, the resulting linear state-space models, representing the aircraft at frozen flight / mass configuration, are of large-scale (state vector of order n around 2000). Even if each model can always be questioned or amended, this large amount of variables comes with an enhanced accuracy, but also renders the control design and optimization tasks even more complex.

This paper reports original results obtained within the joint collaboration between Onera and DLR, on the development of advanced methodologies for load control design applied to a complex flexible large-scale aircraft model, at one single load dimensioning flight and mass configuration. More specifically, with reference to Figure 1, the paper is attached to approximate the large-scale model \mathbf{H} (blue block) and, grounded on the low-order model $\hat{\mathbf{H}}$, design a dedicated flight and load control law that should fulfil flight performance in normal situations and prevent load limitations *i.e.* saturations, when critical manoeuvre occurs (red blocks).

Designing such a controller, involving large-scale dynamical model, is a challenging problem (Gadient et al. (2012)), indeed:

- the large number of states involved in the dynamical model results in computational complexity,
- the load preservation specifications are given as strong time-domain constraints on the wing root bending moment ($WRM_x(t)$), an output of the model,
- the nominal flight control law performances, when no critical load are detected, must be ensured (*e.g.* load

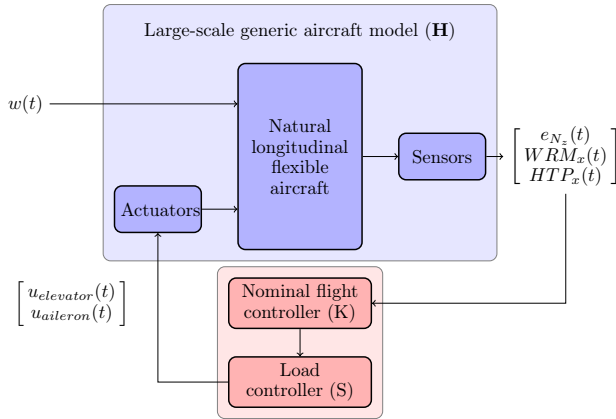


Fig. 1. Flexible aircraft model (\mathbf{H}) and load controller.

factor $N_z(t)$ should tracks its reference $N_z^*(t)$, thus $\lim_{t \rightarrow \infty} e_{N_z}(t) = 0$, $e_{N_z}(t) = N_z(t) - N_z^*(t)$, and,

- high frequency flexible - lightly - damped modes must remain stable, and unmodified.

1.2 Paper notations and structure

The flexible aircraft modelling and approximation steps are briefly described in Section 2. Then, Section 3 describes the core contribution, *i.e.* a combined flight and load control strategy, allowing to provide *good flight quality while preserving load saturation*. The complete validation of the proposed load control is performed on the full order flexible aircraft model, using flight certification criterion, assessing the interest and effectiveness of the proposed controller. Conclusions are given in Section 4.

Throughout the paper, the following notations will be used: \mathbf{H} (*resp.* $H(s)$) denotes the full order state-space model realization (*resp.* transfer function, which is a $\mathcal{H}_p^{n_y \times n_u}$ matrix complex-valued function²) of order n and $\hat{\mathbf{H}}$ (*resp.* $\hat{H}(s)$) stands for the reduced order state-space model realization (*resp.* transfer function) of order $r \ll n$. Given the matrices $M = \begin{bmatrix} M_{11} & M_{12} \\ M_{21} & M_{22} \end{bmatrix}$ and K of suitable dimensions, $\mathcal{F}_l(M, K)_{w \rightarrow z} = M_{11} + M_{12}K(I - M_{22}K)^{-1}M_{21}$ denotes the transfer from w to z of the lower linear fractional transformation operator that interconnects M with K .

2. LARGE-SCALE LONG RANGE FLEXIBLE AIRCRAFT MODELLING, APPROXIMATION AND PROBLEM FORMULATION

2.1 Large-scale modelling

The considered dynamical aircraft model, represents a longitudinal long range generic aircraft, linearised at varying mass and flight configurations (mass, flight altitude and speed). This model is obtained by merging the mass and geometry of the aircraft (*e.g.* obtained from finite element mapping) using a flexible tool for simulation of loads

² the $\mathcal{H}_p^{n_y \times n_u}$ denotes the set of $n_y \times n_u$ matrix-valued complex-valued functions $H(s)$ with component $h_{ij}(s)$ that are analytic in the open right half-plane \mathbb{C}^+ , and wher the $\|\cdot\|_{\mathcal{H}_p}$ -norm is defined.

analysis models (see Hofstee et al. (2003)), with method and equations of integrating gust and manoeuvre models (see Kier and Looye (2009)). The entire procedure is made available through the use of FlightDynLib, an integrated tool (see Looye et al. (2005)). When combined with flight, load and aerodynamical delays dynamical equations, a complete integrated model is thus generated at different flight configurations.

In this study, *one single* linear large-scale dynamical model, valid at one single mass/flight configuration will be considered. The resulting aeroservoelastic model form includes the aeroelastic model coupled to the load recovery (see Figure 1). This system can be represented by its transfer function $H(s) = C(sI_n - A)^{-1}B + D$, or equivalent state-space realization \mathbf{H} as:

$$\mathbf{H} : \begin{cases} \dot{x}(t) = Ax(t) + Bu(t) \\ y(t) = Cx(t) + Du(t) \end{cases}, \quad (1)$$

where $A \in \mathbb{R}^{n \times n}$, $B \in \mathbb{R}^{n \times n_u}$, $C \in \mathbb{R}^{n_y \times n}$ and $D \in \mathbb{R}^{n_y \times n_u}$ (with $n \approx 1700$, $n_u = 3$ and $n_y = 3$ are the number of states, inputs and outputs, respectively). In the considered application, the input vector is composed of

- $w(t)$, the external disturbance input representing a gust impact on the entire wing and fuselage,
- $u_{elevator}(t)$ and $u_{aileron}(t)$, representing elevator and outer aileron equivalent control surfaces action,

and the output vector is composed of

- $N_z(t)$, the vertical load factor, representing the *flight dynamic performance*,
- $WRM_x(t)$, the wing root bending moment, which is the value to be monitored to ensure *load saturation preservation* (this value represents the effort at the fuselage/wing connection and is thus dimensioning for safety certification purpose),
- $HTP_x(t)$, the root bending moment at the tail of the aircraft, which should be monitored as well (but the variable is not load-dimensioning).

2.2 \mathcal{H}_2 -optimal model approximation

As the original system is of large-scale ($n \approx 1700$), the application of the standard control optimization tools is no longer adapted for numerical and memory management reasons. This is why an open-loop model approximation step is firstly done (see Antoulas (2005)). Since the aim of model approximation is to construct a reduced-order model $\hat{\mathbf{H}}$ (or $\hat{H}(s)$) that captures the main original system dynamics input/output behaviour while preserving stability, the \mathcal{H}_2 -norm mismatch error is often addressed (see Gugercin et al. (2008)). More specifically, in the applicative context of - load - control, it is more convenient to consider the mismatch error over a limited frequency range (*e.g.* the range on which the control law will act). This consideration has been addressed in recent model approximation results through the use of the frequency-limited \mathcal{H}_2 -norm, denoted $\mathcal{H}_{2,\Omega}$ -norm (Ω stands for the frequency support). The resulting approximation problem consists of seeking an approximation $\hat{H}(s)$ of $H(s)$, so that

$$\hat{H} := \arg \min_{\substack{G \in \mathcal{H}_{\infty}^{n_y \times n_u} \\ \text{rank}(G) = r \ll n}} \|H - G\|_{\mathcal{H}_{2,\Omega}}. \quad (2)$$

Beside the fact that problem (2) is non convex, some algorithm have been proposed to solve it, reaching the so-called first order optimality conditions, ensuring that a local (hopefully global) optimum is reached. In this paper context, the aircraft model described above has been approximated using different reduction techniques. Figure 2 reports the $\mathcal{H}_{2,\Omega}$ -norm mismatch error ($\Omega = [0 \ 100]$ Hz) as a function of the order of the approximated model r , using either the best MATLAB³ method, the **ISTIA** proposed in Poussot-Vassal (2011) and extended in Vuillemin et al. (2013) and **DARPO**, a Descent Algorithm for Residues and Poles Optimization of Vuillemin et al. (2014).

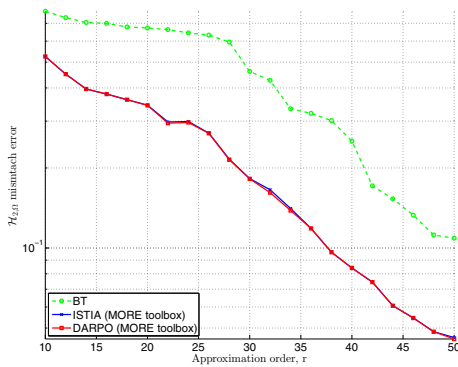


Fig. 2. $\mathcal{H}_{2,\Omega}$ -norm mismatch error as a function of the order r of the approximated model for: **BT** (green rounded line) and **ISTIA** of the MORE toolbox (blue crossed line) and **DARPO** of the MORE toolbox (red solid squared line).

With reference to Figure 2, it is clear that the **ISTIA** and **DARPO** provide better approximated models over the bounded frequency support than the standard **BT** and will thus be preferred in the following. Without loss of generality, from now on, when $\hat{\mathbf{H}}$ (or $\hat{H}(s)$) is mentioned, it will refer to approximated model of order $r = 50$ obtained with the **DARPO**, providing an relative error of $\approx 4\%$.

Remark 1. (Model approximation). As it is not the topic of the paper, the **ISTIA** and **DARPO** methods are not described here. However, interested reader may refer to the MORE toolbox for additional details⁴.

2.3 Performance specifications and constraints

At the considered dimensioning mass and flight configuration, as stated in the Section 1, let us formalize the performance and constraints as follows:

- FQ1 Flight qualities 1 (frequency domain):** ensure load tracking, *i.e.* $N_z(t)$ should follow $N_z^*(t)$ reference.
- LP1 Load performances 1 (frequency domain):** ensure wing root bending moment ($WRM_x(t)$) attenuation in low frequency until the first load mode, in response to wind disturbance, with negligible impact

³ In most of the case the best result is obtained when using the Balanced Truncation (**BT**) method.

⁴ Webpage <http://w3.onera.fr/more> Poussot-Vassal and Vuillemin (2012).

on higher modes. This performance is also evaluated through a frequency-limited \mathcal{H}_2 -norm improvement,

$$100 \frac{|\mathcal{J}^{\text{nom}} - \mathcal{J}|}{\mathcal{J}^{\text{nom}}}, \quad (3)$$

where $\mathcal{J}^{\text{nom}} = \|T_{w \rightarrow WRM_x}\|_{\mathcal{H}_{2,[0.1 \ 100]}}$ without control, and $\mathcal{J} = \|T_{w \rightarrow WRM_x}\|_{\mathcal{H}_{2,[0.1 \ 100]}}$ when the controller is connected.

- LP2 Load performance 2 (time domain):** ensure that the wing root bending moment $WRM_x(t)$ remains within lower and upper limits, critic for load clearance, $WRM_x^{\text{min}} \leq WRM_x(t) \leq WRM_x^{\text{max}}$.
- Const1 Controller constraints (frequency domain):** the control should not act above 10Hz in order to not deteriorate lightly damped flexible modes.
- Const2 Structural constraints (structure):** the controller should have a simple structure. Moreover, it is likely for aircraft engineers to dissociate the nominal law with the load clearance one, as illustrated in Figure 1.

Note that item **LP2** is a very far to be a trivial task since it cannot be handled in an efficient way through linear approaches. It is why in the next section, a dedicated load controller will be added to the nominal flight control to monitor the wing root bending moment and guarantee that the limitations are kept.

3. MANOEUVRE-LOAD ALLEVIATION CONTROLLER DESIGN

3.1 (Nominal) flight controller design (K)

To achieve flight and load control performances in nominal situation (when no wing root bending moment limitations are reached), *i.e.* to address objectives **FQ1** and **LP1**, while ensuring constraints **Const1** and **Const2**, a linear structured controller is designed with \mathcal{H}_∞ -norm minimization objective, as

$$K := \arg \min_{\substack{C \in \mathcal{H}_2^{n_u \times n_y} \\ \text{rank}(C) = n_c}} \|F_l^*(\hat{H}, C)\|_{\mathcal{H}_\infty}, \quad (4)$$

where, to avoid \mathcal{H}_∞ -norm cross minimization transfer, $F_l^*(\hat{H}, C)$ is structured as,

$$F_l^*(\hat{H}, C) = \text{diag} \left(\begin{array}{c} W_i F_l(\hat{H}, C)_{N_z^* \rightarrow e_{N_z}} W_o, \\ W_i F_l(\hat{H}, C)_{w \rightarrow e_{N_z}, WRM_x, HTP_x} W_o, \\ W_i F_l(\hat{H}, C)_{N_z^*, w \rightarrow u_{\text{aileron}, u_{\text{elevator}}} } W_o \end{array} \right), \quad (5)$$

where W_i and W_o are the weighting function classically used in frequency controller synthesis to address **FQ1** and **LP1** objectives. Without loss of generality and with reference to (4), to address (i) **Const1**, the controller is structured such that the control rolls-off above 10Hz and enforcing the controller to belong $\mathcal{H}_2^{n_u \times n_y}$, and (ii) **Const2**, by imposing a rank constraint on the controller. This is achieved through used of standard algorithm made available by Apkarian and Noll (2006) (see Figure 3).

3.2 Output saturation design of the wing root bending moment $WRM_x(t)$

Additionally - and this is the specificity of the treated problem to handle the fact that the wing root bending mo-

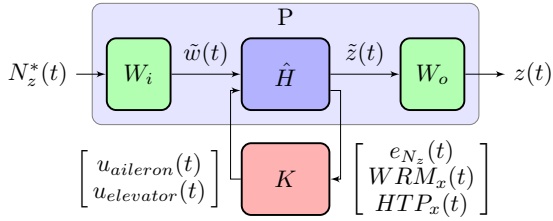


Fig. 3. Flexible aircraft model (\hat{H}), weighting filters (W_i , W_o) and load controller (K).

ment must remain inside a specified interval (e.g. for structural limitations purpose) an output saturation constraint must be specified (**LP2**). Mathematically, it consists in guaranteeing $WRM_x^{\min} < WRM_x(t) < WRM_x^{\max}$. In the following, this specificity is treated through a reformulation of the output saturation into an input saturation one, on which a performance-oriented controller will be applied. Note that the objective of the load saturation is to alleviate loads at the wing/fuselage location. However, to achieve flight performance, loads still have to be maintained elsewhere on the aircraft. Consequently, the objective is to balance the load of the WRM_x to the elevator surface HTP_x . Therefore, in what follows, the actuator ensuring the output saturation will be the elevator ($u_{elevator}$), only. The proposed approach does not require any on-line optimization procedure, unless standard approaches based on predictive control (Haghighat et al. (2012)).

3.3 Output to input saturation transform (S)

General result: The general method which consists in converting an interval constraint on an output $z(t)$ into a saturation on the control law $u(t)$ is described in Burlion (2012). The first step consists in computing the relative degree (denoted $d_u^{rel}(z)$) of the constrained output $z(t)$ with respect to the control value $u(t)$. In the context of the paper, we have $d_{u_{elevator}}^{rel}(WRM_x) = 0$, which means that the value of $u_{elevator}$ instantaneously changes the value of WRM_x .

Proposition 1. (OIST). Let us assume $z = WRM_x$ and the wind disturbance w to be measured and let us note (where $B_{WRM_x, u_e} \neq 0$)

$$WRM_x \hat{x}(t) = C_{WRM_x} \hat{x}(t) + B_{WRM_x, w} w(t) + B_{WRM_x, u_a} u_{aileron}(t) + B_{WRM_x, u_e} u_{elevator}(t), \quad (6)$$

and

$$\begin{cases} WRM_x^{\min}(\hat{x}, w, u_{aileron}) = WRM_x^{\min} - C_{WRM_x} \hat{x} - B_{WRM_x, w} w - B_{WRM_x, u_a} u_{aileron} \\ WRM_x^{\max}(\hat{x}, w, u_{aileron}) = WRM_x^{\max} - C_{WRM_x} \hat{x} - B_{WRM_x, w} w - B_{WRM_x, u_a} u_{aileron} \end{cases}$$

In the simple case of relative degree 0, the Output to Input Saturation Transform (**OIST**) (Burlion (2012), Burlion and de Plinval (2013)) boils down saying that

$$\begin{cases} \forall t \geq 0, & B_{WRM_x, u_e} u_{elevator}(t) \in \\ & [WRM_x^{\min}(\hat{x}, w, u_{aileron}), WRM_x^{\max}(\hat{x}, w, u_{aileron})] \end{cases}$$

then,

$$\forall t \geq 0, \quad WRM_x(t) \in [WRM_x^{\min}, WRM_x^{\max}]$$

providing the state $\hat{x}(t)$ remains stable when $u_{elevator}(t)$ saturates.

One remarks that the output interval constraint has been replaced by a saturation on $u_{elevator}$ whose bounds are time varying and depend on the internal state and on the other inputs.

In the relative degree $d_{u_{elevator}}^{rel}(WRM_x) = 0$, the method is rather simple but requires that the internal state x remains stable when the control law saturates. This proposition is closely related to the stability of the zeros associated to the transfers whose output is WRM_x since it is necessary that the zero dynamics associated to the output WRM_x remain stable when the constraint is activated. In the considered benchmark, the transfer functions $WRM_x(s)/u_{elevator}(s)$, $WRM_x(s)/u_{aileron}(s)$ and $WRM_x(s)/w(s)$ unfortunately possess unstable zeros and it is then not possible to apply the input saturation which is obtained through the application of Proposition 1.

Relaxation of the method by approximating the non minimum phase constrained output: The application of this saturation on $u_{elevator}(t)$ ensures that $WRM_x(t)$ remains inside its interval.

To alleviate this limitation, we propose to relax our saturation function by considering a saturation on an approximation of $WRM_x(t)$ instead of a saturation on $WRM_x(t)$. Let us note $WRM_x^{approx}(t)$ this new output: it must be close enough to $WRM_x(t)$ to have very similar bounds but must be a minimum phase.

The transfer functions from the inputs to $WRM_x(t)$, exhibits zeros in the right half plane with high magnitude. Therefore we propose to remove them in this stable plane by changing their real value sign (see Figure 4). Associated to these new transfer functions, we obtain a new output, namely WRM_x^{approx} which is minimum phase and whose behavior is very close to the original non minimum phase output WRM_x . This is not so surprising since moving the zeros leads to bad effects since they have relatively large real value in our model values. Indeed, for instance moving a given pure real zero named $a \gg 0$, means that the ratio between the approximated transfer function and the original one is:

$$\frac{a-s}{a+s} \approx e^{-\frac{2}{a}s},$$

according to the well known Padé's first order approximation method, this ratio means there is approximately a delay between the outputs and its value is thus very small ($\frac{2}{a} \ll 1$). Finally, the controlled input saturation is based on a minimum phase output of the same system and noting:

$$WRM_x^{approx}(t) = C_{WRM_x}^{approx} x^{approx}(t) + B_{WRM_x, w}^{approx} w(t) + B_{WRM_x, u_a}^{approx} u_{aileron}(t) + B_{WRM_x, u_e}^{approx} u_{elevator}(t), \quad (7)$$

we finally saturate our elevator control law accordingly i.e.

$$\begin{cases} \forall t \geq 0, & B_{WRM_x, u_e}^{approx} u_{elevator}(t) \in \\ & [WRM_x^{\min, approx}(t), WRM_x^{\max, approx}(t)] \end{cases} \quad (8)$$

3.4 Large-scale numerical validation

In order to validate the proposed approach, a commonly used certification scenario in aeronautics to assess the manoeuvre load control, will be used and applied on

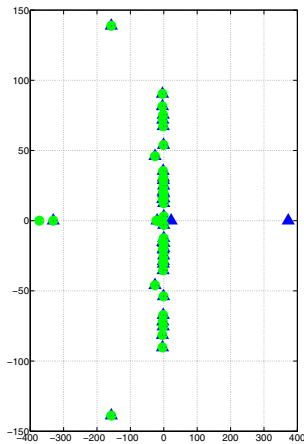


Fig. 4. Illustration of the approximation: the zeros of the transfer $WRM_x(s)/u_{elevator}(s)$ (resp. $WRM_x^{approx}(s)/u_{elevator}(s)$) are plotted in blue triangle (resp. in green round).

the large-scale model. This scenario, called "Manoeuvre Vertical Stretched" (MVS), consists in considering the aircraft flying at 1g and applying the following stick trajectory: (i) push the pilot stick with a sine shape until a load factor of 2.5g is reached, then (ii) released to turn back to 1g with a sine like function (see black solid line on Figure 5 top middle frame). The main objectives and results are reported on Figure 5.

With reference to the left frames, the frequency responses from the wind to the controlled outputs are reported. One can first notice that the closed-loop responses (solid red) with respect to the open-loop ones (dashed blue) are attenuated in low frequency and at the first resonance pick around 3Hz, while higher frequencies (above 10Hz) are not modified thanks to the controller structure that rolls-off above 10Hz. When considering the middle frames, the time responses to a MVS are reported. These frames compare the responses either with (solid red) or without (dashed blue) the load clearance controller presented in Section 3.3. First, top frame illustrates the fact that the load factor $N_z(t)$ reference is well tracked with both controller. The only slight difference occurs at $t = 10s$ and $t = 15s$ when the wing root bending moment is saturated (middle frame). Indeed, as illustrated in the middle frame, the proposed load saturation control allows to prevent limitation overshoot, maintaining the wing root bending moment within load limitations. This is a strong property and very important for certification purpose since it allows to guarantee that, whatever the exogenous input, the load envelope is preserved. Indeed, the nominal flight control is not able to prevent saturation without a significant diminution of the flight performances.

To quantify the effectiveness of the anti-load controller, the attenuation metric (3) indicates a gain of 25% in load attenuation, which is very encouraging for further developments. Finally, bottom right frame shows the control signal, illustrating the smoothness of the control law, even in saturation situations, which is a demand from aircraft engineers.

4. CONCLUSIONS AND PERSPECTIVES

In this paper, a strategy for manoeuvre load control has been presented and validated on a large-scale high fidelity model, constructed to faithfully reproduce the flexible aircraft behaviour at one single flight point. The proposed control design is based on a frequency-limited model approximation, followed by an innovative structured controller linked with an appropriate output saturation mechanism. This output saturation mechanism recast a controls input saturation one, allows to use the nominal controller and ensures good flight performance in most of the case, while guaranteeing wing root bending moment limitation only when it is necessary. Both frequency and time domain results emphasize the effectiveness of the proposed structure. Forthcoming work will address the robustness property by considering additional flight points/mass.

ACKNOWLEDGEMENT

The research leading to these results has received funding from the European Union's Seventh Framework Program (FP7/2007-2013) for the Clean Sky Joint Technology Initiative under grant agreement CSJU-GAM-SFWA-2008-001.

REFERENCES

- Antoulas, A.C. (2005). *Approximation of Large-Scale Dynamical Systems*. Advanced Design and Control, SIAM, Philadelphia.
- Apkarian, P. and Noll, D. (2006). Nonsmooth \mathcal{H}_∞ Synthesis. *IEEE Transaction on Automatic Control*, 51(1), 71–86.
- Burlion, L. (2012). A new saturation function to convert an output constraint into an input constraint. In *Proceedings of the 20th Mediterranean Conference on Control and Automation*, 1211–1216.
- Burlion, L. and de Plinval, H. (2013). Keeping a ground point in the camera field of view of a landing uav. In *Proceedings of the IEEE International Conference on Robotics and Automation*, 5763–5768.
- Gadient, R., Lavretsky, E., and Wise, K. (2012). Very Flexible Aircraft Control Challenge Problem. In *Proceedings of the AIAA Guidance, Navigation, and Control Conference*. Minneapolis, Minnesota, USA.
- Gardonio, P. (2002). Review of Active Techniques for Aerospace Vibro-Acoustic Control. *Journal of Aircraft*, 39(2), 206–214.
- Gaulocher, S., Roos, C., and Cumer, C. (2007). Aircraft load alleviation during maneuvers using optimal control surface combinations. *AIAA Journal of Guidance, Control and Dynamics*, 30(2), 591–600.
- Gugercin, S., Antoulas, A.C., and Beattie, C.A. (2008). \mathcal{H}_2 Model Reduction for Large Scale Linear Dynamical Systems. *SIAM Journal on Matrix Analysis and Applications*, 30(2), 609–638.
- Haghighat, S., Liu, H., and Martins, J. (2012). A model predictive gust load alleviation controller for a highly flexible aircraft. *Journal of Guidance, Control and Dynamics*.
- Hofstee, J., Kier, T., Cerulli, C., and Looye, G. (2003). A Variable, Fully Flexible Dynamic Response Tool for

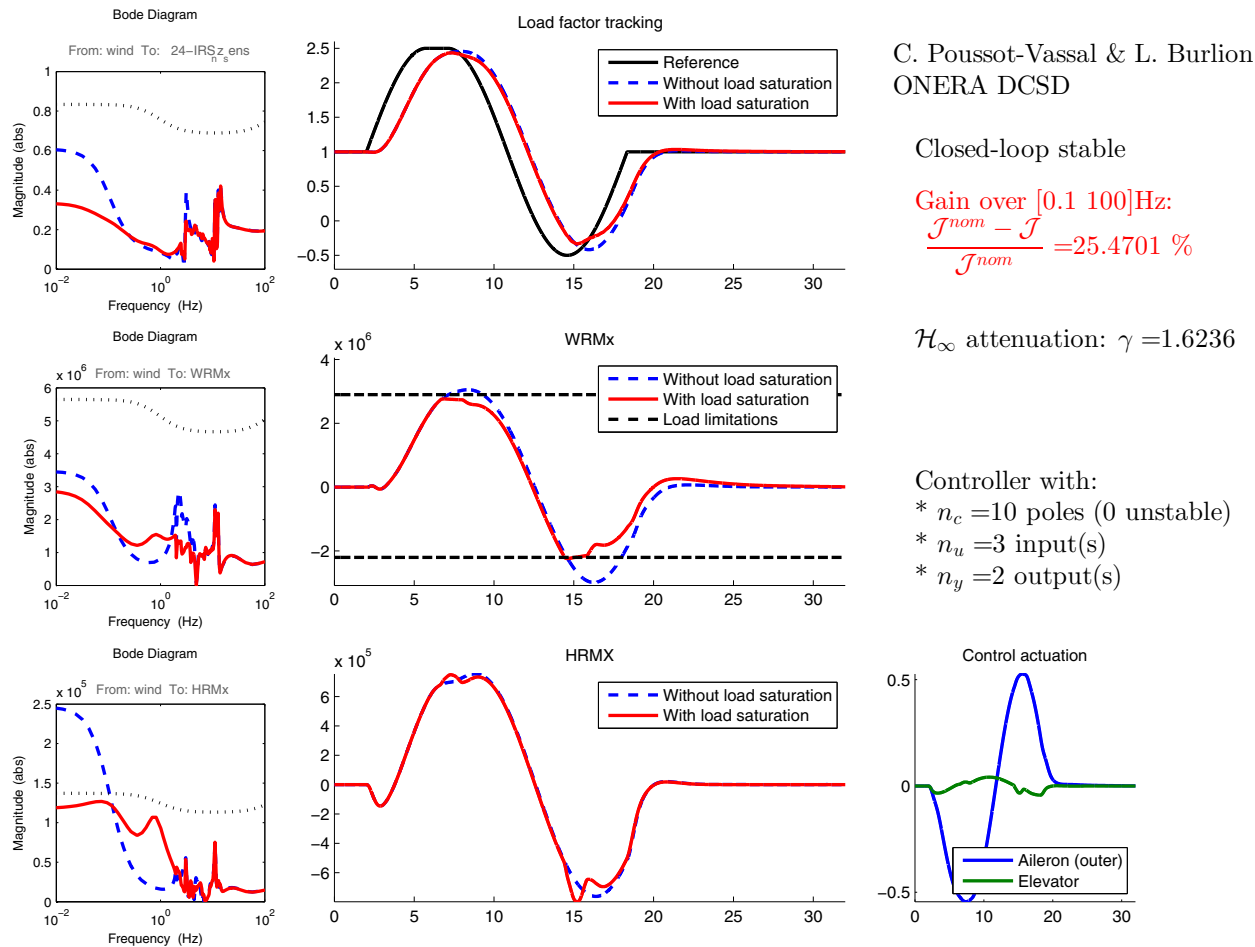


Fig. 5. Control results, applied on the large-scale flexible aircraft model. Left frames: frequency domain responses of the load factor (N_z), wing root bending moment (WRM_x) and tail root bending moment (HTP_x) in response to a wind disturbance (w) - open-loop: dashed blue, closed-loop: solid red, weighting filter used in the synthesis: dotted black. Middle frame: time domain behaviour in response to the MVS. Top frame: load factor tracking; Middle frame: wing root bending moment; and Bottom frame: HTP behaviour. Right side: attenuation criteria, property of the controller and control signal of the controller with load saturation.

Special Investigations (VarLoads). In *International Forum on Aeroelasticity and Structural Dynamics*.

Kier, T. and Looye, G. (2009). Unifying Manoeuvre and Gust Loads Analysis. In *International Forum on Aeroelasticity and Structural Dynamics*, IFASD-2009-106.

Looye, G., Hecker, S., Kier, T., and Reschke, C. (2005). FlightDynLib: An Object-Oriented Model Component Library for Constructing Multi-Disciplinary Aircraft Dynamics Models. In *International Forum on Aeroelasticity and Structural Dynamics*, IF-045. CEAS/DLR/AIAA.

Poussot-Vassal, C. (2011). An Iterative SVD-Tangential Interpolation Method for Medium-Scale MIMO Systems Approximation with Application on Flexible Aircraft. In *Proceedings of the 50th IEEE Conference on Decision and Control - European Control Conference*, 7117–7122. Orlando, Florida, USA.

Poussot-Vassal, C. and Vuillemin, P. (2012). Introduction to MORE: a MODEL REDuction Toolbox. In *Proceedings of the IEEE Multi-conference on Systems and Control*, 776–781. Dubrovnik, Croatia.

Vuillemin, P., Poussot-Vassal, C., and Alazard, D. (2013). \mathcal{H}_2 optimal and frequency limited approximation methods for large-scale LTI dynamical systems. In *Proceedings of the 6th IFAC Symposium on Systems Structure and Control*, 719–724. Grenoble, France.

Vuillemin, P., Poussot-Vassal, C., and Alazard, D. (2014). Poles Residues Descent Algorithm for Optimal Frequency-Limited \mathcal{H}_2 Model Approximation. In *Proceedings of the European Control Conference*. Strasbourg, France.

Time-response shaping using output to input saturation transformation

E. Chambon, L. Burlion and P. Apkarian

Onera – The French Aerospace Lab, Toulouse, France

ABSTRACT

For linear systems, the control law design is often performed so that the resulting closed loop meets specific frequency-domain requirements. However, in many cases, it may be observed that the obtained controller does not enforce time-domain requirements amongst which the objective of keeping a scalar output variable in a given interval. In this article, a transformation is proposed to convert prescribed bounds on an output variable into time-varying saturations on the synthesised linear scalar control law. This transformation uses some well-chosen time-varying coefficients so that the resulting time-varying saturation bounds do not overlap in the presence of disturbances. Using an anti-windup approach, it is obtained that the origin of the resulting closed loop is globally asymptotically stable and that the constrained output variable satisfies the time-domain constraints in the presence of an unknown finite-energy-bounded disturbance. An application to a linear ball and beam model is presented.

ARTICLE HISTORY

Received 12 October 2015
Accepted 19 January 2017

KEYWORDS

Constrained control; linear systems; unknown disturbance; interval constraint; time-domain constraint; anti-windup

1. Introduction

To stabilise a given system, many techniques exist to obtain a control law satisfying to specified constraints. As far as linear systems are concerned, H_∞ loop-shaping can, for example, be used to enforce frequency-domain requirements. However it is possible that, using such control law, time-domain requirements on a *constrained variable* $\alpha = C_\alpha y \in \mathbb{R}$ are not fulfilled. This is illustrated on [Figure 1](#) where α time response violates expected bounds $[\underline{\alpha}(t), \bar{\alpha}(t)]$. In practice, a good knowledge of the studied system is often sufficient to shape its time response. However, designing controllers satisfying to such prescribed time-domain requirements remains tedious and relies on numerous trial and errors involving simulations. Consequently, for more complex systems, and from the theoretical point of view, dedicated methods are often required to enforce both stability and time-domain constraints.

Amongst existing strategies to enforce time-domain requirements like time response or overshoot limitation, it is possible to mention the work presented in [Gevers \(2002\)](#) which introduced the notion of iterative feedback tuning (IFT). The idea is to shape the closed loop in response to specific input signals so as to satisfy time-domain constraints. In the PID-tuning case, a comparison with practitioners methods was performed in [Mossberg, Gevers, and Lequin \(2002\)](#), which gives a hint on how to achieve time-domain requirements using this method. Time-domain specifications are also

treated through optimal control strategies as extensively presented in [Goodwin, Seron, and de Doná \(2005\)](#). These approaches include model predictive control (MPC) in which the optimisation problem can take constraints into account (see, for example, [Chen and Allgöwer, 1996, 1999](#)). Computationally effective methods close to MPC are reported in [Ghaemi, Sun, and Kolmanovsky \(2012\)](#). The notion of reference-governor to adjust the reference trajectory so that the constraints on the system are satisfied is also noticeable. It was presented in [Gilbert and Kolmanovsky \(2002\)](#) with an application to aerospace systems in [Polóni, Kalabić, McDonough, and Kolmanovsky \(2014\)](#). The combination of frequency-domain and time-domain constraints has been explored in [Apkarian, Ravanbod-Hosseini, and Noll \(2011\)](#) and references therein. This method makes use of non-smooth bundle optimisation methods and is referred to as ‘constrained structured H_∞ -synthesis’. It combines simulation optimisation with H_∞ -synthesis to enforce both frequency-domain and time-domain requirements.

Despite interesting numerical performance, this simulation-based technique does not guarantee the time-domain constraints satisfaction with respect to any type of input signals but those considered in the simulation.

These strategies often include the control law design, especially when an optimising scheme is used. Alternative schemes including anti-windup systems were proposed, for example, in [Turner and Postlethwaite \(2002\)](#) and [Rojas and Goodwin \(2002\)](#). Compared to the

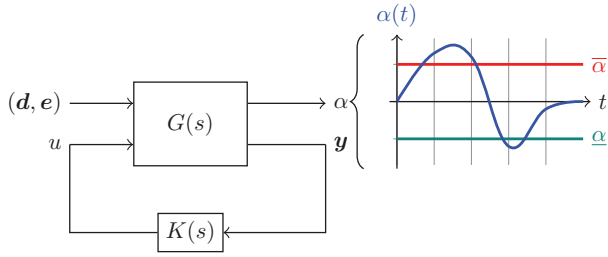


Figure 1. Illustration of system (G) in closed loop with controller K . The requirement on the constrained output variable $\alpha(t)$ is violated.

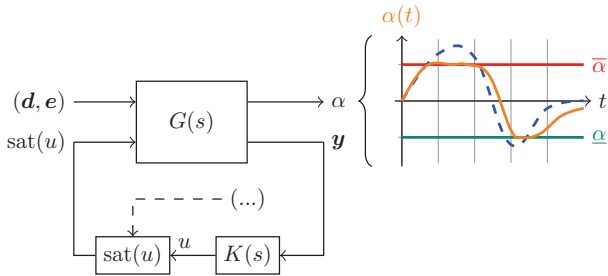


Figure 2. Illustration of system (G) in closed loop with the saturations obtained using OIST, and expected performance result.

aforementioned results, the anti-windup design is interesting because the nominal control law remains unchanged when acting far from the constraints. Also, an extensive literature on the subject is available (see Tarbouriech & Turner, 2009, or Galeani, Tarbouriech, Turner, & Zaccarian, 2009, for instance). However, there is not necessarily a guarantee on the fact that the time-domain constraints will actually be satisfied. In this article, the approach presented in Burlion (2012) and applied in Burlion and de Plinval (2013) and Burlion, Poussot-Vassal, Vuillemin, Leitner, and Kier (2014) is presented in-depth for state-feedback minimum-phase linear systems subject to disturbances. The output-to-input saturation transformation (OIST) theory proposes to reformulate prescribed bounds on the constrained variable α into state-dependent saturations on the control input u . This approach is illustrated in Figure 2 where an *ad hoc* saturating block is inserted before the system control input. As indicated in this figure, additional information may be required to express these saturations. Using this method along with some assumptions, it is possible to obtain guarantees on the fulfilment of the time-domain constraints when an unsatisfactory control law has already been designed.

This article is an extension of the works presented in Burlion (2012) and Chambron, Burlion, and Apkarian (2015a) in the LTI framework. It gives a comprehensive description of the OIST method for minimum-phase linear systems with unknown finite-energy-bounded

Table 1. Acronyms.

Acronym	Definition
CIBS	Converging input-bounded state
CICS	Converging input-converging state
GAS	Globally asymptotically stable (system)
GES	Globally exponentially stable (system)
ISS	Input-to-state stable (system)
LQR	Linear quadratic regulator
LTI	Linear time invariant
OIST	Output-to-input saturation transformation
OIST-LTI	Output-to-input saturation transformation for LTI systems

disturbances, leading to the OIST-LTI method. Further, it develops new results to bring guarantees to the method: the OIST design parameters are chosen time varying to accommodate for saturation bounds overlap and a solution is provided to enforce the stability of the resulting saturated closed loop.

The article is organised as follows: notations and definitions along with some function properties are presented in Section 2 before introducing the ball and beam example. This example is used as a case study to highlight some problems linked to the application of OIST. Formal statements of the two considered problems are presented in Section 3 along with some assumptions which were used to obtain the results presented here. Then, the output-to-input saturation transformation proposed to solve the first problem is presented in Section 4. Due to the conservatism introduced by the bounds on the disturbances, special attention is paid in the selection of the design parameters so that the resulting time-varying saturation bounds do not overlap. The second problem deals with the asymptotic stability of the origin of the system in closed loop with the obtained saturated control. It is solved in Section 5 using an anti-windup structure. Finally, the whole approach is applied to the linear ball and beam model in Section 6. Conclusions and perspectives are then presented in Section 7.

2. Definitions and a motivating case study

2.1 Definitions and notations

2.1.1 Acronyms

The acronyms listed in Table 1 are used throughout the article.

2.1.2 Notations

Throughout this paper, linear systems with the following realisation are considered:

$$(G) \begin{cases} \dot{x} = Ax + B_u u + B_d d \\ y = x & + D_e e \\ \alpha = C_\alpha x & + D_\alpha e \end{cases} \quad (1)$$

where $\mathbf{A} \in \mathbb{R}^{n \times n}$, $\mathbf{B} = [\mathbf{B}_u \ \mathbf{B}_d \ \mathbf{0}] \in \mathbb{R}^{n \times m}$, $\mathbf{D} = [\mathbf{0} \ \mathbf{0} \ \mathbf{D}_e] \in \mathbb{R}^{n \times m}$, $\mathbf{C}_\alpha \in \mathbb{R}^{1 \times n}$ and $\mathbf{D}_\alpha = \mathbf{C}_\alpha \mathbf{D}_e \in \mathbb{R}$. The state vector is denoted by $\mathbf{x} \in \mathbb{R}^n$ and the measurements vector is denoted by $\mathbf{y} \in \mathbb{R}^n$. It is assumed that the measurement vector equals the state vector plus eventually a disturbance vector $\mathbf{D}_e \mathbf{e}$. The input vector lying in \mathbb{R}^m is divided between the scalar control input denoted by $u \in \mathbb{R}$ and the unknown inputs which are denoted by $[\mathbf{d}, \mathbf{e}] \in \mathbb{R}^{m-1}$ (respectively: state and measurement disturbances). The scalar output α is called the constrained output and its meaning is detailed later on in the paper. Let (K) denote a dynamic controller designed to achieve some frequency-domain constraints. Its state-space representation is given by

$$(K) \begin{cases} \dot{\mathbf{x}}_K = \mathbf{A}_K \mathbf{x}_K + \mathbf{B}_K u_K \\ y_K = \mathbf{C}_K \mathbf{x}_K + \mathbf{D}_K u_K \end{cases} \quad (2)$$

where $\mathbf{x}_K \in \mathbb{R}^{n_K}$, $\mathbf{u}_K = \mathbf{y}$ and $u = y_K$ - at least before applying OIST or considering additional stabilising structures like anti-windups. The transfer function from an input u to an output y is denoted by $T_{u \rightarrow y}(s)$ where s is the Laplace variable.

Inequalities involving matrices of identical dimensions are understood component-wise: let $(\mathbf{A}, \mathbf{B}) \in \mathbb{R}^{n \times m}$, then, $\mathbf{A} \leq \mathbf{B} \Leftrightarrow \forall (i, j)$ s.t. $1 \leq i \leq n, 1 \leq j \leq m$, $A_{ij} \leq B_{ij}$.

For a given bounded vector $\mathbf{x}(t)$, if the bounds are known, they are denoted by $\underline{\mathbf{x}}(t)$ and $\bar{\mathbf{x}}(t)$, i.e. $\underline{\mathbf{x}}(t) \leq \mathbf{x}(t) \leq \bar{\mathbf{x}}(t), \forall t$.

The saturation and dead-zone functions applied to a bounded variable x are, respectively, denoted by $\text{sat}_{\underline{\mathbf{x}}}^{\bar{\mathbf{x}}}(x)$ and $\text{Dz}_{\underline{\mathbf{x}}}^{\bar{\mathbf{x}}}(x)$. They are related to each other by

$$\text{sat}_{\underline{\mathbf{x}}}^{\bar{\mathbf{x}}}(x) = x - \text{Dz}_{\underline{\mathbf{x}}}^{\bar{\mathbf{x}}}(x) \quad (3)$$

In case the signals $\underline{\mathbf{x}}$ and $\bar{\mathbf{x}}$ are determined from other variables, as is the case in the OIST methodology, it may happen that $\bar{\mathbf{x}} \leq \underline{\mathbf{x}}$ due to sign inversions. For the saturating operator to be *robust* to such situations, it is defined as follows:

$$\text{sat}_{\underline{\mathbf{x}}}^{\bar{\mathbf{x}}}(\mathbf{x}) := \max(\min(\underline{\mathbf{x}}, \bar{\mathbf{x}}), \min(\mathbf{x}, \max(\underline{\mathbf{x}}, \bar{\mathbf{x}}))) \quad (4)$$

The standard Euclidean norm of a given signal $\mathbf{x}(t)$ defined for $t \geq 0$ is denoted $\|\mathbf{x}\|$. The L_2 -norm of the same signal is denoted $\|\mathbf{x}\|_2$ and is given by

$$\|\mathbf{x}\|_2 = \sqrt{\int_0^\infty |\mathbf{x}(t)|^2 dt} \quad (5)$$

2.1.3 Definitions

Some definitions are now introduced. In the article, the term ‘overlap’ is used to refer to two signals taking the same value at a given instant and possibly changing order:

Definition 2.1: Two unidimensional signals $\underline{s}(t)$ and $\bar{s}(t)$ are said to overlap if $\exists t_1 > 0, \delta > 0$ such that $\forall t < t_1, \underline{s}(t) \leq \bar{s}(t)$ and $\forall t \in [t_1, t_1 + \delta], \underline{s}(t) > \bar{s}(t)$.

The notion is illustrated on Figure 3. Next, the Lambert function is used to define some constants. It is defined as follows:

Definition 2.2: Let $\forall x \in \mathbb{R}, F(x) = xe^x$. The inverse function of F is the Lambert function denoted by $W_0(y)$ which fulfils $\forall y, F(W_0(y)) = W_0(y)e^{W_0(y)} = y$.

This definition is used to define constants which in turn will help to define differentiable approximates of non-differentiable functions:

Definition 2.3: Let us define the constants $\xi := \frac{1}{2}W_0\left(\frac{1}{e}\right) + \frac{1}{2}$ and $\Xi := \xi - \tanh(\xi)\xi > 0$. Using these notations, let us also define the following functions,

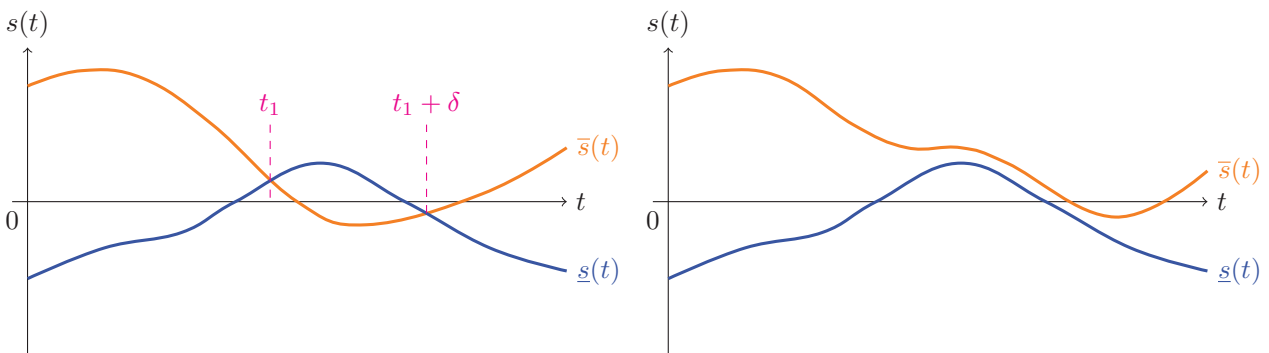


Figure 3. Left: example of overlap of two signals $\underline{s}(t)$ and $\bar{s}(t)$, overlap starts at time t_1 and stops at $t_1 + \delta$. Right: the represented signals do not overlap over the considered interval of time.

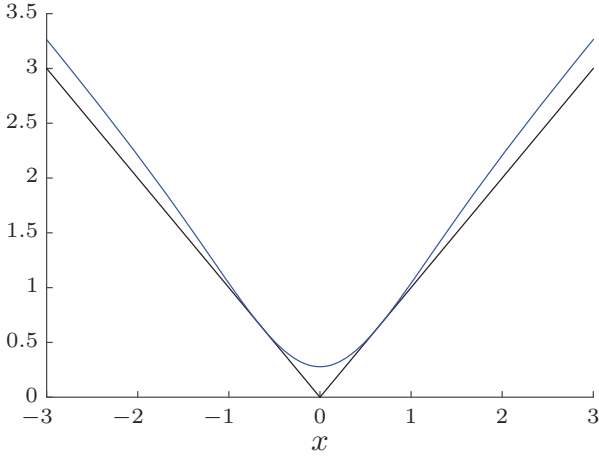


Figure 4. (Colour online) Representation of the absolute value function (in black) and its differentiable approximate f_{abs} (in blue) over the interval $[-3, 3]$.

$\forall (x, y) \in \mathbb{R}^2$:

$$\begin{aligned} f_{\text{abs}}(x) &:= \tanh(x)x + \Xi \\ f_{\text{max}}(x, y) &:= \frac{1}{2} [x + y + f_{\text{abs}}(x - y)] \\ g(x, y) &:= f_{\text{max}}(f_{\text{abs}}(x), f_{\text{abs}}(y)) \end{aligned} \quad (6)$$

in which definition is extended to vectors $(\mathbf{x}, \mathbf{y}) \in \mathbb{R}^{n \times 2}$ in a component-wise manner. The absolute value and its differentiable over-approximating function $f_{\text{abs}}(x)$ are represented on Figure 4 over an interval of \mathbb{R} . This definition triggers some remarks:

Remark 2.1: Note that ξ is the solution to the equation $(2x - 1)e^{2x} = 1$. Also, note that $f_{\text{abs}}, f_{\text{max}}$ and g are continuous differentiable over \mathbb{R} or \mathbb{R}^2 . Moreover,

- $\forall x \in \mathbb{R}, f_{\text{abs}}(x) \geq |x|$;
- $\forall (x, y) \in \mathbb{R}^2, f_{\text{max}}(x, y) \geq \max(x, y)$.

Proof: These inequalities can be proved using basic real analysis. ■

The following definitions are directly related to the implementation of the OIST method.

Definition 2.4: Let $k \in \mathbb{N}$. Considering the LTI system in Equation (1) and supposing the disturbance signal \mathbf{e} is independent from u , the *constrained output variable* $\alpha \in \mathbb{R}$ is said to be of relative degree k with respect to u , if and only if

$$\forall i \text{ s.t. } 0 \leq i < k - 1, \mathbf{C}_\alpha \mathbf{A}^i \mathbf{B}_u = 0 \text{ and } \mathbf{C}_\alpha \mathbf{A}^{k-1} \mathbf{B}_u \neq 0 \quad (7)$$

2.2 Motivating case study

In this section, an example is introduced where the control synthesis problem has been solved without considering any time-domain constraint on the selected constrained output variable α . In this case, there is a violation of the expected time-domain performance of this constrained variable which motivates the use of a dedicated method such as OIST. However, two problems related to the application of this method as presented in Burlion (2012) arise. This paper proposes solutions to both problems.

Note that a more thorough control design study may be sufficient to enforce the time-domain requirement. However, this is not considered in this article for two reasons:

- The OIST method was proposed to enforce time-domain requirements when the controller is not able to do so, hence the failing controller is kept for illustrative purposes.
- Other criteria often enter in the control design. Enforcing the time-domain criterion may degrade nominal performance from other points of view.

2.2.1 Considered ball and beam model

This case study is dedicated to the position control of a ball on a beam. The physical system and the notations are represented in Figure 5.

The beam is actuated using a lever arm. An unknown disturbance force d is eventually applied to the ball acceleration. The disturbance signal used in simulation is represented in plain blue on Figure 6. The state vector of the system is defined by $\mathbf{x} = \begin{bmatrix} r \\ \dot{r} \end{bmatrix}$ and the measurements vector by $\mathbf{y} = \mathbf{x}$. Note that $\mathbf{e} = \mathbf{0}$ in this example meaning

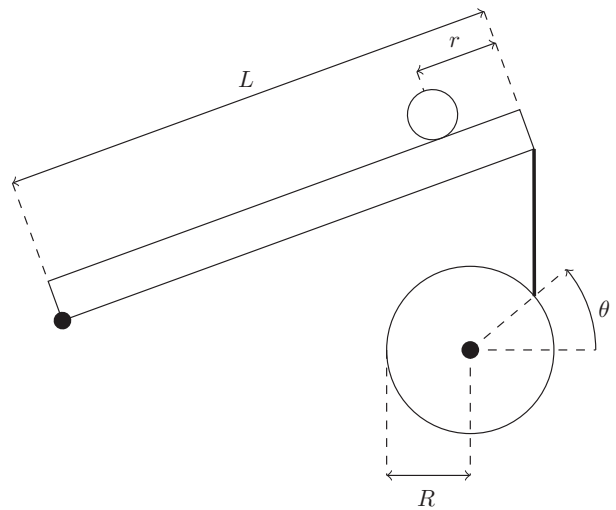


Figure 5. Ball and beam system example, thick dots represent fixed axes of rotation.

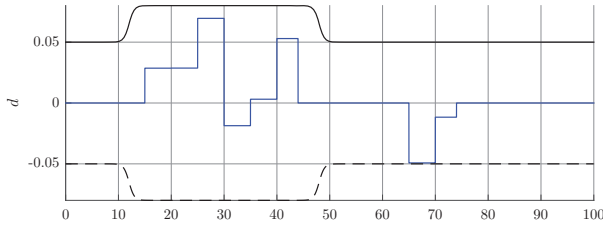


Figure 6. Considered state disturbance d (in simulation) and its known bounds \underline{d} and \bar{d} .

that the measurements vector is undisturbed and equals the state vector exactly. The constrained output variable expression simplifies to $\alpha = \mathbf{C}_\alpha \mathbf{x}$ with $\mathbf{C}_\alpha = [1 \ 0]$. This is used to constrain the ball position on the beam.

The reason for monitoring this variable is quite obvious. The beam length is limited to $L = 1$ m which means that even a theoretically stabilising control law can result in the ball falling off the beam especially in the presence of a disturbance. The time-domain requirement is thus to satisfy $0.1 \leq \alpha(t) \leq 0.9$ (in metres), $\forall t$ while driving the system from $r_0 = 0.5$ m to the set point $r_s = 0.6$ m. More exotic time-varying requirements can also be considered as follows. The system state-space representation is given by

$$\begin{aligned} \mathbf{A} &= \begin{bmatrix} 0 & 1 \\ 0 & 0 \end{bmatrix}, \mathbf{B} = \begin{bmatrix} 0 & 0 \\ -0.21 & 1 \end{bmatrix}, \\ \mathbf{C} &= \mathbf{I}_2, \mathbf{D} = \begin{bmatrix} 0 & 0 \\ 0 & 0 \end{bmatrix} \end{aligned} \quad (8)$$

where the inputs are, respectively, u and d . As far as the nominal control design is concerned, a state-feedback controller with integral action is implemented to achieve

steady-state accuracy. The considered controller state-space representation is given by Equation (2), where

$$\begin{aligned} \mathbf{A}_K &= -1.5779, \mathbf{B}_K = [0.0322 \quad 0.2339], \\ \mathbf{C}_K &= -0.0644, \mathbf{D}_K = [-0.3156 \quad -2.0937] \end{aligned} \quad (9)$$

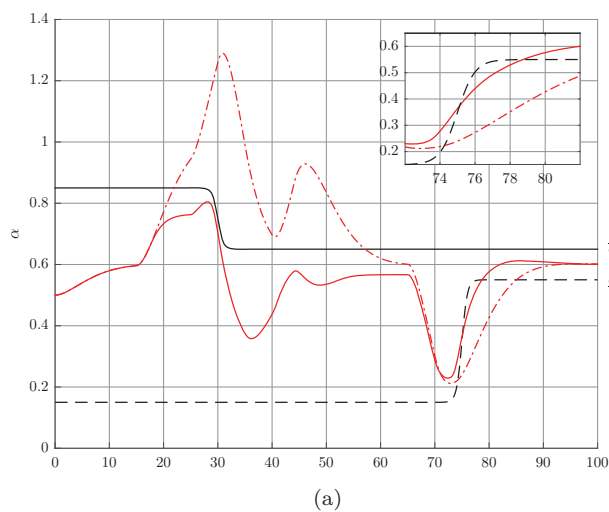
and $\mathbf{u}_K = \mathbf{y}_s - \mathbf{y}$ with $\mathbf{y}_s = [r_s \ 0]^\top$.

This dynamic controller stabilises the system and yields good results in r_s -set-point tracking. However, using this controller, the constrained output variable represented in dashed-dotted red line in Figure 7(a) violates the time-varying time-domain requirement represented in black lines.

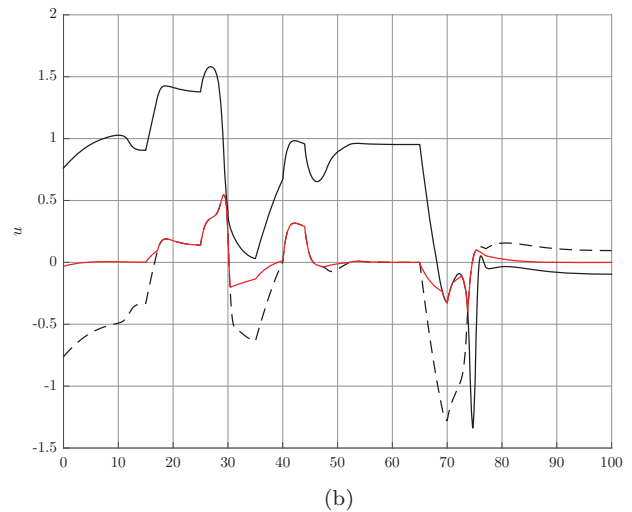
2.2.2 Application of the original OIST method

To enforce the time-domain requirement, it is proposed to use the OIST approach as presented in Burlion (2012). In this article, the author uses a specific transformation which allows to transform a constraint on an output into saturations on the input. By appropriately choosing the saturations, the reachable set is restricted such that the constrained variable satisfies the considered requirement even in the presence of unknown disturbances. The only required information are bounds \underline{d} and \bar{d} on the disturbance d as illustrated in Figure 6. For the sake of simplicity, the formulas are not described in this section. Please refer to Section 4 for a complete description of the method.

In the mentioned article, the design parameters used in the method are chosen constant. Let us consider $\kappa_1 = 1$ and $\kappa_2 = 0.6$. The OIST approach is then implemented on the system. Simulation results are represented in plain red



(a)



(b)

Figure 7. (Colour online) Case study: simulation results w/ (plain red) or w/o (dashed-dotted red) OIST in the loop. (a) Time-domain requirement (in black) and simulation results for the constrained variable α . The dashed-dotted red line is obtained when using the nominal controller and the plain red line is obtained when using OIST as in Burlion (2012). (b) Control signal (in red) and saturation bounds obtained using OIST as in Burlion (2012). Saturation bounds overlap starts around $t_1 = 73$ s.

line in Figure 7. At first, it seems that the constrained variable satisfies the requirement. However, it appears that violation of the constraint occurs at $t = 75$ s. This results from the two saturation bounds overlap starting at time t_1 as illustrated in Figure 7(b). This could be avoided using time-varying coefficients $\kappa_1(t)$ and $\kappa_2(t)$. This was mentioned in Burlion (2012), but not detailed. The first main contribution of the current work is thus to propose guarantees within the OIST method such that saturation bounds overlap never occurs and the time-domain requirement is guaranteed (see Section 4).

Moreover, inserting saturations in the loop is never harmless, especially when the controller is unstable. In most cases, however, theoretical guarantees on the closed-loop stability are expected. This is the second main contribution of the paper (see Section 5).

3. Problems statement

Let us consider the LTI system (G) in Equation (1) in closed loop with the controller (K) in Equation (2) ($\mathbf{u}_k = \mathbf{y}$ and $u = y_K$). Both the state and measurements are supposed to be disturbed. A time-domain constraint is expressed on its constrained output variable $\alpha \in \mathbb{R}$. It consists in ensuring $\alpha(t) \in [\underline{\alpha}(t), \bar{\alpha}(t)]$, $\forall t$, where $\underline{\alpha}(t)$ and $\bar{\alpha}(t)$ are design parameters such that $\bar{\alpha}(t) \geq \underline{\alpha}(t)$, $\forall t$. Before stating the tackled problems, some assumptions are now introduced.

3.1 Assumptions

To be able to use the transformation presented in Section 4, the considered system has to fulfil some assumptions which are recalled here. These assumptions are capital to be able to provide solutions to the considered problems. For example, it would be fanciful to enforce the time-domain constraint without having more information on the disturbances. First, the design signals of the time-domain requirement need to converge:

Assumption 3.1: *The time-domain requirement signals are supposed to converge towards constant values:*

$$\lim_{t \rightarrow \infty} \underline{\alpha}(t) = \underline{\alpha}^*, \quad \lim_{t \rightarrow \infty} \bar{\alpha}(t) = \bar{\alpha}^* \quad (10)$$

where $\underline{\alpha}^* \leq \bar{\alpha}^*$.

Second, the relative degrees of the constrained variable with respect to the inputs are detailed:

Assumption 3.2: *Let $(k, l) \in \mathbb{N}^2$ such that $1 \leq l \leq k$. It is supposed the constrained output variable α is of relative degree k (resp. l) with respect to u (resp. the state disturbance input \mathbf{d}).*

Note that since \mathbf{D}_α is supposed to be non-null, then the constrained variable α is of null relative degree with respect to the measurement noise \mathbf{e} . Let $\mathcal{D}(t) = [\mathbf{d} \dot{\mathbf{d}} \dots \mathbf{d}^{(k-l-1)}]^\top \in \mathbb{R}^{k-l}$ and $\mathcal{E}(t) = [\mathbf{e} \dot{\mathbf{e}} \dots \mathbf{e}^{(k)}]^\top \in \mathbb{R}^{k+1}$. The next assumption makes sure that these quantities are bounded by known time-varying matrices.

Assumption 3.3: *Continuous time-varying bounds $[\underline{\mathcal{D}}(t), \bar{\mathcal{D}}(t)]$ on the unknown disturbances and their derivatives $\mathcal{D}(t)$ are supposed to be known, that is,*

$$\underline{\mathcal{D}}(t) \leq \mathcal{D}(t) \leq \bar{\mathcal{D}}(t), \quad \forall t \quad (11)$$

or, more precisely,

$$\forall i \text{ s.t. } 0 \leq i \leq k-l-1, \quad \underline{d}^{(i)}(t) \leq d^{(i)}(t) \leq \bar{d}^{(i)}(t), \quad \forall t \quad (12)$$

The same holds for the measurement disturbance and its derivatives $\mathcal{E}(t)$ with time-varying bounds $[\underline{\mathcal{E}}(t), \bar{\mathcal{E}}(t)]$. Also,

$$\begin{aligned} \lim_{t \rightarrow \infty} \underline{\mathcal{D}}(t) = \mathbf{0}, \quad \lim_{t \rightarrow \infty} \bar{\mathcal{D}}(t) = \mathbf{0}, \quad \lim_{t \rightarrow \infty} \underline{\mathcal{E}}(t) \\ = \mathbf{0} \text{ and } \lim_{t \rightarrow \infty} \bar{\mathcal{E}}(t) = \mathbf{0} \end{aligned} \quad (13)$$

As conservative as this assumption may be, it is not so different from supposing the disturbances follow some theoretical model. The following assumptions will be used in the proof of the closed-loop system state convergence to the origin:

Assumption 3.4: *The disturbance \mathbf{d} is supposed to be of finite energy $\|\mathbf{d}\|_2 < \infty$. The same holds for \mathbf{e} with energy $\|\mathbf{e}\|_2 < \infty$.*

Assumption 3.5: *The controller in Equation (2) is supposed to stabilise asymptotically (resp. exponentially) system (G) to the origin $\mathbf{x}^* = \mathbf{0}$, under Assumption 3.4 (resp. $\mathbf{d} = \mathbf{0}$ and $\mathbf{e} = \mathbf{0}$). The controller state at the equilibrium is denoted $\mathbf{x}_K^* = \mathbf{0}$.*

In this article, only minimum-phase systems are considered. In the non-minimum-phase case, additional analysis is required to ensure stability, which is considered as a perspective for future works.

Assumption 3.6: *The zeros of the SISO transfer function $T_{u \rightarrow \alpha}(s)$ from the control input u to the constrained variable α are supposed to be with strictly negative real part.*

To simplify the formulation of iterative expressions for the saturations components, the following assumption is made to ensure some terms will not re-appear upon derivation of the components:

Assumption 3.7: *The relative degrees in Assumption 3.2 satisfy to the relation $2l > k$.*

For any system fulfilling these hypotheses, the two following problems are considered:

- Enforce the considered time-domain requirement on the considered constrained variable. This is formulated in Problem 3.1 and a solution is provided in Section 4. As illustrated in Section 2.2, this implicitly requires to avoid saturation bounds overlap;
- Guarantee the closed-loop stability in the presence of OIST saturations. This is formulated in Problem 3.2 and a solution is provided in Section 5.

3.2 Considered problems

The problem of enforcing this time-domain constraint was introduced in Burlion (2012) and translated in the linear framework in Chambon et al. (2015a):

Problem 3.1 (Guaranteed satisfaction of a time-domain requirement, LTI framework): Find $[\underline{u}(t), \bar{u}(t)]$ such that for two design signals $\underline{\alpha}(t)$ and $\bar{\alpha}(t)$ fulfilling $\underline{\alpha}(t) \leq \bar{\alpha}(t)$, $\forall t$:

$$\alpha(t) \in [\underline{\alpha}(t), \bar{\alpha}(t)], \forall t \quad (14)$$

for the system (G) in Equation (1) in closed loop with controller (K) in Equation (2) and satisfying to Assumptions 3.1–3.7:

$$\begin{cases} \dot{\mathbf{x}}(t) = \mathbf{A}\mathbf{x}(t) + \mathbf{B}_u u(t) + \mathbf{B}_d \mathbf{d}(t) \\ \mathbf{y}(t) = \mathbf{C}\mathbf{x}(t) + \mathbf{D}_e \mathbf{e}(t) \\ \alpha(t) = \mathbf{C}_\alpha \mathbf{x}(t) + \mathbf{D}_\alpha \mathbf{e}(t) \\ \alpha(0) \in [\underline{\alpha}(0), \bar{\alpha}(0)] \\ \dot{\mathbf{x}}_K(t) = \mathbf{A}_K \mathbf{x}_K(t) + \mathbf{B}_K \mathbf{y}(t) \\ u(t) = \text{sat}_{\underline{u}(t)}^{\bar{u}(t)}(\mathbf{C}_K \mathbf{x}_K(t) + \mathbf{D}_K \mathbf{y}(t)) \end{cases} \quad (15)$$

where $\alpha \in \mathbb{R}$ is the considered constrained output variable.

Finding a solution to this problem motivates the output-to-input saturation Transformation (OIST) where a constraint on the output α as in Equation (14) is transformed into saturations $[\underline{u}(t), \bar{u}(t)]$ on the control input u .

Remark 3.1: The problem of avoiding saturation bounds overlap may not be obvious when considering the chosen formulation for Problem 3.1. However, as illustrated in Section 2.2, finding a solution to Problem 3.1 implicitly requires to avoid such overlap. Otherwise, no guarantee can be offered.

A guaranteed solution of this problem is proposed in Section 4. The introduction of saturations is critical in

most cases. In the presence of saturations, the state of the closed-loop system may diverge: this is the well-known windup effect. Hence, a second problem should be considered in addition to Problem 3.1:

Problem 3.2 (Guaranteed closed-loop stability using OIST): Guarantee that the origin of the saturated closed loop in Equation (15) is asymptotically stable.

A solution to this problem is proposed in Section 5 using the saturations provided by the OIST approach in Section 4.

4. OIST-LTI with saturation bounds overlap avoidance

The output-to-input saturation transformation is presented in this section as a solution to Problem 3.1 in the case of known LTI systems fulfilling Assumptions 3.1–3.7. Time-varying design coefficients are introduced in the saturation bounds for the first time so as to avoid overlap. Their expressions are derived from the known bounds on $\mathcal{D}(t)$ and $\mathcal{E}(t)$. This is detailed in the following sections.

4.1 Constrained output variable differentiation and relative degree

Using Assumptions 3.2 and 3.7, the k th derivative of the constrained variable α in function of u and \mathbf{d} has the following expression:

$$\begin{aligned} \alpha^{(k)}(t) &= \mathbf{C}_\alpha \mathbf{A}^k \mathbf{x}(t) + \mathbf{D}_\alpha \mathbf{e}^{(k)}(t) + \mathbf{C}_\alpha \mathbf{A}^{k-1} \mathbf{B}_u u(t) \\ &\quad + \sum_{j=1}^k \mathbf{C}_\alpha \mathbf{A}^{j-1} \mathbf{B}_d \mathbf{d}^{(k-j)}(t) \end{aligned} \quad (16)$$

By definition of the relative degree (Definition 2.4), the k th derivative of the constrained variable α thus depends on the control input signal $u(t)$. In the next section, a lemma will be formulated so that properly differentiated design bounds on α can lead to saturations on u , using Equation (16).

4.2 Fulfilling the time-domain requirement

Considering Problem 3.1, the objective is to ensure $\alpha(t) \in [\underline{\alpha}(t), \bar{\alpha}(t)]$, $\forall t$. In this section, it is shown how adequate constraints on the successive derivatives of α can be used to fulfil this requirement. Let us consider a vector of known positive time-varying signals

$$\boldsymbol{\kappa}(t) = [\kappa_1(t) \cdots \kappa_k(t)] \in \mathbb{R}_+^k \quad (17)$$

which will act as ‘design parameters’. The following lemma is proposed and proved:

Lemma 4.1: *Let us define $\underline{\alpha}_0(t) := \underline{\alpha}(t)$, $\bar{\alpha}_0(t) := \bar{\alpha}(t)$ by convention and $\forall j$ s.t. $1 \leq j \leq k, \forall t$:*

$$\begin{aligned}\underline{\alpha}_j(t) &:= \kappa_j(t)(\underline{\alpha}_{j-1}(t) - \alpha^{(j-1)}(t)) + \underbrace{\underline{\alpha}_{j-1}(t)} \\ \bar{\alpha}_j(t) &:= \kappa_j(t)(\bar{\alpha}_{j-1}(t) - \alpha^{(j-1)}(t)) + \underbrace{\bar{\alpha}_{j-1}(t)}\end{aligned}\quad (18)$$

Supposing that $\forall i$ s.t. $0 \leq i \leq k$, $\alpha^{(i)}(0) \in [\underline{\alpha}_i(0), \bar{\alpha}_i(0)]$, then

$$\begin{aligned}\alpha^{(k)}(t) \in [\underline{\alpha}_k(t), \bar{\alpha}_k(t)], \forall t &\Rightarrow \alpha(t) \in [\underline{\alpha}_0(t), \bar{\alpha}_0(t)] \\ &= [\underline{\alpha}(t), \bar{\alpha}(t)], \forall t\end{aligned}$$

Proof: See Appendix 1. ■

Remark 4.1: The time-varying signal $\kappa(t)$ components $\kappa_j(t)$ in Equation (18) are the design parameters of the method. Their selection is crucial to avoid saturation bounds overlap as detailed in Section 4.4.

Remark 4.2: Note this lemma is still valid when introducing more conservative bounds $\underline{\beta}_j(t)$ and $\bar{\beta}_j(t)$ on $\alpha^{(j)}(t)$, i.e. satisfying for any given j such that $1 \leq j \leq k$:

$$\underline{\alpha}_j(t) \leq \underline{\beta}_j(t), \bar{\beta}_j(t) \leq \bar{\alpha}_j(t), \forall t \quad (19)$$

Also, note these more conservative bounds are not necessarily defined by an iterative relation as in Equation (18).

This lemma is directly inspired by Assumption 3.2 on the relative degree of α with respect to u . It can be used to enforce a time-domain constraint on α by considering a time-domain constraint on its k th derivative $\alpha^{(k)}$. Since the latter depends on u as highlighted in Equation (16), appropriate saturations on the control input can be obtained. This is detailed in the next section.

4.3 Detailed expressions of the control saturation bounds

Given Assumption 3.2, there is $\mathbf{C}_\alpha \mathbf{A}^{k-1} \mathbf{B}_u \neq 0$. Let us also suppose that $\mathbf{C}_\alpha \mathbf{A}^{k-1} \mathbf{B}_u > 0$. Considering Lemma 4.1 and Equation (16), and supposing that the expressions of $\underline{\alpha}_k(t)$ and $\bar{\alpha}_k(t)$ are known $\forall t$, the saturations to apply to the control input u can be obtained. In the undisturbed case ($\mathbf{d}(t) = 0$ and $\mathbf{e}(t) = 0, \forall t$), these saturations would

simply be given by

$$\begin{aligned}\underline{u}(t) &= \frac{1}{\mathbf{C}_\alpha \mathbf{A}^{k-1} \mathbf{B}_u} [\underline{\alpha}_k(t) - \mathbf{C}_\alpha \mathbf{A}^k \mathbf{x}(t)] \\ \bar{u}(t) &= \frac{1}{\mathbf{C}_\alpha \mathbf{A}^{k-1} \mathbf{B}_u} [\bar{\alpha}_k(t) - \mathbf{C}_\alpha \mathbf{A}^k \mathbf{x}(t)]\end{aligned}\quad (20)$$

In the more general considered case, the saturation expressions should account for the presence of unknown disturbances. This is possible using Assumption 3.3:

$$\begin{aligned}\underline{u}(t) &= \frac{1}{\mathbf{C}_\alpha \mathbf{A}^{k-1} \mathbf{B}_u} \left[\underline{\alpha}_k(t) - \mathbf{C}_\alpha \mathbf{A}^k \mathbf{x}(t) + |D_\alpha| \max \left(\left| \underline{\mathbf{e}}^{(k)}(t) \right|, \left| \bar{\mathbf{e}}^{(k)}(t) \right| \right) \right. \\ &\quad \left. + \sum_{j=1}^k |\mathbf{C}_\alpha \mathbf{A}^{j-1} \mathbf{B}_d| \max \left(\left| \underline{\mathbf{d}}^{(k-j)}(t) \right|, \left| \bar{\mathbf{d}}^{(k-j)}(t) \right| \right) \right] \\ \bar{u}(t) &= \frac{1}{\mathbf{C}_\alpha \mathbf{A}^{k-1} \mathbf{B}_u} \left[\bar{\alpha}_k(t) - \mathbf{C}_\alpha \mathbf{A}^k \mathbf{x}(t) - |D_\alpha| \max \left(\left| \underline{\mathbf{e}}^{(k)}(t) \right|, \left| \bar{\mathbf{e}}^{(k)}(t) \right| \right) \right. \\ &\quad \left. - \sum_{j=1}^k |\mathbf{C}_\alpha \mathbf{A}^{j-1} \mathbf{B}_d| \max \left(\left| \underline{\mathbf{d}}^{(k-j)}(t) \right|, \left| \bar{\mathbf{d}}^{(k-j)}(t) \right| \right) \right]\end{aligned}\quad (21)$$

To be appropriately defined, the saturations in both Equations (20) and (21) should not overlap, i.e. $\bar{u}(t) \geq \underline{u}(t), \forall t$. This can be ensured using appropriate time-varying design parameters $\kappa(t)$. This is discussed in Section 4.4.

Remark 4.3: In case $\mathbf{C}_\alpha \mathbf{A}^{k-1} \mathbf{B}_u < 0$ and to avoid loss of generality, proper re-ordering of $\underline{u}(t)$ and $\bar{u}(t)$ is required. This is obtained using the definition in Equation (4) of the saturation operator.

Expressions of the control saturation bounds have been obtained. Using these saturations, one can enforce the considered time-domain constraint as shown in Lemma 4.1. As seen in Equations (20) and (21), these saturations depend on two quantities $\underline{\alpha}_k(t)$ and $\bar{\alpha}_k(t)$ which are iteratively defined in Equation (18). A finer study of these quantities is performed here. For any integer j such that $1 \leq j \leq k$, let us define the two following vectors:

- $\mathbf{U}^j(t) = [u_0^j(t) \cdots u_k^j(t)] \in \mathbb{R}^{1 \times (k+1)}$ where $u_j^j(t) = 1$ and $\forall i > j, u_i^j(t) = 0$;
- $\mathbf{V}^j(t) = [v_0^j(t) \cdots v_{k-l-1}^j(t)] \in \mathbb{R}^{1 \times (k-l)}$ where $\forall i > \max(-1, j-l-1), v_i^j(t) = 0$ and

$$v_0^{l+1}(t) = u_{l-1}^l(t) \mathbf{C}_\alpha \mathbf{A}^{l-1} \mathbf{B}_d$$

Let $\underline{\mathbf{A}} = [\underline{\alpha} \ \underline{\alpha} \ \cdots \ (\underline{\alpha})^{(k)}]^\top \in \mathbb{R}^{k+1}$, $\bar{\mathbf{A}} = [\bar{\alpha} \ \bar{\alpha} \ \cdots \ (\bar{\alpha})^{(k)}]^\top$ and $\boldsymbol{\Theta} = [\mathbf{C}_\alpha \ \mathbf{C}_\alpha \mathbf{A} \ \cdots \ \mathbf{C}_\alpha \mathbf{A}^k]^\top \in \mathbb{R}^{(k+1) \times n}$. Using the iterative definition in Equation (18) and notations in Section 3.1, the

following expressions are obtained for $\underline{\alpha}_j(t)$ and $\bar{\alpha}_j(t)$:

$$\begin{aligned}\underline{\alpha}_j(t) &= \mathbf{U}^j(t) \{ \underline{\mathcal{A}}(t) - \Theta \mathbf{x}(t) - \mathcal{E}(t) \mathbf{D}_\alpha^\top \} \\ &\quad + \mathbf{C}_\alpha \mathbf{A}^j \mathbf{x}(t) + \mathbf{D}_\alpha \mathbf{e}^{(j)}(t) - \mathbf{V}^j(t) \mathcal{D}(t) \\ \bar{\alpha}_j(t) &= \mathbf{U}^j(t) \{ \bar{\mathcal{A}}(t) - \Theta \mathbf{x}(t) - \mathcal{E}(t) \mathbf{D}_\alpha^\top \} \\ &\quad + \mathbf{C}_\alpha \mathbf{A}^j \mathbf{x}(t) + \mathbf{D}_\alpha \mathbf{e}^{(j)}(t) - \mathbf{V}^j(t) \mathcal{D}(t)\end{aligned}\quad (22)$$

The vectors \mathbf{U}^j and \mathbf{V}^j can be defined iteratively when applying Equations (18)–(22). This is detailed in Appendix 2.

Remark 4.4: Using the obtained iterative expressions and the fact that $u_0^j(t) = \kappa_1(t)$, one can determine that $\forall j, 0 \leq j < k, u_j^{j+1}(t) = \sum_{w=1}^{j+1} \kappa_w(t)$.

However, the expressions obtained in Equation (22) cannot be used since $\mathcal{D}(t)$ and $\mathcal{E}(t)$ are unknown quantities. As stated in Remark 4.2, Lemma 4.1 is still valid if more conservative bounds are considered for the application on the derivatives $\alpha^{(j)}(t)$. Under Assumption 3.3, the disturbances are known to be bounded by known quantities. This is used along with Definition 2.3 to obtain differentiable known expressions instead of the original ones in Equation (22):

$$\begin{aligned}\underline{\beta}_j(t) &= \mathbf{U}^j(t) \{ \underline{\mathcal{A}}(t) - \Theta \mathbf{x}(t) \} \\ &\quad + f_{\text{abs}}(\mathbf{U}^j(t)) g(\underline{\mathcal{E}}(t), \bar{\mathcal{E}}(t)) |\mathbf{D}_\alpha^\top| + \mathbf{C}_\alpha \mathbf{A}^j \mathbf{x}(t) \\ &\quad + |\mathbf{D}_\alpha| g(\underline{\mathbf{e}}^{(j)}(t), \bar{\mathbf{e}}^{(j)}(t)) + f_{\text{abs}}(\mathbf{V}^j(t)) g(\underline{\mathcal{D}}(t), \bar{\mathcal{D}}(t)) \\ \bar{\beta}_j(t) &= \mathbf{U}^j(t) \{ \bar{\mathcal{A}}(t) - \Theta \mathbf{x}(t) \} \\ &\quad - f_{\text{abs}}(\mathbf{U}^j(t)) g(\underline{\mathcal{E}}(t), \bar{\mathcal{E}}(t)) |\mathbf{D}_\alpha^\top| + \mathbf{C}_\alpha \mathbf{A}^j \mathbf{x}(t) \\ &\quad - |\mathbf{D}_\alpha| g(\underline{\mathbf{e}}^{(j)}(t), \bar{\mathbf{e}}^{(j)}(t)) - f_{\text{abs}}(\mathbf{V}^j(t)) g(\underline{\mathcal{D}}(t), \bar{\mathcal{D}}(t))\end{aligned}\quad (23)$$

As stated in Remark 4.2, these bounds are not longer defined by iterative expressions as in Equation (18). They satisfy the following relations:

$$\underline{\alpha}_j(t) \leq \underline{\beta}_j(t), \bar{\alpha}_j(t) \geq \bar{\beta}_j(t)\quad (24)$$

which is compatible with the use of Lemma 4.1, as already mentioned. In the next section, the selection of the coefficients in $\kappa(t)$ which were introduced in Section 4.2 is discussed. This selection is critical to avoid saturation bounds overlap.

4.4 Saturation bounds overlap avoidance

Let us use the differentiable expressions of Equation (23) with $j = k$ in place of $\underline{\alpha}_k(t)$ and $\bar{\alpha}_k(t)$ in Equation (21). This is then possible to ensure that $\alpha^{(k)}(t) \in [\underline{\beta}^k(t), \bar{\beta}^k(t)]$, $\forall t$, so that, after using Lemma 4.1 and Remark 4.2, the time-domain requirement is

fulfilled:

$$\begin{aligned}\underline{u}(t) &= \frac{1}{\mathbf{C}_\alpha \mathbf{A}^{k-1} \mathbf{B}_u} \left[\underline{\beta}_k(t) - \mathbf{C}_\alpha \mathbf{A}^k \mathbf{x}(t) + |\mathbf{D}_\alpha| \max(|\underline{\mathbf{e}}^{(k)}(t)|, |\bar{\mathbf{e}}^{(k)}(t)|) \right. \\ &\quad \left. + \sum_{j=1}^k |\mathbf{C}_\alpha \mathbf{A}^{j-1} \mathbf{B}_d| \max(|\underline{\mathbf{d}}^{(k-j)}(t)|, |\bar{\mathbf{d}}^{(k-j)}(t)|) \right] \\ \bar{u}(t) &= \frac{1}{\mathbf{C}_\alpha \mathbf{A}^{k-1} \mathbf{B}_u} \left[\bar{\beta}_k(t) - \mathbf{C}_\alpha \mathbf{A}^k \mathbf{x}(t) - |\mathbf{D}_\alpha| \max(|\underline{\mathbf{e}}^{(k)}(t)|, |\bar{\mathbf{e}}^{(k)}(t)|) \right. \\ &\quad \left. - \sum_{j=1}^k |\mathbf{C}_\alpha \mathbf{A}^{j-1} \mathbf{B}_d| \max(|\underline{\mathbf{d}}^{(k-j)}(t)|, |\bar{\mathbf{d}}^{(k-j)}(t)|) \right]\end{aligned}\quad (25)$$

The obtained saturations depend on the design parameters $\kappa(t)$ from Equation (17), $\underline{\mathcal{A}}(t)$ and $\bar{\mathcal{A}}(t)$ and on the signals describing the limited knowledge of the disturbances: $\underline{\mathcal{D}}(t)$, $\bar{\mathcal{D}}(t)$, $\underline{\mathcal{E}}(t)$ and $\bar{\mathcal{E}}(t)$. Some further analysis is, however, required. As highlighted in the case study of Section 2.2, it is particularly important to detect possible saturation bounds overlap.

To study the possible saturation bounds overlap, the successive differences $\bar{\beta}_j(t) - \underline{\beta}_j(t)$ are considered up to $j = k - 1$. For $j = k$, one also has to consider the additional terms in $\bar{u}(t) - \underline{u}(t)$ (see Equation (25)). Let us define $\Delta_0(t) := \bar{\alpha}(t) - \underline{\alpha}(t)$ and, $\forall 1 \leq j \leq k$, $\Delta_j(t) := \bar{\beta}_j(t) - \underline{\beta}_j(t)$. Thus,

$$\begin{aligned}\Delta_j(t) &= \mathbf{U}^j(t) \{ \bar{\mathcal{A}}(t) - \underline{\mathcal{A}}(t) \} \\ &\quad - 2 f_{\text{abs}}(\mathbf{U}^j(t)) g(\underline{\mathcal{E}}(t), \bar{\mathcal{E}}(t)) |\mathbf{D}_\alpha^\top| \\ &\quad - 2 f_{\text{abs}}(\mathbf{V}^j(t)) g(\underline{\mathcal{D}}(t), \bar{\mathcal{D}}(t)) \\ &\quad - 2 |\mathbf{D}_\alpha| g(\underline{\mathbf{e}}^{(j)}, \bar{\mathbf{e}}^{(j)})\end{aligned}\quad (26)$$

Considering the iterative definitions in Equation (50), the difference in Equation (26) can be factorised by $\kappa_j(t)$. The expression is straightforward to obtain and can be written in the following form:

$$\Delta_j(t) = \kappa_j(t) \lambda_j^d(t) + \lambda_j^n(t)\quad (27)$$

where $\lambda_j^d(t)$ and $\lambda_j^n(t)$ only depend on the coefficients $\kappa_l(t)$ with $1 \leq l < j$. Using Equation (27), it seems possible to force $\Delta_j(t) \geq 0$, $\forall t$ by appropriately defining the coefficient $\kappa_j(t)$. The following lemma recalls the conditions under which saturation bounds overlap is avoided:

Lemma 4.2: Saturation bounds overlap is avoided if both conditions

- $\forall j$ s.t. $0 \leq j < k$, $\Delta_j(t) \geq 0$, $\forall t$;
- and, $\Delta_k(t) \geq 2 |\mathbf{D}_\alpha| \max(|\underline{\mathbf{e}}^{(k)}|, |\bar{\mathbf{e}}^{(k)}|) + 2 \sum_{j=1}^k |\mathbf{C}_\alpha \mathbf{A}^{j-1} \mathbf{B}_d| \max(|\underline{\mathbf{d}}^{(k-j)}|, |\bar{\mathbf{d}}^{(k-j)}|)$, $\forall t$.

are satisfied.

The last condition ensures that $\bar{u}(t) - \underline{u}(t) \geq 0$, $\forall t$ after considering Equation (25). A constructive definition of the coefficients $\kappa_j(t)$ in Equation (17) can be used to fulfil Lemma 4.2:

Theorem 4.1: *Supposing that $\bar{\alpha}(t) \geq \underline{\alpha}(t)$ (see Problem 3.1) and $\lambda_1^d(t) \neq 0$, $\forall t$, saturation bounds overlap is avoided by selecting the time-varying coefficients $\kappa(t)$ as follows:*

$$\begin{aligned} \forall 1 \leq j < k, \quad \kappa_j(t) &= \frac{\check{\kappa}_j - \lambda_j^n(t)}{\lambda_j^d(t)}, \quad \forall t \\ \text{and } \kappa_k(t) &= \frac{1}{\lambda_k^d(t)} \left[\check{\kappa}_k - \lambda_k^n(t) + 2|\mathbf{D}_\alpha| \max(|\underline{\mathbf{e}}^{(k)}|, |\overline{\mathbf{e}}^{(k)}|) \right. \\ &\quad \left. + 2 \sum_{j=1}^k |\mathbf{C}_\alpha \mathbf{A}^{j-1} \mathbf{B}_d| \max(|\underline{\mathbf{d}}^{(k-j)}|, |\overline{\mathbf{d}}^{(k-j)}|) \right], \quad \forall t \end{aligned} \quad (28)$$

with $\check{\kappa}_j > 0$ such that $\kappa_1(t) > \frac{1}{2}$, $\forall j > 1$, $\kappa_j(t) > 1$ and $\lambda_{j+1}^d(t) \neq 0$, and $\check{\kappa}_k > 0$ such that $\kappa_k(t) > \frac{1}{2}$.

Proof: Straightforward using Lemma 4.2 and Equation (27). As far as the minimal values for the $\kappa_j(t)$ are concerned, this is discussed in the proof of Proposition 5.2 in Appendix 3. ■

Remark 4.5: Note that $\kappa_k(t)$ is not differentiable with respect to t by definition but this is not required contrary to the other coefficients.

By the end of this section, a vector of design parameters $\check{\kappa} = [\check{\kappa}_1 \ \dots \ \check{\kappa}_k]$ is obtained, ensuring the absence of saturation bounds overlap and the differentiability of $\kappa(t)$ (to the exception of $\kappa_k(t)$). The stability of the system in closed loop with the saturated nominal controller is studied in the next section.

5. Guaranteed closed-loop stability using OIST-LTI

Due to the introduction of saturations, the controller state may diverge upon saturation of the control. This is the well-known ‘windup’ effect. Hence, even if a solution to Problem 3.1 was provided in Section 4, there is actually no guarantee that the closed-loop system state won’t diverge, as required in Problem 3.2.

In this section, a solution to Problem 3.2 is provided. The stability of the system in closed loop with the saturated control signal $\text{sat}_{\underline{u}(t)}^{\bar{u}(t)}(\mathbf{C}_K \mathbf{x}_K(t) + \mathbf{D}_K \mathbf{y}(t))$ (where $\underline{u}(t)$ and $\bar{u}(t)$ have been obtained using the approach presented in Section 4) is enforced using an anti-windup approach. However, to be able to state stability analysis results, some analysis of the OIST saturations is required. This is performed in the next section.

5.1 OIST saturations analysis

To ease the stability analysis of the saturated closed loop, a transformation of the OIST saturations is proposed here. Also, under the assumptions stated in Section 3.1, it is shown that these saturations converge towards constant values. This allows to state asymptotic stability results.

5.1.1 Reformulation as state-independent saturations

It is interesting to note that only one term depends on the state vector $\mathbf{x}(t)$ in the expressions of the control input saturations obtained using the definitions of $\underline{\gamma}_k$ and $\bar{\gamma}_k$ in Equation (23). Let us define

$$\forall t, \mathbf{K}_{\text{oist}}(t) := \frac{\mathbf{U}^k(t) \Theta}{\mathbf{C}_\alpha \mathbf{A}^{k-1} \mathbf{B}_u} \in \mathbb{R}^{1 \times n} \quad (29)$$

It is observed that introducing saturations on the control input u is equivalent to saturating the signal v defined as

$$\begin{aligned} v(t) &:= u(t) + \mathbf{K}_{\text{oist}}(t) \mathbf{y}(t) = u(t) \\ &\quad + \mathbf{K}_{\text{oist}}(t) \mathbf{x}(t) + \mathbf{K}_{\text{oist}}(t) \mathbf{D}_e \mathbf{e}(t), \quad \forall t \end{aligned} \quad (30)$$

by the following state-free saturations:

$$\begin{aligned} \underline{v}(t) &= \underline{u}(t) + \mathbf{K}_{\text{oist}}(t) \mathbf{x}(t) + |\mathbf{K}_{\text{oist}}(t) \mathbf{D}_e| \max(|\underline{\mathbf{e}}(t)|, |\bar{\mathbf{e}}(t)|) \\ \bar{v}(t) &= \bar{u}(t) + \mathbf{K}_{\text{oist}}(t) \mathbf{x}(t) - |\mathbf{K}_{\text{oist}}(t) \mathbf{D}_e| \max(|\underline{\mathbf{e}}(t)|, |\bar{\mathbf{e}}(t)|) \end{aligned} \quad (31)$$

Remark 5.1: Positivity of $\bar{v}(t) - \underline{v}(t)$, $\forall t$, is ensured using similar considerations than in Theorem 4.1.

Using v instead of u as the new input to system (G) in Equation (1), the saturated system becomes

$$\begin{aligned} \dot{\mathbf{x}}(t) &= [\mathbf{A} - \mathbf{B}_u \mathbf{K}_{\text{oist}}(t)] \mathbf{x}(t) + \mathbf{B}_u \text{sat}_{\underline{v}(t)}^{\bar{v}(t)}(v(t)) \\ &\quad - \mathbf{B}_u \mathbf{K}_{\text{oist}}(t) \mathbf{D}_e \mathbf{e}(t) + \mathbf{B}_d \mathbf{d}(t) \end{aligned} \quad (32)$$

5.1.2 Admissible asymptotic equilibrium

Using Equation (25) and the definitions of the state-free saturations in Equation (31), the saturations on the new input v can be obtained. Using Assumption 3.1, there is also

$$\lim_{t \rightarrow \infty} \underline{\mathcal{A}}(t) = [\underline{\alpha}^* \ 0 \ \dots \ 0]^\top, \quad \lim_{t \rightarrow \infty} \bar{\mathcal{A}}(t) = [\bar{\alpha}^* \ 0 \ \dots \ 0] \quad (33)$$

Considering Theorem 4.1 along with Assumption 3.4, it can be observed that the design signal $\kappa(t)$ in Equation (17) converges towards a constant value. Thus, this is also the case of vectors $\mathbf{U}^j(t)$ and $\mathbf{V}^j(t)$, $\forall j$, s.t. $1 \leq j \leq k$, and $\lim_{t \rightarrow \infty} \mathbf{K}_{\text{oist}}(t) = \mathbf{K}_{\text{oist}}^*$. Consequently, as far as the saturations in Equation (31) are concerned and using Assumption 3.3, they tend towards finite values and the

unsaturated control becomes

$$v^* = \mathbf{C}_K \mathbf{x}_K^* + (\mathbf{D}_K + \mathbf{K}_{\text{oist}}^*) (\mathbf{x}^* + \mathbf{D}_e \mathbf{e}^*) = 0 \quad (34)$$

In the following proposition, it is shown that the origin is an admissible equilibrium under some condition. This condition can be evaluated during the analysis phase of the unconstrained closed-loop system.

Proposition 5.1: *Let $\mathbf{x}^* \in \mathbb{R}^n$ and suppose Assumptions 3.1–3.4 are satisfied. In the non-restrictive case where $\mathbf{x}^* = 0$, this is an admissible asymptotic equilibrium, if*

$$v^* = 0 \in [\underline{v}^*, \bar{v}^*] \quad (35)$$

or, more precisely, if

$$\frac{u_0^{k,*} \underline{\alpha}^*}{\mathbf{C}_\alpha \mathbf{A}^{k-1} \mathbf{B}_u} \leq 0 \leq \frac{u_0^{k,*} \bar{\alpha}^*}{\mathbf{C}_\alpha \mathbf{A}^{k-1} \mathbf{B}_u} \quad (36)$$

5.2 Closed-loop representation

As mentioned in Section 5.1.1, the control signal saturations depend on the system state $x(t)$. Changing the control signal into $v(t) = u(t) + \mathbf{K}_{\text{oist}}(t)y(t)$, the system studied in this section is equivalent to the system in Equation (37) where the saturations on $v(t)$ do not depend on the state vector anymore:

$$(G) \begin{cases} \dot{\mathbf{x}}(t) = [\mathbf{A} - \mathbf{B}_u \mathbf{K}_{\text{oist}}(t)] \mathbf{x}(t) + \mathbf{B}_u \text{sat}_{\underline{v}(t)}^{\bar{v}(t)}(v(t)) \\ \quad - \mathbf{B}_u \mathbf{K}_{\text{oist}}(t) \mathbf{D}_e \mathbf{e}(t) + \mathbf{B}_d \mathbf{d}(t) \\ \mathbf{y}(t) = \mathbf{x}(t) + \mathbf{D}_e \mathbf{e}(t) \\ \dot{\mathbf{x}}_K(t) = \mathbf{A}_K \mathbf{x}_K(t) + \mathbf{B}_K \mathbf{y}(t) \\ v(t) = \mathbf{C}_K \mathbf{x}_K(t) + (\mathbf{D}_K + \mathbf{K}_{\text{oist}}(t)) \mathbf{y}(t) \\ \alpha(t) = \mathbf{C}_\alpha \mathbf{x}(t) + \mathbf{D}_\alpha \mathbf{e}(t) \end{cases} \quad (37)$$

The following lemma will be used to demonstrate the final theorem of this paper:

Lemma 5.1: $\forall \mathbf{x}(t) \in \mathbb{R}^n, \forall t$, the function $-\mathbf{K}_{\text{oist}}(t)\mathbf{x}(t)$ is Lipschitz (with respect to \mathbf{x}). Moreover, $-\mathbf{K}_{\text{oist}}(t)\mathbf{x}(t)$ is K_1 -Lipschitz, where $K_1 = \max_t \|\mathbf{K}_{\text{oist}}(t)\| \in \mathbb{R}$.

Proof: Let us define, $\forall \mathbf{x} \in \mathbb{R}^n, \forall t, f(\mathbf{x}, t) = -\mathbf{K}_{\text{oist}}(t)\mathbf{x}(t)$. Then, $\forall \mathbf{x} \in \mathbb{R}^n, \frac{\partial f}{\partial \mathbf{x}}(\mathbf{x}, t) = -\mathbf{K}_{\text{oist}}(t)$. Since $\mathbf{K}_{\text{oist}}(t)$ is continuous $\forall t$ by definition of the coefficients $\kappa(t)$ and continuity of $[\underline{\mathcal{D}}(t), \overline{\mathcal{D}}(t), \underline{\mathcal{E}}(t), \overline{\mathcal{E}}(t)]$ (see Assumption 3.3), the function f is continuously differentiable with respect to the state \mathbf{x} . This implies that $\mathbf{K}_{\text{oist}}(t)\mathbf{x}(t)$ is a Lipschitz continuous function with respect to \mathbf{x} . ■

5.3 Guaranteeing the closed-loop stability with an anti-windup approach

Due to the presence of a dynamic controller and saturations, unexpected closed-loop behaviour is expected. Anti-windup techniques have been widely studied and used to avoid behaviours like controller state divergence. Some of these techniques are presented in Grimm et al. (2003), Kapoor, Teel, and Daoutidis (1998) and Tarbouriech and Turner (2009). The approach proposed in Menon, Herrmann, Turner, Bates, and Postlethwaite (2006) and Herrmann, Menon, Turner, Bates, and Postlethwaite (2010) deals with a specific class of nonlinear systems to which the system presented in Equation (37) belongs. In this article, the anti-windup framework is used to enforce the closed-loop stability of the system in Equation (37) where the time-varying gain $\mathbf{K}_{\text{oist}}(t)$ and saturations are, respectively, given by Equations (29) and (31). This provides an answer to Problem 3.2.

Proposition 5.2: *The open-loop system*

$$\dot{\mathbf{x}}(t) = [\mathbf{A} - \mathbf{B}_u \mathbf{K}_{\text{oist}}(t)] \mathbf{x}(t) \quad (38)$$

is GES.

The proof is inspired by Herrmann et al. (2010).

Proof: See Appendix 3. ■

To ensure asymptotic stability of the saturated closed loop, it is necessary to use an anti-windup. Considering the system in Equation (37), the following anti-windup with state $\mathbf{x}_a \in \mathbb{R}^n$ is introduced:

$$(G_a) \begin{cases} \dot{\mathbf{x}}_a(t) = \mathbf{A} \mathbf{x}_a(t) + \mathbf{B}_u u_a(t) \\ \mathbf{y}_a(t) = \mathbf{x}_a(t) \\ u_a(t) = -\mathbf{K}_{\text{oist}}(t) \mathbf{y}_a(t) - \mathbf{D} \mathbf{Z}_{\underline{v}(t)}^{\bar{v}(t)}(v(t)) \\ v_1(t) = -[K(s) + \mathbf{K}_{\text{oist}}(t)] \mathbf{y}_a(t) \end{cases} \quad (39)$$

The control v is then modified into

$$\begin{aligned} v(t) &= u(t) + \mathbf{K}_{\text{oist}}(t) \mathbf{y}(t) + v_1(t) \\ &= \mathbf{C}_K \mathbf{x}_K(t) + \mathbf{D}_K (\mathbf{y}(t) - \mathbf{y}_a(t)) \\ &\quad + \mathbf{K}_{\text{oist}}(t) (\mathbf{y}(t) - \mathbf{y}_a(t)) \end{aligned} \quad (40)$$

The main result of this section is the following theorem which proves the stability of the origin of the system in closed loop with the saturated nominal controller. Both this theorem and its proof are inspired by Menon et al. (2006) and Herrmann et al. (2010).

Theorem 5.1: *If Assumptions 3.1–3.7 are satisfied (resulting in Theorem 4.1 and Proposition 5.2), the origin of the closed-loop system consisting of the system in Equation (32) – where the time-varying saturations are given*

in Equation (31) – the control law in Equation (40) and the anti-windup compensator given in Equation (39) is GAS.

Proof: See Appendix 4. ■

An illustration of the system in closed loop with the anti-windup and saturating block is given in Figure 8. This is the typical structure obtained when implementing OIST on a linear system.

6. Example: back to the case study

The ball and beam example which served as a case study in Section 2.2 is considered again for the application of the method which was presented in Section 4.

Remark 6.1: In this example, there is no disturbance on the measurements. The theory presented in Section 5 would, however, be applicable, for example, in the case where $\alpha = \mathbf{C}_\alpha \mathbf{x} + e$ with e , an unknown but bounded disturbance.

6.1 Assumptions

In this section, the assumptions in Section 3.1 are reviewed in the case of the ball and beam example introduced in Section 2.2.

- As far as the relative degrees are concerned, $k = 2$ and $l = 2$ which fulfils Assumptions 3.2 and 3.7.
- The disturbance and its bounds are represented on Figure 6. They fulfil Assumption 3.3.

- Assumption 3.4 is satisfied.
- The state-feedback controller with integral action proposed in Equation (9) asymptotically stabilises the ball and beam system. Hence, Assumption 3.5 is satisfied.
- The system is equivalent to a double integrator with no transmission zero: $T_{u \rightarrow \alpha}(s) = -\frac{0.21}{s^2}$. Assumption 3.6 is fulfilled.

Remark 6.2: Note that the set point $r_s = 0.6$ m (and $\dot{r}_s = 0$ m/s) is not the origin of the system (it is still a feasible equilibrium). However, using some transformation equivalent to a translation, one can obtain a set point on the origin of the system. Hence Theorem 5.1 and its proof are still valid.

6.2 OIST-LTI implementation, with no saturation bounds overlap

Using results in Section 4 and considering $\underline{\alpha} = 0.1$ m, $\bar{\alpha} = 0.9$ m, the following expressions are obtained for the successive $\Delta_i(t)$:

$$\forall t, \begin{cases} \Delta_0(t) = 0.8 \\ \Delta_1(t) = \kappa_1(t) \lambda_1^d(t) + \lambda_1^n(t) \\ \Delta_2(t) = \kappa_2(t) \lambda_2^d(t) + \lambda_2^n(t) \end{cases} \quad (41)$$

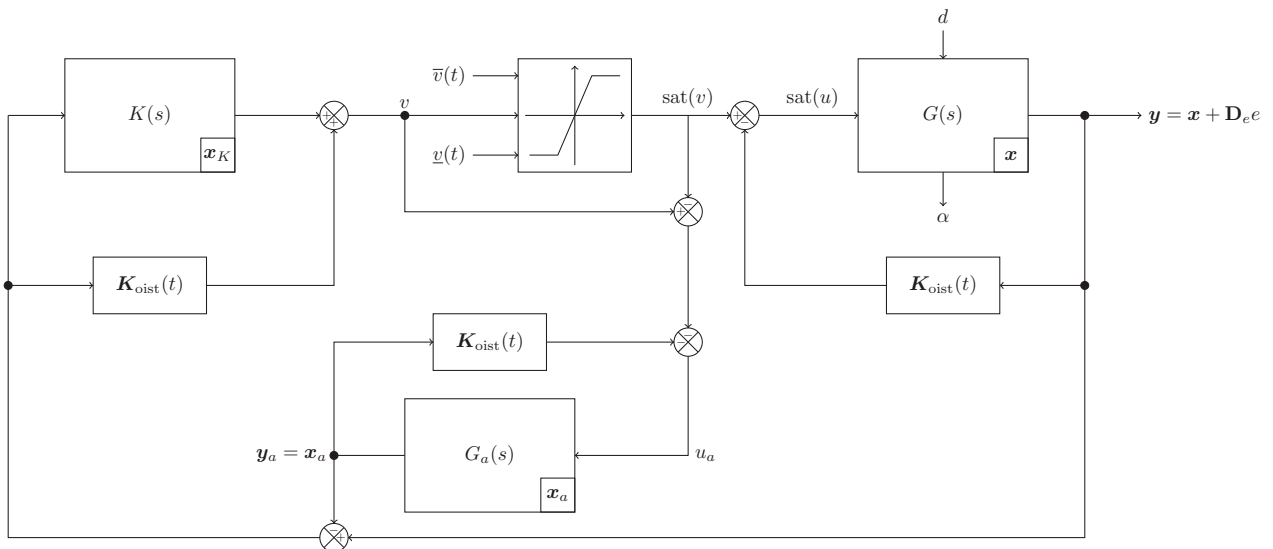


Figure 8. Closed-loop illustration.

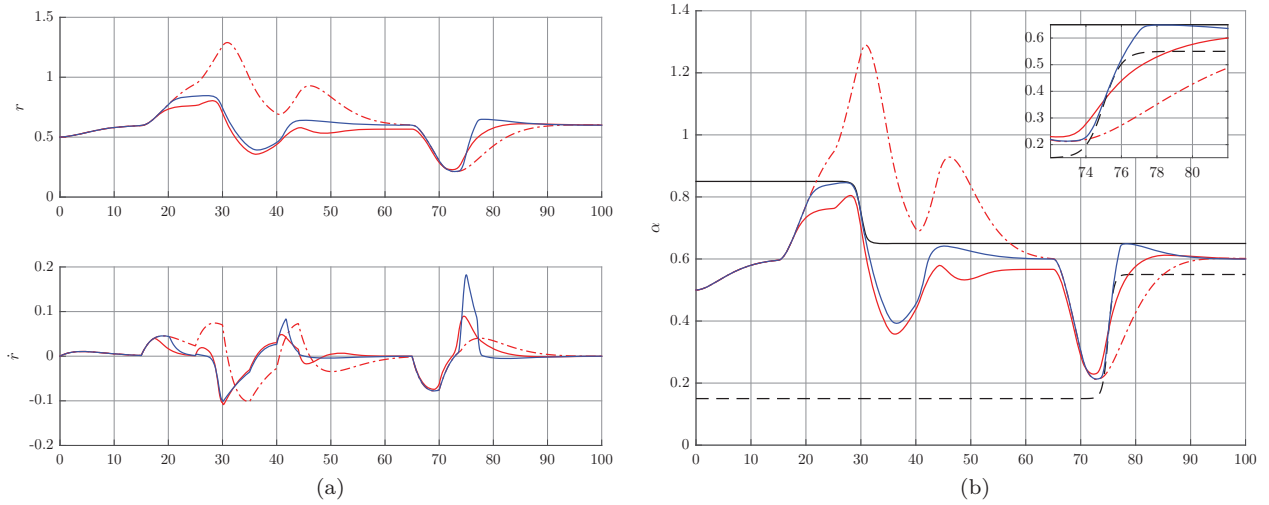


Figure 9. (Colour online) System state and constrained output variable $\alpha = r$ simulation results. (a) System state using time-varying coefficients (in blue), using constant coefficients (plain red), or, without using OIST (dashed-dotted red). (b) Constrained output simulation using time-varying coefficients (in blue), using constant coefficients (plain red), or, without using OIST (dashed-dotted red). A zoom is performed for $72 \leq t \leq 82$ s. In the time-varying coefficients case, the requirement is guaranteed.

where

$$\begin{aligned} \lambda_1^d(t) &= \bar{\alpha}(t) - \underline{\alpha}(t) \\ \lambda_1^n(t) &= \dot{\bar{\alpha}} - \dot{\underline{\alpha}} \\ \lambda_2^d(t) &= [\kappa_1(t) \ 1 \ 0] \{ \bar{\mathcal{A}}(t) - \underline{\mathcal{A}}(t) \} \\ \lambda_2^n(t) &= [\dot{\kappa}_1(t) \ \kappa_1(t) \ 1] \{ \bar{\mathcal{A}}(t) - \underline{\mathcal{A}}(t) \} \end{aligned} \quad (42)$$

Then, the values of the design signals $\kappa_i(t)$ are deduced from these expressions and Theorem 4.1:

$$\begin{aligned} \kappa_1(t) &= \frac{\check{\kappa}_1 - \lambda_1^n(t)}{\lambda_1^d(t)} \\ \kappa_2(t) &= \frac{\check{\kappa}_2 - \lambda_2^n(t) + 2|\mathbf{C}_\alpha \mathbf{A} \mathbf{B}_d| \max(|\underline{d}(t)|, |\bar{d}(t)|)}{\lambda_2^d(t)} \end{aligned} \quad (43)$$

where $\check{\kappa} = [\check{\kappa}_1 \ \check{\kappa}_2] = [0.5 \ 5]$ are chosen so that the conditions in Theorem 4.1 are satisfied. It is then possible to obtain saturations on the control signal. Note that $\mathbf{C}_\alpha \mathbf{A} \mathbf{B}_u = -0.21 < 0$ in this example, so the operator in Equation (4) is used to obtain the adequate saturations.

6.3 Guaranteed closed-loop stability

In this example, the controller is stable and using an anti-windup is not necessary. For illustrative purposes and to illustrate the action of such structure, an anti-windup is, however, designed following the results in Section 5.

The time-varying coefficient $\mathbf{K}_{\text{oist}}(t)$ is defined as follows:

$$\mathbf{K}_{\text{oist}}(t) = \frac{\mathbf{U}^2(t) \Theta}{\mathbf{C}_\alpha \mathbf{A} \mathbf{B}_u} \quad (44)$$

where $\mathbf{U}^2(t) = [\kappa_2(t) \kappa_1(t) + \dot{\kappa}_1(t) \ \kappa_1(t) + \kappa_2(t) \ 1]$ and $\Theta = [\mathbf{C}_\alpha \ \mathbf{C}_\alpha \mathbf{A} \ \mathbf{C}_\alpha \mathbf{A}^2]^\top$. The simulation results w/ or w/o an anti-windup structure in the loop are compared in Section 6.4.2.

6.4 Simulations and results

Using the results in Section 6.2, simulations are performed over 100 s. The disturbance signal used in simulation is shown in Figure 6.

6.4.1 Simulation results w/o anti-windup structure

The simulation results are represented on Figures 9 and 10. The data are represented in dashed-dotted red when considering the nominal control law only (no saturations), in plain red when considering OIST with constant coefficients (see the case study in Section 2.2) and in plain blue when the saturations obtained using OIST are introduced in the closed loop and the OIST coefficients are chosen time varying as in Theorem 4.1 or Equation (43). As mentioned in Section 2.2, the synthesised controller is not efficient enough and the ball falls off the beam. Using OIST and the knowledge on the

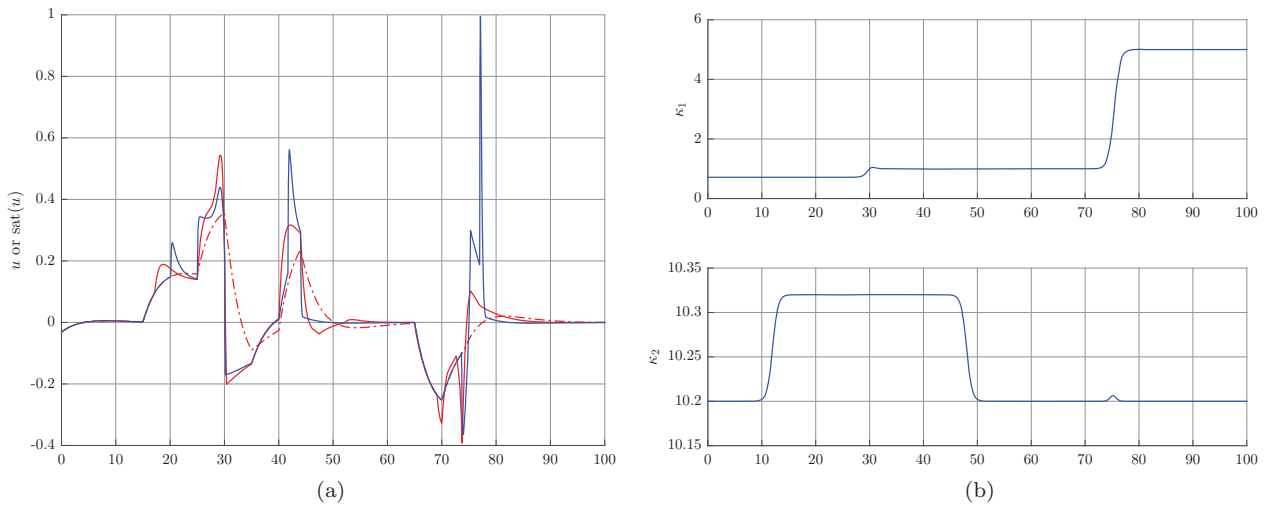


Figure 10. (Colour online) Control signal and OIST design parameters $\kappa(t)$ simulation results. (a) Control signal obtained using time-varying coefficients (in blue), using constant coefficients (plain red), or, without using OIST (dashed–dotted red). (b) OIST-LTI design parameters $\kappa(t)$ obtained (time-varying case only) through the application of Theorem 4.1.

disturbances bounds, the time-domain constraint is satisfied and nominal performance is recovered whenever the constraint is not violated. Note that the proposed approach leads to some conservatism due to the lack of knowledge on d , especially around $t = 45$ s. Also, some conservatism could be introduced by using differentiable upper approximates of the absolute value and maximum functions.

Contrary to the constant coefficients case, it can be noted on Figure 9(b) that the use of time-varying

coefficients as defined in Theorem 4.1 offers guarantees on the time-domain requirement satisfaction at all times. This results from the saturation bounds not overlapping in this case, whatever the choice of $\check{\kappa}$.

It appears in Figure 10(a) that the control law variations are much sharper in the saturated cases. This is a trade-off required for complying with the time-domain requirement. Optimisation of the constants $\check{\kappa}$ may help to obtain less demanding although satisfying control laws. This is considered future works.

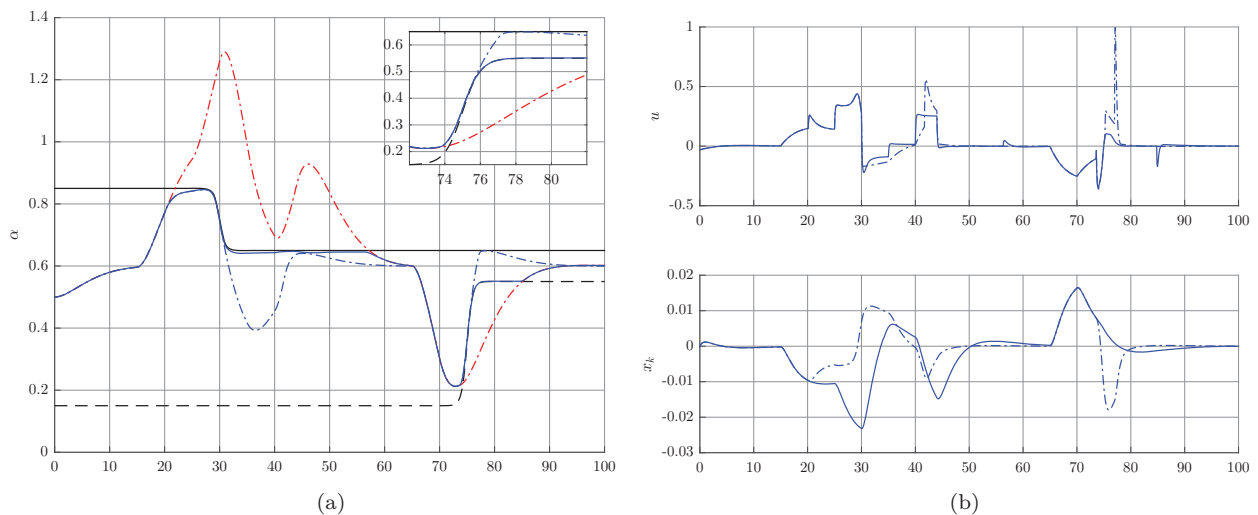


Figure 11. (Colour online) Comparison of the simulation results obtained w/ (plain blue) or w/o (dashed–dotted blue) an anti-windup. (a) Comparison of the constrained output simulation results. (b) Comparison of the control signal u and controller state x_k .

6.4.2 Comparison of simulation results w/ or w/o an anti-windup structure

In the previous section, satisfying results were obtained without using an anti-windup structure in the feedback loop. The influence of such structure is illustrated in Figure 11. The simulation results obtained with (resp. without) the anti-windup in the feedback loop are represented in plain (resp. dashed-dotted) blue. It appears that the use of an anti-windup allows the control law to stay longer on the saturations. This results in the constrained variable sticking to the time-domain requirement limits. In an informal way, this means that the nominal performance is less degraded since the control law tries to copy the original control as much as possible.

6.5 Conclusions on the simulation results

The results obtained in simulation are highly satisfactory. Using time-varying design parameters in the OIST approach as proposed in Theorem 4.1, a time-domain requirement on a given constrained output can be fulfilled *with guarantees*. Moreover, the closed-loop stability is ensured as demonstrated in Section 5. In practice, using an anti-windup structure is not mandatory. However, it has been observed on the illustrating example that the constrained variable sticks to the requirement bounds to copy the original system response as much as possible when using such structure.

7. Conclusion

In this article, the problem of keeping a linear system output in an interval has been formalised. A solution based on a transformation from the output expected 'saturation' to a saturation on the existing linear control input has been proposed. A constructive method to apply this transformation has been introduced. Time-varying saturations are obtained and used in closed loop. Special attention has been paid to choose the time-varying design parameters $\kappa_i(t)$ in Equation (17) in order to avoid saturation bounds overlap. Also, using results from the anti-windup design community, the stability of the system in closed loop with the resulting nonlinear control has been guaranteed under the considered assumptions. An application to a linear ball and beam model has been proposed, showing satisfactory results and illustrating the influence of the anti-windup structure.

However, throughout this article, the specific class of minimum-phase linear systems has been considered. Also, it has been supposed that the whole state is measured. Future works will be dedicated to extend the approach to non-minimum-phase systems and to systems with output feedback. Some hints on the last aspect

were already drawn in Chambon, Burlion, and Apkarian (2015b). Optimisation of the coefficients $\check{\kappa}$ will also be considered.

Notes

1. Output-to-input saturation transformation for LTI systems.
2. For more details on how this notion is used in the following, the reader should refer to Definition 2.1.
3. In the non-pathological case where \mathbf{d} is a physical signal converging to zero under Assumption 3.4.
4. And excluding the pathological case where \mathbf{d} is a non-converging finite energy distribution, which is not a realistic physical case.

Disclosure statement

No potential conflict of interest was reported by the authors.

Funding

This work was funded by Onera.

References

- Apkarian, P., Ravanbod-Hosseini, L., & Noll, D. (2011). Time domain constrained H_∞ -synthesis. *International Journal of Robust and Nonlinear Control*, 21(2), 197–217.
- Burlion, L. (B. Morcego, F. Nejari, R. Pérez, J. Quevedo, R. Sarrate, & S. Tornil (2012). A new Saturation function to convert an output constraint into an input constraint (Eds), *20th Mediterranean Conference on Control and Automation* (pp. 1218–1222). Barcelona.
- Burlion, L., & de Plinval, H. (2013). Keeping a ground point in the camera field of view of a landing UAV. In *Proceedings of the IEEE International Conference on Robotics and Automation* (pp. 5763–5768). Karlsruhe.
- Burlion, L., Poussot-Vassal, C., Vuillemin, P., Leitner, M., & Kier, T. (2014). Longitudinal manoeuvre load control of a flexible large-scale aircraft. In *Proceedings of the 19th IFAC World Congress* (pp. 3413–3418). Cape Town.
- Chambon, E., Burlion, L., & Apkarian, P. (2015a). Output to input saturation transformation: Demonstration and application to disturbed linear systems. In *Proceedings of the 54th IEEE Conference on Decision and Control* (pp. 7566–7571). Osaka.
- Chambon, E., Burlion, L., & Apkarian, P. (2015b). Robust output interval constraint using O/I saturation transformation with application to uncertain linear launch vehicle. In *Proceedings of the 14th European Control Conference* (pp. 1796–1801). Linz.
- Chen, H., & Allgöwer, F. (1996). A quasi-infinite horizon predictive control scheme for constrained nonlinear systems. In *Proceedings of the 16th Chinese Control Conference* (pp. 309–316). Qindao.
- Chen, H., & Allgöwer, F. (1999). Nonlinear model predictive control schemes with guaranteed stability. In R. Berber C. Kravaris (Eds.), *Nonlinear model based process control* (pp. 465–494). Dordrecht: Kluwer Academic.

- Galeani, S., Tarbouriech, S., Turner, M., & Zaccarian, L. (2009). A tutorial on modern anti-windup design. *European Journal of Control*, 15(3-4), 418–440.
- Gevers, M. (2002). A decade of progress in iterative process control design: from theory to practice. *Journal of Process Control*, 12, 519–531.
- Ghaemi, R., Sun, J., & Kolmanovsky, I. (2012). Robust control of constrained linear systems with bounded disturbances. *IEEE Transactions on Automatic Control*, 57(10), 2683–2688.
- Gilbert, E., & Kolmanovsky, I. (2002). Nonlinear tracking control in the presence of state and control constraints: A generalized reference governor. *Automatica*, 38(12), 2063–2073.
- Goodwin, G.C., Seron, M.M., & de Doná, J.A. (2005). *Constrained control and estimation*. London: Springer-Verlag.
- Grimm, G., Hatfield, J., Postlethwaite, I., Teel, A.R., Turner, M.C., & Zaccarian, L. (2003). Antiwindup for stable linear systems with input saturation: An LMI-based synthesis. *IEEE Transactions on Automatic Control*, 48(9), 1509–1525.
- Herrmann, G., Menon, P.P., Turner, M.C., Bates, D.G., & Postlethwaite, I. (2010). Anti-windup synthesis for nonlinear dynamic inversion control schemes. *International Journal of Robust and Nonlinear Control*, 1465–1482.
- Hu, X., Lindquist, A., Mari, J., & Sand, J. (2012). *Geometric control theory* [Lecture notes]. Sweden: KTH, Royal Institute of Technology.
- Isidori, A. (1999). *Nonlinear control systems II*. London: Springer.
- Kapoor, N., & Daoutidis, P. (1999). An observer-based anti-windup scheme for non-linear systems with input constraints. *International Journal of Control*, 72(1), 18–29.
- Kapoor, N., Teel, A.R., & Daoutidis, P. (1998). An anti-windup design for linear systems with input saturation. *Automatica*, 34(5), 559–574.
- Khalil, H.K. (1996). *Nonlinear systems*. Upper Saddle River, NJ: Prentice Hall.
- Menon, P.P., Herrmann, G., Turner, M.C., Bates, D.G., & Postlethwaite, I. (2006). General anti-windup synthesis for input constrained nonlinear systems controlled using nonlinear dynamic inversion. In *Proceedings of the 45th IEEE Conference on Decision and Control* (pp. 5435–5440). San Diego, CA.
- Mossberg, M., Gevers, M., & Lequin, O. (2002). A comparison of iterative feedback tuning and classical PID tuning schemes. In *Proceedings of the International Conference on Signal Processing, Robotics and Automation*. Cadiz.
- Polóni, T., Kalabić, U., McDonough, K., & Kolmanovsky, I. (2014). Disturbance canceling control based on simple input observers with constraint enforcement for aerospace applications. In *IEEE Conference on Control Applications* (pp. 158–165).
- Rojas, O.J., & Goodwin, G.C. (2002). A simple anti-windup strategy for state constrained linear control. In *Proceedings of the 15th IFAC World Congress*. Barcelona.
- Sontag, E.D. (1989). Remarks on stabilization and input-to-state stability. In *Proceedings of the 28th IEEE Conference on Decision and Control* (pp. 1376–1378). Tampa, FL: IEEE.
- Tarbouriech, S., & Turner, M. (2009). Anti-windup design: An overview of some recent advances and open problems. *IET Control Theory and Applications*, 3(1), 1–19.

- Terrell, W.J. (2009). *Stability and stabilization: An introduction*, Princeton, NJ: Princeton University Press.
- Turner, M.C., & Postlethwaite, I. (2002). Output violation compensation for systems with output constraints. *IEEE Transactions on Automatic Control*, 47(9), 1540–1546.

Appendix 1. Proof of Lemma 4.1

The proof is performed iteratively with fixed k . Let an integer j such that $1 \leq j \leq k$. Suppose that $\alpha^{(k)}(t) \in [\underline{\alpha}_k(t), \bar{\alpha}_k(t)] \Rightarrow \alpha^{(j)}(t) \in [\underline{\alpha}_j(t), \bar{\alpha}_j(t)]$, $\forall t$. Also, $\alpha^{(j-1)}(0) \in [\underline{\alpha}_{j-1}(0), \bar{\alpha}_{j-1}(0)]$. Only the lower bound is considered. The demonstration is similar in the upper bound case. Suppose

$$\exists t_2 > 0, \alpha^{(j-1)}(t_2) < \underline{\alpha}_{j-1}(t_2) \quad (\text{A1})$$

then, since $\alpha^{(j-1)}(0) \in [\underline{\alpha}_{j-1}(0), \bar{\alpha}_{j-1}(0)]$ and, by continuity of $\alpha^{(j-1)}$ and $\underline{\alpha}_{j-1}$,

$$\exists t_1, 0 < t_1 < t_2, \begin{cases} \alpha^{(j-1)}(t_1) = \underline{\alpha}_{j-1}(t_1) \\ \forall t \in [t_1, t_2], \alpha^{(j-1)}(t) \leq \underline{\alpha}_{j-1}(t) \end{cases} \quad (\text{A2})$$

But, using the recurrence hypothesis, the definition of $\underline{\alpha}_j(t)$ and the fact that $\forall t, \kappa_j(t) \geq 0$, one obtains, $\forall t \in [t_1, t_2]$,

$$\begin{aligned} \alpha^{(j)}(t) &\geq \underline{\alpha}_j(t) \\ &\geq \kappa_j(t) \left(\underline{\alpha}_{j-1}(t) - \alpha^{(j-1)}(t) \right) + \widehat{\underline{\alpha}}_{j-1}(t) \quad (\text{A3}) \\ &\geq \widehat{\underline{\alpha}}_{j-1}(t) \end{aligned}$$

hence, using the property of integrals,

$$\begin{aligned} \int_{t_1}^{t_2} \alpha^{(j)}(\lambda) d\lambda &\geq \int_{t_1}^{t_2} \widehat{\underline{\alpha}}_{j-1}(\lambda) d\lambda \quad (\text{A4}) \\ \alpha^{(j-1)}(t_2) - \alpha^{(j-1)}(t_1) &\geq \underline{\alpha}_{j-1}(t_2) - \underline{\alpha}_{j-1}(t_1) \end{aligned}$$

which contradicts Equation (A1). In other words,

$$\forall t > 0, \alpha^{(j-1)}(t) \geq \underline{\alpha}_{j-1}(t) \quad (\text{A5})$$

which proves the lemma.

Appendix 2. Vectors U^j and V^j iterative definitions

The vectors U^j and V^j are given by the following iterative expressions:

$$\begin{aligned}
 U^0(t) &= [1 \ 0 \ \dots \ 0] \\
 \forall j \text{ s.t. } 1 \leq j \leq k, U^j(t) &= \kappa_j(t)U^{j-1}(t) \\
 &+ \dot{U}^{j-1}(t) + \sigma(U^{j-1}(t)) \\
 \forall j \text{ s.t. } 0 \leq j \leq l, V^j(t) &= 0 \\
 \forall j \text{ s.t. } l < j \leq k, V^j(t) &= \kappa_j(t)(V^{j-1}(t) \\
 &+ C_\alpha A^{j-l-1}[A^{l-1}B_d \dots A^{2l-j}B_d]) + \dot{V}^{j-1}(t) \\
 &+ \sigma(V^{j-1}(t)) + \left[\sum_{w=0}^{j-l-1} u_{l-1+w}^{j-1}(t) C_\alpha A^{l-1+w} B_d \ 0 \ \dots \ 0 \right]
 \end{aligned} \tag{B1}$$

where $\sigma(U^{j-1})(t)$ is the cyclic permutation of length $k+1$ on the elements of $U^{j-1}(t)$:

Definition 9.1: Let $S = [s_0 \ \dots \ s_k] \in \mathbb{R}^{k+1}$. The function

$$\sigma(S) = [\sigma(s_0) \ \dots \ \sigma(s_k)] \tag{B2}$$

where

$$\sigma(s_i) := \begin{cases} s_{i-1} & \text{if } 1 \leq i \leq k \\ s_k & \text{if } i = 0 \end{cases} \tag{B3}$$

is called the cyclic permutation of length $k+1$ on the elements of S .

Proof: Tedious rewriting of Equation (22) in explicit form and using Equation (18) to express $\underline{\alpha}_{j+1}$ for $j \geq 0$ starting with $\underline{\alpha}_0(t) = \underline{\alpha}(t)$ leads to Equation (B1). The same calculus is performed as far as the upper bound is concerned. ■

Appendix 3. Proof of Proposition 5.2

Considering Equation (30) and the system in Equation (37), this problem is equivalent to studying the stability of the system $\dot{\mathbf{x}}(t) = \mathbf{A}\mathbf{x}(t) + \mathbf{B}_u u(t)$ in closed-loop with $v(t) = 0$ or $u(t) = -K_{\text{oist}}(t)\mathbf{x}(t)$ ($\mathbf{d}(t) = 0$ and $\mathbf{e}(t) = 0$). The transfer function between u and the constrained variable α is given by

$$\begin{aligned}
 \alpha &= T_{u \rightarrow \alpha}(s) \\
 &= \frac{s^m + p_1 s^{m-1} + \dots + p_{m-1} s + p_m}{s^n + d_1 s^{n-1} + \dots + d_{n-1} s + d_n} u
 \end{aligned} \tag{C1}$$

with $k = n - m$ (see Assumption 3.2). Theoretically speaking, a minimum state-space representation of this transfer can be represented in the canonical form which can in turn be expressed as a chain of integrators in addition to the considered transfer zero dynamics (see Hu, Lindquist, Mari, & Sand, 2012, Chapter 4). The chain of integrators is given by

$$\begin{cases} \dot{\alpha} = \alpha \\ \vdots \\ \dot{\alpha}^{(k-2)} = \alpha^{(k-1)} \\ \dot{\alpha}^{(k-1)} = \alpha^{(k)} \\ = -U^k(t)\Theta\mathbf{x} + C_\alpha A^k \mathbf{x} \end{cases} \tag{C2}$$

where the last equality is obtained by observing that $u = -K_{\text{oist}}(t)\mathbf{x}$ (and $\mathbf{d} = 0$, $\mathbf{e} = 0$). Let $\forall 0 \leq j \leq k-1$, $\gamma_j = \alpha^{(j)} + U^j(t)\Theta\mathbf{x} - C_\alpha A^j \mathbf{x}$ and $\Gamma = [\gamma_0 \ \dots \ \gamma_{k-1}] \in \mathbb{R}^k$. Using Equations (18) and (22) with null disturbances, the chain of integrators in Equation (C2) can be rewritten as

$$\begin{aligned}
 \dot{\Gamma} &= \begin{bmatrix} -\kappa_1 & 1 & 0 & \dots & 0 \\ 0 & \ddots & \ddots & \ddots & \vdots \\ \vdots & \ddots & \ddots & \ddots & 0 \\ 0 & \dots & 0 & -\kappa_{k-1} & 1 \\ 0 & \dots & 0 & -\kappa_k & 0 \end{bmatrix} \Gamma \\
 &= \mathbf{A}_\Gamma \Gamma
 \end{aligned} \tag{C3}$$

This is completed by the zero dynamics as shown in Hu et al. (2012, Chapter 4) which results in the open-loop transfer in Equation (C1) being equivalent to the following state-space representation:

$$\begin{bmatrix} \dot{\Gamma} \\ \dot{Z} \end{bmatrix} = \begin{bmatrix} \mathbf{A}_\Gamma & 0 \\ \mathbf{A}_{Z\Gamma} & \mathbf{A}_Z \end{bmatrix} \begin{bmatrix} \Gamma \\ Z \end{bmatrix} \tag{C4}$$

where

$$\mathbf{A}_Z = \begin{bmatrix} 0 & 1 & 0 & \dots & 0 \\ \vdots & \ddots & \ddots & \ddots & \vdots \\ \vdots & & \ddots & \ddots & 0 \\ 0 & \dots & \dots & 0 & 1 \\ -p_m & -p_{m-1} & \dots & -p_2 & -p_1 \end{bmatrix} \tag{C5}$$

and $\mathbf{A}_{Z\Gamma}$ is the null matrix except for the coefficient $\mathbf{A}_{Z\Gamma}(n-k, 1) = 1$. Considering Assumption 3.6, \mathbf{A}_Z

eigenvalues are with strictly negative real parts. As far as the dynamics of Equation (C4) is concerned, the following candidate Lyapunov positive definite function is considered:

$$V(\Gamma, Z) = \frac{1}{2}\Gamma^\top \Gamma + \frac{\epsilon}{2}Z^\top Z \quad (\text{C6})$$

where ϵ is a positive constant. Then,

$$\dot{V}(\Gamma, Z) = \Gamma^\top \mathbf{A}_\Gamma \Gamma + \epsilon Z^\top \mathbf{A}_Z Z + \epsilon Z^\top \mathbf{A}_{Z\Gamma} \Gamma \quad (\text{C7})$$

where, using the logarithmic function concavity and the fact that $\forall 1 \leq i \leq k, \gamma_{i-1}\gamma_i \leq |\gamma_{i-1}\gamma_i|$,

$$\begin{aligned} \Gamma^\top \mathbf{A}_\Gamma \Gamma &= -\sum_{i=0}^{k-1} \kappa_{i+1} \gamma_i^2 + \sum_{i=1}^{k-1} \gamma_{i-1} \gamma_i \\ &\leq -\sum_{i=0}^{k-1} \kappa_{i+1} \gamma_i^2 + \frac{1}{2} \sum_{i=1}^{k-1} \gamma_i^2 + \frac{1}{2} \sum_{i=0}^{k-2} \gamma_i^2 \\ \Gamma^\top \mathbf{A}_\Gamma \Gamma &\leq -\Gamma^\top \mathbf{D}_{V\Gamma} \Gamma \\ &\leq -\Gamma^\top \text{diag} \left(\kappa_1 - \frac{1}{2}, \kappa_2 - 1, \dots, \kappa_{k-1} - 1, \kappa_k - \frac{1}{2} \right) \Gamma \end{aligned} \quad (\text{C8})$$

so that $\mathbf{D}_{V\Gamma}$ is a positive definite diagonal matrix upon adapted selection of the positive time-varying coefficients $\kappa_i(t)$. In the same vein,

$$\epsilon Z^\top \mathbf{A}_{Z\Gamma} \Gamma \leq \frac{\epsilon \nu}{2} (\mathbf{A}_{Z\Gamma}^\top Z)^\top \mathbf{A}_{Z\Gamma}^\top Z + \frac{\epsilon}{2\nu} \Gamma^\top \Gamma \quad (\text{C9})$$

where ν is a positive constant. It comes that

$$\begin{aligned} \dot{V}(\Gamma, Z) &\leq -\Gamma^\top \mathbf{D}_{V\Gamma} \Gamma + \frac{\epsilon}{2\nu} \Gamma^\top \Gamma \\ &\quad + \epsilon \left(Z^\top \mathbf{A}_Z Z + \frac{\nu}{2} Z^\top (\mathbf{A}_{Z\Gamma} \mathbf{A}_{Z\Gamma}^\top) Z \right) \end{aligned} \quad (\text{C10})$$

Using the notations $\lambda_{\min}(\mathbf{M})$ and $\lambda_{\max}(\mathbf{M})$ to denote the minimal and maximal real parts of the eigenvalues of the matrix \mathbf{M} , it is observed that

$$\begin{aligned} Z^\top \mathbf{A}_Z Z + \frac{\nu}{2} Z^\top (\mathbf{A}_{Z\Gamma} \mathbf{A}_{Z\Gamma}^\top) Z &\leq \lambda_{\max}(\mathbf{A}_Z) Z^\top Z \\ &\quad + \frac{\nu}{2} \lambda_{\max}(\mathbf{A}_{Z\Gamma} \mathbf{A}_{Z\Gamma}^\top) Z^\top Z \end{aligned} \quad (\text{C11})$$

and

$$-\Gamma^\top \mathbf{D}_{V\Gamma} \Gamma + \frac{\epsilon}{2\nu} \Gamma^\top \Gamma \leq -\lambda_{\min}(\mathbf{D}_{V\Gamma}) \Gamma^\top \Gamma + \frac{\epsilon}{2\nu} \Gamma^\top \Gamma \quad (\text{C12})$$

By choosing $\nu = -\frac{\lambda_{\max}(\mathbf{A}_Z)}{\lambda_{\max}(\mathbf{A}_{Z\Gamma} \mathbf{A}_{Z\Gamma}^\top)} > 0$ (since $\mathbf{A}_{Z\Gamma} \mathbf{A}_{Z\Gamma}^\top$ is positive semi-definite) and $\epsilon = \nu \lambda_{\min}(\mathbf{D}_{V\Gamma}) > 0$ and by observing that the eigenvalues of \mathbf{A}_Z are with strictly

negative real parts (see Assumption 3.6) and $\mathbf{D}_{V\Gamma}$ is a positive definite matrix, one obtains

$$\begin{aligned} \dot{V}(\Gamma, Z) &\leq -\frac{1}{2} \lambda_{\min}(\mathbf{D}_{V\Gamma}) \Gamma^\top \Gamma + \frac{1}{2} \lambda_{\max}(\mathbf{A}_Z) Z^\top Z \\ &\leq -\min(\lambda_{\min}(\mathbf{D}_{V\Gamma}), -\frac{1}{\epsilon} \lambda_{\max}(\mathbf{A}_Z)) V(\Gamma, Z) \\ &\leq -k_1 V(\Gamma, Z) \end{aligned}$$

where $k_1 > 0$. Also note that $\dot{V}(0, 0) = 0$. As a consequence, the candidate function V is a Lyapunov function and the open-loop system $\dot{x} = [\mathbf{A} - \mathbf{B}_u \mathbf{K}_{\text{oist}}(t)] x$ is GES.

Appendix 4. Proof of Theorem 5.1

First, considering Proposition 5.1, the origin is a reachable equilibrium of the system in closed loop with the saturated control signal. Thus, it is of some interest to study the asymptotic stability of this equilibrium. Using Equation (3), the state equation in Equation (32) can be rewritten as

$$\begin{aligned} \dot{x}(t) &= \mathbf{A}x(t) + \mathbf{B}_u \left[-\mathbf{K}_{\text{oist}}(t)x_a(t) + \mathbf{C}_K x_K(t) \right. \\ &\quad \left. + \mathbf{D}_K (y(t) - x_a(t)) - \mathbf{D}z_{\underline{v}}^{\bar{v}(t)}(v(t)) \right] + \mathbf{B}_d d(t) \end{aligned} \quad (\text{D1})$$

Using a similar approach to Kapoor and Daoutidis (1999), let us define $e_x(t) := x(t) - x_a(t)$. It follows that

$$\begin{aligned} \dot{e}_x(t) &= (\mathbf{A} + \mathbf{B}_u \mathbf{D}_K) e_x(t) + \mathbf{B}_u \mathbf{C}_K x_K(t) \\ &\quad + \mathbf{B}_d d(t) + \mathbf{B}_u \mathbf{D}_K \mathbf{D}_e e(t) \end{aligned} \quad (\text{D2})$$

$$\dot{x}_K(t) = \mathbf{A}_K x_K(t) + \mathbf{B}_K e_x(t) + \mathbf{B}_K \mathbf{D}_e e(t)$$

Let $X = [e_x \ x_K]^\top$ and $W = [d \ e]^\top$, then

$$\begin{aligned} \dot{X} &= \begin{bmatrix} \mathbf{A} + \mathbf{B}_u \mathbf{D}_K & \mathbf{B}_u \mathbf{C}_K \\ \mathbf{B}_K & \mathbf{A}_K \end{bmatrix} X + \begin{bmatrix} \mathbf{B}_d & \mathbf{B}_u \mathbf{D}_K \mathbf{D}_e \\ 0 & \mathbf{B}_K \mathbf{D}_e \end{bmatrix} \begin{bmatrix} d \\ e \end{bmatrix} \\ &= \mathbf{A}_X X + \mathbf{B}_X W \end{aligned} \quad (\text{D3})$$

Under Assumptions 3.3 and 3.4, $\|W\|_2$ is finite and $\|W\|$ is bounded. It follows that $\|X\|_2$ is finite and $\|X\|$ converges to zero. In case $W = 0$, the state X converges exponentially to zero. Replacing v in Equation (39) by its expression in Equation (40), one obtains the following equation:

$$\begin{aligned} \dot{x}_a(t) &= [\mathbf{A} - \mathbf{B}_u \mathbf{K}_{\text{oist}}(t)] x_a(t) \\ &\quad - \mathbf{B}_u \mathbf{D}z_{\underline{v}}^{\bar{v}(t)}(\mathbf{K}_{\text{oist}}(t)e_x(t) + \mathbf{K}_{\text{oist}}(t)\mathbf{D}_e e(t) \\ &\quad + \mathbf{D}_K e_x(t) + \mathbf{D}_K \mathbf{D}_e e(t) + \mathbf{C}_K x_K(t)) \end{aligned} \quad (\text{D4})$$

Considering Proposition 5.2, the open-loop system $\dot{x}_a = [\mathbf{A} - \mathbf{B}_u \mathbf{K}_{\text{oist}}(t)] x_a(t)$ is exponentially stable. Thus,

for some positive definite function $V(\mathbf{x}_a)$, there exists by the converse Lyapunov theorem (see Khalil, 1996), constants α_i , $1 \leq i \leq 4$, such that

$$\begin{aligned} \alpha_1 \|\mathbf{x}_a\|^2 &\leq V(\mathbf{x}_a) \leq \alpha_2 \|\mathbf{x}_a\|^2 \\ \left\| \frac{\partial V(\mathbf{x}_a)}{\partial \mathbf{x}_a} \right\| &\leq \alpha_3 \|\mathbf{x}_a\| \end{aligned} \quad (\text{D5})$$

$$\frac{\partial V(\mathbf{x}_a)}{\partial \mathbf{x}_a} [\mathbf{A}\mathbf{x}_a - \mathbf{B}_u \mathbf{K}_{\text{oist}}(t) \mathbf{x}_a] \leq -\alpha_4 \|\mathbf{x}_a\|^2$$

Since, by Equation (D4),

$$\begin{aligned} \dot{V}(\mathbf{x}_a) &= \frac{\partial V(\mathbf{x}_a)}{\partial \mathbf{x}_a} [\mathbf{A}\mathbf{x}_a - \mathbf{B}_u \mathbf{K}_{\text{oist}}(t) \mathbf{x}_a] \\ &\quad - \frac{\partial V(\mathbf{x}_a)}{\partial \mathbf{x}_a} \mathbf{B}_u \text{Dz}_{\underline{v}(t)}^{\bar{v}(t)}(\mathbf{K}_{\text{oist}}(t) \mathbf{e}_x(t) \\ &\quad + \mathbf{D}_K \mathbf{e}_x(t) + \mathbf{C}_K \mathbf{x}_K(t) + (\mathbf{D}_K \\ &\quad + \mathbf{K}_{\text{oist}}(t)) \mathbf{D}_e \mathbf{e}(t)) \end{aligned} \quad (\text{D6})$$

it comes

$$\begin{aligned} \dot{V}(\mathbf{x}_a) &\leq -\alpha_4 \|\mathbf{x}_a\|^2 \\ &\quad + \alpha_3 \|\mathbf{x}_a\| \|\mathbf{B}_u\| \left\| \text{Dz}_{\underline{v}(t)}^{\bar{v}(t)}(\mathbf{K}_{\text{oist}}(t) \mathbf{e}_x(t) \right. \\ &\quad + \mathbf{D}_K \mathbf{e}_x(t) + \mathbf{C}_K \mathbf{x}_K(t) \\ &\quad \left. + (\mathbf{D}_K + \mathbf{K}_{\text{oist}}(t)) \mathbf{D}_e \mathbf{e}(t) \right\| \end{aligned} \quad (\text{D7})$$

First, using Lemma 5.1 and $\mathbf{e}_x := \mathbf{x} - \mathbf{x}_a$, it is observed that since $\mathbf{K}_{\text{oist}}(t) \mathbf{x}$ is K_1 -Lipschitz, then

$$\|\mathbf{K}_{\text{oist}}(t) \mathbf{e}_x\| \leq K_1 \|\mathbf{e}_x\|, \forall t \quad (\text{D8})$$

Second, by property of the dead-zone function, $\|\text{Dz}_{\underline{v}(t)}^{\bar{v}(t)}(v(t))\| \leq \|v(t)\|, \forall t$. It comes that

$$\begin{aligned} \dot{V}(\mathbf{x}_a) &\leq -\alpha_4 \|\mathbf{x}_a\|^2 + \alpha_3 \|\mathbf{B}_u\| \|\mathbf{x}_a\| \{ [K_1 + \|\mathbf{D}_K\|] (\|\mathbf{e}_x\| \\ &\quad + \|\mathbf{D}_e\| \|\mathbf{e}\|) + \|\mathbf{C}_K\| \|\mathbf{x}_K\| \} \\ &\leq -\alpha_4 \|\mathbf{x}_a\|^2 + \alpha_3 \|\mathbf{B}_u\| \|\mathbf{x}_a\| [K_1 + \|\mathbf{D}_K \mathbf{C}_K\|] \|\mathbf{X}\| \\ &\quad + \alpha_3 \|\mathbf{B}_u\| \|\mathbf{x}_a\| [K_1 + \|[0 \mathbf{D}_K]\|] \|\mathbf{D}_e\| \|\mathbf{W}\| \end{aligned} \quad (\text{D9})$$

Using $k_1 > 0$ and $k_2 > 0$ such that

$$\begin{aligned} k_1 &\geq \alpha_3 \|\mathbf{B}_u\| [K_1 + \|\mathbf{D}_K \mathbf{C}_K\|] \in \mathbb{R} \\ k_2 &\geq \alpha_3 \|\mathbf{B}_u\| [K_1 + \|[0 \mathbf{D}_K]\|] \|\mathbf{D}_e\| \in \mathbb{R} \end{aligned} \quad (\text{D10})$$

then Equation (D9) becomes

$$\dot{V}(\mathbf{x}_a) \leq -\alpha_4 \|\mathbf{x}_a\|^2 + \|\mathbf{x}_a\| [k_1 \|\mathbf{X}\| + k_2 \|\mathbf{W}\|] \quad (\text{D11})$$

Applying the inequality $2\epsilon \|\mathbf{x}_a\| \|\mathbf{X}\| \leq \epsilon^2 \|\mathbf{x}_a\|^2 + \frac{\|\mathbf{X}\|^2}{\epsilon^2}$ for $\epsilon > 0$, Equation (D11) is rewritten as

$$\begin{aligned} \dot{V}(\mathbf{x}_a) &\leq -\alpha_4 \|\mathbf{x}_a\|^2 + \frac{1}{2} k_1^2 \epsilon_1^2 \|\mathbf{x}_a\|^2 + \frac{1}{2} k_2^2 \epsilon_2^2 \|\mathbf{x}_a\|^2 \\ &\quad + \frac{k_1^2}{2\epsilon_1^2} \|\mathbf{X}\|^2 + \frac{k_2^2}{2\epsilon_2^2} \|\mathbf{W}\|^2 \\ &\leq \left(-\alpha_4 + \frac{1}{2} k_1^2 \epsilon_1^2 + \frac{1}{2} k_2^2 \epsilon_2^2 \right) \|\mathbf{x}_a\|^2 + \frac{k_1^2}{2\epsilon_1^2} \|\mathbf{X}\|^2 + \frac{k_2^2}{2\epsilon_2^2} \|\mathbf{W}\|^2 \\ &\leq -\alpha_5 \|\mathbf{x}_a\|^2 + \frac{k_1^2}{2\epsilon_1^2} \|\mathbf{X}\|^2 + \frac{k_2^2}{2\epsilon_2^2} \|\mathbf{W}\|^2 \end{aligned} \quad (\text{D12})$$

where $\alpha_5 = \alpha_4 - \frac{1}{2} k_1^2 \epsilon_1^2 - \frac{1}{2} k_2^2 \epsilon_2^2 > 0$ if the constants ϵ_1 and ϵ_2 are chosen small enough so that $\alpha_4 > \frac{1}{2} k_1^2 \epsilon_1^2 + \frac{1}{2} k_2^2 \epsilon_2^2$. Using Isidori (1999, Lemma 10.4.2, p. 21), V is thus an ISS-Lyapunov function for the system

$$\dot{\mathbf{x}}_a = f_1 \left(\mathbf{x}_a, \begin{bmatrix} \mathbf{X} \\ \mathbf{W} \end{bmatrix} \right) \quad (\text{D13})$$

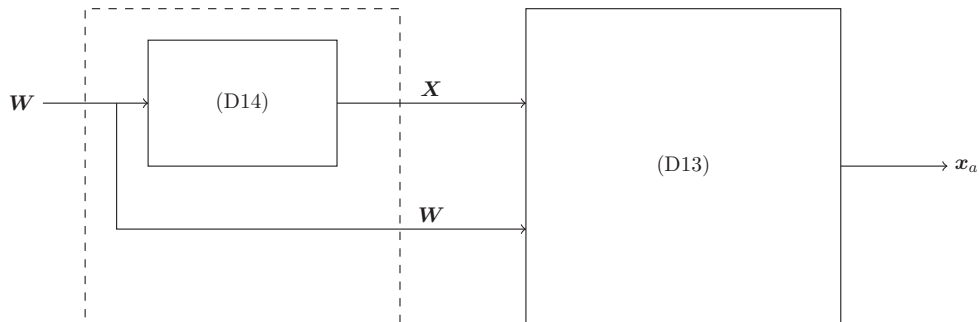


Figure D1. Illustration of the interconnections in the cascade described by Equation (D15).

where f_1 is a nonlinear function adequately defined. According to Isidori (1999, Theorem 10.4.1, p. 21), the system in Equation (D13) is thus ISS. At the beginning of this proof, it has been shown that – for a specific class of bounded finite energy disturbances \mathbf{d} and \mathbf{e} – $\|\mathbf{X}\|_2$ is finite and $\|\mathbf{X}\|$ converges to zero. Using a similar approach to the previous case, there exists V_X and strictly positive constants β_1, β_2 such that $\dot{V}_X(\mathbf{X}) \leq -\beta_1 \|\mathbf{X}\|^2 + \beta_2 \|\mathbf{W}\|^2$. This function is an ISS-Lyapunov function to the following system:

$$\dot{\mathbf{X}} = f_2(\mathbf{X}, \mathbf{W}) \quad (\text{D14})$$

where f_2 is a linear function adequately defined. Using Isidori (1999, Theorem 10.5.2, p. 34), it is possible to conclude that the cascade of systems in Equation (D15)

is ISS. The cascade is illustrated on Figure 12. Note that in case $\mathbf{d} = 0$ and $\mathbf{e} = 0$ and using Isidori (1999, Corollary 10.5.3, p. 35), the origin $(\mathbf{x}_a, \mathbf{X}) = (0, 0)$ is GAS for the cascade.

$$\begin{cases} \dot{\mathbf{x}}_a = f_1\left(\mathbf{x}_a, \begin{bmatrix} \mathbf{X} \\ \mathbf{W} \end{bmatrix}\right) \\ \dot{\mathbf{X}} = f_2(\mathbf{X}, \mathbf{W}) \end{cases} \quad (\text{D15})$$

Using the relation between ISS and CICS property, as stated in Terrell (2009, Theorem 16.4, p. 373), it comes that the cascade in Equation (D15) is CICS. Hence, using the theorem in Sontag (1989) (where CIBS property is a weaker property than CICS), the origin $(\mathbf{x}_a, \mathbf{X}) = (0, 0)$ is GAS for the cascade. This concludes the proof.

Attitude tracking control of a flexible spacecraft under angular velocity constraints

Laurent Burlion^a, Jean-Marc Biannic^a and Tarek Ahmed-Ali^b

^aONERA, The French Aerospace Lab, Toulouse, France; ^bLaboratoire GREYC, UMR CNRS 6072, Université de Caen Basse-Normandie/ENSICAEN, Caen, France

ABSTRACT

In this paper, a new technique is proposed for trajectory tracking of a flexible spacecraft subject to angular velocity constraints. The problem is addressed using an output to input saturation transformation (OIST) which converts the prescribed bounds into state-dependent saturations on the control input signals. It is shown that an interval observer can be used in combination with the OIST technique to ensure that the constraints remain satisfied despite unmeasured flexible modes and torque disturbances. Some realistic simulations conclude the paper and validate our approach.

ARTICLE HISTORY

Received 23 February 2017
Accepted 24 October 2017

KEYWORDS

Constrained control; interval observers; anti-windup; spacecraft; attitude stabilisation; time-domain constraint

1. Introduction

State constraints arise in numerous engineering applications. Among several approaches summarised in Goodwin, Seron, and de Dona (2004) and Glattfelder and Schaufelberger (2003), a popular idea consists of modifying a nominal controller whenever the constraints are about to be violated. Following this line, the output to input saturation transformation (OIST) approach was recently proposed in Burlion (2012) and Chambon, Burlion, and Apkarian (2015a) to replace the state constraints by some state-dependent control saturations. Such an approach is attractive because it enables use of the vast literature on control saturation problems and may especially lead to consider anti-windup loops which are now well understood (see e.g. Galeani, Tarbouriech, Turner, & Zaccarian, 2009; Tarbouriech & Turner, 2009).

On the other hand, the spacecraft attitude pointing and tracking control problems have been extensively studied in the past decades (see e.g. Akella, Thakur, & Mazenc, 2015; Chen & Huang, 2009; Di Gennaro, 2002; Gennaro, 2003; Lovera & Astolfi, 2004; Tayebi, 2008; Trégouët, Arzelier, Peaucelle, Pittet, & Zaccarian, 2015; Zhang & Cheng, 2012; Zhang, Wang, & Trivailo, 2008, and the references therein). Of particular interest are the studies carried out in Xiao, Yin, and Kaynak (2017) and Xiao, Yin, and Wu (2017) where a nonlinear observer-based attitude control was tailored to reject both external disturbances and flexible vibrations. The effectiveness of the approach was verified through a testbed which uses thruster and reaction wheels as actuators. However, reaction wheels' rotation speed limitations were not studied in these papers.

Most of the papers dealing with satellite attitude control subject to constraints use model predictive control (MPC) techniques (see e.g. Gupta, Kalabic, Cairano, Bloch, & Kolmanovsky, 2015; Hegrehaes, Gravdahl, & Tondel, 2005). Although MPC provides very efficient solutions, the full state is most of the time assumed to be available. As an alternative to MPC, only a few papers deal with state-constraints, especially with the problem

of limiting the angular velocity of a spacecraft as in Hu (2009) and Luzi, Peaucelle, Biannic, Pittet, and Mignot (2014). This is a significant problem because the limitations of the satellite reaction wheels require a response with a limited speed when the pointing error is too large (Biannic, Roos, & Pittet, 2011; Pittet & Arzelier, 2006).

In this paper, the problem of spacecraft attitude reference trajectory tracking is considered. To cope with angular velocity limitations, a nominal controller is combined with the so-called OIST methodology (Chambon, Burlion, & Apkarian, 2017). Since in its preliminary form, this technique requires the full state to be measured, an interval observer is proposed developing the ideas introduced in Chambon, Burlion, and Apkarian (2015b) (note that this last paper did not prove the stability of the resulting closed-loop system). Such an observer is here used to compute the upper and lower bounds of the torque induced by the unmeasured flexible modes and external disturbances. The main contribution of the paper is to extend the OIST technique (which was initially detailed for linear systems in Chambon et al. (2017)) to a nonlinear spacecraft model. Also, we establish the closed-loop system stability by using an anti-windup recipe.

The paper is organised as follows. In Section 2, the mathematical model of the flexible spacecraft is recalled, while in Section 3, the control problem is stated. In Section 4, a novel OIST which uses a time-varying interval observer is proposed to deal with the angular velocity constraints. The obtained closed-loop saturated system is studied in Section 5: it is demonstrated that asymptotic stability properties are achieved when a nonlinear anti-windup loop is combined with a nominal control law. Finally, the effectiveness of the proposed approach is illustrated by numerical simulations in Section 6.

2. Preliminaries

2.1 Definitions and notation

Notation: The classical unit quaternion representation for satellite orientation with respect to an inertial frame is denoted

$q = [q_0, q_v^T]^T$, where $q_0 \in \mathcal{R}$ is the scalar component and $q_v \in \mathcal{R}^3$ is the vector component. The quaternion is unit when $q_0^2 + q_v^T q_v = 1$. The inverse of q is denoted $q^{-1} = [q_0, -q_v^T]^T$ and the product of two quaternions q_1 and q_2 is denoted $q_1 * q_2$. The following notation will be useful when developing the equations for satellite attitude dynamics:

$$S(v) = \begin{bmatrix} 0 & -v_3 & v_2 \\ v_3 & 0 & -v_1 \\ -v_2 & v_1 & 0 \end{bmatrix} \quad E(q) = \begin{bmatrix} -q_v^T \\ q_0 I_3 + S(q_v) \end{bmatrix} \quad (1)$$

$$R(q) = (q_0^2 - q_v^T q_v) I_3 + 2q_v q_v^T - 2q_0 S(q_v)$$

where $v = [v_1, v_2, v_3]^T$. Note that $S(\cdot)$ is the skew symmetric operator and that $E(q) \in \mathcal{R}^{4 \times 3}$ is classically used in the expression of \dot{q} . Moreover, $R(q) \in SO(3)$ is the rotation matrix that corresponds with q .

Notation: Given two vectors $x_1, x_2 \in \mathbb{R}^n$, the relation $x_1 \leq x_2$, is understood element-wise.

Notation: For any vector $x \in \mathcal{R}^n$, and any matrix $A \in \mathcal{R}^{m \times n}$, $|x|$ and $|A|$ denote, respectively, the Euclidean norm of x and the induced norm of A . The Frobenius norm is denoted by $|A|_F := \sqrt{\text{trace}(A^T A)}$. Moreover, given any positive definite matrix Q , $\lambda_{\min}(Q)$ (resp. $\lambda_{\max}(Q)$) denotes the minimal (resp. maximal) eigenvalue value of Q .

Definition 2.1: A square matrix $M = (M_{ij}) \in \mathcal{R}^{n \times n}$ is said to be Metzler if $M_{ij} \geq 0, \forall i \neq j$.

Definition 2.2: Given two scalar functions $\underline{u}, \bar{u} : \mathcal{R} \rightarrow \mathcal{R}$ such that $\forall t, \underline{u}(t) \leq \bar{u}(t)$, the following saturation operator with time-varying bounds is defined:

$$\forall u \in \mathcal{R}, \quad \text{Sat}_{\underline{u}(t)}^{\bar{u}(t)}(u) = \max\{\underline{u}(t), \min\{\bar{u}(t), u\}\} \quad (2)$$

When applied to a vector, this operator is understood component-wise.

2.2 Flexible spacecraft modelling

In this paper, we consider the flexible spacecraft model used in Di Gennaro (2002):

$$\dot{q}_e = \frac{1}{2} E(q_e) \omega_e \quad (3a)$$

$$J_{mb} \dot{\omega}_e = -N(\omega, \omega_e, z_e, \omega_r^b) + u + d + C_z z_e + D_z \omega_e - J_{mb} \dot{\omega}_r^b \quad (3b)$$

$$\dot{z}_e = A_z z_e + B_{1,z} \omega_e + B_{2,z} \dot{\omega}_r^b \quad (3c)$$

where

- $q_e = q * q_r^{-1} = [q_{e0}, q_{ev}^T]^T$ is the error between the spacecraft quaternion q and the reference quaternion q_r
- $\omega_e = \omega - \omega_r^b \in \mathcal{R}^3$ is the error between the angular velocity of the spacecraft ω and ω_r^b which is the reference angular velocity ω_r expressed in the body-fixed frame. In other words, ω_r^b is defined by

$$\omega_r^b = R(q_e) \omega_r = R(q) R(q_r)^T \omega_r \quad (4)$$

- $u \in \mathcal{R}^3$ are the control inputs produced by gas jets.
- $d \in \mathcal{R}^3$ are the torque disturbances.
- $z_e = z - z_r$, where $z = [\eta; \psi] = [\eta; \dot{\eta} + \delta \omega]$ ($\eta \in \mathcal{R}^N$ being the vector of the modal displacements) and $z_r := [O_{N,1}; \delta \omega_r^b]$.
- $J_{mb} = J - \delta^T \delta$ is the main body symmetric inertia matrix where $J \in \mathcal{R}^{3 \times 3}$ is the symmetric inertia matrix of the undeformed structure and $\delta \in \mathcal{R}^{N \times 3}$ is the coupling matrix between elastic and rigid dynamics
- $(A_z, B_{1,z}, B_{2,z}, C_z, D_z)$ are matrices expressed with respect to the damping (resp. stiffness) matrix $C = \text{diag}\{2\xi_i \omega_i, i = 1, \dots, N\}$ (resp. $K = \text{diag}\{\omega_i^2, i = 1, \dots, N\}$) of the N flexible modes:

$$A_z = \begin{bmatrix} O_N & I_N \\ -K & -C \end{bmatrix}, \quad B_{2,z} = - \begin{bmatrix} O_N \\ I_N \end{bmatrix} \delta, \quad B_{1,z} = A_z B_{2,z}$$

$$C_z = \delta^T [K C], \quad D_z = -\delta^T C \delta \quad (5)$$

- the function N is defined by the following relation:

$$\forall e, f, g \in \mathcal{R}^3, \forall z \in \mathcal{R}^{2N}, N(e, f, z, h) = S(e)(J_{mb} f + G_z z + J h) \quad (6)$$

where $G_z = [O_{3,N} \delta^T]$

Remark 2.1: The expression retained for z_r corresponds to the absence of modal displacements. Indeed, z_r can be rewritten as $z_r := [\eta_r; \dot{\eta}_r + \delta \omega_r^b]$ where $\eta_r = \dot{\eta}_r = O_{N,1}$. Moreover, considering the expressions of $A_z, B_{1,z}$ and $B_{2,z}$ (5), it can be easily shown that z_r verifies $\dot{z}_r = A_z z_r + B_{1,z} \dot{\omega}_r^b - B_{2,z} \dot{\omega}_r^b$.

Remark 2.2: Control inputs u are merely produced by gas jets in the retained model of Di Gennaro (2002). Considering additional control inputs like reaction wheels and magnetorquers is postponed to future studies. However, being able to limit the satellite angular velocity is of practical interest because it is a first step before successfully dealing with the reaction wheels' speed limitations. See, for more details, Pittet and Arzelier (2006) and Luzi et al. (2014).

3. Problem formulation

3.1 Main assumptions

In the remainder of the paper, the following 'not so restrictive' assumptions have been made:

- (A1) Although it might be poorly damped, the spacecraft structure is assumed strictly stable so that A_z is Hurwitz (all eigenvalues lie strictly inside the open left half-plane),
- (A2) The torque disturbance signal is bounded. More precisely, we assume that

$$d \in \mathcal{L}_2 \cap \mathcal{L}_\infty \quad (7)$$

which implies

$$\exists \bar{d} > 0 / d(t) \in [-\bar{d}, \bar{d}] \quad (8)$$

(A3) The initial state vector $z(0) \in \mathbb{R}^{2N}$ associated to the flexible modes is assumed to belong to a bounded interval. Then, there exist $z_0^-, z_0^+ \in \mathbb{R}^{2N}$ such that $z_0^- \leq z(0) \leq z_0^+$ or equivalently:

$$z(0) \in [z_0^-, z_0^+] \quad (9)$$

(A4) The reference angular velocity ω_r and the acceleration $\dot{\omega}_r$ are assumed to be bounded. More precisely, we will consider:

$$\omega_r \in \mathcal{L}_\infty \quad ; \quad \dot{\omega}_r \in \mathcal{L}_2 \cap \mathcal{L}_\infty \quad (10)$$

3.2 Problem statement

The starting point of the paper is the following nominal control law which does not take into account the angular velocity constraints and requires the whole state to be measured:

Lemma 3.1: Under Assumptions (A2) and (A4) and further considering that the whole state is measurable, let the following static state-feedback controller be applied to system (3a)–(3c)

$$\begin{aligned} u &= u_{nom}(q_{e0}, x_e, \omega_r^b, \dot{\omega}_r^b) \\ &= -k_p q_{ev} - k_d \omega_e - J_{mb} \dot{q}_{ev} + N(\omega, \omega_e, z_e, \omega_r^b) \\ &\quad - C_z z_e - D_z \omega_e + J_{mb} \dot{\omega}_r^b \end{aligned} \quad (11)$$

where the controller gains k_p and k_d are strictly positive scalars. Then, the error state $x_e = [q_{ev}; \omega_e; z_e]$ asymptotically converges to the origin for any initial condition $x(0)$.

Proof: The control law is similar to the one of Di Gennaro (2002, Theorem 1). There are two slight differences in the proof of the result:

- (1) in our modelling, we consider a torque disturbance d which introduces an additional term in the derivative of the Lyapunov function V (see (8) and (9) in Di Gennaro, 2002). This is treated in the same manner that of the $\dot{\omega}_r$ term. Indeed, using Assumption (A2), one can still conclude the proof by invoking Barbalat's lemma.
- (2) we do not impose any lower bound on k_d since the proof is unchanged when P is replaced by εP where the positive real ε is an extra degree of freedom which can be chosen sufficiently small so that $Q > 0$ no matter the value of $k_d > 0$ (see (11) in Di Gennaro, 2002) \square

Remark 3.1: Note that q_{ev} tends to 0 while q_{e0} is driven to ± 1 which in all cases make $R(q_e)$ converge to the same rotation I_3 . Akella et al. (2015) propose to adopt the notion of 'almost' global asymptotic stability for this problem.

In this paper, the problem at hand is thus to redesign the nominal full state feedback control law (11) in the case where

- the modal displacements η and their time derivatives $\dot{\eta}$ are not measured, which means that z is no longer available for feedback,

- the angular velocity vector ω must satisfy the following asymmetric constraints:

$$\forall t, \quad \underline{\omega} \leq \omega(t) \leq \bar{\omega} \quad (12)$$

with

$$\underline{\omega} < 0 < \bar{\omega} \quad (13)$$

4. Output to input saturation transformation extended for robustness (OISTeR)

Before stating our main results and for clarity of presentation, we first recall the OIST technique when both the full state and the disturbance are measured. Then, we propose an extended technique using the upper and lower bounds of the unmeasured states which are thus provided by the interval observer. This new technique called OISTeR means OIST extended with Robustness properties (with respect to both the uncertain initial condition $z(0) \in [z_0^-, z_0^+]$ and uncertainties on $d \in [-\bar{d}, \bar{d}]$).

4.1 The 'classical' OIST methodology

For clarity of presentation, let us first recall the OIST methodology when the full state and the disturbance d are measured.

Lemma 4.1: Let k_O be a strictly positive real number. Let $u \in \mathcal{L}_2$. Suppose that the whole state and the disturbance torque d are available for feedback. Suppose that $\omega(0) \in [\underline{\omega}, \bar{\omega}]$ and consider the following input saturated system:

$$J_{mb} \dot{\omega} = -N(\omega, \omega, z, 0) + OISat(u) + d + C_z z + D_z \omega \quad (14a)$$

$$\dot{z} = A_z z + B_{1,z} \omega \quad (14b)$$

where

$$\begin{aligned} OISat(u) &:= J_{mb} (\text{Sat}_{k_O \underline{\omega}}^{k_O \bar{\omega}}(\alpha + k_O \omega) - k_O \omega) \\ &\quad + N(\omega, \omega, z, 0) - d - C_z z - D_z \omega \end{aligned} \quad (15)$$

with

$$\alpha = J_{mb}^{-1} (-N(\omega, \omega, z, 0) + u + d + C_z z + D_z \omega) \quad (16)$$

Then, $\forall t \geq 0, \omega(t) \in [\underline{\omega}, \bar{\omega}]$

Proof: The proof is straightforward using the OIST technique as defined in Burlion (2012) and Chambon et al. (2015a) in the relative degree 1 case (i.e. when u appears in the expression of the first derivative of ω with respect to time). For clarity, we develop the basic computations. Using (14a)–(15), it is readily seen that ω undergoes the following dynamics:

$$\dot{\omega} = \text{Sat}_{k_O \underline{\omega}}^{k_O \bar{\omega}}(\alpha + k_O \omega) - k_O \omega \quad (17)$$

which implies that $\forall t,$

$$-k_O(\omega - \underline{\omega}) \leq \dot{\omega} \leq -k_O(\omega - \bar{\omega}) \quad (18)$$

from this, the result is easily deduced using the fact that $\omega(0) \in [\underline{\omega}, \bar{\omega}]$ and $k_O > 0$. \square

Remark 4.1: ‘OISat(u)’ denotes a saturation of the control input u . This notation is preferred to ‘Sat’ since it is a state-dependent saturation element which comes from an OIST.

4.2 The OISter methodology

The OISter methodology is now developed: it extends the above result when neither z nor d are no longer measured. Following the preliminary ideas of Chambon et al. (2015b), we first build an interval observer in order to obtain the lower and upper bounds of the missing variables. Then, we propose a novel ‘OISat’ function which exploits these bounds. Note that the use of an interval observer is the key idea to respect the angular velocity constraints (using an estimation of z in combination with the OIST methodology presented in Lemma 3.1 would not be sufficient to make sure that these constraints are fulfilled). The following result is then established:

Lemma 4.2: Let k_O be a strictly positive real number. Let $d \in \mathcal{L}_2$. Let Assumptions (A2) and (A3) hold and suppose that $\omega(0) \in [\underline{\omega}, \bar{\omega}]$. Then, there exists a time-varying vector \bar{e}_y taking its values in $\mathbb{R}_{\geq 0}^3$ such that the input saturated system (14a)–(14b) with

$$\text{OISat}(u) := J_{mb}(\text{Sat}_{k(t)\underline{\omega} + \bar{e}_y}^{k(t)\bar{\omega} - \bar{e}_y}(\alpha + k(t)\omega) - k(t)\omega) + N(\omega, \omega, \hat{z}, 0) - C_z \hat{z} - D_z \omega \quad (19)$$

and

$$\alpha = J_{mb}^{-1}(-N(\omega, \omega, \hat{z}, 0) + u + C_z \hat{z} + D_z \omega) \quad (20a)$$

$$k(t) = k_O + \frac{2\bar{e}_y}{\bar{\omega} - \underline{\omega}} \quad (20b)$$

$$\dot{\hat{z}} = A_z \hat{z} + B_{1,z} \omega \quad (20c)$$

$$\hat{z}(0) = \frac{z_0^- + z_0^+}{2} \quad (20d)$$

satisfies

$$\forall t \geq 0, \quad \omega(t) \in [\underline{\omega}, \bar{\omega}] \quad (21)$$

Proof: Let us denote $e_z = z - \hat{z}$, where \hat{z} is defined by (20c) and (20d).

Let us also note

$$e_y = J_{mb}^{-1}(-S(\omega)G_z e_z + C_z e_z + d) \quad (22)$$

Using these notations, it is clear that (3b) can be rewritten as follows:

$$J_{mb} \dot{\omega}_e = -N(\omega, \omega_e, \hat{z}_e, \omega_r^b) + u + C_z \hat{z}_e + D_z \omega_e - J_{mb} \dot{\omega}_r^b + J_{mb} e_y \quad (23)$$

Note that e_y is thus the total disturbance torque induced by both the disturbance d and the observation error. Then, as detailed in Appendix 1, one can easily construct the lower bounds $-\bar{e}_y$ and the upper bounds \bar{e}_y of the missing variables e_y using the interval observer proposed in Mazenc and Bernard (2011).

Using (14a), (22) and (23), it is readily checked that ω undergoes the following dynamics:

$$\dot{\omega} = \text{Sat}_{k(t)\underline{\omega} + \bar{e}_y}^{k(t)\bar{\omega} - \bar{e}_y}(\alpha + k(t)\omega) - k(t)\omega + e_y \quad (24)$$

when one applies the control action (19).

Note that here the saturation function is well defined because (20b) implies that

$$\forall t \geq 0, \quad k(t)\bar{\omega} - \bar{e}_y \geq k(t)\underline{\omega} + \bar{e}_y \quad (25)$$

it follows from (24) that

$$\forall t \geq 0, \quad -k(t)(\omega - \underline{\omega}) + e_y + \bar{e}_y \leq \dot{\omega} \leq e_y - \bar{e}_y - k(t)(\omega - \bar{\omega}) \quad (26)$$

which implies that

$$\forall t \geq 0, \quad -k(t)(\omega - \underline{\omega}) \leq \dot{\omega} \leq -k(t)(\omega - \bar{\omega}) \quad (27)$$

Recalling that $\omega(0) \in [\underline{\omega}, \bar{\omega}]$ and noting from (13) and (20b) that $k(t) \geq k_O > 0$, the final result (21) immediately follows from (27) which concludes the proof. \square

5. Main result: attitude tracking under velocity constraints

Based on the notation introduced in the preceding section and more specifically on equations, the flexible spacecraft model (3a)–(3c) is now rewritten as follows:

$$\dot{q}_e = \frac{1}{2} E(q_e) \omega_e \quad (28a)$$

$$J_{mb} \dot{\omega}_e = -N(\omega, \omega_e, \hat{z}_e, \omega_r^b) + u + C_z \hat{z}_e + D_z \omega_e + J_{mb} (e_y - \dot{\omega}_r^b) \quad (28b)$$

$$\dot{\hat{z}}_e = A_z \hat{z}_e + B_{1,z} \omega_e + B_{2,z} \dot{\omega}_r^b \quad (28c)$$

$$\dot{e}_z = A_z e_z \quad (28d)$$

with

$$\hat{z}_e = \hat{z} - z_r \quad (29)$$

$$e_z = z - \hat{z} \quad (30)$$

$$e_y = J_{mb}^{-1}(-S(\omega)G_z e_z + C_z e_z + d) \quad (31)$$

and the main result of the paper, summarised in the following theorem, may now be stated.

Theorem 5.1: Let k_O, k_a be strictly positive real numbers. Let $d \in \mathcal{L}_2$. Let Assumptions (A2)–(A4) hold and suppose that $\omega(0) \in [\underline{\omega}, \bar{\omega}]$. Consider a closed-loop system consisting of the plant (28a)–(28d) and the dynamic control law:

$$u = OISat(\tilde{u}_n + u_a) \quad (32)$$

$$= J_{mb} \left(Sat_{k(t)\omega + \bar{e}_y}^{k(t)\bar{\omega} - \bar{e}_y}(\alpha + k(t)\omega) - k(t)\omega \right) + N(\omega, \omega, \hat{z}, 0) - C_z \hat{z} - D_z \omega \quad (33)$$

$$\dot{q}_a = \frac{1}{2} E(q_a) \omega_a := \frac{1}{2} E(q_a) R(q_e) R(q_a)^T \omega_a^{be} \quad (34)$$

$$J_{mb} \dot{\omega}_a^{be} = (N(\tilde{\omega} + \omega_r^b, \tilde{\omega}, \hat{z}, \omega_r^b) - N(\omega, \omega_e, \hat{z}_e, \omega_r^b)) + C_z z_a + D_z \omega_a^{be} \quad (35)$$

$$+ OISat(\tilde{u}_n + u_a) - \tilde{u}_n \quad (36)$$

$$\dot{z}_a = A_z z_a + B_{1,z} \omega_a^{be} \quad (37)$$

with

$$\tilde{u}_n = u_{nom}(\tilde{q}_0, \hat{x}, \omega_r^b, \dot{\omega}_r^b) \quad (38a)$$

$$\alpha = J_{mb}^{-1} (-N(\omega, \omega, \hat{z}, 0) + \tilde{u}_n + u_a + C_z \hat{z} + D_z \omega) \quad (38b)$$

$$u_a = J_{mb} (-k_a q_{av} - k(t) \omega_a^{be}) + N(\omega, \omega_a^{be}, z_a, 0) - C_z z_a - D_z \omega_a^{be} \quad (38c)$$

where

- $\hat{z} = \hat{z}_e - z_a$, $\tilde{\omega} = \omega_e - \omega_a^{be}$, $\tilde{q} = q_e * q_a^{-1}$.
- \bar{e}_y (resp. $k(t)$) is given by (A9) (resp. (20b)).

Then, $\forall t \geq 0$, $\omega(t) \in [\underline{\omega}, \bar{\omega}]$ and there exists k_O such that the error $x_e = [q_{ev}; \omega_e; z_e]$ is asymptotically stabilised to the origin for $k_O \geq k_O$.

Remark 5.1: Note that the dynamic part of the control law described by Equations (34)–(37) is the anti-windup loop.

Proof: The proof of the result is divided into two parts. In the first part, it is shown that the error system whose state $\tilde{x} = [\tilde{q}_v; \tilde{\omega}; \tilde{z}]$ asymptotically converges to 0. The second part of the proof establishes that the anti-windup state denoted by $x_a = [q_{av}; \omega_a^{be}; z_a]$ asymptotically converges to the origin as well. As a consequence, the state of the error system $x_e = [q_{ev}; \omega_e; z_e]$ tends asymptotically to 0.

Part 1. Let us consider the error system whose state is \tilde{x} . After straightforward computations, one obtains

$$\begin{cases} \dot{\tilde{q}} = \frac{1}{2} E(\tilde{q}) \tilde{\omega} \\ J_{mb} \dot{\tilde{\omega}} = -N(\tilde{\omega} + \omega_r^b, \tilde{\omega}, \hat{z}, \omega_r^b) + u_{nom}(\tilde{q}_0, \hat{x}, \omega_r^b, \dot{\omega}_r^b) \\ \quad + C_z \tilde{z} + D_z \tilde{\omega} + J_{mb}(e_y - \dot{\omega}_r^b) \\ \dot{\tilde{z}} = A_z \tilde{z} + B_{1,z} \tilde{\omega} + B_{2,z} \dot{\omega}_r^b \end{cases} \quad (39)$$

Following the ideas of the proof of (Di Gennaro, 2002, Theorem 1), we first consider the following Lyapunov

function:

$$V(t, \tilde{x}) = (k_p + k_d)[(1 - \tilde{q}_0)^2 + |\tilde{q}_v|^2] + \frac{1}{2} (\tilde{q}_v + \tilde{\omega})^T J_{mb} (\tilde{q}_v + \tilde{\omega}) + \frac{\varepsilon}{2} \tilde{z}^T P_z \tilde{z} + \gamma e_z^T P_z e_z \quad (40)$$

where $\varepsilon, \gamma > 0$ and $P_z = P_z^T > 0$ is a solution to

$$P_z A_z + A_z^T P_z = -2Q_z \quad (41)$$

for any fixed $Q_z = Q_z^T > 0$. (P_z exists because A_z is strictly Hurwitz stable).

Computing the derivative of V , one gets

$$\dot{V}(t, \tilde{x}) = -\tilde{x}^T Q \tilde{x} - \gamma e_z^T Q_z e_z + (\tilde{q}_v + \tilde{\omega})^T (e_y - \dot{\omega}_r^b) \quad (42)$$

with

$$Q = \begin{bmatrix} k_p I_3 & O & O \\ O & k_d I_3 & \frac{\varepsilon}{2} B_{1,z}^T P_z \\ O & \frac{\varepsilon}{2} P_z B_{1,z} & \varepsilon Q_z \end{bmatrix} \quad (43)$$

which, for sufficiently small $\varepsilon > 0$, is positive definite.

Then, using (31) and the boundedness of ω (which follows from (33) and Lemma 4.2), there exist $\lambda_1, \lambda_2, \lambda_3 > 0$ such that

$$\dot{V}(t, \tilde{x}) = -\lambda_{\min}(Q) |\tilde{x}|^2 - \gamma e_z^T Q_z e_z + \lambda_1 |\tilde{x}| |e_z| + \lambda_2 |\tilde{x}| |d| + \lambda_3 |\tilde{x}| |\dot{\omega}_r| \quad (44)$$

which, for $\gamma > 0$ chosen sufficiently large, yields

$$\dot{V}(t, \tilde{x}) \leq -\frac{\lambda_{\min}(Q)}{2} |\tilde{x}|^2 - \frac{\gamma}{2} e_z^T Q_z e_z + \lambda_2 |\tilde{x}| |d| + \lambda_3 |\tilde{x}| |\dot{\omega}_r| \quad (45)$$

where $d, \dot{\omega}_r \in \mathcal{L}_2$ in virtue of Assumptions (A2) and (A4). The proof of this part ends by invoking Barbalat's lemma as in the proof of [Theorem 1, Di Gennaro (2002)]. \square

Remark 5.2: As a result, \tilde{x} is uniformly bounded. Furthermore, ω being bounded implies that $\omega_a^b := \omega - \tilde{\omega} - \omega_r^{ba}$ is bounded. From Assumption (A1) and Equation (37), it readily follows that z_a is bounded. Moreover, q_a being a unit quaternion, q_{av} is bounded. As a consequence, there exist well-defined positive constants \tilde{c}, c_a such that

$$\forall t, \quad |\tilde{x}(t)| \leq \tilde{c} \quad |x_a(t)| \leq c_a \quad (46)$$

Part 2.

On the other hand, the nonlinear anti-windup loop (34)–(37) is now rewritten as follows:

$$\begin{cases} \dot{q}_a = \frac{1}{2} E(q_a) (\omega_a^{be} + \Delta_q) \\ J_{mb} \dot{\omega}_a^{be} = (-N(\omega, \omega_a^{be}, z_a, 0) + C_z z_a + D_z \omega_a^{be}) \\ \quad + OISat(u_a) + \Delta_\omega \\ \dot{z}_a = A_z z_a + B_{1,z} \omega_a^{be} \end{cases} \quad (47)$$

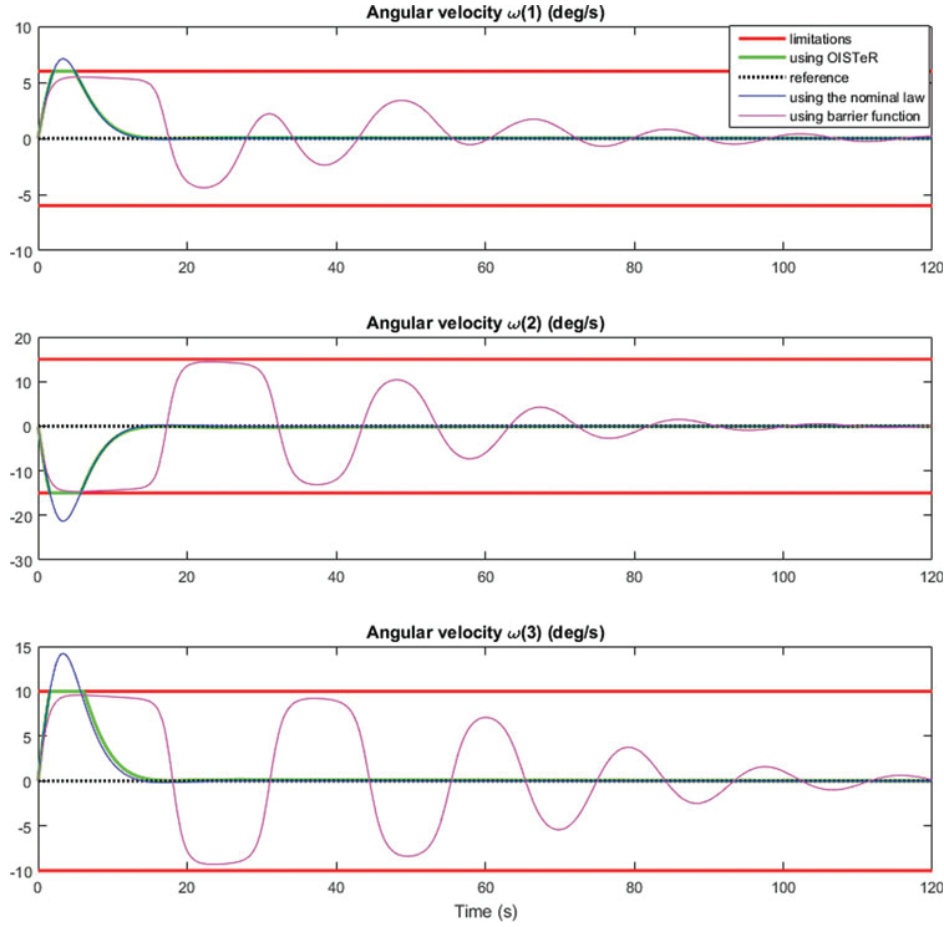


Figure 1. Scenario 1: comparison of the angular velocities on each axis with the nominal, BLF-based and enhanced (OISter-based) control systems.

where

$$\Delta_q = (R(\tilde{q})^T - I_3) \omega_a^{be} \quad (48)$$

$$\Delta_\omega = OISat(u_a + \tilde{u}_n) - OISat(u_a) - \tilde{u}_n + N(\tilde{\omega}) + \omega_r^b, \tilde{\omega}, \hat{z}, \omega_r^b \quad (49)$$

$$+ (N(\omega, \omega_a^{be}, z_a, 0) - N(\omega, \omega_e, \hat{z}_e, \omega_r^b)) \quad (50)$$

$$OISat(u_a) = J_{mb} \left(Sat_{k(t)\underline{\omega} + \bar{e}_y}^{k(t)\bar{\omega} - \bar{e}_y}(\alpha_a + k(t)\omega_a^{be}) - k(t)\omega_a^{be} \right) \quad (51)$$

$$+ N(\omega, \omega_a^{be}, z_a, 0) - C_z z_a - D_z \omega_a^{be} \quad (52)$$

$$\alpha_a = J_{mb}^{-1} (-N(\omega, \omega_a^{be}, z_a, 0) + u_a + C_z z_a + D_z \omega_a^{be}) \quad (53)$$

Substituting (52) in (47) results in the following subsystem:

$$\begin{cases} \dot{q}_a = \frac{1}{2} E(q_a) (\omega_a^{be} + \Delta_q) \\ J_{mb} \dot{\omega}_a^{be} = J_{mb} \left(Sat_{k(t)\underline{\omega} + \bar{e}_y}^{k(t)\bar{\omega} - \bar{e}_y}(\alpha_a + k(t)\omega_a^{be}) - k(t)\omega_a^{be} \right) + \Delta_\omega \\ \dot{z}_a = A_z z_a + B_{1,z} \omega_a^{be} \end{cases} \quad (54)$$

Let us now apply the control law u_a defined by (38c). It readily follows from (53) and (54) that

$$\begin{cases} \dot{q}_a = \frac{1}{2} E(q_a) (\omega_a^{be} + \Delta_q) \\ J_{mb} \dot{\omega}_a^{be} = J_{mb} \left(Sat_{k(t)\underline{\omega} + \bar{e}_y}^{k(t)\bar{\omega} - \bar{e}_y}(-k_a q_{av}) - k(t)\omega_a^{be} \right) + \Delta_\omega \\ \dot{z}_a = A_z z_a + B_{1,z} \omega_a^{be} \end{cases} \quad (55)$$

Now considering the time-varying bounds of the saturation operator and substitute $k(t)$ as in (20b), one obtains

$$\begin{cases} k(t)\bar{\omega} - \bar{e}_y = k_O \bar{\omega} + \frac{\bar{\omega} + \underline{\omega}}{\bar{\omega} - \underline{\omega}} \bar{e}_y \\ k(t)\underline{\omega} + \bar{e}_y = k_O \underline{\omega} + \frac{\bar{\omega} + \underline{\omega}}{\bar{\omega} - \underline{\omega}} \bar{e}_y \end{cases} \quad (56)$$

From (A4), (A8) and (A9), it readily follows that \tilde{y} tends asymptotically to $|J_{mb}^{-1}| \bar{d}$. Thus, there exists $T \geq 0$ such that

$$\forall t \geq T, |J_{mb}^{-1}| \bar{d} \leq \bar{e}_y \leq 2|J_{mb}^{-1}| \bar{d} \quad (57)$$

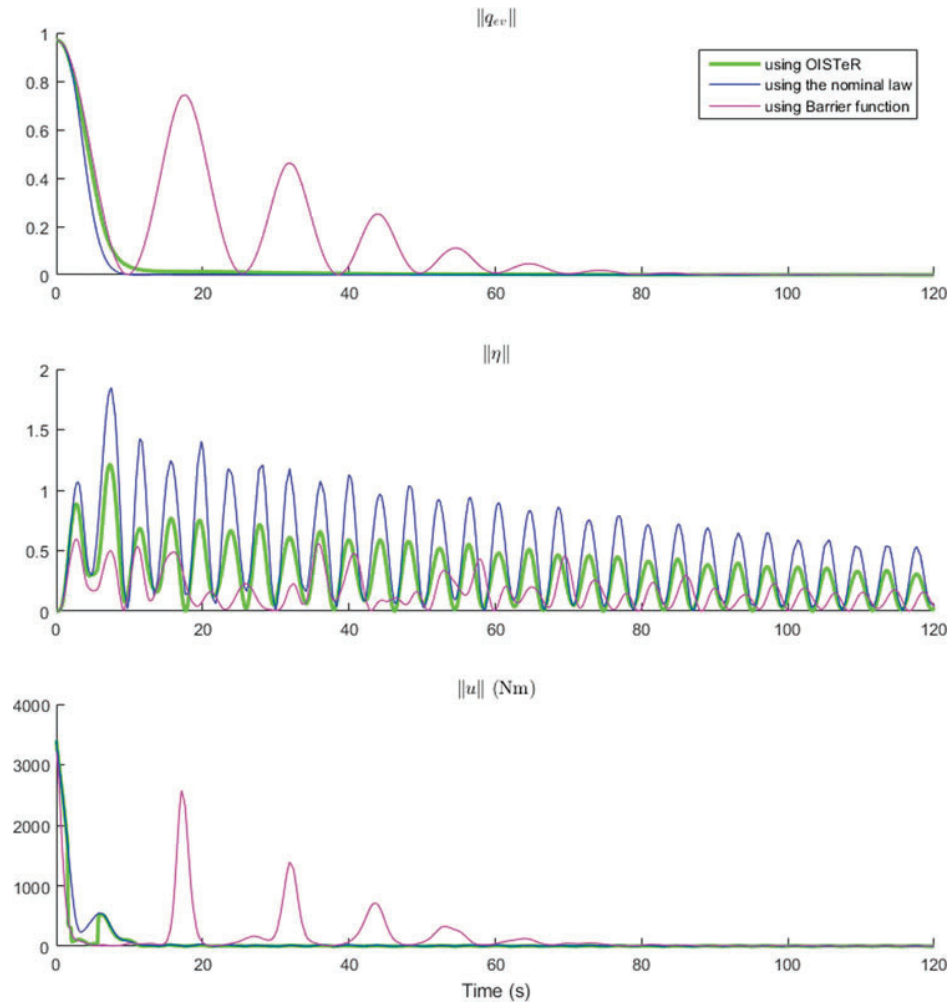


Figure 2. Scenario 1: further comparison of the nominal and enhanced controllers through the tracking error ($\|q_{ev}(t)\|$), the activity of the flexible modes ($\|\eta(t)\|$) and the control effort ($\|u(t)\|$).

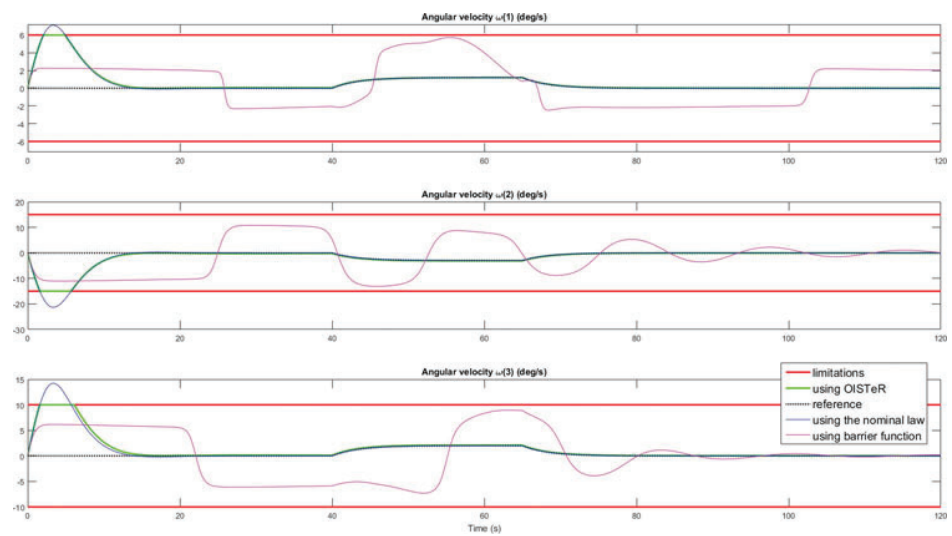


Figure 3. Scenario 2: comparison of the angular velocities on each axis with the nominal, BLF-based and enhanced (OISTeR-based) control systems.

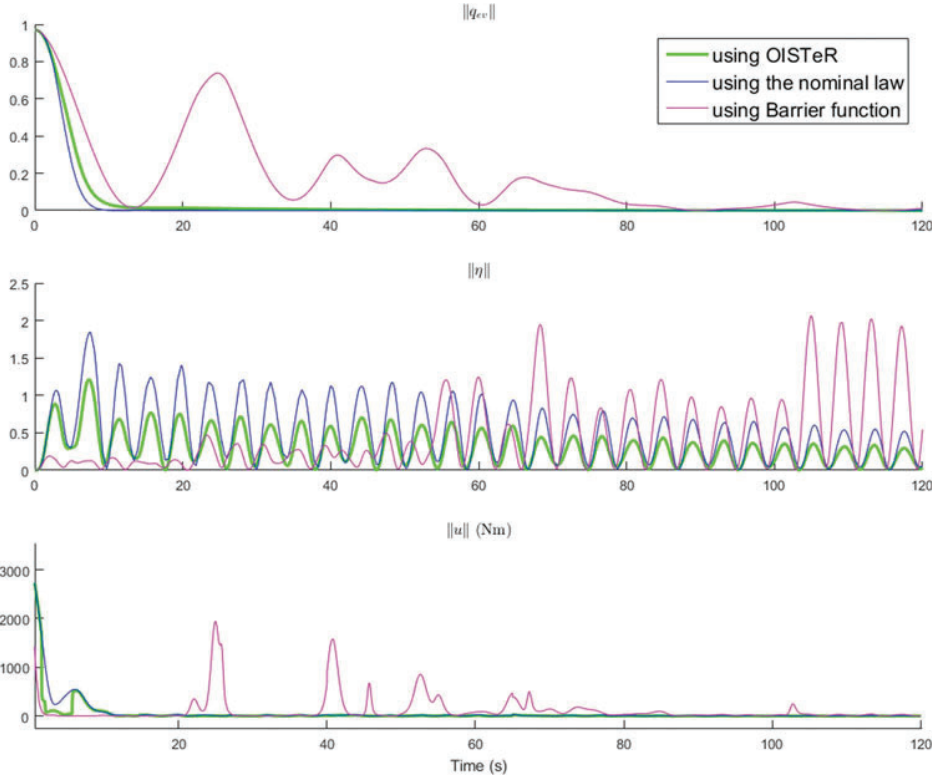


Figure 4. Scenario 2: further comparison of the nominal and enhanced controllers through the tracking error ($\|q_{ev}(t)\|$), the activity of the flexible modes ($\|\eta(t)\|$) and the control effort ($\|u(t)\|$).

which together with (56) implies that

$$\forall t \geq T, \begin{cases} k(t)\bar{\omega} - \bar{e}_y \geq k_O\bar{\omega} + \frac{\bar{\omega} + \omega}{\bar{\omega} - \omega} |J_{mb}^{-1}| \bar{d} \\ k(t)\underline{\omega} + \bar{e}_y \leq k_O\underline{\omega} + 2\frac{\bar{\omega} + \omega}{\bar{\omega} - \omega} |J_{mb}^{-1}| \bar{d} \end{cases} \quad (58)$$

Thus, choosing

$$k_O > \max \left\{ 0, \frac{1}{\bar{\omega}} \left(k_a - \frac{\bar{\omega} + \omega}{\bar{\omega} - \omega} |J_{mb}^{-1}| \bar{d} \right), \frac{-1}{\underline{\omega}} \left(k_a + 2\frac{\bar{\omega} + \omega}{\bar{\omega} - \omega} |J_{mb}^{-1}| \bar{d} \right) \right\} \quad (59)$$

one gets

$$\forall t \geq T, \begin{cases} k(t)\bar{\omega} - \bar{e}_y \geq k_a \\ k(t)\underline{\omega} + \bar{e}_y \leq -k_a \end{cases} \quad (60)$$

As a consequence,

$$\forall t \geq T, \text{Sat}_{k(t)\underline{\omega} + \bar{e}_y}^{k(t)\bar{\omega} - \bar{e}_y}(-k_a q_{av}) = -k_a q_{av} \quad (61)$$

Hence, the solutions being bounded for all time in virtue of (46), the asymptotic stability of x_a is now proven by studying the following system on $t \in [T, +\infty[$:

$$\begin{cases} \dot{q}_a = \frac{1}{2} E(q_a) (\omega_a^{be} + \Delta_q) \\ \dot{\omega}_a^{be} = -k_a q_{av} - k(t) \omega_a^{be} + J_{mb}^{-1} \Delta_\omega \\ \dot{z}_a = A_z z_a + B_{1,z} \omega_a^{be} \end{cases} \quad (62)$$

To this aim, we consider the following function:

$$V_a(t, x_a) = k_a [(1 - q_{a0})^2 + |q_{av}|^2] + \frac{1}{2} |\omega_a^{be}|^2 + \frac{\varepsilon}{2} z_a^T P_z z_a + \mu q_{av}^T \omega_a^{be} \quad (63)$$

where ε is a small positive constant to be clarified next and $\mu > 0$ is a tuning parameter.

From a simple completion of squares,

$$-\frac{\mu}{2} |q_{av}|^2 - \frac{\mu}{2} |\omega_a^{be}|^2 \leq \mu q_{av}^T \omega_a^{be} \leq \frac{\mu}{2} |q_{av}|^2 + \frac{\mu}{2} |\omega_a^{be}|^2 \quad (64)$$

it is readily checked that V_a is a Lyapunov candidate function since it verifies

$$\begin{aligned} k_a (1 - q_{a0})^2 + \frac{k_a}{2} |q_{av}|^2 + \frac{1}{4} |\omega_a^{be}|^2 + \frac{\varepsilon}{2} z_a^T P_z z_a &\leq V_a \\ &\leq k_a (1 - q_{a0})^2 + \frac{3k_a}{2} |q_{av}|^2 + \frac{3}{4} |\omega_a^{be}|^2 + \frac{\varepsilon}{2} z_a^T P_z z_a \end{aligned} \quad (65)$$

when $0 < \mu \leq \min \{k_a, \frac{1}{2}\}$.

Next, differentiating V_a with respect to time and using (54) yields $\forall t \geq T$

$$\begin{aligned} \dot{V}_a &= k_a q_{av}^T (\omega_a^{be} + \Delta_q) + (\omega_a^{be} + \mu q_{av})^T \\ &\quad \times (-k_a q_{av} - k(t) \omega_a^{be} + J_{mb}^{-1} \Delta_\omega) - \varepsilon z_a^T Q_z z_a \end{aligned} \quad (66)$$

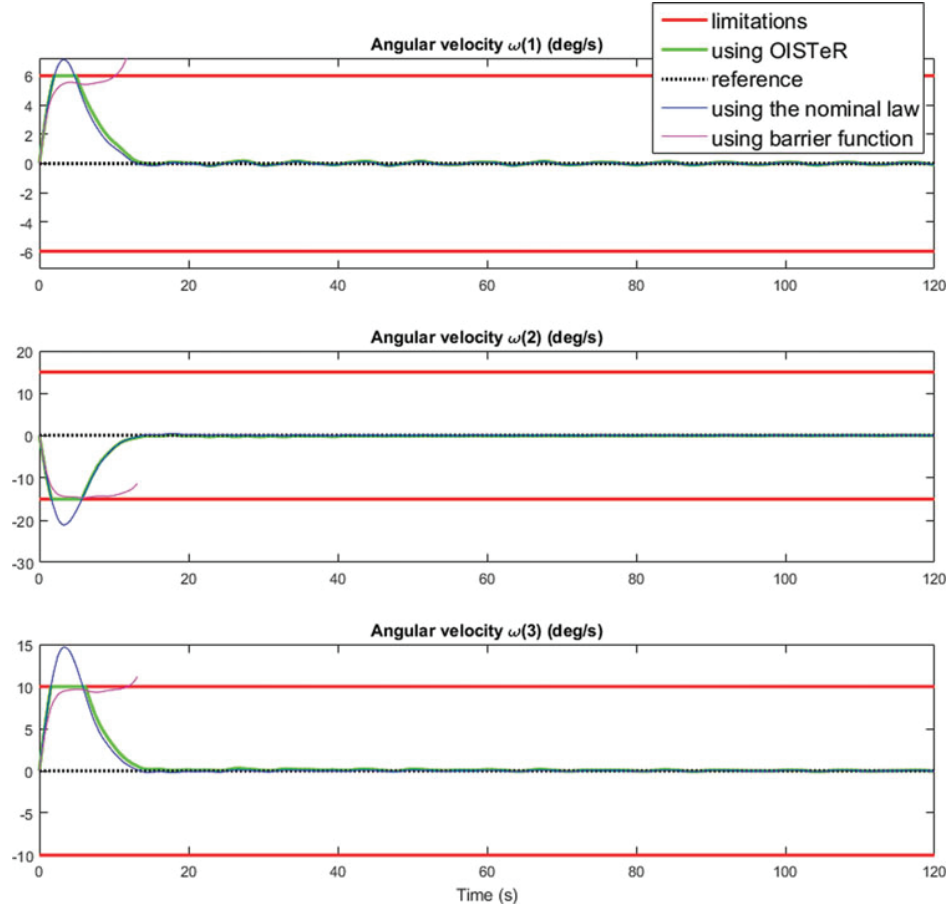


Figure 5. Scenario 3: comparison of the angular velocities on each axis with the nominal, BLF-based and enhanced (OISTeR-based) control systems.

$$+\varepsilon z_a^T P_z B_{1,z} \omega_a^{be} + \frac{\mu}{2} ((q_{a0} I_3 + S(q_{av})) \omega_a^{be})^T \omega_a^{be} \quad (67)$$

$$\leq -\mu k_a |q_{av}|^2 - k(t) |\omega_a^{be}|^2 - \varepsilon z_a^T Q_z z_a - \mu k(t) q_{av}^T \omega_a^{be} \quad (68)$$

$$+\varepsilon z_a^T P_z B_{1,z} \omega_a^{be} + \frac{\mu}{2} |\omega_a^{be}|^2 + k_a q_{av}^T \Delta_q + (\omega_a^{be} + \mu q_{av})^T J_{mb}^{-1} \Delta_\omega \quad (69)$$

Considering Equations (56) and (57), it is easily checked that

$$\forall t \geq T, \quad k_{\min} \leq k(t) \leq k_{\max} \quad (70)$$

with

$$k_{\min} = k_O + \frac{2}{\bar{\omega} - \underline{\omega}} |J_{mb}^{-1}| \bar{d}, \quad k_{\max} = k_O + \frac{4}{\bar{\omega} - \underline{\omega}} |J_{mb}^{-1}| \bar{d} \quad (71)$$

Combining (69) with (70) yields $\forall t \geq T$:

$$\dot{V}_a \leq -\mu k_a |q_{av}|^2 - k_{\min} |\omega_a^{be}|^2 - \varepsilon z_a^T Q_z z_a + \mu k_{\max} |q_{av}| |\omega_a^{be}| \quad (72)$$

$$+\varepsilon z_a^T P_z B_{1,z} \omega_a^{be} + \frac{\mu}{2} |\omega_a^{be}|^2 + k_a q_{av}^T \Delta_q + (\omega_a^{be} + \mu q_{av})^T J_{mb}^{-1} \Delta_\omega \quad (73)$$

$$\leq -x_a^T Q_a x_a + k_a q_{av}^T \Delta_q + (\omega_a^{be} + \mu q_{av})^T J_{mb}^{-1} \Delta_\omega \quad (74)$$

where

$$Q_a = \begin{bmatrix} \mu k_a & \frac{\mu k_{\max}}{2} & O \\ \frac{\mu k_{\max}}{2} & k_{\min} - \frac{\mu}{2} & -\frac{\varepsilon}{2} P_z B_{1,z} \\ O & -\frac{\varepsilon}{2} P_z B_{1,z} & \varepsilon Q_z \end{bmatrix} \quad (75)$$

which is positive definite for small values of μ and $\varepsilon > 0$.

Finally, it is convenient to bound the coupling terms between the \tilde{x} and x_a subsystems, which is the scope of the following lemma (its proof is detailed in Appendix 2)

Lemma 5.1: *there exists $\lambda > 0$ such that $\forall t \geq T$*

$$k_a q_{av}^T \Delta_q + (\omega_a^{be} + \mu q_{av})^T J_{mb}^{-1} \Delta_\omega \leq \lambda |x_a| (|\tilde{x}| + |e_z| + |\omega_r|) \quad (76)$$

Consequently, $\forall t \geq T$

$$\dot{V}_a \leq -x_a^T Q_a x_a + \lambda |x_a| (|\tilde{x}| + |e_z| + |\omega_r|) \quad (77)$$

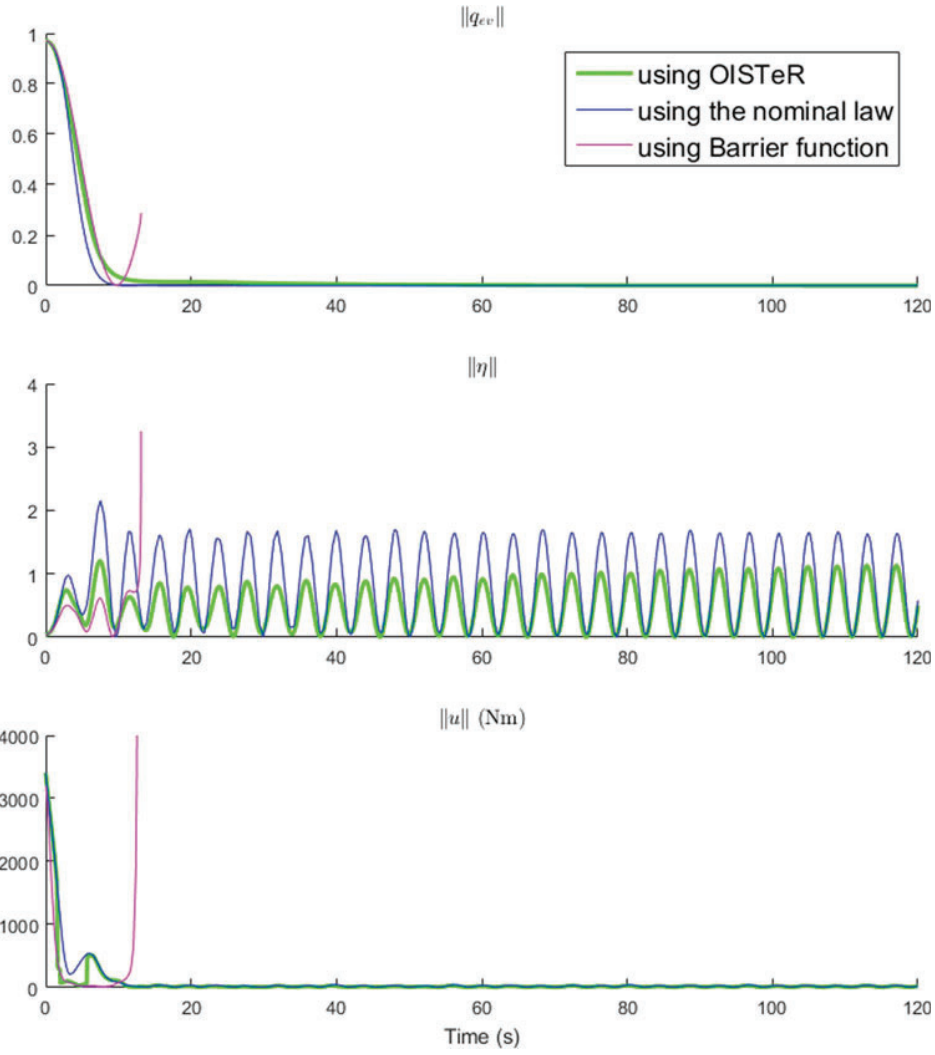


Figure 6. Scenario 3: further comparison of the nominal and enhanced controllers through the tracking error ($\|q_{ev}(t)\|$), the activity of the flexible modes ($\|\eta(t)\|$) and the control effort ($\|u(t)\|$).

ω_r (resp. \tilde{x} and e_z) being in \mathcal{L}_2 from Assumption (A4) (resp. from the proof of part 1), it readily follows from the application of Barbalat's lemma that x_a asymptotically converges to the origin. The proof is now completed.

6. Application to a flexible spacecraft attitude control problem

A realistic application to a flexible spacecraft attitude control problem of the proposed design methodology is now presented.

6.1 Numerical data

In this application, the spacecraft model described in Section 2.2 is considered with the following numerical data (borrowed from Hu, 2009):

$$J_{mb} = \begin{bmatrix} 350 & 3 & 4 \\ 3 & 270 & 10 \\ 4 & 10 & 190 \end{bmatrix} \text{ kg m}^2, \quad \delta = \begin{bmatrix} 6.46 & 1.28 & 2.16 \\ -1.26 & 0.92 & -1.67 \\ 1.12 & 2.49 & -0.84 \end{bmatrix} \text{ kg}^{1/2} \text{ m s}^{-2} \quad (78)$$

Table 1. Characteristics of the flexible modes.

	Pulsation	Damping ratio
Flexible mode #1	$\omega_1 = 0.77$ rad/s	$\xi_1 = 0.0056$
Flexible mode #2	$\omega_2 = 1.10$ rad/s	$\xi_2 = 0.0086$
Flexible mode #3	$\omega_3 = 1.87$ rad/s	$\xi_3 = 0.0130$

The characteristics of the three flexible modes are summarised in Table 1, and the angular velocity constraints are as follows:

$$\bar{\omega} = -\underline{\omega} = [6 \ 15 \ 10]^T \text{ deg/s} \quad (79)$$

6.2 Scenarios

The simulation starts from the initial state below:

$$\begin{cases} q(0) = [0.173648 & -0.263201 & 0.789603 & -0.526402]^T \\ \omega(0) = \eta(0) = \dot{\eta}(0) = [0 \ 0 \ 0]^T \end{cases}$$

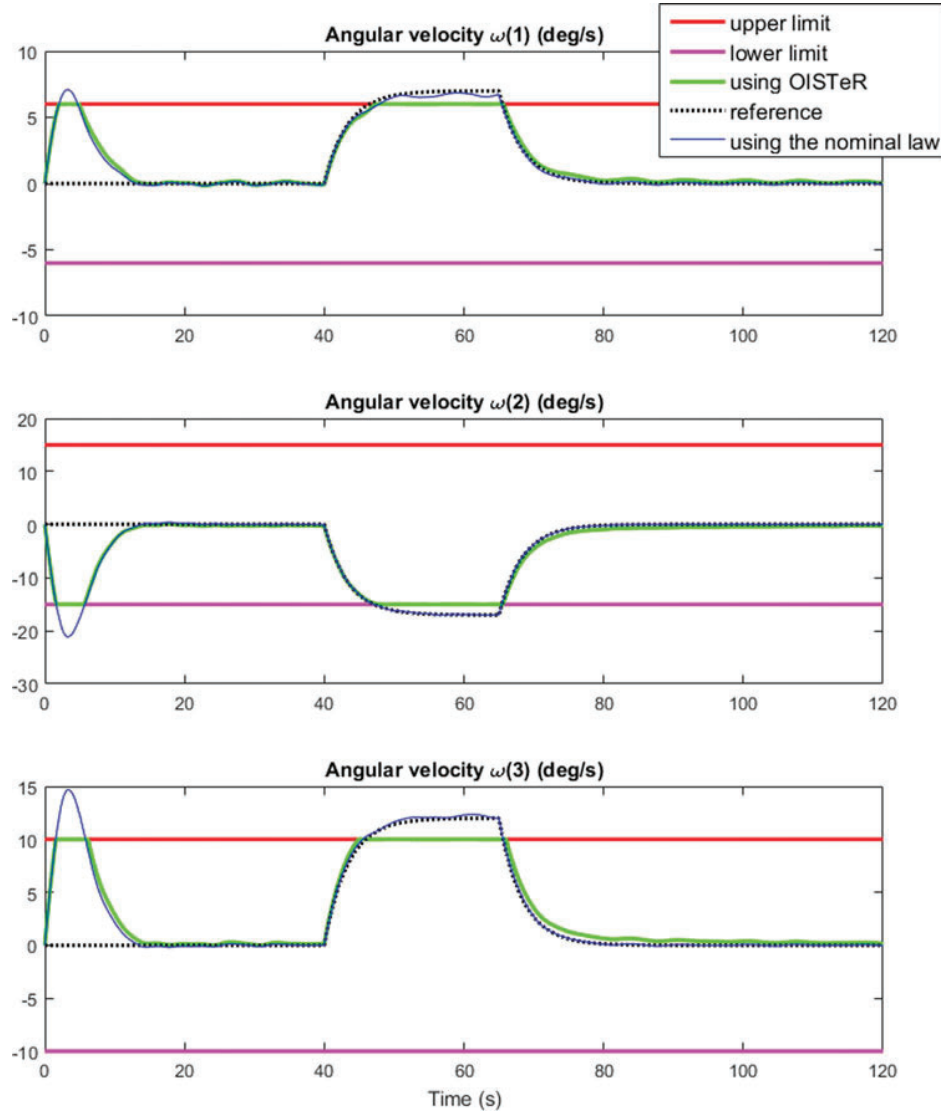


Figure 7. Scenario 4: comparison of the angular velocities on each axis with the nominal and enhanced (OISTeR-based) control systems.

We study four scenarios which are summarised in Table 2. In the stabilisation mode, the flexible satellite attitude must be set to $q_r = [1 \ 0 \ 0 \ 0]^T$.

In the tracking mode, the flexible satellite attitude shall track a reference signal $q_r(t)$ defined by its initial value $q_r(0) = [1 \ 0 \ 0 \ 0]^T$ and its time-domain variation ω_r , generated by a two-step response of a first-order filter $F_r(s) = (1 + 0.3s)^{-1}$.

Moreover, in Scenarios 2 and 4, a periodic disturbance torque is applied to the satellite:

$$d(t) = [0.3 \cos(0.01t) + 0.1 \ 0.15 \sin(0.02t) + 0.3 \cos(0.025t) \ 0.3 \sin(0.01t) + 0.1]^T \text{ N m} \quad (80)$$

Table 2. Scenarios.

	Mode	Flexible modes	Disturbance
Scenario #1	Stabilisation	Measured	Off
Scenario #2	Tracking	Measured	Off
Scenario #3	Stabilisation	Unmeasured	On
Scenario #4	Tracking	Unmeasured	On

In our interval observer design, we will then use the bound $\bar{d} = [0.5 \ 0.5 \ 0.5]^T$ N m.

6.3 Controller gains tuning and Barrier Lyapunov function-based controller design

For comparison purpose, we consider the nominal (state-feedback) control law resulting from Lemma 3.1, the enhanced (output-feedback) version resulting from Theorem 5.1 and the design of another controller using a Barrier Lyapunov function:

- the nominal control law gains are simply chosen by poles placement of the following system:

$$\dot{q}_{ev} = \omega_e \quad (81a)$$

$$J_{mb}\omega_e = -k_p q_{ev} - k_d \omega_e \quad (81b)$$

which simply consists of a linearisation of the rigid part of the closed-loop system (3a)–(3c) and (11). Here, a

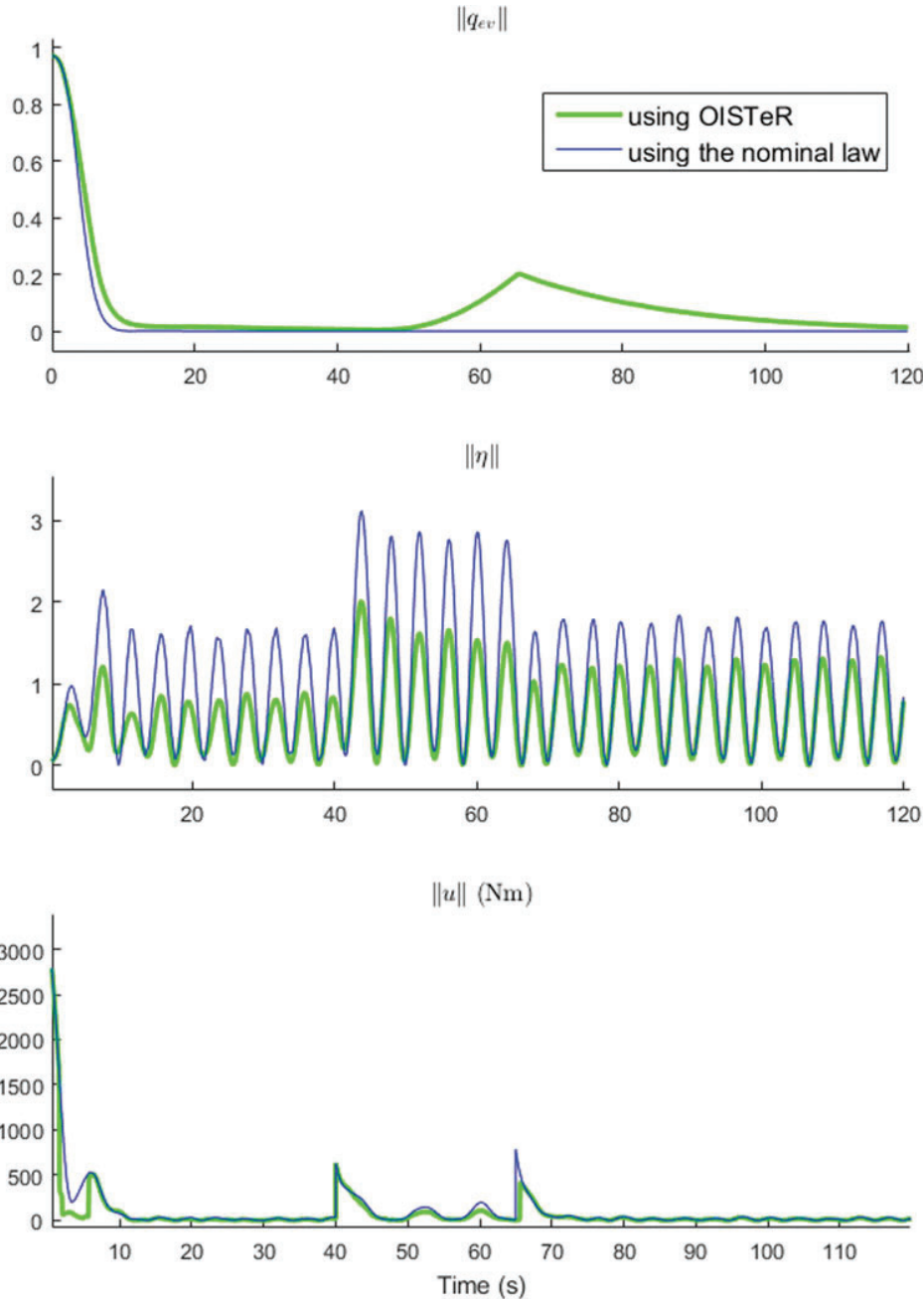


Figure 8. Further comparison of the nominal and enhanced controllers through the tracking error ($\|q_{ev}(t)\|$), the activity of the flexible modes ($\|\eta(t)\|$) and the control effort ($\|u(t)\|$).

satisfying pole placement was obtained for

$$k_p = 0.25J_{mb}(1, 1), \quad k_d = 0.1J_{mb}(1, 1) \quad (82)$$

- our enhanced control law is tuned by choosing the gains k_O , $k_a > 0$ which must satisfy inequalities (59). Given \underline{d} , $\bar{\omega}$, $\underline{\omega}$, we selected $k_a = 2$ in order to obtain $k_O \cong k_d$.
- the last controller is designed, thanks to a widely used method that is based on a Barrier Lyapunov function (BLF) (detailed e.g. in Tee, Ge, & Tay, 2009); such a Lyapunov

function grows to infinity whenever the state reaches some constraints. To facilitate reading this section, the design of such a controller is detailed in Appendix 3.

The tuning gains k_p , k_d are those defined above; it remains to choose the gains $\chi > 0$ and $k_{bi} > 0$ ($i \in \{1, 3\}$). According to Appendix 3 and given a reference ω_r which satisfies for all time and for all $i \in \{1, 3\}$, $|\omega_r(i)| < \bar{\omega}_r$, these gains must satisfy

$$\forall i \in \{1, 3\}, 0 \leq k_{bi} + \bar{\omega}_r + \chi \leq \min\{\underline{\omega}(i), \bar{\omega}(i)\} \quad (83)$$

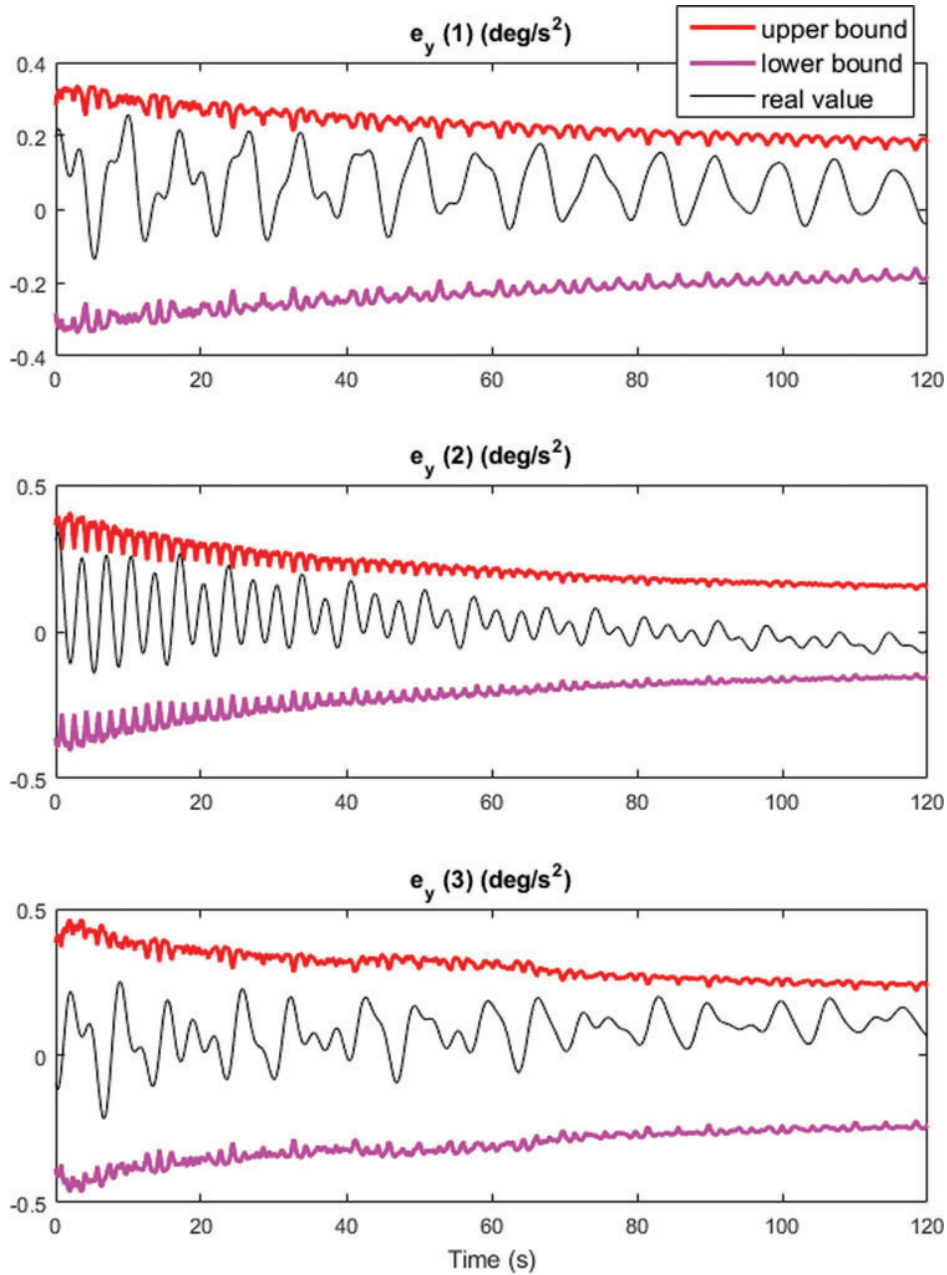


Figure 9. Scenario 4: interval observer (bounds detection on the unmeasured disturbance torque e_y).

We then choose $\chi = 0.1$ to allow k_{bi} being large and obtain

$$k_{bi} = \min\{\underline{\omega}(i), \bar{\omega}(i)\} - \bar{\omega}_r - \chi \quad (84)$$

Note that the condition $k_{bi} \geq 0$ limits the value of $\bar{\omega}_r$ and so the reference to follow.

6.4 Nonlinear simulations results

The spacecraft model with both nominal and enhanced control laws has been implemented in SIMULINKTM files. Following the scenarios presented in Section 6.2, nonlinear simulations have been performed on a time range from 0 to 120 s.

6.4.1 Scenario 1 (state feedback stabilisation in the absence of a disturbance)

The results are presented in Figures 1 and 2.

Next, the angular velocities on the three axes are displayed in Figure 1 where a comparison between the nominal, BFL and enhanced controllers is proposed. As expected, every time a step input is applied, the angular velocities exceed the constraints on each axis when the nominal controller is used. This is however no longer the case with both the BLF and enhanced control systems. In this case indeed, the velocities are always kept in the prescribed limits. However, the limitations of the BLF synthesis (6.4.4) impose choosing $\chi > 0$ sufficiently small which increases the time response. As a result, our enhanced controller (which

is not subjected to such limitations) outperforms the BLF controller.

6.4.2 Scenario 2 (state feedback reference tracking in the absence of a disturbance)

The results are presented in Figures 3 and 4.

We can make the same comments as in Scenario 1. In addition, note that one more time the use of a BLF constrains the reference to follow to be very small in virtue of (6.4.4).

6.4.3 Scenario 3 (output feedback stabilisation in the presence of a disturbance)

The results are presented in Figures 5 and 6. Since now the flexible modes z are unmeasured, all the controllers here use \hat{z} (defined by Equation (20c)). This time the BLF controller diverges: it is not robust to the disturbance and to the observation error. Note that our enhanced controller still continues to give satisfactory responses.

6.4.4 Scenario 4 (output feedback reference tracking in the presence of a disturbance)

As before, the results are presented in Figures 7 and 8. This scenario appears to be the more demanding and deserves more comments. Note that here the BLF controller is not applied; indeed, as discussed before, it is not robust and cannot be applied here because the use of a reference signal which can exceed the ω limitations (for a while) cannot be taken into account with such a method because of the limitations. As clarified in the paper, the use of an interval observer of the unmeasured disturbance torque is essential in our approach to enforce the angular rates constraints in Scenarios 3 and 4. Note that an additional Figure 9 illustrates the behaviour of the interval observer. The tightness of the computed bounds as a function of time is clearly visualised.

The comparison of the nominal and enhanced controllers is further investigated in Figure 8.

- The first subplot (upper) illustrates the time-domain evolution of the tracking error (via the norm of the quaternion error $\|q_{ev}(t)\|$). It is easily observed that the nominal controller outperforms the OISTeR-based solution. But this is not surprising since velocity constraints are not respected in the first case. More precisely, when comparing both plots, the price to pay for constraints satisfaction is clearly visualised between $t \cong 50$ s and $t \cong 65$ s. During this time interval, the reference quaternion is no longer tracked by the enhanced system. Next, the error starts to decrease as soon as the anti-windup loop becomes active.
- The second subplot (middle) illustrates the activity of the flexible mode. Quite interestingly, it is observed that the excitation of the flexible modes is considerably lower when the enhanced controller is used. Here again, this is not surprising since the angular velocities are now controlled.
- The last and third subplot (lower) illustrates the control activity which, as expected also, is significantly lower when the OISTeR-based system is used.

7. Conclusions

The problem of output-feedback trajectory tracking of flexible spacecraft attitude under angular velocity constraints has been addressed in this paper. Given a nominal controller which solves the tracking problem in the full state-feedback case without velocity constraints, it is proven that the general problem can be solved by saturating the nominal controller by an output to input saturation. Such a saturated control law is then applied in combination with a nonlinear anti-windup loop. Note that one key feature of this result is to use an interval observer not only to estimate the flexible modes but also to provide at each instant their lower and upper bounds, which is crucial to ultimately guarantee the satisfaction of the velocity constraints.

As discussed earlier, limiting the angular velocity is a first step towards using a more detailed spacecraft model incorporating some reaction wheels. In future research, we plan to keep up our efforts in this direction and thus to validate our methodology on a benchmark of the DEMETER satellite (Pittet & Arzelier, 2006).

Disclosure statement

No potential conflict of interest was reported by the authors.

References

- Akella, M., Thakur, D., & Mazenc, F. (2015). Partial Lyapunov stratification: Smooth angular velocity observers for attitude tracking control. *Journal of Guidance, Control, and Dynamics*, 38(3), 442–451.
- Biannic, J.-M., Roos, C., & Pittet, C. (2011). Linear parameter varying analysis of switched controllers for attitude control systems. *Journal of Guidance, Control, and Dynamics*, 34(5), 1561–1567.
- Burlion, L. (2012). A new saturation function to convert an output constraint into an input constraint. In *20th Mediterranean conference on control automation (MED)* (pp. 1217–1222). Barcelona: IEEE.
- Chambon, E., Burlion, L., & Apkarian, P. (2015a). Output to input saturation transformation: Demonstration and application to disturbed linear systems. In *IEEE 54th annual conference on decision and control (CDC)* (pp. 7566–7571).
- Chambon, E., Burlion, L., & Apkarian, P. (2015b). Robust output interval constraint using O/I saturation transformation with application to uncertain linear launch vehicle. In *European control conference (ECC)* (pp. 1802–1807). Linz: IEEE.
- Chambon, E., Burlion, L., & Apkarian, P. (2017). Time-response shaping using output to input saturation transformation. *International Journal of Control*. doi:10.1080/00207179.2017.1286043
- Chen, Z., & Huang, J. (2009). Attitude tracking and disturbance rejection of rigid spacecraft by adaptive control. *IEEE Transactions on Automatic Control*, 54(3), 600–605.
- Di Gennaro, S. (2002). Output attitude tracking for flexible spacecraft. *Automatica*, 38(10), 1719–1726.
- Galeani, S., Tarbouriech, S., Turner, M., & Zaccarian, L. (2009). A tutorial on modern anti-windup design. *European Journal of Control*, 15(3-4), 418–440.
- Gennaro, S. D. (2003). Output stabilization of flexible spacecraft with active vibration suppression. *IEEE Transactions on Aerospace and Electronic Systems*, 39(3), 747–759.
- Glattfelder, A., & Schaufelberger, W. (2003). *Control systems with input and output constraints*. London: Springer.
- Goodwin, G. C., Seron, M., & de Dona, J. (2004). *Constrained control and estimation: An optimization approach*. London: Springer.
- Gupta, R., Kalabic, U. V., Cairano, S. D., Bloch, A. M., & Kolmanovskiy, I. V. (2015). Constrained spacecraft attitude control on SO(3) using fast nonlinear model predictive control. In *American control conference (ACC)* (pp. 2980–2986). Chicago: IEEE.
- Hegrenæs, O., Gravdahl, J., & Tondel, P. (2005). Spacecraft attitude control using explicit model predictive control. *Automatica*, 41(12), 2107–2114.

- Hu, Q. (2009). Robust adaptive backstepping attitude and vibration control with L_2 -gain performance for flexible spacecraft under angular velocity constraint. *Journal of Sound and Vibration*, 327(35), 285–298.
- Lovera, M., & Astolfi, A. (2004). Spacecraft attitude control using magnetic actuators. *Automatica*, 40(8), 1405–1414.
- Luzi, A.-R., Peaucelle, D., Biannic, J.-M., Pittet, C., & Mignot, J. (2014). Structured adaptive attitude control of a satellite. *International Journal of Adaptive Control and Signal Processing*, 28(7–8), 664–685.
- Mazenc, F., & Bernard, O. (2010). Asymptotically stable interval observers for planar systems with complex poles. *IEEE Transactions on Automatic Control*, 55(2), 523–527.
- Mazenc, F., & Bernard, O. (2011). Interval observers for linear time-invariant systems with disturbances. *Automatica*, 47(1), 140–147.
- Pittet, C., & Arzelier, D. (2006). DEMETER: A benchmark for robust analysis and control of the attitude of flexible micro satellites. *IFAC Proceedings Volumes*, 39(9), 661–666 (5th IFAC symposium on robust control design).
- Tarbouriech, S., & Turner, M. (2009). Anti-windup design: An overview of some recent advances and open problems. *Control Theory Applications, IET*, 3(1), 1–19.
- Tayebi, A. (2008). Unit quaternion-based output feedback for the attitude tracking problem. *IEEE Transactions on Automatic Control*, 53(6), 1516–1520.
- Tee, K., Ge, S., & Tay, E. (2009). Barrier Lyapunov functions for the control of output-constrained nonlinear systems. *Automatica*, 45(4), 918–927.
- Tréguët, J.-F., Arzelier, D., Peaucelle, D., Pittet, C., & Zaccarian, L. (2015). Reaction wheels desaturation using magnetorquers and static input allocation. *IEEE Transactions on Control Systems Technology*, 23(2), 525–539.
- Xiao, B., Yin, S., & Kaynak, O. (2017). Attitude stabilization control of flexible satellites with high accuracy: An estimator-based approach. *IEEE/ASME Transactions on Mechatronics*, 22(1), 349–358.
- Xiao, B., Yin, S., & Wu, L. (2017). A structure simple controller for satellite attitude tracking maneuver. *IEEE Transactions on Industrial Electronics*, 64(2), 1436–1446.
- Zhang, X., & Cheng, D. (2012). Nonlinear internal model based attitude tracking and disturbance rejection. *Asian Journal of Control*, 14(5), 1397–1402.
- Zhang, H.-H., Wang, F., & Trivailo, P. (2008). Spin-axis stabilisation of underactuated rigid spacecraft under sinusoidal disturbance. *International Journal of Control*, 81(12), 1901–1909.

Appendix 1. Construction of the lower and upper bounds of the missing variables

First of all, let us introduce the following notation. Note that this notation (which is very specific and merely used in this appendix) was not given before to avoid breaking the flow of the paper derivations.

Notation: we introduce the following two functions (as in Mazenc & Bernard, 2010):

$$\mathcal{L}(s) = \max\{0, s\}, \quad \mathcal{M}(s) = \min\{0, s\} \quad (\text{A1})$$

Then, given a time-varying matrix $\Pi(t)$, we define

$$\Pi_p(t) = (\mathcal{L}(\Pi_{i,j}(t))), \quad \Pi_m(t) = (\mathcal{M}(\Pi_{i,j}(t))), \quad (\text{A2})$$

As a consequence of $|s| = \mathcal{L}(s) - \mathcal{M}(s)$, one has $|\Pi(t)| = \Pi_p(t) - \Pi_m(t)$, such an equality being understood element-wise.

Let us now detail the procedure we applied to compute some lower and upper bounds for the missing quantity e_y defined by (22).

Clearly, the observation error $e_z = z - \hat{z}$ undergoes the following dynamics:

$$\dot{e}_z = A_z e_z \quad (\text{A3})$$

A_z being Hurwitz, an interval observer can be easily designed for e_z . Indeed, using the results of Mazenc and Bernard (2011), there exists a change of coordinates $\zeta = Q(t)e_z$ and a Hurwitz Metzler matrix M such that the following is an interval observer for ζ

$$\begin{cases} \dot{\zeta}^+ = M\zeta^+ \\ \dot{\zeta}^- = M\zeta^- \end{cases} \quad (\text{A4})$$

where $\zeta^+(0) = \zeta_0^+$ (resp. $\zeta^-(0) = \zeta_0^-$) are given by

$$\begin{cases} \zeta_0^+ = Q_p(0) \frac{z_0^+ - z_0^-}{2} - Q_m(0) \frac{z_0^+ - z_0^-}{2} = |Q(0)| \frac{z_0^+ - z_0^-}{2} \\ \zeta_0^- = Q_m(0) \frac{z_0^+ - z_0^-}{2} - Q_p(0) \frac{z_0^+ - z_0^-}{2} = -|Q(0)| \frac{z_0^+ - z_0^-}{2} \end{cases} \quad (\text{A5})$$

Then, it is possible to bound the output e_y since

$$e_y = J_{mb}^{-1} (-S(\omega)G_z e_z + C_z e_z + d) \quad (\text{A6})$$

$$= J_{mb}^{-1} ((-S(\omega)G_z + C_z)Q(t)^{-1}\zeta + d) \quad (\text{A7})$$

$$:= \Pi(t, \omega)\zeta + J_{mb}^{-1}d \quad (\text{A8})$$

Indeed, it is readily seen that $e_y \in [\underline{e}_y, \bar{e}_y]$ where

$$\begin{cases} \bar{e}_y := \Pi_p(t, \omega)\zeta^+ + \Pi_m(t, \omega)\zeta^- + |J_{mb}^{-1}|\bar{d} \\ \underline{e}_y := \Pi_m(t, \omega)\zeta^+ + \Pi_p(t, \omega)\zeta^- - |J_{mb}^{-1}|\bar{d} \end{cases} \quad (\text{A9})$$

which simplifies as follows:

$$\begin{cases} \bar{e}_y := |\Pi(t, \omega)|\zeta^+ + |J_{mb}^{-1}|\bar{d} \\ \underline{e}_y := -\bar{e}_y \end{cases} \quad (\text{A10})$$

Indeed, it readily follows from (A4) and (A5) that $\forall t, \zeta^+(t) = -\zeta^-(t)$.

Appendix 2. Proof of Lemma 5.1

The proof of Lemma 5.1 readily follows from the proofs of the two following inequalities:

- (1) there exists $\lambda_4, \lambda_5, \lambda_6 > 0$ such that $\forall t \geq T$:

$$(\omega_a^b + \mu q_{av})^T \Delta_\omega \leq \lambda_4 |x_a| |\tilde{x}| + \lambda_5 |x_a| |e_z| + \lambda_6 |x_a| |\omega_r| \quad (\text{B1})$$

- (2) there exists $\lambda_7 > 0$ such that

$$q_{av}^T \Delta_q \leq \lambda_7 |x_a| |\tilde{x}| \quad (\text{B2})$$

B1 Part 1

Starting from Equation (50), we obtain (B4) by using (11), (38a)–(38c) and (52) :

$$\begin{aligned} (\omega_a^b + \mu q_{av})^T \Delta_\omega &= (\omega_a^b + \mu q_{av})^T (OISat(u_a + \tilde{u}_n) - OISat(u_a) \\ &\quad - \tilde{u}_n + N(\tilde{\omega} + \omega_r^b, \tilde{\omega}, \hat{z}, \omega_r^b) \\ &\quad + (N(\omega, \omega_a^{be}, z_a, 0) - N(\omega, \omega_e, \hat{z}_e, \omega_r^b))) \\ &\leq 3(1 + \mu)|x_a|(\lambda_{\max}(J_{mb})|\Delta_S| + |\tilde{\Delta}|) \end{aligned} \quad (B4)$$

where

$$\Delta_S := Sat_{k(t)\tilde{\omega} + \tilde{e}_y}^{k(t)\tilde{\omega} - \tilde{e}_y}(\alpha + k(t)\omega) - Sat_{k(t)\tilde{\omega} + \tilde{e}_y}^{k(t)\tilde{\omega} - \tilde{e}_y}(\alpha_a + k(t)\omega_a^{be}) \quad (B5)$$

$$\begin{aligned} \tilde{\Delta} &:= J_{mb}(-k(t)\tilde{\omega}) - C_z \tilde{z} - D_z \tilde{\omega} - \tilde{u}_n - N(\omega, \tilde{\omega}, \hat{z}, \omega_r^b) \\ &\quad - C_z(z_r - e_z) - (J_{mb}k(t) + D_z)\omega_r^b \end{aligned} \quad (B6)$$

Looking at (38b)–(53), we observe that

$$\begin{aligned} \alpha + k(t)\omega &= \alpha_a + k(t)\omega_a^{be} + k(t)(\tilde{\omega} + \omega_r^b) \\ &\quad + J_{mb}^{-1}(N(\omega, \omega_a^{be}, z_a, 0) - N(\omega, \omega, \hat{z}, 0) \\ &\quad + \tilde{u}_n + C_z(\tilde{z} - e_z + z_r) + D_z(\tilde{\omega} + \omega_r)) \end{aligned} \quad (B7)$$

Substituting (B7) in (B5) and using the fact that *Sat* is 1-Lipschitz yields

$$|\Delta_S| \leq |k(t)(\tilde{\omega} + \omega_r^b) + J_{mb}^{-1}(N(\omega, \omega_a^{be}, z_a, 0) - N(\omega, \omega, \hat{z}, 0) + \tilde{u}_n + C_z(\tilde{z} - e_z + z_r) + D_z(\tilde{\omega} + \omega_r))| \quad (B8)$$

$$\leq |k(t)(\tilde{\omega} + \omega_r^b) + J_{mb}^{-1}(-N(\omega, \tilde{\omega} + \omega_r^b, \hat{z} + z_r, 0) + \tilde{u}_n + C_z(\tilde{z} - e_z + z_r) + D_z(\tilde{\omega} + \omega_r))| \quad (B9)$$

Looking at the expressions (6) (resp. (11)–(38a)) of *N* (resp. \tilde{u}) and bearing in mind the fact that ω is bounded and $k(t)$ is dominated by a constant $k_{\max} > 0$ for $t \geq T$, it is not difficult to see that $|\Delta_S|$ (resp. $|\tilde{\Delta}|$) given by (B9) (resp. (B6)) is Lipschitz with respect to the variables \tilde{x} , e_z and ω_r for all $t \geq T$. The proof of (B1) readily follows from this fact plus the use of (B4).

B2 Part 2

Starting from Equation (48), one can successively prove that

$$\begin{aligned} q_{av}^T \Delta_q &= q_{av}^T (R(\tilde{q})^T - I_3) \omega_a^{be} \\ &= q_{av}^T ((\tilde{q}_0^2 - \tilde{q}_v^T \tilde{q}_v - 1)I_3 + 2\tilde{q}_v \tilde{q}_v^T - 2\tilde{q}_0 S(\tilde{q}_v)) \omega_a^{be} \\ &= q_{av}^T (-2\tilde{q}_v^T \tilde{q}_v I_3 + 2\tilde{q}_v \tilde{q}_v^T - 2\tilde{q}_0 S(\tilde{q}_v)) \omega_a^{be} \\ &= q_{av}^T (2S(\tilde{q}_v)^2 - 2\tilde{q}_0 S(\tilde{q}_v)) \omega_a^{be} \\ &= 2q_{av}^T (S(\tilde{q}_v) - \tilde{q}_0 I_3) S(\tilde{q}_v) \omega_a^{be} \end{aligned} \quad (B10)$$

$$\leq 2|q_{av}|(\sqrt{2}|\tilde{q}_v| + 1)\sqrt{2}|\tilde{q}_v| |\omega_a^{be}| \quad (B11)$$

$$\begin{aligned} &\leq 2(2 + \sqrt{2})|\tilde{q}_v| |\omega_a^{be}| \\ &\leq 8|\tilde{x}| |x_a| \end{aligned} \quad (B12)$$

where (B10) is obtained by using the relation $S(x)^2 = -(x^T x)I_3 + xx^T$, where (B11) is obtained by using the relation $|S(q_v)| \leq \sqrt{2}|q_v|^2 = \sqrt{2}|q_v|$ which readily follows from the well-known relation $|A| \leq |A|_F = \sqrt{\text{trace}(A^T A)}$ (substituting A for $S(q_v)$).

The proof is thus completed for any $\lambda_7 \geq 8$.

Appendix 3. Barrier Lyapunov function construction

Our Lyapunov-based control method is naturally compared to the most used one known as barrier function Lyapunov function-based control design. To the best of our knowledge, such a method has been mainly used in the state feedback context in the absence of disturbance. Of course, extending here such a method is outside the scope of the present work.

Let us then consider the following error system:

$$\dot{q}_e = \frac{1}{2}E(q_e)\omega_e \quad (C1a)$$

$$J_{mb}\dot{\omega}_e = -N(\omega, \omega_e, z_e, \omega_r^b) + u + C_z z_e + D_z \omega_e - J_{mb}\dot{\omega}_r^b \quad (C1b)$$

$$\dot{z}_e = A_z z_e + B_{1,z}\omega_e + B_{2,z}\dot{\omega}_r^b \quad (C1c)$$

$$(C1d)$$

Lemma 3.1 suggests using the following Lyapunov function in the absence of angular velocity constraints:

$$\begin{aligned} V &= (k_p + \chi k_d)((1 - q_{e0}^2) + |q_{ev}|^2) + \frac{1}{2}(\chi q_{ev} \\ &\quad + \omega_e)^T J_{mb}(\chi q_v + \omega_e) + \frac{\varepsilon}{2}z_e^T P_z z_e \end{aligned} \quad (C2)$$

note that here we introduce an additional tuning parameter $\chi > 0$ which will be discussed below. (note that when $\chi = 1$, one finds again the Lyapunov function used in Lemma 3.1). After a few computations, choosing the following control law:

$$\begin{aligned} u &= -k_p q_{ev} - k_d \omega_e - \chi J_{mb} \dot{q}_{ev} + N(\omega, \omega_e, z_e, \omega_r^b) \\ &\quad - C_z z_e - D_z \omega_e + J_{mb} \dot{\omega}_r^b \end{aligned} \quad (C3)$$

one obtains

$$\dot{V} \leq -[q_{ev} \ \omega_e \ z_e] Q [q_{ev} \ \omega_e \ z_e]^T \quad (C4)$$

where matrix Q (given by (43)) is positive definite for $\varepsilon > 0$ sufficiently small. As a result, the closed-loop system is GAS.

Following the ideas of Tee et al. (2009), the proposed design procedure is the following one:

- Step 1: redesign V as follows:

$$\begin{aligned} W &= (k_p + \chi k_d)((1 - q_{e0}^2) + |q_{ev}|^2) \\ &\quad + \frac{1}{2} \sum_{i=1:3} J_{mb}(i, i) k_{b_i}^2 \log \left(\frac{k_{b_i}^2}{k_{b_i}^2 - (\chi q_{ev}(i) + \omega_e(i))^2} \right) \\ &\quad + \frac{\varepsilon}{2} z_e^T P_z z_e \end{aligned} \quad (C5)$$

where $k_{b_i} > 0$ ($i \in \{1, 3\}$).

- Step 2: computing the derivative of W , the control law is finally designed as

$$u = \mathcal{B}(q_{ev}, \omega_e)(-k_p q_{ev} - k_d \omega_e) - \chi J_{mb} \dot{q}_{ev} + N(\omega, \omega_e, z_e, \omega_r^b) - C_z z_e - D_z \omega_e + J_{mb} \dot{\omega}_r^b \quad (C6)$$

where

$$\mathcal{B}(q_{ev}, \omega_e) = J_{mb} \begin{bmatrix} \frac{k_{b_1}^2 - (\chi q_{ev}(1) + \omega_e(1))^2}{k_{b_1}^2 J_{mb}(1, 1)} & 0 & 0 & 0 \\ 0 & \frac{k_{b_2}^2 - (\chi q_{ev}(2) + \omega_e(2))^2}{k_{b_2}^2 J_{mb}(2, 2)} & 0 & 0 \\ 0 & 0 & \frac{k_{b_3}^2 - (\chi q_{ev}(3) + \omega_e(3))^2}{k_{b_3}^2 J_{mb}(3, 3)} & 0 \end{bmatrix} \quad (C7)$$

Indeed, using such a controller one obtains

$$\dot{W} \leq -[q_{ev} \ \omega_e \ z_e] Q [q_{ev} \ \omega_e \ z_e]^T \quad (C8)$$

which proves that the closed-loop system is GAS.

- Step 3: according to Lemma 1 of Tee et al. (2009), we have

$$\forall t > 0, \forall i \in \{1, 3\}, |\chi q_{ev}(i) + \omega_e(i)| < k_{b_i} \quad (C9)$$

provided such inequalities are satisfied at $t = 0$. So, given a reference $\omega_r(t)$ which satisfies $\forall t, \forall i \in \{1, 3\}, |\omega_r(i)| < \bar{\omega}_r$ where $\bar{\omega}_r > 0$, it is clear that $\forall t, \forall i \in \{1, 3\}, |\omega_r^b(i)| \leq \bar{\omega}_r$ and that

$$|\omega(i)| < k_{b_i} + \bar{\omega}_r + \chi \quad (C10)$$

since $|q_{ev}(i)| \leq 1$. Therefore, $\omega(i)$ will finally satisfy its constraints $-\underline{\omega}(i) \leq \omega(i) \leq \bar{\omega}(i)$ if:

$$0 \leq k_{b_i} + \bar{\omega}_r + \chi \leq \min\{\underline{\omega}(i), \bar{\omega}(i)\}. \quad (C11)$$

Overview of linear time-invariant interval observer design: towards a non-smooth optimisation-based approach

Emmanuel Chambon , Laurent Burlion, Pierre Apkarian

Onera – The French Aerospace Lab, 2 avenue Édouard Belin, FR-31055 Toulouse Cedex 4, France

✉ E-mail: Emmanuel.Chambon@onera.fr

ISSN 1751-8644

Received on 31st July 2015

Revised on 3rd March 2016

Accepted on 13th March 2016

doi: 10.1049/iet-cta.2015.0742

www.ietdl.org

Abstract: Some applications in control require the state vector of a system to be expressed in the appropriate coordinates so as to satisfy to some mathematical properties which constrain the studied system dynamics. This is the case with the theory of linear interval observers which are trivial to implement on cooperative systems, a rather limited class of control systems. The available literature shows how to enforce this limiting cooperativity condition for any considered system through a state-coordinate transformation. This study proposes an overview of the existing numerical techniques to determine such a transformation. It is shown that in spite of being practical, these techniques have some limitations. Consequently, a reformulation of the problem is proposed so as to apply non-smooth control design techniques. A solution is obtained in both the continuous- and discrete-time frameworks. Interestingly, the new method allows to formulate additional control constraints. Simulations are performed on three examples.

1 Introduction

To be applicable, many observation and control strategies applied to linear systems are required to comply with some constraints on the designed dynamics. These constraints are expressed through mathematical properties which should be satisfied by the resulting system state-space representation matrices. For example, considering the case of interval observers [1], a constructive cooperativity condition [2] on the observation error dynamics is looked for, which is linked to properties of the resulting state matrix. In the continuous-time (CT) case, this matrix should be Metzler which means that its off-diagonal elements should be positive. For a given system, this property is rarely satisfied in the original state coordinates. However, a change of coordinates can be calculated so that cooperativity is satisfied in the new coordinates [3, 4]. Various techniques – which are detailed in this paper – currently exist to determine such a transformation. Their advantages lie in their simplicity. However, they rely on ‘first guess’ and are hardly compatible with additional constraints related to control performance. In the case of interval observers, it may be expected that the error dynamics should satisfy to additional constraints like disturbances rejection. To the authors opinion, the fact that the observer gain and the state-coordinate transform cannot be simultaneously computed to satisfy to the Metzler property and to an additional disturbance rejection constraint is a limit to these methods.

An overview of the aforementioned existing techniques is presented in this paper. Their limitations motivate a reformulation of the problem. This is presented in this paper both in the CT and discrete-time (DT) frameworks. This leads to an optimisation problem which is solved using non-smooth optimisation techniques usually dedicated to control design. Using such techniques, additional control constraints can be taken into account in the determination of the appropriate state-coordinate transformation. This paper extends the preliminary results presented in [5]. This approach was motivated by the interval observers cooperativity requirement, but it is expected to be generalisable to any problem requiring specific structures of the matrices of the studied system. It is important to understand that no theoretical addition is brought to the existing interval observer framework, but rather on a computation-related sub-problem. Note that the use of time-varying changes of coordinates [3] is not considered since our method is not applicable in this case.

The core of the technique is to reformulate the mathematical conditions on a matrix – like the Metzler requirement on the state-matrix – into a stabilisation control problem. Using recent theoretical results [6] of the structured controller synthesis field, a control law synthesis is then performed on multiple models in view of the specified control requirements. The approach is applied to various examples of interval observer problems. Numerical and simulation results are compared to the ones obtained using the existing techniques.

This paper is organised as follows. The notations and definitions required to understand the motivations and the resulting computation-related problems are presented in Section 2. The theory of interval observers is recalled in Section 3. In the same section, an overview of the existing techniques to compute the necessary state-coordinate transformation is performed. This raises a difficult numerical problem which is described in Section 4. A solution based on multiple models control law synthesis is proposed in Section 5 for both the CT and DT frameworks. The approach is then applied on various examples in Section 6 before concluding in Section 7.

2 Notations and definitions

The Laplace transform is denoted s and the Z-transform is denoted z . Let denote \mathbb{Z} is the set of integers, \mathbb{R} is the set of real numbers and \mathbb{R}_+ is the set of positive real numbers. Let $\mathbb{Z}_+ = \mathbb{Z} \cap \mathbb{R}_+$. If not otherwise stated, the indices (i, j, k, l, m, n) are integers in \mathbb{Z}_+ . The H_2 -norm of a transfer function $T(s)$ (resp. $T(z)$) is denoted $\|T(s)\|_2$ (resp. $\|T(z)\|_2$) and is defined as

$$\|T(s)\|_2 = \sqrt{\frac{1}{2\pi} \int_{-\infty}^{\infty} \text{tr} [T(j\omega)^* T(j\omega)] d\omega}$$

resp. $\|T(z)\|_2 = \sqrt{(1/2\pi) \int_{-\pi}^{\pi} \text{tr} [T(e^{j\omega})^* T(e^{j\omega})] d\omega}$, where ‘tr’ is the trace operator and $T(j\omega)^*$ the conjugate transpose of $T(j\omega)$. The elements of a matrix $A \in \mathbb{R}^{n \times m}$ are referred to using the lower-case notation a_{ij} where $i \leq n$ and $j \leq m$. The ordering operators $>$, $<$, \leq and \geq are understood component-wise when applied to multi-dimensional signals. Known (or computed) time-varying bounds on

a multi-dimensional signal $x \in \mathbb{R}^n$ are denoted $\underline{x}(t)$ and $\bar{x}(t)$

$$\forall t, \underline{x}(t) \leq x(t) \leq \bar{x}(t) \quad (1)$$

In this paper, only linear time-invariant (LTI) systems are considered. In the CT case, let an LTI system (G) be defined by

$$(G) \begin{cases} \dot{x} = Ax + B_1u + B_2d \\ y = Cx \\ x(0) = x_0 \end{cases} \quad (2)$$

where $x \in \mathbb{R}^n$, $u \in \mathbb{R}$, $d \in \mathbb{R}$ and matrices are of appropriate dimensions.

Definition 1 (Interval observer, CT): Suppose quantities $\underline{x}_0, \bar{x}_0$ and signals $\underline{d}(t), \bar{d}(t)$ are known such that $\underline{x}_0 \leq x_0 \leq \bar{x}_0$ and $\underline{d}(t) \leq d(t) \leq \bar{d}(t), \forall t$. Then, the dynamical system

$$(G^\sharp) \begin{cases} \dot{z} = A^\sharp z + B_1^\sharp u + B_2^\sharp \begin{bmatrix} \underline{d} \\ \bar{d} \end{bmatrix} \in \mathbb{R}^{2n} \\ \begin{bmatrix} x \\ \bar{x} \end{bmatrix} = C^\sharp z \end{cases} \quad \text{with rank}(C^\sharp) = 2n \quad (3)$$

associated with the initial condition $z_0 = (C^{\sharp\top} C^\sharp)^{-1} [\underline{x}_0 \ \bar{x}_0]^\top$, where the newly defined matrices are of appropriate dimensions, is a linear interval observer of the system (G) in (2) if, see [7, Definition 4]:

- i. (G^\sharp) is input-to-state stable.
- ii. The solutions to (2) and (3) with, respectively, x_0 and z_0 as initial conditions are defined $\forall t \in \mathbb{R}_+$ and fulfil

$$\underline{x}(t) \leq x(t) \leq \bar{x}(t), \quad \forall t$$

- iii. If $|\bar{d}(t) - \underline{d}(t)|$ is uniformly bounded then $\|\bar{x}(t) - \underline{x}(t)\|$ is also uniformly bounded and if $\underline{d}(t) = \bar{d}(t), \forall t \in \mathbb{R}_+$ then $\|\bar{x}(t) - \underline{x}(t)\| \rightarrow 0$.

A similar definition is obtained in the DT case. This definition means that any system can be an interval observer as long as the two conditions are satisfied. However, this is quite hard in general to find the required matrices $A^\sharp, B_1^\sharp, B_2^\sharp$ and C^\sharp . To do so, some constructive assumptions are gradually made on the considered systems structures so as to easily satisfy both conditions. For a given matrix $A \in \mathbb{R}^{n \times m}$, let define $A^+ = \max(A, 0)$ and $A^- = A^+ - A$. To determine matrices B_2^\sharp and C^\sharp , the following lemma will be used.

Lemma 1 (see [8, Lemma 1] and the associated proof): Let $x \in \mathbb{R}^n$ s.t. $\underline{x}(t) \leq x(t) \leq \bar{x}(t)$ and $A \in \mathbb{R}^{m \times n}$ a constant matrix s.t. $A = A^+ - A^-$. Then $\forall t$

$$A^+ \underline{x}(t) - A^- \bar{x}(t) \leq Ax(t) \leq A^+ \bar{x}(t) - A^- \underline{x}(t) \quad (4)$$

The following definitions will be useful to define A^\sharp and obtain interval observers on linear systems.

Definition 2 (Metzler matrix): Let $A = (a_{ij}) \in \mathbb{R}^{n \times n}$. The matrix A is said to be Metzler if

$$\forall i \neq j, \quad a_{ij} \geq 0 \quad (5)$$

Definition 3 (Non-negative matrix): Let $A_d = (a_{ij}) \in \mathbb{R}^{n \times n}$. The matrix A_d is said to be non-negative if

$$\forall (i, j), \quad a_{ij} \geq 0 \quad (6)$$

The theory of cooperative systems is extensively used when designing interval observers. Such systems have interesting properties as far as trajectory ordering is considered. This is used to fulfil the second condition in Definition 1 straightforwardly.

Definition 4 (Cooperative system, CT): An autonomous CT linear system (G) is said to be cooperative if its state matrix A is a Metzler matrix.

Remark 1: In the case of a CT linear system with inputs (and $D = 0$), it is said to be cooperative if A is Metzler, $B \in \mathbb{R}_+^{n \times l}$ and $C \in \mathbb{R}_+^{m \times n}$. A cooperative CT system is thus a positive system.

Of course, DT systems can also be cooperative under slightly different conditions.

Definition 5 (Cooperative system, DT): An autonomous DT linear system (G_d) is said to be cooperative if its state matrix A_d is a non-negative matrix.

3 Motivations

In many control applications, it is required to enforce specific properties on a system state-space representation. This is the case when designing interval observers as defined in Definition 1.

3.1 Motivating problem

The linear interval observer framework and existing techniques to compute a state-coordinate transformation such that the state-matrix is Metzler or non-negative are now presented.

3.1.1 Interval observer literature: The theory of interval observers was first introduced in [1, 9] as a deterministic state ‘framing’ method in the case of cooperative systems [2] disturbed by unknown disturbances with known bounds. When the original system is not cooperative, a state-coordinate transformation is considered. In [10], the authors show (on a precise class of systems) exponential stability of a time-varying interval observer obtained using a time-varying state-coordinate change. This is applied in [3] on a broader class. A similar transformation is also proposed in [11]. The approach is extended in [12] to linear time varying (LTV) systems. In other works, a more classical approach leads to time-invariant linear interval observers with weaker stability guarantees, but broader system classes. In [4], a time-invariant state coordinate transform is used to obtain a cooperative observation error dynamics on which an interval observer is designed. This is extended to a class of non-linear and LPV (linear parameter varying)/LTV systems in [8, 13]. Another formulation is proposed in [14]. An extensive study of these techniques is available in [15, 16].

The theory of interval observers applied to DT systems [17] is very similar to the CT case. Extensions to DT LPV systems have been proposed in [18]. An extension to CT systems with discrete measurements is proposed in [16].

Note there exists other approaches based on internal positive representations of systems [7, 17]. Those are not considered in this paper.

In this paper, the considered systems are LTI systems and the results in [4] are used.

3.1.2 Interval observer design using a classical observer: Let consider an LTI CT system with a state-space representation as in (2) where $u \in \mathbb{R}$ is the control signal, $d \in \mathbb{R}$ is an unknown state disturbance and $x_0 \in \mathbb{R}^n$ is the initial condition. The following hypotheses are considered

$$\text{Hypothesis 1: Couples } (\underline{x}_0, \bar{x}_0) \text{ and } (\underline{d}, \bar{d}) \text{ are known s.t. } \underline{x}_0 \leq x_0 \leq \bar{x}_0 \text{ and } \forall t \geq 0, \quad \underline{d}(t) \leq d(t) \leq \bar{d}(t) \quad (7)$$

Hypothesis 2: The pair (A, C) in (2) is detectable.

To fulfil the first condition in Definition 1, a classical observer of the system in (2) is used

$$(G_{\text{obs}}) \begin{cases} \dot{\hat{x}} = A\hat{x} + B_1u + L(y - C\hat{x}) \\ \hat{y} = C\hat{x} \\ \hat{x}(0) = \hat{x}_0 \end{cases} \quad (8)$$

where $L \in \mathbb{R}^{n \times m}$ is defined such that $A - LC$ is Hurwitz. The underlying estimation error dynamics is deduced from both (2) and (8)

$$(G_e) \begin{cases} \dot{e} = (A - LC)e + B_2d \\ e_0 = x_0 - \hat{x}_0 \end{cases} \quad (9)$$

where $e = x - \hat{x}$. If $A - LC$ is not Metzler, (G_e) is not cooperative and it is not possible to fulfil the second condition in Definition 1 without a state coordinate change. Under Hypothesis 1 one obtains bounds on the initial error e_0 : $\underline{e}_0 = \underline{x}_0 - \hat{x}_0$ and $\bar{e}_0 = \bar{x}_0 - \hat{x}_0$.

Hypothesis 3: A state coordinate transformation $P \in \mathbb{R}^{n \times n}$ is known s.t. $M = P(A - LC)P^{-1}$ is Metzler.

The error dynamics in (9) expressed in the new coordinates becomes

$$(G_{e_z}) \begin{cases} \dot{e}_z = Me_z + B'_2d \\ e_z(0) = Pe_0 \end{cases} \quad (10)$$

where $e_z = Pe$ and $B'_2 = PB_2$. According to Definition 1 and using Lemma 1 and Hypothesis 3, an interval observer (G^\sharp) on the system in (10) is defined by the following dynamic system

$$(G^\sharp_{e_z}) \begin{cases} \dot{e}_z = Me_z + B'^+_2d - B'^-_2\bar{d} \\ \dot{\bar{e}}_z = M\bar{e}_z + B'^+_2\bar{d} - B'^-_2d \\ e_z(0) = P^+\underline{e}_0 - P^-\bar{e}_0 \\ \bar{e}_z(0) = P^+\bar{e}_0 - P^-\underline{e}_0 \end{cases} \quad (11)$$

Let $T = P^{-1}$. To obtain bounds in the original coordinates $e = Te_z$, the following relations are used

$$\begin{cases} \underline{e} = T^+\underline{e}_z - T^-\bar{e}_z \\ \bar{e} = T^+\bar{e}_z - T^-\underline{e}_z \end{cases} \quad (12)$$

which preserve state ordering under Lemma 1. Thus, for any $e_0 \in [\underline{e}_0, \bar{e}_0]$ the following framing is obtained

$$\forall t \geq 0, \quad \underline{e}(t) \leq e(t) \leq \bar{e}(t) \quad (13)$$

which in turn leads to

$$\forall t \geq 0, \quad \underline{x}(t) = \hat{x}(t) + \underline{e}(t) \leq x(t) \leq \hat{x}(t) + \bar{e}(t) = \bar{x}(t) \quad (14)$$

Using an appropriate state coordinate transformation, the state of a generic disturbed LTI CT system can thus be bounded.

In the DT case, the formalism is very close to the CT case with a slight difference on the properties to be satisfied by the state matrix, since it should be Schur-stable and non-negative, as stated in Definition 5:

Hypothesis 4: A state coordinate transformation $P \in \mathbb{R}^{n \times n}$ is known s.t. $M = P(A - LC)P^{-1}$ is non-negative.

3.2 Overview of existing techniques to find an appropriate state coordinate transform

In the framework presented in Section 3.1.2, Hypothesis 3 and 4 are strong hypotheses. In the case of high-order systems, choosing a satisfying state coordinate transformation matrix P is not obvious:

Problem 1 (CT case): Find $P \in \mathbb{R}^{n \times n}$ and $L \in \mathbb{R}^{n \times m}$ such that $M = P(A - LC)P^{-1}$ is Hurwitz–Metzler.

Problem 2 (DT case): Find $P \in \mathbb{R}^{n \times n}$ and $L \in \mathbb{R}^{n \times m}$ such that $M = P(A - LC)P^{-1}$ is Schur-stable and non-negative.

In this section, the existing methods to determine a solution to Problems 1 and 2 are presented along with their advantages and limitations.

3.2.1 Real-constrained pole placement (trivial solution):

This trivial solution is obtained by noticing that diagonal matrices satisfy to Definition 2. Supposing that the pair (A, C) is observable (or that the unobservable eigenvalues are real negative, which is stronger than simple detectability), the matrix L is chosen such that $A - LC$ only has negative real eigenvalues. Then, choosing P as the matrix of the right-hand eigenvectors means $M = P(A - LC)P^{-1}$ is diagonal hence is a Metzler matrix.

The advantage of this technique is its simplicity since it only requires a pole placement and an eigenstructure determination algorithm. Three main limitations can, however, be mentioned:

- placing real poles can result in very large observation gains L resulting in sensitivity problems;
- an observer with complex poles may achieve better results;
- due to floating-point computations precision errors, the computed matrix M is Metzler up to the machine precision.

Remark 2: In the DT case, the poles have to be placed on real values between 0 and 1 to comply with the definitions of Schur-stability and non-negativity.

3.2.2 Resolution of a Sylvester equation: To find a solution to Problem 1, another approach can be used

- choose $M \in \mathbb{R}^{n \times n}$ to be a Metzler matrix;
- choose $Q \in \mathbb{R}^{n \times m}$, this will represent the matrix product PL ;
- using algorithms, for example proposed in [19] or [20], solve the following Sylvester equation in P

$$-MP + PA = PLC = QC \quad (15)$$

If M and A have no common eigenvalues, this equation has a unique solution for any Q .

One thus obtains a Metzler matrix $M = P(A - LC)P^{-1}$ where the observer gain is defined by $L = P^{-1}Q$. This method was proposed in [4] along with a constructive lemma [4, Lemma 1, p. 261] to solve the equation using observability criteria. However this lemma is difficult to apply in case complex eigenvalues are looked for since there is no trivial (i.e. diagonal or triangular) Metzler matrix M with complex eigenvalues. Numerical errors may also occur in case of badly-conditioned matrices. A solution to the Sylvester equation can be obtained, for example using [20].

Remark 3: In the DT case, Remark 2 is still valid here.

3.3 Conclusions on the interests of an alternative approach

Both techniques proposed in the literature bring the advantage of simplicity and only use built-in functions of any numerical computation software. This will be sufficient in most considered cases.

However, in more complex cases – high-order systems, ill-conditioned system matrices, additional constraints like observer error dynamics decay rate optimisation and so on – it seems more difficult to obtain satisfying results due to numerical precision problems as well as to the method philosophy. Indeed, the chosen matrices M and Q could lead to non-optimal results in view of other control constraints. Moreover, it seems difficult to obtain an expression of a Metzler matrix from expected complex eigenvalues.

An alternative technique is hereby proposed which could complement the existing methods by taking these more complex cases into account.

4 Problems statement

In this section, the different problems which arise in the proposed approach are exposed. As far as the state coordinate transformation determination is concerned, a reformulation into a control law synthesis problem is proposed, as exposed in [5]. A numerical approach to find a solution simultaneously satisfying to these problems is then proposed in Section 5. It uses existing controller synthesis techniques as permitted by the reformulation.

4.1 State coordinate transformation determination

In Section 3, the design of interval observers has motivated the need for state coordinate transformation determination methods. This paper proposes a new approach based on solving a control design problem.

4.1.1 Initial problem: Let recall the initial state coordinate transformation problem as stated in Problem 1.

Problem 3 (Mathematical formulation): Given (A, C) detectable, determine simultaneously $P \in \mathbb{R}^{n \times n}$ and $L \in \mathbb{R}^{n \times m}$ such that $M = P(A - LC)P^{-1}$ is

- Metzler and Hurwitz (CT case);
- non-negative and Schur-stable (DT case).

In other words, finding a solution to Problem 3 in the CT case is equivalent to finding P and L under $n(n - 1)$ positivity requirements on the off-diagonal elements of $M = (m_{ij}) \in \mathbb{R}^{n \times n}$. This directly comes from Definition 2 of a Metzler matrix

$$m_{ij} \geq 0, \quad \forall i \neq j \Leftrightarrow -m_{ij} \leq 0, \quad \forall i \neq j$$

In terms of control theory, these last inequalities are reminiscent of the stabilisation condition on a ‘fictitious’ mono-dimensional system having its real pole located at $-m_{ij}$.

4.1.2 Reformulation into a control design problem: A reformulation of Problem 3 into a control design problem is done in the following proposition.

Proposition 1 (Equivalent control design problem, CT case): Let (A, C) detectable and

$$m_{ij}(P, L) = \left[P(A - LC)P^{-1} \right]_{ij}$$

for $P \in \mathbb{R}^{n \times n}$ and $L \in \mathbb{R}^{n \times m}$. If the following system

$$(G_c) \begin{cases} \dot{x}_1 = (A - LC)x_1 \\ \dot{x}_{ij} = -m_{ij}(P, L)x_{ij} \quad \forall i \neq j \end{cases} \quad (16)$$

is a Hurwitz stable for given P and L then $P(A - LC)P^{-1}$ is Metzler and Hurwitz.

Proof: Straightforward considering the definition of a Metzler matrix, see Definition 2, and the definitions of the coefficients

$m_{ij}(P, L)$. In particular, ensuring positiveness of $m_{ij}(P, L)$ is equivalent to stabilising $\dot{x}_{ij} = -m_{ij}(P, L)x_{ij}$. \square

The states $x_{ij} \in \mathbb{R}$ are called ‘fictitious’ states since they do not have any physical meaning. For an initial matrix $A \in \mathbb{R}^{n \times n}$, $n(n - 1)$ ‘fictitious’ states are considered.

Remark 4: Proposition 1 is reminiscent of a structured control design problem which is NP-hard in general. It is usually solved using algorithms with local optimality certificates which are known to work in practice. There is however no guarantee that the locally optimal solution stabilises (16).

Remark 5: In the DT case, n^2 ‘fictitious’ states are considered since the diagonal elements of matrix M should also be non-negative. However, due to the definition of Schur stability, using Proposition 1 would lead to $-m_{ij}(P, L) \in [-1, 1], \forall (i, j)$ which does not comply with the definition of non-negativity. In that case, the system in (16) is replaced by the following system

$$(G_{c,d}) \begin{cases} x_{1,t+1} = (A - LC)x_{1,t} \\ x_{ij,t+1} = f(-m_{ij}(P, L))x_{ij,t} \quad \forall (i, j) \end{cases} \quad (17)$$

where $f: \mathbb{R} \rightarrow \mathbb{R}$ is a linear function which maps $[-m_{ij}^{\max}, 0]$ onto $[-1, 1]$ with $m_{ij}^{\max} > 0$ a design parameter which will be useful later

$$f(x) = \frac{2}{m_{ij}^{\max}}x + 1 \quad (18)$$

Using this function has proved to be effective in practice.

4.2 Adding control requirements: resulting optimisation problem

As already mentioned in Section 3.3, choosing P and L simultaneously such that additional control constraints are fulfilled is difficult. For example, considering the observation error dynamics in (9), it may be beneficial in terms of estimation quality to minimise a normalised value of the H_2 -norm of the transfer from the disturbance d to the observation error e

$$\min_{P, L} \max \{ \|W(s)T_{d \rightarrow e}(s, L)\|_2, \|T_2(s, P, L)\|_2, \|T_3(s, P, L)\|_\infty, \dots \}$$

subject to $G_c(P, L)$ ((16)) is stable. (19)

where $W(s)$ is an appropriate weighting and $T_2(s, P, L)$ and $T_3(s, P, L)$ are additional design transfer functions. Note that the cost function is non-smooth. This type of optimisation problem is typical of the kind of problem encountered when synthesising structured controllers against multiple requirements over multiple models. The idea is thus to use such formalism to find at least a local minimiser to this problem.

4.3 Structured controller synthesis

The synthesis of full-order controllers through H_∞ methods has been widely studied and used in the past two decades. Solutions to the problem of H_∞ synthesis in the case of multiple-input multiple-output systems were provided, for example in [21, 22]. When considering controllers with a fixed order much lower than the original plant, the problem of finding a controller is a non-convex optimisation problem. A local solution to this problem was proposed in [23] and implemented in consecutive works [24]. Other implementations for computing fixed-order controllers include [25]. More recent works [6, 26, 27] consider the case of finding a controller satisfying to multiple requirements on multiple models. Considering these techniques, it appears possible to solve the minimisation problem in (19).

5 Non-smooth optimisation-based approach

In this section, the *structured controller synthesis* approach is detailed to solve the optimisation problem in Section 4.2. An illustration of the technique to determine an interval observer state coordinate transformation is also proposed, which is then applied to three examples in Section 6.

5.1 Structured controller synthesis algorithm

As mentioned in Section 4.2, it appears that the reformulation proposed in Proposition 1 joined to additional control requirements leads to a structured controller synthesis problem. As already mentioned, this problem has been solved in [6, 23]. In this article, the `systune` function – along with the `TuningGoal` structure – from the MATLAB Robust Control Toolbox [28] is used to solve the problem. This function uses non-smooth optimisation algorithms to solve non-smooth non-convex optimisation problems. The method is provably convergent and computes certified locally optimal solutions from any remote starting point.

In the following sections, the models and requirements needed to solve the optimisation problem in Section 4.2 using these tools are detailed.

5.2 Models definition

As was already mentioned, recent control synthesis techniques allow to set multiple requirements on multiple models, be they are describing an existing physical system or mathematical constraints, as is the case with the ‘fictitious’ states used in Proposition 1. In the CT case, let define $n(n-1)$ fictitious systems

$$\left(G_M^{ij}\right) \dot{x}_{ij} = -m_{ij}(P, L) x_{ij}, \quad \forall i \neq j \quad (20)$$

and, in the DT case, let define the following n^2 fictitious systems:

$$\left(G_{M,d}^{ij}\right) x_{ij,t+1} = f(-m_{ij}(P, L) x_{ij,t}), \quad \forall (i, j) \quad (21)$$

The required synthesis models are enumerated here in the form of *collections* of models. Note that some collections only apply to the CT or DT case.

(C1–CT) $n(n-1)$ unidimensional fictitious systems $\left\{G_M^{ij}\right\}_{i,j,i \neq j}$ as defined in (20).

(C1–DT) n^2 unidimensional fictitious systems $\left\{G_{M,d}^{ij}\right\}_{i,j}$ as defined in (21) with f a linear function mapping $\left[-m_{ij}^{\max}, 0\right]$ onto $[-1, 1]$ where m_{ij}^{\max} is a design parameter playing the same role as in **(C2–CT)** (see Remark 5).

(C2–CT) (optional) $n(n-1)$ unidimensional fictitious systems $\left\{G_M^{ij}\right\}_{i,j,i \neq j}$ with state matrix $m_{ij}(P, L) - m_{ij}^{\max} \in \mathbb{R}$. This helps to restrict the set of acceptable solutions when $0 < m_{ij}^{\max} < +\infty$. The initialising variables excursion is thus limited around a smaller set of potential local optima.

(C3) Any other model in state-space representation, describing the control or observation problem, thus including tunable controller or observer parameters.

A series of requirements are now expressed on each collection.

5.3 Requirements

For each collection in Section 5.2, a set of requirements (or constraints, see Section 4.3) is expressed.

(R1–CT) a requirement on the closed-loop poles location is expressed on **(C1–CT)** in the form of a constraint on the minimum decay rate. This ensures negativity of $-m_{ij}(P, L)$ hence positivity of m_{ij} , $\forall i \neq j$ (CT case).

(R1–DT) similar requirement to **(R1–CT)**, but expressed on the n^2 models in **(C1–DT)**.

(R2–CT) similar to previous requirements sets, but applied on **(C2–CT)**. This ensures negativity of $m_{ij} - m_{ij}^{\max}$, $\forall i \neq j$;

(R3) Any control requirement to enforce on **(C3)** like disturbance rejection, closed-loop poles and so on.

6 Applications

In this section, the method proposed in Section 5 is applied to three examples, including an unstable system, using the interval observers formalism presented in Section 3. A comparison with the methods proposed in the literature is also provided.

6.1 CT stable sixth-order example

The formalism of interval observers in the CT case is presented in Section 3.1.2. The method presented in this paper proposes to enforce Hypothesis 3 by computing P and L such that M is Hurwitz–Metzler.

The following example is inspired from [3]. The considered system dynamics is given by

$$\begin{cases} \dot{x} = Ax + B_1 u \\ y = Cx + d \end{cases} \quad (22)$$

where $x \in \mathbb{R}^6$, $u(t) = \sin(t)$ and $d(t)$ is an unknown but bounded measurement disturbance with $\underline{d} = -2 \leq d(t) \leq 1 = \bar{d}$, $\forall t$. A random number generator with limited range is used in simulation. The system matrices are numerically given by

$$A = \begin{bmatrix} -1 & 1 & 0 & 0 & -1 & 0 \\ -1 & -2 & 0 & -1 & 0 & 1 \\ -2 & 0 & -3 & -2 & 0 & 0 \\ -1 & 0 & -2 & -3 & 0 & 1 \\ -1 & 0 & 2 & 0 & -4 & 0 \\ -1 & -1 & 0 & 1 & 0 & -1 \end{bmatrix}, \quad B_1 = \begin{bmatrix} -18 \\ -13 \\ -5 \\ -4 \\ -10 \\ 22 \end{bmatrix}, \quad C = [1 \ 0 \ 0 \ 0 \ 0 \ 0] \quad (23)$$

The system is stable and it is initialised at $x_0 = [20 \ 10 \ 6 \ 20 \ 30 \ 40]^T$. The Luenberger observer is initialised at $\hat{x}_0 = 0$ and the initial state is supposed to lie in $[-\bar{x}_0, \bar{x}_0]$ where $\bar{x}_0 = 50 [1 \ 1 \ 1 \ 1 \ 1 \ 1]^T$. Thus, the initial observation error e_0 lies in $[e_0, \bar{e}_0] = [-\bar{x}_0 - \hat{x}_0, \bar{x}_0 - \hat{x}_0]$.

The observation error dynamics is defined by

$$\begin{cases} \dot{e} = (A - LC)e - Ld \\ e_0 = x_0 - \hat{x}_0 \end{cases} \quad (24)$$

which is not cooperative. Under Hypothesis 3, the following system is an interval observer for the observation error dynamics in (24), where $P_L^+ = \max(PL, 0)$ and $P_L^- = P_L^+ - PL$

$$\begin{cases} \underline{e}_z = M \underline{e}_z + P_L^+ \underline{d} - P_L^- \bar{d} \\ \bar{e}_z = M \bar{e}_z + P_L^+ \bar{d} - P_L^- \underline{d} \\ \underline{e}_z(0) = P^+ \underline{e}_0 - P^- \bar{e}_0 \\ \bar{e}_z(0) = P^+ \bar{e}_0 - P^- \underline{e}_0 \end{cases} \quad (25)$$

Reverting back to the initial coordinates is done using (12). The three following methods are considered to determine P and L :

- real pole placement allowing state matrix diagonalisation;
- resolution of a Sylvester equation;
- application of the non-smooth control-based method.

6.1.1 Existing techniques: The numerical results obtained using existing techniques are presented here.

Real pole placement: The following pole placement gives rather good results in simulation as far as the convergence speed of the observer is concerned

$$p = [-4.7 \quad -4.6 \quad -2.1 \quad -1.2 \quad -1.1 \quad -0.3] \quad (26)$$

Using the pole placement and diagonalisation approach in Section 6.3.1, one obtains the following P and L matrices (see (27))

which leads to the following matrix $M = P(A - LC)P^{-1}$

$$M = \begin{bmatrix} -4.7000 & 0.0000 & -0.0000 & 0.0000 & 0.0000 & -0.0000 \\ -0.0000 & -4.6000 & -0.0000 & 0.0000 & 0.0000 & -0.0000 \\ -0.0000 & 0.0000 & -2.1000 & 0.0000 & 0.0000 & 0.0000 \\ 0.0000 & -0.0000 & -0.0000 & -1.2000 & -0.0000 & 0.0000 \\ -0.0000 & 0.0000 & 0.0000 & 0.0000 & -1.1000 & -0.0000 \\ -0.0000 & 0.0000 & -0.0000 & -0.0000 & -0.0000 & -0.3000 \end{bmatrix} \quad (28)$$

Due to numerical errors, the observation error dynamics is, however, not certified to be cooperative.

Sylvester equation: The approach in Section 3.2.2 is applied to the considered system. The following upper-triangular Metzler matrix M is proposed

$$M = \begin{bmatrix} -4.7000 & 1.0000 & 1.0000 & 1.0000 & 1.0000 & 1.0000 \\ 0 & -4.6000 & 1.0000 & 1.0000 & 1.0000 & 1.0000 \\ 0 & 0 & -2.1000 & 1.0000 & 1.0000 & 1.0000 \\ 0 & 0 & 0 & -1.2000 & 1.0000 & 1.0000 \\ 0 & 0 & 0 & 0 & -1.1000 & 1.0000 \\ 0 & 0 & 0 & 0 & 0 & -0.3000 \end{bmatrix} \quad (29)$$

along with $Q = [1 \quad 2 \quad 3 \quad 4 \quad 5 \quad 6]^T$. Solving (15) for these values, one obtains

$$P = \begin{bmatrix} 11.1557 & -23.0016 & -41.8920 & 58.6245 & -3.1677 & 54.8212 \\ 8.6278 & -19.1428 & -35.4258 & 48.3810 & -2.9658 & 45.4833 \\ 15.8575 & -28.1624 & -53.0607 & 70.9787 & -6.0558 & 71.5056 \\ 11.3015 & -26.6410 & -53.7302 & 70.7881 & -3.8611 & 64.4377 \\ 1.8712 & -16.6031 & -28.5216 & 38.4000 & -0.7267 & 32.0343 \\ -0.8742 & -15.2203 & -24.0624 & 32.7206 & 0.2363 & 25.0003 \end{bmatrix}, \quad L = \begin{bmatrix} 0.0000 \\ -1.2981 \\ -1.1800 \\ -1.0496 \\ -0.0981 \\ -0.3113 \end{bmatrix} \quad (30)$$

Table 1 Control-based approach parameters for the example described in Section 6.1, $p_{(A-LC)}$ refers to the poles of the observer error dynamics (24)

Syn. model	Requirement	Settings
(C1-CT)	(R1-CT)	$m_{ij}^{\max} = 200$ $\text{Re}(p_{A-LC}) \in]-\infty, -3.10^{-3}]$ $\left\ \frac{1}{0.4} T_{d \rightarrow e}(s) \right\ \leq 1$
(C2-CT)	(R2-CT)	
(C3)	(R3)-1	
	(R3)-2	

which leads to the following matrix $M = P(A - LC)P^{-1}$

$$M = \begin{bmatrix} -4.7000 & 1.0000 & 1.0000 & 1.0000 & 1.0000 & 1.0000 \\ 0.0000 & -4.6000 & 1.0000 & 1.0000 & 1.0000 & 1.0000 \\ -0.0000 & -0.0000 & -2.1000 & 1.0000 & 1.0000 & 1.0000 \\ 0.0000 & -0.0000 & 0.0000 & -1.2000 & 1.0000 & 1.0000 \\ -0.0000 & -0.0000 & 0.0000 & -0.0000 & -1.1000 & 1.0000 \\ -0.0000 & -0.0000 & 0.0000 & -0.0000 & 0.0000 & -0.3000 \end{bmatrix} \quad (31)$$

In this case, numerical errors also appear in the final result.

6.1.2 Control-based approach: The method proposed in Sections 4 and 5 is used. The synthesis models and requirements used are recalled in Table 1 and refer to notations used in Section 5.

Using the control law synthesis algorithm presented in Section 5.1, a locally optimal solution is found in 287 s after 3 restarts and requiring 1107 iterations. The following results are obtained, where $M = P(A - LC)P^{-1}$ is Hurwitz-Metzler

$$M = \begin{bmatrix} -0.9015 & 0.0000 & 22.5484 & 0.0002 & 0.0054 & 0.0001 \\ 0.0231 & -2.5523 & 0.1372 & 0.0000 & 0.4259 & 0.0589 \\ 0.0000 & 0.0114 & -1.4533 & 0.0001 & 0.0622 & 0.0000 \\ 0.0831 & 26.4981 & 0.0000 & -4.4748 & 4.3388 & 2.7824 \\ 0.0000 & 0.0000 & 0.0050 & 0.5871 & -3.4814 & 0.0335 \\ 1.3946 & 0.0000 & 0.5513 & 0.0010 & 0.0032 & -1.0506 \end{bmatrix}, \quad P = \begin{bmatrix} -0.5886 & -0.9537 & -1.2910 & 1.7496 & 0.3504 & 0.3355 \\ 0.0110 & 0.0364 & -0.1391 & 0.1713 & -0.0840 & 0.0965 \\ 0.0398 & 0.0055 & -0.0037 & 0.0087 & -0.0221 & 0.0337 \\ 1.4422 & -0.3846 & -0.7972 & 3.8482 & -0.4497 & 2.3833 \\ 0.1262 & 0.0438 & -0.8724 & 0.3191 & 0.2818 & 0.4526 \\ 0.2464 & -1.0668 & -0.7884 & 1.4262 & -0.2453 & 2.5864 \end{bmatrix}, \quad L = \begin{bmatrix} -0.0862 \\ 0.0583 \\ -0.1903 \\ 0.0349 \\ 0.0366 \\ -0.1631 \end{bmatrix} \quad (32)$$

6.1.3 Simulations and comparisons: The system is initialised at x_0 and simulated over 40s using $u(t) = \sin(t)$ and a random-number-generated signal $d(t) \in [-2, 1]$. Results are shown in Figs. 1 and 2.

The results obtained using the control-based approach are highly satisfying. Although the obtained interval observer seems slower than the one obtained using real pole placement, it converges closer to the system state. Additional requirements could be used to deal with the convergence speed. The results obtained using the Sylvester equation approach are very bad due to the difficulty of selecting appropriate matrices M and Q . Moreover, P is used to determine L while this is not the case in the other methods.

$$P = \begin{bmatrix} -2.5932 & 1.9801 & -9.9547 & -12.1661 & -3.7046 & 2.7530 \\ -2.8007 & 2.1553 & -9.4734 & -12.2466 & -4.6679 & 2.8031 \\ 1.6458 & -0.1905 & 1.6282 & -1.5989 & -0.8662 & 1.6268 \\ -20.6249 & -16.3609 & -11.6690 & 17.8681 & 7.3660 & -7.5362 \\ 19.8606 & 16.2310 & 10.4293 & -16.7563 & -6.8485 & 5.2526 \\ 0.0250 & 0.4350 & 0.6878 & -0.9352 & -0.0068 & -0.7146 \end{bmatrix}, \quad L = \begin{bmatrix} -0.0000 \\ -1.2981 \\ -1.1800 \\ -1.0496 \\ -0.0981 \\ -0.3113 \end{bmatrix} \quad (27)$$

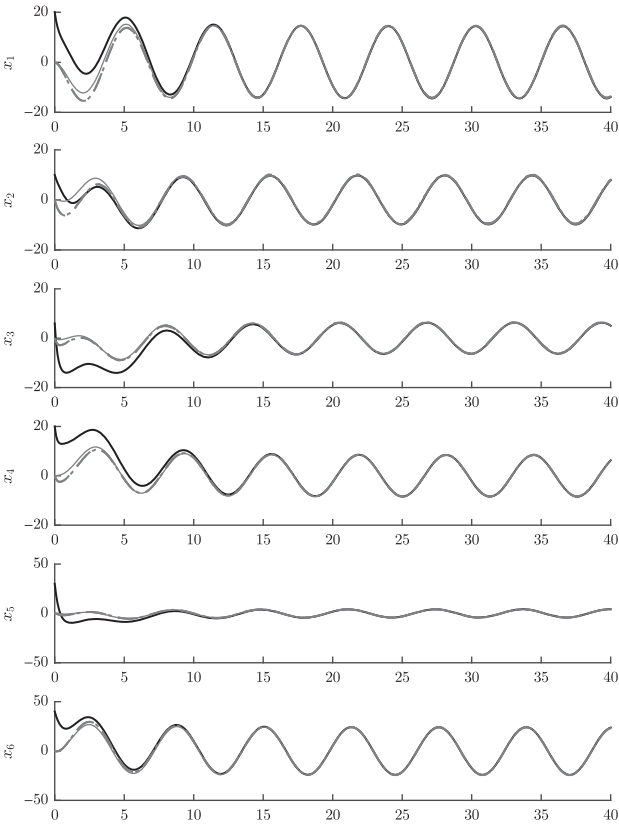


Fig. 1 In black, simulation results for the system in (22) and in grey solid (resp. dashed/dashed-dotted) line, for the classical observer in (8) obtained using the observer gain L in (32) [resp. (27) or (30)] produced by the control-based approach (resp. real pole placement or Sylvester equation resolution)

6.2 CT unstable third-order example

The following example is adapted from [4]. The considered system dynamics is given by

$$\begin{cases} \dot{x} = Ax + Bd \\ y = Cx \end{cases} \quad (33)$$

where $x \in \mathbb{R}^3$ and $d(t)$ is an unknown, but bounded state disturbance with $\underline{d}(t) = -1 \leq d(t) \leq 1 = \bar{d}(t)$, $\forall t$. The signal $d(t) = \sin(2t)$ will be used in simulation. The system matrices are defined as follows

$$A = \begin{bmatrix} 2 & 0 & 0 \\ 1 & -4 & \sqrt{3} \\ -1 & -\sqrt{3} & -4 \end{bmatrix}, \quad B = \begin{bmatrix} -1 \\ 0 \\ 1 \end{bmatrix}, \quad C = [1 \quad 0 \quad 0] \quad (34)$$

This system is unstable and detectable. The initial state is given by $x_0 = [-2 \quad 1.5 \quad -1]^\top$ and the initial observer state by $\hat{x}_0 = 0$. Bounds on the initial state are supposed to equal $\underline{x}_0 = [-2 \quad -2 \quad -2]^\top$ and $\bar{x}_0 = -x_0$. The initial observation error e_0 lies in $[\underline{e}_0, \bar{e}_0] = [x_0 - \hat{x}_0, -x_0 - \hat{x}_0]$.

The observation error dynamics is defined by

$$\begin{cases} \dot{e} = (A - LC)e + Bd \\ e_0 = x_0 - \hat{x}_0 \end{cases} \quad (35)$$

which is not cooperative. Under Hypothesis 3, the following system is an interval observer for the observation error dynamics in (35),

where $P_B^+ = \max(PB, 0)$ and $P_B^- = P_B^+ - PB$

$$\begin{cases} \underline{e}_z = M\underline{e}_z + P_B^+\underline{d} - P_B^-\bar{d} \\ \bar{e}_z = M\bar{e}_z + P_B^+\bar{d} - P_B^-\underline{d} \\ \underline{e}_z(0) = P^+\underline{e}_0 - P^-\bar{e}_0 \\ \bar{e}_z(0) = P^+\bar{e}_0 - P^-\underline{e}_0 \end{cases} \quad (36)$$

Reverting back to the initial coordinates is done using (12). The two following methods are considered to determine P and L :

- application of [4, Lemma 1, p. 261];
- application of the non-smooth control-based method.

6.2.1 Application of the constructive lemma: In this section, Lemma 1 in [4, p. 261] is used as a practical method to solve the Sylvester equation presented in Section 3.2.2. At first, one has to choose the observer gain so that $A - LC$ is Hurwitz. For example $L = [3 \quad 0 \quad 0]^\top$. Then, a targeted matrix M is selected such that it is Metzler and has the same eigenvalues as $A - LC$

$$M = \begin{bmatrix} -3 & 2 & 0 \\ 0 & -3 & 2 \\ 2 & 0 & -3 \end{bmatrix} \quad (37)$$

Using [4, Lemma 1, p. 261] with $e_1 = [1 \quad 0 \quad 1]^\top$ and $e_2 = [1 \quad 1 \quad 0]^\top$, one obtains

$$P = \begin{bmatrix} 0.4085 & 0.8660 & 0.5000 \\ 0.5915 & -0.8660 & 0.5000 \\ -0.0915 & 0.0000 & -1.0000 \end{bmatrix},$$

$$M = P(A - LC)P^{-1} = \begin{bmatrix} -3.0000 & 2.0000 & -0.0000 \\ -0.0000 & -3.0000 & 2.0000 \\ 2.0000 & 0.0000 & -3.0000 \end{bmatrix} \quad (38)$$

6.2.2 Control-based approach: In this section, the approach proposed in Sections 4 and 5 is used. The synthesis models and requirements used, along with the settings values, are presented in Table 2.

Using the control law synthesis algorithm presented in Section 5.1, a locally optimal solution is found after 5 restarts requiring less than 400 iterations each. The execution time rises to 15 s. The result is given below

$$P = \begin{bmatrix} 0.4622 & -1.1708 & -1.6588 \\ 0.3043 & 2.0962 & -0.0391 \\ 0.0021 & -0.0165 & 0.0372 \end{bmatrix}, \quad L = \begin{bmatrix} 2.9830 \\ 1.2172 \\ -1.2948 \end{bmatrix},$$

$$M = \begin{bmatrix} -2.8253 & 2.0267 & 0.0000 \\ 0.0000 & -3.1910 & 98.5812 \\ 0.0404 & 0.0000 & -2.9666 \end{bmatrix} \quad (39)$$

where $M = P(A - LC)P^{-1}$ with no numerical error.

6.2.3 Simulations and comparisons: The system initialised at x_0 is simulated over 10 s with $d(t) = \sin(2t)$. As expected, the system state diverges. However, considering the observation error e rather than the state x , the bounds \underline{e} and \bar{e} obtained using the interval observer in (36) are expected to converge. Simulation results are displayed in Figs. 3 and 4.

In this particular example, the results obtained using the proposed control-based approach are better. The obtained matrix M is certified to be Hurwitz-Metzler. By adding control requirements and simultaneously synthesising P and L , the disturbance can be better rejected.

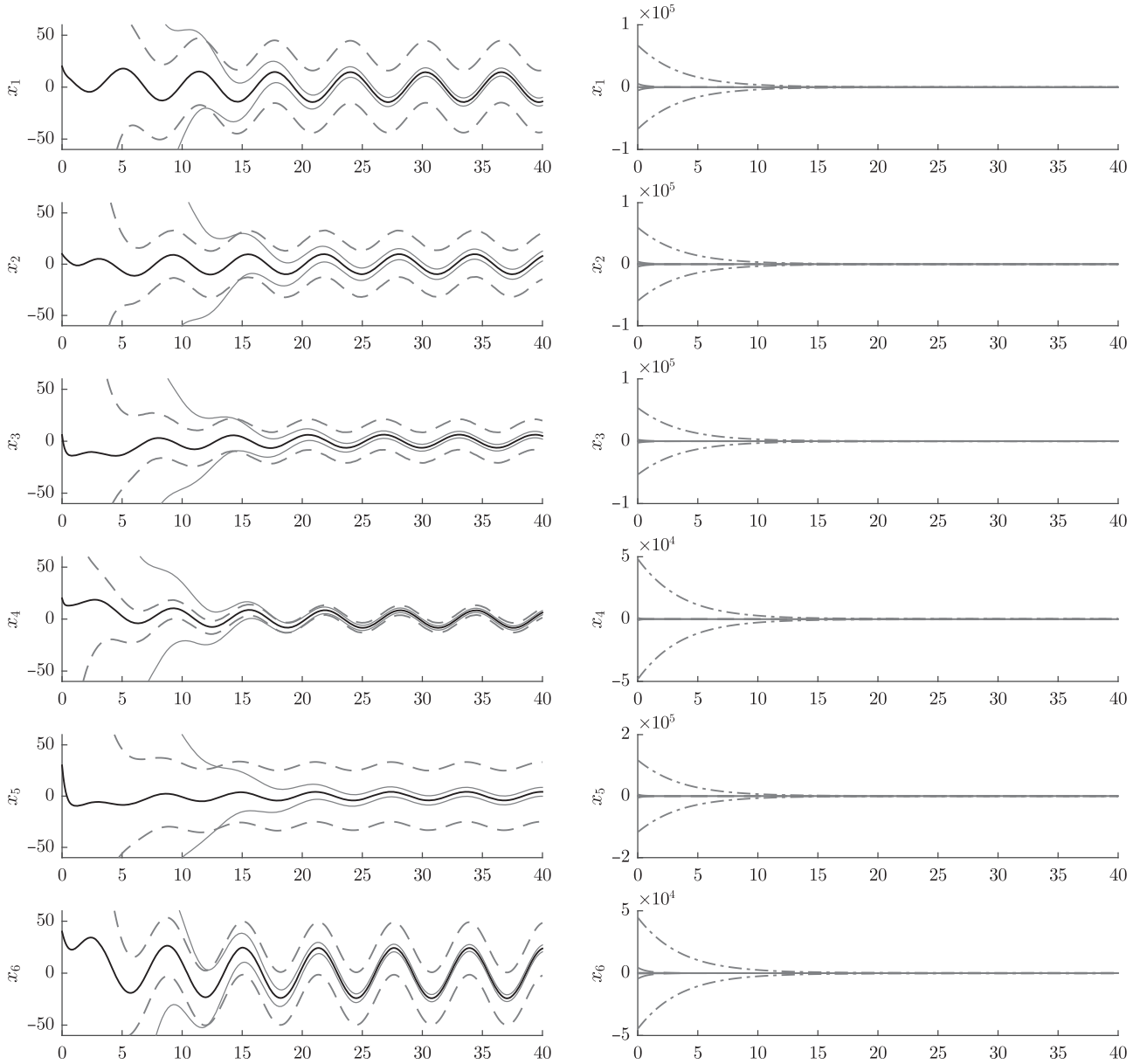


Fig. 2 In black, simulation results for the system in (22) and in grey solid (resp. dashed/dashed-dotted) line, bounds of the interval observer obtained using the control-based approach (resp. real pole placement/Sylvester equation resolution). The plots on the left are the same as the plots on the right but with limited ordinate excursion

6.3 Discrete-time example

This example is adapted from [18]. The following DT system with sample time $T_s = 1$ s is considered

$$\begin{cases} x_{t+1} = A_d x_t + B_d d_t \\ y_t = C_d x_t \end{cases} \quad (40)$$

where $x_t \in \mathbb{R}^5$ and d_t is an unknown disturbance bounded by $[-1, 1]$ and which is simulated by a random number generator on a limited range and with a time sampling of T_s . The numerical values used for the system matrices are

$$A_d = \begin{bmatrix} -0.54 & 0.45 & 0.36 & 0 & 0 \\ 0.63 & 0.45 & 0.18 & 0.36 & 0 \\ 0.09 & 0.45 & 0.27 & 0.09 & 0.18 \\ 0 & 0 & 0.25 & 0.25\sqrt{2} & -0.25\sqrt{2} \\ 0 & 0 & 0 & 0.25\sqrt{2} & 0.25\sqrt{2} \end{bmatrix},$$

Table 2 Control-based approach parameters for the example described in Section 6.2, $p_{(A-LC)}$ refers to the poles of the observer error dynamics (35)

Syn. model	Requirement	Settings
(C1-CT)	(R1-CT)	$m_{ij}^{\max} = 100$ $\text{Re}(p_{A-LC}) \in [-10, -3 \cdot 10^{-3}]$ $\left\ \frac{1}{0.8} T_{d \rightarrow e}(s) \right\ \leq 1$
(C2-CT)	(R2-CT)	
(C3)	(R3)-1	
	(R3)-2	

$$B_d = \begin{bmatrix} -1 \\ 0 \\ 0 \\ 0 \\ 1 \end{bmatrix}^T, \quad C_d = \begin{bmatrix} 1 & 0 & 0 & 0 & 0 \\ 0 & 0 & 0 & 1 & 0 \end{bmatrix} \quad (41)$$

The system is Schur stable. It is initialised at $x_0 = [-0.3 \ -0.5 \ 0.6 \ 0.9 \ -0.2]^T$. The Luenberger observer is

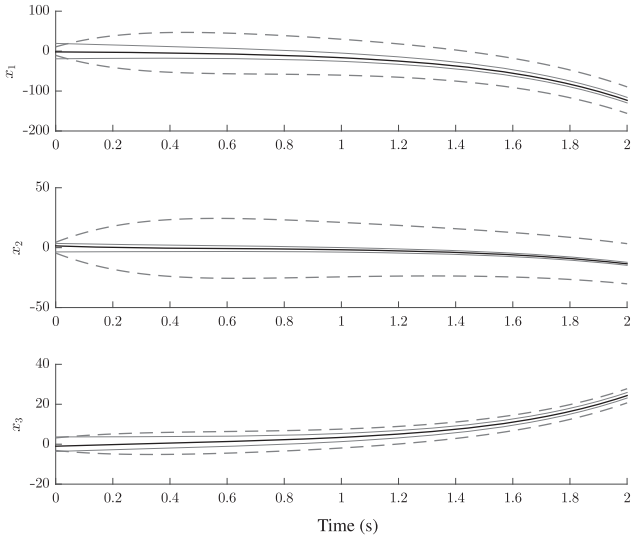


Fig. 3 In black, simulation results over 2s for the system in (33) and in grey solid (resp. dashed) line, bounds of the interval observer obtained using the control-based approach (resp. Lemma 1 in [4])

initialised at $\hat{x}_0 = 0$ and the initial state is supposed to lie in $[-\bar{x}_0, \bar{x}_0]$ where $\bar{x}_0 = [1 \ 1 \ 1 \ 1 \ 1]^T$. The initial observation error e_0 lies in $[\underline{e}_0, \bar{e}_0] = [-\bar{x}_0 - \hat{x}_0, \bar{x}_0 - \hat{x}_0]$. The observation error dynamics is defined by

$$\begin{cases} e_{t+1} = (A_d - LC_d)e_t + B_d d_t \\ e_0 = x_0 - \hat{x}_0 \end{cases} \quad (42)$$

which is not cooperative for any value of L . Under Hypothesis 4, the following system is an interval observer for the observation error dynamics defined in (42), where $P_B^+ = \max(PB_d, 0)$ and $P_B^- = P_B^+ - PB_d$

$$\begin{cases} \underline{e}_{z,t+1} = M_d \underline{e}_{z,t} + P_B^+ d_t - P_B^- \bar{d}_t \\ \bar{e}_{z,t+1} = M_d \bar{e}_{z,t} + P_B^+ \bar{d}_t - P_B^- d_t \\ \underline{e}_{z,0} = P^+ \underline{e}_0 - P^- \bar{e}_0 \\ \bar{e}_{z,0} = P^+ \bar{e}_0 - P^- \underline{e}_0 \end{cases} \quad (43)$$

Reverting back to the initial coordinates is performed using (12). In that case, the Sylvester method proposed in Remark 3 yields very poor results with the chosen arbitrary pole placement and non-negative matrix M_d . The two remaining methods: real pole placement as described in Remark 2 and the approach proposed in this paper are compared.

6.3.1 Real pole placement and diagonalisation: A pole placement is used as described in Remark 2 in Section 6.3.1. The desired poles are chosen arbitrarily as real numbers inferior to 1 and positive

$$p_3 = [0.1 \ 0.3 \ 0.5 \ 0.7 \ 0.9] \quad (44)$$

The following P and L matrices are thus obtained

$$P = \begin{bmatrix} -0.4816 & -1.3788 & -0.8972 & -0.5748 & 0.0763 \\ -0.3375 & -0.5564 & 0.0284 & 0.9356 & -0.9400 \\ -0.1471 & -0.9124 & 0.8567 & 0.2861 & -0.2092 \\ 0.5944 & -1.4806 & -0.7589 & -0.4881 & 0.2457 \\ -0.1690 & 0.0094 & 0.1658 & 0.2565 & 1.1357 \end{bmatrix}, \quad L = \begin{bmatrix} -1.1993 & -0.2234 \\ 0.6217 & 0.2992 \\ -0.0161 & 0.2228 \\ -0.0205 & -0.4136 \\ -0.0333 & 0.4069 \end{bmatrix} \quad (45)$$

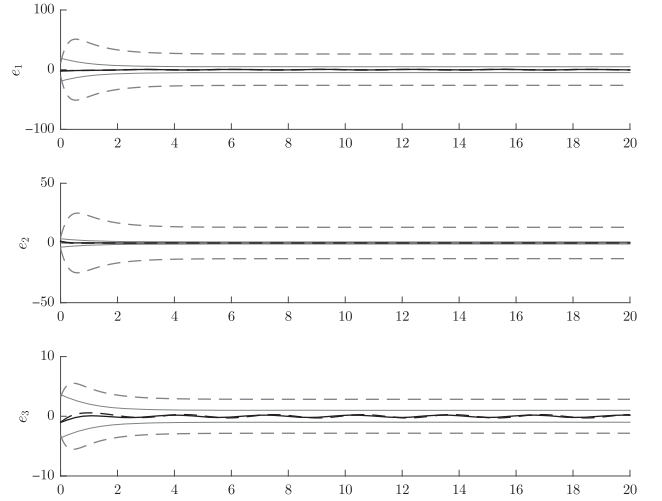


Fig. 4 In black, simulation results over 20s for the system in (35) and in grey solid line, bounds of the interval observer obtained using the control-based approach. The results obtained using Lemma 1 in [4] are represented in dashed lines

Table 3 Control-based approach parameters for the example described in Section 6.3, $T_{d_t \rightarrow e_t}(z)$ refers to the transfer function from e_t to d_t , stability of the observation error dynamics is also ensured

Syn. model	Requirement	Settings
(C1-DT) (C3)	(R1-DT) (R3)-1 (R3)-2	$m_{ij}^{\max} = 100$ Stab. (42) $\ T_{d_t \rightarrow e_t}(z)\ _2 \leq 1$

which leads to the following matrix $M = P(A - LC)P^{-1}$

$$M = \begin{bmatrix} 0.9000 & 0.0000 & -0.0000 & 0.0000 & -0.0000 \\ -0.0000 & 0.7000 & -0.0000 & 0.0000 & 0.0000 \\ -0.0000 & -0.0000 & 0.1000 & -0.0000 & 0.0000 \\ 0.0000 & 0.0000 & 0.0000 & 0.5000 & -0.0000 \\ -0.0000 & -0.0000 & 0 & -0.0000 & 0.3000 \end{bmatrix} \quad (46)$$

Due to numerical errors, the matrix M is not non-negative up to the machine precision.

6.3.2 Control-based approach: The approach proposed in Sections 4 and 5 is used, in the case of DT systems. The synthesis models and requirements used are recalled in Table 3.

Using the control law synthesis algorithm presented in Section 5.1, a local optimal solution is found after 3 restarts and 400 iterations at maximum. The execution time rises to 41 s. The following matrices are obtained

$$M_d = \begin{bmatrix} 0.1552 & 0.0166 & 0.0000 & 3.9459 & 0.0000 \\ 0.0108 & 0.3773 & 0.1110 & 0.0035 & 0.0240 \\ 0.0000 & 0.1725 & 0.0529 & 0.0281 & 0.0050 \\ 0.0000 & 0.0761 & 0.0877 & 0.1050 & 0.0000 \\ 0.4027 & 0.0181 & 0.1069 & 0.0066 & 0.4067 \end{bmatrix}, \quad P = \begin{bmatrix} 0.9952 & 0.4521 & 0.0923 & 0.2680 & -0.0638 \\ -0.3055 & 1.0187 & 0.1835 & 0.2143 & -0.3359 \\ -0.5536 & 0.0632 & 0.9009 & 0.1155 & -0.5773 \\ -0.0634 & 0.1535 & 0.1303 & 0.2667 & -0.0216 \\ 0.1970 & 0.2770 & 0.2393 & 0.1984 & 1.2526 \end{bmatrix}, \quad L = \begin{bmatrix} -0.5400 & -0.9321 \\ 0.6300 & 0.1244 \\ -0.0900 & -0.4325 \\ 0.3536 & 0.3300 \\ -0.3536 & 0.4908 \end{bmatrix} \quad (47)$$

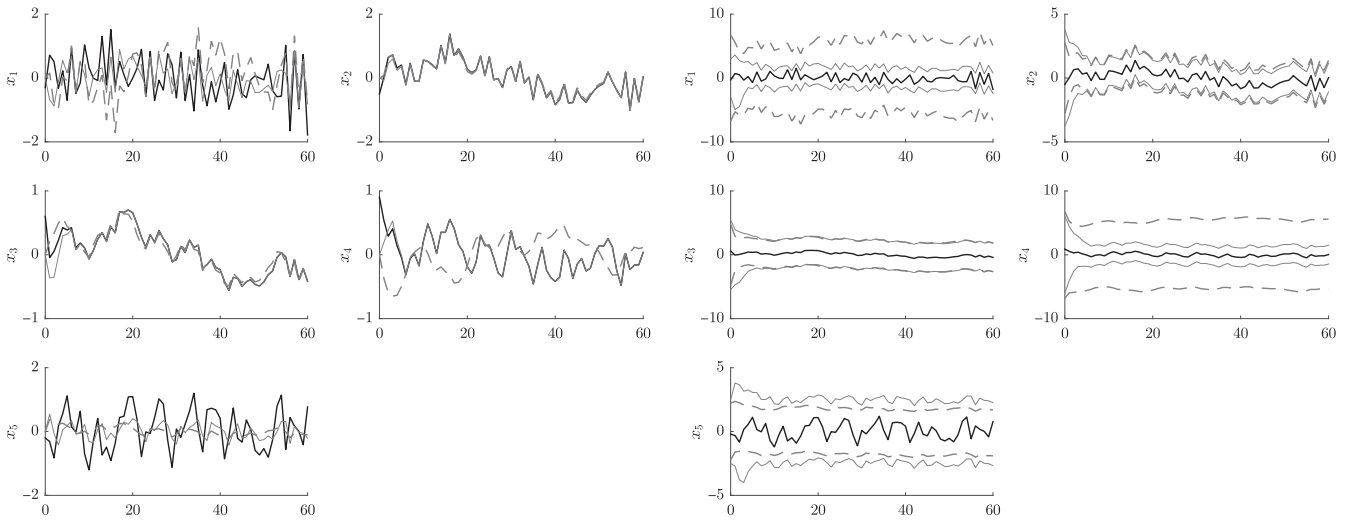


Fig. 5 Left: in black, simulation results for system (40) and in grey solid (resp. dashed) line, for the DT formulation of the classical observer in (8) obtained using the observer gain L produced by the control-based approach (resp. real pole placement). Right: bounds of the interval observer compared to the simulated state

where $M_d = P(A_d - LC_d)P^{-1}$ is Schur-stable and non-negative as required.

6.3.3 Simulations and comparisons: The disturbance d_t used for the simulation is randomly generated with $d_t \in [-1, 1]$. The simulation results are shown in Fig. 5.

The results obtained using the control-based approach are very satisfactory. The simultaneous synthesis of P and L leads to a more precise observer. An arbitrary choice of the poles is not required anymore since it is included in the optimisation process.

7 Conclusions

In this paper, a new approach to compute an appropriate change of coordinates for a system to be cooperative in these new coordinates has been introduced following preliminary results in [5]. Both the CT and DT cases have been considered. An overview of the existing techniques to determine such transformation has been performed. The new approach has been applied on three examples and compared with the existing techniques.

The proposed method is based on structured controller synthesis techniques [6, 23]. It is used to enforce specific properties on the state-space matrices of a system. The main addition of the method in comparison with existing ones is the possibility to satisfy additional constraints dealing with the dynamics of the observer. Also, in the case of interval observers, matrices P and L are determined simultaneously while other methods require to choose a targeted Metzler matrix M with the same eigenvalues as $A - LC$, which is not an easy task from the authors point of view.

The current limitation of the method is the computation time which increases with the order of the system. Also, it uses algorithms which were not specifically designed for this task. The consequence is a loss in computational efficiency. As far as the theory of interval observers is concerned, the proposed method currently only applies to determining a time-invariant change of coordinates in the linear time-invariant case. A perspective of this work could be to extend the approach to the time-varying case for which theoretical results have been proposed [8].

8 References

- 1 Gouzé, J.L., Rapaport, A., Hadj-Sadok, M.Z.: 'Interval observers for uncertain biological systems', *Ecol. Model.*, 2000, **133**, (1–2), pp. 45–56
- 2 Smith, H.L.: 'Monotone dynamical systems: an introduction to the theory of competitive and cooperative systems. Mathematical Surveys and Monographs'

- vol. 41, (American Mathematical Society, Providence, Rhode Island, 1995)
- 3 Mazenc, F., Bernard, O.: 'Interval observers for linear time-invariant systems with disturbances', *Automatica*, 2011, **47**, (1), pp. 140–147
- 4 Răssi, T., Efimov, D., Zolghadri, A.: 'Interval state estimation for a class of nonlinear systems', *IEEE Trans. Autom. Control*, 2012, **57**, (1), pp. 260–265
- 5 Chambon, E., Apkarian, P., Burlion, L.: 'Metzler matrix transform determination using a non-smooth optimization technique with an application to interval observers'. Proc. SIAM Conf. on Control and its Applications, Paris, France, 2015, p. 205–211
- 6 Apkarian, P.: 'Tuning controllers against multiple design requirements'. Proc. American Control Conf. Washington, USA, 2013, pp. 3888–3893
- 7 Cacace, F., Germani, A., Manes, C.: 'A new approach to design interval observers for linear systems', *IEEE Trans. Autom. Control*, 2015, **60**, (6), pp. 1665–1670
- 8 Efimov, D., Raïssi, T., Chebotarev, S. *et al.*: 'Interval state observer for nonlinear time varying systems', *Automatica*, 2013, **49**, (1), pp. 200–205
- 9 Rapaport, A., Gouzé, J.L.: 'Parallelotopic and practical observers for nonlinear uncertain systems', *Int. J. Control*, 2002, **76**, pp. 237–251
- 10 Mazenc, F., Bernard, O.: 'Asymptotically stable interval observers for planar systems with complex poles', *IEEE Trans. Autom. Control*, 2010, **55**, (2), pp. 523–527
- 11 Combastel, C., Raka, S.A.: 'A stable interval observer for LTI systems with no multiple poles'. Proc. 18th IFAC World Congress. Milano, Italy, 2011, pp. 14335–14341
- 12 Thabet, R.E.H., Raïssi, T., Combastel, C., *et al.*: 'An effective method to interval observer design for time-varying systems', *Automatica*, 2014, **50**, (1), pp. 2677–2684
- 13 Efimov, D., Raïssi, T., Zolghadri, A.: 'Control of nonlinear and LPV systems: interval observer-based framework', *IEEE Trans. Autom. Control*, 2013, **58**, (3), pp. 773–778
- 14 Dinh, T.N., Mazenc, F., Niculescu, S.I.: 'Interval observer composed of observers for nonlinear systems'. Proc. European Control Conf. Strasbourg, France, 2014, pp. 660–665
- 15 Efimov, D., Raïssi, T.: 'Design of interval observers for uncertain dynamical systems', *Autom. Remote Control*, 2015, **77**, (2), pp. 191–225
- 16 Dinh, T.N.: 'Interval observer and positive observer'. PhD thesis, Université Paris-Sud. Paris, France, 2014
- 17 Efimov, D., Perruquetti, W., Răssi, T. *et al.*: 'On interval observer design for time-invariant discrete-time systems'. Proc. European Control Conf., Zürich, Switzerland, 2013, pp. 2651–2656
- 18 Efimov, D., Raïssi, T., Perruquetti, W., *et al.*: 'Estimation and control of discrete-time LPV systems using interval observers'. Proc. 52nd IEEE Conf. on Decision and Control, Florence, Italy, 2013, pp. 5036–5041
- 19 Golub, G.H., Nash, S., Van Loan, C.: 'A Hessenberg-Schur method for the problem $AX + XB = C$ ', *IEEE Trans. Autom. Control*, 1979, **24**, (6), pp. 909–913
- 20 Bartels, R.H., Stewart, G.W., *et al.*: 'Solution of the matrix equation $AX + XB = C$ ', *Commun. ACM*, 1972, **15**, (9), pp. 820–826
- 21 Doyle, J.C., Glover, K., Khargonekar, P., *et al.*: 'State-space solutions to standard H_2 and H_∞ control problems', *IEEE Trans. Autom. Control*, 1989, **34**, pp. 831–847
- 22 Apkarian, C.: 'The Riccati inequality and state-space H_∞ -optimal control'. PhD thesis, University of Würzburg, 1990
- 23 Apkarian, P., Noll, D.: 'Nonsmooth H_∞ synthesis', *IEEE Trans. Autom. Control*, 2006, **51**, (1), pp. 71–86
- 24 Gahinet, P., Apkarian, P.: 'Structured H_∞ synthesis in MATLAB'. Proc. 18th IFAC World Congress, Milan, 2011, pp. 1435–1440

- 25 Burke, J.V., Henrion, D., Lewis, A.S., *et al.*: 'HIFOO – a MATLAB package for fixed-order controller design and H_∞ optimization'. Proc. Fifth IFAC Symp. on Robust Control Design, Toulouse, France, 2006
- 26 Gahinet, P., Apkarian, P.: 'Frequency-domain tuning of fixed-structure control systems'. Proc. UKACC Int. Conf. on Control. Cardiff, UK, 2012, pp. 178–183
- 27 Apkarian, P., Gahinet, P., Buhr, C.: 'Multi-model, multi-objective tuning of fixed-structure controllers'. Proc. European Control Conf. Strasbourg, France, 2014, pp. 856–861
- 28 MATLAB: 'Robust Control Toolbox version 5.2 (R2014b)'. The MathWorks Inc., Natick, Massachusetts, 2014

Chapitre 7

Analyse, synthèse ou observation non linéaires pour l'atterrissage basé vision de systèmes aérospatiaux

Résumé du chapitre : nous présentons ici un problème particulier d'atterrissage basé vision sous un angle qui nous a permis de proposer quelques résultats originaux en terme d'observation, analyse ou commande robustes.

- Dans un premier temps, nous effectuons un certain nombre de rappels sur les asservissements visuels et posons le problème de l'atterrissage automatique d'un Airbus en utilisant une caméra et des capteurs inertiels embarqués.
 - Dans un second temps, nous présentons des travaux d'analyse d'observabilité et de synthèse d'observateurs non linéaires permettant d'estimer la profondeur de la scène observée par la caméra.
 - Enfin, nous présentons quelques travaux basés sur l'anti-windup appliqué à la dynamique longitudinale du guidage basé vision de l'avion lorsque la commande est saturée. Nous avons notamment proposé trois solutions :
 1. la synthèse d'une boucle anti-windup basée sur l'estimation de la profondeur,
 2. la synthèse d'une boucle anti-windup robuste à la méconnaissance de la profondeur,
 3. l'analyse de stabilité d'une loi de guidage utilisant une boucle anti-windup synthétisée pour une valeur "probable" de la profondeur.
-

7.1 Introduction

Nos travaux de recherche sur la commande basée vision ont commencé en 2011 par l'encadrement de la thèse de Guillaume Sabiron (2011-2013) qui consistait à utiliser des capteurs de flux optique pour l'atterrissage lunaire autonome. Nous avons montré que de tels capteurs bas coûts et très légers (quelques grammes) pouvaient apporter une solution de secours intéressante en cas de défaillance des capteurs inertiels. Ensuite, nous avons développé des solutions de guidage basé vision pour la phase d'atterrissage d'aéronefs en coordonnant le projet ANR VISIOLAND (2013-2017) et en co-encadrant la thèse de Victor Gibert (2013-2016). Dans ces deux cas, le problème consistait à utiliser dans une boucle de guidage des informations imprécises. L'imprécision provenait de la profondeur de la scène qui est perdue lorsque l'espace 3D est projeté sur le plan image 2D de la caméra. Sur le plan théorique cela signifiait qu'une grandeur incertaine et temps variant pouvait potentiellement déstabiliser la boucle de guidage.

7.2 Contexte et positionnement de nos travaux

Comme nous allons le voir, c'est dans un double contexte industriel et académique que se situent nos travaux de recherche en asservissements visuels.

7.2.1 Utilisation de la vision dans l'industrie aéronautique

La plupart des drones commerciaux sont aujourd'hui équipés d'une ou plusieurs caméras. Celles-ci leur permettent de réaliser un certain nombre de tâches comme par exemple la fonction "follow-me". Enfin, la localisation et cartographie simultanées, connue en anglais sous le nom de SLAM, contribue actuellement à rendre les drones plus autonomes en leur permettant d'évoluer dans un environnement incertain. Les méthodes basées sur l'apprentissage et la vision sont aussi en train de prendre beaucoup d'importance dans le domaine des drones (voir par exemple [37, 104]).

L'industrie aéronautique n'est pas en reste et s'intéresse elle-aussi de plus en plus aux systèmes de vision. En effet, l'utilisation d'une caméra pourrait s'avérer extrêmement utile pour réaliser des tâches de localisation, d'exploration mais aussi d'évitement d'obstacles. En particulier, l'aviation civile et militaire se sont intéressées à l'utilisation de la vision pour améliorer la phase

d'atterrissage. Par exemple, les projets suivants et relativement récents ont permis une collaboration étroite entre l'industrie et la recherche :

- le projet Européen PEGASE (2006-2009) [48, 99], coordonné par Dassault Aviation, s'est intéressé à l'atterrissage basé vision sur une piste totalement connue,
- le projet ANR VISIOLAND (2013-2017) que nous avons coordonné et monté à la demande d'Airbus s'est intéressé à l'atterrissage basé vision sur une piste méconnue.
- Dans la continuité de VISIOLAND, Airbus a ensuite intensifié ses travaux sur la vision et a lancé deux projets : EAGLE et ATTOL. Le projet ATTOL, démarré en 2018, vise notamment à effectuer des tests approfondis sur un A320 modifié et à certifier des logiciels de vols utilisant des informations visuelles. Enfin, son projet de voiture volante 'VAHANA' emporte des caméras, lidars et radars pour réaliser la tâche 'sense and avoid'.
- le projet Européano-Japonais VISION (2016-2019) vise à fusionner les informations visuelles et inertielles d'un aéronef pour le rendre plus robuste aux pannes ou lui permettre de détecter un obstacle surgissant. Ce projet a pour partenaires industriels Airbus, Dassault Aviation, Ricoh, Enri ou Mitsubishi Space Software.

Les travaux que nous avons menés dans le cadre du projet VISIOLAND s'inscrivent ainsi dans un contexte stimulant où l'utilisation de capteurs visuels prend de plus en plus d'importance.

7.2.2 Asservissements visuels "classiques" puis "saturés"

La commande référencée vision, aussi appelée asservissement visuel, consiste à contrôler les mouvements d'un système en utilisant des informations issues d'un capteur vision. L'utilisation de la vision peut paraître de prime abord naturelle mais il a fallu attendre que le traitement des images puisse se faire en temps réel pour pouvoir utiliser des informations visuelles dans une boucle de rétroaction. Ainsi, les premières utilisations de la vision dans un système en boucle fermée datent des années 70 [106, 71] et ont d'abord permis d'améliorer la précision des bras manipulateurs. Aujourd'hui, le contrôle basé sur la vision est de plus en plus utilisé dans des environnements incertains avec des applications automobiles et aérospatiales.

Les asservissements visuels appartiennent généralement à deux familles de méthodes [72, 35, 36] selon que l'on cherche ou pas à reconstituer la POSE (position et orientation) du système contrôlé à partir des images. En effet,

- soit on reconstruit la POSE de manière à utiliser "telle quelle" la loi de commande qui serait utiliser si on la connaissait précisément. On dit alors que l'asservissement visuel est de type PBVS (pour Pose Based Visual Servoing) ;
- soit on cherche à contrôler directement la position des indices visuelles dans l'image observée de manière à superposer l'image courante et l'image désirée. On dit alors que l'asservissement visuel est de type IBVS (pour Image based Visual Servoing).

Des solutions intermédiaires [85, 47] existent aussi de manière à combiner ces deux approches. C'est d'ailleurs sur cette voie que nous nous sommes engagés dans le projet VISIOLAND puisque nous nous sommes demandés s'il était nécessaire de reconstituer partiellement ou totalement la POSE relative entre un aéronef et sa piste d'atterrissage pour le faire atterrir automatiquement à l'aide d'une caméra. En effet, il était possible à partir d'une seule image et des capteurs inertiels de reconstituer l'attitude relative ainsi que la position relative à une grandeur près (ici la profondeur du champ de la caméra). La question était alors d'estimer ou pas cette information manquante . Notons ici qu'il s'agissait d'un problème d'estimation d'une grandeur qui apparaît de manière non linéaire dans le système à étudier [1, 43, 76]. Nous avons collaboré avec le LS2N (A. Chriette et F. Plestan) sur cette thématique.

Une autre question qui nous a amenés à effectuer un certain nombre de travaux de recherche était de savoir comment prendre en compte les saturations des actionneurs (et/ou des contraintes de sorties) lorsque l'on utilise des informations visuelles dans une boucle de commande et comment apporter des garanties théoriques sur le système bouclé. Plusieurs chercheurs avaient déjà étudié des schémas de commande saturée utilisant des informations visuelles imprécises [40, 45, 46] mais les classes de systèmes non linéaires différaient de celles que nous avons à traiter. Nous avons collaboré avec le LAAS CNRS (S. Tarbouriech et L. Zaccarian) sur cette seconde thématique.

7.3 Problématique

Le projet VISIOLAND dont l'ensemble des tâches a été décrit au chapitre précédent nous a conduit à étudier la dynamique de guidage d'un avion qui évolue à vitesse constante et doit s'aligner avec sa piste d'atterrissage avant d'effectuer l'arrondi final (flare) lui permettant de se poser sur la piste. Rappelons que le but du projet était de pouvoir se passer des équipements au sol (type ILS, GLS) et d'utiliser seulement des capteurs embarqués (ici les centrales inertielles et une simple caméra). Dans ce contexte, aligner l'avion consiste à lui faire rejoindre et suivre à vitesse constante une pente d'approche (ou glide) en utilisant uniquement ses capteurs embarqués. Le schéma suivant donne les principales notations utilisées dans la discussion qui suit :

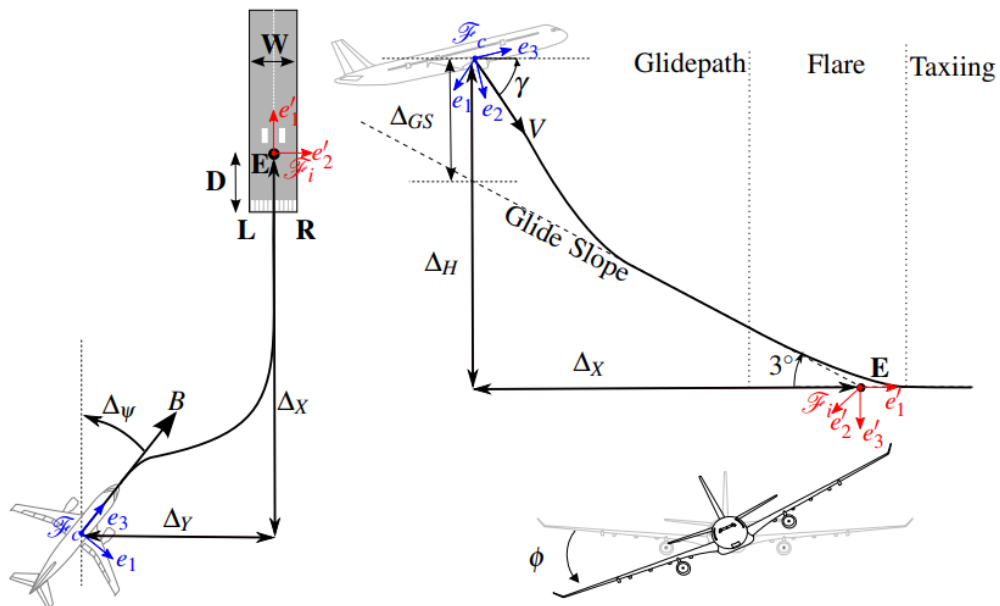


FIGURE 7.1 – Notations

- (E, e'_1, e'_2, e'_3) est le repère piste positionné au point d'aboutissement. La piste est supposée parfaitement plate.
- (G, e_1, e_2, e_3) est le repère avion (G étant le centre de gravité de l'avion)
- $\Delta\psi, \gamma, \phi$ représentent respectivement le cap de l'avion par rapport à la piste, la pente de l'avion (ou assiette) et le roulis de l'avion.

- $\Delta_X, \Delta_Y, \Delta_H$ sont les écarts de position entre l'avion et le point d'aboutissement exprimés dans le repère piste.
- $\Delta_{GS} = \Delta_H - \tan(\gamma_c)\Delta_X$ représente l'écart vertical entre le glide et l'avion ($\gamma_c = 3deg$ est l'angle entre la piste et le glide)
- V est la vitesse constante de l'avion

Notons à présent $\Delta_\gamma = \gamma - \gamma_c$. Aligner l'avion signifie alors annuler les variables $\Delta_{GS}, \Delta_Y, \Delta_\gamma, \Delta_\psi, \phi$.

En utilisant les relations liant ces variables et en introduisant les entrées de commande de la boucle de guidage de l'avion, l'alignement revient à stabiliser autour de l'origine les deux systèmes suivants :

$$\begin{cases} \dot{\Delta}_{GS} &= V \sin(\Delta_\gamma) + V \cos(\Delta_\gamma + \gamma_c) \sin(\gamma_c)(1 - \cos(\Delta_\psi)) \\ \dot{\Delta}_\gamma &= u_1 \end{cases} \quad (7.1)$$

$$\begin{cases} \dot{\Delta}_Y &= V \cos(\Delta_\gamma + \gamma_c) \sin(\Delta_\psi) \\ \dot{\Delta}_\psi &= \frac{g}{V} \tan(\phi) \\ \dot{\phi} &= u_2 \end{cases} \quad (7.2)$$

Ces systèmes représentent les dynamiques de guidage longitudinal et latéral de l'avion en phase d'approche. Nous remarquons qu'il y a des termes de couplage entre ces deux dynamiques qui peuvent être négligés lorsque Δ_ψ est faible.

Nous remarquons aussi que les linéarisés tangents de ces deux systèmes sont des chaînes d'intégrateurs :

$$\begin{cases} \dot{\Delta}_{GS} &= V \Delta_\gamma \\ \dot{\Delta}_\gamma &= u_1 \end{cases} \quad (7.3)$$

$$\begin{cases} \dot{\Delta}_Y &= V \Delta_\psi \\ \dot{\Delta}_\psi &= \frac{g}{V} \phi \\ \dot{\phi} &= u_2 \end{cases} \quad (7.4)$$

Ce problème de guidage peut sembler de prime abord simple ; pourtant, il peut devenir relativement complexe lorsqu'on ne mesure pas tout l'état du système et que l'on prend en compte les saturations des entrées de commande u_1 et u_2 .

En effet, il est possible de montrer [22] que l'utilisation d'informations visuelles et de capteurs inertiels 'idéaux' permet d'extraire les informations suivantes :

$$Y = \begin{cases} \frac{\Delta_{GS}}{\Delta_X} \\ \Delta_\gamma \\ \frac{\Delta_Y}{\Delta_X} \\ \Delta_\psi \\ \phi \end{cases} \quad (7.5)$$

Autrement dit la première composante de l'état de chacun de ces systèmes n'est connue qu'à un facteur d'échelle près et temps variant $\frac{1}{\Delta_x}$. Le point de départ de notre étude a été d'observer que les lois de guidage classiques d'un airbus (synthétisées par placement de pôles sur les systèmes linéarisés) peuvent déstabiliser ces systèmes lorsqu'on utilise non plus l'état du système mais le vecteur des sorties Y et qu'on a un modèle d'avion complet prenant en compte les saturations des entrées de guidage. D'un point de vue opérationnel, déstabiliser les boucles de guidage revient à activer les lois de protection puis à redonner la main au pilote humain : ce n'est donc pas dramatique mais ça revient à abandonner notre objectif initial qui était de réaliser automatiquement l'alignement.

7.4 Nos contributions

7.4.1 Estimation de la profondeur

La thèse de Victor Gibert nous a amené à étudier de près la synthèse d'estimateurs de la grandeur non mesurée $\frac{1}{\Delta_x}$. Plus précisément, nous avons :

- effectué un travail important sur l'analyse d'observabilité qui a permis de définir les indices visuels utilisables dans l'image pour garantir l'observabilité du système tout au long de la phase d'approche
- nous avons proposés et comparés plusieurs solutions d'estimation [75, 73, 76, 62, 61] de la grandeur manquante Δ_x . Nous avons notamment étudié la sensibilité de différents observateurs aux bruits de mesure et erreurs de calibration de la camera.
- nous avons confrontés ces estimateurs à des mesures réalistes en utilisant des images synthétiques ou des images enregistrées à bord d'un Airbus d'essai.

Nous présentons une partie de ces travaux dans un article ci-joint et paru dans la revue *Control Engineering Practice* en 2018 [63].

7.4.2 Analyse et commande de la dynamique longitudinale

Les solutions PBVS s'avèrent préférables pour les applications industrielles puisque les lois de guidage, d'ores et déjà validées par les autorités de certification telles que l'EASA ou la FAA, peuvent être réutilisées et l'effort de certification se limite seulement aux algorithmes d'estimation. Pourtant, la synthèse d'estimateurs "seule" ne permettait pas de répondre à la problématique initiale consistant à apporter des garanties théoriques sur la stabilité

de la boucle fermée. C'est pour cette raison que nous avons ensuite effectué un certain nombre de travaux de recherche sur la synthèse anti-windup.

- Partant d'un schéma d'estimation donné, nous avons pu démontrer la stabilité de la boucle fermée en combinant la solution PBVS associée avec une boucle d'anti windup. Nous avons démontré que le système bouclé était globalement uniformément asymptotiquement stable en utilisant la notion de iISS (stabilité intégrale entrée-état) [107]. En effet, le système bouclé n'était pas ISS (stabilité entrée-état) pour une entrée (ici l'erreur d'estimation) bornée mais la propriété iISS a permis de prendre en compte que cette erreur d'estimation tendait asymptotiquement vers 0.
- Nous avons proposé un nouveau schéma d'anti-windup nous permettant de stabiliser le système sans avoir à estimer Δ_X et ce malgré la mesure imprécise et la saturation de la loi de commande. Nous avons démontré la convergence globale asymptotique et uniforme du système bouclé en utilisant le principe d'invariance étendu aux systèmes hybrides [65, 103].
- De nouveaux outils d'analyse basés sur des fonctions de Lyapunov à paramètres dépendants (PDLF) ont aussi été développés pour valider une loi de guidage basé vision (ne cherchant pas à estimer Δ_X) en temps asymptotique ou en temps fini. Le temps fini est particulièrement intéressant dans notre contexte puisque nous devons aligner l'avion avec la piste avant de commencer l'arrondi.

Nous présentons ces différents travaux dans les articles ci-joints et parus respectivement à l'IFAC World Congress 2017 [22], Automatica 2019 [27] et l'IFAC LPVS 2018 [13]. Ces travaux de commande ont été illustrés sur la dynamique longitudinale de l'avion. Leur généralisation à la dynamique latérale demandent encore quelques travaux de recherche.

Enfin, le guidage basé vision de l'avion en phase d'approche a fait l'objet d'autres travaux (présentés dans le chapitre suivant). Ces derniers se basent sur une technique de commande dénommée "Backstepping borné".



Contents lists available at ScienceDirect

Control Engineering Practice

journal homepage: www.elsevier.com/locate/conengprac

Visual estimation of deviations for the civil aircraft landing

V. Gibert^a, F. Plestan^{b,*}, L. Burlion^c, J. Boada-Bauxell^a, A. Chriette^b^a Department of Stability and Control, Airbus Operations SAS, Toulouse, France^b Ecole Centrale de Nantes-LS2N, UMR CNRS 6004, Nantes, France^c Onera, Toulouse, France

ARTICLE INFO

Keywords:

Visual estimation
Nonlinear observers
Aircraft landing

ABSTRACT

This paper presents a new scheme for the visual estimation of deviation of a system with respect to an object for which no feature is known (position, dimensions, ...). This scheme is based on nonlinear observers and, thanks to an adequate combination of the visual information, requires reduced computation for its design. It is evaluated on a scenario describing the landing of an aircraft on an unknown runway and is validated with synthetic images.

1. Introduction

In future aircraft, Airbus wishes to develop automatic landing “everywhere and every time”. The proposed solution based on cameras would allow operation of an aircraft as a pilot would operate it nowadays in case of DGPS loss and ILS unavailability, *i.e.* in visual flight rules. Then, the camera and observation scheme can be considered a sensor in case of failure of other sensors, even if the conditions of visibility are not ideal, thanks to infra-red or multimeter-waves cameras. The camera coupled, in this paper, to an observer (called software sensor) is also very interesting in the frame of data fusion and would appear as an additional redundant sensor. In this case, it could be used to verify readings from other measurement systems (GBAS/SBAS that equipped civil aircrafts, IRS), to re-calibrate them versus camera informations, to detect sensors failure or to ensure redundancy.

Not all airport runways are equipped with ILS (Instrument Landing System) technology, and GPS (Global Positioning System) is not always available; yet both of these systems are required to ensure automatic landing. A solution to overcome the lack of external information consists of using an embedded visual system for retrieving the deviation information of the aircraft versus the runway. Given that camera sensors and image processing algorithms have made large technological leaps in the last few decades, visual informations coupled with IRS (Inertial Reference System) measurements could induce a solution to perform automatic landing. Then, the camera provides informations for the control of the aircraft, which is called visual servoing. It consists of using a vision sensor and computer vision algorithms in order to control the motion of the system (see tutorial in Chaumette & Hutchinson, 2006). Note that, in civil aircraft applications, embedded sensors such as accelerometer or gyros provide accurate information so that the attitude

(yaw, pitch, roll angles) and the motion of the aircraft can be considered well-known; hence, the use of dynamics of visual features between several images is sufficient to estimate deviations with respect to (*w.r.t.*) the runway.

The first class of visual servoing control is named PBVS (Pose Based Visual Servoing) and consists of using visual measurements in order to estimate the pose of the camera, whereas the second class of control, named IBVS (Image Based Visual Servoing), consists of controlling the coordinates of visual features in the image plane.

IBVS solutions applied to the automatic landing of an aircraft have been intensively studied during the last decade. Guidance solutions are proposed in Azinheira and Rives (2008) and Le Bras, Hamel, Barat, and Mahony (2009) in order to reach and track the desired trajectory by using only lines coordinates detected in the image of the runway, or in Coutard, Chaumette, and Pflimlin (2011) and Gibert and Puyou (2013) in which the control is based on centerline and touchdown point coordinates. Nevertheless, these scheme imply the development of new guidance laws with a completely new structure (composed of image capture, image processing and guidance algorithms) which might be difficult to certify by the authorities and strongly increases the cost of these solutions. In fact, the use of already certified guidance laws is a key-point for aircraft manufacturers; it is the main reason why the IBVS solution is not the “ideal” one. Therefore, it is desired to introduce visual servoing, but without changing the control structure; this is why the PBVS described in the sequel presents a great interest.

The PBVS scheme could be divided in two steps: the first one is to estimate the deviations of the aircraft *w.r.t.* the runway, and, in the second step, the estimated deviations are used in the certified guidance laws. Note that a single camera provides a 2D view of the scene, but 3D

* Corresponding author.

E-mail address: franck.plestan@ec-nantes.fr (F. Plestan).

deviation estimation is required for the control of a landing aircraft. The estimation of the 3D deviations can be obtained by using more than one camera (Trisiripisal, Parks, Abbott, Liu, & Fleming, 2006). Nevertheless, stereo-vision appears difficult in civil aircraft application because, when the landing operations start, the distance from runway is important; thus, calibration of both the cameras must be very precise which is a hard task in an industrial context. Another solution is based on knowledge of objects (here, the runway) dimensions (Gui et al., 2013). However, this paper considers a generic runway whose size and markers are not known: geometric reconstruction solutions using these informations cannot be applied. The last solution consists in using a monocular camera by taking into account its motion (Dahl, Nyberg, Holst, & Heyden, 2005; Giordano, De Luca, & Oriolo, 2008; Karagiannis & Astolfi, 2005). Note that these preliminary results with such approach are limited to the use of one single point in the image and there is not application with a landing scenario.

This last solution is selected to solve the 3D estimation problem and consists of using state observers. Thanks to this solution, the unknown scale factor can be estimated, and an estimation of the 3D information becomes available. Hence, there is a real interest to develop solutions in order to estimate the deviations of the camera *w.r.t.* the runway. For this purpose, the available information is the knowledge of attitude, velocities and accelerations provided by the Inertial Measurement Unit and visual measurements; *no geometric information of the runway is required*. The visual informations, provided by image processing algorithms, correspond to the perspective projection of the 3D corners of the runway in the image plane. To sum up, the problem remains to estimate a 3D information from 2D measurements. The authors of the current paper have already proposed estimation solutions of the deviations during an aircraft landing scenario. In Gibert, Burlion, Chriette, Boada-Bauxell, and Plestan (2015a), an extended observer solution of Karagiannis and Astolfi (2005) using more than 1 point has been proposed, with a detailed observability analysis of the system. In Gibert, Burlion, Chriette, Boada-Bauxell, and Plestan (2015b), observer solutions based on high gain approach and sliding mode theory have been designed in conditions such that the observability along the landing is guaranteed. However, these solutions do not have formal convergence proof, are quite complex to design and have been tested in simulation but not by using real image processing experiments.

The main contribution of this paper is to propose observation solutions, based on a new simplified formulation thanks to the use of a virtual frame. This new formulation provides a simple dynamic system that makes the design of the observers easy and guarantees the observability all along the landing trajectory. Then, a robust observer based on sliding mode theory is designed and compared to a high gain observer. Realistic results based on synthetic images and real image processing are detailed; the aircraft landing is made assuming that runway features are not known.

The paper is organized as follows. First, the problem under interest is presented with its simplified formulation. Then, the new observation scheme is presented by assuming that two points are tracked in the image; sliding mode and high gain observers are designed. Finally, results in realistic conditions thanks to synthetic images are proposed.

2. Problem formulation

The problem of range estimation based on a standard formulation in the camera frame has been tackled with different observers (Giordano et al., 2008; Karagiannis & Astolfi, 2005). However, it has been shown in Gibert et al. (2015a) that, if the objective is to estimate the deviations of the aircraft with respect to the runway, there are singularities of observability during the landing phase, when only a single point of the image is used. Therefore, a new problem formulation is proposed by introducing a *virtual frame* that allows to simplify the problem formulation and to get some interesting properties.

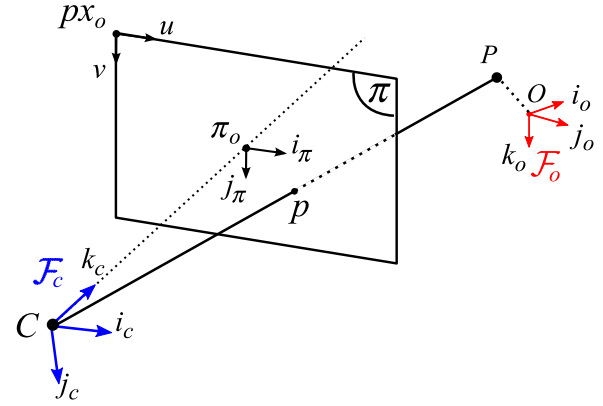


Fig. 1. Perspective projection of a point P in the image plane.

2.1. Standard formulation in the camera frame

Consider the following notations (see Fig. 1)

- $F_o = (O, i_o, j_o, k_o)$ an inertial frame (in the current application, it will be a frame linked to the runway);
- $P_o = (P_{o1}, P_{o2}, P_{o3})$ the 3D coordinates of a point P in F_o ;
- $F_c = (C, i_c, j_c, k_c)$ the camera frame whose origin, C , is the optical center of the camera;
- $P_c = (P_{c1}, P_{c2}, P_{c3})$ the coordinates of P in the frame F_c ;
- $F_\pi = (\pi_0, i_\pi, j_\pi)$ the image frame whose origin π_0 has coordinates in F_c , $\pi_0 = (0, 0, f)$ where f is the focal length of the camera.
- $F_{px} = (px_0, u, v)$ the pixelic frame whose origin is at the upper-left corner of the image.

The standard expression for the dynamics of the point P (that is fixed in F_o) in the camera frame F_c is (Dahl et al., 2005):

$$\begin{bmatrix} \dot{P}_{c1} \\ \dot{P}_{c2} \\ \dot{P}_{c3} \end{bmatrix} = A_c \cdot \begin{bmatrix} P_{c1} \\ P_{c2} \\ P_{c3} \end{bmatrix} + b_c \quad (1)$$

with $A_c \in M_{3,3}(\mathbb{R})$ and $b_c = [b_{c1} \ b_{c2} \ b_{c3}]^T \in \mathbb{R}^3$ respectively representing the skew matrix of the known rotational and translational velocities of the camera in the camera frame F_c .

The problem is that the state of (1) is not directly measured. Thanks to the vision system based on perspective projection camera model (Hartley & Zisserman, 2003), the available measurement of the 3D coordinates of the point P is a 2D vector y_c expressed in the image plane π and given by

$$y_c = \begin{bmatrix} y_{c1} \\ y_{c2} \end{bmatrix} = f \cdot \begin{bmatrix} \frac{P_{c1}}{P_{c3}} & \frac{P_{c2}}{P_{c3}} \end{bmatrix}^T \quad (2)$$

with f the focal length of the camera. For the rest of the paper, without loss of generality, the focal length is considered equal to 1.

The objective of the paper is to get an estimate of the state vector $[P_{c1} \ P_{c2} \ P_{c3}]^T$ from the knowledge of A_c , b_c , and y_c .

A necessary condition to design an observer for system (1) is that this latter is observable. Given that observability condition (Karagiannis & Astolfi, 2005) is fulfilled, solutions based on nonlinear observers have been proposed (Chen & Kano, 2002; Dahl et al., 2005; Karagiannis & Astolfi, 2005). However, in Gibert et al. (2015a), it has been shown that, *in the case of aircraft landing*, if the tracked point is the aiming guidance point on the runway, observability is not maintained all along the landing phase.

Then, in order to ensure observability all along the landing phase, a solution consists in using *at least* two points on the runway (*i.e.* which belong to the runway plane). This way, if one of the points is not providing observability, the second guarantees that the whole

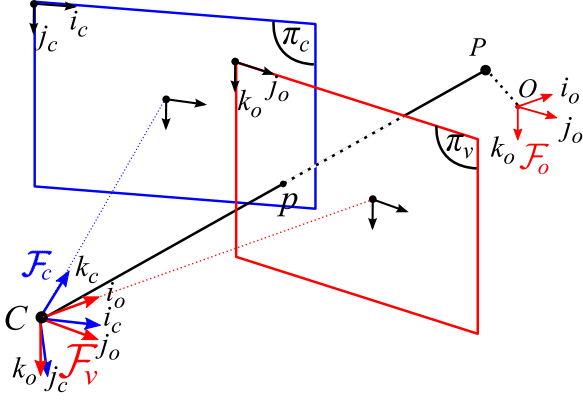


Fig. 2. Perspective projection of a point P in the image plane π_c , and in a virtual plan π_v .

system is observable. For estimation, any point in the runway plane can be considered and will provide the relative altitude of the aircraft *w.r.t.* the runway. The depth estimation problem is then solved. But the final objective is to guide the aircraft on a predefined trajectory, the selected points should have a physical meaning with respect to the guidance aiming point. Any points on the center line or symmetrically located *w.r.t.* the center line (on side lines for example) provide enough information for lateral control. However, for longitudinal control, the points should be chosen *w.r.t.* the aiming point of the glide slope trajectory. Selecting the two corners of the runway threshold, estimating the deviation of the aircraft *w.r.t.* these points and knowing that the aiming point is placed 400m after threshold, it is possible to estimate the pose of the aircraft *w.r.t.* the glide slope trajectory aiming point. The use of two points P' and P'' requires the use of two systems (1), each of these systems having measurement vectors $y'_c \in \mathbb{R}^2$ and $y''_c \in \mathbb{R}^2$ respectively for P' and P'' . A solution consists of designing two observers (one for each point) and in using a switching strategy (El Tannoury, Moussaoui, Plestan, Romani, & Pita-Gil, 2013) between both the observers. This strategy evaluates the observability for both the dynamic systems describing the motion of P' and P'' in the camera frame, and allows switching from one observer to the other one in case of loss of observability. This strategy involves designing two observation structures, and tuning a parameter allowing to evaluate the rate of observability.

In order to reduce the tuning task, the solution proposed in the sequel introduces a virtual frame in order to “link” P' and P'' using the fact that the points belong to the runway plane ; as a consequence, a single and simpler observation solution can be designed.

2.2. Simplified formulation in a virtual frame

In order to link the two points P' and P'' , a virtual frame F_v (see Fig. 2) is introduced. This virtual frame has the same orientation as the ground frame F_o and its origin is placed in the center of the camera C as F_c . The use of this virtual frame is standard in cases of image stabilization. However, the context of this paper makes its use original given that the final objective is system observation and not image stabilization.

In fact, the virtual frame can be viewed as a frame linked to a *virtual camera* that will rotate in order to have a virtual image plane π_v always parallel to (j_o, k_o) -plane of F_o . As a consequence, in F_v , the coordinates of P' and P'' do not depend on the rotation of the camera. Furthermore, recalling the context of aircraft landing, the points P' and P'' are located on the runway and then, at least their coordinates along k_o -vector are the same (by supposing that both the points have the same altitude). All these features mean that the dynamics of the system expressed in F_v are simpler and have a reduced dimension. This implies that the

design of the observation structure developed in the sequel is simplified. Considering the Euler angles respectively the yaw ψ , pitch θ and roll ϕ between the camera frame F_c and the ground frame F_o , it is possible to write the coordinates of these two points in the virtual frame.

Denoting $[P'_{v1} \ P'_{v2} \ P'_{v3}]^T$ the coordinates of P' in the virtual frame F_v and $[P'_{c1} \ P'_{c2} \ P'_{c3}]^T$ the coordinates of P' in F_c , one has¹

$$\begin{bmatrix} P'_{v1} \\ P'_{v2} \\ P'_{v3} \end{bmatrix} = {}^vR_c \begin{bmatrix} P'_{c1} \\ P'_{c2} \\ P'_{c3} \end{bmatrix} \quad (3)$$

with vR_c the rotational matrix from F_c to F_v , respecting “pitch-roll-yaw” Euler angles convention, defined as

$$\begin{aligned} {}^vR_c &= \begin{bmatrix} \cos \psi & -\sin \psi & 0 \\ \sin \psi & \cos \psi & 0 \\ 0 & 0 & 1 \end{bmatrix} \cdot \begin{bmatrix} \cos \theta & 0 & \sin \theta \\ 0 & 1 & 0 \\ -\sin \theta & 0 & \cos \theta \end{bmatrix} \\ &\cdot \begin{bmatrix} 1 & 0 & 0 \\ 0 & \cos \phi & -\sin \phi \\ 0 & \sin \phi & \cos \phi \end{bmatrix} \cdot \begin{bmatrix} 0 & 0 & 1 \\ 1 & 0 & 0 \\ 0 & 1 & 0 \end{bmatrix} \\ &:= \begin{bmatrix} r_{11} & r_{12} & r_{13} \\ r_{21} & r_{22} & r_{23} \\ r_{31} & r_{32} & r_{33} \end{bmatrix}. \end{aligned} \quad (4)$$

Introduce the vector y_v , called the *virtual measurement vector* as

$$y_v = \begin{bmatrix} P'_{v1} & P'_{v2} & P'_{v3} \\ P''_{v1} & P''_{v2} & P''_{v3} \end{bmatrix}^T = [y'_1 \ y'_2 \ y''_1 \ y''_2]^T. \quad (5)$$

As it is shown in the sequel, this vector can be written as a function of only available measured variables. For example, the first component y_{v1} of y_v reads as

$$\begin{aligned} y_{v1} &= \frac{P'_{v1}}{P'_{v3}} = \frac{r_{11}P'_{c1} + r_{12}P'_{c2} + r_{13}P'_{c3}}{r_{31}P'_{c1} + r_{32}P'_{c2} + r_{33}P'_{c3}} \\ &= \frac{r_{11} \frac{P'_{c1}}{P'_{c3}} + r_{12} \frac{P'_{c2}}{P'_{c3}} + r_{13}}{r_{31} \frac{P'_{c1}}{P'_{c3}} + r_{32} \frac{P'_{c2}}{P'_{c3}} + r_{33}} \\ &= \frac{r_{11}y'_{c1} + r_{12}y'_{c2} + r_{13}}{r_{31}y'_{c1} + r_{32}y'_{c2} + r_{33}}. \end{aligned} \quad (6)$$

Remark 1. The virtual measurement vector y_v can be seen as the perspective projection of points P' and P'' in the virtual image frame π_v (see Fig. 2). Contrary to the camera image frame π_c that moves with the camera rotation, the virtual image frame π_v is always normal to the vector i_o in the F_o frame, and is aligned with j_o, k_o as depicted by Fig. 2. ■

Remark 2. In the field of application considered in the paper, the runway is coplanar to i_o and j_o . Therefore, the two points P' and P'' belong to the same plane so that, in the virtual frame, F_v , $P'_{v3} = P''_{v3}$. This assumption is weak since it is only assumed that the runway is at a constant altitude. ■

When expressing the dynamics of P' and P'' , the use of F_v allows the dynamics of both these points to be independent of the rotation velocities of the camera. Then, given Remark 2, dynamics of P' and P'' in F_v read as

$$\begin{bmatrix} \dot{P}'_{v1} \\ \dot{P}'_{v2} \\ \dot{P}'_{v3} \end{bmatrix} = - \begin{bmatrix} b_{v1} \\ b_{v2} \\ b_{v3} \end{bmatrix} \quad (7)$$

¹ Similar equation can be obtained for $[P''_{v1} \ P''_{v2} \ P''_{v3}]^T$, the virtual coordinates of P'' .

where $\mathbf{b}_v = [b_{v1} \ b_{v2} \ b_{v3}]^T$ is the known velocity vector of the camera with respect to the ground expressed in the virtual frame; the velocities b_{v1} , b_{v2} and b_{v3} are known thanks to the IRS.

2.3. Estimation problem

It would be possible to design an observer for system (7)–(5) but a similar formulation, as in Karagiannis and Astolfi (2005), is more convenient because it shows up the observability condition, allows a reduced order observer design and expresses the problem in a classical nonlinear state formulation. Indeed, defining the unmeasurable variable η , the inverse of the altitude, as

$$\eta = \frac{1}{P'_{v3}}, \quad (8)$$

the estimation problem of system (7)–(5) is equivalent to the estimation problem of the following system

$$\begin{aligned} \dot{y}'_1 &= -(b_{v1} - b_{v3}y'_1)\eta \\ \dot{y}'_2 &= -(b_{v2} - b_{v3}y'_2)\eta \\ \dot{y}''_1 &= -(b_{v1} - b_{v3}y''_1)\eta \\ \dot{y}''_2 &= -(b_{v2} - b_{v3}y''_2)\eta \\ \dot{\eta} &= b_{v3}\eta^2 \end{aligned} \quad (9)$$

where $\mathbf{y}_v = [y'_1 \ y'_2 \ y''_1 \ y''_2]^T$ is the measured vector and η is the single state variable that must be estimated.

To summarize, consider the nonlinear system

$$\begin{aligned} \dot{\mathbf{y}}_v &= F(\mathbf{b}_v, \mathbf{y}_v) \cdot \eta \\ \dot{\eta} &= b_{v3} \cdot \eta^2 \end{aligned} \quad (10)$$

with $\mathbf{y}_v \in \mathbb{R}^4$ the measured output and $\mathbf{b}_v \in \mathbb{R}^3$ the control input; both of these vectors are known. The state variable η is not measured. Then, an observer has to be designed in order to get an estimated value $\hat{\eta}$ of η , from the knowledge of \mathbf{y}_v and \mathbf{b}_v .

Observability analysis.

Proposition 1. System (9) is observable if the condition

$$(b_{v1} - b_{v3}y'_1)^2 + (b_{v2} - b_{v3}y'_2)^2 + (b_{v1} - b_{v3}y''_1)^2 + (b_{v2} - b_{v3}y''_2)^2 > 0 \quad (11)$$

is fulfilled. ■

It is obvious that, given (9), the state variable η can be reconstructed from one of the measured variables' dynamics if condition (11) is fulfilled. In the context of this paper, considering that two separated point P' and P'' of the runway are chosen (see in the sequel), it has been shown in Gibert et al. (2015a) that condition (11) is always respected during a civil aircraft landing.

Estimation of P'_{c1} , P'_{c2} and P'_{c3} . Once the estimation $\hat{\eta}$ of η obtained, one gets the estimation of P'_{v3} and P''_{v3} from

$$\hat{P}'_{v3} = \hat{P}''_{v3} = \frac{1}{\hat{\eta}}.$$

Then, from \mathbf{y}_v (5), one gets

$$\hat{P}'_{v1} = y'_1 \cdot \hat{P}'_{v3}, \quad \hat{P}''_{v1} = y''_1 \cdot \hat{P}''_{v3}$$

$$\hat{P}'_{v2} = y'_2 \cdot \hat{P}'_{v3}, \quad \hat{P}''_{v2} = y''_2 \cdot \hat{P}''_{v3}.$$

Finally, from (3), one derives the estimated values of the coordinates of P' and P'' in the camera frame, that are (only P' is shown; similar result is obtained for P'')

$$\begin{bmatrix} \hat{P}'_{c1} \\ \hat{P}'_{c2} \\ \hat{P}'_{c3} \end{bmatrix} = {}^v\mathcal{R}_c^{-1} \cdot \begin{bmatrix} \hat{P}'_{v1} \\ \hat{P}'_{v2} \\ \hat{P}'_{v3} \end{bmatrix} = {}^v\mathcal{R}_c^{-1} \cdot \begin{bmatrix} y'_1 \cdot \hat{P}'_{v3} \\ y'_2 \cdot \hat{P}'_{v3} \\ \frac{1}{\hat{\eta}} \end{bmatrix}. \quad (12)$$

3. Observer design

In order to take into account the measurement of the two points P' and P'' , an observer is designed and is based on a reduced form thanks to a state coordinates transformation. Thus, one gets a simpler system that induces the use of a reduced observer providing an estimation of η ; as previously displayed, the estimation of η allows to get estimation of P_{c1} , P_{c2} and P_{c3} .

3.1. Measurement combination

Suppose

H1. The measured vector \mathbf{y}_v and the control input vector \mathbf{b}_v are known and sufficiently differentiable. ■

H2. Condition (11) is fulfilled. ■

Considering the measurement vector \mathbf{y}_v (5), define the variable z_1 as

$$\begin{aligned} z_1 &= b_{v1}y'_1 - \frac{1}{2}b_{v3}y'^2_1 + b_{v2}y'_2 - \frac{1}{2}b_{v3}y'^2_2 + b_{v1}y''_1 \\ &\quad - \frac{1}{2}b_{v3}y''^2_1 + b_{v2}y''_2 - \frac{1}{2}b_{v3}y''^2_2. \end{aligned} \quad (13)$$

Then, the z_1 dynamics read as

$$\dot{z}_1 = \Delta_y \eta + \gamma(\mathbf{y}_v, \dot{\mathbf{b}}_v) \quad (14)$$

with

$$\begin{aligned} \Delta_y &= (b_{v1} - b_{v3}y'_1)^2 + (b_{v2} - b_{v3}y'_2)^2 + (b_{v1} - b_{v3}y''_1)^2 + (b_{v2} - b_{v3}y''_2)^2 \\ \gamma &= \dot{b}_{v1}y'_1 - \frac{1}{2}\dot{b}_{v3}y'^2_1 + \dot{b}_{v2}y'_2 - \frac{1}{2}\dot{b}_{v3}y'^2_2 \\ &\quad + \dot{b}_{v1}y''_1 - \frac{1}{2}\dot{b}_{v3}y''^2_1 + \dot{b}_{v2}y''_2 - \frac{1}{2}\dot{b}_{v3}y''^2_2. \end{aligned} \quad (15)$$

Then, thanks to (13), system (9) can be reformulated as

$$\begin{aligned} \dot{z}_1 &= \Delta_y \eta + \gamma(\mathbf{y}_v, \dot{\mathbf{b}}_v) \\ \dot{\eta} &= b_{v3}\eta^2 \end{aligned} \quad (16)$$

with z_1 the measured variable. Given hypothesis H2, the function Δ_y is strictly positive; then, z_1 being the measured variable of system (16), it is obvious to conclude that this latter is observable.

3.2. Observer design

Note that, in system (16), the term $\gamma(\mathbf{y}_v, \dot{\mathbf{b}}_v)$ only depends on the known variables. As shown in Moog, Plestan, Conte, and Perdon (1993) and Plestan and Glumineau (1997), this term is not required for the observer design, and can be removed thanks to an input–output injection function $-\gamma(\mathbf{y}_v, \dot{\mathbf{b}}_v)$ which does not change the observability property. It follows that the system (16) is transformed into (with abuse of notation)

$$\begin{aligned} \dot{z}_1 &= \Delta_y \eta \\ \dot{\eta} &= b_{v3}\eta^2. \end{aligned} \quad (17)$$

Consider the transformation

$$\Psi = \begin{bmatrix} z_1 \\ \dot{z}_1 \end{bmatrix} = \begin{bmatrix} z_1 \\ \Delta_y \eta \end{bmatrix} \quad (18)$$

Δ_y (15) can be re-written as $\Delta_y = 2b^2_{v1} + 2b^2_{v2} - 2b_{v3}z_1$, one gets

$$\Psi = \begin{bmatrix} z_1 \\ (2b^2_{v1} + 2b^2_{v2} - 2b_{v3}z_1) \eta \end{bmatrix}. \quad (19)$$

Given that system (17) is supposed to be observable, then the previous transformation is invertible and can be viewed as a state coordinates one. Defining the new state vector $\xi = [z_1 \ \dot{z}_1]^T = [\xi_1 \ \xi_2]^T$, one gets

$$\dot{\xi} = \underbrace{\begin{bmatrix} 0 & 1 \\ 0 & 0 \end{bmatrix}}_A \xi + \underbrace{\begin{bmatrix} 0 \\ \Phi_2(\eta, \mathbf{b}_v, \dot{\mathbf{b}}_v, \mathbf{y}_v) \end{bmatrix}}_{\Phi(\eta, \mathbf{b}_v, \dot{\mathbf{b}}_v, \mathbf{y}_v)}. \quad (20)$$

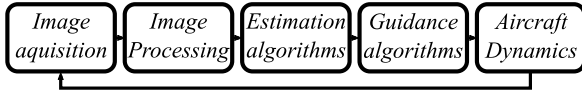


Fig. 3. Visual servoing diagram.

The matrix $\Phi(\cdot)$ is supposed to be composed by a nominal part (known) Φ_N and an uncertain part $\Delta\Phi$ such that

$$\Phi(\cdot) = \Phi_N + \Delta\Phi. \quad (21)$$

Proposition 2. An observer for system (20) reads as

$$\dot{\hat{\xi}} = A\hat{\xi} + \Phi_N(\hat{\eta}, \mathbf{b}_v, \dot{\mathbf{b}}_v, \mathbf{y}) + \kappa(\xi_1, \hat{\xi}_1) \quad (22)$$

with $\hat{\xi}$ the estimated state of ξ , and the function $\kappa(\xi_1, \hat{\xi}_1)$ called “correction term” that forces $\hat{\xi} \rightarrow \xi$. ■

Notice that the correction term $\kappa(\xi_1, \hat{\xi}_1)$ only depends on the measured variable ξ_1 and estimated state vector $\hat{\xi}$; it is not unique and can be obtained by several different methods depending on the desired features (robustness, finite time convergence, ...). Estimation error dynamics reads as (with $e = \hat{\xi} - \xi$)

$$\dot{e} = Ae + \Phi_N(\hat{\eta}, \mathbf{b}_v, \dot{\mathbf{b}}_v, \mathbf{y}) - \Phi(\eta, \mathbf{b}_v, \dot{\mathbf{b}}_v, \mathbf{y}) + \kappa(\xi_1, \hat{\xi}_1). \quad (23)$$

As previously introduced, $\kappa(\xi_1, \hat{\xi}_1)$ has to make the observer converge to the system in spite of the initial error $e(0)$ and the uncertainties/perturbations $\Delta\Phi$. From $\hat{\xi} = \Psi(\hat{z})$ ($\hat{z} = [\hat{z}_1 \ \hat{\eta}]^T$), one gets

$$\dot{\hat{\xi}} = \frac{\partial \Psi}{\partial \hat{z}} \dot{\hat{z}} \rightarrow \dot{\hat{z}} = \left[\frac{\partial \Psi}{\partial \hat{z}} \right]^{-1} \dot{\hat{\xi}} \quad (24)$$

with the Jacobian matrix $\frac{\partial \Psi}{\partial \hat{z}} = \begin{bmatrix} 1 & 0 \\ -2b_{v3}\hat{\eta} & \Delta_y \end{bmatrix}$. Then, as in El Tannoury et al. (2013), an observer for system (17) reads as

$$\begin{bmatrix} \dot{\hat{z}}_1 \\ \dot{\hat{\eta}} \end{bmatrix} = \begin{bmatrix} \Delta_y \hat{\eta} \\ b_{v3} \hat{\eta}^2 \end{bmatrix} + \left[\frac{\partial \Psi}{\partial \hat{z}} \right]^{-1} \kappa(z_1, \hat{z}_1). \quad (25)$$

The application of the inverse input-output injection transformation allows one to get an observer for system (16)

$$\begin{bmatrix} \dot{\hat{z}}_1 \\ \dot{\hat{\eta}} \end{bmatrix} = \begin{bmatrix} \Delta_y \hat{\eta} + \gamma(\mathbf{y}, \dot{\mathbf{b}}_v) \\ b_{v3} \hat{\eta}^2 \end{bmatrix} + \left[\frac{\partial \Psi}{\partial \hat{z}} \right]^{-1} \kappa(z_1, \hat{z}_1). \quad (26)$$

To summarize, the observer (26) allows one to obtain

$$\hat{\eta} = \frac{1}{\hat{P}'_{v3}} = \frac{1}{\hat{P}''_{v3}}.$$

As previously detailed in Section 2.3, from the estimated state and the measured vector \mathbf{y}_v (5), one gets, for both the points P' and P'' ,

$$\begin{bmatrix} \hat{P}'_{c1} \\ \hat{P}'_{c2} \\ \hat{P}'_{c3} \end{bmatrix} = {}^v\mathcal{R}_c^{-1} \cdot \begin{bmatrix} \hat{y}'_1 \\ \hat{\eta} \\ \hat{y}'_2 \\ \hat{\eta} \\ 1 \\ \hat{\eta} \end{bmatrix} \quad \text{and} \quad \begin{bmatrix} \hat{P}''_{c1} \\ \hat{P}''_{c2} \\ \hat{P}''_{c3} \end{bmatrix} = {}^v\mathcal{R}_c^{-1} \cdot \begin{bmatrix} \hat{y}''_1 \\ \hat{\eta} \\ \hat{y}''_2 \\ \hat{\eta} \\ 1 \\ \hat{\eta} \end{bmatrix}. \quad (27)$$

A positive feature of the proposed observer structure is that the “most intensive” computation is the inversion of Ψ -Jacobian; this is not a hard task given the reduced dimension of this matrix (2×2). In the sequel, the correction term $\kappa(z_1, \hat{z}_1)$ is detailed, the objective being to propose both nonlinear solutions: the first one being based on high gain approach whereas the second one is based on sliding mode theory.

High-gain observer (Gauthier, Hammouri, & Othman, 1992). The observer (26) for the system (17) admits a correction term $\kappa(z_1, \hat{z}_1)$ defined as

$$\kappa(z_1, \hat{z}_1) = \Lambda^{-1}K(z_1 - \hat{z}_1) \quad (28)$$

with the observer gain matrix K defined as

$$K = \begin{bmatrix} K_1 \\ K_2 \end{bmatrix} \quad (29)$$

so that $A - KC$ is Hurwitz with $C = [1 \ 0]$, and

$$A = \begin{bmatrix} \tau & 0 \\ 0 & \tau^2 \end{bmatrix} \quad (30)$$

with τ strictly positive. ■

Second-order sliding-mode observer (Levant, 2003). This solution is proposed in order to obtain an accurate and robust estimation of z_1 and η , and is based on high-order sliding-mode differentiation. Consider the system (22) and suppose that $|\Phi(\cdot)| \leq L_\Phi$ with L_Φ being the known Lipschitz positive constant. Then, an observer based on high-order sliding-mode (Levant, 2003, 2012) for system (22) reads as

$$\dot{\hat{\xi}}_1 = \hat{\xi}_2 + a_1 \underbrace{L_\Phi^{\frac{1}{2}} |\xi_1 - \hat{\xi}_1|^{\frac{1}{2}} \text{sign}(\xi_1 - \hat{\xi}_1)}_{\gamma_1} \quad (31)$$

$$\dot{\hat{\xi}}_2 = \Phi_{2N}(\cdot) + a_2 L_\Phi \text{sign}(\gamma_1).$$

Coefficients a_1 and a_2 must be fixed as proposed in Levant (2003)

$$a_1 = 1.5, \quad a_2 = 1.1. \quad (32)$$

A finite time convergence of the estimation $\hat{\xi} - \xi$ to the vicinity of 0 (see Theorem 6 in Levant (2003)) can be proven by rewriting (31) using the differential inclusion. Then, the observer (26) for the system (17) admits a correction term $\kappa(z_1, \hat{z}_1)$ defined as

$$\kappa(z_1, \hat{z}_1) = \begin{bmatrix} a_1 L_\Phi^{\frac{1}{2}} |\xi_1 - \hat{\xi}_1|^{\frac{1}{2}} \text{sign}(\xi_1 - \hat{\xi}_1) \\ a_2 L_\Phi \text{sign} \left(a_1 L_\Phi^{\frac{1}{2}} |\xi_1 - \hat{\xi}_1|^{\frac{1}{2}} \text{sign}(\xi_1 - \hat{\xi}_1) \right) \end{bmatrix}. \quad \blacksquare \quad (33)$$

Remark 3. For sake of clarity, the problem considered previously is just using two points. It is the minimal amount of information in order to theoretically guarantee observability. Nevertheless, the proposed observer could easily be extended to more than two points. ■

4. Civil aircraft landing application

The final objective is the use of visual servoing for the landing of an aircraft without knowledge of the runway features. Visual servoing is composed of different blocks (Fig. 3) that are image acquisition, image processing, estimation and guidance. The estimation block has to estimate the deviation of the aircraft with respect to the runway while the guidance algorithms force the aircraft to track a desired trajectory called “glide path”.

In Fig. 3, the estimation algorithms based on previously described state observers are included in the control loop, which is its final goal. However, in the current paper, the estimation solutions will be not included in the control loop, but will be evaluated in an “open-loop” context (the system is controlled by a standard way, and the estimator is evaluated through its capability to estimate the unmeasured state variables but without providing information to the controllers).²

In the sequel, results obtained from the previously displayed observation solutions are presented in order to estimate the deviation of the aircraft with respect to the runway; they are based on image processing algorithms that have been applied on synthetic images derived from a scenario of an Airbus civil aircraft landing at Toulouse Airport, France.

² The introduction of the estimator in the closed loop will be the subject of future works.

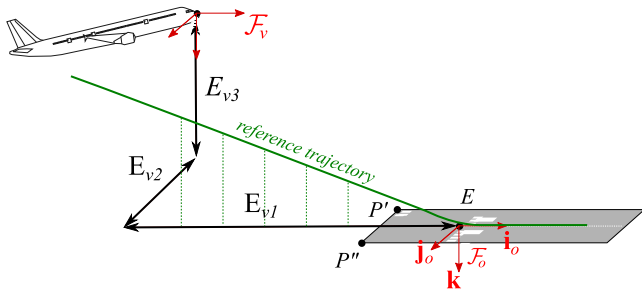


Fig. 4. Reference trajectory (glide path) and deviation notations.

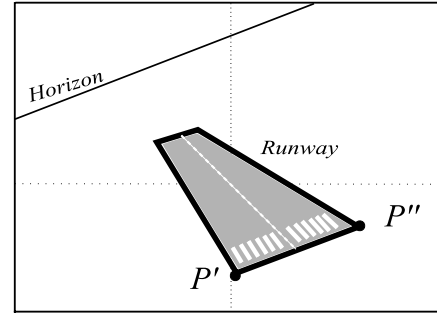


Fig. 5. Runway corners P' and P'' .

4.1. Context and tests conditions

During the final approach of the aircraft towards the runway, the glide path ends on the runway at a point E attached to the runway frame \mathcal{F}_o . One solution would be to estimate the position of the aircraft with respect to the aiming point E ; however, in this case, when the aircraft is aligned on the desired trajectory, observability is not respected and the estimation of the 3D-coordinates of E is not possible from its perspective projection in the image frame (Gibert et al., 2015a, b). In these previous references, it has been shown that the minimal required image information is two points, which can be the two first corners of the runway P' and P'' (see Fig. 4). From the estimation of P' and P'' in the virtual frame and knowing the position of E from the threshold of the runway (300 m along the runway axis), the position of E (whose the coordinates in the virtual frame are denoted $[E_{v1} E_{v2} E_{v3}]^T$) can be easily computed without knowing the width of the runway.

The results presented in the sequel are based on a conventional landing trajectory with initial real positions defined as (in m)

$$[E_{v1} E_{v2} E_{v3}]^T = [5000 \quad -200 \quad 220]^T \quad (34)$$

whereas the sliding mode/high gain observers will be initialized from (in m)

$$[\hat{P}'_{v1} \hat{P}'_{v2} \hat{P}''_{v1} \hat{P}''_{v2} \hat{P}'_{v3}]^T = [7500 \quad -340 \quad 7500 \quad -260 \quad 330]^T \quad (35)$$

which make an important initial estimation error (50% relative error).³

Simulation scenarios. Before using image processing algorithms and in order to validate the observers behavior, one first supposes that this processing is ideal (this scenario will be called “Ideal images”), that the measurement y is perfect with respect to the real deviations $[E_{v1} E_{v2} E_{v3}]^T$, and that it is expressed in the virtual frame \mathcal{F}_v .

In this frame, in Gibert et al. (2015a, b), it has been shown that the minimal required image information is two points, which can be the two first corners of the runway P' and P'' . See Fig. 5.

From the knowledge of both these points coordinates in the image frame (2), the expression of these coordinates in the virtual frame (5) is possible but requires the knowledge of the rotation between \mathcal{F}_c and \mathcal{F}_v . The bank angle ϕ and the pitch angle θ are very precisely known in a civil aircraft thanks to the *Inertial Reference System (IRS)*. The heading difference Δ_ψ can be obtained by knowing the runway heading or by using the image coordinates of the vanishing point of the runway side lines.⁴ Thus, in the following simulations, the rotation matrix ${}^v\mathcal{R}_c$

³ The initial values of \hat{P}'_{v2} and \hat{P}''_{v2} have been arbitrary chosen for the biggest runway width (i.e. 80 m). However, Toulouse airport runway width is 60 m.

⁴ Indeed, even if there is no information concerning the runway, as detailed in Gibert et al. (2015a), thanks to center or sides lines detection by image processing, and the use of roll and pitch angles to estimate the horizontal line in the image, the vanishing point of the runway can be evaluated. From the image coordinates of the vanishing point, it is possible to retrieve the heading difference between aircraft and runway. Then, the roll, pitch and yaw angles can be used to determine the rotation matrix between \mathcal{F}_c and \mathcal{F}_v .

between \mathcal{F}_c and \mathcal{F}_v is assumed to be known which is not a strong assumption.

Other required information includes the dynamics of the camera and is provided by the IRS and is assumed to be available for all time and with sufficient accuracy. This information is expressed through (9) and is used in the observers.

4.2. Results with “ideal images”

Results obtained with the observers based on (26) (which are sliding mode (33) and high gain (28) ones) are displayed in Figs. 6–7. The results show convergence of both the observers even in spite of significant initial estimation errors of the observers (see (34) and (35)). Note that the high gain observer induces a static estimation error close to zero whereas the sliding mode observer presents a reduced phenomenon of chattering (high frequency oscillations). For the sake of clarity, the estimation errors during the transient phase are shown in Fig. 7.

Of course, the interesting results are the estimated deviations of the aircraft with respect to the runway along the glide path, which are presented in Fig. 8. One gets a fast and efficient convergence to real values, which validates the observers design on a conventional trajectory with perfect measurement.

4.3. Results with synthetic images including image processing

In order to get more realistic evaluations of estimation schemes performances, simulations based on synthetic images and real image processing algorithms are now presented. The synthetic images are created by Oktal-SE and based on trajectories used in the previous subsection. They provide a good representation of the Toulouse Airport runway as shown in Fig. 9. The results of image processing algorithms applied to these synthetic images are used by the observers to estimate the deviations of the aircraft with respect to the runway.

Remark 4. Image processing is a critical point for detection, tracking and extraction of features. The used algorithms are not discussed in this paper; if necessary, the reader could refer to Dickmanns, Schubert, Boada-Bauxell, and Gibert (2015) and Schertler (2014). These algorithms are able to extract, from each image of a sequence, visual features which are linked with the runway (centerline, border, markers) and are used in the estimation process. ■

Remark 5. Some other robustness evaluations have been made by considering noisy measurements, bias on velocities and camera calibration errors ; a detailed analysis (not appearing here due to a lack of space) with several different estimation procedures has been made in Gibert (2016) and shows that the estimation process provides acceptable results in the presence of bias. ■

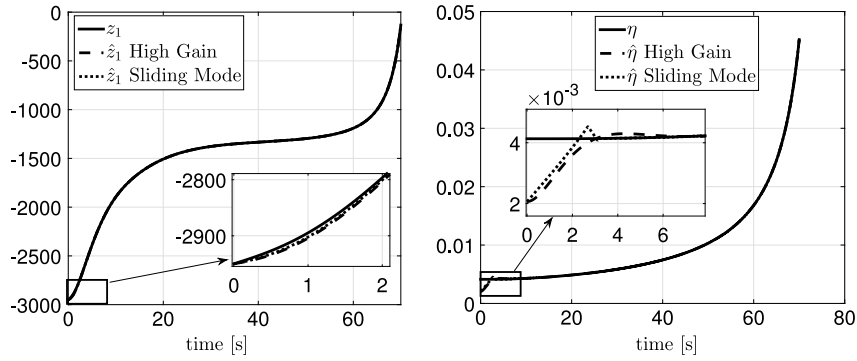


Fig. 6. Left. State variable z_1 (m) and its estimations (m) versus time (s). Right. State variable η (m^{-1}) and its estimations (m^{-1}) versus time (s).

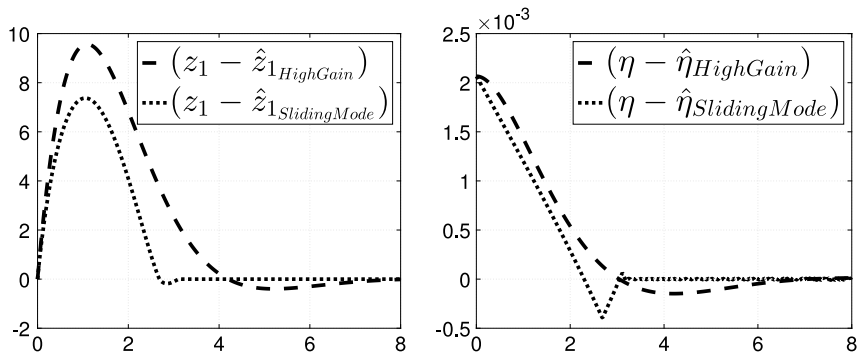


Fig. 7. Left. Error between state variable z_1 (m) and its estimation (m) versus time (s). Right. Error between state variable η (m^{-1}) and its estimation (m^{-1}) versus time (s).

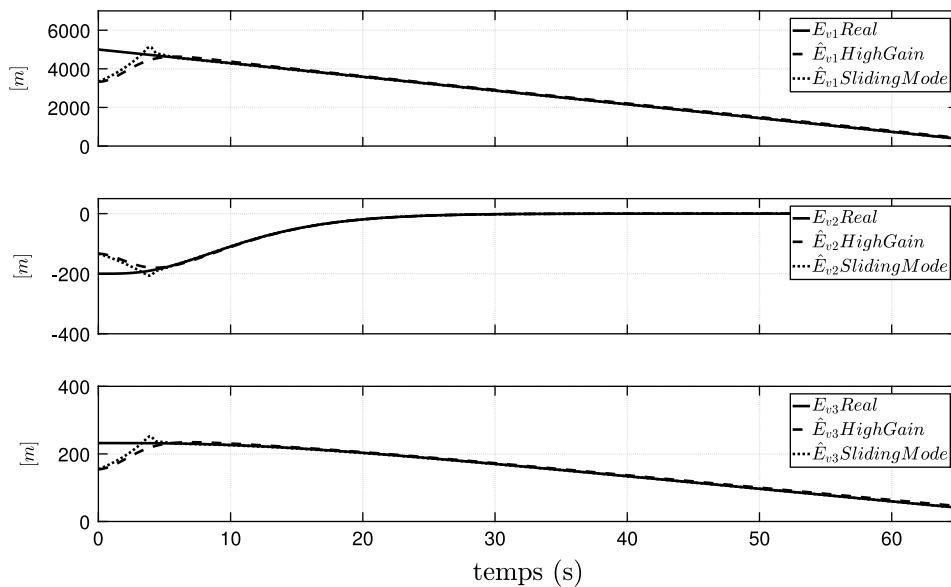


Fig. 8. Top. E_{v1} (m) and its estimations versus time (s). Middle. E_{v2} (m) and its estimations versus time (s). Bottom. E_{v3} (m) and its estimations versus time (s).

The measurements obtained by the image processing algorithms are presented in Fig. 10 and are compared to the expected ones computed from the knowledge of the real trajectory. The accuracy of image processing results is good ; the obtained coordinates are tracking the expected ones all along the landing. Notice a reduced noise (less than

3 pixels) between 30 and 40 s. The frequency used for the image acquisition is 25 Hz.

Fig. 11 displays the estimation of the deviations obtained by both observers (26)–(33) and (26)–(28), using the measurements issued from image processing (Fig. 10). It is shown that the observers converge to the

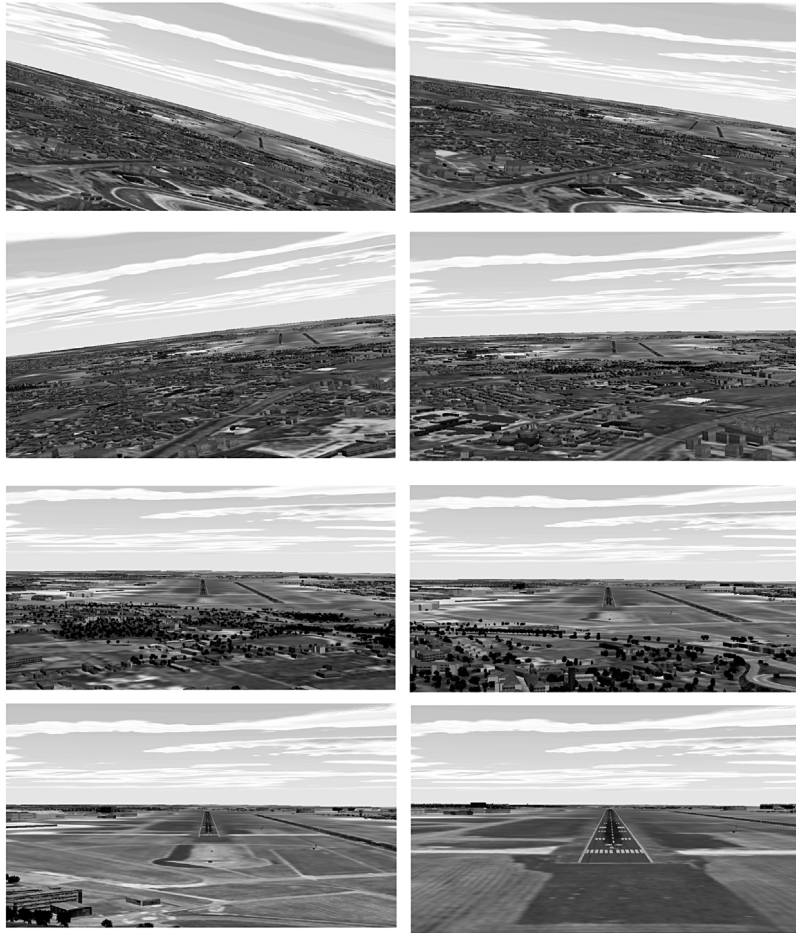


Fig. 9. Oktal-SE synthetic landing in Toulouse Airport runway 32L.

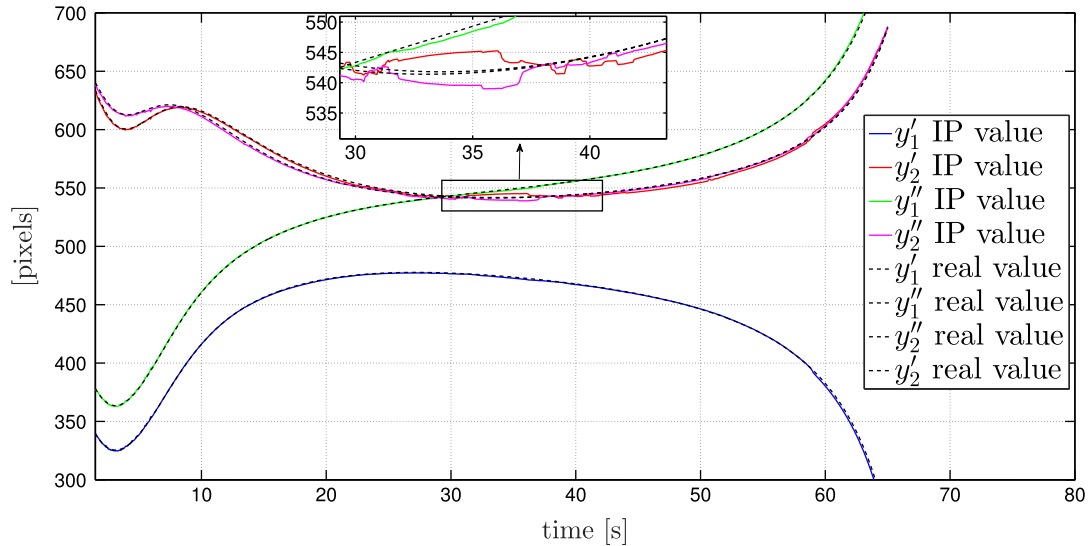


Fig. 10. Coordinates (pixel) in the image of points P' (y_1' and y_2') and P'' (y_1'' and y_2'') versus time (s) obtained from real values (dotted line) and image processing algorithm (solid line).

real values. The high gain observer static error is in the vicinity of zero whereas the sliding mode observer maintains some oscillating behavior due to its sensitivity to the noisy measurements due to image processing. These results show the feasibility of the observer design w.r.t estimating the deviations of the aircraft.

5. Conclusion

In this paper, two new observers based on a high gain approach and sliding mode theory are designed and applied to a vision-based landing solution for civil aircraft. The proposed scheme guarantees observability

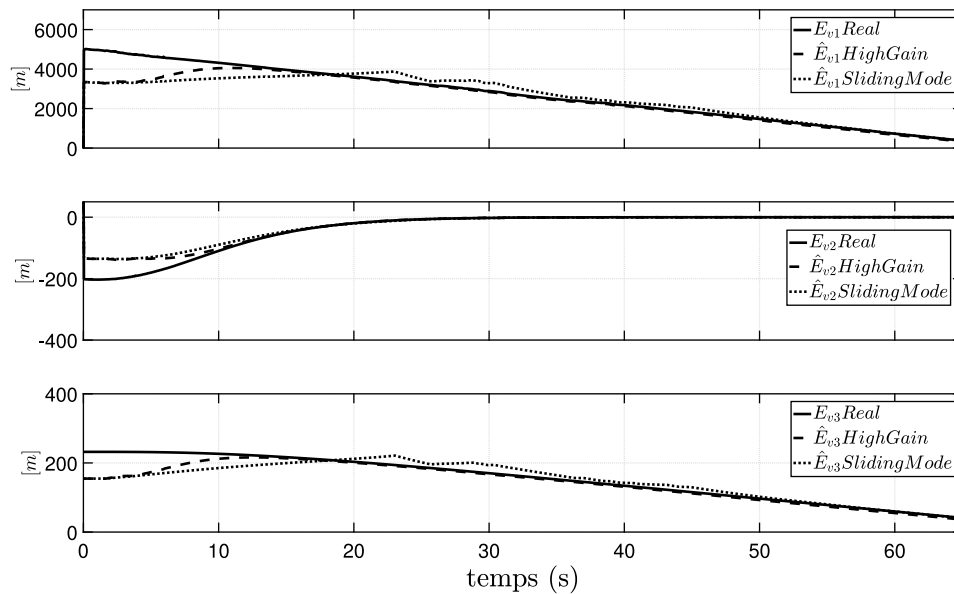


Fig. 11. **Top.** E_{v1} (m) and its estimates versus time (s). **Middle.** E_{v2} (m) and its estimates versus time (s). **Bottom.** E_{v3} (m) and its estimates versus time (s).

thanks to an adequate combination of coordinates of specific points in the image, and allows a simple design solution. The results have been validated in simulation of an aircraft landing scenario by including image processing algorithms on synthetic images.

This work is only a first step on the way towards real applications and future works are numerous. A short-term objective is the application of the estimation scheme to real images, and then the use (and stability analysis) of the observers in the control closed loop. Another research direction is to study the behavior of the observation scheme with temporarily missing or unavailable measurements. The use of observers as redundant sensors (thanks to data fusion algorithm with other measurements) is also a key point in order to ensure sensor redundancy, detect sensors failure, etc. Then, analysis of the behavior of the observation solutions in more complete scenarios, such as imposed for certification, will be necessary.

Acknowledgments

This work has been with the financial support of *Agence Nationale de la Recherche et de la Technologie* (grant 2013/0142) and *Agence Nationale de la Recherche* (grant ANR-13-CORD-0012 VISIOLAND.)

References

- Azinheira, J. R., & Rives, P. (2008). Image-based visual servoing for vanishing features and ground lines tracking: Application to a UAV automatic landing. *International Journal of Optomechatronics*, 2, 275–295.
- Chaumette, F., & Hutchinson, S. (2006). Visual servo control. I. Basic approaches. *IEEE Magazine on Robotics and Automation*, 13(4), 82–90.
- Chen, X., & Kano, H. (2002). A new state observer for perspective systems. *IEEE Transactions on Automatic Control*, 47(4), 658–663.
- Coutard, L., Chaumette, F., & Pflimlin, J.-M. (2011). Automatic landing on aircraft carrier by visual servoing. In *IEEE/RSJ international conference on intelligent robots and systems*.
- Dahl, O., Nyberg, F., Holst, J., & Heyden, A. (2005). Linear design of a nonlinear observer for perspective systems. In *IEEE international conference on robotics and automation*.
- Dickmanns, D., Schubert, F., Boada-Bauxell, J., & Gibert, V. (2015). Vision based landing for commercial aircraft. In *European conference for aeronautics and space sciences*.
- El Tannoury, C., Moussaoui, S., Plestan, F., Romani, N., & Pita-Gil, G. (2013). Synthesis and application of nonlinear observers for the estimation of tire effective radius and rolling resistance of an automotive vehicle. *IEEE Transactions on Control Systems Technology*, 21(6), 2408–2416.
- Gauthier, J. P., Hammouri, H., & Othman, S. (1992). A simple observer for nonlinear systems, application to bioreactors. *IEEE Transactions on Automatic Control*, 37(6), 875–880.
- Gibert, V. (2016). Analyse d'observabilité et synthèse d'observateurs robustes pour l'atterrissage basé vision d'avions de ligne sur des pistes inconnues (in French). Available at <https://hal.archives-ouvertes.fr/tel-01464342>.
- Gibert, V., Burlion, L., Chriette, A., Boada-Bauxell, J., & Plestan, F. (2015a). New pose estimation scheme in perspective vision system during civil aircraft landing. In *IFAC symposium on robot control*.
- Gibert, V., Burlion, L., Chriette, A., Boada-Bauxell, J., & Plestan, F. (2015b). Nonlinear observers in vision system : Application to civil aircraft landing. In *European control conference*.
- Gibert, V., & Puyou, G. (2013). Landing of a transport aircraft using image based visual servoing. In *IFAC symposium on nonlinear control systems*.
- Giordano, P., De Luca, A., & Oriolo, G. (2008). 3D structure identification from image moments. In *IEEE international conference on robotics and automation*.
- Gui, Y., Guo, P., Zhang, H., Lei, Z., Zhou, X., Du, J., & Yu, Q. (2013). Airborne vision-based navigation method for uav accuracy landing using infrared lamps. *Journal of Intelligent and Robotic Systems*, 72(2), 197–218.
- Hartley, R., & Zisserman, A. (2003). *Multiple view geometry in computer vision*. Cambridge, UK: Cambridge University Press.
- Karagiannis, D., & Astolfi, A. (2005). A new solution to the problem of range identification in perspective vision systems. *IEEE Transactions on Automatic Control*, 50(12), 2074–2077.
- Le Bras, F., Hamel, T., Barat, C., & Mahony, R. (2009). Nonlinear image-based visual servo controller for automatic landing guidance of a fixed-wing aircraft. In *European control conference* (pp. 1836–1841).
- Levant, A. (2003). Higher-order sliding modes, differentiation and output-feedback control. *International Journal of Control*, 76(9–10), 924–941.
- Levant, A. (2012). Finite-time stability and high relative degrees in sliding-mode control. In L. Fridman, J. Moreno, & R. Iriarte (Eds.), *Lecture notes in control and information sciences: vol. 412. Sliding modes after the first decade of the 21st century* (pp. 59–92). Springer Berlin Heidelberg.
- Moog, C., Plestan, F., Conte, G., & Perdon, A. (1993). On canonical forms of nonlinear systems. In *European control conference*.
- Plestan, F., & Glumineau, A. (1997). Linearization by generalized input-output injection. *Systems & Control Letters*, 31(2), 115–128.
- Schertler, K. (2014). Method and device for image-assisted runway localization. Patent WO/2014/075657.
- Trisripisal, P., Parks, M., Abbott, A., Liu, T., & Fleming, G. (2006). Stereo analysis for vision-based guidance and control of aircraft landing. In *AIAA aerospace science meeting and exhibit*.

Vision based anti-windup design with application to the landing of an Airliner

Laurent Burlion* Henry de Plinval*

* ONERA-Toulouse (e-mail: lburlion (at) onera.fr).

Abstract: In this article, we present a novel anti-windup method for vision based control. Technically speaking, this method aims at controlling a second order chain of integrators with the first component being known up to an unknown, time-varying scaling factor, and including control saturations. This complex problem is of practical relevance since it appears naturally in the context of vision-based control, the position of an object being determined from bi-dimensional images, so that it is known up to a factor. Saturations are also obviously present in such a context. To address this issue, we combine a tailored observer together with an anti-windup scheme. Uniform global asymptotic stability of the closed loop system is proven. Finally, simulation results demonstrate the effectiveness of the method.

© 2017, IFAC (International Federation of Automatic Control) Hosting by Elsevier Ltd. All rights reserved.

Keywords: Saturated systems, anti-windup, vision-based control, range identification, nonlinear observers.

1. INTRODUCTION

1.1 Motivation

In order to cope with control saturations, a number of anti-windup techniques have been developed Tarbouriech and Turner (2009); Galeani et al. (2009); Zaccarian et al. (2011). They are aiming at recovering stability and performance under saturation. Among these methods, we have retained the Model Recovery Anti-Windup (MRAW), whose key idea Teel and Kapoor (1997) is to combine a nominal control law with a global one. The nominal one is also called local, since it is designed so as to show optimized performance in the absence of saturation. On the other hand, the global one guarantees Global Stability properties with the saturation. With this approach, the desirable performances of the nominal control laws are recovered when the saturation limits are not reached.

Much effort has been undergone to apply the MRAW design technique in different contexts, not only to deal with control saturation Forni et al. (2012); Galeani et al. (2007); Forni and Galeani (2010); Herrmann et al. (2010) but also in different areas like active vibration isolation Teel et al. (2006), input allocation Zaccarian (2009), output saturated plants Sassano and Zaccarian (2015) or output constraints Chambon et al. (2015).

Plant uncertainties issues have also been dealt with through MRAW design Turner et al. (2007), Prempain et al. (2009), Roos and Biannic (2008). Among these works, a switching adaptation algorithm has been defined in order to make the Anti-Windup compensator more robust in the presence of large uncertainties on constant parameters Bruckner et al. (2013).

The use of vision in the control loops often leads to challenging control problems. Thus, in most works, the control saturations are neglected, assuming the saturation limits will not be reached, although no mechanism is implemented to force it, and although no proof is provided that it will, indeed, not hap-

pen. An important distinction which is often made Chaumette and Hutchinson (2006, 2007) distinguish Position Based Visual Servoing (PBVS) a set of techniques where the 3D position information is recovered from the image information- and Image Based Visual Servoing (IBVS) where the control loops are directly fed with the visual inputs without an explicit 3D reconstruction. As for the PBVS, estimating the range of the visual features is an important issue for which number of works have been completed Jankovic and Ghosh (1995); Karagiannis and Astolfi (2005); Aguiar and Hespanha (2006); Dahl et al. (2010); Vasconcelos et al. (2010); Gibert et al. (2015b)). Indeed, with a single videocamera, this piece of information is not directly available. On the other hand, convergence proofs for PBVS schemes under input saturations have almost never been addressed. Also, the observability conditions necessary to recover a fine estimate has almost never been addressed. In such situations, the problem can be tackled by changing the control law to optimize the observation process Spica et al. (2014) but at the price of more complexity.

1.2 Purpose

This paper will study a vision based control design problem in the presence of control saturation. More specifically, we propose a novel solution to the MRAW design problem for a double integrator when the first component of the state is known up to a time varying scaling factor which is, again, the case of visual-based landing. As compared to other saturated control schemes de Plinval et al. (2012, 2017), an anti-windup problem is addressed where the local control dynamics is pre-specified (it is here an image based PID controller). Here, we propose an observer based MRAW approach because of the fact that the classical MRAW approach requires use of plant dynamics which is here partially unknown due to the image projection, which hides the depth information. Then the closed loop system stability was studied.

The paper is organized as follows. In section 2, we expose the

* This work was partly supported by ANR VISIOLAND project ANR-13-CORD-0012 dedicated to VISIOn based aircraft LANDING techniques

problem of the vision based landing of an aircraft in presence of an actuator saturation. In section 3, we select an existing image-based observer and show that the observability is guaranteed all along the descent by using a well chosen visual cue. Our observer based MRAW solution is then proposed and the GUAS property of the closed-loop system is proved in section 4. Lastly, section 5 applies the result to a numerical example.

Notation Function $|\cdot|$ denotes the Euclidean norm. Given a scalar $L_a > 0$, the notation sat_{L_a} refers to the classical symmetric saturation function defined as follows:

$$\forall u \in \mathcal{R}, \quad \text{sat}_{L_a}(u) := \max\{-L_a, \min\{L_a, u\}\} \quad (1)$$

2. A SATURATED CONTROL PROBLEM

2.1 Context and main assumptions

In this preliminary work, we will focus on the glide slope phase (see Figure 1) during which the autopilot system must maintain a constant slope $\gamma_0 = -3\text{deg}$ and a constant airspeed despite external perturbations.

$$V = 70\text{ms}^{-1} \quad (2)$$

Deviations from the nominal trajectory are usually provided

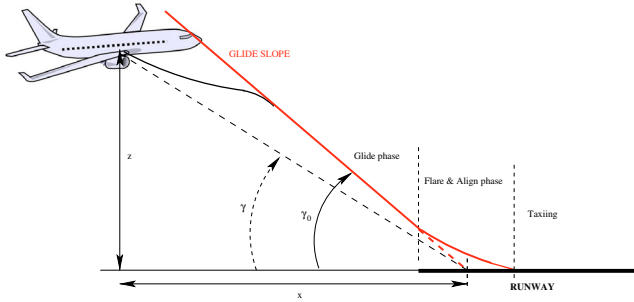


Fig. 1. Landing phases

by the ILS. In our context they are derived by image processing from a body fixed monocular camera thanks to which the slope γ is available as a novel output:

$$y_1 = \gamma = \frac{z}{x} \quad (3)$$

another output is extracted from each image:

$$y_2 = \frac{w}{x} \quad (4)$$

where w is the runway width. To avoid breaking the flow of reading, we explain in the appendix how these two outputs can be obtained by using the attitude of the aircraft (given by the IMU¹) plus some visual features which are extracted from the images. Moreover, it is assumed that all the required visual features remain in the field of view of the camera all along the descent (see for example Burlion and de Plinval (2013) for an illustration of how to enforce it).

Assuming that an inner-loop controller enables to track the vertical acceleration² $a_z = \ddot{z} = \text{sat}_{L_a}(u)$, and that, under low wind conditions, the horizontal speed verifies the approximation $\dot{x} \approx V$, the studied open-loop system initially reduces to:

$$\dot{x} = V \quad (5a)$$

$$\ddot{z} = \text{sat}_{L_a}(u) \quad (5b)$$

¹ Inertial Measurement Unit

² provided that it remains below a given range $|\ddot{z}| \leq L_a$

2.2 Preliminary Closed-loop model

Using the first vision-based output y_1 and considering that the vertical speed \dot{z} (via the IMU) is also available for feedback, the following PID controller may be defined:

$$\begin{cases} \dot{x}_i = x_0(y_1 - \gamma_0) \\ u_c = -k_i x_i - k_p x_0(y_1 - \gamma_0) - k_d(\dot{z} - \gamma_0 V) \end{cases} \quad (6)$$

where the gains $k_p > 0$ and $k_d > 0$ are tuned such that, at the beginning of the glide phase (approximately starting at $x_0 = -5000\text{m}$), the system is well-damped and the slope is tracked with a response time below 20s:

$$\begin{cases} k_p = \omega^2, \quad \omega = 0.2 \\ k_d = 2\eta\omega, \quad \eta = 0.75 \end{cases} \quad (7)$$

Moreover, $k_i > 0$ is tuned such that any steady state error will be cancelled. Typically, one chooses:

$$k_i = \frac{k_p}{20} \quad (8)$$

Let us now define the following change of variable:

$$\begin{cases} \xi_1 = z - \gamma_0 x \\ \xi_2 = \Delta v_z = \dot{z} - \gamma_0 V \end{cases} \quad (9)$$

Then, the closed-loop system, combining equations (5b) and (6), reads:

$$\begin{cases} \dot{x}_i = \frac{x_0}{x} \xi_1 \\ \dot{\xi}_1 = \xi_2 \\ \dot{\xi}_2 = \text{sat}_{L_a} \left(-k_i x_i - k_p \frac{x_0}{x} \xi_1 - k_d \xi_2 \right) \end{cases} \quad (10)$$

As claimed in the introduction, the use of vision-based outputs introduces a time-varying term:

$$\lambda(t) = \frac{x_0}{x(t)} \quad (11)$$

which may destabilize the system. From equation (5a), it is easily checked that, during the landing phase this varying term is increasing:

$$\dot{\lambda}(t) = -\frac{V}{x_0} \lambda(t)^2 > 0 \quad (12)$$

In this paper, we focus on the final part of the glide phase, just before switching to the flare mode. This phase during which the position x of the aircraft is varying in the interval $[-5000\text{m}, -400\text{m}]$, is critical since the parameter $\lambda(t)$ will significantly increase. Indeed, from (31), (11) and (12), one computes the following intervals:

$$\begin{cases} \lambda(t) \in [1, 12.5] \\ \dot{\lambda}(t) = 0.014 \lambda(t)^2 \in [0.0014, 0.218] \end{cases} \quad (13)$$

2.3 Problem statement

The combined effects of the saturation, integral term and the parametric variations $\lambda(t)$ in (10) may destabilize the system as discussed further in the numerical results section. To retrieve some good stability properties, we propose to redesign this preliminary control law by:

- synthesizing a vision based observer in order to estimate the unknown term x and to replace x_0 by its estimate \hat{x} in the control law
- designing an anti-windup solution to guarantee the stability of the closed loop system (especially during the transient of the observer error)

3. IMAGE BASED OBSERVER DESIGN

The second vision based output y_2 is now used for the observer design.

Let us note $\chi = -\frac{1}{x} > 0$, one has:

$$\begin{cases} \dot{y}_2 = Vy_2\chi \\ \dot{\chi} = V\chi^2 \end{cases} \quad (14)$$

Then, given $\lambda > 0$ we may select the following estimator $\hat{\chi}$ of χ :

$$\begin{cases} \dot{\hat{\chi}} = (V - \lambda V^2 y_2^2) e^{\xi + \beta(y_2)} \\ \hat{\chi} = e^{\xi + \beta(y_2)} \end{cases} \quad (15)$$

where

$$\beta(y_2) = \frac{\lambda}{2} V y_2^2 \quad (16)$$

Lemma 1. Suppose for all $t, x(t) < 0$, then for any $\lambda > \frac{1}{Vy_2^2}$, $\lim_{t \rightarrow \infty} \hat{\chi}(t) - \chi(t) = 0$

proof: the proof of the result readily follows the result of (Sassano et al. (2010), proposition 1). To be able to apply this proposition however, there is an observability condition to be verified (a nonnegative scalar function satisfying an inequality) : in our case, this condition boils down to verifying that:

$$V - \lambda V^2 y_2^2 < 0 \quad (17)$$

which is ensured by our selection of λ . \square

Remark 1. Such an observer is of interest from our control since the observability is always guaranteed. (up to the standard assumption in vision based control that x does not change its sign)

Remark 2. The runway width w being typically inside the interval $[30m, 60m]$, λ must verify in our application:

$$\lambda > \frac{x^2}{Vw^2} \geq \frac{5000^2}{70.30^2} = 1.7 \cdot 10^3 \quad (18)$$

4. ANTI-WINDUP COMPENSATOR DESIGN

Let us consider the observer (15) and let us note $\hat{x} = -\frac{1}{\hat{\chi}}$. The unconstrained controller is now selected as follows:

$$\begin{cases} \dot{x}_i = \hat{x}(y_1 - \gamma_0) \\ u_c(x_i, \hat{x}(y_1 - \gamma_0), \xi_2) = -k_i x_i - k_p \hat{x}(y_1 - \gamma_0) - k_d \xi_2 \end{cases} \quad (19)$$

Moreover, the following global controller $u_g(z, \dot{z})$ is chosen for the constrained dynamics (5b)

$$u_g(z, \dot{z}) = -k_1 \varphi_1(z) - k_2 \text{Sat}_1(\dot{z}) \quad (20)$$

where $\varphi_1(z) = \frac{2}{\pi} \arctan(k_{1z} z)$ with $k_{1z} > 0$ is chosen as a differentiable saturation function

where $k_2 > k_1 > 0$, $k_2 + k_1 \leq L_a$.

This control law is inspired from (de Plinval et al. (2012)) and has the following property

Lemma 2. the closed-loop system (5b)-(20) is GAS.

Proof: Consider the following candidate Lyapunov function

$$V_1 = k_1 \int_0^z \varphi_1(s) ds + \frac{1}{2} \dot{z}^2 \quad (21)$$

Computing its derivative, one gets:

$$\dot{V}_1 = -k_2 \dot{z} \text{Sat}_1(\dot{z}) \leq 0 \quad (22)$$

The GAS property is simply obtained by invoking LaSalle's invariance Theorem. \square

Then, we propose the following MRAW (Model Recovery Anti-Windup) design to combine the control law u_c and u_g into a unique controller which achieves the desirable local performance induced by u_c and the global stability induced by u_g . To this end, we suggest the following compensator:

$$\begin{cases} u = u_c \left(\xi_i, \hat{x} \frac{\xi_1}{x} - z_a, \xi_2 - \dot{z}_a \right) + u_g(z_a, \dot{z}_a) \\ \dot{\xi}_i = \hat{x} \frac{\xi_1}{x} - z_a \\ \dot{z}_a = \text{sat}_{L_a}(u) - u_c \left(\xi_i, \hat{x} \frac{\xi_1}{x} - z_a, \xi_2 - \dot{z}_a \right) \end{cases} \quad (23)$$

Theorem 1. (main result) Let $x_{\min} < x_{\max} < 0$. Suppose for all $t, x_{\min} \leq x(t) \leq x_{\max} < 0$, then for any $\lambda > \frac{1}{Vy_2^2}$, the closed-loop system (5b)-(15)-(23) is Globally Uniformly Asymptotically Stable (GUAS).

Sketch of the proof. The proof is divided into several parts:

Part A: Study of the observation error.

Let us first introduce the following notation:

$$\delta = \frac{\hat{x}}{x} - 1 = \frac{\chi}{\hat{\chi}} - 1 \quad (24)$$

from (15), it is readily checked that δ undergoes the following dynamics:

$$\dot{\delta} = f_o(t, \delta) \quad (25)$$

with $f_o(t, \delta) = -V\chi(\lambda Vy_2^2 - 1)\delta = -\frac{V}{x(t)} \left(\frac{\lambda Vw^2}{x^2(t)} - 1 \right) \delta$. We then consider $V_e = \frac{1}{2} \delta^2$ and easily show that there exists $\alpha_e > 0$ such that:

$$\dot{V}_e \leq -\alpha_e V_e \quad (26)$$

As a consequence,

$$\int_0^\infty |\delta(s)| ds < \infty \quad (27)$$

Part B: Study of \tilde{X}

Using (19) and the notation (25), the local control law of (23) is rewritten as follows:

$$\begin{cases} \dot{\xi}_i = \xi_i - z_a + \delta \xi_1 \\ u_c = -k_i \xi_i - k_p (\xi_i - z_a) - k_d (\xi_2 - \dot{z}_a) - k_p \delta \xi_1 \end{cases} \quad (28)$$

Let us now note $\tilde{X} = [\xi_i, \xi_1 - z_a, \xi_2 - \dot{z}_a]^T$ and $X_a = [z_a, \dot{z}_a]^T$. From (5b)-(23)-(28), it can be checked that \tilde{X} undergoes the following dynamics:

$$\dot{\tilde{X}} = A\tilde{X} + \delta (B\tilde{X} + B_a X_a) \quad (29)$$

where:

$$A = \begin{bmatrix} 0 & 1 & 0 \\ 0 & 0 & 1 \\ -k_i & -k_p & -k_v \end{bmatrix} \quad B = \begin{bmatrix} 0 & 1 & 0 \\ 0 & 0 & 0 \\ 0 & -k_p & 0 \end{bmatrix} \quad B_a = \begin{bmatrix} 1 & 0 \\ 0 & 0 \\ -k_p & 0 \end{bmatrix} \quad (30)$$

Since k_i, k_p and k_v are strictly positive, A is strictly Hurwitz ; as a consequence, there exist $P = P^T > 0, Q > 0$ such that $A^T P + PA = -Q$. We then define the following candidate Lyapunov function :

$$V_0(\tilde{X}) = \tilde{X}^T P \tilde{X} \quad (31)$$

which will be used in Part D.

Part C: Study of the anti-windup state X_a

Let us now consider the anti-windup loop whose state is $X_a = [z_a, \dot{z}_a]^T$. Observe that the last equation of (23) can be rewritten as follows:

$$\dot{z}_a = u_g(z_a, \dot{z}_a) + \delta u \quad (32)$$

where:

$$\delta_u = \text{sat}_{L_a}(u) - u_c \left(\xi_i, \hat{x} \frac{\xi_1}{x} - z_a, \xi_2 - \dot{z}_a \right) - u_g(z_a, \dot{z}_a) \quad (33)$$

$|u_g|$ being bounded by L_a it is clear that there exists $c_a, c_1, c_2, c_3 > 0$ such that:

$$|\delta_u| \leq c_a |u_c(\xi_i, (\xi_1 - z_a) + \delta \xi_1, \xi_2 - \dot{z}_a)| \quad (34)$$

$$\leq (c_1 + c_2 |\delta|) |\tilde{X}| + c_3 |\delta| |X_a| \quad (35)$$

Consider $V_a(X_a) = k_1 \int_0^{z_a} \varphi_1(s) ds + \frac{1}{2} \dot{z}_a^2 + \kappa_1 \varphi_1(z_a) \varphi_1(\dot{z}_a)$ which can be easily shown to be definite positive for any $\kappa_1 > 0$ sufficiently small (see (de Plinval et al. (2012), Appendix) for more details). Such a function can be interpreted as the strictification of V_1 . We compute its derivative using (20)-(32):

$$\begin{aligned} \dot{V}_a = & -(\kappa_1 k_1 \partial \varphi_1(\dot{z}_a)) \varphi_1(z_a)^2 - k_2 \dot{z}_a \text{Sat}_1(\dot{z}_a) \\ & + \kappa_1 [\partial \varphi_1(z_a) \varphi_1(\dot{z}_a) \dot{z}_a - k_2 \varphi_1(z_a) \partial \varphi_1(\dot{z}_a) \text{Sat}_1(\dot{z}_a)] \\ & + [\dot{z}_a + \kappa_1 \varphi_1(z_a) \partial \varphi_1(\dot{z}_a)] \delta_u \end{aligned} \quad (36)$$

with $\partial \varphi_1(s) = \frac{2k_{1z}}{\pi(1+k_{1z}^2 s^2)}$.

Part D: Study of the full state $[\tilde{X}^T, X_a^T]^T$

Finally, we consider the full state $[\tilde{X}^T, X_a^T]^T$ and the following candidate Lyapunov function:

$$W = \log(1 + V_0(\tilde{X}) + \varepsilon V_a(X_a)) \quad (37)$$

where $\varepsilon > 0$. Using the preceding computations and some majorations, it can be shown that for ε sufficiently small, there exists a continuous positive definite function $\alpha : \mathbb{R}_{\geq 0} \rightarrow \mathbb{R}_{\geq 0}$ and $\gamma > 0$ such that:

$$\dot{W} \leq -\alpha(|[\tilde{X}^T, X_a^T]^T|) + \gamma |\delta| \quad (38)$$

it follows from (Angeli et al. (2000)) that $[\tilde{X}^T, X_a^T]^T$ is iISS with respect to the input δ which satisfies (27). Following (Sontag (1998), proposition 6), it can be shown that the closed-loop system (5b)-(15)-(23) is (GUAS).

□

5. NUMERICAL RESULTS

The saturation bound is $L_a = 0.3$.

The novel anti-windup compensator (23) is now illustrated on the vision based automatic landing problem of an autonomous fixed-wing aircraft. For this specific problem, we consider the global controller u_g :

$$u_g(z_a, \dot{z}_a) = -\frac{2k_1}{\pi} \arctan(k_{1z} z_a) - k_2 \text{Sat}_1(\dot{z}_a) \quad (39)$$

with $k_{1z} = 0.12$, $k_1 = 0.7L_a/1.7 = 0.12$ and $k_2 = L_a/1.7 = 0.17$. It is fair to say that the potential of the method is illustrated on an example which goes beyond what is proven in this paper: indeed, due to the physical limitation $x < 0$ and to the saturations limits, no control law can succeed to make the airplane follow its reference trajectory for any initial error. However, the advantages of the anti-windup can be illustrated on several initial points. For instance, we consider an error of $15m$ at a distance of $5000m$.

The anti-windup law (23) was compared then with the nominal PID control law (6) which motivated the anti-windup design and with the local control law (14) which uses the observer (15).

As shown on figure (2) and (3), the windup phenomenon is observed when one applies control laws (6) or (14) : the control

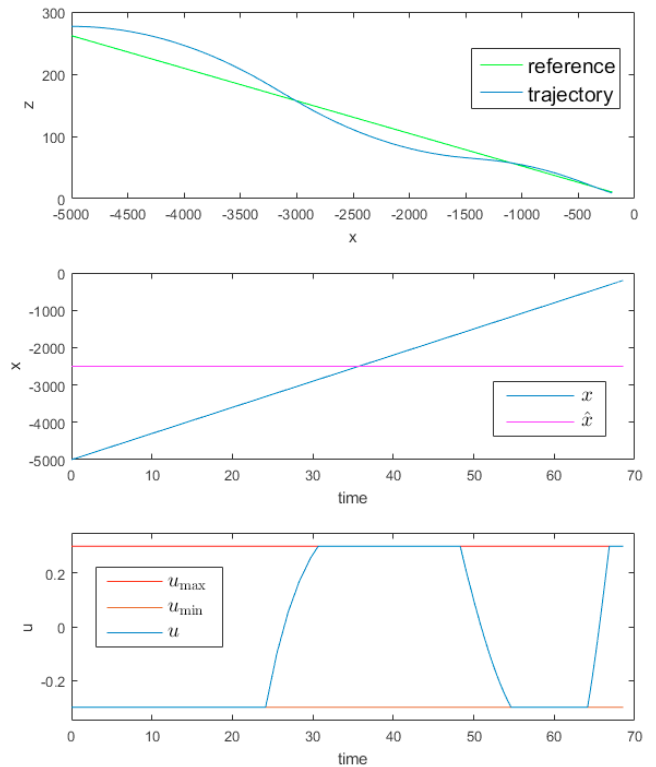


Fig. 2. Numerical results when one uses the controller (6)

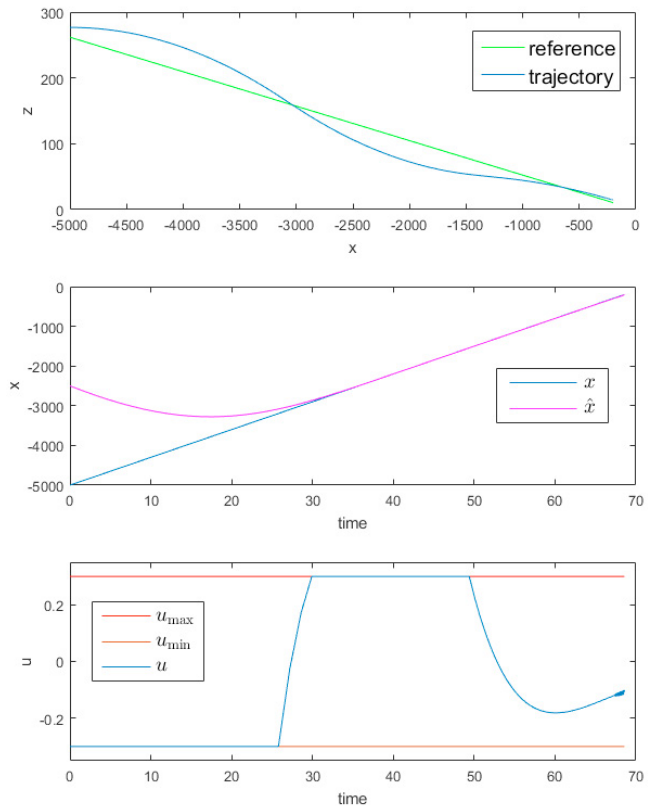


Fig. 3. Numerical results when one uses controller (19)

input is continuously trying to act beyond its limits and undesirable input and output oscillations occur. Note that the observer works well and is able to estimate x within 30s. As expected and as shown in figure (4), the 'Anti-windup' augmentation

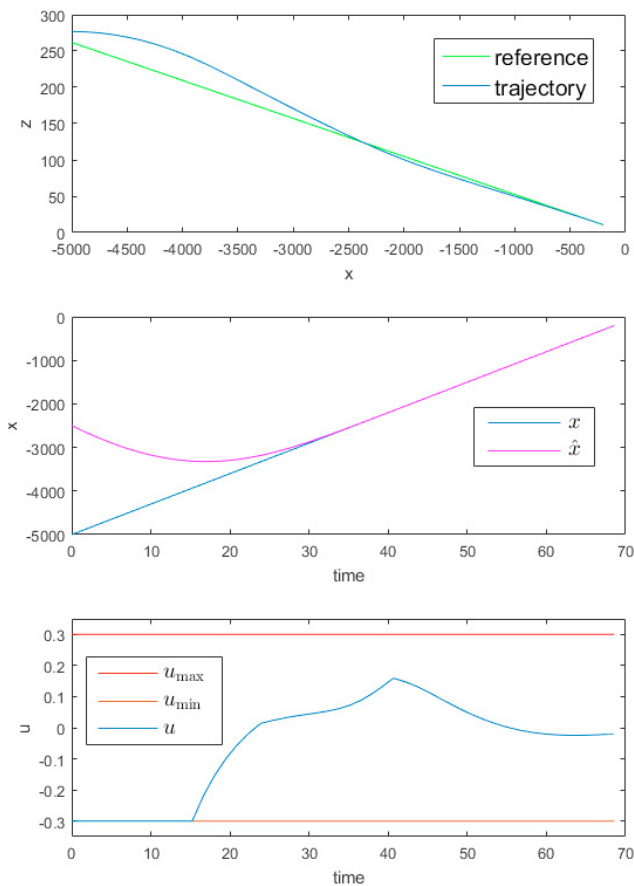


Fig. 4. Numerical results when one uses controller (23)

succeeds to eliminate the oscillations of the response of the position error which occur when the control law reaches several times its magnitude limit.

6. CONCLUSION

A novel MRAW design problem was defined and solved for a second order chain of integrators when the first component of the state is known up to a time-varying scaling factor. The major difficulty is that the plant model is not fully known. The main Theorem of our paper shows that a MRAW design in combination with a vision based observer is suitable for this class of systems. The simulation results show the effectiveness of the method on the vision based control problem design of a landing aircraft. Future work will be devoted to apply such a result on a more complex modelling of the landing aircraft.

7. APPENDIX: ABOUT THE EXTRACTION OF THE TWO VISION OUTPUTS

For simplicity, consider that the video camera frame is the aircraft body frame and that the camera focal length equals 1. Then the vision outputs are computed as follows:

- (1) the runway is detected and then tracked in each image (5).
- (2) the visual cue d_F is computed. As explained in (Gibert et al. (2015a), equation (15)), the heading difference between the runway and the aircraft δ_ψ can be computed by using d_F . The aircraft pitch angle θ and roll angle ϕ being obtained from the IMU measurements, the rotation matrix

$R_{(\phi, \theta, \delta_\psi)}$ between the aircraft body frame and the runway inertial frame is thus fully known.

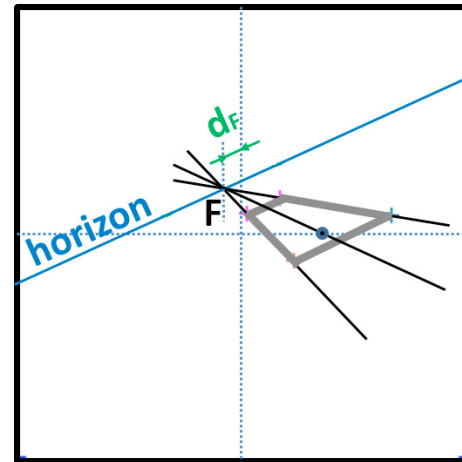


Fig. 5. illustration inspired from (Gibert et al. (2015a), figure 5)

- (3) To each 2D image point (u, v) corresponds a 3D point $(1, u, v)$ (the focal length being equalled to 1). Then, we apply the following transformation to each image point (u, v)

$$\begin{cases} \begin{bmatrix} x_1 \\ u_1 \\ v_1 \end{bmatrix} = R_{\phi, \theta, \delta_\psi}^T \begin{bmatrix} 1 \\ u \\ v \end{bmatrix} \\ \begin{bmatrix} u_2 \\ v_2 \end{bmatrix} = \frac{1}{x_1} \begin{bmatrix} u_1 \\ v_1 \end{bmatrix} \end{cases} \quad (40)$$

and obtain a novel image (6) whose points coordinates are (u_2, v_2) . Such a transformation which we call 'derotation' enables to visualize the runway in the case the camera frame would be the inertial frame.

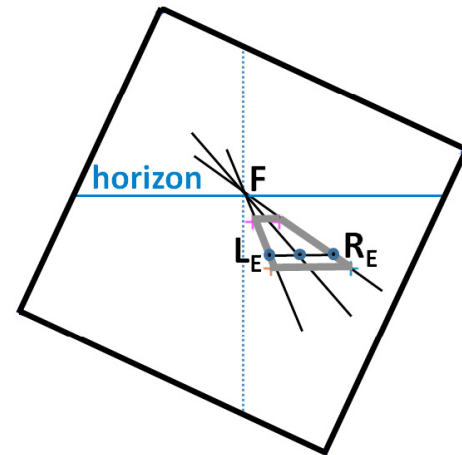


Fig. 6. Our figure (5) after the 'derotation'

- (4) On the image (6), it is rather easy to compute the desired vision based outputs. Let us draw a line parallel to the horizon and passing through the touch down point: this line intersects the runway borders line at L_E and R_E . Then, from the coordinates (u_{L_e}, v_{L_e}) (resp. (u_{R_e}, v_{R_e})) of L_E (resp. R_E) in the 'derotated' image, one can easily compute the desired quantities:

$$\begin{cases} y_1 = -u_{L_e} = \frac{z}{x} \\ y_2 = -v_{L_e} + v_{R_e} = \frac{w}{x} \end{cases} \quad (41)$$

REFERENCES

- Aguiar, A. and Hespanha, J. (2006). Minimum-energy state estimation for systems with perspective outputs. *Automatic Control, IEEE Transactions on*, 51(2), 226–241.
- Angeli, D., Sontag, E.D., and Wang, Y. (2000). A characterization of integral input-to-state stability. *IEEE Transactions on Automatic Control*, 45(6), 1082–1097.
- Bruckner, M., Galeani, S., and del Re, L. (2013). Robustified anti-windup via switching adaptation. *Automatic Control, IEEE Transactions on*, 58(3), 731–737.
- Burlion, L. and de Plinval, H. (2013). Keeping a ground point in the camera field of view of a landing UAV. In *Robotics and Automation (ICRA), 2013 IEEE International Conference on*, 5763–5768.
- Chambon, E., Burlion, L., and Apkarian, P. (2015). Output to input saturation transformation: Demonstration and application to disturbed linear systems. In *Decision and Control (CDC), 2015 IEEE 54th Annual Conference on*, 7566–7571.
- Chaumette, F. and Hutchinson, S. (2006). Visual servo control. i. basic approaches. *Robotics Automation Magazine, IEEE*, 13(4), 82–90.
- Chaumette, F. and Hutchinson, S. (2007). Visual servo control. ii. advanced approaches [tutorial]. *Robotics Automation Magazine, IEEE*, 14(1), 109–118.
- Dahl, O., Wang, Y., Lynch, A., and Heyden, A. (2010). Observer forms for perspective systems. *Automatica*, 46(11), 1829 – 1834.
- de Plinval, H., Morin, P., and Mouyon, P. (2012). Nonlinear control of underactuated vehicles with uncertain position measurements and application to visual servoing. In *American Control Conference (ACC), 2012*, 3253–3259.
- de Plinval, H., Morin, P., and Mouyon, P. (2017). Stabilization of a class of underactuated vehicles with uncertain position measurements and application to visual servoing. *Automatica*, 77, 155 – 169.
- Forni, F. and Galeani, S. (2010). Gain-scheduled, model-based anti-windup for lpv systems. *Automatica*, 46(1), 222 – 225.
- Forni, F., Galeani, S., and Zaccarian, L. (2012). Model recovery anti-windup for continuous-time rate and magnitude saturated linear plants. *Automatica*, 48(8), 1502 – 1513.
- Galeani, S., Tarbouriech, S., Turner, M., and Zaccarian, L. (2009). A tutorial on modern anti-windup design. *European Journal of Control*, 15(34), 418 – 440.
- Galeani, S., Teel, A., and Zaccarian, L. (2007). Constructive nonlinear anti-windup design for exponentially unstable linear plants. *Systems & Control Letters*, 56(5), 357 – 365.
- Gibert, G., Burlion, L., Chriette, A., Boada, J., and Plestan, F. (2015a). New pose estimation scheme in perspective vision system during civil aircraft landing. *IFAC-PapersOnLine*, 48(19), 238 – 243. 11th IFAC Symposium on Robot Control, SYROCO 2015, Salvador, Brazil, August 2015.
- Gibert, V., Burlion, L., Chriette, A., Boada, J., and Plestan, F. (2015b). Nonlinear observers in vision system: Application to civil aircraft landing. In *Control Conference (ECC), 2015 European*, 1818–1823.
- Herrmann, G., Menon, P.P., Turner, M.C., Bates, D.G., and Postlethwaite, I. (2010). Anti-windup synthesis for nonlinear dynamic inversion control schemes. *Int. J. Robust Nonlinear Control*, 20, 1465 – 1482.
- Jankovic, M. and Ghosh, B. (1995). Visually guided ranging from observations of points, lines and curves via an identifier based nonlinear observer. *Systems & Control Letters*, 25(1), 63 – 73.
- Karagiannis, D. and Astolfi, A. (2005). A new solution to the problem of range identification in perspective vision systems. *Automatic Control, IEEE Transactions on*, 50(12), 2074–2077.
- Prempain, E., Turner, M., and Postlethwaite, I. (2009). Coprime factor based anti-windup synthesis for parameter-dependent systems. *Systems & Control Letters*, 58(12), 810 – 817.
- Roos, C. and Biannic, J.M. (2008). A convex characterization of dynamically-constrained anti-windup controllers. *Automatica*, 44(9), 2449 – 2452.
- Sassano, M., Carnevale, D., and Astolfi, A. (2010). Observer design for range and orientation identification. *Automatica*, 46(8), 1369 – 1375.
- Sassano, M. and Zaccarian, L. (2015). Model recovery anti-windup for output saturated SISO linear closed loops. *Systems & Control Letters*, 85, 109 – 117.
- Sontag, E. (1998). Comments on integral variants of iss. *Systems & Control Letters*, 34(1-2), 93 – 100.
- Spica, R., Giordano, P.R., and Chaumette, F. (2014). Active structure from motion: Application to point, sphere, and cylinder. *IEEE Transactions on Robotics*, 30(6), 1499–1513.
- Tarbouriech, S. and Turner, M. (2009). Anti-windup design: an overview of some recent advances and open problems. *Control Theory Applications, IET*, 3(1), 1–19.
- Teel, A. and Kapoor, N. (1997). The L2 anti-windup problem: its definition and solution. In *European Control Conference (ECC)*, 1897–1902.
- Teel, A., Zaccarian, L., and J.J., M. (2006). An anti-windup strategy for active vibration isolation systems. *Control Engineering Practice*, 14(1), 17 – 27.
- Turner, M., Herrmann, G., and Postlethwaite, I. (2007). Incorporating robustness requirements into antiwindup design. *Automatic Control, IEEE Transactions on*, 52(10), 1842–1855.
- Vasconcelos, J., Cunha, R., Silvestre, C., and Oliveira, P. (2010). A nonlinear position and attitude observer on SE(3) using landmark measurements. *Systems & Control Letters*, 59(3-4), 155 – 166.
- Zaccarian, L., , and Teel, A. (2011). *Modern anti-windup synthesis: control augmentation for actuator saturation*. Princeton University Press.
- Zaccarian, L. (2009). Dynamic allocation for input redundant control systems. *Automatica*, 45(6), 1431 – 1438.



Contents lists available at ScienceDirect

Automatica

journal homepage: www.elsevier.com/locate/automatica



Brief paper

Discontinuous model recovery anti-windup for image based visual servoing[☆]



Laurent Burlion^{a,*}, Luca Zaccarian^{b,c}, Henry de Plinval^a, Sophie Tarbouriech^b

^a ONERA, The French Aerospace Lab, F-31055 Toulouse, France

^b LAAS-CNRS, Université de Toulouse, CNRS, Toulouse, France

^c Dipartimento di Ingegneria Industriale, University of Trento, Italy

ARTICLE INFO

Article history:

Received 27 January 2017
Received in revised form 2 January 2019
Accepted 13 February 2019
Available online 12 March 2019

Keywords:

Model recovery anti-windup
Image-based visual servo control
Time-varying systems
Uncertain systems

ABSTRACT

A discontinuous model recovery anti-windup technique is proposed for a double integrator with the output measurement corrupted by a time-varying scaling factor. This challenging measurement configuration arises in vision-based control, where the position of an object moving in the three-dimensional space is determined using two-dimensional images. We prove uniform global asymptotic stability of the closed loop by applying an invariance principle argument to the regularized dynamics. The effectiveness of the proposed approach is illustrated on a visual aircraft landing simulation example.

© 2019 Elsevier Ltd. All rights reserved.

1. Introduction

Anti-windup deals with the problem of stability and performance degradation due to control saturation (Galeani, Tarbouriech, Turner, & Zaccarian, 2009). Model Recovery Anti-Windup (MRAW) merges a local control law (that should be followed before saturation) with a global one (guaranteeing global stability despite control saturation). MRAW designs are perhaps the only effective architectures in the presence of saturated plants that are not linear time-invariant (see Todeschini, Formentin, Panzani, Corno, Savaresi, and Zaccarian (2016) and references therein for some examples). Visual servoing is in general challenging enough, so that most works conducted in this area have assumed no control saturation. Most vision-based control papers distinguish between Position Based Visual Servoing (PBVS), where the image information is used to recover 3D position information (Aguilar & Hespanha, 2006; Jankovic & Ghosh, 1995; Karagiannis & Astolfi, 2005 and references therein), and Image Based Visual Servoing (IBVS) where the visual information is directly used in the control loops (Chaumette & Hutchinson, 2007 and references therein). The second approach offers more

robustness against camera calibration errors with reduced design complexity (Hamel & Mahony, 2002) unless control saturation needs to be considered from the design phase (de Plinval, Morin, & Mouyon, 2017).

Saturated IBVS design with an anti-windup approach is the contribution of this paper. We propose (1) a robust local stabilizer, (2) a robust global stabilizer (both of them extending previous results) and, most importantly, (3) a novel solution to the MRAW design problem for a double integrator with measurement corrupted by a time-varying scaling factor. As compared to other saturated IBVS schemes (de Plinval et al., 2017), an anti-windup problem is addressed where the local control dynamics is pre-specified—a key feature of the proposed approach.

The paper is organized as follows. In Section 2, we introduce the problem and in Section 3 we give our main results. A visual landing example is discussed in Section 4 and proofs are reported in Section 5.

Notation: Function $|\cdot|$ denotes the Euclidean norm. Given a scalar $\delta > 0$, the classical symmetric saturation function is: $\text{sat}_\delta(w) := \max\{-\delta, \min\{\delta, w\}\}$, $\forall w \in \mathcal{R}$.

2. System description and assumptions

Consider the input-saturated plant:

$$\begin{aligned} \dot{p} &= v \\ \dot{v} &= u_s := \text{sat}_i(u), \quad y = \begin{bmatrix} m(t)p \\ v \end{bmatrix} \end{aligned} \quad (1)$$

where $p, v, u \in \mathbb{R}$, $x = \begin{bmatrix} p \\ v \end{bmatrix}$ is the state, $u \in \mathbb{R}$ is the control input and $y := \begin{bmatrix} y_1 \\ y_2 \end{bmatrix} \in \mathbb{R}^2$ is the measurement output. In this model,

[☆] First author's work was partly supported by ANR, France VISIOLAND project ANR-13-CORD-0012. The material in this paper was not presented at any conference. This paper was recommended for publication in revised form by Associate Editor Zongli Lin under the direction of Editor Daniel Liberzon.

* Corresponding author.

E-mail addresses: laurent.burlion@rutgers.edu (L. Burlion), zaccarian@laas.fr (L. Zaccarian), henry.de_plinval@onera.fr (H. de Plinval), tarbour@laas.fr (S. Tarbouriech).

y_1 is obtained from a video-camera, so that function $t \mapsto m(t)$ is a continuously differentiable function equal to the reverse of the uncertain image depth due to the image projection. With video-camera measurements, function m is not available, but we can measure the time variation of its inverse, corresponding to the time variation v_d of the depth (where we select $t_0 = 0$ without loss of generality):

$$v_d(t) := \frac{d}{dt} m^{-1}(t) = -\frac{\dot{m}(t)}{m^2(t)}, \quad |v_d(t)| \leq v_{\max}, \quad \forall t \geq 0. \quad (2)$$

For the previous property to make sense, a typical assumption enforced on function m is that it has constant positive upper and lower bounds (λ_0, λ_m) (as for the helicopters in de Plinval et al. (2017)). We consider here less conservative time-varying bounds possibly arising from a better knowledge of the plant dynamics. For example, time-varying bounds may arise from some worst case analysis based on the measurement in (2):

$$0 < \lambda_0 \leq \lambda_1(t) \leq m(t) \leq \lambda_2(t) \leq \lambda_m, \quad \forall t \geq 0. \quad (3)$$

Indeed, if $m^{-1}(0) \in [1/\lambda_2(0), 1/\lambda_1(0)]$, then one computes $\lambda_i(t) = \frac{\lambda_i(0)}{1 + \lambda_i(0) \int_0^t v_d(s) ds}$ where $i \in \{1, 2\}$, by integrating (2). Based on the above, we make the following assumption.

Assumption 1. There exist (possibly unknown) positive scalars ($\lambda_0, \lambda_m, v_{\max}$) and accessible functions $t \mapsto \lambda_1(t)$, $t \mapsto \lambda_2(t)$, $t \mapsto v_d(t)$ satisfying (2) and (3).

Remark 1. These models and assumptions come from a challenging application illustrated in Section 4: a vision-based automatic aircraft landing problem, where $m(t)$ corresponds to the inverse of the distance to the runway. This is why its inverse derivative is bounded, because it corresponds to the aircraft velocity, which may be estimated or proven to be between two measurable bounds (Burlion & de Plinval, 2015). \lrcorner

An interesting consequence of Assumption 1, arising from (3) is that the following bound holds for all $t \geq 0$:

$$\frac{\lambda_0}{\lambda_m} \leq \frac{m(t)}{\lambda_m} \leq \frac{m(t)}{\lambda_2(t)} \leq 1 \leq \frac{m(t)}{\lambda_1(t)} \leq \frac{m(t)}{\lambda_0} \leq \frac{\lambda_m}{\lambda_0} \quad (4)$$

Remark 2. Using (2), it is readily checked that system (1) can be rewritten as the following time-varying dynamics with full state measurement:

$$\dot{y}_1 = m(t)(v - v_d y_1), \quad \dot{v} = \text{sat}_{\bar{u}}(u) \quad (5)$$

where y_1 denotes the first component of y . However the representation (1) is more convenient for our derivations. \lrcorner

3. Main results

Towards providing a globally bounded stabilizer of the origin for (1) the anti-windup approach is based on merging a *local* and a *global* controller, in the spirit of Teel and Kapoor (1997), even though those results are inapplicable because m is not accessible. The following *local controller* stabilizes the origin of (1) from u_s (namely disregarding saturation). We propose the following discontinuous law:

$$u_s = u_c(t, y) := -k_p \gamma(t, y) y_1 - k_v v \quad (6a)$$

$$\gamma(t, y) := \begin{cases} \frac{1}{\lambda_1(t)}, & \text{if } y_1 v \geq 0 \\ \frac{1}{\lambda_2(t)}, & \text{otherwise,} \end{cases} \quad (6b)$$

The discontinuous term γ deals with the inaccurate knowledge of the distance while ensuring stability, in the sense of the generalized solutions discussed in Goebel, Sanfelice, and Teel (2012, Ch. 4) as certified by the following lemma, whose proof is given in Section 5.

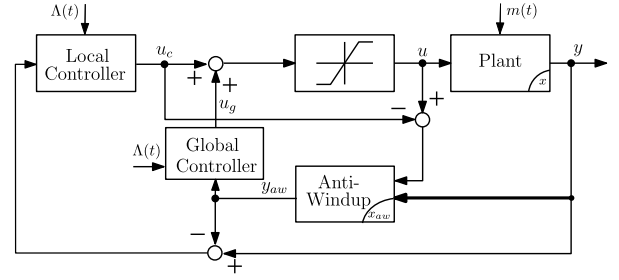


Fig. 1. The proposed model recovery anti-windup architecture for merging the local and global components.

Lemma 1. Under Assumption 1, consider any gain values $k_p, k_v > 0$. Then, the static output feedback (6), ensures that the origin of the closed loop with (1) is robustly globally asymptotically stable (GAS) in the sense of Goebel et al. (2012, Def. 7.5).

The following *global controller* stabilizes the origin of (1) from u (namely accounting for saturation) but is typically associated with poor small signal performance (thereby motivating the anti-windup approach). We use the following nonlinear output feedback stabilizer

$$u = u_g(t, y) := -\text{sat}_{\bar{u}_p}(k_p^g \gamma(t, y) y_1) - \text{sat}_{\bar{u}_v}(k_v^g v), \quad (7)$$

with γ as in (6b), $k_p^g, k_v^g > 0$ are scalar gains and scalars $\bar{u}_p > 0, \bar{u}_v > 0$ satisfy the bound:

$$\bar{u}_p + \bar{u}_v < \bar{u}. \quad (8)$$

The next lemma establishes stability with the global stabilizer while parameter tuning is discussed in Remark 3.

Lemma 2. Under Assumption 1, consider any values $\bar{u}_p > 0, \bar{u}_v > 0$ satisfying (8) and any pair of positive gains $k_p^g, k_v^g > 0$. Then, the static feedback stabilizer $u = u_g$, with u_g defined in (7), (6b), ensures robust GAS of the origin for (1).

Remark 3. The controller parameters $\bar{u}_p, \bar{u}_g, k_p^g, k_v^g > 0$ can be tuned following the state-feedback procedure, i.e. replacing $\gamma(t, y) y_1$ by p . Then, there exist many strategies to stabilize system (1) (see e.g. Rao and Bernstein (2001) or the twisting controller (Levant, 2003)). Indeed it is possible to make our controller exactly match some of these controllers when the saturations are active. For instance, the classical twisting controller being of the form:

$$u_{twisting} = -\frac{\bar{u}}{1 + \chi} (\text{sign}(p) + \chi \text{sign}(v)), \quad \chi \in]0, 1[, \quad (9)$$

we may choose $\bar{u}_p = \frac{\bar{u}}{1 + \chi}$ and $\bar{u}_v = \frac{\chi \bar{u}}{1 + \chi}$. Finally, the gains k_p^g and k_v^g can be tuned, for instance, by pole placement. \lrcorner

The proposed anti-windup solution for controlling (1) combines the above local and global controllers into a unique controller achieving the desirable local performance induced by u_c and the desirable global stability (on the saturated plant) induced by u_g . To this end, as shown in Fig. 1, we suggest this input selection for saturated plant (1):

$$u(t, y - y_{aw}, y_{aw}) = u_c(t, y - y_{aw}) + u_g(t, y_{aw}), \quad (10)$$

where signal y_{aw} is the state of the following novel form of anti-windup compensator:

$$\begin{aligned} \dot{y}_{1,aw} &= \hat{m}(t, y, y_{aw})(v_{aw} - v_d y_{1,aw}) \\ \dot{v}_{aw} &= \text{sat}_{\bar{u}}(u(t, y - y_{aw})) - u_c(t, y - y_{aw}), \end{aligned} \quad (11)$$

and where we used

$$\hat{m}(t, y, y_{aw}) := \begin{cases} \lambda_1(t), & \text{if } [k_p \kappa] \tilde{y}(v_{aw} - v_d(t)y_{1,aw}) \leq 0 \\ \lambda_2(t), & \text{otherwise} \end{cases}$$

$$y_{aw} := \begin{bmatrix} y_{1,aw} \\ v_{aw} \end{bmatrix}, \quad \tilde{y} := y - y_{aw}. \quad (12)$$

The only parameter to be chosen in (10)–(12) is the scalar gain κ , which should satisfy the two inequalities below:

$$\kappa < \sqrt{2k_p\lambda_0}, \quad \frac{\kappa}{\lambda_0} + \frac{\kappa^2\lambda_m}{2k_p\lambda_0} \left(v_{\max} + \frac{k_v}{\lambda_0} \right)^2 < k_v. \quad (13)$$

The novelty of this approach is to use function \hat{m} to account for the unknown time-varying term m appearing in (1). This may be seen as an adaptive MRAW solution ($m(t)$ being replaced by $\hat{m}(t)$) and is a peculiar dynamical interconnection of the local and global controllers by way of filter (11), as shown in Fig. 1. Note that the plant depends on the unknown term $m(t)$ and that both controllers use the time-varying bounds $\Lambda(t) = [\lambda_1(t), \lambda_2(t)]$. The anti-windup filter allows merging the two actions. To this end, not only it uses the term $\text{sat}_{\bar{u}}(u) - u_c$ but also y , which is necessary to compute $\hat{m}(t)$. This fact often characterizes anti-windup schemes for nonlinear systems. To highlight this fact, the arrow coming from y is drawn in bold. Our main result below is proven in Section 5 using Lemmas 1 and 2.

Theorem 1. Suppose that Assumption 1 holds. Consider any selection of the local and global stabilizers u_c and u_g in (6) and (7) satisfying the assumptions of Lemmas 1 and 2, respectively. Then for any value $\kappa > 0$ satisfying bounds (13), the control law (10)–(12), ensures that the origin of the saturated closed loop with plant (1) is GAS.

Remark 4. An important outcome of the Lyapunov-based approach adopted in this work is that it paves the road for possible extensions and enhancements of the proposed MRAW solution. As an example, one may consider the need of using extra dynamics in the local controller (6) of the following form:

$$u_c(t, y) = -k_p\gamma(t, y)y_1 - k_v v - K_c x_c$$

$$\dot{x}_c = A_c x_c + B_c v$$

where $x_c \in R^n$ and A_c is Hurwitz, and then generalizing the construction of function V_0 presented later in (23), in our proofs section. In particular, V_0 will be chosen as

$$V_0(x) = k_p \frac{1}{2} p^2 + \frac{1}{2} v^2 + \frac{1}{2} x_c^T P_c x_c$$

where $P_c = P_c^T > 0$ satisfies $P_c A_c + A_c^T P_c \leq -2I_{n_c}$. The local controller will be:

$$u_c(t, y, x_c) = -k_p\gamma(t, y)y_1 - k_v v - B_c^T P_c x_c$$

It is not difficult to see that the proof of the main result can still be done in this case with slight modifications. For the application study considered in Section 4, this extra dynamics is not necessary and it is therefore omitted for the sake of conciseness. \square

4. Numerical example

We consider a vision-based automatic landing problem of an autonomous fixed-wing aircraft. The guidance objective is to make the aircraft follow a reference glide slope knowing its velocity plus a quantity which is proportional to the position error with respect to the desired trajectory (Burlion & de Plinval, 2015) (see Remark 1). Using the notation of Burlion and de Plinval

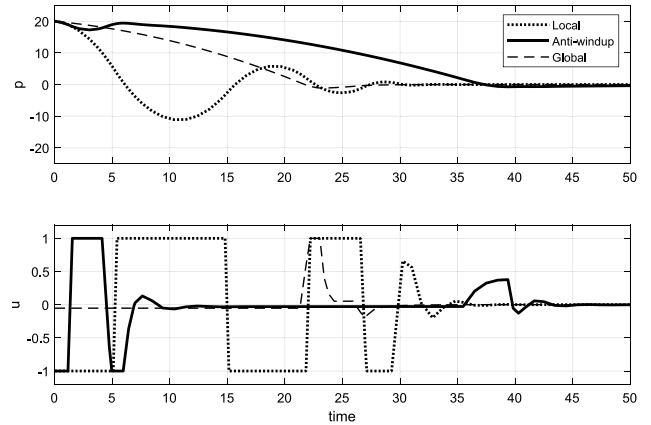


Fig. 2. Numerical results when $x(0) = [20, -1]^T$ and $\Delta_x(0) = 3000$.

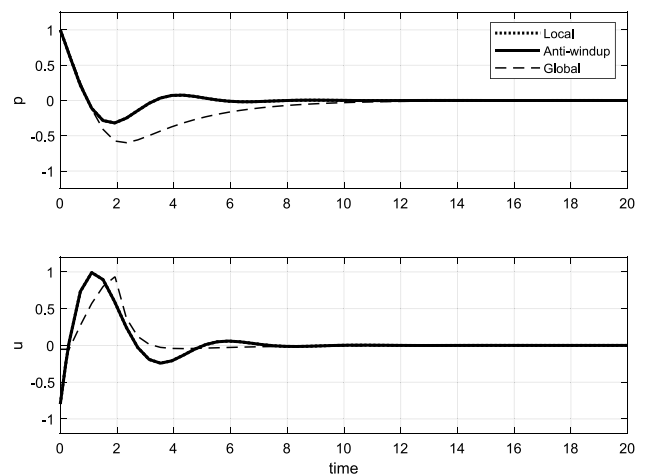


Fig. 3. Numerical results when $x(0) = [1, -3]^T$ and $\Delta_x(0) = 3000$. Local and Anti-windup controllers give the same response.

(2015), the guidance problem boils down to stabilizing a system of the form (1) where

$$p = \Delta_z - \tan(\gamma^c)\Delta_x, \quad v = V(\gamma - \gamma^c),$$

$$u = g u_{lon}, \quad \bar{u} = g \bar{u}_{lon}, \quad m(t) = \frac{1}{\Delta_x}, \quad v_d = V \quad (14)$$

with Δ_x and Δ_z being the horizontal and vertical deviations between the aircraft and the runway touchdown point (see Burlion and de Plinval (2015) for details). The longitudinal control u_{lon} is the vertical load factor (the vertical acceleration divided by acceleration due to gravity). At the beginning of the simulation, we assume that $\Delta_x(0) \in [3000 \text{ m}, 15000 \text{ m}]$. In other words, $m(0)$ is known up to a scaling factor of 5. Using a constant speed $v_d = \Delta_x = -20 \text{ m/s}$, it is thus necessary that each simulation stops before $t = 3000/20 = 150 \text{ s}$ to respect Assumption 1 on this practical application (since $m = +\infty$ when the aircraft touches the runway). We decide to stop our simulations before $t = (3000 - 400)/20 = 130 \text{ s}$ since the (next) flare phase usually starts when $\Delta_x = 400 \text{ m}$. We thus choose: $\lambda_0 = \frac{1}{15000}$ and $\lambda_m = \frac{1}{400}$. For this example, the most challenging situation is when $m(t) = \lambda_2(t)$. Indeed, in this case, $|y_1| = |m(t)p|$ is maximum at each time for a given position error p and the actuator saturation occurs more often. Given $\bar{u} = 1$, we choose the following control gains: $k_p = 0.7$, $k_v = 1.2$, $\bar{u}_p = 0.52$, $k_p^g = 0.18$, $\bar{u}_v = 0.47$ and $k_v^g = 1.63$. We then solve inequalities (13) and obtain $0 < \kappa < 9.1 \cdot 10^{-5}$.

In Figs. 2 and 3, we compare the anti-windup controller from Theorem 1 to the local and global controllers from Lemmas 1 and

2 in a large signal and a small signal response. From Fig. 2, the “Anti-windup” law (solid) eliminates the oscillations of the large signal position error exhibited by the local control law (dotted). The anti-windup solution gives however a slower large signal response than that of the global controller (dashed). However, Fig. 3 shows that the anti-windup scheme fully recovers the local controller response when facing small signals, thus achieving a good tradeoff between the local and global control laws.

5. Proofs

We report here the proofs of our main results in Lemmas 1 and 2 and Theorem 1. Special care is taken with our discontinuous dynamics, which may be generically represented as:

$$\dot{\xi} = f(\xi, t), \quad \xi(t_0) = \xi_0, \quad (15)$$

where f may be discontinuous. To characterize stability properties of (15) we insist on generalized solutions and Krasovskii regularizations (see, e.g., Hermes (1967), Goebel et al. (2012, Ch. 4)). In particular, we introduce the regularized dynamics:

$$\dot{\xi} \in F(\xi), \quad \xi(t_0) = \xi_0, \quad (16)$$

such that all solutions to (15) are also solutions to (16) (this is ensured by imposing $f(\xi, t) \in F(\xi)$ for all ξ and for all t), and that the set-valued mapping F in (16) is sufficiently regular to guarantee existence and well-posedness of solutions (in the sense of Goebel et al. (2012, Ch. 6)). Based on the above, the robust GAS stated in Lemmas 1, 2 and Theorem 1 will be proven by focusing on the regularized dynamics (16) and using the following result from Seuret, Prieur, Tarbouriech, Teel, and Zaccarian (2017), together with the equivalence between robust and non-robust versions of asymptotic stability established in Goebel et al. (2012, Thm 7.21).

Proposition 1 (Seuret et al., 2017). Consider system (16) where F is locally bounded (namely compact sets are mapped to compact sets (Goebel et al., 2012, Def. 5.14)) and outer semi-continuous (namely, it has a closed graph), with $F(x)$ nonempty and convex for each value of its argument. Assume that there exists a locally Lipschitz function V , positive definite and radially unbounded, which is a non-strict Lyapunov function for (16), namely assume that:

$$\dot{V}(\xi) := \max_{f \in F(\xi), v \in \partial V(\xi)} \langle v, f \rangle \leq 0, \quad \forall \xi \in \mathbb{R}^n, \quad (17)$$

where $\partial V(\xi)$ denotes the generalized gradient (Clarke, 1990) of V at ξ . Assume also that no complete solution to (16) keeps V constant and nonzero, namely no solution ξ exists satisfying $V(\xi(t)) = V(\xi(0)) \neq 0$, for all $t \geq 0$. Then the origin is robustly GAS for (16).

For constructing the regularized dynamics (16), given the two positive scalars $\lambda_0, \lambda_m > 0$ introduced in Assumption 1, let us introduce the following set-valued maps¹ $M, M_I, \Delta_M : \mathbb{R} \rightrightarrows \mathbb{R}$, essentially capturing the worst case values of pair $(t, m(t))$ satisfying the stated assumption (4). We denote by “ s ” a generic argument of these functions.

$$M(s) := \begin{cases} \lambda_m, & \text{if } s > 0 \\ [\lambda_0, \lambda_m], & \text{if } s = 0 \\ \lambda_0, & \text{if } s < 0 \end{cases} \quad M_I(s) := \begin{cases} \frac{1}{\lambda_0}, & \text{if } s > 0 \\ \left[\frac{1}{\lambda_m}, \frac{1}{\lambda_0} \right], & \text{if } s = 0 \\ \frac{1}{\lambda_m}, & \text{if } s < 0 \end{cases} \quad (18)$$

$$\Delta_M(s) := [\lambda_0, \lambda_m] \times M_I(s) = \begin{cases} \left[1, \frac{\lambda_m}{\lambda_0} \right], & \text{if } s > 0 \\ \left[\frac{\lambda_0}{\lambda_m}, \frac{\lambda_m}{\lambda_0} \right], & \text{if } s = 0 \\ \left[\frac{\lambda_0}{\lambda_m}, 1 \right], & \text{if } s < 0 \end{cases}$$

¹ The double arrow notation \rightrightarrows distinguishes a set-valued mapping from a function (Goebel et al., 2012).

These mappings are (locally) bounded and outer semi-continuous (because their graphs are closed). For each value of s they are non-empty and convex. Another property of M and Δ_M , which will be used in our proofs, is the following:

$$\max_{\xi \in M(s)} \left\{ \left(1 - \frac{\xi}{m(t)} \right) s \right\} \leq 0, \quad \max_{\xi \in \Delta_M(s)} \{(1 - \xi)s\} \leq 0. \quad (19)$$

We are now ready to prove our main results.

Proof of Lemma 1. Let us recall that $x = \begin{bmatrix} p \\ v \end{bmatrix}$. To properly define the solutions to the closed-loop system (1), (6), we introduce the following set-valued mapping $\mathcal{E} : \mathbb{R}^2 \rightrightarrows \mathbb{R}^2$:

$$\mathcal{E}(x) = \left\{ \begin{bmatrix} v \\ -k_p \xi p - k_v v \end{bmatrix} : \xi \in \Delta_M(pv) \right\} \quad (20)$$

where Δ_M is defined in (18). By composition (see Rockafellar and Wets (2009, Prop. 5.52)), mapping \mathcal{E} is locally bounded, outer semicontinuous, and for each x it is non-empty and convex.

Using the property in (4) implied by Assumption 1, we get

$$m(t)\gamma(t, y) \in \Delta_M(m(t)pv) = \Delta_M(pv), \quad \forall t \geq 0, \quad (21)$$

where the second equality follows from the fact that $m(t) \geq \lambda_0 > 0$ for all times. Then the solutions to the closed-loop (1), (6) are also solutions to the following differential inclusion

$$\dot{x} = \begin{bmatrix} \dot{p} \\ \dot{v} \end{bmatrix} \in \mathcal{E}(x), \quad (22)$$

therefore establishing GAS of the origin for (22) implies GAS of the origin for (1), (6). To this end, consider the candidate Lyapunov function

$$V_0(x) := k_p \frac{1}{2} p^2 + \frac{1}{2} v^2 \quad (23)$$

Computing its derivative along the solutions to (22) gives:

$$\dot{V}_0(x) \leq k_p p v - k_v v^2 + \max_{\xi \in \Delta_M(pv)} \{-k_p \xi p v\} \leq -k_v v^2, \quad (24)$$

where we used the right bound in (19). The proof is then completed by applying Proposition 1 using V_0 . Indeed, to see that no complete solution keeps V_0 constant and nonzero, note that from (24) the only possibility for such a solution to exist is that v be identically zero, which is only possible for the trivial solution $x(t) \equiv 0$ along which we have $V_0(x(t)) \equiv 0$. \square

Proof of Lemma 2. First, using (8), it is readily checked that $\text{sat}_{\bar{u}}(u_g) = u_g$. Then, the closed-loop system (1)–(7) is equivalent to the following system:

$$\dot{p} = v, \quad \dot{v} = -\text{sat}_{\bar{u}_p}(k_p^g \gamma(t, y) y_1) - \text{sat}_{\bar{u}_v}(k_v^g v). \quad (25)$$

Proceeding in similar ways to the proof of Lemma 1, define now the set-valued mapping $\Pi : \mathbb{R}^2 \rightrightarrows \mathbb{R}^2$ as:

$$\Pi(x) = \left\{ \begin{bmatrix} v \\ -\text{sat}_{\bar{u}_p}(k_p^g \xi p) - \text{sat}_{\bar{u}_v}(k_v^g v) \end{bmatrix} : \xi \in \Delta_M(pv) \right\}, \quad (26)$$

where Δ_M is defined in (18). By composition, the mapping Π is outer semi-continuous, non empty and convex for all x . Using Assumption 1 and its implications in (21), we easily verify that the solutions to the closed-loop system (25) are also solutions to the differential inclusion: $\dot{x} \in \Pi(x)$. Let us consider the candidate Lyapunov function:

$$V_1(x) = \int_0^p \text{sat}_{\bar{u}_p}(k_p^g \tau) d\tau + \frac{1}{2} v^2. \quad (27)$$

The derivative of V_1 along the solutions of $\dot{x} \in \mathcal{I}(x)$ reads

$$\begin{aligned} \dot{V}_1 &\leq \text{sat}_{\bar{u}_p}(k_p^g p)v + \max_{\xi \in \Delta_M(p\bar{v})} \{-(\text{sat}_{\bar{u}_p}(k_p^g \xi p) + \text{sat}_{\bar{u}_v}(k_v^g v))v\} \\ &\leq -v \text{sat}_{\bar{u}_v}(k_v^g v), \end{aligned} \quad (28)$$

where the last inequality follows from similar reasoning to those behind the right inequality in (19). From (28), the proof is completed using Proposition 1 as in Lemma 1. \square

Proof of Theorem 1. Let us use incremental coordinates

$$x_{aw} := \begin{bmatrix} p_{aw} \\ v_{aw} \end{bmatrix} := \begin{bmatrix} y_{1,aw} \\ v_{aw} \end{bmatrix}, \quad \tilde{x} := x - x_{aw}, \quad (29)$$

which are compatible with the definition of $\tilde{y} = y - y_{aw}$ in (12). Then (similar to Morabito, Teel, and Zaccarian (2004)), consider the closed-loop coordinate representation (\tilde{x}, x) . These dynamics are simplified by using the following incremental quantities:

$$\delta(t, y, y_{aw}) := (m(t) - \hat{m}(t, y, y_{aw}))(v_{aw} - v_d(t)y_{1,aw}), \quad (30)$$

$$\delta_u(t, \tilde{y}, y) := \text{sat}_{\bar{u}}(u(t, \tilde{y}, y - \tilde{y})) - u_g(t, y). \quad (31)$$

The advantage of the coordinate representation (\tilde{x}, x) is that the discontinuous term $\delta(t, \tilde{y}, y_{aw})$ only appears in the \tilde{x} subsystem. Indeed, we get, after some simplifications:

$$\dot{\tilde{x}} = \begin{bmatrix} \tilde{v} + \frac{1}{m(t)}\delta(t, y, y_{aw}) \\ u_c(t, \tilde{y}) \end{bmatrix}, \quad \dot{x} = \begin{bmatrix} v \\ u_g(t, y) + \delta_u(t, \tilde{y}, y) \end{bmatrix}, \quad (32)$$

which corresponds to a peculiar interconnection of the two closed-loop systems analyzed in Lemmas 1 and 2, by way of coupling terms represented by the perturbation functions δ and δ_u introduced in (30)–(31).

The rest of the proof is carried out by showing that the origin is robustly GAS for the closed-loop dynamics (32). For clarity, the proof of the result is divided into three parts. In part 1, we establish the exponential convergence properties of the \tilde{x} dynamics, regardless of the perturbation term δ . Then in part 2, we analyze a modified system where the \tilde{x} component is replaced by a suitable upper bound, which enables applying the invariance principle of Proposition 1. Finally, in part 3, we combine the derived bounds to obtain global asymptotic stability of the origin for (32).

Part 1. Global exponential stability of the \tilde{x} subsystem. Let us focus on the dynamics of the \tilde{x} component of the overall state in (32). Following similar constructions to the ones proposed before, we obtain that all solutions to (32) have an \tilde{x} component that is also a solution to the following time-varying differential inclusion (note that the signals generated by the second substate x are seen here as a time-varying input):

$$\begin{aligned} \dot{\tilde{x}} &\in \tilde{F}(t, \tilde{x}) \\ &:= \left\{ \begin{bmatrix} \tilde{v} + \frac{m(t) - \bar{m}}{m(t)}(v_{aw}(t) - v_d(t)y_{1,aw}(t)) \\ -k_p \xi \tilde{p} - k_v \tilde{v} \end{bmatrix} \text{ where } \right. \\ &\quad \left. \begin{matrix} \bar{m} \in M((k_p \tilde{y}_1 + \kappa \tilde{v})(v_{aw}(t) - v_d(t)y_{1,aw}(t))) \\ \xi \in \Delta_M(\tilde{p}\tilde{v}) \end{matrix} \right\}. \end{aligned} \quad (33)$$

Proceeding as in the proof of Lemma 1 (but adding an extra term to strictify the weak Lyapunov function V_0 in (23)) we get

$$W_0(t, \tilde{x}) := V_0(\tilde{x}) + \kappa \tilde{p} \frac{\tilde{v}}{m(t)}. \quad (34)$$

In view of a few computations, which involve bounding $m(t)^{-1}$, completing squares and using the left inequality in (13), we

obtain that W_0 is uniformly positive definite with respect to \tilde{x} . Indeed, it can be easily shown that $\forall \tilde{x}$,

$$\begin{aligned} W_0(t, \tilde{x}) &\geq \underline{c}_0 |\tilde{x}|^2 := \min \left\{ k_p - \frac{\kappa^2}{2\lambda_0^2}, \frac{1}{2} \right\} |\tilde{x}|^2 \\ W_0(t, \tilde{x}) &\leq \bar{c}_0 |\tilde{x}|^2 := \max \left\{ k_p + \frac{\kappa^2}{2\lambda_0^2}, \frac{3}{2} \right\} |\tilde{x}|^2. \end{aligned} \quad (35)$$

We then compute the derivative of W_0 along the solutions to (33). Let us briefly note $s = (k_p \tilde{y}_1 + \kappa \tilde{v})(v_{aw} - v_d y_{1,aw})$. In particular, using the left bound in (19), implying that $s \frac{m(t) - \bar{m}}{m(t)} \leq 0$ for all $s \in \mathbb{R}$ and $\bar{m} \in M(s)$, we obtain

$$\begin{aligned} \dot{W}_0 &\leq \frac{1}{m(t)} \max_{\bar{m} \in M(s)} \left(\frac{m(t) - \bar{m}}{m(t)} s \right) + \max_{\xi \in \Delta_M(\tilde{p}\tilde{v})} (k_p (1 - \xi) \tilde{p} \tilde{v}) \\ &\quad + \max_{\xi \in \Delta_M(\tilde{p}\tilde{v})} \left(-\kappa k_p \frac{\xi}{m(t)} \tilde{p}^2 \right) - k_v \tilde{v}^2 + \kappa \frac{\tilde{v}^2}{m(t)} \\ &\quad - \kappa k_v \frac{\tilde{p}}{m(t)} \tilde{v} + \kappa v_d \tilde{p} \tilde{v} \\ &\leq -\kappa \left(\frac{k_p}{\lambda_0} - \varepsilon_1 \right) \tilde{p}^2 - \left[k_v - \frac{\kappa}{\lambda_0} - \frac{\kappa^2}{4\varepsilon_1} \left(v_{\max} + \frac{k_v}{\lambda_0} \right)^2 \right] \tilde{v}^2, \end{aligned} \quad (36)$$

where the last inequality uses Assumption 1 and Young's inequality with the free parameter $\varepsilon_1 > 0$. In particular, by selecting ε_1 as $\varepsilon_1 := \frac{k_p}{2\lambda_0}$, using (35), it is readily checked with $\alpha_0 = \frac{1}{\bar{c}_0} \min \left\{ \kappa \frac{k_p}{2\lambda_0}, k_v - \frac{\kappa}{\lambda_0} - \frac{\kappa^2 \lambda_0}{2k_p} \left(v_{\max} + \frac{k_v}{\lambda_0} \right)^2 \right\} > 0$ that $\dot{W}_0 \leq -\alpha_0 W_0$. By standard comparison theory, we obtain $W_0(t, \tilde{x}(t)) \leq e^{-\alpha_0(t-t_0)} W_0(t_0, \tilde{x}(t_0))$ for all $t \geq t_0$, and for all solutions to (33), which establishes GAS of (33).

Part 2. Construction of an auxiliary LTI inclusion. From the exponential bound of Part 1, we now replace the first component \tilde{x} of the overall state of (32) by an exponentially decaying state w_0 representing the interconnection with the time-varying dynamics (33), by way of a time-invariant equivalent form. To this end, consider δ_u in (32) and (31), and add and subtract $u_g(t, y_{aw}) = \text{sat}_{\bar{u}}(u_g(t, y_{aw}))$ to get

$$\begin{aligned} \delta_u(t, \tilde{y}, y) &= \text{sat}_{\bar{u}}(u_c(t, \tilde{y}) + u_g(t, y_{aw})) - \text{sat}_{\bar{u}}(u_g(t, y_{aw})) \\ &\quad + u_g(t, y_{aw}) - u_g(t, y) \\ &= \delta_{u0}(t, \tilde{y}, y) + \delta_{up}(t, \tilde{y}, y), \end{aligned} \quad (37)$$

where

$$\begin{aligned} \delta_{u0}(t, \tilde{y}, y) &:= \text{sat}_{\bar{u}}(u_c(t, \tilde{y}) + u_g(t, y_{aw})) - \text{sat}_{\bar{u}}(u_g(t, y_{aw})) \\ &\quad + \text{sat}_{\bar{u}_v}(k_v^g v) - \text{sat}_{\bar{u}_v}(k_v^g (v - \tilde{v})) \\ \delta_{up}(t, \tilde{y}, y) &:= \text{sat}_{\bar{u}_p}(k_p^g \gamma(t, y)m(t)p) \\ &\quad - \text{sat}_{\bar{u}_p}(k_p^g \gamma(t, y_{aw})m(t)p_{aw}) \end{aligned}$$

We may now use the global Lipschitz property of the saturation function and the bounds in (4) to prove that

$$|\delta_{u0}(t, \tilde{y}, y)| \leq |u_c(t, \tilde{y})| + |k_v^g| |\tilde{v}| \leq c_\delta |\tilde{x}|, \quad (38)$$

where $c_\delta := k_p \frac{\lambda_m}{\lambda_0} + k_v + k_v^g > 0$. About the second term in (37), we may use inclusion (21) to embed it in a larger but more regular set-valued map independent of t :

$$\begin{aligned} \delta_{up}(t, \tilde{y}, y) &\in \mathcal{Y}(\tilde{x}, x) \\ &:= \left\{ \delta_p = \text{sat}_{\bar{u}_p}(k_p^g \zeta \mu p) - \text{sat}_{\bar{u}_p}(k_p^g \zeta_{aw} \mu (p - \tilde{p})), \right. \\ &\quad \left. \zeta \in M_I(pv), \zeta_{aw} \in M_I((p - \tilde{p})(v - \tilde{v})), \mu \in [\lambda_0, \lambda_m] \right\}. \end{aligned} \quad (39)$$

A useful property enjoined by map Υ defined above is clarified in the following technical lemma, whose proof simply arises from brute force enumeration of all possible cases and can be found in [Burlion, Zaccarian, de Plinval, and Tarbouriech \(2017\)](#).

Lemma 3. For any selection of $(\tilde{x}, x) = (\tilde{p}, \tilde{v}, p, v) \in \mathbb{R}^4$, it holds that

$$\max_{\delta_p \in \Upsilon(\tilde{x}, x)} v \delta_p \leq k_p^g \frac{\lambda_m}{\lambda_0} \left(2|\tilde{x}||v| + |\tilde{x}|^2 \right) + 3\tilde{u}_p |\tilde{x}|. \quad (40)$$

In light of the decomposition in (37), we study (32) using the time-invariant differential inclusion (where we use $x_a := (p_a, v_a)$ and subscript “a” stands for “auxiliary”):

$$\begin{bmatrix} \dot{w}_0 \\ \dot{x}_a \end{bmatrix} \in \Theta \left(\begin{bmatrix} w_0 \\ x_a \end{bmatrix} \right), \quad (41a)$$

where the definition of Θ generalizes (26) due to the presence of an extra disturbance input:

$$\Theta \left(\begin{bmatrix} w_0 \\ x_a \end{bmatrix} \right) := \left\{ \begin{bmatrix} -\frac{\alpha_0}{2} w_0 \\ \frac{v_a}{2} \\ -\text{sat}_{\tilde{u}_p}(k_p^g \xi p_a) - \text{sat}_{\tilde{u}_v}(k_v^g v_a) + \delta_0 + \delta_p \\ \text{for all } |\delta_0| \leq c_\delta |w_0|, \delta_p \in \bigcup_{\tilde{x}: |\tilde{x}_a| \leq |w_0|} \Upsilon(\tilde{x}_a, x_a) \\ \text{and } \xi \in \Delta_M(p_a v_a) \end{bmatrix} \right\} \quad (41b)$$

where $c_\delta := k_p \frac{\lambda_m}{\lambda_0} + k_v + k_p^g > 0$.

Part 3. Global asymptotic stability of the auxiliary inclusion.

The advantage of dynamics (41) as compared to (32) is that it is time-invariant, so that we may use the invariance principle of [Proposition 1](#) to prove GAS of the origin. To this end, consider the Lyapunov function V_1 introduced in (27). Using (28) and (40), we obtain:

$$\dot{V}_1 \leq -v_a \text{sat}_{\tilde{u}_v}(k_v^g v_a) + \varphi(|w_0|, |v_a|), \quad \text{with} \quad (42)$$

$$\begin{aligned} \varphi(|w_0|, |v_a|) &:= \left(c_\delta + 2k_p^g \frac{\lambda_m}{\lambda_0} \right) |v_a| |w_0| + k_p^g \frac{\lambda_m}{\lambda_0} |w_0|^2 \\ &+ 3\tilde{u}_p |w_0| \\ &\leq k_\varphi (|w_0| |v_a| + |w_0|^2 + |w_0|) := \tilde{\varphi}(|w_0|, |v_a|), \end{aligned} \quad (43)$$

where $k_\varphi := \max \left\{ c_\delta + 2k_p^g \frac{\lambda_m}{\lambda_0}, 3\tilde{u}_p \right\}$, and where φ (or its upper bound $\tilde{\varphi}$) can be seen as a perturbation term as compared to the analysis of [Lemma 2](#).

Let us now consider the following positive definite and radially unbounded function

$$W_1(w_0, x_a) := \log(1 + V_1(x_a)) + \eta \left(2\sqrt{U_1(w_0)} + U_1(w_0) \right),$$

where $U_1(w_0) = \frac{1}{2} w_0^2$ and where $\eta > 0$ is selected below. Note that due to the square root, W_1 is not differentiable in the set where $w_0 = 0$, but it is locally Lipschitz. Using (42), as long as $w_0 \neq 0$, the gradient of W_1 is well defined and we may compute the derivative of W_1 along the solutions of (41):

$$\begin{aligned} \dot{W}_1 &\leq \frac{-v_a \text{sat}_{\tilde{u}_v}(k_v^g v_a) + k_\varphi (|w_0| |v_a| + |w_0|^2 + |w_0|)}{1 + V_1(x_a)} \\ &\quad - \eta \left(\frac{\alpha_0}{\sqrt{2}} |w_0| + \frac{\alpha_0}{2} |w_0|^2 \right) \\ &\leq -\frac{v_a \text{sat}_{\tilde{u}_v}(k_v^g v_a)}{1 + V_1(x_a)} - \left(\eta \frac{\alpha_0}{\sqrt{2}} - k_\varphi \left(\frac{1}{\sqrt{2}} + 1 \right) \right) |w_0| \\ &\quad - \left(\eta \frac{\alpha_0}{2} - k_\varphi \right) |w_0|^2, \end{aligned} \quad (44)$$

where we used $\left| \frac{2|v_a|}{2+|v_a|^2} \right| \leq \frac{1}{\sqrt{2}}$. For the remaining set where $w_0 = 0$, it is easily checked that the non-differentiable part of

W_1 satisfies² $\partial \sqrt{U_1(w_0)}|_{w_0=0} = \left[-\frac{1}{\sqrt{2}}, \frac{1}{\sqrt{2}} \right]$, and then, keeping in mind that $\dot{w}_0 = -\frac{\alpha_0}{2} w_0$ (which is zero at zero) that term gives a zero contribution to \dot{W}_1 . This implies that bound (44) holds globally. Choosing the free parameter $\eta := \frac{2}{\alpha_0} \max\{1 + k_\varphi, k_\varphi(\frac{1}{\sqrt{2}} + 1)\} > 0$, we obtain:

$$\dot{W}_1 \leq -\frac{v_a \text{sat}_{\tilde{u}_v}(k_v^g v_a)}{1 + V_1(x_a)} - |w_0|^2, \quad \forall (w_0, x_a), \quad (45)$$

which provides a non-strict decrease of W_1 along the solutions. Global asymptotic stability of the origin for the time-invariant dynamics (41) then follows from the Lipschitz version of the invariance principle given in [Proposition 1](#), noticing that no solution exists, except for the trivial one, which keeps W_1 constant. Indeed, any solution except for those at the origin necessarily keeps revisiting areas where $v_a \neq 0$. Due to the equivalences in [Goebel et al. \(2012, Thm 7.12\)](#) we then have a class \mathcal{KL} bound for all solutions. Performing some class \mathcal{K}_∞ transformations, this implies the existence of a function $\beta \in \mathcal{KL}$ such that all solutions to (41) satisfy

$$|x_a(t)|^2 + |w_0(t)|^2 \leq \beta(|x_a(0)|^2 + |w_0(0)|^2, t), \quad \forall t \geq 0. \quad (46)$$

Part 4. Global \mathcal{KL} stability of the closed loop.

We conclude by proving that bound (46) for solutions of (41) implies a class \mathcal{KL} bound for the solutions to the original dynamics (32). To this end, consider any solution $t \mapsto (\tilde{x}(t), x(t))$ of (32). We prove below that there exists a solution $t \mapsto (w_0(t), x_a(t))$ to the auxiliary dynamics (41) starting from $(w_0(0), x_a(0)) = \left(\sqrt{\frac{c_0}{c_0}} |\tilde{x}(0)|, x(0) \right)$, where $(\bar{c}_0, \underline{c}_0)$ comes from (35), such that $x_a(t) = x(t)$ for all $t \geq 0$. To prove this fact, first note that (35) implies

$$|w_0(0)|^2 = \frac{\bar{c}_0}{\underline{c}_0} |\tilde{x}(0)|^2 \geq \frac{1}{\underline{c}_0} W_0(0, \tilde{x}(0)). \quad (47)$$

Moreover, solution w_0 to the linear dynamics in (41) is $w_0(t) := e^{-\frac{\alpha_0}{2} t} w_0(0)$, and function $W_0(\cdot, \tilde{x}(\cdot))$ satisfies $W_0(t, \tilde{x}(t)) \leq e^{-\alpha_0 t} W_0(0, \tilde{x}(0))$, because of comparison theory. Then (47) with (35) gives:

$$|w_0(t)|^2 = e^{-\alpha_0 t} |w_0(0)|^2 \geq \frac{1}{\underline{c}_0} W_0(t, \tilde{x}(t)) \geq |\tilde{x}(t)|^2, \quad \forall t \geq 0. \quad (48)$$

As a consequence of (48), for each $t \geq 0$ there exists a selection of $\delta_0(t)$ and $\delta_p(t)$ in (41b) such that:

$$\begin{aligned} \delta_0(t) &= \delta_{i0}(t, \tilde{y}(t), y(t)) \leq c_\delta |\tilde{x}(t)| \leq c_\delta |w_0(t)|, \\ \delta_p(t) &= \delta_{up}(t, \tilde{y}(t), y(t)) \in \Upsilon(\tilde{x}(t), x(t)) \\ &\subset \bigcup_{\tilde{x}_a: |\tilde{x}_a| \leq |w_0(t)|} \Upsilon(\tilde{x}_a, x(t)). \end{aligned}$$

Thus it holds that $x_a(t) = x(t)$ for all $t \geq 0$, as claimed above.

The proof is completed by noting that (48), together with bound (46), implies:

$$\begin{aligned} |x(t)|^2 + |\tilde{x}(t)|^2 &\leq |x_a(t)|^2 + |w_0(t)|^2 \\ &\leq \beta \left(|x(0)|^2 + \frac{\bar{c}_0}{\underline{c}_0} |\tilde{x}(0)|^2, t \right), \end{aligned}$$

which establishes a uniform class \mathcal{KL} bound on all solutions to (32), establishing GAS. \square

6. Conclusions

The MRAW design problem was defined and solved for a second order chain of integrators when the first component of

² One way to recognize this is to keep in mind that the generalized gradient is the convex hull of all the proximal gradients ([Clarke, 1990](#), page 11, eq. (4)).

the state is known up to a time-varying scaling factor. The main difficulty is that the plant state is not accessible. Our main theorem establishes desirable properties of a novel MRAW design using a discontinuous term. Simulation results show the effectiveness of the method on a vision-based landing aircraft control. Future work will be devoted to extending this novel anti-windup architecture to a larger class of systems.

References

- Aguiar, A. P., & Hespanha, J. P. (2006). Minimum-energy state estimation for systems with perspective outputs. *IEEE Transactions on Automatic Control*, *51*(2), 226–241.
- Burlion, L., & de Plinval, H. (2015). Visual landing insensitive to the depth with velocity and control constraints: A twisting based solution. In *23th Mediterranean conference on control and automation* (pp. 603–610).
- Burlion, L., Zaccarian, L., de Plinval, H., & Tarbouriech, S. (2017). Detailed proof of the Lemma 1 used in this manuscript. <https://hal.archives-ouvertes.fr/hal-01593178>.
- Chaumette, F., & Hutchinson, S. (2007). Visual servo control. II. Advanced approaches [Tutorial]. *IEEE Robotics & Automation Magazine*, *14*(1), 109–118.
- Clarke, F. H. (1990). *Optimization and nonsmooth analysis*. Society of Industrial and Applied Mathematics.
- Galeani, S., Tarbouriech, S., Turner, M., & Zaccarian, L. (2009). A tutorial on modern anti-windup design. *European Journal of Control*, *15*(3–4), 418–440.
- Goebel, R., Sanfelice, R. G., & Teel, A. R. (2012). *Hybrid dynamical systems: modeling, stability, and robustness*. Princeton University Press.
- Hamel, T., & Mahony, R. (2002). Visual servoing of an under-actuated dynamic rigid-body system: an image-based approach. *IEEE Transactions on Robotics and Automation*, *18*(2), 187–198.
- Hermes, H. (1967). Discontinuous vector fields and feedback control, discussing stability under perturbations and Filippov solutions. *Differential Equations and Dynamical Systems*, 155–165.
- Jankovic, M., & Ghosh, B. K. (1995). Visually guided ranging from observations of points, lines and curves via an identifier based nonlinear observer. *Systems & Control Letters*, *25*(1), 63–73.
- Karagiannis, D., & Astolfi, A. (2005). A new solution to the problem of range identification in perspective vision systems. *IEEE Transactions on Automatic Control*, *50*(12), 2074–2077.
- Levant, A. (2003). Higher-order sliding modes, differentiation and output-feedback control. *International Journal of Control*, *76*(9), 924–941.
- Morabito, F., Teel, A. R., & Zaccarian, L. (2004). Nonlinear anti-windup applied to Euler-Lagrange systems. *IEEE Transactions on Robotics and Automation*, *20*(3), 526–537.
- de Plinval, H., Morin, P., & Mouyon, P. (2017). Stabilization of a class of under-actuated vehicles with uncertain position measurements and application to visual servoing. *Automatica*, *77*, 155–169.
- Rao, V. G., & Bernstein, D. S. (2001). Naive control of the double integrator. *IEEE Control Systems*, *21*(5), 86–97.
- Rockafellar, R. T., & Wets, R. J. B. (2009). *Variational analysis: Vol. 317*. Springer Science & Business Media.
- Seuret, A., Prieur, C., Tarbouriech, S., Teel, A. R., & Zaccarian, L. (2017). A nonsmooth hybrid invariance principle applied to robust event-triggered design. *IEEE Transactions on Automatic Control*, (in press).
- Teel, A. R., & Kapoor, N. (1997). Uniting local and global controllers. In *European control conference*.
- Todeschini, F., Formentin, S., Panzani, G., Corno, M., Savaresi, S., & Zaccarian, L. (2016). Nonlinear pressure control for BBW systems via dead zone and anti-windup compensation. *IEEE Transactions on Control Systems Technology*, *4*, 1419–1431.



Laurent Burlion obtained his Ph.D. degree from the University of Orsay-Paris Sud within the L2S-CNRS in 2007. He was a research scientist at the French Aerospace Lab (ONERA) between 2010 and 2018. He has made a long-term visit at the University of Michigan in 2017. Since 2019, he has been an Assistant Professor at Rutgers, the state University of New Jersey. His areas of interest include control and observation of Aerospace systems, with a particular focus on visual servoing or constrained control. He is a member of the IFAC technical committee on Aerospace and the IEEE-CSS Technical Committee on Aerospace Controls.



Luca Zaccarian received the Ph.D. degree from the University of Roma Tor Vergata (Italy) in 2000, where he has been Assistant and then Associate Professor until 2011. Since 2011 he is Directeur de Recherche at the LAAS-CNRS, Toulouse (France) and since 2013 he holds a part-time associate professor position at the University of Trento, Italy. Luca Zaccarian's main research interests include analysis and design of nonlinear and hybrid control systems, modeling and control of mechatronic systems. He has been an associate editor for *Systems and Control Letters* and *IEEE Transactions on Automatic Control*. He is currently an associate editor for the IFAC journal *Automatica* and for the *European Journal of Control*. He was a nominated member of the Board of Governors of the IEEE-CSS in 2014, where he was an elected member in 2017–2019. He is a fellow of the IEEE since 2016. He was a recipient of the 2001 O. Hugo Schuck Best Paper Award given by the American Automatic Control Council.



Henry de Plinval graduated from Ecole Polytechnique, France, in 2006 and received his M.Sc. in Aeronautics and Astronautics in 2006 from MIT (USA) and his Ph.D. in automatic control from the University of Toulouse in 2014. Since 2008, he is working with Onera—the French Aerospace Lab. His areas of interest include guidance, navigation and control, mostly for UAVs, with a particular focus on visual servoing for VTOL UAVs. Since 2015, he is the UAVs Program Director at ONERA, covering the related activities in the areas of automatic control, artificial intelligence, fluid mechanics, optronics, radar, telecommunications, etc.



Sophie Tarbouriech received the Ph.D. degree in Control Theory in 1991 and the HDR degree (Habilitation à Diriger des Recherches) in 1998 from University Paul Sabatier, Toulouse, France. Currently, she is full-time researcher (Directeur de Recherche) in LAAS-CNRS, Toulouse. Her main research interests include analysis and control of linear and nonlinear systems with constraints (limited information), hybrid dynamical systems. She is currently Associate Editor for *IEEE Transactions on Automatic Control*, *Automatica* and *European Journal of Control*. She is also Senior Editor for *IEEE Control Systems Letters*. Since 1999, she is Associate Editor at the Conference Editorial Board of the IEEE Control Systems Society. She is also a member of the IFAC technical committee on Robust Control and Nonlinear Systems, and of the IEEE Technical Committee on Hybrid Systems.

Finite-Time LPV Analysis of a Vision Based Landing System with Anti-Windup Augmentation

Jean-Marc Biannic* Laurent Burlion* Sophie Tarbouriech**

* ONERA-Toulouse (e-mail: biannic@onera.fr).
University of Toulouse, France.

** LAAS-CNRS
University of Toulouse, France.

Abstract: In contrast to standard ILS-based landing control systems, vision-based strategies rely on specific measures that introduce non-linearities into the control laws. Moreover, during the landing phase high gains are often used to improve performances at the expense of stability which is then degraded. This is not much an issue since both final approach and flare segments are short-time maneuvers. However, high gains induce saturations which in turn lead to performances degradation. For these reasons, vision-based landing systems design and tuning require a specific attention which generally involves a time-consuming trial-and-error process. The latter could certainly be fasten and improved with the help of adapted analysis tools providing a reliable estimate of the finite-time performance level of the aforementioned saturated nonlinear closed-loop system. As observed in Biannic and Burlion (2017), it can be rewritten as a saturated Linear Parameter Varying (LPV) system for which many tools exist or can be extended. In this contribution, original discrete-time extensions are then proposed to characterize finite-time performance indexes for a vision-based landing system including an anti-windup device.

© 2018, IFAC (International Federation of Automatic Control) Hosting by Elsevier Ltd. All rights reserved.

Keywords: Saturated systems, LPV systems, Finite-time analysis, vision-based control.

1. INTRODUCTION

Many airports are now equipped with Instrument Landing Systems (ILS) that significantly secure the landing phase in poor visibility conditions. However, the installation and maintenance of such equipment remain very expensive and is not always available. This is generally the case for small airports and especially for unprepared runways, which could, however, be used for emergency landings. In such cases (but not only) vision landing systems offer an attractive and inexpensive alternative. This is why such solutions have been studied in recent years (see for example: Bourquardez and Chaumette (2007); Azinheira and Rives (2008); Le Bras et al. (2009); Huh and Shim (2010)) and are currently being explored further by the aviation industry (see: Gibert and Puyou (2013); Dickmanns et al. (2015); Gibert et al. (2015)). Despite the very promising results obtained in simulations with IBVS (Image-Based Visual Servoing) or PBVS (Pose-Based Visual Servoing) or a combination of both, there are still some obstacles before these solutions can be used on commercial aircraft:

- thorough evaluations under real conditions must be carried out using "true" images captured from video sequences,

- the computational requirements must be carefully evaluated to check compatibility with on-board computers,
- a specific validation process must be defined for certification needs.

Based on the Finite-Time-Stability (FTS) concept for Linear Time Varying (LTV) systems (see Dorato (1961); Garcia et al. (2009)), preliminary results of Biannic and Burlion (2017) are extended here to provide reliable estimates of finite-time performance indexes for saturated parameter-varying systems. As was indeed clarified in Biannic and Burlion (2017), unlike ILS-based controllers, the vision-based landing control system introduces in the closed-loop plant a specific nonlinearity that can be replaced by a varying parameter which constantly grows during the landing phase until flare is activated. Moreover, during this critical phase, high gains tend to be used to maintain the aircraft on its nominal path with a good accuracy despite perturbations. This however induces saturations. The development of specific tools for analysis of saturated LPV systems along given parametric trajectories is then very useful in the context of vision-based control assessment and improvement. The solution proposed in Biannic and Burlion (2017) provides an initial response without however taking into account the finite-time horizon property of the problem which is essential here. The proposed extension detailed in this paper is based on a discrete-time reformulation as described in

* This work was partly supported by ANR VISIOLAND project ANR-13-CORD-0012 dedicated to VISIO based aircraft LANDING techniques

section 2. Next, the main performance analysis results are detailed in section 3 and applied to the evaluation of a vision-based landing system in section 4. The interest of an anti-windup device is clearly demonstrated there. Finally concluding comments and future directions are proposed in section 5.

2. A BOUNDED-HORIZON TIME-VARYING ANALYSIS PROBLEM WITH SATURATIONS

2.1 System description & preliminary analysis

As detailed in Biannic and Burlion (2017), we focus on the glide slope phase illustrated in Figure 1 during which the autopilot system must maintain a constant slope $\gamma_0 = -3^\circ$ and a constant airspeed V despite external perturbations.

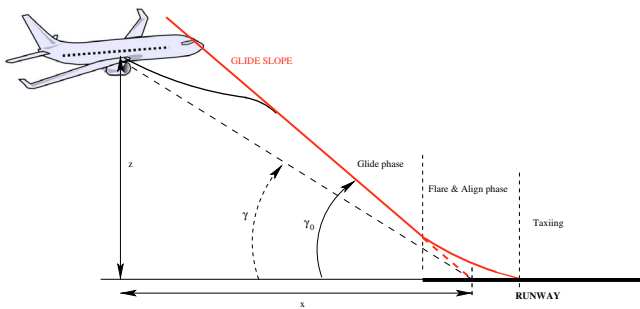


Fig. 1. Landing phases

It is assumed that an inner-loop controller has been defined to track the vertical acceleration \ddot{z} as long as it remains bounded ($|\ddot{z}| \leq L_a$). Moreover, under low wind conditions, the horizontal speed verifies the approximation $\dot{x} \approx V$, so that the studied open-loop system reduces to:

$$\begin{cases} \dot{x} = V \\ \ddot{z} = \text{sat}_{L_a}(u) \end{cases} \quad (1)$$

In a vision-based landing context (see for example Gibert et al. (2015) for further details) this system is initially controlled by a nonlinear proportional-derivative controller:

$$u_0 = k_p \left(\frac{z}{x} - \gamma_0 \right) - k_d (\dot{z} - \gamma_0 V) \quad (2)$$

whose gains $k_p > 0$ and $k_d > 0$ are tuned such that, at the beginning of the glide phase, the system is well-damped and the desired slope is rapidly reached. The non-linearity $\gamma_m = z/x$ is introduced by the visual features. After a variable change $\xi_1 = z - \gamma_0 x$ and $\xi_2 = \Delta v_z = \dot{z} - \gamma_0 V$, one obtains a linear time-varying (LTV) system:

$$\begin{cases} \dot{\xi}_1 = \xi_2 \\ \dot{\xi}_2 = \text{sat}_{L_a}(-\lambda(t)\xi_1 - k_d \xi_2) \end{cases} \quad (3)$$

with:

$$\lambda(t) = -k_p/x(t) \quad (4)$$

The above system has been studied in Biannic and Burlion (2017) with $k_d = 0.3$ and an increasing parameter $\lambda(t)$ such that:

$$\lambda(t) \in [0.1, 0.5], \quad \dot{\lambda}(t) = 0.35 \lambda(t)^2 \quad (5)$$

which corresponds to the final approach phase starting approximately 2000 m before the runway threshold with a constant speed $V = 70 \text{ m s}^{-1}$. This preliminary study

has revealed that the combined effects of the parametric variations with the saturated acceleration were responsible for a severe performance degradation.

2.2 Model-Recovery Anti-Windup (MRAW) design

In this section, it is proposed to enhance the control law (2) with an anti-windup augmentation defined as follows:

- if λ were known, a conventional model-recovery anti-windup scheme Zaccarian and Teel (2011) would consist in choosing:

$$u = -\lambda(\xi_1 - \xi_{1,aw}) - k_d(\xi_2 - \xi_{2,aw}) + u_{aw} \quad (6)$$

$$\begin{cases} \dot{\xi}_{1,aw} = \xi_{2,aw} \\ \dot{\xi}_{2,aw} = \text{sat}_{L_a}(u) - (u - u_{aw}) \\ u_{aw} = -k_{1,aw} \cdot \xi_{1,aw} - k_{2,aw} \cdot \xi_{2,aw} \end{cases} \quad (7)$$

- in the case λ is unknown (which is our case), Burlion and de Plinval (2017) used an estimate $\hat{\lambda}$ in its anti-windup scheme and proved that the closed-loop system was stable using a well-chosen Lyapunov function. Here, we propose to use a more intuitive anti-windup loop which uses a constant value λ_a . Doing so, the anti-windup design is simple but one needs new analysis techniques (especially in the finite-time case) to guarantee that the closed-loop system remains stable.

We thus consider the following control law:

$$u = -\lambda \xi_1 + \lambda_a \xi_{1,aw} - k_d(\xi_2 - \xi_{2,aw}) + u_{aw} \quad (8)$$

with

$$\begin{cases} \dot{\xi}_{1,aw} = \xi_{2,aw} \\ \dot{\xi}_{2,aw} = \text{sat}_{L_a}(u) - (u - u_{aw}) \\ u_{aw} = -k_{1,aw} \cdot \xi_{1,aw} - k_{2,aw} \cdot \xi_{2,aw} \end{cases} \quad (9)$$

Let us choose $\lambda_a = 0.3$, which corresponds to the mean value of the set to which $\lambda(t)$ belongs.

The gains $k_{1,aw}$ and $k_{2,aw}$ of this anti-windup device are tuned according to a low gain strategy as exposed in Lin (1998). For the considered parameter-varying application they were chosen as $k_{1,aw} = 0.1$ and $k_{2,aw} = 0.7$. Next, the global closed-loop system is discretized and the saturation is replaced by a deadzone operator. The following fourth-order system is then obtained:

$$\begin{aligned} \xi_{k+1} &= \underbrace{\begin{pmatrix} 1 & \tau & 0 & 0 \\ -\tau \lambda_k & 1 - 0.3\tau & 0.2\tau & -0.4\tau \\ 0 & 0 & 1 & \tau \\ 0 & 0 & -0.1\tau & 1 - 0.7\tau \end{pmatrix}}_{A_k} \xi_k + \underbrace{\begin{pmatrix} 0 \\ \tau L \\ 0 \\ \tau L \end{pmatrix}}_{B_k} \phi(v_k) \\ v_k &= \underbrace{\begin{pmatrix} \lambda_k L^{-1} & 0.3L^{-1} & -0.2L^{-1} & 0.4L^{-1} \end{pmatrix}}_{C_k} \xi_k \end{aligned} \quad (10)$$

with $\xi = [\xi_1 \ \xi_2 \ \xi_{1,aw} \ \xi_{2,aw}]'$ and where $\phi(\cdot)$ denotes the standard, normalized deadzone operator and τ is the sampling time.

2.3 A preliminary simulation-based analysis

A preliminary simulation-based analysis of the above system is now performed with the initial condition $\xi_0 = [0 \ 2 \ 0 \ 0]'$ and $\tau = 0.3$.

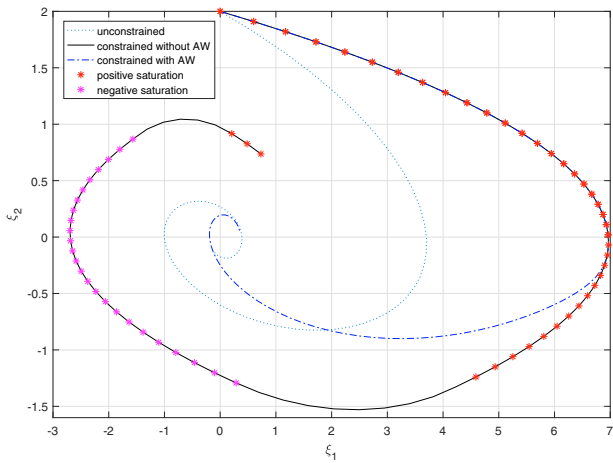


Fig. 2. A preliminary simulation-based analysis: phase portraits illustration.

Phase portraits are plotted in Figure 2 where the discrete-time values λ_k of the varying parameter starting from 0.1 are computed according to equation (5). The effect of the anti-windup system (whose response is visualized by the dash-dotted line) is clearly visible. The phase-portrait trajectory is indeed very close to the origin at the end of the considered horizon $[0, N]$ for which $\lambda_N = 0.5$ and the control system is about to switch to the flare mode. Without anti-windup device, it is observed that the acceleration remains saturated (switching from L to $-L$) on large portions of the trajectory.

The next plots, visualized in Figure 3, show the evolution of $\|\xi\|$, the norm of the state vector as a function of time for the same three configurations as above (unconstrained, constrained without anti-windup and constrained with anti-windup). From this simulation, it can be concluded for the given initial state, that the vision-based control system, equipped with the anti-windup filter, is able to precisely track the glide slope trajectory despite a limited vertical acceleration capacity.

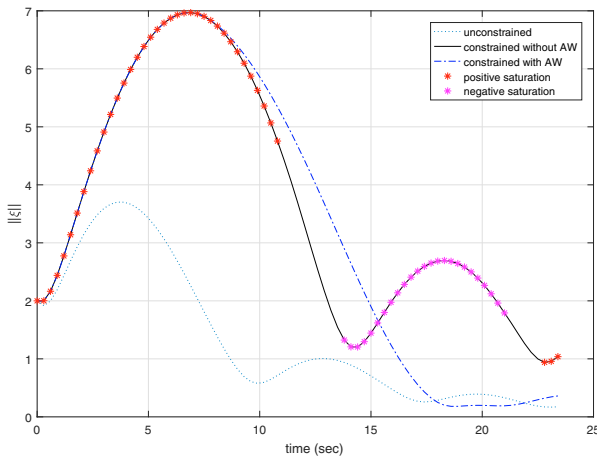


Fig. 3. A preliminary simulation-based analysis: time-domain results

However, the above simulation results do not provide any guarantees at least for different initial conditions. The remainder of the paper is then devoted to the evaluation of a guaranteed performance level without intensive simulations.

3. FINITE-TIME PERFORMANCE ANALYSIS RESULTS

Extending the infinite-horizon and continuous-time analysis results of Biannic and Burlion (2017) to a finite-time horizon analysis, the core of this paper is based on the study of discrete-time saturated LTV systems. The main result, presented next in Theorem 1 generalizes to the bounded horizon and time-varying case a previous result of Gomes da Silva Jr. and Tarbouriech (2006).

3.1 Main result

Theorem 1. (Finite-Time Performance of a Discrete-Time Saturated LTV System). Consider the discrete-time saturated LTV system, defined on the **bounded-horizon** $\{0, 1, \dots, N\}$ by:

$$\begin{cases} \xi_{k+1} = A_k \xi_k + B_k \phi(z_k), & k = 0 \dots N \\ z_k = C_k \xi_k \end{cases} \quad (11)$$

where $\phi(\cdot)$ denotes a normalized deadzone function. If there exist a set of positive definite matrices $Q_k \in \mathbb{R}^{n \times n}$, a set of diagonal matrices $S_k \in \mathbb{R}^{m \times m}$, a set of matrices $Z_k \in \mathbb{R}^{m \times n}$ and a positive real r such that:

$$\begin{pmatrix} Q_{k+1} & A_k Q_k & B_k S_k \\ Q_k A_k' & Q_k & Z_k' \\ S_k B_k' & Z_k & 2S_k \end{pmatrix} > 0, \quad k = 0 \dots N \quad (12)$$

$$\begin{pmatrix} Q_k & Z_k' + Q_k C_k' \\ Z_k + C_k Q_k & 1 \end{pmatrix} > 0, \quad k = 0 \dots N \quad (13)$$

$$Q_0 > \xi_0 \xi_0' \quad (14)$$

$$Q_N < \rho I \quad (15)$$

then, any trajectory ξ_k of system (11) starting from the ellipsoidal set \mathcal{E}_0 that contains the initial vector ξ_0 :

$$\mathcal{E}_0 = \{\xi \in \mathbb{R}^n / \xi' Q_0^{-1} \xi \leq 1\} \ni \xi_0 \quad (16)$$

will verify:

$$\xi_k \in \mathcal{E}_k, \quad i.e. \quad \xi_k' Q_k^{-1} \xi_k \leq 1, \quad k = 1 \dots N \quad (17)$$

and

$$\|\xi_N\| < \sqrt{\rho} \quad (18)$$

□

Sketch of proof: This theorem is easily established with the help of a time-varying quadratic Lyapunov function $V_k = \xi_k' P_k \xi_k$. The matrix inequality (12) in which $Q_k = P_k^{-1}$ clearly implies: $V_{k+1} < V_k$. The same auxiliary variables S_k et Z_k as those introduced in the continuous-time case Biannic and Burlion (2017) are used. This variables are a direct consequence of the use of the modified sector condition originally proposed by Gomes da Silva Jr. and Tarbouriech (2005). The set of inequalities (13) are also linked to the sector conditions and the same formulation is observed in the continuous-time case. The inequality (14) enforces the inclusion of the initial state vector ξ_0

inside the ellipsoidal set \mathcal{E}_0 . One has indeed: $\xi_0' P_0 \xi_0 < 1 \Leftrightarrow Q_0 > \xi_0 \xi_0'$. Finally, the last inequality (15) $Q_N < \rho I$ also reads $P_N > \rho^{-1} I$, from which one obtains $\xi_N' \xi_N = \|\xi_N\|^2 < \rho \xi_N' P_N \xi_N$. The result claimed by inequality (18) stems from the following fact: $V_N = x_N' P_N x_N < 1$ since, by assumption, $V_0 \leq 1$ and also from (12) which implies $V_{k+1} < V_k$. ■

3.2 Numerical complexity and resolution aspects

From a numerical viewpoint, the results stated in Theorem 1 are of high practical interest since they correspond to the minimization of the positive scalar ρ (i.e a linear objective) under linear matrix inequalities (LMI) constraints. However, both the number of constraints:

$$N_c = 2(N + 2) \quad (19)$$

and the number of scalar decision variables:

$$N_v = 1 + (1 + \frac{n}{2})(1 + n)(1 + N) \quad (20)$$

may grow rapidly with the order n of the plant and the number of samples N . At the expense of precision, the latter (N) can be slightly reduced to some extent by increasing the sampling time. But the main options are based on relaxation strategies detailed next.

Reduction in the number of variables. The best option to limit complexity in the LMI optimization problem involved in Theorem 1 is to reduce the number of variables. This is rather easily performed here since the time-varying system matrices depend on a scalar parameter λ . The inequalities (12)- (15) can thus be rewritten:

$$\begin{pmatrix} Q(\lambda_{k+1}) & \star & \star \\ Q(\lambda_k)A'(\lambda_k) & Q(\lambda_k) & \star \\ S(\lambda_k)B'(\lambda_k) & Z(\lambda_k) & 2S(\lambda_k) \end{pmatrix} > 0, \quad k = 0 \dots N \quad (21)$$

$$\begin{pmatrix} Q(\lambda_k) & \star \\ Z(\lambda_k) + C(\lambda_k)Q(\lambda_k) & 1 \end{pmatrix} > 0, \quad k = 0 \dots N \quad (22)$$

$$Q(\lambda_0) > \xi_0 \xi_0' \quad (23)$$

$$Q(\lambda_N) < \rho I \quad (24)$$

and the variables can be chosen, for example, as polynomial functions with respect to λ . Let n_p denote the order of such polynomials, the total number of scalar decision variables now reduces to:

$$N_v = 1 + (1 + \frac{n}{2})(1 + n)(1 + n_p) \quad (25)$$

Reduced number of constraints. A trivial approach to reduce the number of constraints consists in increasing the sampling time in the discretization process to decrease N . This is however infeasible without a possibly significant loss of accuracy. Based on the above characterization, using parameterized functions, there is yet a possible alternative which consists in gridding the parameter space. Then, in inequalities (21) and (22), the index k will no longer evolve in the set $\{0, 1, \dots, N\}$ but in a much smaller subset $\{i_0, i_1, \dots, i_{N_r}\}$ such that $i_0 = 0$, $i_{N_r} = N$ and of course $N_r \ll N$. As a result, the number of constraints reduces to:

$$N_c = 2(N_r + 2) \quad (26)$$

The validity of the inequalities (21) and (22) on the entire set must however be checked *a posteriori* on the initial set and additional constraints must then be considered in case of failure which leads to a (possibly time-consuming) iterative process...

A specialized algorithm for affine parametrically dependent systems. As it can be noticed from equation (10), the state-space data $A_k = A(\lambda_k)$, $B_k = B(\lambda_k)$ and $C_k = C(\lambda_k)$ of the considered time-varying system depend affinely¹ on the parameter λ at each sampling time. In the context of LMI optimization, such a property is useful to guarantee that a parameter-dependent inequality holds by only testing the vertices of the parametric domain. This property forms the basis of the following algorithm with which both the number of variables (without using polynomial expressions) and the number of constraints can be simultaneously limited. As proposed above the algorithm is essentially based on a selection of sampling times:

$$\mathcal{I}_R = \{i_0, i_1, \dots, i_{N_r}\} \quad (27)$$

with $i_0 = 0$ and $i_{N_r} = N$. Next, for each interval $I_k = [i_k \ i_{k+1}]$ (with $k = 0 \dots N_r - 1$), piecewise constant Lyapunov functions $V_k = x_k' P_k x_k$ and relaxation variables Z_k and S_k are used. Then, the $2(N + 2)$ inequalities (21)-(24) become:

$$\begin{pmatrix} Q_k & \star & \star \\ Q_k A'(\lambda_{i_k}) & Q_k & \star \\ S_k B'(\lambda_{i_k}) & Z_k & 2S_k \end{pmatrix} > 0, \quad k = 0 \dots N_r - 1 \quad (28)$$

$$\begin{pmatrix} Q_k & \star & \star \\ Q_k A'(\lambda_{i_{k+1}-1}) & Q_k & \star \\ S_k B'(\lambda_{i_{k+1}-1}) & Z_k & 2S_k \end{pmatrix} > 0, \quad k = 0 \dots N_r - 1 \quad (29)$$

$$\begin{pmatrix} Q_{k+1} & \star & \star \\ Q_k A'(\lambda_{i_{k+1}}) & Q_k & \star \\ S_k B'(\lambda_{i_{k+1}}) & Z_k & 2S_k \end{pmatrix} > 0, \quad k = 0 \dots N_r - 1 \quad (30)$$

$$\begin{pmatrix} Q_k & \star \\ Z_k + C(\lambda_{i_k})Q_k & 1 \end{pmatrix} > 0, \quad k = 0 \dots N_r - 1 \quad (31)$$

$$\begin{pmatrix} Q_k & \star \\ Z_k + C(\lambda_{i_{k+1}})Q_k & 1 \end{pmatrix} > 0, \quad k = 0 \dots N_r - 1 \quad (32)$$

$$Q_0 > \xi_0 \xi_0' \quad (33)$$

$$Q_{N_r} < \rho I \quad (34)$$

Remark 2. Since an affine parametric dependence is assumed here, the above inequalities, by a standard convexity argument, imply that (21) and (22) are satisfied with $Q(\lambda) = Q_k$, $S(\lambda) = S_k$ and $Z(\lambda) = Z_k$ if $\lambda \in [i_k \ i_{k+1}]$.

Algorithm 1. Finite time performance analysis of affine parametrically dependent systems.

(1) Define a subset $\mathcal{I}_R = \{i_0, i_1, \dots, i_{N_r}\}$

(2) Solve the LMI optimization problem:

$$\min \rho / (28), (29), (30), (31), (32)$$

(3) Go back to step (1) and update \mathcal{I}_R to possibly reduce ρ otherwise stop the algorithm.

Remark 3. The number of constraints and variables involved in the above algorithm are respectively reduced to:

$$N_c = 5N_r + 2 \quad (35)$$

and

$$N_v = 1 + (1 + \frac{n}{2})(1 + n)N_r \quad (36)$$

Remark 4. The use of a piecewise constant Lyapunov function possibly leads to conservative results when there

¹ Note that $B(\lambda_k)$ is even a constant, but this additional property will not be exploited in the proposed algorithm.

are not enough points in the selected subset. In such as case, as is proposed in Algorithm 1, a new (denser) set must be provided at the expense of a higher computational burden. An alternative option consists of using piecewise affine functions:

$$Q(\lambda) = \frac{\lambda_{k+1} - \lambda}{\lambda_{k+1} - \lambda_k} Q_k + \frac{\lambda - \lambda_k}{\lambda_{k+1} - \lambda_k} Q_{k+1} \quad (37)$$

with $\lambda \in [\lambda_k \lambda_{k+1}]$. In this case the matrix inequalities (28)-(32) are now second-order polynomials in λ and must then be checked a posteriori to establish their validity for each interval I_k . An efficient alternative option to ensure their validity a priori can also be proposed with the help of additional constraints to enforce a multi-convexity property (see Apkarian and Tuan (2000)).

4. APPLICATION TO THE VISION-BASED LANDING ANALYSIS PROBLEM

The proposed finite-time performance characterizations are now applied to evaluate the vision-based landing system detailed in Section 2. The total order of the system including anti-windup augmentation is limited to $n = 4$. Moreover, the studied horizon is bounded by $T = 25$ s and N is thus no larger than 80 (with sampling time $\tau = 0.3$ s). For these moderate dimensions, the main result stated by Theorem 1 is directly applicable. As emphasized in equations (19) and (20), the LMI problem to be solved involves around 160 constraints and 1200 decision variables.

The results of the application of Theorem 1 are visualized in Figure 4. The problem is solved iteratively over increasing time horizons T_i from 3 s to 24 s. In each case, a guaranteed upper-bound $\rho(T_i)$ (visualized by a magenta star) is computed as well as an ellipsoidal set of initial conditions that includes ξ_0 . As in subsection 2.3, the latter is fixed to $\xi_0 = [0 \ 2 \ 0 \ 0]'$. The lower-bound, represented by the blue solid line curve is simply obtained by the discrete-time trajectory starting from the initial condition ξ_0 .

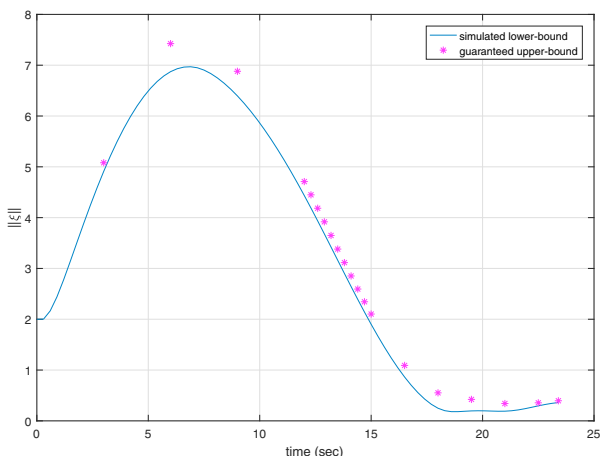


Fig. 4. Finite-time performance analysis: a simulated lower-bound and guaranteed upper-bounds

As one could expect, the conservatism of the proposed characterization in Theorem 1 is reasonably low. At the end of the studied horizon, the gap between upper and lower bounds is very tight indeed and the analysis technique thus captures the beneficial effects of the anti-windup system after 15 s. Unfortunately, this approach is limited to moderate dimensions problems. The computational burden may however be significantly reduced with the help of Algorithm 1 which has also been applied on the same study case for various subset \mathcal{I}_R with growing size. The results are summarized in Table 1.

N_r	10	20	30	Theorem 1
N_c	62	102	152	160
N_v	166	316	466	1196
ρ	infeasible	1.89	0.478	0.396

Table 1. Application of Algorithm 1

The good compromise between accuracy and computational complexity is obtained here with $N_r = 30$. Note that for this choice, the number of constraints is not significantly reduced in comparison with theorem 1. However the number of variables is much smaller. As suggested in Remark 4, less conservative results can be obtained with piecewise affine functions.

5. CONCLUSION AND FUTURE WORK

New performance analysis results have been presented in this paper for time-varying saturated systems over a bounded horizon. The proposed characterization has been successfully tested to evaluate the performance of a landing system with an anti-windup loop. Thanks to well-chosen relaxation techniques the computational complexity can be limited which makes the proposed approach applicable to higher order systems than those considered in this paper. Moreover, extensions (possibly using the IQC framework as proposed in Fry et al. (2017); Seiler et al. (2017)) may also be investigated to introduce robustness aspects with respect to parametric uncertainties. On the application level, more complex vision-based landing control systems, including the flare phase, will also be studied with similar tools in a near future.

REFERENCES

- Apkarian, P. and Tuan, H. (2000). Parameterized LMIs in Control Theory. *SIAM Journal on Control and Optimization*, 38(4), 1241–1264.
- Azinheira, J. and Rives, P. (2008). Image-based visual servoing for vanishing features and ground lines tracking: Application to a uav automatic landing. *International Journal of Optomechatronics*, 2, 275–295.
- Biannic, J.M. and Burlion, L. (2017). Performance analysis of saturated parameter-varying systems with application to vision-based landing assessment. In *20th IFAC World Congress*. Toulouse, France.
- Bourquardez, O. and Chaumette, F. (2007). Visual servoing of an airplane for auto-landing. In *Proceedings of the IEEE/RSJ International Conference on Intelligent Robots and Systems*. San Diego, CA, USA.

- Burlion, L. and de Plinval, H. (2017). Vision based anti-windup design with application to the landing of an Airliner. In *20th IFAC World Congress*. Toulouse, France.
- Dickmanns, D., Boada, J., Gibert, V., and Schubert, F. (2015). Vision based landing for commercial aircraft. In *Proceedings of the 6th European Conference for Aeronautics and Space Sciences*. Krakow, Poland.
- Dorato, P. (1961). Short time stability in linear time-varying systems. In *Proceedings of IRE International Convention Record, Part 4.*, 83–87.
- Fry, J., Farhood, M., and Seiler, P. (2017). IQC-based robustness analysis of discrete-time linear time-varying systems. *International Journal of Robust and Nonlinear Control*, 27(16), 3135–3157.
- Garcia, G., Tarbouriech, S., and Bernussou, J. (2009). Finite-Time Stabilization of Linear Time-Varying Continuous Systems. *IEEE Transactions on Automatic Control*, 54(2), 364–369.
- Gibert, V., Burlion, L., Chriette, A., Boada, J., and Plestan, F. (2015). Vision based automatic landing of a civil aircraft by using nonlinear pose estimation. In *Proceedings of the 6th European Conference for Aerospace Sciences*. Krakow, Poland.
- Gibert, V. and Puyou, G. (2013). Landing of an airliner using image-based visual servoing. In *9th IFAC Symposium on nonlinear control systems*. Toulouse, France.
- Gomes da Silva Jr., J. and Tarbouriech, S. (2005). Anti-windup design with guaranteed regions of stability: An LMI-based approach. *IEEE Transactions on Automatic Control*, 50(1), 106–111.
- Gomes da Silva Jr., J. and Tarbouriech, S. (2006). Anti-windup design with guaranteed regions of stability for discrete-time linear systems. *Systems & Control Letters*, 55, 184–192.
- Huh, S. and Shim, D. (2010). A vision-based automatic landing method for fixed-wing uavs. *Journal of Intelligent and Robotic Systems*, 57, 217–231.
- Le Bras, F., Hamel, T., Barat, C., and Mahony, R. (2009). Nonlinear image-based visual servo controller for automatic landing guidance of a fixed-wing aircraft. In *Proceedings of the European Control Conference*. Budapest, Hungary.
- Lin, Z. (1998). *Low Gain Feedback*. Springer, Berlin, New-York, London.
- Seiler, P., Moore, R., Meissen, C., Arcak, M., and Packard, A. (2017). Finite horizon robustness analysis of LTV systems using integral quadratic constraints. *CoRR*. URL <http://arxiv.org/abs/1711.07248>.
- Zaccarian, L. and Teel, A. (2011). *Modern Anti-Windup Synthesis*. Princeton University Press.

Chapitre 8

Commande et observation de systèmes aérospatiaux à dynamique non linéaire

Résumé du chapitre : Ce chapitre présente des travaux de recherche portant uniquement sur la commande par Backstepping. Nous présentons des résultats lorsque 1) la commande est échantillonnée, 2) des dynamiques méconnues (des modes souples) affectent le système contrôlé ou 3) des mesures sont imprécises (comme dans le problème de l'atterrissage basé vision étudié dans le chapitre précédent).

8.1 Introduction

Nos travaux de recherche sur la commande ou l'observation des systèmes à dynamique non linéaire ont démarré en 2003 avec notre stage de DEA : nous avons utilisé la commande par backstepping et différents observateurs non linéaires pour piloter un planeur sous-marin [19]. Nos travaux de thèse (2003-2006) se sont ensuite focalisés sur le problème de la commande échantillonnée des systèmes non linéaires : nous avons notamment proposé une nouvelle méthodologie basée sur une approximation de Taylor Lie pour améliorer la performance de plusieurs types de commandes non linéaires (Backstepping, Forwarding et Backstepping adaptatif) lorsqu'on les échantillonne [16, 18, 100]. Par la suite, nos encadrants ont continué à travailler sur ce thème des systèmes échantillonnés en dimension finie puis infinie : nous avons régulièrement collaboré avec eux sur des problèmes d'estimation lorsque les sorties mesurées sont échantillonnées ou retardées [56, 2, 3].

En 2011, peu de temps après notre arrivée à l'Onera, nous avons repris des travaux sur le Backstepping et nous avons proposé et coencadré la thèse d'Elodie Duraffourg qui consistait à examiner comment nous pouvions appliquer et étendre le Backstepping à des systèmes aérospatiaux flexibles [49]. Un peu plus tard, nos travaux portant sur l'atterrissage basé vision nous ont permis de travailler sur le backstepping borné et de proposer des solutions complémentaires aux travaux d'observation ou de commande anti-windup décrits dans le chapitre précédent.

Enfin, les deux dernières thèses que nous avons coencadrées se sont aussi intéressées à la commande de systèmes à dynamique non linéaire :

- Torbjørn Cunis a proposé des solutions d'analyse et de commande d'un aéronef qui a décroché. Il a notamment utilisé des techniques d'analyse et de synthèse en utilisant la programmation semi-définie basées sur la positivité de polynômes (SOS) [41, 42],
- Anthony Bourdelle a conduit des travaux de recherche en modélisation, estimation et commande afin de compenser le couple perturbateur induit par les ballottements d'ergol à bord des satellites d'observation. Nous avons travaillé sur un modèle non linéaire puisque la dynamique des ballottements dépendait du mouvement du corps rigide [14].

8.2 La commande par Backstepping

8.2.1 Principe de la méthode

La commande par Backstepping [28, 78, 74] est aujourd'hui une méthode de commande non linéaire standard permettant de stabiliser globalement et asymptotiquement des systèmes sous forme "strict-feedback" ayant une **structure récurrente** bien particulière de la forme suivante :

$$\begin{cases} \dot{x}_1 &= f_1(x_1) + x_2 \\ \dot{x}_2 &= f_2(x_1, x_2) + x_3 \\ &\vdots \\ \dot{x}_n &= f_n(x_1, \dots, x_n) + u \end{cases} \quad (8.1)$$

où les x_i et u sont des vecteurs de même dimension. Si les fonctions f_i sont suffisamment régulières, il est alors possible de construire la loi de commande de manière récursive en partant du premier sous-système à stabiliser ($\dot{x}_1 = f_1(x_1) + x_2$, dont l'entrée de commande est temporairement x_2). L'idée clef est alors de rajouter un intégrateur et de remonter après un nombre suffisant d'intégrateur à la commande u . Cette méthode permet notamment de résoudre un certain nombre de problèmes de robustesse ou de commande adaptative [81, 82].

8.2.2 Positionnement de nos travaux

Nos travaux sur la commande par Backstepping ont porté sur deux aspects (qui se sont avérés être étroitement liés) :

- l'extension de la commande par Backstepping à d'autres classes de systèmes. Par exemple, au cours de notre thèse, nous nous sommes demandé comment étendre la commande par Backstepping au cas où la commande est échantillonnée. Nous nous sommes alors intéressés au discretisé exact du système continu et avons considéré les classes de systèmes obtenus en l'approximant par des séries de Taylor-Lie [9]. Le discrétisé exact pouvait alors être de plus en plus finement approximé par une telle série mais la structure en cascade du système (nécessaire à la synthèse par backstepping) était alors perdue lorsque l'ordre de cette série dépassait un.
- l'application du Backstepping aux systèmes aéronautiques et spatiaux. Le Backstepping s'applique en effet aux modèles cinématiques d'engins pilotés comme les drones [10, 52, 38, 12] (quitte à supposer une séparation des échelles de temps pour simplifier la synthèse) puisque

la position est contrôlée par la vitesse, la vitesse par l'accélération etc...Le Backstepping était d'ailleurs un bon candidat pour le guidage basé vision puisque le modèle est alors cinématique (à ceci près qu'on ne mesure pas tout l'état du système comme nous l'avons vu dans le chapitre précédent). Pourtant, la synthèse des lois de guidage-pilotage des engins aérospatiaux se fait souvent sur des modèles non pas cinématiques mais dynamiques prenant en compte les effets aéroélastiques (forces aérodynamiques et structurelles) ; nous nous sommes alors demandés comment appliquer le Backstepping dans un tel contexte.

8.3 Nos contributions

8.3.1 Backstepping et commande échantillonnée

Nos travaux de thèse ont porté sur le redesign du Backstepping en présence de l'échantillonnage de la commande. En effet, en appliquant la méthode proposée dans [9] nous pouvions approximer le discretisé exact du système par une série de Taylor Lie si toutefois le pas d'échantillonnage est suffisamment petit. Le problème de cette approche provenait du fait qu'un système sous forme strict-feedback perdait sa structure particulière lorsque l'ordre de la série était supérieur à 1. Pour y remédier, nous avons synthétisé une loi de commande par Backstepping basée elle-aussi sur une série de Taylor [18]. Nous avons ensuite considéré le problème des paramètres incertains ; nous avons alors étendu le Backstepping adaptatif au cas échantillonné : cette fois, nous avons dû non seulement redesigner le Backstepping comme précédemment mais avons dû aussi "reparamétriser" le système (au sens de [97]) à cause de l'apparition de puissances des paramètres incertains [100]. Nous donnons à titre d'illustration la publication [18] en fin de chapitre.

8.3.2 Backstepping et modes souples

Le Backstepping peut perdre ses bonnes propriétés en présence de dynamiques négligées : par exemple, la thèse de M. Arcaç s'est intéressée à la dynamique des actionneurs et a proposé de robustifier la commande par Backstepping lorsqu'on prend en compte les actionneurs [8].

Un autre problème d'importance est celui des modes souples ou vibrations indésirables que l'on trouve sur les systèmes aérospatiaux. Ces systèmes n'ont souvent pas d'actionneurs dédiés à l'amortissement des modes souples. Le domaine de la robotique présente d'ailleurs une large littérature de systèmes sous-actionnés à contrôler [53, 98]. Seulement ces résultats ne sont pas tou-

jours transposables au domaine de l'aérospatial (présence des forces aérodynamiques, incertitudes paramétriques ou absence de mesure de l'état complet du système).

Partant de quelques travaux de commande non linéaire de systèmes aérospatiaux flexibles [54, 70] (ces derniers prenaient en compte les modes flexibles dans la preuve de stabilité du système bouclé mais ne cherchaient pas forcément à amortir ces modes), nous avons cherché à modifier le Backstepping qu'on synthétiserait sur le modèle rigide de manière à amortir davantage les modes flexibles. Nous avons dénommé notre approche Backstepping flexible [51]. Nous avons montré comment appliquer le Backstepping à deux classes de systèmes non linéaires pouvant représenter des systèmes aérospatiaux [23]. Enfin, nous nous sommes aussi intéressés aux problèmes des incertitudes paramétriques et de la synthèse d'observateurs dans ce contexte. Par exemple, nous avons combiné l'observation d'état et l'estimation paramétrique de manière à obtenir en temps fini l'estimation de quelques paramètres et de l'état complet d'un lanceur [50]. Ces travaux se sont appuyés sur une méthode d'estimation algébrique [55]. Les publications [23, 50] sont données à la suite de ce chapitre. La suite logique de ces travaux est la thèse d'Anthony Bourdelle qui nous a permis d'étudier cette fois des modes de ballotement d'ergol dans un satellite d'observation.

8.3.3 Backstepping borné et atterrissage basé vision

Durant très longtemps, la communauté scientifique pensait que la technique d'ajout d'intégrateurs ne permettait pas d'obtenir une loi de commande bornée. Les premiers travaux qui ont permis d'obtenir une telle propriété datent de la fin des années 90. [57, 110]. Ces résultats ont fait ensuite l'objet d'extensions notamment pour contrôler des systèmes non autonomes [92]. Des retards ont même été introduits de manière à se passer du fait de calculer les dérivées successives des pseudo-contrôleurs dans la synthèse de la commande par Backstepping [93, 95]. C'est ce dernier point qui a retenu toute notre attention lorsque nous avons travaillé sur notre problème d'atterrissage basé vision. En effet, nous ne disposions que d'une information partielle de l'état à cause de la projection perspective et ne souhaitions donc pas avoir à déterminer les dérivées successives des pseudo-contrôleurs dans la synthèse d'une commande par Backstepping. Nous avons alors entamé une collaboration avec l'Inria (F. Mazenc) et l'Université d'état de la Louisiane (M. Malisoff) sur ce thème [94, 90] et avons ainsi proposé une nouvelle méthode permettant de réaliser le guidage basé vision d'un aéronef sans avoir à estimer la profondeur de champ de la caméra [89, 88]. Nous avons notamment étudié ce problème lorsque les mesures provenant de l'image sont retardées

et échantillonnées à cause de l'acquisition et du traitement des images : [88] a été récemment acceptée à la revue *Systems & Control Letters* et est donnée ci-après. Enfin, nous avons aussi pu nous passer du découplage guidage longitudinal/latéral grâce à ce type de méthode [88].

AUTHOR'S PERSONAL COPY

On the stabilization of sampled-data non-linear systems by using backstepping on the higher order approximate models

L. BURLION*†‡, T. AHMED-ALI§ and F. LAMNABHI-LAGARRIGUE†

†Laboratoire des Signaux et Systèmes, école SUPérieure d'ELECTricité – Centre National de la Recherche Scientifique, Université Paris-XI Sud, 3 Rue Joliot Curie, 91192 Gif-sur-Yvette, France

‡Délégation Générale pour l'Armement, Laboratoire de Recherches Balistiques et Aérodynamiques, BP 914, 27207 Vernon Cedex, France

§Ecole Nationale Supérieure des Ingénieurs des Etudes et Techniques de l'Armement, 2 Rue François Verny, 29806 Brest Cedex 9, France

(Received 17 September 2005; in final form 5 May 2006)

In this paper, we study the stabilization of non-linear sampled-data feedback control systems. Our controller design is based on a backstepping procedure applied on the higher order approximations of the exact discretized associated systems.

1. Introduction

This paper deals with the stabilization problem of non-linear sampled-data feedback control systems. Non-linear sampled-data feedback control systems consist of a non-linear plant (described by a system of first order ordinary differential equation) and a digital controller. Thus, they mix continuous and discrete variables and therefore, belong to the large class of hybrid systems. Moreover, when we use a discretized dynamical feedback and add the control in the state variables, the sampled-data system is included into the subclass of the time-dependent impulsive dynamical systems as explained in Ye *et al.* (1998) and Burlion *et al.* (2004).

There exist two main methods to design controllers for sampled-data systems: the first one is known as the 'CTD' method (also called emulation) and involves discretizing a continuous controller (see for instance Hermann *et al.* (1999) and Burlion *et al.* (2004)); the second method is called the 'DTD' method and involves designing a controller for an approximation of the exact discretized system (see for instance Netic *et al.* (1999), Netic and Teel (2001) and Arcat and Netic (2004)), which is unknown most of the time.

The CTD method does not need the exact knowledge of the sampling period and can achieve global asymptotic stabilization. The DTD method based on approximation can only achieve semi-global stabilization but takes into account the sampling time value in the controller design. Of course, both these methods require that the sampling time is small enough to work. Indeed, very high frequencies are required in order to preserve the properties of the continuous controller in the CTD method and to obtain good approximations of the discretized system in the DTD method. In this paper, we use the DTD method. In the last few years, when people used this method, they only considered the first order approximation of the exact discretized system which was due to the difficulty of the computations and to the appearance of some power series of the controller that render the design very difficult by changing the structure of the continuous non-linear system. For instance, the Euler approximation is used in Netic and Teel (2001) because it preserves the feedback structure of the continuous-time plant.

More recently, the higher order approximations have been introduced in the control design of sampled-data systems (Netic and Grüne 2005, Burlion *et al.* 2005) and this new technique paves the way for several extensions.

We address the problem of extending the backstepping procedure used in Netic and Teel (2001) to the higher order approximation of some non-linear

*Corresponding author. Email: burlion@lss.supelec.fr

sampled-data systems. As we shall see, although the higher order approximations of the discretized system seem to destroy the initial structure of the system at first glance, it is still possible to apply a kind of Backstepping design by assigning to the pseudo-controllers and finally to the controller a specific structure based on some powers extension of the sampling period.

The paper is organized as follows: we first discuss the control design problem for one dimensional non-linear sampled systems. In the §3, we address the problem for a class of higher dimensional non-linear systems by using a backstepping procedure. We finally illustrate our result by an example and some numerical results.

1.1 Notations and mathematical preliminaries

We introduce the multi-index notations

- $I_k := (i_0, \dots, i_k)$
- $|I_k| := i_0 + \dots + i_k$.

We denote by Newton’s multinomial formula the following expression:

$$\left(\sum_{i=0}^r a_i\right)^n = \sum_{\substack{I_r \in \{0,1\}^{r+1} \\ |I_r|=n}} \frac{n!}{i_0! \dots i_r!} a_0^{i_0} \dots a_r^{i_r}.$$

We recall the notation of Lie derivative (i.e derivative of a function along a vector field)

- $L_f h(x) := d/dt[h(x(t))]_{\dot{x}=f(x)} = \partial h/\partial x \cdot f(x)$
- $L_g L_f h(x) := L_g(L_f h(x))$.

A function $\gamma: \mathbb{R}^{+*} \rightarrow \mathbb{R}^{+*}$ is of class \mathcal{K}^∞ if it is continuous, cancels at zero and is strictly increasing and unbounded.

As in Netic and Grüne (2005), we say that a real function $R(T, x)$ is of order T^r and we write $R(T, x) = \mathcal{O}(T^r)$ if whenever R is defined, there exist $\bar{T}, \Delta > 0, \gamma \in \mathcal{K}^\infty$ such that

$$\forall T, x \text{ s.t } T \in [0, \bar{T}], \|x\| \leq \Delta, \implies |R(T, x)| \leq T^r \gamma(\|x\|).$$

2. Stabilization of one-dimensional sampled-data systems

Since the first controlled systems were analog, continuous-control theory has been widely developed and the simplest way to design a controller for a sampled-data system (now digital controllers prevail) is to use continuous-time controller design tools and to discretize the controller using fast sampling. As explained in the introduction, this method is called CTD method or Emulation.

This technique is limited and completely ignores sampling which is why alternative techniques based on approximation of the exact discretized systems have been developed. These techniques are the DTD methods (the reader interested in a more complete introduction on sampled-data systems can find more details in Netic *et al.* (1999), Laila (2005) and Chen and Francis (1995)).

In this paper, we use the DTD method and propose to adapt a well known control design technique for continuous control theory named backstepping to the DTD designs. In this section, we consider one-dimensional sampled-data systems and we give the ideas that will be used in our result.

Given a fixed sampling period $T > 0$, we consider the following non-linear sampled-data system: $\forall k \in \mathbb{N}, \forall t \in [kT, (k+1)T[$

$$\dot{x} = f_1(x) + u_k, \tag{1}$$

where $x \in \mathbb{R}, u := u_k \in \mathbb{R}$ are the state and input variables and f_1 is an analytic function. The notation ‘ u_k ’ means that the controller u is constant on each sampling interval $[kT, (k+1)T[$.

For a given initial condition x_0 , the solution $t \mapsto x(x_0, t)$ of (1) coincides with the solution of the exact discretized system at each time $t = kT, k \in \mathbb{N}$. We note this solution $x_k = x(x_0, kT)$. The exact discretized system associated to (1) is

$$x_{k+1} = x_k + \int_{kT}^{(k+1)T} f_1(x(s)) + u_k ds. \tag{2}$$

In order to prove that the state $x(t)$ in (1) tends to 0 (for a given initial condition x_0 and a sampling period T) as t tends to $+\infty$, we only need to prove that $x(kT)$ tends to 0 as $k \rightarrow +\infty$ when the dynamics of the system are sufficiently smooth. Indeed, in this case there exists $h \in K_\infty$ such that

$$\forall k \in \mathbb{N}, \forall t \in [kT, (k+1)T[, \|x(t)\| \leq h(\|x(kT)\|).$$

This last inequality is satisfied by using Gronwall’s lemma and smooth properties of the functions governing the dynamic of the continuous state $x(t)$. So, if we succeed in proving that $x(kT)$ tends to 0 as $k \rightarrow +\infty$, we prove that $x(t)$ tends to $+\infty$ which was the initial goal.

That is why DTD methods only deal with discrete systems. Since the exact expression of (2) cannot be computed in general, we consider Taylor series. There exists $\bar{T} > 0$ such that for all $T \in [0, \bar{T}[$

$$x_{k+1} = x_k + T(f_1(x_k) + u_k) + \sum_{i=2}^{\infty} \frac{T^i}{i!} x^{(i)}(kT^+).$$

We can now give a simple result which is at the root of many extensions and which has spurred the next section.

Lemma 1: For all $r \in \mathbb{N}^*$, there exist $\alpha \in \mathbb{R}^{+*}$, a controller $u_k := u_k(x(k), r, \alpha)$ such that the solution of (1) taken at the sampling times satisfies

$$x(kT) = (1 - \alpha T)^k x(0) + \mathcal{O}(T^{r+1}).$$

Hence, if $T \in]0, \min\{\bar{T}, 1/\alpha\}[$, the system (2) is stabilized to $0 + \mathcal{O}(T^r + 1)$.

Proof: To simplify the notations, in the remaining of the paper, we will use the notation x (resp. x^+ , resp. u) instead of $x(kT)$ (resp. $x((k+1)T)$, resp. u_k). These notations are often used for difference equations.

Considering the sampled-data system (1), there exists $\bar{T} > 0$ such that for all $T \in [0, \bar{T}]$, its exact discretized system coincides with

$$x^+ = x + T(f_1(x) + u) + \sum_{i=2}^r \frac{T^i}{i!} x^{(i)} + \mathcal{O}(T^{r+1}), \quad (3)$$

where $\mathcal{O}(T^r + 1)$ contains the remaining higher order terms.

Since $\dot{u}_k = 0$ on $[kT, (k+1)T]$, one can express $x^{(i)}$, by using Lie derivatives,

$$x^{(i)} := \sum_{\{k_1, \dots, k_i\} \in \{0, 1\}^i} (L_{g_{k_1}} \dots L_{g_{k_i}} x) u^{|\mathcal{K}_i|},$$

where $|\mathcal{K}_i| := k_1 + \dots + k_i$, $g_0 := f_1$ and $g_1 := 1$.

Thus, noting

$$h_{ij} := \sum_{\substack{\{k_1, \dots, k_j\} \in \{0, 1\}^j \\ |\mathcal{K}_j|=i}} (L_{g_{k_1}} \dots L_{g_{k_j}} x),$$

one can express $x^{(i)}$ in the following form in powers of u :

$$x^{(i)} := \sum_{j=0}^i h_{ij}(x) u^j. \quad (4)$$

Then, we apply the following controller:

$$u = \sum_{i=1}^r \frac{T^{i-1}}{i!} u_i. \quad (5)$$

Using equations (3), (4) and (5) we have

$$\begin{aligned} x^+ &= x + T(u_1 + f_1(x)) \\ &+ \sum_{i=2}^r \frac{T^i}{i!} \left(u_i + \sum_{j=0}^i h_{ij}(x) \left(\sum_{i=1}^r \frac{T^{i-1}}{i!} u_i \right)^j \right) + \mathcal{O}(T^{r+1}). \end{aligned}$$

So, using Newton's multinomial formula in order to collect the terms in powers of the sampling period T , one obtains an expression of the form

$$x^+ = x + \sum_{i=1}^r \frac{T^i}{i!} (u_i + f_i(x, u_1, \dots, u_{i-1})) + \mathcal{O}(T^{r+1}).$$

Then, one chooses the control in this way,

$$\begin{cases} u_1 = -f_1(x) - \alpha x \\ u_2 = -f_2(x, u_1) \\ \vdots \\ u_r = -f_r(x, u_1, \dots, u_{r-1}), \end{cases}$$

where $\alpha \in \mathbb{R}^{+*}$.

Thus, the closed loop system is

$$x^+ = (1 - \alpha T)x + \mathcal{O}(T^{r+1}).$$

Therefore, by a recursive procedure, we obtain

$$x(kT) = (1 - \alpha T)^k x(0) + \mathcal{O}(T^{r+1}).$$

The power expansion of the exact discretized system is convergent for all $T \in]0, \bar{T}[$ and $(1 - \alpha T)^k$ converges to 0 for $|T| < 1/\alpha$. Hence, the result. \square

3. Backstepping design for higher-dimensional sampled-data systems

The idea of the first part stated for one dimensional systems has already been developed in the work of Netic and Grüne (2005) for higher dimensional systems, indeed, in Theorem 3.1 of that paper, a similar expansion in powers of the sampling period was obtained in the difference of a Lyapunov function between two successive sampling points. Similarly to our Lemma 1, considering the class of n -dimensional sampled-data systems of the form

$$\dot{x} = g_0(x) + g_1(x)u_k$$

and given a Lyapunov function V , Netic and Grüne (2005) obtained an expression of the form

$$\begin{aligned} V(x^+) &= V(x) + T(L_{g_0} V(x) + L_{g_1} V(x)u_1) \\ &+ \sum_{i=2}^r \frac{T^i}{i!} (L_{g_1} V(x)u_i + f_i(x, u_1, \dots, u_{i-1})) + \mathcal{O}(T^{r+1}). \end{aligned}$$

This expression was used to redesign controllers for sampled-data systems but it was observed that the controller can not in general cancel the higher order terms since it is too strong to assume that each $f_i(x, u_1, \dots, u_{i-1})$ can be divided by $L_{g_1} V(x)$ and therefore cancelled by u_i . So they proposed to minimize each term $(L_{g_1} V(x)u_i + f_i(x, u_1, \dots, u_{i-1}))$.

The purpose of the next result is to show that for one special class of high dimensional non linear systems named strict feedback systems, the u_i 's can be computed in order to 'cancel' exactly the remaining higher order terms of the higher order approximations of the exact

and (7) is equivalently rewritten as

$$\eta^+ = \eta + Tf^s(\eta, T) + T(\xi - \bar{\xi})R(\eta, T, \xi - \bar{\xi}) + \mathcal{O}(T^{r+1})$$

and such that the following properties hold.

1. There exists a positive definite function W and a function $\alpha_T \in K_\infty$

$$\Delta W := W(\eta^+(\bar{\xi})) - W(\eta) \leq -\alpha_T(\eta) + \mathcal{O}(T^{r+1}).$$

2. There exist $M_\eta, M_\xi, \lambda_T > 0$ such that

$$\begin{cases} V(\eta) \leq M_\eta + \mathcal{O}(T^{r+1}) \\ |\xi - \bar{\xi}(\eta)| \leq M_\xi + \mathcal{O}(T^{r+1}) \end{cases} \implies \|R(\eta, T, \xi - \bar{\xi})\| \leq \lambda_T(1 + |\xi - \bar{\xi}|)(1 + V(\eta)) + \mathcal{O}(T^{r+1}).$$

discretized systems.

Let $r \in \mathbb{N}$ be fixed. Given a fixed sampling period $T > 0$, we consider the following form of non-linear sampled-data system, $\forall k \in \mathbb{N}, \forall t \in [kT, (k+1)T]$

$$\begin{cases} \dot{\eta} = f(\eta) + g(\eta)\xi \\ \dot{\xi} = u_k, \end{cases} \quad (6)$$

where $\eta \in \mathbb{R}^n, \xi \in \mathbb{R}, u_k \in \mathbb{R}$, and f, g are analytic functions. Its associated exact discretized system is

$$\begin{cases} \eta^+ = \eta + T(f(\eta) + g(\eta)\xi) + \sum_{i=2}^r \frac{T^i}{i!} \eta^{(i)}(kT) + \mathcal{O}(T^{r+1}) \\ \xi^+ = \xi + Tu. \end{cases}$$

Computations of the derivatives $\eta^{(i)}$'s show that they can be expressed as functions of (η, ξ, u) . We note that $\eta^{(i)}(kT) := \Gamma_i(\eta, \xi, u)$. The above discrete system is then rewritten in the following form:

$$\eta^+ = \eta + T(f(\eta) + g(\eta)\xi) + \sum_{i=1}^r \frac{T^i}{i!} \Gamma_i(\eta, \xi, u) + \mathcal{O}(T^{r+1}) \quad (7)$$

$$\xi^+ = \xi + Tu. \quad (8)$$

Theorem 1: *Let us first consider the subsystem (7) and let us suppose that there exists \bar{T} such that for all $T \in]0, \bar{T}[$, for any function $u_T: (\eta, \xi) \mapsto \sum_{i=1}^{r-1} (T^{i-1}/i!) \times u_i(\eta, \xi) + \mathcal{O}(T^r)$ sufficiently smooth, there exists $\bar{\xi}_T(\eta) = \sum_{i=1}^r (T^{i-1}/i!) \bar{\xi}_i(\eta)$ (where $\bar{\xi}_i$ is a differential operator of $(u_1, \dots, u_{i-1}, \bar{\xi}_1, \dots, \bar{\xi}_{i-1})$) such that by substituting $\xi := \bar{\xi}$ in (7) we obtain*

$$\eta^+(\bar{\xi}) = \eta + Tf^s(\eta, T) + \mathcal{O}(T^{r+1})$$

Then, considering the full system (7), (8), for all $T \in]0, \bar{T}[$, there exist a controller $u_T: (\eta, \xi) \mapsto \sum_{i=1}^r (T^{i-1}/i!) u_i(\eta, \xi) + \mathcal{O}(T^r)$ (where u_i is a differential operator of $(u_1, \dots, u_{i-1}, \bar{\xi}_1, \dots, \bar{\xi}_{i-1})$), $M_0 > 0$, some positive constant real numbers $M_T, c > 0$, a function $\gamma \in K_\infty$ such that $\forall \eta_0 \in \{\eta, V(\eta) \leq M_0\}, \forall \xi_0 \in \{\xi, |\xi - \bar{\xi}(\eta_0)| \leq M_\xi\}, \forall k \in \mathbb{N}$

$$\begin{aligned} \Delta V(k) := V(\eta((k+1)T)) - V(\eta(kT)) &\leq -\alpha_T(\eta(kT)) \\ &+ \lambda_T M_\eta (1 - cT)^k \gamma(|\xi_0 - \bar{\xi}(\eta_0)|) + \mathcal{O}(T^{r+1}) \end{aligned}$$

and

$$\xi(kT) - \bar{\xi}(\eta(kT)) \xrightarrow[k \rightarrow +\infty]{} 0 + \mathcal{O}(T^{r+1})$$

where $V(\eta) := \ln(1 + W(\eta))$ (it is also a definite positive function) and the expression of R is given by the proof.

Remarks:

- The last inequality amounts to saying that $V(\eta(kT)) \xrightarrow[k \rightarrow +\infty]{} 0 + \mathcal{O}(T^{r+1})$.
- Every notation of the form c_T denotes a form like $c_T := \sum (T^i/i!) c_i$ so it is not unbounded as $T \rightarrow 0$.
- In this theorem, according to the hypothesis, $\bar{\xi}_i$ is a differential operator of $(u_1, \dots, u_{i-1}, \bar{\xi}_1, \dots, \bar{\xi}_{i-1})$, note that there is no contradiction in building a controller where u_i is a differential operator of $(u_1, \dots, u_{i-1}, \bar{\xi}_1, \dots, \bar{\xi}_i)$. Indeed, given $\bar{\xi}_1$ one first computes u_1 , then it is possible to compute $\bar{\xi}_2$, then u_2 is computed and so on.

Proof: Let $T \in]0, \bar{T}[$.

Step 1 (controller design). We note that $\eta^+(\bar{\xi}) = \eta + T(f^s(\eta, T)) + \mathcal{O}(T^{r+1})$.

We then consider

$$\begin{aligned} \eta^+(\xi) &= \eta + T(f(\eta) + g(\eta)\xi) + \sum_{i=2}^r \frac{T^i}{i!} \Gamma_i(\eta, \xi, u) + \mathcal{O}(T^{r+1}) \\ &= \eta + T(f^s(\eta, T)) + Tg(\eta)(\xi - \bar{\xi}) + \sum_{i=2}^r \frac{T^i}{i!} \\ &\quad \times (\Gamma_i(\eta, \xi, u(\eta, \xi)) - \Gamma_i(\eta, \bar{\xi}, u(\eta, \bar{\xi}))) + \mathcal{O}(T^{r+1}) \\ &= \eta + T(f^s(\eta, T)) + (\xi - \bar{\xi}) \\ &\quad \times \left[Tg(\eta) + \sum_{i=2}^r \frac{T^i}{i!} \int_0^1 \frac{\partial \Gamma_i}{\partial \alpha} \Big|_{\alpha=(\eta, \bar{\xi}+s(\xi-\bar{\xi}), u(\eta, \bar{\xi}+s(\xi-\bar{\xi}))} ds \right] \\ &\quad + \mathcal{O}(T^{r+1}) \\ &:= \eta + T(f^s(\eta, T)) + T(\xi - \bar{\xi})R(\eta, T, \xi - \bar{\xi}) \\ &\quad + \mathcal{O}(T^{r+1}). \end{aligned}$$

By using, the decomposition in power expansions of T , $u_T = \sum_{i=1}^r (T^{i-1}/i!)u_i$, $\bar{\xi} = \sum_{i=1}^r (T^{i-1}/i!)\bar{\xi}_i$, and by decomposing the expression of $\eta^+(\xi)$ in power expansions of T , one obtain the following form:

$$\begin{aligned} \eta^+ &= \eta + Tf^s(\eta, T) + Tg(\eta)(\xi - \bar{\xi}) \\ &\quad + \sum_{i=2}^r \frac{T^i}{i!} G_i(\eta, \xi, u_1(\eta, \xi), \dots, u_{i-1}(\eta, \xi)) \\ &\quad + \sum_{i=2}^r \frac{T^i}{i!} H_i(\eta, \bar{\xi}_1, \dots, \bar{\xi}_{i-1}, u_1(\eta, \bar{\xi}_1), \frac{\partial u_1}{\partial \xi}(\eta, \bar{\xi}_1), \dots, \\ &\quad \frac{\partial^{i-1} u_1}{\partial \xi^{i-1}}(\eta, \bar{\xi}_1), \dots, u_{i-2}(\eta, \bar{\xi}_1), \frac{\partial u_{i-2}}{\partial \xi}, u_{i-1}(\eta, \bar{\xi}_1)) \\ &\quad + \mathcal{O}(T^{r+1}), \end{aligned}$$

where the H_i, G_i 's are sufficiently smooth and obtained by computations. Moreover, the same can be done for $\bar{\xi}(\eta^+)$

$$\begin{aligned} \bar{\xi}^+ &:= \bar{\xi}(\eta^+) \\ &= \bar{\xi}(\eta) + \sum_{i=1}^r \frac{T^i}{i!} M_i(\eta, \xi, u_1(\eta, \xi), \dots, u_{i-1}(\eta, \xi)) \\ &\quad + \sum_{i=1}^r \frac{T^i}{i!} N_i(\eta, \bar{\xi}_1, \dots, \bar{\xi}_i, u_1(\eta, \bar{\xi}_1), \frac{\partial u_1}{\partial \xi}(\eta, \bar{\xi}_1), \dots, \end{aligned}$$

$$\begin{aligned} &\frac{\partial^{i-1} u_1}{\partial \xi^{i-1}}(\eta, \bar{\xi}_1), \dots, u_{i-2}(\eta, \bar{\xi}_1), \frac{\partial u_{i-2}}{\partial \xi}, u_{i-1}(\eta, \bar{\xi}_1)) \\ &\quad + \mathcal{O}(T^{r+1}) \\ &:= \bar{\xi}(\eta) + T\Delta\bar{\xi} + \mathcal{O}(T^{r+1}), \end{aligned} \tag{9}$$

where the M_i 's and N_i 's are sufficiently smooth and obtained by computations.

We then use the controller

$$u = -c(\xi - \bar{\xi}) + \Delta\bar{\xi}, \tag{10}$$

where $c > 0$ and verifies $cT < 1$.

Remark: More exactly, if we look at the decomposition in powers of T , we obtain:

$$\begin{aligned} u_1 &= -c(\xi - \bar{\xi}_1) + M_1(\eta, \xi) + N_1(\eta, \bar{\xi}_1) \\ u_i &\stackrel{\forall i \in \{2, \dots, r\}}{=} c\bar{\xi}_i + M_i(\eta, \xi, u_1(\eta, \xi), \dots, u_{i-1}(\eta, \xi)) \\ &\quad + N_i(\eta, \bar{\xi}_1, \dots, \bar{\xi}_i, u_1(\eta, \bar{\xi}_1), \frac{\partial u_1}{\partial \xi}(\eta, \bar{\xi}_1), \dots, \\ &\quad \frac{\partial^{i-1} u_1}{\partial \xi^{i-1}}(\eta, \bar{\xi}_1), \dots, u_{i-2}(\eta, \bar{\xi}_1), \frac{\partial u_{i-2}}{\partial \xi}, u_{i-1}(\eta, \bar{\xi}_1)) \end{aligned}$$

so, we compute u_1 , then $\bar{\xi}_2$, then u_2 and so on.

Step 2 (Proof of the convergence). Let us first consider $\xi - \bar{\xi}$.

By computing $\xi^+ - \bar{\xi}^+$ and by using the controller (10), we obtain

$$\xi^+ - \bar{\xi}(\eta^+) = (1 - cT)(\xi - \bar{\xi}(\eta)) + \mathcal{O}(T^{r+1}).$$

Hence, since $0 < cT < 1$,

$$\begin{aligned} \xi(kT) - \bar{\xi}(\eta(kT)) &= (1 - cT)^k (\xi_0 - \bar{\xi}(\eta_0)) \\ &\quad + \mathcal{O}(T^{r+1}) \xrightarrow[k \rightarrow +\infty]{} 0 + \mathcal{O}(T^{r+1}). \end{aligned} \tag{11}$$

Let us now consider η .

We choose the following candidate Lyapunov function:

$$V(\eta) := \ln(1 + W(\eta)).$$

We choose this function because it has an interesting property: indeed, $|\partial V/\partial \eta| \leq 1$

$$\begin{aligned}
 V(\eta^+) - V(\eta) &= V(\eta + Tf^s(\eta, T) + T(\xi - \bar{\xi})R(\eta, T, \xi - \bar{\xi})) \\
 &\quad + \mathcal{O}(T^{r+1}) - V(\eta) \\
 &= V(\eta + Tf^s(\eta, T) + T(\xi - \bar{\xi})R(\eta, T, \xi - \bar{\xi})) \\
 &\quad + \mathcal{O}(T^{r+1}) - V(\eta + Tf^s(\eta, T)) \\
 &\quad + V(\eta + Tf^s(\eta, T)) - V(\eta) \\
 &= V(\eta + Tf^s(\eta, T)) - V(\eta) \\
 &\quad + \left(\int_0^1 \frac{\partial V}{\partial \alpha} \Big|_{\alpha=\eta+Tf^s(\eta, T)+\tau T(\xi-\bar{\xi})R(\eta, T, \xi-\bar{\xi})} d\tau \right) \\
 &\quad \times T(\xi - \bar{\xi})R(\eta, T, \xi - \bar{\xi}) + \mathcal{O}(T^{r+1}) \\
 &\leq -\alpha_T(\eta) + T|(\xi - \bar{\xi})R(\eta, T, \xi - \bar{\xi})| + \mathcal{O}(T^{r+1}) \\
 &\leq -\alpha_T(\eta) + T\lambda_T|\xi - \bar{\xi}|(1 + |\xi - \bar{\xi}|) \\
 &\quad \times (1 + V(\eta)) + \mathcal{O}(T^{r+1}). \tag{12}
 \end{aligned}$$

The last inequality is obtained by assuming that

$$V(\eta) \leq M_\eta + \mathcal{O}(T^{r+1}) \tag{13}$$

$$|\xi - \bar{\xi}(\eta)| \leq M_\xi + \mathcal{O}(T^{r+1}). \tag{14}$$

The assumption (14) is easily verified by considering equation (11) plus the assumption $\xi_0 \in \{\xi, |\xi - \bar{\xi}(\eta_0)| \leq M_\xi\}$.

By using (12) and (11), we define $\gamma_T \in K_\infty$ by

$$\gamma_T(|\xi_0 - \bar{\xi}_0|) = \lambda_T|\xi_0 - \bar{\xi}_0|(1 + |\xi_0 - \bar{\xi}_0|).$$

In particular, $\forall k \in \mathbb{N}$

$$\begin{aligned}
 &V(\eta((k+1)T)) - V(\eta(kT)) \\
 &\leq (1 - cT)^k T\gamma_T(|\xi_0 - \bar{\xi}_0|)(1 + V(\eta(kT))) + \mathcal{O}(T^{r+1}).
 \end{aligned}$$

Hence,

$$\begin{aligned}
 \frac{V(\eta((k+1)T)) + 1}{V(\eta(kT)) + 1} &\leq 1 + (1 - cT)^k T\gamma_T(|\xi_0 - \bar{\xi}_0|) \\
 &\quad + \mathcal{O}(T^{r+1})
 \end{aligned}$$

$$\begin{aligned}
 &\ln(V(\eta((k+1)T)) + 1) \\
 &\leq \ln(V(\eta_0) + 1) + \sum_{j=0}^k \ln(1 + T\gamma_T(|\xi_0 - \bar{\xi}_0|)(1 - cT)^j) \\
 &\quad + \mathcal{O}(T^{r+1})
 \end{aligned}$$

$$\begin{aligned}
 &\leq \ln(V(\eta_0) + 1) + \sum_{j=0}^k T\gamma_T(|\xi_0 - \bar{\xi}_0|)(1 - cT)^j \\
 &\quad + \mathcal{O}(T^{r+1}) \\
 &\leq \ln(V(\eta_0) + 1) + \sum_{j=0}^{+\infty} T\gamma_T(|\xi_0 - \bar{\xi}_0|)(1 - cT)^j \\
 &\quad + \mathcal{O}(T^{r+1}) \\
 &= \ln(V(\eta_0) + 1) + \frac{1}{c}\gamma_T(|\xi_0 - \bar{\xi}_0|).
 \end{aligned}$$

Hence, $\forall k \in \mathbb{N}$

$$V(\eta(kT)) + 1 \leq (V(\eta_0) + 1)\exp\left(\frac{1}{c}\gamma_T(|\xi_0 - \bar{\xi}_0|)\right) + \mathcal{O}(T^{r+1}).$$

Thus, by choosing M_0 such that

$$(M_0 + 1)\exp\left(\frac{1}{c}\gamma_T(|\xi_0 - \bar{\xi}_0|)\right) \leq M_\eta$$

the assumption (13) is always verified i.e starting from the subset $V(\eta_0) \leq M_0$, $V(\eta)$ will always satisfy $V(\eta) \leq M_\eta$.

Moreover, by using these last inequalities and (12), we finally obtain the expected result i.e

$$\begin{aligned}
 &V(\eta((k+1)T)) - V(\eta(kT)) \\
 &\leq -\alpha_T(\eta(kT)) + \lambda_T M_\eta (1 - cT)^k \gamma(|\xi_0 - \bar{\xi}(\eta_0)|) \\
 &\quad + \mathcal{O}(T^{r+1}). \quad \square
 \end{aligned}$$

4. Example and numerical results

4.1 Example

Let us consider the following example of two dimensional strict-feedback systems:

$$\begin{cases} \dot{\eta} = \eta^2 + \xi \\ \dot{\xi} = u. \end{cases} \tag{15}$$

A classical backstepping design gives the following continuous controller:

$$u_c(\eta, \xi) = -2\eta - \eta^2 - \xi - (2\eta + 1)(\xi + \eta^2).$$

When the controller is blocked on some intervals of time by a zero order hold, the performances were shown (Nesic and Teel 2001) to be better by using a controller based on the Euler approximation of the dynamic

$$u_T^{\text{Euler}}(\eta, \xi) = u_c(\eta, \xi) - \frac{1}{2}T(\eta^2 + \xi - \eta + 2(\xi + \eta^2)^2).$$

Thanks to this controller, the system was semi-globally stabilized to a ball of a given real radius (independent of T). Thanks to our method, we achieve a stabilization toward a ball of radius tending to $0 + \mathcal{O}(T^3)$.

Proposition 1: *If $T \in]0, 1[$, the system (15) is stabilized to $0 + \mathcal{O}(T^3)$ by the controller*

$$u = -2\eta^3 - 2\eta^2 - 2\eta\xi - \eta - 2\xi + T\left(-\eta^4 + 2\eta^3 - 2\xi\eta^2 + \frac{3}{2}\eta^2 + 2\eta\xi - \xi^2 + \frac{1}{2}\xi\right).$$

Proof: Considering the system (15), its exact discretized system is written

$$\begin{cases} \eta^+ = \eta + T(\eta^2 + \xi) + \frac{T^2}{2}(2\eta^3 + 2\eta\xi + u) + \mathcal{O}(T^3) \\ \xi^+ = \xi + Tu. \end{cases}$$

We note that $\bar{\xi} = \bar{\xi}_1 + (T/2)\bar{\xi}_2$ and $u(\eta, \xi) = u_1(\eta, \xi) + (T/2)u_2(\eta, \xi)$. Considering the subsystem

$$\begin{aligned} \eta^+ &= \eta + T(\eta^2 + \bar{\xi}) + \frac{T^2}{2}(2\eta^3 + 2\eta\bar{\xi} + u(\eta, \bar{\xi})) + \mathcal{O}(T^3) \\ &= \eta + T(\eta^2 + \bar{\xi}_1) + \frac{T^2}{2}(\bar{\xi}_2 + 2\eta^3 + 2\eta\bar{\xi}_1 + u_1(\eta, \bar{\xi}_1)) \\ &\quad + \mathcal{O}(T^3). \end{aligned}$$

We choose

$$\begin{cases} \bar{\xi}_1 = -\eta^2 - \eta \\ \bar{\xi}_2 = -2\eta^3 - 2\eta\bar{\xi}_1 - u_1(\eta, \bar{\xi}_1) = 2\eta^2 - u_1(\eta, \bar{\xi}_1(\eta)). \end{cases}$$

We then have

$$\begin{aligned} \eta^+ &= (1 - T)\eta + T(\xi - \bar{\xi}) + \frac{T^2}{2}(2\eta(\xi - \bar{\xi}) + u_1(\eta, \xi) \\ &\quad - u_1(\eta, \bar{\xi})) + \mathcal{O}(T^3). \end{aligned}$$

Hence

$$\begin{aligned} \bar{\xi}_1^+ &= \bar{\xi}_1 + T\frac{\partial\bar{\xi}_1}{\partial\eta}(-\eta + \xi - \bar{\xi}) \\ &\quad + T^2\frac{\partial\bar{\xi}_1}{\partial\eta}\eta(\xi - \bar{\xi}) + \frac{T^2}{2}\frac{\partial\bar{\xi}_1}{\partial\eta}(u_1(\eta, \xi) - u_1(\eta, \bar{\xi})) \\ &\quad + \frac{T^2}{2}\frac{\partial^2\bar{\xi}_1}{\partial\eta^2}(-\eta + \xi - \bar{\xi})^2 + \mathcal{O}(T^3) \\ \bar{\xi}_2^+ &= \bar{\xi}_2 + T\frac{\partial\bar{\xi}_2}{\partial\eta}(-\eta + \xi - \bar{\xi}) + \mathcal{O}(T^2). \end{aligned}$$

Hence

$$\begin{aligned} u_1 &= -(\xi - \bar{\xi}_1) + \frac{\partial\bar{\xi}_1}{\partial\eta}(-\eta + \xi - \bar{\xi}_1) \\ &= -2\eta^3 - 2\eta^2 - 2\eta\xi - \eta - 2\xi. \end{aligned} \quad (16)$$

Hence

$$\begin{aligned} \bar{\xi}_2 &= 2\eta^2 - u_1(\eta, \bar{\xi}_1(\eta)) \\ &= 2\eta^2 + 2\eta^3 + 2\eta^2 + 2\eta(-\eta^2 - \eta) + \eta + 2(-\eta^2 - \eta) \\ &= -\eta. \end{aligned} \quad (17)$$

Moreover

$$\begin{aligned} u_2 &= \bar{\xi}_2 - \frac{\partial\bar{\xi}_1}{\partial\eta}\bar{\xi}_2 + 2\frac{\partial\bar{\xi}_1}{\partial\eta}\eta(\xi - \bar{\xi}_1) + \frac{\partial\bar{\xi}_1}{\partial\eta}(u_1(\eta, \xi) - u_1(\eta, \bar{\xi}_1)) \\ &\quad + \frac{\partial^2\bar{\xi}_1}{\partial\eta^2}(-\eta + \xi - \bar{\xi}_1)^2 - \frac{\partial\bar{\xi}_2}{\partial\eta}(-\eta + \xi - \bar{\xi}) \\ &= \bar{\xi}_2 - (2\eta + 1)(-\bar{\xi}_2 - 2(\xi - \bar{\xi}_1)) - 2(-\eta + \xi - \bar{\xi}_1)^2 \\ &\quad - (-\eta + \xi - \bar{\xi}) \\ &= -\eta - (2\eta + 1)(\eta - 2(\xi + \eta + \eta^2)) - 2(\xi + \eta^2)^2 - (\xi + \eta^2) \\ &= -2\eta^4 + 4\eta^3 - 4\xi\eta^2 + 3\eta^2 + 4\eta\xi - 2\xi^2 + \xi. \end{aligned}$$

Hence, the controller

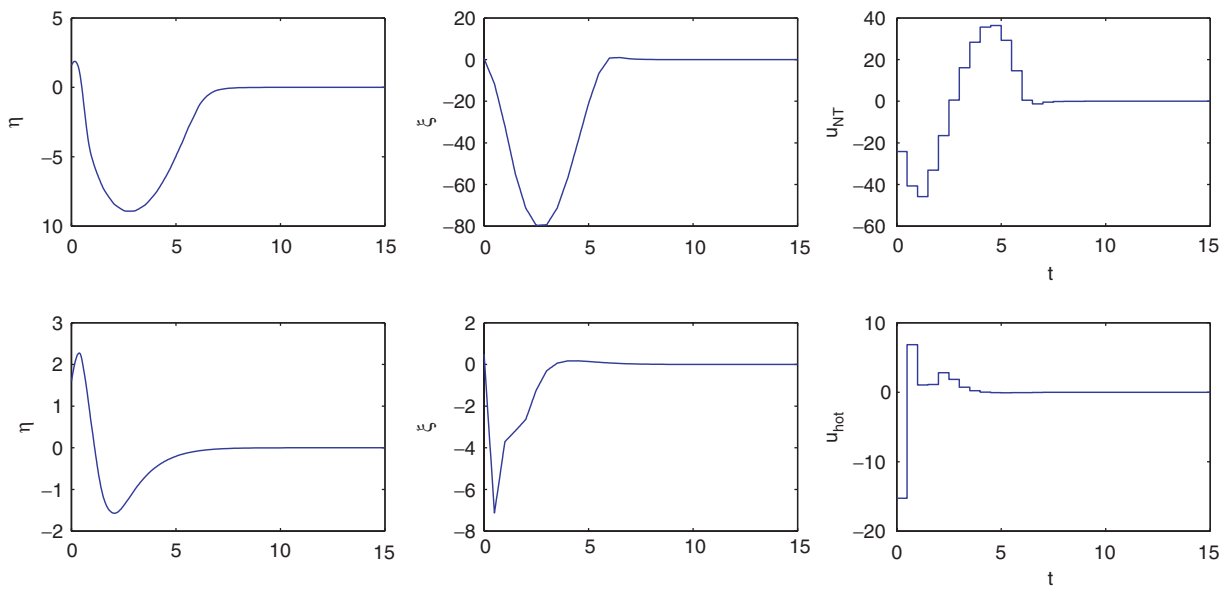
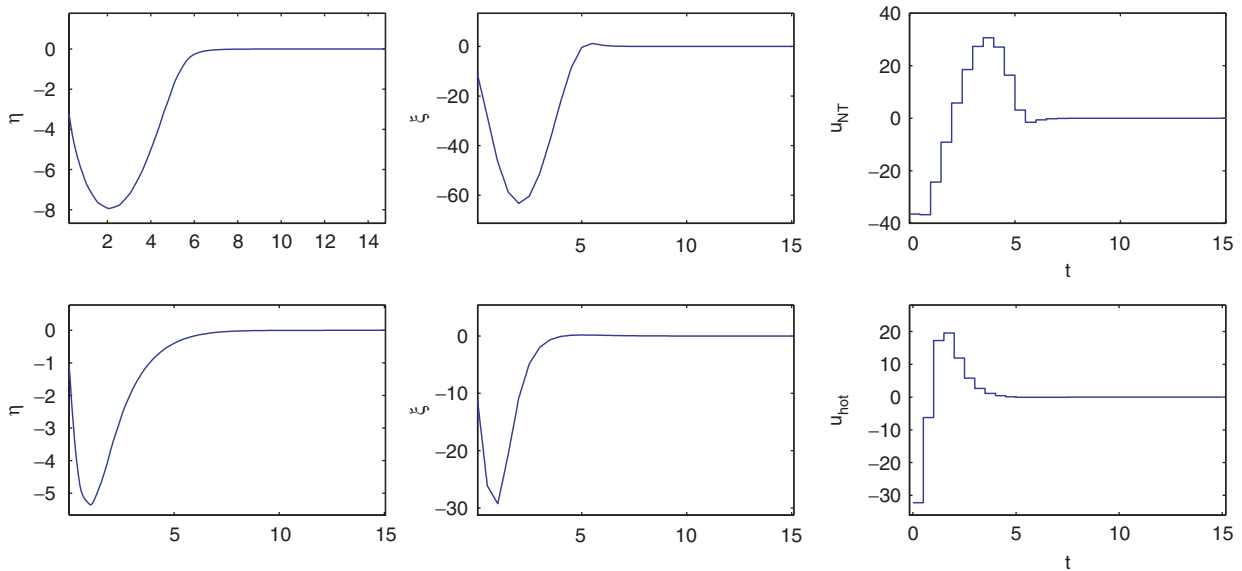
$$\begin{aligned} u &= u_1 + \frac{T}{2}u_2 = -2\eta^3 - 2\eta^2 - 2\eta\xi - \eta - 2\xi \\ &\quad + T\left(-\eta^4 + 2\eta^3 - 2\xi\eta^2 + \frac{3}{2}\eta^2 + 2\eta\xi - \xi^2 + \frac{1}{2}\xi\right). \quad \square \end{aligned}$$

We computed a controller of order 2 and its design required many computations. Since the computations are more and more huge as the order increases, it is difficult to use our technique and this is its weakness. However, to deal with this drawback, one can implement the algorithm on Maple software. For instance, going up to the order 3, the controller would be

$$\begin{aligned} u &= -2\eta^3 - 2\eta^2 - 2\eta\xi - \eta - 2\xi \\ &\quad + T\left(-\eta^4 + 2\eta^3 - 2\xi\eta^2 + \frac{3}{2}\eta^2 + 2\eta\xi - \xi^2 + \frac{1}{2}\xi\right) \\ &\quad + T^2\left(\frac{1}{3}\eta\xi^2 + \frac{13}{6}\xi^2 + \frac{2}{3}\xi\eta^3 + \frac{3}{2}\eta^4 + \frac{1}{3}\eta^5 + \frac{1}{2}\eta^3\right. \\ &\quad \left.+ \frac{11}{3}\xi\eta^2 + \frac{5}{6}\eta\xi + \frac{1}{6}\eta^2\right). \end{aligned}$$

4.2 Numerical results

$T = 0.5$, u_{NT} denotes the controller of Nescic and Teel (2001). u_{hot} denotes our controller (which according

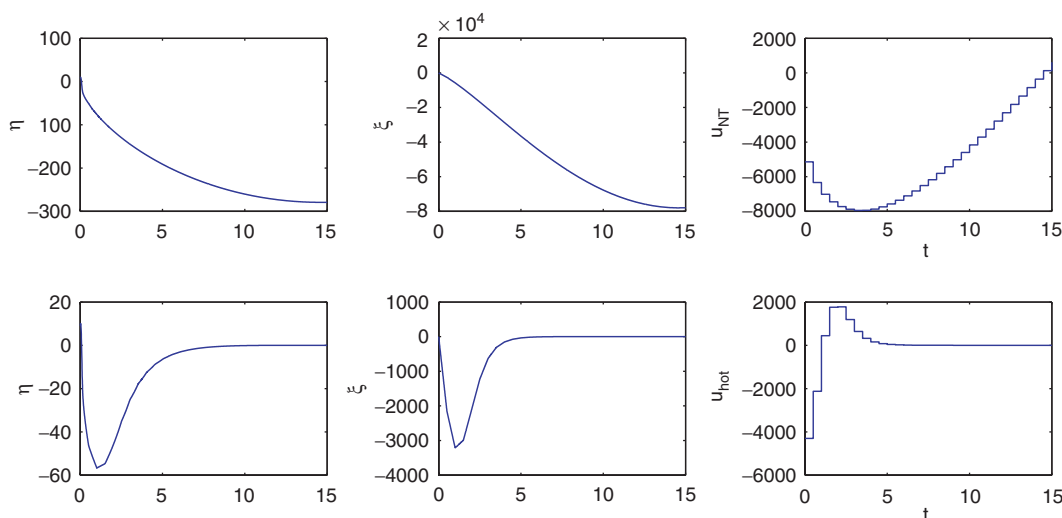
Figure 1. $(\eta(0), \xi(0)) = (1.6, 0.5)$.Figure 2. $(\eta(0), \xi(0)) = (-1, -10)$.

to our method can be refined by using higher order terms in the control design and then it is possible to obtain better results at the sake of more computations).

For figures 1–3, the upper graphs are the results obtained by using the controller u_{NT} and whereas the graphs below illustrate the results obtained with controller u_{hot} method. It seems that our controller is a bit faster and most of the time with less overshoot.

5. Conclusion and future work

In this paper, we have used higher order approximations of the exact-discretized system of a given one dimensional sampled-data system and we have deduced a way to design a stabilizing feedback with a given precision. This precision improves as the order of the approximations of the exact-discretized system increases

Figure 3. $(\eta(0), \xi(0)) = (9, 2)$.

but this is at the price of more computations in order to obtain the controller terms. The main idea of decomposing the controller into a series in powers of the sampling time T has then been applied to a class of higher order non-linear sampled-data systems and we have proposed a kind of new backstepping design for this specific class. However, the proposed design requires many computations and we suggest the use of computer algebra softwares to systematically get the higher order terms of the controller.

Further extensions of the method are currently under investigation. Other classes of non-linear sampled-data systems can be considered and further research may also be carried out in the field of robust and adaptive control of non linear sampled-data systems.

References

T. Ahmed-Ali, L. Burlion and F. Lamnabhi-Lagarrigue, "On the stabilization of sampled-data systems by using higher order

- approximations of the exact discretized systems", in *Proc. of IMACS World Congress*, July, 2005, Paris, CD-ROM.
- M. Arcat and D. Nesić, "A framework for nonlinear sampled-data observer design via approximate discrete-time models and emulation", *Automatica*, 40, pp. 1931–1938, 2004.
- L. Burlion, T. Ahmed-Ali and F. Lamnabhi-Lagarrigue, "On the stability of a class of nonlinear hybrid systems", in *Proc. of NOLCOS 04*, Stuttgart, 2004, pp. 573–578.
- T. Chen and B.A. Francis, *Optimal Sampled-data Control Systems*, London: Springer-Verlag, 1995.
- G. Hermann, S.K. Spurgeon and C. Edwards, "Discretization of sliding mode based control schemes", in *Proc. of the IEEE Conference on Decision and Control*, Phoenix, AZ, 1999, pp. 4257–4262.
- D.S. Laila, "Design and analysis of nonlinear sampled-data control systems". PhD thesis, University of Melbourne (2005).
- D. Nesić and L. Grüne, "Lyapunov based continuous-time nonlinear controller redesign for sampled-data implementation", *Automatica*, 41, pp. 1143–1156, 2005.
- D. Nesić and A.R. Teel, "Backstepping on the Euler approximate model for stabilization of sampled-data systems", in *Proc. of Conf. Decision Control*, Orlando, FL, 2001, pp. 1737–1742.
- D. Nesić, A.R. Teel and P.V. Kokotović, "Sufficient conditions for stabilization of sampled-data systems via discrete-time approximations", *Systems and Control Letters*, 38, pp. 259–270, 1999.
- H. Ye, A.N. Michel and L. Hou, "Stability theory for hybrid dynamical systems", *IEEE Transactions on Automatic Control*, 43, pp. 461–474, 1998.

Global asymptotic stabilization for some nonlinear models of flexible aerospace vehicles

Laurent Burlion¹, Elodie Duraffourg¹, Tarek Ahmed-Ali² and Françoise Lamnabhi-Lagarrigue³

Abstract—New strategies are proposed to design GAS controllers for two significant classes of nonlinear flexible systems. Inspired by a non affine control technique, we have designed some novel nonlinear control laws which use the full state in order to enhance the damping of the flexible modes: this new design is all the more interesting than the classes of considered systems belong to non triangular nonlinear systems. Finally, the effectiveness of our approach is illustrated on simplified models of a flexible launcher and spacecraft.

I. INTRODUCTION

In the last years the stabilization problem of flexible nonlinear systems has received a great attention. This interest is motivated by the fact that flexible modes can generate a very bad transient even if the system is a minimum-phase one. Several results concerning this topic exist in the literature : a typical design is to combine a nominal nonlinear controller with a vibration absorber controller.

This 'vibration absorber' is often based on the well known method of Input Shaping [1],[2],[3],[4] which has the major advantage to require merely relatively good approximation of modeling coefficients instead of direct measurements of the flexible modes : however, this useful method is by nature a linear method which can be used when the initial conditions are known and when the interaction between the flexible state and rigid ones is linear (although a few results exist in the nonlinear case e.g [5]). Another approach is to combine a nonlinear controller with a linear controller which uses the flexible modes and (only) locally damps them out [6],[7]. Open loop or robust feedforward methods can also be used to design a reference trajectory for the rigid state such that the oscillations of the flexible modes remain relatively low [8],[5],[9] but it seems tricky to apply these methods on a large nonlinear operating domain when the systems parameters are uncertain and when there is a lot of flexible modes.

Recently, new nonlinear Lyapunov based approaches have been proposed for the stabilization problem of flexible aerospace systems when there is a large number of flexible modes and a strong nonlinear coupling between flexible and rigid modes [10],[11],[12],[13] : technically speaking, although these systems are minimum phase, they belong to the

class of underactuated non triangular nonlinear systems [15], which renders tedious the twofold objective of stabilizing the system and damping out the oscillations of the flexible modes. In this paper, we propose to enlarge these results by either adding more damping to the flexible dynamics [10],[12],[13] either studying larger classes of systems [11]. The control schemes developed in this paper are based on the result of [16] which is a systematic design approach to add Lyapunov decrease to non affine nonlinear systems whose free dynamics are stable. Moreover, the major difference of our approach compared to classical methods is the fact that the controllers are first designed to stabilize the flexible modes (i.e the zero dynamics) and then extended to stabilize the full state.

The present paper is organized as follows : in section II, the class of nonlinear systems studied here are presented and motivated by some examples of flexible nonlinear systems. Then, we briefly recall the result of [16] used to determine the new control laws proposed in this paper : we show how one can both globally stabilize these classes of systems and add damping to the flexible dynamics. The two following sections illustrate our results on a flexible launch vehicle and a spacecraft model. We finally give our conclusions and some future research directions.

A. Notations

Let $m \in \mathcal{N}$. Throughout the paper, the following notations will be used:

- $\|\cdot\|$ is the Euclidean norm in \mathcal{R}^m
- Given a smooth function $V : \mathcal{R}^{2m} \rightarrow \mathcal{R}$ and a vector field $g : \mathcal{R}^{2m} \rightarrow \mathcal{R}^{2m}$, $L_g V := \frac{\partial V}{\partial x} g$ denotes the Lie-derivative of V with respect to g
- a continuous function $\sigma : \mathcal{R}_{>0} \rightarrow \mathcal{R}_{>0}$ belongs to class \mathcal{K} it is monotonic increasing and $\sigma(0) = 0$
- a continuous function σ of class \mathcal{K} belongs to class \mathcal{K}_∞ if it is unbounded
- given a symmetric matrix P , its minimal (resp. maximal) eigenvalue is denoted by $\lambda_{\min}(P)$ (resp. $\lambda_{\max}(P)$)

II. PROBLEM FORMULATION

In this paper, we consider the stabilization problem of the following classes of minimum-phase nonlinear systems :

A. Class I

$$\begin{cases} \dot{x}_1 &= x_2 \\ \dot{x}_2 &= u \\ \dot{\eta}_1 &= \eta_2 \\ \dot{\eta}_2 &= A_\eta \eta + B_\eta u + P_\eta^1(x_1) + P_\eta^2(x_1)x_2 \end{cases} \quad (1)$$

¹ L. Burlion and E. Duraffourg are with Onera - The French Aerospace Lab, F-31055 Toulouse, France. Laurent.Burlion (at) onera.fr Elodie.Duraffourg (at) onera.fr

² T. Ahmed-Ali is with Ecole Nationale Supérieure d'Ingénieurs de Caen (ENSICAEN), 6 boulevard du Marchal Juin 14050 Caen Cedex 4, France. tarek.ahmed-ali (at) greyc.ensicaen.fr

³ F. Lamnabhi-Lagarrigue is with L2S-CNRS, Supélec, 3 rue Joliot Curie, 91192 Gif-sur-Yvette, France. lamnabhi (at) lss.supelec.fr

This class of systems satisfies the following properties :

- $x_1, x_2, u \in \mathcal{R}$ and $\eta := [\eta_1; \eta_2] \in \mathcal{R}^{2m}$, $m \in \mathcal{N}$
- $\begin{bmatrix} 0 & I_m \\ A_\eta \end{bmatrix}$ is a real Hurwitz matrix and its eigenvalues are all complex conjugates
- η_1 is a vector whose coordinates are called the flexible modes
- the dynamics of $x = [x_1; x_2]$ (resp. $[\eta_1; \eta_2]$) is called the rigid (resp. flexible) dynamics
- all the $e_i^T P_\eta^1$, $i \in \{1, m\}$ are polynomials of degrees $\leq d_1$, where $d_1 \in \mathcal{N}$. Moreover, each $e_i^T P_\eta^1$, $i \in \{1, m\}$ vanishes at 0.
- all the $e_i^T P_\eta^2$, $i \in \{1, m\}$ are polynomials of degrees $\leq d_2$, where $d_2 \in \mathcal{N}$

B. Class II

$$\begin{cases} \dot{x}_1 &= x_2 \\ \dot{x}_2 &= u \\ \dot{\eta}_1 &= \eta_2 \\ \dot{\eta}_2 &= A_\eta \eta + B_\eta u + f_\eta(x_1) + g_\eta(x_1, \eta_1)x_2^2 \end{cases} \quad (2)$$

which verifies the following properties:

- $x_1, x_2, u \in \mathcal{R}$ and $\eta := [\eta_1; \eta_2] \in \mathcal{R}^{2m}$, $m \in \mathcal{N}$
- $\begin{bmatrix} 0 & I_m \\ A_\eta \end{bmatrix}$ is a real Hurwitz matrix and its eigenvalues are all complex conjugates
- η_1 is a vector whose coordinates are called the flexible modes
- the dynamics of $x = [x_1; x_2]$ (resp. $[\eta_1; \eta_2]$) is called the rigid (resp. flexible) dynamics
- f_η (resp. g_η) is a smooth and globally k_f - (resp. k_g) Lipschitz function and all the $e_i^T P_\eta$, $i \in \{1, m\}$ are polynomials of degrees $\leq l$, where $l \in \mathcal{N}$

It has to be noticed that there exist several flexible aerospace vehicles which are described by the above two classes of nonlinear systems. We can cite for instance :

- the rotational dynamics of a flexible hypersonic vehicle belongs to *class I* (see for more details the modeling in [17] and some changes of coordinates leading to the *class I* form in [11]).
- the longitudinal dynamics of a flexible launch vehicle belongs to *class I* (see [18])
- the model of a spacecraft with a flexible attachment belongs to *class II* (see [14])
- the rotational dynamics of space vehicles with propellant sloshing mode belongs to *class II* (see [12], [13] when $a_x = a_z = 0$)

It is well-known that if the zero dynamics of the above systems are supposed asymptotically stable and by considering the state x_1 as output, then there exist several classical methods (e.g Backstepping [19] and Input/Output Linearization [20]), which solve the global asymptotic stabilization problem of these classes of systems. The most important drawback of these methods is that they do not integrate the zero dynamics in the design of the proposed

controllers. This fact generates bad performances of the zero dynamics transients, which means that the flexible modes of several aerospace vehicles will exhibit some undesired oscillations. In the present work, we shall design some nonlinear controllers which simultaneously ensure a global asymptotic stability in closed loop and also improve the transient dynamics of the flexible modes. The major difference of the proposed schemes compared to the classical methods is in the fact that the controller is at first designed to stabilize the zero dynamics. This fact induces an improvement of the flexible modes behavior quality.

III. MAIN RESULTS

Before presenting our main results, we need to give the following important technical result which is largely derived from the work of [16] :

Lemma 1[Wei Lin, [16]] : *Consider a single-input non affine nonlinear system of the following form :*

$$\dot{z} = f_0(z) + g_0(z)u + \sum_{i=2}^l g_i(z)u^i \quad (3)$$

where $u \in \mathcal{R}$, $g_i : \mathcal{R}^{2m} \rightarrow \mathcal{R}^{2m}$, $2 \leq i \leq l$, are smooth functions. Suppose the unforced dynamics f_0 is such that there exists a function $V : \mathcal{R}^{2m} \rightarrow \mathcal{R}$, α_0 of class \mathcal{K} , and α_1, α_2 of class \mathcal{K}_∞ such that $\forall z$

$$\alpha_1(\|z\|) \leq V(z) \leq \alpha_2(\|z\|) \quad (4)$$

$$\dot{V}|_{u=0} = \frac{\partial V}{\partial z} f_0(z) \leq -\alpha_0(z) \quad (5)$$

then the unforced system is GAS and the following control law

$$u(z) = \varphi(z) := \frac{-\beta}{1 + \|\partial V / \partial z\|^2 \rho(z)^2} \frac{L_{g_0} V(z)}{1 + (L_{g_0} V(z))^2} \quad (6)$$

where

$$\rho(z) \geq \sum_{i=2}^l 1 + \|g_i(z)\|^2 \quad (7)$$

and $\beta \in]0, 1[$ still renders system (3) GAS such that :

$$\dot{V} \leq \dot{V}|_{u=0} - \frac{(1-\beta)}{1 + \|\partial V / \partial z\|^2 \rho(z)^2} \frac{(L_{g_0} V(z))^2}{1 + (L_{g_0} V(z))^2} \leq \dot{V}|_{u=0} \quad (8)$$

In this case, we say that u adds damping to system (3) since it achieves more Lyapunov decrease.

Now, we are able to give the following propositions:

A. Stabilization of Class I

Proposition 1: *let us consider the class of systems (1), then there exists a nonlinear feedback control law which simultaneously ensures the global asymptotic stability of the origin of the closed loop system and improves the transient of its corresponding zero dynamics.*

Proof:

In order to prove the above proposition, let us consider the following change of coordinates:

$$\begin{cases} \bar{\eta}_1 &= \eta_1 - B_\eta x_1 \\ \bar{\eta}_2 &= \eta_2 - B_\eta x_2 \end{cases} \quad (9)$$

then, we obtain :

$$\begin{cases} \dot{x}_1 &= x_2 \\ \dot{x}_2 &= u \\ \dot{\bar{\eta}}_1 &= \bar{\eta}_2 \\ \dot{\bar{\eta}}_2 &= A_\eta \bar{\eta} + P_\eta^1(x_1) + P_\eta^2(x_1)x_2 \end{cases} \quad (10)$$

where :

$$\begin{aligned} P_\eta^1(x_1) &:= P_\eta^1(x_1) + A_\eta \begin{bmatrix} B_\eta \\ 0 \end{bmatrix} x_1 \\ P_\eta^2(x_1) &:= P_\eta^2(x_1) + A_\eta \begin{bmatrix} 0 \\ B_\eta \end{bmatrix} \end{aligned}$$

From this, we can easily see that system (10) is a non-triangular nonlinear system non affine in x_1 but affine in x_2 according to the classification of underactuated nonlinear systems proposed in [15]. In order to remove x_2 in the flexible dynamics, let us use the following change of coordinates:

$$\begin{cases} z_1 &= \bar{\eta}_1 \\ z_2 &= \bar{\eta}_2 - \left[\int_0^1 P_\eta^2(sx_1) ds \right] x_1 \\ &:= \bar{\eta}_2 - P_\eta^3(x_1)x_1 \end{cases} \quad (11)$$

Indeed, one can check that :

$$\frac{d}{dt} P_\eta^3(x_1)x_1 = P_\eta^2(x_1)x_2$$

and that $P_\eta^3(x_1)x_1$ is a polynomial of degree $\leq d_2$, then we obtain

$$\begin{cases} \dot{x}_1 &= x_2 \\ \dot{x}_2 &= u \\ \dot{z}_1 &= z_2 + P_\eta^3(x_1)x_1 \\ \dot{z}_2 &= A_\eta z + P_\eta^4(x_1) \end{cases} \quad (12)$$

where

$$P_\eta^4(x_1) = A_\eta \begin{bmatrix} 0 \\ P_\eta^3(x_1)x_1 \end{bmatrix} + P_\eta^1(x_1)$$

is of degree $\leq \max\{d_1, d_2\}$.

Let us set $z = [z_1; z_2]$. As we can see from (12), the z -dynamics of the above system can now be viewed as a non affine triangular nonlinear system with respect to the input x_1 .

Since $\begin{bmatrix} 0 & I_m \\ A_\eta \end{bmatrix}$ is Hurwitz, then there exists $P_z = P_z^T, Q_z > 0$ such that :

$$\begin{bmatrix} 0 & I_m \\ A_\eta \end{bmatrix}^T P_z + P_z \begin{bmatrix} 0 & I_m \\ A_\eta \end{bmatrix} \leq -Q_z. \quad (13)$$

We thus propose to use $V_z = z^T P_z z$ and we compute φ according to (6) where :

$$\begin{aligned} V &:= V_z \\ g_0(z) &= g_0 = \begin{bmatrix} P_\eta^3(0) \\ \frac{d}{dx_1} P_\eta^4(0) \end{bmatrix} \\ g_i(z) \stackrel{\forall i \in \{2, l\}}{=} &g_i = \begin{bmatrix} (i-1)! \frac{d^{i-1}}{dx_1^{i-1}} P_\eta^3(0) \\ i! \frac{d^i}{dx_1^i} P_\eta^4(0) \end{bmatrix} \end{aligned} \quad (14)$$

We choose

$$\delta_1 = x_1 - \varphi(z) \quad (15)$$

Using (8) and the fact that :

$$\forall i \in \mathcal{N}, \quad x_1^i = [\varphi + \delta_1]^i = \varphi^i + \sum_{k=0}^{i-1} C_i^k \varphi^k \delta_1^{i-k}$$

then we have

$$\begin{aligned} \dot{V} &\leq -z^T Q_z z - \frac{(1-\beta)}{1 + \|\partial V / \partial z\|^2 \rho(z)^2} \frac{(L_{g_0} V(z))^2}{1 + (L_{g_0} V(z))^2} \\ &\quad + \left[(L_{g_0} V) + \sum_{\substack{2 \leq i \leq l \\ 0 \leq k \leq i-1}} C_i^k \varphi^k (L_{g_i} V) \delta_1^{i-k-1} \right] \delta_1 \end{aligned}$$

Now, in order to design our controller, we shall use the classical Backstepping design [19] and consider the following Lyapunov function:

$$W_1 = V(z) + \frac{1}{2} \delta_1^2 + \frac{1}{2} \delta_2^2 \quad (16)$$

where $\delta_2 := x_2 - \bar{x}_2$ and

$$\bar{x}_2 = -k_1 \delta_1 + \dot{\varphi} - \left[(L_{g_0} V) + \sum_{\substack{2 \leq i \leq l \\ 0 \leq k \leq i-1}} C_i^k \varphi^k (L_{g_i} V) \delta_1^{i-k-1} \right] \quad (17)$$

where $k_1 > 0$. If we choose the following control law :

$$u = -\delta_1 - k_2 \delta_2 + \frac{d}{dt}(\bar{x}_2) \quad (18)$$

where $k_2 > 0$, then we obtain

$$\begin{aligned} \dot{W}_1 &= -z^T Q_z z - \frac{(1-\beta)}{1 + \|\partial V / \partial z\|^2 \rho(z)^2} \frac{(L_{g_0} V(z))^2}{1 + (L_{g_0} V(z))^2} \\ &\quad - k_1 \delta_1^2 - k_2 \delta_2^2 \end{aligned} \quad (19)$$

which means the origin is GAS. This ends the proof.

B. Stabilization of Class II

Proposition 2: *let us consider the class of systems (2) and define a bounded C^1 function χ and a positive constant $M_\chi > 0$ such that $\forall x_1$,*

$$\begin{cases} |\chi(x_1)| &\leq M_\chi \min(|x_1|, 1) \\ x_1 \chi(x_1) &\leq -M_\chi \|x_1\| \end{cases} \quad (20)$$

then there exists a nonlinear feedback control law which simultaneously ensures the global asymptotic stability of the origin of the closed loop system and improves the transient of the corresponding zero dynamics.

Proof:

Let us give step by step the control law design:

1) Firstly, as for the above proposition, let us introduce a change of coordinates to eliminate u from the flexible dynamics:

$$\begin{cases} \bar{\eta}_1 &= \eta_1 - B_\eta x_1 \\ \bar{\eta}_2 &= \eta_2 - B_\eta x_2 \end{cases} \quad (21)$$

in order to obtain a non linear system of the following form :

$$\begin{cases} \dot{x}_1 = x_2 \\ \dot{x}_2 = u \\ \dot{\bar{\eta}}_1 = \bar{\eta}_2 \\ \dot{\bar{\eta}}_2 = A_\eta \bar{\eta} + \bar{f}_\eta(x_1) + \bar{g}_2 x_2 + \bar{g}_\eta(x_1, \bar{\eta}_1) x_2^2 \end{cases} \quad (22)$$

where $\bar{g}_2 := A_\eta \begin{bmatrix} 0 \\ B_\eta \end{bmatrix}$, $\bar{f}_\eta(x_1) = f_\eta(x_1) + A_\eta \begin{bmatrix} B_\eta \\ 0 \end{bmatrix}$ and $\bar{g}_\eta(x_1, \bar{\eta}_1) = g(x_1, \bar{\eta}_1)$.

It is worth noting that such a system is a nontriangular nonlinear system non affine in x_1 and x_2 according to the classification of underactuated nonlinear systems proposed in [15].

- 2) Let us note $z = [x_1; \bar{\eta}_1; \bar{\eta}_2]$ and let us use the fact that $x_2 = \chi(x_1) + (x_2 - \chi(x_1))$. Then, let us write the dynamics of z :

$$\dot{z} = f_0(z) + g_0(z)(x_2 - \chi(x_1)) + g_2(z)(x_2 - \chi(x_1))^2 \quad (23)$$

where:

$$\begin{aligned} f_0(z) &= \begin{cases} \chi(x_1) \\ \bar{\eta}_2 \\ A_\eta \bar{\eta} + \bar{f}_\eta(x_1) + \bar{g}_2 \chi + \bar{g}_\eta(x_1, \bar{\eta}_1) \chi^2 \end{cases} \\ g_0(z) &= \begin{cases} 1 \\ 0 \\ \bar{g}_2 + 2\bar{g}_\eta(x_1, \bar{\eta}_1) \chi(x_1) \end{cases} \\ g_2(z) &= \begin{cases} 0 \\ 0 \\ \bar{g}_\eta(x_1, \bar{\eta}_1) \end{cases} \end{aligned}$$

- 3) then, given $P_z = P_z^T, Q_z > 0$ satisfying (13), we propose:

$$\begin{aligned} V &= \log(1 + \bar{\eta}^T P_z \bar{\eta}) + \frac{c_1}{2} x_1^2 \\ &:= \log(1 + V_{\bar{\eta}}) + \frac{c_1}{2} x_1^2 \end{aligned} \quad (24)$$

where $c_1, c_2 > 0$ are given below.

From this we obtain :

$$\begin{aligned} \dot{V} &= \frac{-\bar{\eta}^T Q_z \bar{\eta}}{1 + V_{\bar{\eta}}} + c_1 x_1 \chi(x_1) \\ &+ 2 \frac{\bar{\eta}^T P_z}{1 + V_{\bar{\eta}}} (\bar{f}_\eta(x_1) + \bar{g}_2 \chi(x_1) + \bar{g}_\eta(x_1, \bar{\eta}_1) \chi^2(x_1)) \\ &+ (L_{g_0(z)} V)(x_2 - \chi(x_1)) + (L_{g_2(z)} V)(x_2 - \chi(x_1))^2 \end{aligned} \quad (25)$$

- 4) Using the fact that $2 \frac{\bar{\eta}^T P_z}{1 + V_{\bar{\eta}}} = \frac{2\bar{\eta}^T P_z^{1/2}}{1 + (P_z^{1/2} \bar{\eta})^T (P_z^{1/2} \bar{\eta})} P_z^{1/2}$ and the assumptions on \bar{f}_η , \bar{g}_η , and χ , then we have :

$$\left\| 2 \frac{\bar{\eta}^T P_z}{1 + V_{\bar{\eta}}} \bar{f}_\eta(x_1) \right\| = \left\| \left(\frac{2\bar{\eta}^T P_z^{1/2}}{1 + V_{\bar{\eta}}} \right) P_z^{1/2} \bar{f}_\eta(x_1) \right\| \leq k_f \lambda_{\max}(P_z^{1/2}) \|x_1\| \quad (26)$$

$$\left\| 2 \frac{\bar{\eta}^T P_z}{1 + V_{\bar{\eta}}} \bar{g}_2 \chi(x_1) \right\| \leq M_\chi \|g_2\| \lambda_{\max}(P_z^{1/2}) \|x_1\| \quad (27)$$

$$\left\| 2 \frac{\bar{\eta}^T P_z}{1 + V_{\bar{\eta}}} \bar{g}_\eta \chi^2(x_1) \right\| \leq M_\chi^2 \lambda_{\max}(P_z^{1/2}) \|x_1\| + 2k_g M_\chi \|x_1\| \quad (28)$$

So, let us choose $c_1 > 0$ such that :

$$c_1 = \frac{\bar{c}_1 + (k_f + M_\chi \|g_2\| + k_g M_\chi^2) \lambda_{\max}(P_z^{1/2}) + 2k_g M_\chi}{M_\chi} \quad (29)$$

with $\bar{c}_1 > 0$, then we obtain,

$$\begin{aligned} \dot{V} &\leq \frac{-\bar{\eta}^T Q_z \bar{\eta}}{1 + V_{\bar{\eta}}} - \bar{c}_1 \|x_1\| + (L_{g_0(z)} V)(x_2 - \chi(x_1)) \\ &+ (L_{g_2(z)} V)(x_2 - \chi(x_1))^2 \end{aligned} \quad (30)$$

- 5) then we use $x_2 - \chi(x_1) = (x_2 - \chi(x_1) - \varphi(z)) + \varphi(z)$ where φ is given by (6). After a few computations, we obtain :

$$\begin{aligned} \dot{V} &\leq \frac{-\bar{\eta}^T Q_z \bar{\eta}}{1 + V_{\bar{\eta}}} - \bar{c}_1 \|x_1\| \\ &- \frac{(1 - \beta)}{1 + \|\partial V / \partial z\|^2 \rho(z)^2} \frac{(L_{g_0} V(z))^2}{1 + (L_{g_0} V(z))^2} \\ &+ [(L_{g_0} V) + 2\varphi(z) L_{g_2} V + (L_{g_2} V) \delta_2] \delta_2 \end{aligned} \quad (31)$$

where

$$\delta_2 := x_2 - \chi(x_1) - \varphi(z) \quad (32)$$

- 6) finally, if we use the following Lyapunov candidate function :

$$W_2 = V + \frac{1}{2} \delta_2^2 \quad (33)$$

and by choosing the following control law :

$$\begin{aligned} u &= -k_2(x_2 - \chi(x_1)) - (L_{g_0} V) - 2\varphi(z) L_{g_2} V \\ &- (L_{g_2} V) \delta_2 + \frac{d}{dt}(\chi(x_1) + \varphi(z)) \end{aligned} \quad (34)$$

where $k_2 > 0$, we derive that :

$$\begin{aligned} \dot{V} &\leq \frac{-\bar{\eta}^T Q_z \bar{\eta}}{1 + V_{\bar{\eta}}} - \bar{c}_1 \|x_1\| - k_2 \delta_2^2 \\ &- \frac{(1 - \beta)}{1 + \|\partial V / \partial z\|^2 \rho(z)^2} \frac{(L_{g_0} V(z))^2}{1 + (L_{g_0} V(z))^2} \end{aligned} \quad (35)$$

from this we conclude that the origin of system (2) is GAS.

IV. APPLICATION TO A NONLINEAR MODEL OF A FLEXIBLE LAUNCH VEHICLE

A. Mathematical Model

From the full Mathematical model of a flexible launch vehicle obtained by using the Lagrange equations, we extract the rotational 'fast' dynamics (for more details, see ([18])):

$$\begin{cases} \dot{\psi} = q \\ \dot{q} = -\frac{I_{\text{aero}}}{I_k} L(\psi) + \frac{T}{I_L} (L_T r - h) \eta_1 + \frac{T L_T}{I_L} \beta \\ \dot{\eta}_1 = -\omega^2 \eta_1 - 2\xi \omega \dot{\eta}_1 + h r T \eta_1 + h T \beta \end{cases} \quad (36)$$

where ψ, η_1 belong to \mathcal{R} (We only consider the first flexible mode which is known to be the only one to be relevant to consider in the control design) and $\beta \in \mathcal{R}$ is the control. where the lift is a non-linear function of the attitude, given by:

$$L(\psi) = \bar{q}S(C_L^1\psi + C_L^2\psi^2) = \bar{L}(\psi)\psi$$

B. Controller design

First we use the notation :

$$u := -\frac{l_{aero}}{I_L}L(\psi) + \frac{T}{I_L}(L_T r - h)\eta_1 + \frac{TL_T}{I_L}\beta$$

By noting $x_1 = \psi, x_2 = q, \dot{\eta}_1 = \eta_2$, we obtain a model which belongs to the Class I:

$$\begin{cases} \dot{x}_1 = x_2 \\ \dot{x}_2 = u \\ \dot{\eta}_1 = \eta_2 \\ \dot{\eta}_2 = -\bar{\omega}^2\eta_1 - 2\xi\omega\eta_2 + \frac{hl_{aero}}{L_T}L(x_1) + \frac{hl_L}{L_T}u \end{cases} \quad (37)$$

with $\bar{\omega}^2 := \omega^2 + \frac{hT}{L_T}(L_T r - h) - hrT$.

Applying the design method described in the proof of proposition 1, then we obtain : the following dynamics :

$$\begin{cases} \dot{x}_1 = x_2 \\ \dot{x}_2 = u \\ \dot{z}_1 = z_2 - 2\xi\omega\frac{hl_L}{L_T}x_1 \\ \dot{z}_2 = -\bar{\omega}^2z_1 - 2\xi\omega z_2 + \frac{h}{L_T}\left(4\xi^2\omega^2I_L - \bar{\omega}^2I_L\right. \\ \left. + l_{aero}\bar{q}SC_L^1\right)x_1 + \frac{hl_{aero}}{L_T}\bar{q}SC_L^2x_1^2 \end{cases}$$

We then numerically solve the Lyapunov equation by considering the equality (instead of the inequality) associated to (13). We obtain :

$$V = z^T P_z z \quad (38)$$

we then compute φ according to (6) ; in this case, we use :

$$g_0 = \frac{h}{L_T} \begin{bmatrix} -2\xi\omega I_L \\ 4\xi^2\omega^2 I_L - \bar{\omega}^2 I_L + l_{aero}\bar{q}SC_L^1 \end{bmatrix} \quad (39)$$

$$g_2 = \frac{h}{L_T} \begin{bmatrix} 0 \\ l_{aero}\bar{q}SC_L^2 \end{bmatrix} \quad (40)$$

Then, given two gains $k_1, k_2 > 0$ the proposed controller is :

$$u = -(x_1 - \varphi(z)) - k_2(x_2 - \bar{x}_2) + \frac{d}{dt}\bar{x}_2 \quad (41)$$

where:

$$\begin{aligned} \bar{x}_2 &= -k_1(x_1 - \varphi(z)) + \dot{\varphi} - L_{g_0}V \\ &\quad - (L_{g_2}V)(x_1 - \varphi(z)) - 2\varphi(z)(L_{g_2}V) \\ &= -k_1(x_1 - \varphi(z)) + \dot{\varphi} - L_{g_0}V - (L_{g_2}V)(x_1 + \varphi(z)) \end{aligned} \quad (42)$$

This law is compared to the following 'nominal' Backstep-law :

$$\begin{aligned} u_0 &= -x_1 - k_2(x_2 - \bar{x}_{20}) + \frac{d}{dt}\bar{x}_{20} \\ &:= -x_1 - k_2(x_2 + k_1x_1) - \frac{d}{dt}(k_1x_1) \\ &= -(1 + k_1k_2)x_1 - (k_1 + k_2)x_2 \end{aligned} \quad (43)$$

C. Numerical results

The damping of the flexible mode is chosen very low (0.01) and the simulations are performed under the initial conditions $\psi(0) = 20$ deg, $q(0) = 20$ deg/s far from the origin.

Figure (1) shows in blue (resp. in orange) the evolution of both ψ and η_1 when the controller u (resp. u_0) is applied to the system. We observe that controller u enhances the transient of the flexible mode.

V. APPLICATION TO A NONLINEAR MODEL OF A FLEXIBLE SPACECRAFT

A. Mathematical Model

We consider the following model of a flexible attachment to a spacecraft which has been obtained after a partial feedback linearization [14]

$$\begin{cases} \dot{x}_1 = x_2 \\ \dot{x}_2 = u \\ \dot{\eta}_1 = \eta_2 \\ \dot{\eta}_2 = -\omega^2\eta_1 - 2\xi\omega\eta_2 + \eta_1x_2^2 - \alpha u \end{cases} \quad (44)$$

B. Controller design

Applying the design method described in the proof of proposition 2, we first use the following change of coordinates :

$$z = \begin{cases} x_1 \\ \bar{\eta}_1 \\ \bar{\eta}_2 \end{cases} := \begin{cases} x_1 \\ \eta_1 + \alpha x_1 \\ \eta_2 + \alpha x_2 \end{cases} \quad (45)$$

We then numerically solve the Lyapunov equation by considering the equality (instead of the inequality) associated to (13). We obtain :

$$V_{\bar{\eta}} = \bar{\eta}^T P_z \bar{\eta} \quad (46)$$

Then we choose (for instance)

$$\chi(x_1) = -M_\chi \tanh(x_1) \quad (47)$$

where $M_\chi > 0$ and we rewrite the dynamics as follows :

$$\begin{aligned} \dot{z} &= f_0(z) + g_0(z)(x_2 - \chi(x_1)) + g_2(z)(x_2 - \chi(x_1))^2 \\ &= f_0(z) + g_0(z)\varphi(z) + g_2(z)\varphi^2 + g_0(z)\delta_2 \\ &\quad v + 2g_2(z)\varphi(z)\delta_2 + g_2(z)\delta_2^2 \end{aligned} \quad (48)$$

we then compute φ according to (6) ; in this case, we use :

$$\begin{aligned} V &= \log(1 + V_{\bar{\eta}}) + \frac{1}{2}c_1x_1^2 \\ f_0 &= \begin{cases} \chi(x_1) \\ \bar{\eta}_2 \\ -\omega^2\bar{\eta}_1 - 2\xi\omega\bar{\eta}_2 + \omega^2\alpha x_1 \\ + 2\xi\omega\alpha\chi(x_1) + (\bar{\eta}_1 - \alpha x_1)\chi^2(x_1) \end{cases} \\ g_0 &= \begin{cases} 1 \\ 0 \\ 2\xi\omega\alpha + 2(\bar{\eta}_1 - \alpha x_1)\chi(x_1) \end{cases} \\ g_2 &= \begin{cases} 0 \\ 0 \\ \bar{\eta}_1 - \alpha x_1 \end{cases} \end{aligned}$$

Our control law is finally given by (41) and compared to the following 'nominal' Backstepping control law :

$$\begin{aligned} u_0 &= -k_2(x_2 - \chi(x_1)) + \dot{\chi}(x_1) \\ &= -k_2(x_2 + M_\chi \tanh(x_1)) - M_\chi(1 - \tanh^2(x_1))x_2 \end{aligned} \quad (49)$$

C. Numerical results

In order to give more importance to the nonlinear term in x_2^2 , we used a high coupling coefficient $\alpha = -1$ (by comparison to the very small value of a real model [14]). Moreover, the damping of the flexible mode is chosen very low (0.01) and the simulation model is run under the following initial conditions $x_1(0) = 45$ deg, $x_2(0) = 0$ deg/s far from the origin. Figure (2) clearly shows the damping enhancement of the flexible mode when we apply our novel controller (in blue).

VI. CONCLUSIONS

New strategies have been proposed to design GAS controllers for two significant classes of nonlinear minimum phase systems. Inspired by a non affine control method [16], we have designed some novel nonlinear control laws which take into account the zero dynamics of the considered systems. In future work, we will extend our results to systems with uncertain parameters and unmeasured flexible states.

VII. FIGURES

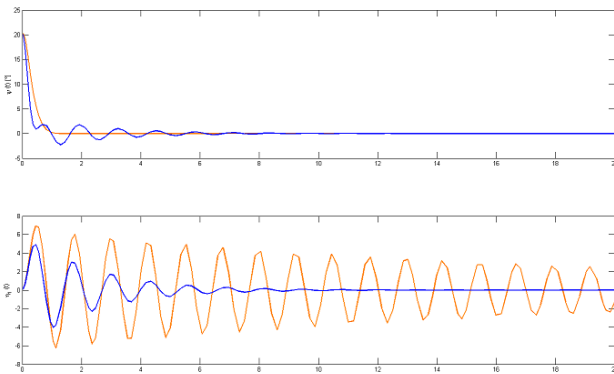


Fig. 1. Application 1 : evolution of $\psi(t)$ and $\eta_1(t)$ (below)

REFERENCES

- [1] K.L. Sorensen, W.E. Singhose and S. Dickerson, A controller enabling precise positioning and sway reduction in bridge and gantry cranes, *Control Engineering Practice*, vol.15, no. 7, pp. 825-837, 2007.
- [2] W. Aribowo, T. Yamashita, K. Terashima and H. Kitagawa, Input shaping control to suppress sloshing on liquid container transfer using multi-joint robot arm, *IEEE International Conference on Intelligent Robots and Systems*, pp. 3489-3494, 2010.
- [3] B. Pridgen, K. Bai and W.E. Singhose, Slosh suppression by robust input shaping, *IEEE International Conference on Decision and Control*, pp. 2316-2321, 2010.
- [4] Q. Hu, Z. Wang and H-J Gao, Sliding mode and shaped input vibration control of flexible systems, *IEEE Transactions on Aerospace and Electronic Systems*, pp. 503-519, 2008.

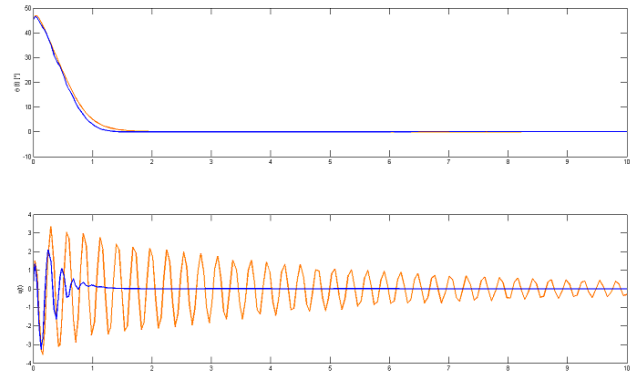


Fig. 2. Application 2 : evolution of $x_1(t)$ and $q(t)$ (below)

- [5] D. Gorinevsky and G. Vukovichz, Nonlinear Input Shaping Control of Flexible Spacecraft Reorientation Maneuver, *AIAA Journal of Guidance, Control, and Dynamics*, vol. 21, no. 2, pp. 264-270, 1998.
- [6] M. Malekzadeh, A. Naghash and H.A Talebi, Heidar, A Robust Nonlinear Control Approach for Tip Position Tracking of Flexible Spacecraft, *IEEE Transactions on Aerospace and Electronic Systems*, pp. 2423-2434, 2011.
- [7] G. Bartolini, A. Pisano and E. Usai, Second-order sliding-mode control of container cranes, *Automatica*, pp. 1783-1790, 2002.
- [8] K. Graichen and M. Zeitz, Feedforward control design for finite time transition problems of non-linear MIMO systems under input constraints, in *International Journal of Control*, vol. 81, no. 3, pp. 417-427, 2008.
- [9] I.A. Shkolnikov and Y.B. Shtessel, Tracking in a class of nonminimum-phase systems with nonlinear internal dynamics via sliding mode control using method of system center, *Automatica*, pp. 837-842, 2002.
- [10] L. Fiorentini, A. Serrani, M. Bolender and D. Doman, Nonlinear Robust Adaptive Control of Flexible Air-Breathing Hypersonic Vehicles, *Journal of Guidance, Control and Dynamics*, vol. 32, no. 2, pp. 402-417, 2009.
- [11] E. Duraffourg, L. Burlion, T. Ahmed-Ali and F. Lamnabhi-Lagarrigue, Nonlinear control of the longitudinal rotational dynamics of a flexible aircraft, in *Proc. European Control Conference, Zürich*, pp. 335-340, 2013.
- [12] M. Reyhanoglu and J. Hervas, Point-to-Point Liquid Container Transfer via a PPR Robot with Sloshing Suppression, in *Proc. American Control Conference, Montréal*, pp. 5490-5494, 2012.
- [13] M. Reyhanoglu and J. Hervas, Nonlinear dynamics and control of space vehicles with multiple fuel slosh modes, *Control Engineering Practice*, vol. 20, pp. 912-918, 2012.
- [14] M. Reyhanoglu, Slewing maneuver of a flexible spacecraft using finite time control, in *Proc. of the 34th IEEE International Conference IECON*, pp. 2667-2671, 2008.
- [15] R. Olfati-Saber, Nonlinear Control of Underactuated Mechanical Systems with Application to Robotics and Aerospace Vehicles, *PHD Thesis*, MIT, Cambridge, MA, February 2001.
- [16] W. Lin, Global asymptotic stabilization of general nonlinear systems with stable free dynamics via passivity and bounded feedback, *Automatica*, Volume 32, Issue 6, 1996, pp. 915-924, 1996.
- [17] M. Bolender and D. Doman, Nonlinear Longitudinal Dynamical Model of an Air-Breathing Hypersonic Vehicle, *Journal of Spacecraft and Rockets*, vol.44, no. 2, pp. 374, 2007.
- [18] E. Duraffourg, L. Burlion and T. Ahmed-Ali, Longitudinal Modeling and Preliminary Control of a Non-linear Flexible Launch Vehicle, in *Proc. IFAC ALCOSP Conference, Caen*, pp. 209-214, 2013.
- [19] R. Sepulchre, M. Jankovic and P.V. Kokotovic, *Constructive nonlinear control*, Springer, 1997.
- [20] A. Isidori, *Nonlinear Control Systems*, Springer, third edition, 1995.

Finite-time observer-based backstepping control of a flexible launch vehicle

Elodie Duraffourg¹, Laurent Burlion¹ and Tarek Ahmed-Ali²

Journal of Vibration and Control
1–16

© The Author(s) 2016

Reprints and permissions:

sagepub.co.uk/journalsPermissions.nav

DOI: 10.1177/1077546316664021

jvc.sagepub.com



Abstract

In this paper, a longitudinal model of a space launch vehicle was developed using the Lagrange mechanism and a free–free Euler–Bernoulli beam model. The aim was to propose a model including one flexible mode plus a nonlinear aerodynamic coefficient for nonlinear control design. We then studied the output feedback problem raised by using such a nonlinear model. The main achievement is to propose a new finite-time state observer when the measured outputs are corrupted by an unidentified flexible mode. This effect may destabilize a classical backstepping control law applied to the rigid model. To achieve this, a backstepping control law was redesigned to damp out the flexible mode, once measured and characterized. Hence a new adaptive finite time observer was developed. Closed-loop simulations show the effectiveness of the observer in combination with a redesigned backstepping control law when sensors and the launcher nozzle are collocated.

Keywords

Nonlinear control, backstepping, observer design, flexible modes

1. Introduction

The problem of finite-time observation for linear and nonlinear systems has been widely investigated over the past decades. Two classes of observers emerge in the series of methods that achieve finite-time convergence. The first one, based on the use of delay, has deserved a lot of attention (Engel and Kreisselmeier, 2002; Menold et al., 2003). Recently, in Karafyllis and Jiang (2011), a novel hybrid dead-beat observer which uses delays has been proposed. The history of the output is used in order to estimate the state of the system. Sliding mode observers, widely researched in the literature, make up the second class (see Ahmed-Ali and Lamnabhi Lagarrigue, 1999; Shtessel et al., 2010, for instance). More recently, homogeneous finite-time observers have been developed for a specific class of nonlinear system in Perruquetti et al. (2008). Most of these approaches make the assumption that the system structure and parameters are known.

In this paper we propose to design a finite-time observer for a space launch vehicle which belongs to the class of uncertain nonlinear systems. Researchers have recently investigated this subject in the field of nonlinear control. Several solutions have been proposed. Some of them, on the one hand, addressed

the problem of unknown parameters and uncertainties using a direct-adaptive, (Fiorentini et al., 2009; Hu et al., 2012), or time varying controller (Hervas and Reyhanoglu, 2012). Nevertheless, only rigid states (attitude angle and pitch rate) are used in these proposed methods. A great deal of further effort has been devoted to stabilize uncertain nonlinear systems with disturbances (Pan et al., 2015a; Yu et al., 2015). Such control methods are also applied to vehicle suspension systems (Pan et al., 2015b; Sun et al., 2016). Current active research in the field of flexible robots also aims at achieving robustness to model uncertainties and disturbances (see, e.g., De Luca, 2015, and references therein).

On the other hand, estimating the flexible states is often necessary for control design purposes: for instance, Hu (2009) uses them to actively reduce the vibrations of a flexible spacecraft. Using a sliding

¹Onera, the French Aerospace Lab, France

²Ecole Nationale Supérieure d'Ingénieurs de Caen (ENSICAEN), France

Received: 27 November 2015; accepted: 18 July 2016

Corresponding author:

Laurent Burlion, The French Aerospace Lab, F-31055 Toulouse, France.
Email: lburlion@onera.fr

mode state observer, Shtessel et al. (2010) estimate the flexible states (mode shape coordinates and their time derivatives) in order to remove the undesirable dynamics from the measurements. These approaches unfortunately require a strong knowledge of the mathematical model of the system, in particular parameters for the flexible modes (natural frequency and damping of the bending modes). However, to the best of our knowledge, the design of a finite-time observer has not been achieved on uncertain nonlinear aerospace models.

Due to mass constraints, space vehicles tend to have lightweight and flexible structures with low natural frequencies, distorting sensor measurements and adding stability problems during flight. Indeed, sensor measurements deliver rigid launcher motion plus flexible displacements at the location of the sensor. Consequently, the location of the sensors has a significant importance (Frosch and Valley, 1967). Notch-filters are usually used to overcome this stability problem by filtering the bending mode and reverting to rigid body behavior. However, this no longer works if the flexible natural frequency is very low because of interaction with rigid dynamics. Another proposed solution consists in estimating the flexible states to filter the outputs.

As far as we are concerned, we recently designed a Lyapunov-based nonlinear controller, which uses the flexible states, to ensure control objectives of both reference path tracking and bending mode damping for a class of nonlinear flexible systems (Burlion et al., 2013); (Duraffourg et al., 2013a); (Duraffourg et al., 2013b). Assuming that the whole state is available, this control law has been applied to the rotational dynamics of a space launch vehicle in Duraffourg et al. (2013c). Such assumptions do not hold in practical applications since flexible states are generally not measured. Consequently, we need to estimate the flexible states. Besides, noting that flexible parameters are subject to uncertainties or variation during flight, this paper aims to extend existing theory by proposing an indirect adaptive hybrid observer that no longer requires system parameter knowledge. The proposed approach, which extends the preliminary conference paper of Duraffourg et al. (2014) consists of estimating flexible parameters (natural frequency and damping) and initial state conditions, using the algebraic tools of Fliess and Sira-Ramirez (2003). The first ones improve the accuracy and the robustness of the observer through the indirect adaptive feature. The second ones are used to regularly update the estimated state and so guarantee a finite-time convergence.

This paper is organized as follows. Section 2 formulates the mathematical model of the flexible launch vehicle using the Lagrange mechanism and a free-free Euler-Bernoulli beam model. In Section 3, the control problem is stated. A nonlinear control law, using the

unmeasured flexible states, and achieving control objectives of stability and bending mode damping, is presented. Since flexible states are required, Section 4 develops a flexible parameter estimator and a flexible state observer which are then mixed to design a hybrid adaptive finite-time observer. Simulation results are given in Section 5. In section 6, the blending of the finite-time observer and nonlinear control law is discussed in addition to the closed-loop simulations. Closed-loop stability properties are also analyzed. Finally, Section 7 contains our conclusions and future research directions.

1.1. Useful notation

Useful notation is reported in Table 1.

Table 1. Nomenclature.

Notation	Meaning	Unit
ψ	Deviation angle around axis w.r.t the guidance attitude reference angle	rad
β	Thruster angle of deflection	rad
η	Mode shape temporal coordinate	
q	Pitch rate	rad/s
y	Drift	m
h_T	Thruster flexible displacement	m
r_T	Thruster flexible rotation	rad
r_{ci}	Inertial unit flexible rotation	rad
r_{gy}	Rategyro flexible rotation	rad
T	Thrust	kg m/s ²
L	Lift	kg m/s ²
D	Drag	kg m/s ²
G_L	Launcher center of mass	
C_T	Gimbal joint	
F_L	Aerodynamic center	
I_L	Launcher body inertia	kg m ²
M_L	Launcher body mass	kg
L_T	Algebraic distance from G_L to C_T	m
l_{aero}	Algebraic distance from F_L to G_L	m
\bar{q}	Dynamic pressure	Pa
S	Reference area of the vehicle	m ²
ω	Natural frequency of the first bending mode	rad/s
\mathcal{R}_n	Frame (G_n, x_n, y_n) linked to the reference trajectory	
ξ	Natural damping of the first bending mode	
\mathcal{R}_L	Frame (G_L, x_L, y_L) linked to the launcher	

2. Modeling of a flexible launch vehicle

This section states the longitudinal dynamics of a launch vehicle during its atmospheric flight.

2.1. Launch vehicle

We consider a flexible, static (masses and inertia stay constant) and symmetric space vehicle moving around its center of mass G_L , as shown in Figure 1. The launcher is propelled thanks to a thrust force T oriented by a deflection angle β . The launcher dynamics is formulated in the fixed and non-Galilean frame $R_n = (G_n, x_n, y_n)$ linked to the reference trajectory. Let us note $R_L = (G_L, x_L, y_L)$ the frame attached to the launcher body, ψ the deviation angle around the body axis with respect to the guidance attitude reference and y the position along the y_n axis.

To capture flexible effects, we assume that the launcher body can be identified with a free-free Euler-Bernoulli beam model on which the separation principle has been applied. Solving the Euler-Lagrange equation gives a general solution (in the free vibration case) which depends on the so-called displacements solutions. It is assumed that the control synthesis can be achieved considering merely the lower frequency displacement solution (also called the first bending mode), the remaining flexible modes being ignored. Indeed, it is well known that this assumption is satisfactory

if the closed-loop bandwidth is below a critical limit. The launcher flexible displacements along the lateral axis y_L caused by the first bending mode is given by

$$u(x, t) = h(x)\eta(t) \tag{1}$$

where $h(x)$ is the first mode shape and $\eta(t)$ is the temporal mode shape coordinate. Let us also define the mode shape derivative with respect to the launcher axis coordinate (that corresponds to a flexible rotation) by

$$r(x) = \frac{dh(x)}{dx} \tag{2}$$

Figure 2 illustrates flexible displacements at a given instant t , along the launcher axis for the first bending mode and gives a schematic representation of the mode shape. The following notations are considered

$$r_T = r(x_T) \quad h_T = h(x_T) \quad r_{ci} = r(x_{ci}) \tag{3}$$

$$r_{gy}^a = r(x_{gy}^a) \quad r_{gy}^b = r(x_{gy}^b)$$

where x_T, x_{ci}, x_{gy}^a and x_{gy}^b respectively are the coordinates of the gimbal joint, inertial unit, rate-gyro ‘‘a’’ and rate-gyro ‘‘b’’ on the launcher body axis x_L .

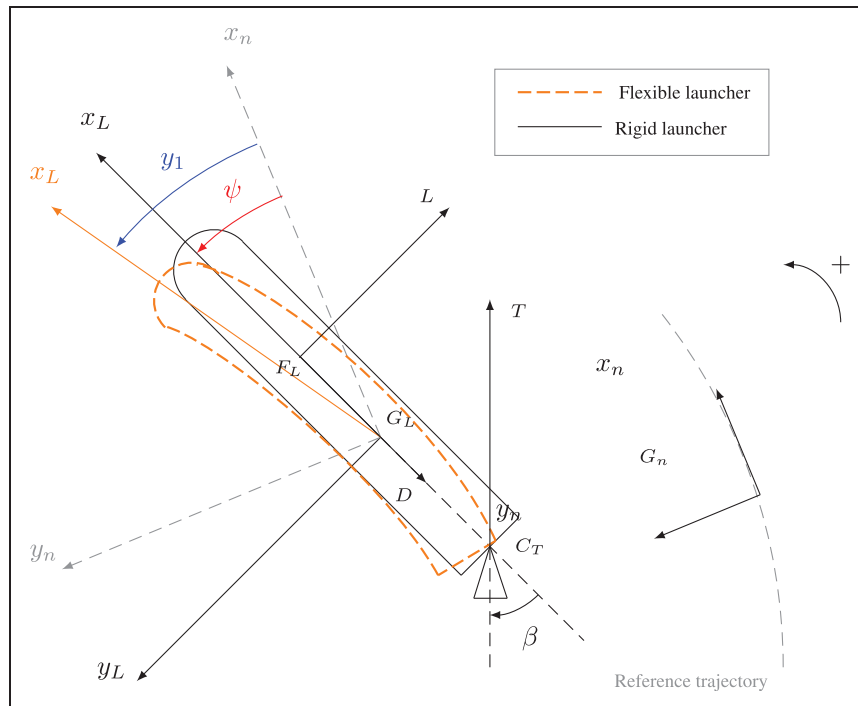


Figure 1. Flexible launch vehicle schematic representation.

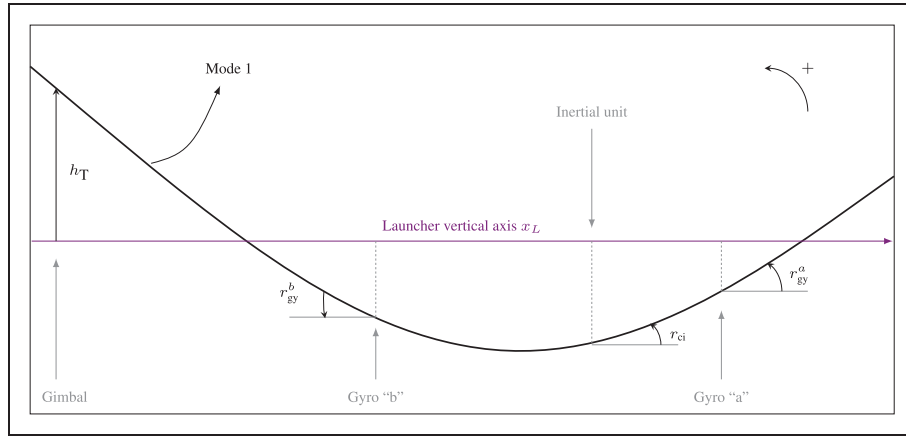


Figure 2. Schematic view of the first mode shape.

2.2. Mathematical model

The launcher mathematical model is extracted from the Lagrangian mechanism. As in Clement (2001) and Clement et al. (2001), this model is a deviation model with respect to a reference model. The Lagrangian generalized coordinates are referred to as $\kappa = (y, \psi, \eta)$ and the Lagrangian takes the form $\mathcal{L} = \mathcal{L}(\kappa, \dot{\kappa})$. Dynamic equations of the flexible launch vehicle are given by

$$\frac{d}{dt} \frac{\partial \mathcal{L}}{\partial \dot{y}} - \frac{\partial \mathcal{L}}{\partial y} = \Phi_y \quad (4)$$

$$\frac{d}{dt} \frac{\partial \mathcal{L}}{\partial \dot{\psi}} - \frac{\partial \mathcal{L}}{\partial \psi} = \Phi_\psi \quad (5)$$

$$\frac{d}{dt} \frac{\partial \mathcal{L}}{\partial \dot{\eta}} - \frac{\partial \mathcal{L}}{\partial \eta} + \frac{\partial \mathcal{R}}{\partial \dot{\eta}} = \Phi_\eta \quad (6)$$

where $\mathcal{R} = \xi \omega \dot{\eta}^2$ is a Rayleigh dissipation function introduced to consider natural energy dissipation of the bending mode and Φ_j is the generalized force relative to Lagrangian coordinate $j \in \{y, \psi, \eta\}$.

Aerodynamic forces (lift L and drag D), thrust T , and inertial forces (since the fixed frame is not Galilean) make up the external forces applied to the launch vehicle. Their generalized forces are formulated as follows

$$\begin{aligned} \Phi_y &= D \sin \psi + L \cos \psi + T \sin(\psi + \beta + r_T \eta) \\ \Phi_\psi &= -L l_{aero} + T L_T \sin(\beta + r_T \eta) - T h_T \eta \cos(\beta + r_T \eta) \\ \Phi_\eta &= h_T T \sin(\beta + r_T \eta) \end{aligned} \quad (7)$$

We compute kinetic and potential energies of the launcher in order to apply the energetic formulation of the Lagrange mechanism. Kinetic energies of the

launch vehicle \mathcal{T}_L and the shape mode \mathcal{T}_f are expressed as follows

$$\mathcal{T}_L = \frac{1}{2} M_L (\dot{x}^2 + \dot{y}^2) + \frac{1}{2} I_L \dot{\psi}^2 \quad (8)$$

$$\mathcal{T}_f = \frac{1}{2} \dot{\eta}^2 \quad (9)$$

The bending mode is identified as a mass-spring system whose stiffness is linked to its natural frequency $k = \omega^2$. Thus, the elastic potential energy is

$$\mathcal{V}_f = \frac{1}{2} \omega^2 \eta^2$$

Note that \mathcal{V}_f is the total potential energy of the deviation model with respect to the reference model, which takes into account the potential energy due to gravity.

Then, the Lagrangian is stated as the difference between the kinetic and the potential energies. That is

$$\mathcal{L} = \mathcal{T}_L + \mathcal{T}_f - \mathcal{V}_f \quad (10)$$

Applying Lagrangian formalism (4)–(6) with the generalized forces (7), the equations of motion of the launch vehicle are obtained

$$\begin{cases} M_L \ddot{y} = D \sin \psi + L \cos \psi + T \sin(\psi + \beta + r_T \eta) \\ I_L \ddot{\psi} = -L l_{aero} + T L_T \sin(\beta + r_T \eta) \\ \quad - T h_T \eta \cos(\beta + r_T \eta) \\ \ddot{\eta} = -\omega^2 \eta - 2\xi \omega \dot{\eta} + h_T T \sin(\beta + r_T \eta) \end{cases} \quad (11)$$

The spacecraft is equipped with two rate-gyros and an inertial unit that delivers measurements corrupted by flexible mode shape, as shown in Figure 1,

where y_1 does not exactly match with ψ

$$\begin{cases} y_1 = \psi + r_{ci}\eta \\ y_2 = q + r_{gy}\dot{\eta} \end{cases} \quad (12)$$

where r_{gy} is equal to r_{gy}^a or r_{gy}^b depending on whether rate-gyro ‘‘a’’ or ‘‘b’’ is considered. These two separate cases will be studied in Section 7.

3. Problem statement

Due to the classical time-scale separation principle, throughout the remainder of the paper, we focus only on fast dynamics (that is, rotational dynamics), and make the assumption of small angles for the actuator and flexible rotations. In other words, we only consider the two last equations of (11) where the trigonometric functions have been linearized. The control input is the thruster angle of deflection β . Using the notation q for the pitch rate, the considered equations of motion are given by

$$\begin{cases} \dot{\psi} = q \\ \dot{q} = -\frac{l_{aero}}{I_L}L(\psi) + \mathbf{C}_N\mathbf{N} + d_N\beta \\ \dot{\mathbf{N}} = \mathbf{A}_N\mathbf{N} + \mathbf{B}_N\beta \end{cases} \quad (13)$$

with $\mathbf{N} = [\eta, \dot{\eta}]^T$ and

$$\mathbf{A}_N = \begin{pmatrix} 0 & 1 \\ -\omega^2 + h_T r_T T - 2\xi\omega & 0 \end{pmatrix}; \quad \mathbf{B}_N = \begin{pmatrix} 0 \\ h_T T \end{pmatrix}$$

$$\mathbf{C}_N = \begin{pmatrix} \frac{T}{I_L}(L_T r_T - h_T) & 0 \end{pmatrix}; \quad d_N = \frac{TL_T}{I_L}$$

In the remainder of the paper, (ψ, q) are referred to as rigid states while $(\eta, \dot{\eta})$ are referred to as flexible states. As stated in Fiorentini et al. (2009), for a hypersonic aircraft lift $L(\psi)$ is classically described by a polynomial function (see also Boiffier (1998) for more details on aerodynamics coefficients)

$$L(\psi) = \bar{q}S(C_L^1\psi - C_L^2\psi^2) \quad (14)$$

Consider system (13). Our objective is twofold:

- to steer the attitude angle to zero so that the vehicle keeps the guidance reference trajectory;
- to add damping to the bending mode.

The challenge consists in considering this problem when:

- the model possesses a polynomial nonlinearity (here $L(\psi)$);
- the natural damping and pulsation of the flexible mode are unknown;

- we do not measure the full state of the system (we only measure (12)).

We address this problem under the following assumptions:

Assumption 1. All parameters are supposed to be known, except ξ and ω which are only bounded.

Remark 1. The parameters which account for flexible dynamics are usually known with a higher level of uncertainty than those which account for rigid dynamics. Therefore, the project focused on studying the uncertainties in damping ratio ξ and the natural frequency ω of the flexible mode. To be more thorough, we should also consider uncertainties of r_T , h_T , r_{ci} and r_{gi} . This would certainly greatly complicate the proposed observer synthesis and is postponed to future studies.

Remark 2. An additional persistence of excitation (PE) assumption, detailed in Section 5, boils down to the fact that the output signals are sufficiently ‘‘rich’’ to estimate the unknown flexible parameters. See Subsection 6.3.2 for more details.

A nonlinear control law which achieves the control objectives has been developed in Duraffourg et al. (2013a). This controller is referred to as ‘‘flexible backstepping,’’ since it uses the flexible states and minimizes the impact of the rigid dynamics on the transience of the flexible one. Despite this, this control law consists in a full-state feedback and requires knowing flexible states and parameters. That’s why we here propose to build a dedicated adaptive observer in order to estimate the flexible states together with the unknown parameters.

3.1. Nonlinear control law design for the rotational dynamics

Before giving the observer synthesis, we firstly show how one can build a state-feedback nonlinear controller which achieves the control objectives when the flexible parameters are known.

Let us note

$$c_\beta = \frac{I_L h_T}{L_T} \quad (15)$$

We firstly rewrite system (13), applying the following change of coordinates to the flexible dynamics

$$\mathbf{z} = \begin{pmatrix} \eta \\ \dot{\eta} \end{pmatrix} - c_\beta \begin{pmatrix} \psi \\ q \end{pmatrix} \quad (16)$$

It yields

$$\begin{aligned}\dot{\psi} &= q \\ \dot{q} &= -\frac{l_{aero}}{I_L} L(\psi) + \mathbf{C}_N \mathbf{N} + d_N \beta \\ \dot{\mathbf{z}} &= \mathbf{A}_z \mathbf{z} + \mathbf{F}(\psi) \psi + \mathbf{G} q\end{aligned}\quad (17)$$

with

$$\begin{aligned}\mathbf{A}_z &= \mathbf{A}_N - c_\beta \begin{pmatrix} 0 & 0 \\ \mathbf{C}_N \end{pmatrix} \\ \mathbf{F}(\psi) \psi &= c_\beta \left(\mathbf{A}_N \begin{pmatrix} \psi \\ 0 \end{pmatrix} + \frac{l_{aero}}{I_L} \begin{pmatrix} 0 \\ L(\psi) \end{pmatrix} \right) \\ \mathbf{G} &= c_\beta \left(\mathbf{A}_N \begin{pmatrix} 0 \\ 1 \end{pmatrix} - \begin{pmatrix} 1 \\ 0 \end{pmatrix} \right)\end{aligned}$$

The remaining q -term in suggests the following second change of coordinates

$$\mathbf{Z} = \mathbf{z} - \mathbf{G} \psi \quad (18)$$

We obtain a nonlinear system in lower triangular form

$$\begin{cases} \dot{\mathbf{Z}} = \mathbf{A}_z \mathbf{Z} + \mathbf{H}(\psi) \psi \\ \dot{\psi} = q \\ \dot{q} = -\frac{l_{aero}}{I_L} L(\psi) + \mathbf{C}_N \mathbf{N} + d_N \beta \end{cases} \quad (19)$$

where $\mathbf{H}(\psi) := \mathbf{F}(\psi) + \mathbf{A}_z \mathbf{G}$

Proposition 1. Consider system (19) with the following feedback control law

$$\begin{aligned}\beta_f(\psi, q, \mathbf{N}) &= \frac{c_\beta}{h_T r_T} \left[\dot{q}_{cmd} + \frac{l_{aero}}{I_L} L(\psi) \right. \\ &\quad \left. - \mathbf{C}_N \mathbf{N} - \frac{1}{c_3^f} (c_1^f \psi + \lambda_q \delta_q) \right]\end{aligned}\quad (20)$$

with $\lambda_q > 0$, $\lambda_\psi > 0$ and where

$$q_{cmd} = -\frac{1}{c_1^f} \left(\lambda_\psi \psi + c_2^f \mathbf{H}(\psi)^T \mathbf{P}_z \mathbf{Z} \right); \quad \delta_q = q - q_{cmd} \quad (21)$$

control parameters c_i^f , $i \in \{1, 2, 3\}$ are positive (tuning) constants and $\mathbf{P}_z \in \mathbb{R}^{2 \times 2}$ is a symmetric positive definite matrix defined hereafter.

So, the closed-loop system is globally asymptotically stable at the origin. This proposed controller also leads to global asymptotic stability (GAS) of the closed-loop system composed by (13) and (20).

Proof. \mathbf{A}_z being Hurwitz, flexible backstepping control law can be applied to system (17) (see Duraffourg

et al., 2013a,b), considering the following Lyapunov function

$$V_f = \frac{c_1^f}{2} \psi^2 + \frac{c_2^f}{2} \mathbf{Z}^T \mathbf{P}_z \mathbf{Z} + \frac{c_3^f}{2} \delta_q^2 \quad (22)$$

where c_i^f are positive constants ($i \in \{1, 2, 3\}$), $\mathbf{P}_z \in \mathbb{R}^{2 \times 2}$ is the positive and symmetric matrix which verifies

$$\mathbf{A}_z^T \mathbf{P}_z + \mathbf{P}_z \mathbf{A}_z = -2\mathbf{Q}_z \quad (23)$$

with \mathbf{Q}_z a positive and symmetric matrix of $\mathbb{R}^{2 \times 2}$. Choosing control law (20), the Lyapunov function time derivative is given by

$$\dot{V} = -\lambda_\psi \psi^2 - c_2^f \mathbf{Z}^T \mathbf{Q}_z \mathbf{Z} - \lambda_q \delta_q^2 \leq 0 \quad (24)$$

that ensures GAS of the origin of the closed-loop system. At that point the convergence to zero of ψ , \mathbf{Z} and δ_q is ensured. Thanks to the changes of coordinates (16), (18) and (21), the flexible states N and the pitch rate q also converge to zero.

Remark 3. When $c_2^f = 0$, one gets the classical backstepping controller. (In this case, the term $\mathbf{C}_N \mathbf{N}$ represents an exogenous disturbance which must be dominated. Note that such an unmeasured disturbance may even destabilize the system). When $c_2^f > 0$, this controller is referred to as flexible backstepping since it clearly acts on the oscillations of the dynamics associated with the under-actuated degree of freedom. Indeed, (24) yields

$$c_2^f \mathbf{Z}^T \mathbf{Q}_z \mathbf{Z} \leq -\dot{V} \quad (25)$$

By integration one gets

$$\int_0^{+\infty} \mathbf{Z}^T(s) \mathbf{Q}_z \mathbf{Z}(s) ds \leq \frac{1}{c_2^f} V(0) \quad (26)$$

This means that increasing c_2^f enables to limit the oscillations of the dynamics of \mathbf{Z} . Coming back to the original system (13), one can check by numerical simulations that the control law adds damping to the dynamics of the flexible mode η .

Remark 4. This ‘‘flexible backstepping’’ controller β_f depends on the full state and requires the knowledge of the unknown parameters. To better understand this fact, we propose to note this control law as follows

$$\beta_f := \beta_f(\psi, q, \mathbf{N}, -2\xi\omega, -\bar{\omega}) \quad (27)$$

where $\bar{\omega} = \omega^2 - h_T r_T T$.

Indeed, β_f depends on ξ and ω since it depends on \mathbf{P}_z , which in turn depends on $\mathbf{A}_z(-2\xi\omega, -\bar{\omega})$ through the

relation (23). To ensure all control objectives and make the use of this law possible, we propose a dedicated estimation scheme in the following section.

4. Main result: An adaptive finite time observer design

Since the bending mode is not measured and flexible parameters are generally distorted, we develop in this section a method to estimate flexible states and parameters and so to make the use of our nonlinear control law possible.

4.1. State observer design with known parameters (ideal case)

Flexible states η and $\dot{\eta}$ must be estimated. They are described by linear differential equations which result from system (13). Since outputs (12) involve both rigid and flexible states, the idea is to consider the augmented state $\mathbf{X} = (\psi \ \eta \ \dot{\eta})^T$ instead of just the required flexible states. It is important to note that this system is linear, contrary to the original nonlinear one (13).

Working with this augmented state gives the possibility to design a linear observer, by focusing on

$$\begin{cases} \dot{\mathbf{X}} = \mathbf{A}\mathbf{X} + \mathbf{B}_y y_2 + \mathbf{B}_\beta \beta \\ \mathbf{y}_1 = \mathbf{C}\mathbf{X} \end{cases} \quad (28)$$

where y_2 acts as an input and

$$\mathbf{A} = \begin{pmatrix} 0 & 0 & -r_{gy} \\ 0 & 0 & 1 \\ 0 & -\bar{\omega}^2 & -2\xi\omega \end{pmatrix} \quad \mathbf{B}_y = \begin{pmatrix} 1 \\ 0 \\ 0 \end{pmatrix}$$

$$\mathbf{B}_\beta = \begin{pmatrix} 0 \\ 0 \\ h_T T \end{pmatrix} \quad \mathbf{C} = (1 \quad r_{ci} \quad 0)$$

with $\bar{\omega} = \omega^2 - h_T r_T T$.

Observability conditions hold for the pair (\mathbf{A}, \mathbf{C}) and estimated state $\hat{\mathbf{X}} = (\hat{\psi} \ \hat{\eta} \ \hat{\dot{\eta}})^T$ is given by the classical Luenberger observer

$$\dot{\hat{\mathbf{X}}} = \mathbf{A}\hat{\mathbf{X}} + \mathbf{B}_y y_2 + \mathbf{B}_\beta \beta + \mathbf{L}_o (y_1 - \mathbf{C}\hat{\mathbf{X}}) \quad (29)$$

where $\mathbf{L}_o \in \mathbb{R}^{3 \times 1}$ is chosen such that $\mathbf{A} - \mathbf{L}_o \mathbf{C}$ is Hurwitz.

4.2. Parameters estimation

Bending mode natural damping and pulsation are generally subject to uncertainties and variations during flight. Besides, since our flight control law intends to attenuate the oscillations of the bending mode—that is,

to add damping—it is important to know these parameters accurately.

Moreover, the accuracy and convergence time of the state observer can be improved by a better knowledge of the initial state conditions.

In this way we choose to estimate the following parameters

$$\theta = \begin{pmatrix} \theta_1 \\ \theta_2 \\ \theta_3 \\ \theta_4 \end{pmatrix} = \begin{pmatrix} -2\xi\omega \\ -\bar{\omega}^2 \\ y_3(0) \\ \dot{y}_3(0) - \dot{y}_2(0) + 2\xi\omega y_3(0) \end{pmatrix} \quad (30)$$

where $y_3 = \dot{y}_1 = y_2 + (r_{ci} - r_{gy})\dot{\eta}$.

The first two parameters (θ_1 and θ_2) give the natural damping and pulsation of the bending mode. The flexible initial state conditions depend on the four parameters θ

$$\eta(0) = \frac{1}{\theta_2} \left(\frac{\theta_4 + \theta_1 y_2(0)}{r_{ci} - r_{gy}} - h_T T \beta(0) \right)$$

$$\dot{\eta}(0) = \frac{\theta_3 - y_2(0)}{r_{ci} - r_{gy}}$$

r_{ci} being small, we use the first initial output to approximate the state initial condition (IC) $\psi(0)$

$$\psi(0) = y_1(0) - r_{ci}\eta(0) \simeq y_1(0) \quad (31)$$

The flexible initial state conditions must be estimated through the outputs and their time derivatives. Noting that $\dot{\eta} = \frac{y_1 - y_2}{r_{ci} - r_{gy}}$, it is the following equation that links the outputs and their time derivatives to the input derivative, and consists in the basic equation of the parameter estimation

$$y_1^{(3)} = \theta_2(\dot{y}_1 - y_2) + \theta_1(\ddot{y}_1 - \dot{y}_2) + h_T T(r_{ci} - r_{gy})\dot{\beta} + \ddot{y}_2 \quad (32)$$

An algebraic methodology for parameter identification is described in Fliess and Sira-Ramirez (2003). This approach was used here to estimate θ . The main steps are presented here.

1. Take the Laplace transformation of (32) to reveal the four parameters to be estimated. So

$$\theta_1 [-s^2 Y_1 + s(Y_2 + y_1(0)s) - y_2(0)] + \theta_2 [-s Y_1 + Y_2 + y_1(0)] - s\theta_3 - \theta_4$$

$$= h_T T(r_{ci} - r_{gy})[sB - \beta(0)] - s^3 Y_1 + s^2[Y_2 + y_1(0)] - sy_2(0) \tag{33}$$

where s represents the Laplace variable and Y_i (resp. B) is the Laplace transformation of signal y_i ($i \in \{1, 2\}$) (resp. β).

2. Take derivatives with respect to s , (three times) to get unknown parameters as equations.
3. Multiply by s^{-3} both sides to avoid time derivations.
4. Come back to the time domain using inverse transformations.
5. Note that the system of time-varying linear equations can be expressed in matrix form as

$$P(t)\theta = Q(t) \tag{34}$$

where $P \in \mathbb{R}^{4 \times 4}$ and $Q \in \mathbb{R}^{4 \times 1}$ (details of the matrices in Appendix 1).

The usual way to conclude the algebraic estimation technique is to use the inverse of matrix P to define θ . But, as P is time varying, it is likely to vanish at some instants. To avoid this problem we make the following assumption

Assumption 2. PE condition: $\exists \tau > 0$ such that

$$\forall t \geq 0, \int_t^{t+\tau} P(s)^T P(s) ds > 0 \tag{35}$$

Remark 5. In view of matrix P coefficients detailed in the Appendix 1, it is clear that the PE condition depends on outputs y_1, y_2 and on the input β of the system.

Under Assumption 2, θ is finally given by

$$\theta = \left(\int_t^{t+\tau} P(s)^T P(s) ds \right)^{-1} \left(\int_t^{t+\tau} P(s)^T Q(s) ds \right) \tag{36}$$

Since τ is unknown, we compute estimated parameters $\hat{\theta}$ and then \hat{A} and \hat{X}_0 at discrete time instants τ_k where $\{\tau_k\}_{k=0}^{+\infty}$ is a partition of \mathbb{R}^+ , using

$$\hat{\theta}(\tau_k) = \left(\int_0^{\tau_k} P(s)^T P(s) ds \right)^{-1} \left(\int_0^{\tau_k} P(s)^T Q(s) ds \right) \tag{37}$$

$$\hat{A}(\tau_k) = \hat{A}_k = \begin{pmatrix} 0 & 0 & -r_{gy} \\ 0 & 0 & 1 \\ 0 & \hat{\theta}_2(\tau_k) & \hat{\theta}_1(\tau_k) \end{pmatrix} \tag{38}$$

$$\hat{X}_0(\tau_k) = \begin{pmatrix} y_1(0) \\ \frac{1}{\hat{\theta}_2(\tau_k)} \left(\frac{\hat{\theta}_4(\tau_k) + \hat{\theta}_1(\tau_k)y_2(0)}{r_{ci} - r_{gy}} - h_T T\beta(0) \right) \\ \frac{\hat{\theta}_3(\tau_k) - y_2(0)}{r_{ci} - r_{gy}} \end{pmatrix} \tag{39}$$

Remark 6. It is important to note that \hat{A} and \hat{X}_0 are not completely described by estimated parameters. Parameters r_{gy}, r_{ci}, h_T and T are supposed to be known, as stated in Assumption 1.

4.3. Adaptive finite-time observer

Mixing the results of the last subsections, it is now possible to design an observer where the parameters are unknown.

Estimated parameters and IC are used to improve the accuracy of the observer. In particular, $\hat{\theta}_1$ and $\hat{\theta}_2$ are used in the design such that the observer no longer depends on the natural damping and pulsation of the bending mode, that are subject to variations.

Proposition 2. Under Assumption 2, the following hybrid observer converges in finite-time

$$\begin{cases} \forall t \in [\tau_k, \tau_{k+1}[\\ \dot{\hat{X}} = \hat{A}_k \hat{X} + B_y y_2 + B_\beta \beta + L_k (y_1 - C \hat{X}) \\ \text{when } t = \tau_k \\ \hat{X}(\tau_k) = e^{\hat{A}_k \tau_k} \hat{X}_0(\tau_k) + \int_0^{\tau_k} e^{\hat{A}_k(\tau_k-s)} [B_y y_2(s) + B_\beta \beta(s)] ds \end{cases} \tag{40}$$

At each τ_k , the state is updated and the dynamics (\hat{A}_k) as well.

L_k is chosen such that $\hat{A}_k - L_k C$ is Hurwitz.

Proof. Using the notations $\tilde{X} = X - \hat{X}$ and $\tilde{A} = A - \hat{A}_k$, it comes

$$\dot{\tilde{X}} = AX - \hat{A}_k \hat{X} - L_k C \tilde{X} = (\hat{A}_k - L_k C) \tilde{X} + \tilde{A} X \tag{41}$$

Because of the PE condition, algebraic parameter estimation converges in finite-time. Thus, there exists k^* such that $\tau_{k^*} > \tau > 0$ and

$$\forall k > k^*, \hat{\theta}(\tau_k) = \theta \tag{42}$$

Consequently $\forall k > k^*, \hat{A}_k = A$ and $L_k = L_0$. The estimation error satisfies

$$\forall t \geq \tau_k^*, \dot{\tilde{X}} = (A - L_0 C) \tilde{X} \tag{43}$$

$A - L_0 C$ being Hurwitz, the estimation error \tilde{X} converges asymptotically to zero.

Besides, the estimated state $\hat{X}(t)$ is updated on $\hat{X}(\tau_k)$ at each τ_k verifying $\tau_k > \tau_{k^*}$

$$\forall t \geq \tau_k^*, \dot{\hat{X}}_0(t) = X_0(t) \text{ ie } \hat{X}(\tau_k) = X(\tau_k) \tag{44}$$

Estimation error is then given by

$$\forall t \geq \tau_k^*, \quad \tilde{\mathbf{X}}(t) = \tilde{\mathbf{X}}(\tau_k) e^{(\mathbf{A} - \mathbf{L}_k \mathbf{C})(t - \tau_k)} = 0 \quad (45)$$

Finally the estimation error vanishes in finite-time.

Remark 7. The proposed observer (40) was inspired by the work of Karafyllis and Jiang (2011). We've added the gain \mathbf{L}_k to account for possible measurement noise. Consider that we measure $y_1 + d_1$ and $y_2 + d_2$ where d_1 and d_2 are measurement noise. This gives: $\forall t \in [\tau_k, \tau_{k+1}[$

$$\dot{\tilde{\mathbf{X}}} = (\hat{\mathbf{A}}_k - \mathbf{L}_k \mathbf{C}) \tilde{\mathbf{X}} + \tilde{\mathbf{A}} \mathbf{X} - B_y d_2 - L_k d_1 \quad (46)$$

This is an input to state stable (ISS) system, since it can be seen as an asymptotically stable linear system driven by the input $\tilde{\mathbf{A}} \mathbf{X} - B_y d_2 - L_k d_1$. Note that the term $\tilde{\mathbf{A}} \mathbf{X}$ disappears once matrix $\tilde{\mathbf{A}}$ is correctly estimated (however, contrary to the above discussion, it might not disappear in

case of noisy measurements). Note that when $L_k = 0$, the observation error dynamics is not an ISS system since $\hat{\mathbf{A}}_k$ is marginally stable according to equation (38).

5. Simulation results

5.1. Parameters estimator

Figure 3 shows in blue (resp. in red) the evolution of flexible estimated parameters ($\hat{\theta}_1, \hat{\theta}_2$) and initial state conditions $\hat{\mathbf{X}}_0 = (\hat{\psi}(0) \hat{\eta}(0) \hat{\eta}(0))$ when the sensors give ideal (resp. noisy) measurements. The red curve was obtained applying a zero-mean periodic noise on signals y_1 and y_2 . The simulation has been performed with the following parameters

$$\begin{aligned} \theta_1 &= -1.2 & \theta_2 &= -35 & \psi(0) &= 20^\circ \\ \eta(0) &= 10 & \dot{\eta}(0) &= 5 \end{aligned}$$

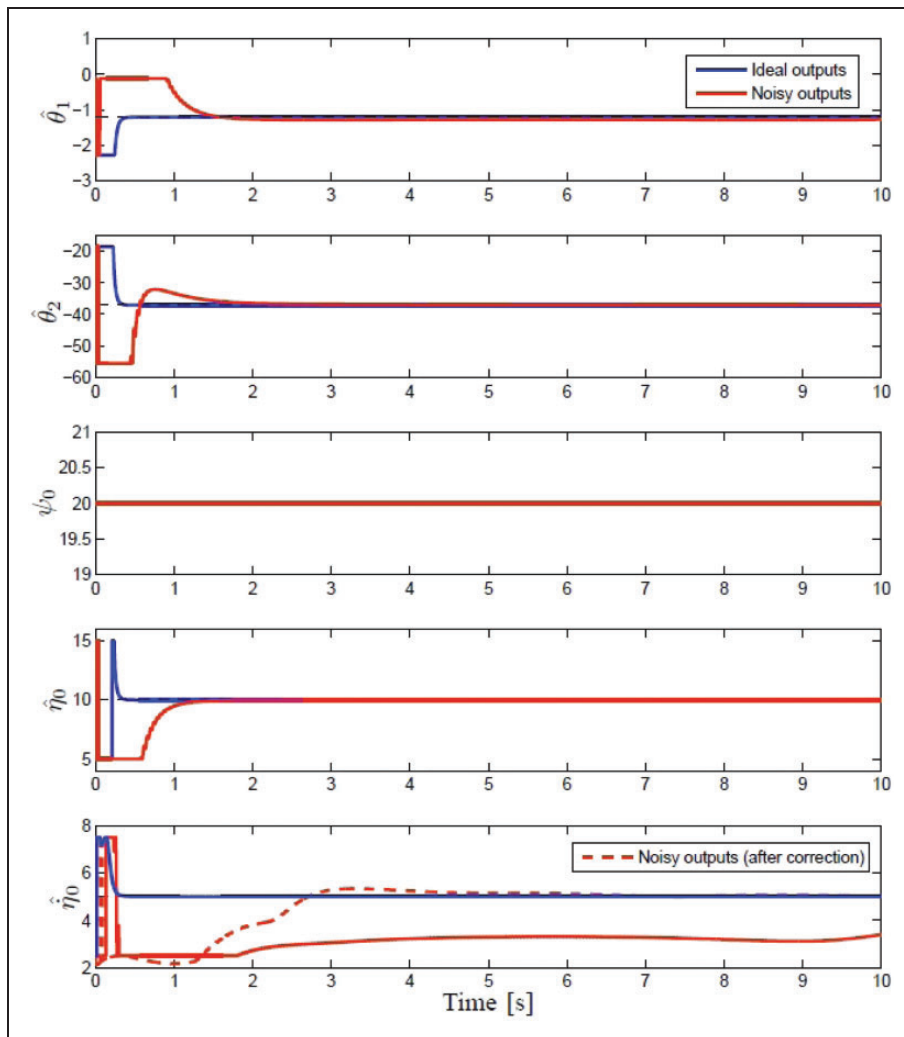


Figure 3. Estimated parameters.

Remark 8. With noisy measurements, estimated parameter $\hat{\eta}(0)$ is biased and the estimation error $\tilde{\eta} = \dot{\eta}(0) - \hat{\eta}(0)$ is quite important (about 1.5). This problem is detailed in the following subsection.

5.2. Robustness improvement of the observer with respect to noisy measurements

An estimation bias appears in simulation on estimated parameter $\hat{\eta}(0)$ when measurements are noisy (solid red curve on the last plot of Figure 3). It is given by

$$\tilde{\eta}(0) = \dot{\eta}(0) - \hat{\eta}(0) = \frac{\theta_3 - \hat{\theta}_3}{r_{ci} - r_{gy}} \quad (47)$$

This bias term is due to the low values of $r_{ci} - r_{gy}$ which accentuates the (low) difference between θ_3 and $\hat{\theta}_3$. This section proposes a way to identify this estimation bias $\tilde{\eta}(0)$ and thus to correct $\hat{\mathbf{X}}_0(\tau_k)$.

From system (28), we have

$$y_1(t) = \mathbf{C}e^{\mathbf{A}t}\mathbf{X}_0(t) + \mathbf{C} \int_0^t e^{\mathbf{A}(t-s)} [\mathbf{B}_y y_2(s) + \mathbf{B}_\beta \beta(s)] ds \quad (48)$$

Similarly, with the estimated state

$$\hat{\mathbf{X}}(t) = e^{\hat{\mathbf{A}}_k t} \hat{\mathbf{X}}_0(t) + \int_0^t e^{\hat{\mathbf{A}}_k(t-s)} [\mathbf{B}_y y_2(s) + \mathbf{B}_\beta \beta(s)] ds \quad (49)$$

Under the PE condition, algebraic parameter estimation still converges in finite-time. Thus, there exists $k^* > 0$ such that for all $k \geq k^*$

$$\hat{\mathbf{A}}_k = \mathbf{A} \quad \text{and} \quad \hat{\mathbf{X}}_0 = (\psi(0) \quad \eta(0) \quad \dot{\eta}(0) - \tilde{\eta}(0))^T \quad (50)$$

This last equation underlines the fact that only the estimated IC $\dot{\eta}$ is biased. Then

$$\forall t > t_{k^*} \quad y_1(t) - \mathbf{C}\hat{\mathbf{X}}(t) = \mathbf{C}e^{\mathbf{A}t}\mathbf{e}_3 \tilde{\eta}(0) \quad (51)$$

with $\mathbf{e}_3 = (0 \quad 0 \quad 1)^T$. That can be written as

$$\int_0^t (\mathbf{C}e^{\mathbf{A}s}\mathbf{e}_3)^2 ds \tilde{\eta}(0) = \int_0^t \mathbf{C}e^{\mathbf{A}s}\mathbf{e}_3 [y_1(s) - \mathbf{C}\hat{\mathbf{X}}(s)] ds \quad (52)$$

Supposing that $\int_0^t (\mathbf{C}e^{\mathbf{A}s}\mathbf{e}_3)^2 ds \neq 0$, estimation error is given by

$$\tilde{\eta}(0) = \frac{\int_0^t \mathbf{C}e^{\mathbf{A}s}\mathbf{e}_3 [y_1(s) - \mathbf{C}\hat{\mathbf{X}}(s)] ds}{\int_0^t (\mathbf{C}e^{\mathbf{A}s}\mathbf{e}_3)^2 ds} \quad (53)$$

This term is added on the last simulation. The result is represented by the dashed red line on Figure 3.

5.3. Finite time observer

Figure 4 compares this finite-time observer that updates the state from the knowledge of the IC (in blue) with the same Luenberger observer without any update of the estimated state (in green). In the two cases, the observer parameter \mathbf{L}_o is the same. Moreover, the ICs of the classical Luenberger observer have been chosen very close to the estimated parameters, so that the comparison is fair. This figure shows how the observer convergence time is improved. The dramatic slope on the blue curve corresponds to the moment where the estimated state is updated.

6. Closed-loop simulations

In this section, the adaptive finite-time observer is blended with the flexible backstepping law and closed-loop simulations are realized for separate locations of sensors.

6.1. Closed-loop system

Before reaching the convergence time τ_k^* , asymptotic stability of the closed-loop system, composed of system (17) and the flexible backstepping law, is not guaranteed. For that reason, the final control law is designed as a switch between:

- classical backstepping law applied to the sole rigid dynamics and consisting of an output-feedback controller, assuming that ψ (resp. q) approximately corresponds to output y_1 (resp. y_2), before reaching convergence time;
- flexible backstepping controller using estimated flexible states and parameters as soon as convergence time is reached.

Using the notation (27), this switching controller is summarized as follows

$$\beta = \begin{cases} \beta_c(y_1, y_2) & \text{when } t < \tau_k^* \\ \hat{\beta}_f := \beta_f(y_1 - r_{ci}\hat{\eta}, y_2 - r_{gy}\hat{\eta}, \hat{\mathbf{N}}, \hat{\theta}_1, \hat{\theta}_2) & \text{else} \end{cases} \quad (54)$$

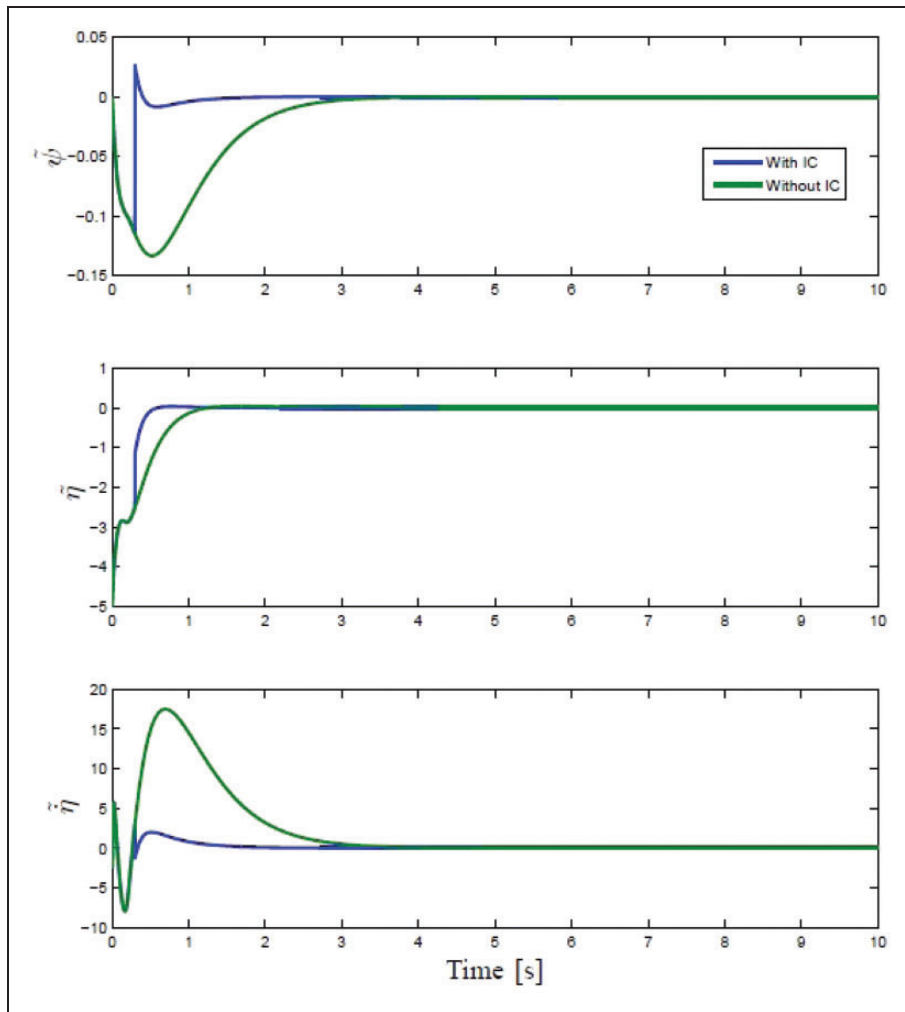


Figure 4. Observation errors.

β^c is the backstepping controller designed on the sole rigid-dynamics, which is in strict-feedback form (Duraffourg et al., 2013c). This control law corresponds to the flexible backstepping (20) without flexible states (the expression of β_c is detailed hereafter (55)).

The closed-loop system is illustrated in Figure 5.

6.2. Closed-loop simulation for a collocated rate-gyro sensor

Collocation occurs if the dynamics between the actuator and sensor show a repeating sequence of anti-resonances and resonances, with the consequence that the phase never drops below -180° , which is beneficial for stability. For noncollocated actuators and sensors this repeating sequence is not guaranteed (for more details see, for instance, Frosch and Vally, 1967; Spector and Flashner, 1990; Spong, 1996; Olfati-Saber, 2000; Preumont, 2011).

Figure 2 illustrates the location of

1. a collocated rate-gyro (gyro “a”): $y_2 = q + r_{gy}^a \dot{\eta}$
2. a noncollocated rate-gyro (gyro “b”): $y_2 = q + r_{gy}^b \dot{\eta}$

This study only considered the collocated case for two reasons:

1. The following assumption was numerically validated:

Assumption 3. *the linearized closed-loop system has all its eigenvalues with strictly negative real parts.*

2. Using assumptions 1 and 3, it is possible to prove that the closed-loop system (13)–(54) possesses (at least) a region of attraction around zero. (This is discussed in the following section.)

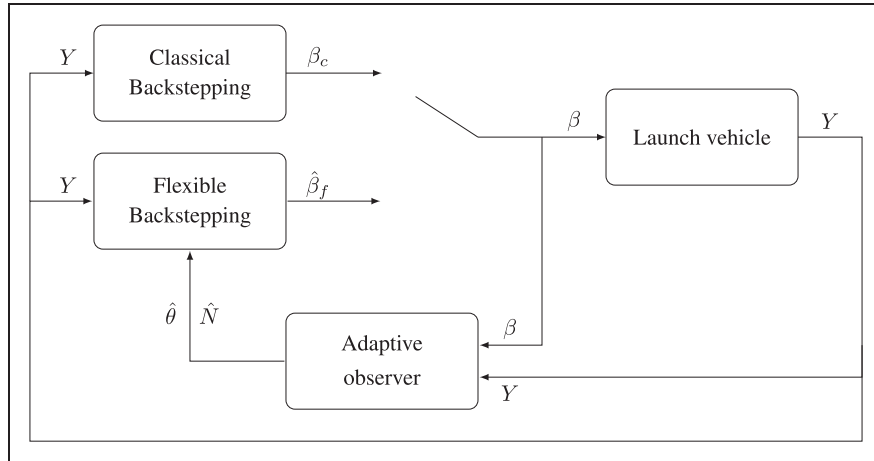


Figure 5. Block diagram of the closed-loop system.

The switching controller (54) is now denoted by Observer Flexible Backstepping. It was compared with:

- the “Classical backstepping control” law β^c (54) which use the outputs y_1 and y_2 ;
- an ideal full-state feedback flexible backstepping law given by (20), assuming the flexible states \mathbf{N} and the parameters ξ and ω are known.

This last controller has demonstrated good performance in terms of stability and bending mode damping. Consequently, it corresponds to a reference law and enables us to judge the efficiency of the designed switching output-feedback controller.

Figure 6 shows the evolution of attitude, pitch rate and flexible states with time. The simulation was performed with natural damping equal to 0.005 and a natural frequency equal to 6 rad.s⁻¹. Control parameters have been tuned so that the time responses are the same.

The three controllers converge asymptotically to the origin.

As expected (see Remark 3), full state-feedback flexible backstepping improves the damping of the bending mode compared to classical backstepping. Moreover, it is remarkable that observer flexible backstepping is able to damp out the bending mode when the flexible states are unmeasured and flexible parameters ξ and ω are uncertain.

6.3. Further discussions on the estimation phase

6.3.1. Closed-loop stability. Thanks to the finite time convergence property of the observer (40), the controller defined by (54) switches once at $t = \tau_k^*$. Such a switch occurs when the parameters θ (30) have converged.

The closed-loop system defined by (17), (40) and (54) inherits the GAS property proved in Proposition 1

when $t \geq \tau_k^*$. Meanwhile, it is necessary to prove that this closed-loop system remains stable for $t \in [0, \tau_k^*]$.

Let us consider system (13).

For $t \in [0, \tau_k^*]$, the following feedback control law is applied

$$\beta_c(y_1, y_2) = \frac{c_\beta}{h_T T} \left[-\frac{1}{c_1^f} \lambda_\psi y_2 + \frac{l_{aero}}{I_L} L(y_1) - \frac{1}{c_3^f} (c_1^f y_1 + \lambda_q \delta_{y_2}) \right] \quad (55)$$

with tuning gains $\lambda_q > 0, \lambda_\psi > 0, c_i^f \quad i \in \{1, 2\}$ and where

$$y_{2,cmd} = -\frac{1}{c_1^f} \lambda_\psi y_1; \quad \delta_{y_2} = y_2 - y_{2,cmd} \quad (56)$$

Considering equations (12), (14) and (55), it is clear that

$$\beta_c(y_1, y_2) = \beta_c(\psi, q) + \mathbf{C}_\beta \mathbf{N} + g(\psi\eta, \eta^2) \quad (57)$$

where

$$\mathbf{C}_\beta = -\frac{c_\beta}{h_T T} \left(\frac{1}{c_3^f} \left(c_1^f + \frac{\lambda_\psi \lambda_q}{c_3^f} \right) r_{ci} \quad \left(\frac{\lambda_\psi}{c_1^f} + \frac{\lambda_q}{c_3^f} \right) r_{gy} \right) \quad (58)$$

$$g(\psi\eta, \eta^2) = -\frac{c_\beta l_{aero}}{h_T T I_L} \bar{q} S C_L^2 r_{ci} (2\psi\eta + r_{ci} \eta^2) \quad (59)$$

Therefore, the closed-loop system (13)–(20) is rewritten as follows

$$\begin{cases} \dot{\psi} = q \\ \dot{q} = -\frac{l_{aero}}{I_L} L(\psi) + \mathbf{C}_{N_y} \mathbf{N} + \mathbf{d}_N (\beta_c(\psi, q) + g(\psi\eta, \eta^2)) \\ \dot{\mathbf{N}} = \mathbf{A}_{N_y} \mathbf{N} + \mathbf{B}_N (\beta_c(\psi, q) + g(\psi\eta, \eta^2)) \end{cases} \quad (60)$$

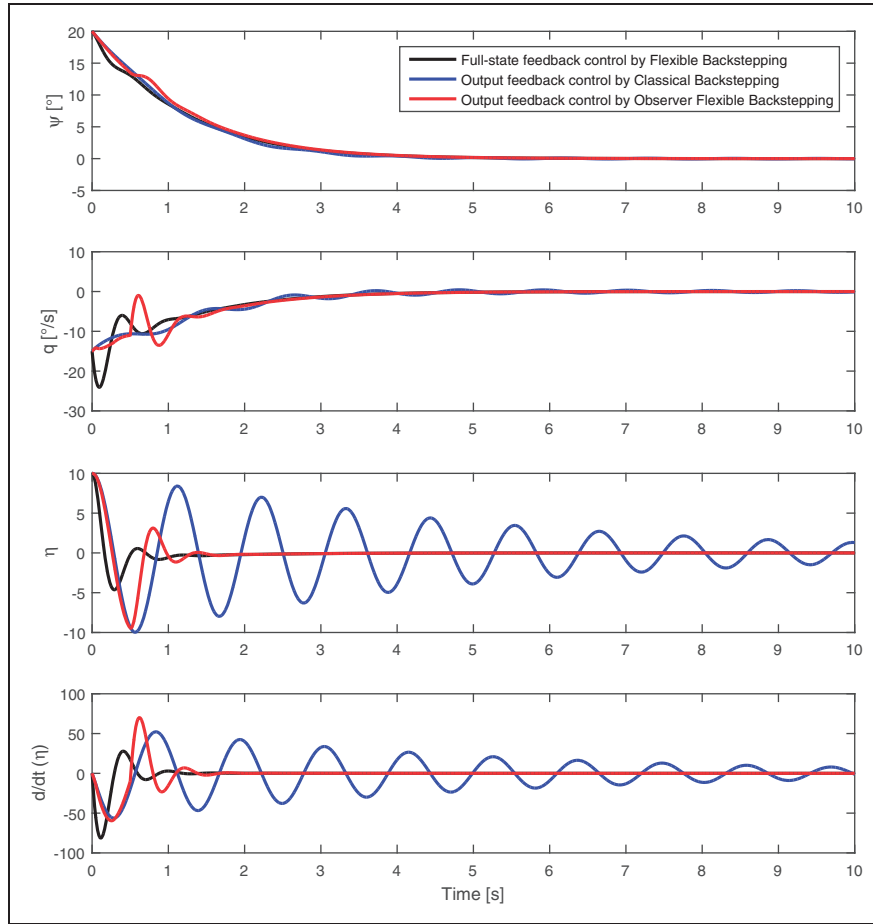


Figure 6. Closed-loop comparison.

where

$$\mathbf{A}_{Ny} = \mathbf{A}_N + \mathbf{B}_N \mathbf{C}_\beta; \quad \mathbf{C}_{Ny} = \mathbf{C}_N + \mathbf{d}_N \mathbf{C}_\beta \quad (61)$$

Discussion:

1. Let us suppose assumptions 1 and 3 hold. The closed-loop system (60) is Locally Asymptotically Stable by virtue of Lyapunov’s indirect method (for more details, see Theorem 3.7 in Khalil (1996). In other words, this means a region of attraction exists around zero.
2. Consider:

Assumption 4.

$$r_{ci} = 0 \quad (62)$$

In this case the nonlinear term $g(\psi\eta, \eta^2)$ disappears! Under Assumptions 1, 3 and 4 (plus some mild assumptions) one can apply the results of Arcak and Kokotovic (2000) to redesign the backstepping controller β_c and prove GAS of the closed-loop system (60)

(For more details, see Theorem 1 in Arcak and Kokotovic, 2000.)

3. Finally, when $r_{ci} \neq 0$ and when Assumptions 1 and 3 hold, the aforementioned redesigned controller might not be able to globally stabilize system (60) because of the nonlinear term $g(\psi\eta, \eta^2)$ (which is also changed by the redesign technique). In this case, a region of attraction might be computed. Future research may be devoted to show that the estimation of the region of attraction is enlarged once the backstepping controller β_c is redesigned. This point will be addressed in the future.

6.3.2. Closed-loop observability. As remarked before (see Remark 5), Assumption 2 depends on the trajectories followed by $y_1(t)$ and $y_2(t)$. (It also depends on β_c , which in turn depends on $y_1(t)$ and $y_2(t)$ in a closed loop)

Thus, another problem consists of using the observer (40) within the transition phase of the closed-loop system (17), (54). Indeed, one must guarantee that the

excitation condition (35) is satisfied. Note that this PE condition is our Assumption 2, which can reasonably be made in open loop. In our closed-loop simulations, this condition was respected.

However, when this assumption is not satisfied, it is necessary to make the system outputs $y_1(t)$, $y_2(t)$ track sufficiently exciting reference signals $y_1^r(t)$, $y_2^r(t)$ (which are set to 0 when $t \geq \tau_k^*$).

Few results deal with the link between the design of such exciting reference signals and the closed-loop PE condition. For a further discussion on this topic, the interested reader is referred to Adetola and Guay (2006), Adetola and Guay (2008) and the references therein.

This is another possible future research direction.

7. Conclusion

A mathematical model for a flexible launch vehicle has been formulated, using the Lagrange mechanism and a free-free Euler-Bernoulli beam model. Next, a full state flexible backstepping controller, which both guarantees GAS of the closed-loop nonlinear system and improves the bending mode damping, was proposed. Then, an adaptive finite-time observer that enables estimation of flexible states with unknown flexible parameters has been specifically designed in order to blend with this control design method. Numerical simulations have been performed in the case of collocation between sensors and actuator: They have clearly shown the efficiency of the designed controller in conjunction with the proposed observer.

For our future work, uncertainties on mode shapes and aerodynamics coefficients will be considered. Moreover, this novel work on using a model of the flexible launch vehicle possessing a nonlinear aerodynamic coefficient in the control design has raised several issues which need further investigation: For example, the estimation of the closed-loop system's region of attraction, the use of noncollocated outputs, and the consideration of several flexible modes. Finally, we plan to apply the flexible backstepping design method to a highly representative flexible satellite simulator. We would also like to experimentally test this method on a flexible robotic arm.

Funding

This research received no specific grant from any funding agency in the public, commercial, or not-for-profit sectors.

References

Adetola V and Guay M (2006) Excitation signal design for parameter convergence in adaptive control of linearizable systems. In: *Proceedings of the 45th IEEE conference on decision and control*, San Diego, CA, pp.447–452. .

- Adetola V and Guay M (2008) Finite-time parameter estimation in adaptive control of nonlinear systems. *IEEE Transactions on Automatic Control* 53(3): 807–811.
- Arcak M and Kokotovic PV (2000) Robust nonlinear control of systems with input unmodeled dynamics. *Systems & Control Letters* 41(2): 115–122.
- Ahmed-Ali T and Lamnabhi Lagarrigue F (1999) Sliding observer-controller design for uncertain triangular nonlinear systems. *IEEE Transactions on Automatic Control* 4(6): 1244–1249.
- Boiffier JL (1998) *The Dynamics of Flight: The Equations*. Hoboken, NJ: Wiley.
- Burlion L, Duraffourg E, Ahmed-Ali T, et al. (2013) Global asymptotic stabilization for some nonlinear models of flexible aerospace vehicles. In: *Proceedings of the 52nd IEEE conference on decision and control*, Florence, Italy, pp.4230–4235.
- Clement B (2001) *Multiobjective synthesis and gain scheduling: Application to an aerospace launcher guidance*. PhD Dissertation, University of Paris XI, Orsay, France.
- Clement B, Duc G and Mauffrey S, et al. (2001) Gain scheduling for an aerospace launcher with bending modes. In: *Proceedings of the 15th IFAC symposium on automatic control in aerospace*, Bologna, Italy, pp.475–480.
- De Luca A (2015) Flexible robots. In: Baillieul J and Samad T (eds) *Encyclopedia of Systems and Control*. London: Springer, pp. 451–458.
- Duraffourg E, Burlion L, Ahmed-Ali T, et al. (2013) Non-linear control of the longitudinal rotational dynamics of a flexible aircraft. In: *Proceedings of the 12th European control conference*, Zürich, Switzerland, pp.335–340.
- Duraffourg E, Burlion L, Ahmed-Ali T, et al. (2013) Non-linear full-state control of a flexible hypersonic vehicle. In: *Proceedings of the 11th IEEE international workshop on electronics control measurement signals and their application to mechatronics*, Toulouse, France.
- Duraffourg E, Burlion L and Ahmed-Ali T (2013) Longitudinal modeling and preliminary control of a nonlinear flexible launch vehicle. In: *Proceedings of the 11th IFAC international workshop on adaptation and learning in control and signal processing*, Caen, France.
- Duraffourg E, Burlion L, Ahmed-Ali T, et al. (2014) Adaptive finite-time observer for a nonlinear and flexible space launch vehicle. In: *Proceedings of 19th world congress of the international federation of automatic control*, Cape Town, South Africa, pp.546–551.
- Engel R and Kreisselmeier G (2002) A continuous-time observer which converges in finite time. *IEEE Transactions on Automatic Control* 47(7): 1202–1204.
- Fiorentini L, Serrani A, Bolender MA, et al. (2009) Nonlinear robust adaptive control of flexible air-breathing hypersonic vehicles. *Journal of Guidance, Control and Dynamics* 32(2): 401–416.
- Fliess M and Sira-Ramirez H (2003) An algebraic framework for linear identification. *ESAIM Control, Optimisation and Calculus of Variations* 9: 151–168.
- Frosch JA and Valley DP (1967) Saturn AS-501/S-IC flight control system design. *Journal of Spacecraft* 4(8): 1003–1009.
- Hervas JR and Reyhanoglu M (2012) Control of a spacecraft with time-varying propellant slosh parameters.

In: *Proceedings of the 12th international conference on control automation and systems*, Jeju Island, Korea.

Hu Q (2009) Robust adaptive backstepping attitude and vibration control with L2-gain performance for flexible spacecraft under angular velocity constraint. *Journal of Sound and Vibration* 327(3–5): 285–298.

Hu X, Wu L, Hu C, et al. (2012) Adaptive sliding mode tracking control for a flexible air-breathing hypersonic vehicle. *Journal of the Franklin Institute* 349(2): 559–577.

Karafyllis I and Jiang ZP (2011) Hybrid dead-beat observers for a class of nonlinear systems. *Systems and Control Letters* 60: 608–617.

Khalil H (1996) *Nonlinear Systems*. Upper Saddle River, NJ: Prentice Hall.

Menold PH, Findeisen R and Allgöwer F (2003) Finite time convergent observers for nonlinear systems. In: *Proceedings of the 42nd IEEE conference on decision and control*, Maui, HI, pp.5673–5678.

Olfati-Saber R (2000) Trajectory tracking for a flexible one-link robot using a nonlinear noncollocated output. In: *Proceedings of the 39th IEEE conference on decision and control*, Sydney, Australia, pp.4024–4029.

Pan H, Sun W, Gao H, et al. (2015a) Disturbance observer-based adaptive tracking control with actuator saturation and its application. *IEEE Transactions in Automation Science and Engineering* 99: 1–8.

Pan H, Sun W, Gao H, et al. (2015b) Finite-time stabilization for vehicle active suspension systems with hard constraints. *IEEE Transactions on Intelligent Transportation Systems* 16(5): 2663–2672.

Perruquetti W, Floquet T and Moulay E (2008) Finite-time observers: Application to secure communication. *IEEE Transactions on Automatic Control* 53(1): 356–360.

Preumont A (2011) *Vibration Control of Active Structures: An Introduction*, 3rd ed. Berlin, Germany: Springer.

Spector VA and Flashner H (1990) Modelling and design implications of non-collocated control in flexible systems. *ASME Journal of Dynamics Systems, Measurement and Control* 11: 186–193.

Spong MW (1996) Energy based control of a class of underactuated mechanical systems. In: *Proceedings of the IFAC world congress*, San Francisco, CA, pp.431–436.

Shtessel YB, Baev S, Edwards C, et al. (2010) HOSM observer for a class of nonminimum phase causal nonlinear MIMO systems. *IEEE Transactions on Automatic Control* 55(2): 543–548.

Shtessel YB, Hall CE, Baev S, et al. (2010) Flexible modes control using sliding mode observers: Application to Ares I. In: *Proceedings of the AIAA guidance, navigation and control conference*, Canada, Toronto.

Sun W, Pan H and Gao H (2016) Filter-based adaptive vibration control for active vehicle suspensions with electrohydraulic actuators. *IEEE Transactions in Vehicular Technology* 65(6): 4619–4626.

Yu P, Shtessel Y and Edwards C (2015) Adaptive continuous higher order sliding mode control of air breathing hypersonic missile for maximum target penetration. In: *AIAA guidance, navigation, and control conference*.

Appendix I. P and Q matrices

Once back in the time domain, the following relation is used to make the implementation easier (Fliess and Sira-Ramirez, 2003)

$$\int_0^t \int_0^{t_{v-1}} \dots \int_0^{t_1} \tau^\alpha x(\tau) dt_{v-1} \dots dt_1 d\tau \quad (63)$$

$$= \int_0^t \frac{(t-\tau)^{v-1}}{(v-1)!} \tau^\alpha x(\tau) d\tau \quad (64)$$

Matrices P and Q are then expressed as

$$\mathbf{P}(t) = \begin{pmatrix} P_{11}(t) & P_{12}(t) & 0 & 0 \\ P_{21}(t) & P_{22}(t) & 0 & 0 \\ P_{31}(t) & P_{32}(t) & P_{33}(t) & 0 \\ P_{41}(t) & P_{42}(t) & 0 & P_{44}(t) \end{pmatrix} \quad (65)$$

$$\mathbf{Q}(t) = (Q_1(t) \quad Q_2(t) \quad Q_3(t) \quad Q_4(t))^T \quad (66)$$

with

$$\begin{aligned} P_{11}(t) &= \int_0^t \left(-\frac{(t-s)^3}{3} s + \frac{(t-s)^2}{2} s^2 \right) y_2(s) ds \\ &+ \int_0^t \left(\frac{(t-s)^3}{3} + 2(t-s)^2 s - (t-s)s^2 \right) y_1(s) ds \\ P_{12}(t) &= \int_0^t \frac{(t-s)^3}{6} s^2 y_2(s) ds \\ &+ \int_0^t \left(\frac{(t-s)^3}{3} s - \frac{(t-s)^2}{2} s^2 \right) y_1(s) ds \\ P_{21}(t) &= \int_0^t \left(\frac{(t-s)^3}{2} s^2 - \frac{(t-s)^2}{2} s^3 \right) y_2(s) ds \\ &+ \int_0^t \left((t-s)^3 s - 3(t-s)^2 s^2 + (t-s)s^3 \right) y_1(s) ds \\ P_{22}(t) &= \int_0^t -\frac{(t-s)^3}{6} s^2 y_2(s) ds \\ &+ \int_0^t \left(-\frac{(t-s)^3}{2} s^2 + \frac{(t-s)^2}{2} s^3 \right) y_1(s) ds \\ P_{31}(t) &= \int_0^t \left(\frac{(t-s)^4}{24} + \frac{(t-s)^3}{6} s - \frac{(t-s)^2}{2} s^2 \right) y_2(s) ds \\ &+ \int_0^t \left(\frac{-3(t-s)^2}{2} s + (t-s)s^2 \right) y_1(s) ds + \frac{t^4}{24} y_1(0) \\ P_{32}(t) &= \int_0^t \left(-\frac{(t-s)^4}{24} s - \frac{(t-s)^3}{6} s^2 \right) y_2(s) ds \\ &+ \int_0^t \left(\frac{-(t-s)^4}{24} - \frac{(t-s)^3}{6} s + \frac{(t-s)^2}{2} s^2 \right) y_1(s) ds \end{aligned}$$

$$\begin{aligned}
P_{33}(t) &= -\frac{t^4}{24} \\
P_{41}(t) &= \int_0^t \frac{(t-s)^2}{2} s y_2(s) ds \\
&\quad + \int_0^t \left(\frac{(t-s)^2}{2} - (t-s)s \right) y_1(s) ds - \frac{t^4}{24} y_2(0) \\
P_{42}(t) &= \int_0^t \left(\frac{(t-s)^4}{24} + \frac{(t-s)^3}{6} s \right) y_2(s) ds \\
&\quad + \int_0^t -\frac{(t-s)^2}{2} s y_1(s) ds + \frac{t^4}{24} y_1(0) \\
P_{44}(t) &= -\frac{t^4}{24}
\end{aligned}$$

$$\begin{aligned}
Q_1(t) &= hT(r_{ci} - r_{gy}) \int_0^t \left(-\frac{(t-s)^3}{6} s + \frac{(t-s)^2}{2} s^2 \right) \beta(s) ds \\
&\quad + \int_0^t \left(\frac{(t-s)^3}{3} - 2(t-s)^2 s + (t-s)s^2 \right) y_2(s) ds \\
&\quad - \int_0^t \left(3(t-s)^2 - 6(t-s)s + s^2 \right) y_1(s) ds + \frac{t^3}{3} y_1(0)
\end{aligned}$$

$$\begin{aligned}
Q_2(t) &= hT(r_{ci} - r_{gy}) \int_0^t \left(\frac{(t-s)^3}{2} s^2 - \frac{(t-s)^2}{2} s^3 \right) \beta(s) ds \\
&\quad + \int_0^t \left(-(t-s)^3 s + 3(t-s)^2 s^2 - (t-s)s^3 \right) y_2(s) ds \\
&\quad + \int_0^t \left(-(t-s)^3 + 9(t-s)^2 s - 9(t-s)s^2 + s^3 \right) \\
&\quad \times y_1(s) ds
\end{aligned}$$

$$\begin{aligned}
Q_3(t) &= -hT(r_{ci} - r_{gy}) \int_0^t \left(-\frac{(t-s)^4}{24} - \frac{(t-s)^3}{6} s \right. \\
&\quad \left. + \frac{(t-s)^2}{2} s^2 \right) \beta(s) ds \\
&\quad + \int_0^t \left(\frac{3(t-s)^2}{2} s - (t-s)s^2 \right) y_2(s) ds \\
&\quad + \int_0^t \left(\frac{3(t-s)^2}{2} - 5(t-s)s + s^2 \right) y_1(s) ds \\
&\quad - \frac{t^4}{24} y_2(0)
\end{aligned}$$

$$\begin{aligned}
Q_4(t) &= -hT(r_{ci} - r_{gy}) \int_0^t -\frac{(t-s)^2}{2} s \beta(s) ds \\
&\quad + \int_0^t \left(-\frac{(t-s)^2}{2} + (t-s)s \right) y_2(s) ds \\
&\quad + \int_0^t \left(2(t-s) - s \right) y_2(s) ds \\
&\quad - \frac{t^2}{2} y_1(0) - K \frac{t^4}{24} \beta(0)
\end{aligned}$$



Contents lists available at ScienceDirect

Systems & Control Letters

journal homepage: www.elsevier.com/locate/sysconle

Stabilization for a chain of saturating integrators arising in the visual landing of aircraft with sampling[☆]



Laurent Burlion^a, Michael Malisoff^b, Frédéric Mazenc^{c,*}

^a Department of Mechanical and Aerospace Engineering, 98 Brett Road, Rutgers University, Piscataway, NJ 08854, USA

^b Department of Mathematics, Louisiana State University, Baton Rouge, LA 70803-4918, USA

^c Inria EPI DISCO, L2S-CNRS-CentraleSupélec, 3 rue Joliot Curie, 91192, Gif-sur-Yvette, France

ARTICLE INFO

Article history:

Received 19 March 2019

Received in revised form 30 October 2019

Accepted 4 November 2019

Available online xxxx

Keywords:

Stabilization

Vision-based control

Backstepping

Aircraft

ABSTRACT

We provide a new output feedback control design for a chain of saturating integrators with imprecise output measurements where the outputs can also contain delays and sampling. Using a backstepping approach that leads to pointwise delays in the control and a dynamic extension, we prove input-to-state stability using a new dynamic extension approach. We utilize our main result to solve a problem in the visual landing of aircraft in the glide phase in the presence of delayed and sampled image processing.

© 2019 Elsevier B.V. All rights reserved.

1. Introduction

This paper continues our development of more effective output feedback stabilization methods for cases where only delayed, imprecise, or sampled output measurements are available. We began by providing a novel backstepping approach in [1,2], where pointwise delays were present in the feedback even if current state values are available. Our work [3,4] then used the preceding backstepping approach to solve an output feedback control problem for a chain of saturated integrators with imprecise output measurements using an unbounded control and sampling. In the present work, we utilize our backstepping approach to solve a more challenging output stabilization problem for a chain of saturating integrators with imprecise measurements, output delays, and output sampling using a new dynamical extension; see the end of Sections 2 and 3.1 for detailed discussions on the potential advantages of this work compared with [3,4].

The work in this paper is a new development in a long history of research on stabilization under delays, bounded controls, and sampling. Some earlier work on bounded feedback controls includes the semi-global state and output feedback stabilization

results [5], which employ linear control laws inside saturations. For some linear and nonlinear systems, crucial regional [6] stability results were presented in [7] (using LMI methods [8,9]). Earlier bounded backstepping and forwarding methods lead to globally asymptotically stabilizing controls for some nonlinear systems; see [10] for bounded backstepping, and see [11,12] for forwarding methods. The delay systems literature consists largely of emulation methods (where the feedback control is designed without taking the delays in the state or output observations into account, and where one then studies the effects of state or output delays on the performance of the feedback control) and either reduction or prediction methods (which both use information about the measurement delays in the control design). However, a potential challenge in implementing standard prediction methods is that the methods usually lead to distributed terms in controls, which are terms involving an integral of past control values (but see [13] for sequential predictor or other alternative prediction methods that are free of distributed terms).

The backstepping designs from [1,2] circumvent the problem of determining Lie derivatives of the fictitious controls by introducing artificial delays in the control (which are called artificial because they are present even if current state values are available for measurement), and therefore are significantly different from prior backstepping methods. The artificial delays approach removes the smoothness requirement on the fictitious control that was present in previous backstepping approaches. The advantages of [1] are also present in the present work, which adapts the approach from [1] to solve a control problem for a chain of saturating integrators for a dynamics with outputs that occurs in the vision based [14] landing of aircraft. Since

[☆] Malisoff was partly supported by US National Science Foundation grant 1711299. A special case (Burlion et al. (2019)) of this work will appear in the Proceedings of the 58th IEEE Conference on Decision and Control; see Section 1 below for a comparison of this work with (Burlion et al. (2019)).

* Corresponding author.

E-mail addresses: laurent.burlion@rutgers.edu (L. Burlion), malisoff@lsu.edu (M. Malisoff), frederic.mazenc@l2s.centralesupelec.fr (F. Mazenc).

only imprecise, delayed, or sampled measurements of the two first state variables are available in this application, the regional or semi-global results mentioned above do not apply, nor can we apply [1] or extensions such as [2]. This motivates our new control, which is inspired by the forwarding theory from [15]. Our controls in the present work ensure input-to-state stability with respect to additive uncertainties in the output measurements using a saturated output feedback. Also, for a positive constant \bar{u} , we can ensure that our control is bounded by \bar{u} . This contrasts with our prior work [3,4] on chains of saturating integrators, where no amplitude constraints on the output feedback control could be satisfied and where the overshoot in the input-to-state stability estimate depends on both the additive uncertainty on the control and the maximum delay in the output measurements. See Section 3.1 for more discussion on the connections between this work and [3].

This paper improves on our preliminary conference version [16], which did not allow sampling or delays in the outputs and did not include complete proofs. Allowing delays or sampling in the outputs is motivated by the image processing in visual landing problems; see our illustration section below. However, methods such as those in [17,18], or [19] for quantifying the effects of sampling in feedback controls would not apply here, in part because of the saturations in the dynamics and imprecise output measurements (with a multiplicative uncertainty) which place our dynamics outside the scope of existing methods for control affine systems.

The notation will be simplified whenever no confusion would arise given the context. Given any constant $T > 0$, C_{in} denotes the set of all continuous functions $\phi : [-T, 0] \rightarrow \mathbb{R}^n$, which we call the set of all *initial functions*. We define $\mathcal{E}_t \in C_{in}$ by $\mathcal{E}_t(s) = \mathcal{E}(t+s)$ for all \mathcal{E} , $s \leq 0$, and $t \geq 0$ such that $t+s$ in the domain of \mathcal{E} . The usual Euclidean norm and the corresponding matrix norm are denoted by $|\cdot|$, and $|\cdot|_S$ (resp., $|\cdot|_\infty$) denotes the corresponding supremum over any set S (resp., essential supremum). For each constant $L > 0$, we use the usual saturation function $\text{sat}_L(x) = \max\{-L, \min\{L, x\}\}$. We use the standard definitions of input-to-state stability and class \mathcal{KL} and \mathcal{K}_∞ functions, as defined in [20, Chapter 4], and \mathcal{M} is the set of all functions of the form $\gamma+c$ where $\gamma \in \mathcal{K}_\infty$ and $c \geq 0$ is a constant. Let z_i denote the i th entry of any vector z for each index i .

2. Problem statement

The following system plays a valuable role in the study of the visual landing of aircraft:

$$\begin{cases} \dot{x}_1 = \text{sat}_{L_1}(x_2) \\ \dot{x}_2 = \text{sat}_{L_2}(x_3) \\ \dot{x}_3 = \text{sat}_{L_3}(u), \end{cases} \quad (1)$$

where $x = (x_1, x_2, x_3)$ is valued in \mathbb{R}^3 , the input u is valued in \mathbb{R} , and $L_i > 0$ is a known constant for $i = 1, 2, 3$. The available output measurements are

$$\begin{aligned} y_1(t) &= \eta(t)x_1(\sigma(t)) + \delta_1(t) \\ y_2(t) &= x_2(\sigma(t)) + \delta_2(t) \\ y_3(t) &= x_3(t), \end{aligned} \quad (2)$$

where δ_1, δ_2 and η are unknown but piecewise continuous functions for which there are known constants $\bar{\eta} > 1$, $\bar{\delta}_1 \geq 0$, and $\bar{\delta}_2 \geq 0$ such that for all $t \geq 0$, we have

$$\eta(t) \in [1, \bar{\eta}] \quad \text{and} \quad |\delta_i(t)| \leq \bar{\delta}_i \quad \text{for } i = 1, 2 \quad (3)$$

and the known piecewise continuous nondecreasing right continuous function $\sigma : \mathbb{R} \rightarrow \mathbb{R}$ admits a constant $\bar{\sigma} \geq 0$ such that

$t - \bar{\sigma} \leq \sigma(t) \leq t$ for all $t \geq 0$ and so can model measurement delays and sampling, e.g., by taking σ of the form $\sigma(t) = t_i - \bar{\sigma}_a$ for all $t \in [t_i, t_{i+1})$ and $i \geq 0$, where the times t_i are such that $t_0 = 0$ and such that there is a constant $\epsilon_0 > 0$ such that $\epsilon_0 \leq t_{i+1} - t_i \leq \bar{\sigma}_b$ for all $i \geq 0$, and where the nonnegative constants $\bar{\sigma}_a$ and $\bar{\sigma}_b$ are such that $\bar{\sigma}_a + \bar{\sigma}_b \leq \bar{\sigma}$; see Section 4. In particular, the delayed state components x_1 and x_2 are not assumed to be available for measurement (because in addition to delays, our y_1 and y_2 formulas allow sampling and additive or multiplicative uncertainty), so the available measurements are not simply the delayed states. This justifies calling (2) outputs, and calling our feedbacks output feedbacks. The assumption that x_3 is available for measurement is justified because only the first two state components are subjected to the sampling and uncertainties from image processing in the aerospace application; see Section 4. The additive uncertainties δ_i can be used to model the effects of uncertainty in the sample times t_i or in the delay $\bar{\sigma}_a$.

Given an appropriate positive constant \bar{u} , our goal is to design a control u that is valued in $[-\bar{u}, \bar{u}]$ and that can be computed from the outputs (2) and that renders (1) input-to-state stable with respect to $\delta = (\delta_1, \delta_2)$. Choosing $\bar{u} \in (0, L_3)$ allows us to avoid the saturation in (1). Since the state space for (1) is \mathbb{R}^3 , this implies as a special case that when $\delta = 0$, all solutions of (1) for all constant initial states $x(0) \in \mathbb{R}^3$ will converge to 0 as $t \rightarrow \infty$. Also, the input-to-state stability estimate will hold for all choices of the initial state. Our control will be a dynamic one that can be expressed the form $U(y_t, z_t)$, where the state $z(t)$ of the dynamic extension is computed using values y of the output, so we use an output feedback control. This contrasts with [4], which also studied (1) with the outputs (2), because in [4], the control was not required to be bounded, and also, [4] required the more stringent condition $\bar{\delta}_2 < L_1(1 - e^{-1})^2/(40(1 + 2e^{-1} + e^{-2}))$ and [4] only proved the weaker conclusion that the closed loop system was input-to-state stable with respect to $(\delta_1, \delta_2, \sigma)$, which produced a positive overshoot in the stability estimate even if the δ_i 's are zero. See also Section 4 for more on how this work is less restrictive than [4]. Hence, this paper provides potential advantages over [4], using a new dynamic extension which was not present in [4].

Requiring $\eta(t) \geq 1$ for all $t \geq 0$ is not restrictive because in practice, η will have known positive upper and lower bounds, and then we can divide the formula for the output component y_1 in (2) by $\inf\{\eta(\ell) : \ell \geq 0\}$ so the rescaled η and δ_1 are such that the rescaled η is bounded below by 1. Also, the outputs (2) are equivalent to assuming that the available measurements are $y_1(t) = \eta(\sigma(t))x_1(\sigma(t)) + \delta_1(t)$, $y_2(t) = x_2(\sigma(t)) + \delta_2(t)$, and $y_3(t) = x_3(t)$, because when the σ is also present in η , then we can define the new uncertainty $\eta_{\text{new}}(t) = \eta(\sigma(t))$ to obtain outputs of the form (2). Throughout this work, we assume that the initial functions are constant at the initial time $t_0 = 0$, so $x_i(t) = x_i(0)$ for all $t \leq 0$ for $i = 1, 2, 3$ and similarly for the other states.

3. Stabilization of the system (1)

3.1. Statement of main result

This section provides formulas for our output feedback control that we described in Section 2. Our construction improves on the main result from [3], because [3] did not allow sampling or delays in the outputs, and because [3] did not provide a way to satisfy input constraints on u , and because [3] only asserted a weaker ultimate boundedness result (without proof) and in particular did not prove convergence to the equilibrium when $\delta = 0$. Given the positive constant saturation levels L_1, L_2 , and L_3 from (1),

and the constant $\bar{\sigma} \geq 0$ from our requirement on σ from our output measurements (2), and the given bounds $\bar{\eta}$, $\bar{\delta}_1$, and $\bar{\delta}_2$ from our conditions (3), our control design will introduce several constants. These additional constants p_1 , p_2 , T , k , L_4 , $\bar{\alpha}_1$, and $\bar{\beta}_1$ will be required to satisfy additional conditions (7); see Section 4 for an illustration where (7) are satisfied, and Section 3.2 about the existence of solutions, and about how our conditions simplify in the significant special case where $\sigma(t) = t$ which is the case where there is no sampling or delays in the outputs.

Theorem 1. Consider the system with outputs (1)–(2). Let the constants $\bar{\sigma} \geq 0$, $\bar{\delta}_1 \geq 0$, $\bar{\delta}_2 \in [0, L_1]$, $L_1 > 0$, $L_2 > 0$, $L_3 > 0$, and $\bar{\eta} > 0$ satisfy the requirements from Section 2. Choose the control

$$u(t) = \begin{cases} 0, & t \in [0, 2T) \\ -\text{sat}_{L_4}(x_3(t) - v_1(z_t) - \beta(t)) \\ \quad + v_2(y_t, z_t) + v_3(y_t, z_t), & t \geq 2T \end{cases}, \text{ where} \quad (4a)$$

$$v_1(z_t) = \frac{k}{(1-e^{-kT})^2} (z_1(t) - z_2(t) - 2e^{-kT}z_1(t-T) + e^{-kT}z_2(t-T) + e^{-2kT}z_1(t-2T)), \quad (4b)$$

$$v_2(y_t, z_t) = \frac{k^2}{(1-e^{-kT})^2} (-2z_1(t) + z_2(t) + 4e^{-kT}z_1(t-T) - e^{-kT}z_2(t-T) - 2e^{-2kT}z_1(t-2T) + \phi(t) - 2e^{-kT}\phi(t-T) + e^{-2kT}\phi(t-2T)), \text{ and} \quad (4c)$$

$$v_3(y_t, z_t) = \frac{k}{1-e^{-kT}} (-z_3(t) + e^{-kT}z_3(t-T) + \omega(t) - e^{-kT}\omega(t-T)) \quad (4d)$$

where the z_i 's are the states of the dynamic extension

$$\begin{cases} \dot{z}_1(t) = k[-z_1(t) + \phi(t)] \\ \dot{z}_2(t) = k[-z_2(t) + z_1(t) - e^{-kT}z_1(t-T)] \\ \dot{z}_3(t) = k[-z_3(t) + \omega(t)] \end{cases} \quad (5)$$

with the initial condition $z(\ell) = 0$ for all $\ell \in [-2T - \bar{\sigma}, 0]$, and where

$$\phi(t) = -\frac{\bar{\alpha}_1}{p_1} \text{sat}_{p_1}(y_1(t)) \text{ and} \quad (6a)$$

$$\omega(t) = -\frac{\bar{\beta}_1}{p_2} \text{sat}_{p_2}(y_2(t) - \alpha(\sigma(t))) \text{ and}$$

$$\alpha(t) = \frac{z_2(t) - e^{-kT}z_2(t-T)}{(1-e^{-kT})^2} \text{ and} \quad (6b)$$

$$\beta(t) = \frac{z_3(t) - e^{-kT}z_3(t-T)}{1-e^{-kT}},$$

and where the positive constants p_1 , p_2 , T , k , L_4 , $\bar{\alpha}_1$, and $\bar{\beta}_1$ and the model parameters are assumed to satisfy

$$\bar{\beta}_1 + \bar{\alpha}_2 < L_2 \quad (7a)$$

$$\bar{\sigma}\bar{\beta}_1 + 2\bar{\alpha}_1 + \bar{\delta}_2 < L_1 \quad (7b)$$

$$L_4 + \bar{\alpha}_3 + \bar{\beta}_2 < L_3 \quad (7c)$$

$$\bar{\eta}(\bar{\sigma} + T)\bar{\alpha}_1 + \bar{\delta}_1 < p_1 \quad (7d)$$

$$\bar{\alpha}_1\bar{\eta}^2(2T + \bar{\sigma}) < p_1 \quad (7e)$$

$$(\bar{\sigma} + T)\bar{\beta}_1 + \bar{\delta}_2 < p_2 \quad (7f)$$

$$2\bar{\beta}_1(T + \bar{\sigma}) < p_2 \quad (7g)$$

$$\frac{\bar{\alpha}_1\bar{\eta}}{p_1}(2T + \bar{\sigma}) \left(\bar{\alpha}_1 + \xi_* + \frac{\bar{\alpha}_1}{p_1}\bar{\delta}_1 \right) + \xi_* + \frac{\bar{\alpha}_1}{p_1}\bar{\delta}_1 < \frac{\bar{\alpha}_1}{\bar{\eta}} \quad (7h)$$

where

$$\xi_* = \frac{\bar{\delta}_2(\bar{\beta}_1(T + \bar{\sigma}) + p_2)}{p_2\sqrt{1 - \frac{2}{p_2}\bar{\beta}_1(T + \bar{\sigma})}}, \quad \bar{\alpha}_2 = \frac{2k\bar{\alpha}_1}{1 - e^{-kT}}, \quad (8)$$

$$\bar{\alpha}_3 = \frac{4k^2\bar{\alpha}_1}{(1 - e^{-kT})^2}, \quad \text{and} \quad \bar{\beta}_2 = \frac{2k\bar{\beta}_1}{1 - e^{-kT}}.$$

Then the following conclusions hold: (a) The control u in (4a) is bounded by $L_4 + \bar{\alpha}_3 + \bar{\beta}_2$ and (b) the system (1) in closed loop with the control (4a) satisfies an input-to-state stability estimate with respect to $\delta = (\delta_1, \delta_2)$ for all initial states $x(0) \in \mathbb{R}^3$.

3.2. Consistency of conditions (7), existence of solutions, and special cases

This section explains how to satisfy (7), how (7) reduces to the type of conditions from [3] in the case $\sigma(t) = t$, and why the existence of solutions of the closed loop system is assured. For given constants $\bar{\sigma}$, L_1 , L_2 , L_3 , $\bar{\eta}$, $\bar{\delta}_1$, and $\bar{\delta}_2$ in our theorem, we can satisfy (7) using the following three step process. First, choose any positive constants k and T . Second, choose the positive constants $\bar{\alpha}_1$, $\bar{\beta}_1$, and L_4 to be small enough so that (7a)–(7c) are satisfied, which can be done because of our assumption that $\bar{\delta}_2 < L_1$ and because of our formulas for $\bar{\alpha}_3$ and $\bar{\beta}_2$ from (8). Finally, choose the positive constants p_1 and p_2 to satisfy the remaining conditions from (7), which can be done when $\bar{\delta}_2$ is small enough, because of the way p_1 and p_2 appear in denominators in (7h) and (8); see Section 4. The existence of a unique solution for each constant initial state (such that the solution is defined for all $t \geq 0$) follows because of the linear growth of the right side of closed loop dynamics, the boundedness of the nonlinear terms, and standard existence and uniqueness results from basic theory of differential equations.

Since Theorem 1 ensures input-to-state stability, it provides robustness with respect to slight modifications of the system (such as the image processing method in the application). In the special case where there is neither sampling nor delays, we can pick $\sigma(t) = t$ for all real t and therefore $\bar{\sigma} = 0$ in (7). However, our method does not allow us to choose $T = 0$, because (4b)–(4d), (6b), and (8) would not be defined for $T = 0$, and because our choices of α and β in (6b) are essential for producing a system in new variables that lends itself to proving stability results; see (15). Hence, the only simplifications in our control when there is no sampling or delays in (2) are that (i) we replace $\sigma(t)$ by t in (2) and in our formula for the function ω in (6a) and (ii) we replace $\bar{\sigma}$ by 0 in (7)–(8). In particular, the control design does not significantly simplify in the absence of delays or sampling. Then our conditions in Theorem 1 are similar to those of [3] (and we recover conditions from [16] in the limit as $\bar{\sigma} \rightarrow 0$), but [3] only asserted a weaker ultimate boundedness result. Another important case is where the δ_i 's are zero, in which case we can set $\bar{\delta}_1 = \bar{\delta}_2 = 0$ in (7) and we can conclude that the closed loop system is uniformly globally asymptotically stable on \mathbb{R}^3 . This highlights a distinction between the delay $T > 0$ in our control design and the output delay that can be represented by our function σ in (2), which is that T is an artificial delay that is introduced in the control (and cannot be removed) and that T does not correspond to a delay in engineering system that is being modeled, while σ can model a delay in the engineering system.

3.3. Key lemmas needed for proving Theorem 1

A key idea in our proof of Theorem 1 is to show that for large enough times, the saturations in our system and in our control

can be removed, because their arguments will lie in the intervals in which the saturations agree with the identity function. To make this idea precise, and to help readers grasp the technical steps of our proof of [Theorem 1](#), we first state lemmas, for which we provide proofs in the appendices below. Our first lemma is as follows, whose conclusions [\(9a\)](#) and [\(9c\)](#) can be combined to give the bound $L_4 + \bar{\alpha}_3 + \bar{\beta}_2$ on our control u :

Lemma 1. *In terms of the notation from [Theorem 1](#), we have*

$$u(t) = -\text{sat}_{L_4}(x_3(t) - \dot{\alpha}(t) - \beta(t)) + \ddot{\alpha}(t) + \dot{\beta}(t), \quad (9a)$$

$$\alpha(t) = \frac{k^2}{(1 - e^{-kT})^2} \int_{t-T}^t \int_{m-T}^m e^{k(\ell-t)} \phi(\ell) d\ell dm, \quad (9b)$$

$$\beta(t) = \frac{k}{1 - e^{-kT}} \int_{t-T}^t e^{k(\ell-t)} \omega(\ell) d\ell,$$

$$\begin{aligned} |\alpha(t)| &\leq \bar{\alpha}_1, & |\dot{\alpha}(t)| &\leq \bar{\alpha}_2, & |\ddot{\alpha}(t)| &\leq \bar{\alpha}_3, \\ |\beta(t)| &\leq \bar{\beta}_1, & \text{and } |\dot{\beta}(t)| &\leq \bar{\beta}_2 \end{aligned} \quad (9c)$$

for all $t \geq 2T$.

The next lemma follows from the Fundamental Theorem of Calculus, so we omit its proof:

Lemma 2. *Let k and T be any positive constants. Then the relations*

$$\begin{aligned} \int_{t-T}^t \int_{m-T}^m e^{k(\ell-t)} d\ell dm &= \frac{1}{k^2} (1 - e^{-kT})^2 \quad \text{and} \\ \int_{t-T}^t e^{k(\ell-t)} d\ell &= \frac{1}{k} (1 - e^{-kT}) \end{aligned} \quad (10)$$

hold for all $t \geq 0$.

To realize our goal of eliminating the effects of the saturations, we will find class \mathcal{M} functions \mathcal{T} so that certain scalar variables $q(t)$ stay within suitable intervals $[-\bar{M}, \bar{M}]$ for all $t \geq \mathcal{T}(|q(T_0)|)$ and suitable times T_0 , which will be useful for realizing our strategy of removing saturations in the course of our proof. The following lemma will allow us to find the required class \mathcal{M} functions, and we prove this lemma in [Appendix B](#):

Lemma 3. *Let $\mathcal{G} : \mathbb{R}^2 \rightarrow \mathbb{R}$ be a bounded continuous function that admits positive constants g_0 , T_0 , and \bar{M} and a function $g : \mathbb{R} \rightarrow [0, \infty)$ such that $\mathcal{G}(t, q) = g(t)q$ for all $t \geq T_0$ and all $q \in [-\bar{M}, \bar{M}]$ and such that $\mathcal{G}(t, q)\text{sign}(q) \geq g_0$ holds for all $t \geq T_0$ and $q \in \mathbb{R} \setminus [-\bar{M}, \bar{M}]$. Let $\mathcal{H} : [0, \infty) \rightarrow \mathbb{R}$ be a bounded continuous function that admits constants $\bar{T} > T_0$ and $\bar{H} > 0$ such that $|\mathcal{H}(t)| \leq \bar{H}$ for all $t \geq \bar{T}$ and such that $\bar{H} < g_0$. Then there exists a function $T_* \in \mathcal{M}$ such that for each C^1 solution $q : [T_0, \infty) \rightarrow \mathbb{R}$ of*

$$\dot{q}(t) = -\mathcal{G}(t, q(t)) + \mathcal{H}(t), \quad (11)$$

we have $|q(t)| \leq \bar{M}$ for all $t \geq T_*(|q(T_0)|)$ and therefore also $\dot{q}(t) = -g(t)q(t) + \mathcal{H}(t)$ for all $t \geq T_*(|q(T_0)|)$.

Finally, we need this variant of Halanay's inequality, which generalizes [\[21, Lemma 4.2\]](#) to allow nonzero values of Δ_1 , and which we prove in [Appendix C](#) and which is used in our Lyapunov analysis in [Section 3.4.2](#):

Lemma 4. *Consider a continuous function $v : [-h, +\infty) \rightarrow [0, +\infty)$ with $h > 0$ being a constant. Assume that there are constants $\Delta_1 \geq 0$, c_1 , and c_2 satisfying $c_1 > c_2 > 0$ such that the inequality*

$$\dot{v}(t) \leq -c_1 v(t) + c_2 \sup_{m \in [t-h, t]} v(m) + \Delta_1 \quad (12)$$

is satisfied for all $t \geq 0$. Choose $c_s > 0$ to be the unique positive value such that $c_s = c_1 - c_2 e^{c_s h}$, and let $l_v > 0$ be a constant such that $l_v e^{-c_s t} > v(t) - \Delta_1 / (c_1 - c_2)$ for all $t \in [-h, 0]$. Then

$$v(t) \leq l_v e^{-c_s t} + \frac{\Delta_1}{c_1 - c_2} \quad (13)$$

holds for all $t \geq 0$.

3.4. Proof of [Theorem 1](#)

The proof is arranged as follows. In the first step, we use a change of variables that produces a useful cascaded system with a globally asymptotically stable subsystem; see [\(16\)](#). In the second step, we perform a Lyapunov function analysis for this new system. In the third step, we use results from the first two steps to find useful bounds on the states of the original system. In the last step, we use linear growth properties of the closed loop system to transform the preceding estimates into the required input-to-state stability estimate.

3.4.1. First step: system in new variables with asymptotically stable subsystem

We use the new variable $\xi = (x_1, \xi_2, \xi_3)$, where

$$\xi_2(t) = x_2(t) - \alpha(t) \quad \text{and} \quad \xi_3(t) = x_3(t) - \dot{\alpha}(t) - \beta(t). \quad (14)$$

Direct calculations then transform [\(1\)](#) into the new system

$$\begin{aligned} \dot{x}_1(t) &= \text{sat}_{L_1}(\alpha(t) + \xi_2(t)), \\ \dot{\xi}_2(t) &= \text{sat}_{L_2}(\beta(t) + \xi_3(t) + \dot{\alpha}(t)) - \dot{\alpha}(t), \\ \dot{\xi}_3(t) &= \text{sat}_{L_3}(u) - \ddot{\alpha}(t) - \dot{\beta}(t). \end{aligned} \quad (15)$$

Notice that the system [\(15\)](#) in closed-loop with [\(4a\)](#) is forward complete, by the forward completeness of our dynamic extension [\(5\)](#), meaning, all of its solutions are defined for all $t \geq 0$ for all constant initial functions at the initial time $t_0 = 0$ (which follows from the boundedness of the nonlinear terms in [\(5\)](#)). Also, [\(9c\)](#) and [\(7c\)](#) imply that $|u(t)| = |\text{sat}_{L_4}(\xi_3(t)) + \ddot{\alpha}(t) + \dot{\beta}(t)| \leq L_4 + \bar{\alpha}_3 + \bar{\beta}_2 < L_3$ holds for all $t \geq 2T$. As an immediate consequence, the system [\(15\)](#) in closed loop with the feedback defined in [\(4a\)](#) admits the representation

$$\begin{aligned} \dot{x}_1(t) &= \text{sat}_{L_1}(\alpha(t) + \xi_2(t)), \\ \dot{\xi}_2(t) &= \text{sat}_{L_2}(\beta(t) + \xi_3(t) + \dot{\alpha}(t)) - \dot{\alpha}(t), \\ \dot{\xi}_3(t) &= -\text{sat}_{L_4}(\xi_3(t)) \end{aligned} \quad (16)$$

for all $t \geq 2T$. Since the ξ_3 subsystem of [\(16\)](#) is globally asymptotically stable to 0 on \mathbb{R} , we deduce from [\(7a\)](#) and the bounds [\(9c\)](#) that there is a class \mathcal{M} function $T_b : [0, +\infty) \rightarrow [2T, +\infty)$ (depending on $\bar{\beta}_1$ and $\bar{\alpha}_2$) such that for all $t \geq T_b(|\xi(0)|)$, we have $|\beta(t) + \xi_3(t) + \dot{\alpha}(t)| \leq \bar{\beta}_1 + \bar{\alpha}_2 + |\xi_3(t)| < L_2$. Hence, we obtain the system

$$\dot{x}_1(t) = \text{sat}_{L_1}(\alpha(t) + \xi_2(t)), \quad \dot{\xi}_2(t) = \beta(t) + \xi_3(t) \quad (17)$$

for all $t \geq T_b(|\xi(0)|)$. Using the formulas $y_1(t) = \eta(t)x_1(\sigma(t)) + \delta_1(t)$ and $y_2(t) = \alpha(\sigma(t)) + \delta_2(t) - \alpha(\sigma(t)) = \xi_2(\sigma(t)) + \delta_2(t)$ for our output components (which follow from [\(2\)](#) and [\(14\)](#)), and also using our formulas for ϕ and ω from [\(6a\)](#) and [\(9b\)](#), we can then rewrite [\(17\)](#) as

$$\left\{ \begin{aligned} \dot{x}_1(t) &= \text{sat}_{L_1} \left(-\frac{k^2 \bar{\alpha}_1}{(1 - e^{-kT})^2 p_1} \right. \\ &\quad \times \int_{t-T}^t \int_{m-T}^m e^{k(\ell-t)} \text{sat}_{p_1}(\eta(\ell)x_1(\sigma(\ell))) d\ell dm \\ &\quad \left. + \mathcal{J}_1(t) \right) \\ \dot{\xi}_2(t) &= -\frac{\bar{\beta}_1 k}{p_2(1 - e^{-kT})} \int_{t-T}^t e^{k(\ell-t)} \text{sat}_{p_2}(\xi_2(\sigma(\ell))) d\ell + \mathcal{J}_2(t), \end{aligned} \right. \quad (18a)$$

where $\mathcal{J}_1(t) = \text{sat}_{L_1} \left(-\frac{k^2 \bar{\alpha}_1}{(1 - e^{-kT})^2 p_1} \right)$
 $\times \int_{t-T}^t \int_{m-T}^m e^{k(\ell-t)} \text{sat}_{p_1}(\eta(\ell)x_1(\sigma(\ell)) + \delta_1(\ell)) d\ell dm + \xi_2(t)$
 $-\text{sat}_{L_1} \left(-\frac{k^2 \bar{\alpha}_1}{(1 - e^{-kT})^2 p_1} \int_{t-T}^t \int_{m-T}^m e^{k(\ell-t)} \text{sat}_{p_1}(\eta(\ell)x_1(\sigma(\ell))) d\ell dm \right)$
 and $\mathcal{J}_2(t) = \frac{\bar{\beta}_1 k}{p_2(1 - e^{-kT})}$
 $\times \int_{t-T}^t e^{k(\ell-t)} [\text{sat}_{p_2}(\xi_2(\sigma(\ell))) - \text{sat}_{p_2}(\xi_2(\sigma(\ell)) + \delta_2(\ell))] d\ell$
 $+ \xi_3(t)$ (18b)

for all $t \geq T_b(|\xi(0)|)$. The formulas (18a) will play an important role in what follows, because we will use the $\xi_2(t)$ formula from (18a) to find an upper bound for $|\xi_2(t)|$ in terms of $|\bar{\delta}_1, \bar{\delta}_2|$ and an additional term that converges to 0, and then we will use the $\dot{x}_1(t)$ formula from (18a) to obtain an analogous bound for $|x_1(t)|$; see (31). This will lead to the desired conclusion for the system in the original variables.

By (7b), we have $\bar{\alpha}_1 < L_1$, and sat_{p_1} is bounded by p_1 , so (18a) and the first equality in (10) give

$$\dot{x}_1(t) = -\frac{k^2 \bar{\alpha}_1}{(1 - e^{-kT})^2 p_1} \times \int_{t-T}^t \int_{m-T}^m e^{k(\ell-t)} \text{sat}_{p_1}(\eta(\ell)x_1(\sigma(\ell))) d\ell dm + \mathcal{J}_1(t)$$
 (19)

for all $t \geq T_b(|\xi(0)|)$. Finally, since saturations have the global Lipschitz constant 1, we can check that

$$|\mathcal{J}_2(t)| \leq |\xi_3(t)| + \frac{\bar{\beta}_1}{p_2} \bar{\delta}_2 \quad \text{and} \quad |\mathcal{J}_1(t)| \leq |\xi_2(t)| + \frac{\bar{\alpha}_1}{p_1} \bar{\delta}_1$$
 (20)
 for all $t \geq T_b(|\xi(0)|)$,

by (10). We next analyze the stability properties of the system (18a).

By adding and subtracting $(\bar{\beta}_1/p_2) \text{sat}_{p_2}(\xi_2(t))$ on the right side of the $\dot{\xi}_2(t)$ formula in (18a) and then using the second equality in (10), it follows that, for all $t \geq T_b(|\xi(0)|) + \bar{\sigma} + T$,

$$\dot{\xi}_2(t) = -\frac{\bar{\beta}_1}{p_2} \text{sat}_{p_2}(\xi_2(t)) + \mathcal{R}_1(t) + \mathcal{J}_2(t), \quad \text{where} \quad (21a)$$

$$\mathcal{R}_1(t) = \frac{\bar{\beta}_1 k}{p_2(1 - e^{-kT})} \times \int_{t-T}^t e^{k(\ell-t)} \left[\text{sat}_{p_2}(\xi_2(t)) - \text{sat}_{p_2} \left(\xi_2(t) - \int_{\sigma(\ell)}^t \dot{\xi}_2(s) ds \right) \right] d\ell.$$
 (21b)

Moreover, by (9c) and (17), we have $|\dot{\xi}_2(t)| \leq |\xi_3(t)| + \bar{\beta}_1$. As a consequence, for all $t \geq T_b(|\xi(0)|) + T + \bar{\sigma}$, we have

$$|\mathcal{R}_1(t)| \leq \frac{\bar{\beta}_1 k}{p_2(1 - e^{-kT})} \times \int_{t-T}^t e^{k(\ell-t)} (t - \sigma(\ell)) d\ell \left(|\xi_3|_{[t-T-\bar{\sigma}, t]} + \bar{\beta}_1 \right) \leq \frac{\bar{\beta}_1}{p_2} (T + \bar{\sigma}) \times (|\xi_3|_{[t-T-\bar{\sigma}, t]} + \bar{\beta}_1)$$
 (22)

where the last inequality in (22) used (10) and the bounds $\ell - \bar{\sigma} \leq \sigma(\ell)$ to get $t - \sigma(\ell) \leq t - \ell + \bar{\sigma} \leq T + \bar{\sigma}$ for all $\ell \in [t - T, t]$. The

second inequality in (22) and the first inequality in (20) yield

$$|\mathcal{R}_1(t)| + |\mathcal{J}_2(t)| \leq \frac{\bar{\beta}_1}{p_2} [(T + \bar{\sigma}) (|\xi_3|_{[t-T-\bar{\sigma}, t]} + \bar{\beta}_1) + \bar{\delta}_2] + |\xi_3(t)|$$
 (23)

for all $t \geq T_b(|\xi(0)|) + T + \bar{\sigma}$. Since the ξ_3 subsystem is globally asymptotically stable to 0, we deduce from (23) and (7f) that there is a class \mathcal{M} function $T_c : [0, +\infty) \rightarrow [0, +\infty)$ and a constant $\delta_0 > 0$ such that

$$\sup_{\ell \geq T_c(|\xi(0)|)} (|\mathcal{R}_1(\ell)| + |\mathcal{J}_2(\ell)|) \leq \frac{\bar{\beta}_1}{p_2} [(T + \bar{\sigma}) \bar{\beta}_1 + \bar{\delta}_2] + \delta_0 < \bar{\beta}_1.$$
 (24)

Hence, by (21a), there is a class \mathcal{M} function $T_d : [0, +\infty) \rightarrow [0, +\infty)$ such that $T_d(s) \geq T_b(s) + T + \bar{\sigma}$ for all $s \geq 0$ and such that $|\xi_2(t)| < p_2$ for all $t \geq T_d(|\xi(0)|)$, because $\dot{\xi}_2 > 0$ (resp., < 0) when $\xi_2(t) \leq -p_2$ (resp., $\geq p_2$). Then for all $t \geq T_d(|\xi(0)|)$, we have $\text{sat}_{p_2}(\xi_2(t)) = \xi_2(t)$, so (21a) gives the reduced order system

$$\begin{cases} \dot{x}_1(t) = -\frac{k^2 \bar{\alpha}_1}{(1 - e^{-kT})^2 p_1} \times \int_{t-T}^t \int_{m-T}^m e^{k(\ell-t)} \text{sat}_{p_1}(\eta(\ell)x_1(\sigma(\ell))) d\ell dm + \mathcal{J}_1(t) \\ \dot{\xi}_2(t) = -\frac{\bar{\beta}_1}{p_2} \xi_2(t) + \mathcal{R}_1(t) + \mathcal{J}_2(t) \end{cases}$$
 (25)

in the new variables from (14) for all $t \geq T_d(|\xi(0)|)$. This follows by applying Lemma 3 to the system (21a), by choosing $q = \xi_2$, $\mathcal{G}(t, q) = (\bar{\beta}_1/p_2) \text{sat}_{p_2}(q)$, $g(t) = \bar{\beta}_1/p_2$, $\bar{M} = p_2$, and $\mathcal{H} = \mathcal{R}_1 + \mathcal{J}_2$ in the lemma, and using the fact that $|\xi| \geq |\xi_2|$.

3.4.2. Second step: Lyapunov analysis for reduced order system (25) in new variables

This step will use the candidate Lyapunov function $\Upsilon(\xi_2) = \frac{1}{2} \xi_2^2$. By (21b) and the second equality in (10), we get

$$|\mathcal{R}_1(t)| \leq \frac{\bar{\beta}_1 k}{p_2(1 - e^{-kT})} \int_{t-T}^t e^{k(\ell-t)} \int_{\sigma(\ell)}^t |\dot{\xi}_2(s)| ds d\ell \leq \frac{\bar{\beta}_1}{p_2} \int_{t-T-\bar{\sigma}}^t |\dot{\xi}_2(s)| ds$$
 (26)

for all $t \geq T_d(|\xi(0)|)$, because sat_{p_2} has the Lipschitz constant 1. By using (18a) to upper bound $|\dot{\xi}_2(s)|$ in (26), we deduce from the second inequality in (26) that for all $t \geq T_d(|\xi(0)|)$, we have

$$|\mathcal{R}_1(t)| \leq \frac{\bar{\beta}_1^2 k}{p_2^2(1 - e^{-kT})} \int_{t-T-\bar{\sigma}}^t \int_{s-T}^s e^{k(\ell-s)} d\ell ds \times \sup_{m \in [t-2T-2\bar{\sigma}, t]} |\xi_2(m)| + \frac{\bar{\beta}_1}{p_2} \int_{t-T-\bar{\sigma}}^t |\mathcal{J}_2(s)| ds \leq \frac{\bar{\beta}_1^2 (T + \bar{\sigma})}{p_2^2} \sup_{m \in [t-2T-2\bar{\sigma}, t]} |\xi_2(m)| + \frac{\bar{\beta}_1 (T + \bar{\sigma})}{p_2} \left(\frac{\bar{\beta}_1}{p_2} \bar{\delta}_2 + |\xi_3|_{[t-T-\bar{\sigma}, t]} \right),$$
 (27)

where the last inequality is a consequence of the second equality in (10) and of the first inequality in (20). By using the first inequality in (20) and (27) to bound \mathcal{R}_1 and \mathcal{J}_2 from (25), we easily deduce from the asymptotic stability of the ξ_3 subsystem

of (16) that for any constant $\omega_0 > 0$, we have

$$\begin{aligned} \dot{\gamma}(t) &\leq \frac{\bar{\beta}_1}{p_2} \left(-\xi_2^2(t) + \frac{\bar{\beta}_1(T + \bar{\sigma})}{p_2} \sup_{m \in [t-2T-2\bar{\sigma}, t]} \xi_2^2(m) \right. \\ &\quad \left. + |\xi_2(t)| \left[\left\{ \left(\frac{\bar{\beta}_1}{p_2}(T + \bar{\sigma}) + 1 \right) \bar{\delta}_2 \right\} + \mu(|\xi(0)|, t) \right] \right) \\ &\leq \frac{\bar{\beta}_1}{p_2} \left(-\gamma(\xi_2(t)) + \frac{2\bar{\beta}_1(T + \bar{\sigma})}{p_2} \right. \\ &\quad \left. \times \sup_{m \in [t-2T-2\bar{\sigma}, t]} \gamma(\xi_2(m)) + \frac{1}{2} B_*(t) \right), \end{aligned} \quad (28)$$

along all solutions of (25) for all $t \geq T_d(|\xi(0)|) + T + \bar{\sigma}$, where

$$\begin{aligned} B_*(t) &= (1 + \omega_0) \left(\frac{\bar{\beta}_1}{p_2}(T + \bar{\sigma}) + 1 \right)^2 \bar{\delta}_2^2 \\ &\quad + \left[\left(1 + \frac{1}{\omega_0} \right) \mu^2(|\xi(0)|, t) \right], \end{aligned} \quad (29)$$

and where the last inequality in (28) used the triangle inequality $ab \leq \frac{1}{2}a^2 + \frac{1}{2}b^2$ with $a = |\xi_2(t)|$ and b being the quantity in squared brackets in (28) (followed by a use of the relation $(r + s)^2 \leq (1 + \omega_0)r^2 + (1 + (1/\omega_0))s^2$ where r is the quantity in curly braces in (28) and $s = \mu(|\xi(0)|, t)$), and where μ is a class \mathcal{KL} function. Since $\mu \in \mathcal{KL}$, we can then find a class \mathcal{M} function $T_d^\# : [0, +\infty) \rightarrow [0, +\infty)$ such that $T_d^\#(s) \geq T_d(s) + T$ for all $s \geq 0$ and such that $\mu(|\xi(0)|, t) \leq \omega_0$ for all $t \geq T_d^\#(|\xi(0)|)$, and therefore such that the quantity in squared brackets in (29) is bounded above by $\omega_0 + \omega_0^2$ for all $t \geq T_d^\#(|\xi(0)|)$. Therefore, for any constant $\epsilon > 0$, we can choose $\omega_0 > 0$ small enough (with ω_0 depending on ϵ and the other parameters) such that

$$\begin{aligned} &\sqrt{B_*(t)\bar{\beta}_1/(p_2(c_1 - c_2))} \\ &\leq \left(\sqrt{1 + \omega_0} \left(\frac{\bar{\beta}_1}{p_2}(T + \bar{\sigma}) + 1 \right) \bar{\delta}_2 + \sqrt{\omega_0 + \omega_0^2} \right) \\ &\quad \times \sqrt{\frac{\bar{\beta}_1}{p_2(c_1 - c_2)}} < \xi_*(1 + \epsilon) \end{aligned} \quad (30)$$

for all $t \geq T_d^\#(|\xi(0)|)$, where ξ_* is from (8), $c_1 = \bar{\beta}_1/p_2$, $c_2 = 2\bar{\beta}_1^2(T + \bar{\sigma})/p_2^2$, and the first inequality in (30) used the subadditivity of the square root; the fact that $c_1 > c_2$ follows because (7g) implies that $1 > 2\bar{\beta}_1(T + \bar{\sigma})/p_2$. Since $1 > 2\bar{\beta}_1(T + \bar{\sigma})/p_2$, it follows from Lemma 4 (applied to $v(t) = \gamma(\xi_2(t + T_d^\#(|\xi(0)|)))$), and with the preceding choices of c_1 and c_2 and the choice $\Delta_1 = \frac{1}{2}(\bar{\beta}_1/p_2) \sup\{B_*(t) : t \geq T_d^\#(|\xi(0)|)\}$ that

$$|\xi_2(t)| \leq \xi_*(1 + \epsilon) + \mu_0(|x(0)| + |\delta|_\infty, t) \text{ for all } t \geq T_d^\#(|\xi(0)|); \quad (31)$$

this is done by using (9b) and (14) to find a $\gamma \in \mathcal{K}_\infty$ such that $|\xi(0)| \leq \gamma(|x(0)| + |\delta|_\infty)$ for all initial states and also using the second equality in (17) and the linear growth of the dynamics to bound $|\xi_2|$ on $[0, T_d^\#(|\xi(0)|)]$, in order to find the required function $\mu_0 \in \mathcal{KL}$. We also used the subadditivity of the square root to transform the upper bound on $\gamma(\xi_2(t))$ that is obtained from Lemma 4 into the upper bound (31) on $|\xi_2(t)|$.

The next part is devoted to the x_1 -subsystem (25). First, we deduce from (25) that $|\dot{x}_1(t)| \leq \bar{\alpha}_1 + |\mathcal{J}_1(t)| \leq \bar{\alpha}_1 + |\xi_2(t)| + \frac{\bar{\alpha}_1}{p_1} \bar{\delta}_1$, using the first equality in (10) and the second inequality in (20),

so (31) gives

$$\begin{aligned} |\dot{x}_1(t)| &\leq \bar{\alpha}_1 + \xi_*(1 + \epsilon) \\ &\quad + \frac{\bar{\alpha}_1}{p_1} \bar{\delta}_1 + \mu_0(|x(0)| + |\delta|_\infty, t) \text{ for all } t \geq T_d^\#(|\xi(0)|). \end{aligned} \quad (32)$$

Also, by adding and subtracting $\text{sat}_{p_1}(\eta(\ell)x_1(t))$ in its integrand, (25) implies that for all $t \geq T_d^\#(|\xi(0)|)$,

$$\begin{aligned} \dot{x}_1(t) &= -\frac{k^2 \bar{\alpha}_1}{(1 - e^{-kT})^2 p_1} \int_{t-T}^t \int_{m-T}^m e^{k(\ell-t)} \text{sat}_{p_1}(\eta(\ell)x_1(t)) \, d\ell dm \\ &\quad + \mathcal{R}_2(t) + \mathcal{J}_1(t), \text{ where} \end{aligned} \quad (33a)$$

$$\begin{aligned} \mathcal{R}_2(t) &= -\frac{k^2 \bar{\alpha}_1}{(1 - e^{-kT})^2 p_1} \int_{t-T}^t \int_{m-T}^m e^{k(\ell-t)} \\ &\quad \times [\text{sat}_{p_1}(\eta(\ell)x_1(\sigma(\ell))) - \text{sat}_{p_1}(\eta(\ell)x_1(t))] \, d\ell dm, \end{aligned} \quad (33b)$$

and where we can use the first equality in (10) and the global Lipschitz constant of 1 for sat_{p_1} to obtain

$$\begin{aligned} |\mathcal{R}_2(t)| &\leq \frac{k^2 \bar{\alpha}_1}{(1 - e^{-kT})^2 p_1} \bar{\eta} \\ &\quad \times \int_{t-T}^t \int_{m-T}^m e^{k(\ell-t)} |x_1(t) - x_1(\sigma(\ell))| \, d\ell dm \\ &\leq \frac{\bar{\alpha}_1 \bar{\eta}}{p_1} \int_{t-2T-\bar{\sigma}}^t |\dot{x}_1(s)| \, ds, \end{aligned} \quad (34)$$

since the Fundamental Theorem of Calculus gives $|x_1(t) - x_1(\sigma(\ell))| \leq \int_{t-2T-\bar{\sigma}}^t |\dot{x}_1(s)| \, ds$ for all $\ell \in [t - 2T - \bar{\sigma}, t]$.

Although we can use the bound L_1 on \dot{x}_1 from (1) and (34) to upper bound $|\mathcal{R}_2(t)|$ by $(\bar{\alpha}_1 \bar{\eta}/p_1)(2T + \bar{\sigma})L_1$, we will instead use (32) to upper bound $|\dot{x}_1(s)|$ in (34) in order to obtain a bound on \mathcal{R}_2 that contains $\bar{\delta}_1$ that is needed to prove our input-to-state stability estimate. To this end, notice that from (32), it follows that for all $t \geq T_d^\#(|\xi(0)|) + 2T + \bar{\sigma}$, we have

$$\begin{aligned} |\mathcal{R}_2(t)| &\leq \frac{\bar{\alpha}_1 \bar{\eta}}{p_1} (2T + \bar{\sigma}) \\ &\quad \times \left(\bar{\alpha}_1 + \xi_*(1 + \epsilon) + \mu_0^b(|x(0)| + |\delta|_\infty, t) + \frac{\bar{\alpha}_1}{p_1} \bar{\delta}_1 \right), \end{aligned} \quad (35)$$

where $\mu_0^b(s, t) = \mu_0(s, t - 2T - \bar{\sigma})$. Combining (35) and the second inequality in (20) with (31), we obtain a class \mathcal{M} function $T_d^\# : [0, +\infty) \rightarrow [0, +\infty)$ such that

$$\sup_{t \geq T_d^\#(|\xi(0)|)} (|\mathcal{R}_2(t)| + |\mathcal{J}_1(t)|) < \frac{\bar{\alpha}_1}{\bar{\eta}}, \quad (36)$$

where the last inequality is a consequence of (7h) and by choosing $\epsilon \in (0, 1)$ to be small enough. Hence, there is a class \mathcal{M} function $T_e : [0, +\infty) \rightarrow [0, +\infty)$ such that $\bar{\eta}|x_1(t)| < p_1$ and so also $|\eta(\ell)x_1(t)| < p_1$ for all $t \geq T_e(|\xi(0)|)$ and $\ell \geq 0$. It follows from (33a) that

$$\begin{aligned} \dot{x}_1(t) &= -\frac{k^2 \bar{\alpha}_1}{(1 - e^{-kT})^2 p_1} \\ &\quad \times \int_{t-T}^t \int_{m-T}^m e^{k(\ell-t)} \eta(\ell)x_1(t) \, d\ell dm + \mathcal{R}_2(t) + \mathcal{J}_1(t) \end{aligned} \quad (37)$$

for all $t \geq T_e(|\xi(0)|)$. This follows from applying Lemma 3 to the system (33a), and choosing $q = x_1$ and $M = p_1/\bar{\eta}$ in the lemma, because $|\xi| \geq |x_1|$. We can assume that $T_e(s) \geq T_d^\#(s) + 2T + \bar{\sigma}$ for all $s \geq 0$.

Let us consider the candidate Lyapunov function $v(x_1) = \frac{1}{2}x_1^2$. Since η is lower bounded by 1, we deduce from the second inequality in (20) and (34) that

$$\begin{aligned} \dot{v}(t) &\leq -\frac{\bar{\alpha}_1}{p_1}x_1^2(t) + x_1(t)[\mathcal{R}_2(t) + \mathcal{J}_1(t)] \\ &\leq -\frac{\bar{\alpha}_1}{p_1}x_1^2(t) + |x_1(t)|\frac{\bar{\alpha}_1\bar{\eta}}{p_1}\int_{t-2T-\bar{\sigma}}^t |\dot{x}_1(s)|ds \\ &\quad + |x_1(t)|\left(|\xi_2(t)| + \frac{\bar{\alpha}_1}{p_1}\bar{\delta}_1\right) \end{aligned} \tag{38}$$

holds along all solutions of (37) for all $t \geq T_e(|\xi(0)|)$, by the first equality in (10). From (25) and the first equality in (10), we deduce that

$$\begin{aligned} |\dot{x}_1(t)| &\leq \frac{k^2\bar{\alpha}_1}{(1-e^{-kT})^2p_1}\int_{t-T}^t\int_{m-T}^m e^{k(\ell-t)}\bar{\eta}|x_1(\sigma(\ell))|d\ell dm \\ &\quad + |\mathcal{J}_1(t)| \\ &\leq \frac{\bar{\alpha}_1\bar{\eta}}{p_1}\sup_{m \in [t-2T-\bar{\sigma}, t]} |x_1(m)| + |\xi_2(t)| + \frac{\bar{\alpha}_1}{p_1}\bar{\delta}_1 \end{aligned} \tag{39}$$

for all $t \geq T_e(|\xi(0)|)$, by our bound $\bar{\eta}$ on η , and where the second inequality is by (20). Hence, (38) gives

$$\begin{aligned} \dot{v}(t) &\leq -\frac{\bar{\alpha}_1}{p_1}x_1^2(t) + |x_1(t)|\frac{\bar{\alpha}_1\bar{\eta}}{p_1} \\ &\quad \times \int_{t-2T-\bar{\sigma}}^t \left(\frac{\bar{\alpha}_1\bar{\eta}}{p_1}\sup_{m \in [s-2T-\bar{\sigma}, s]} |x_1(m)| + |\xi_2(s)|\right) ds \\ &\quad + |x_1(t)|\left(\frac{\bar{\alpha}_1\bar{\eta}}{p_1}(2T+\bar{\sigma})\frac{\bar{\alpha}_1}{p_1}\bar{\delta}_1 + |\xi_2(t)| + \frac{\bar{\alpha}_1}{p_1}\bar{\delta}_1\right) \\ &\leq -\frac{\bar{\alpha}_1}{p_1}x_1^2(t) + \frac{\bar{\alpha}_1^2\bar{\eta}^2}{p_1^2}(2T+\bar{\sigma})\sup_{m \in [t-4T-2\bar{\sigma}, t]} |x_1(m)|^2 \\ &\quad + |x_1(t)|\left[\frac{\bar{\alpha}_1\bar{\eta}}{p_1}\int_{t-2T-\bar{\sigma}}^t |\xi_2(s)|ds\right. \\ &\quad \left. + \frac{\bar{\alpha}_1^2\bar{\eta}}{p_1^2}(2T+\bar{\sigma})\bar{\delta}_1 + |\xi_2(t)| + \frac{\bar{\alpha}_1}{p_1}\bar{\delta}_1\right] \end{aligned} \tag{40}$$

for all $t \geq T_e(|\xi(0)|) + 2T + \bar{\sigma}$. Setting $\xi_*^\sharp = \xi_*(1 + \epsilon)$, it follows from (31) that, for all $t \geq T_e(|\xi(0)|) + 2T + \bar{\sigma}$,

$$\begin{aligned} \dot{v}(t) &\leq -\frac{\bar{\alpha}_1}{p_1}x_1^2(t) + \frac{\bar{\alpha}_1^2\bar{\eta}^2}{p_1^2}(2T+\bar{\sigma})\sup_{m \in [t-4T-2\bar{\sigma}, t]} |x_1(m)|^2 \\ &\quad + \{ |x_1(t)| \left\{ \frac{\bar{\alpha}_1\bar{\eta}}{p_1}(2T+\bar{\sigma})(\xi_*^\sharp + \mu_0(|x(0)| + |\delta|_\infty, t)) \right. \right. \\ &\quad \left. \left. + \frac{\bar{\alpha}_1^2\bar{\eta}(2T+\bar{\sigma})\bar{\delta}_1}{p_1^2} + \xi_*^\sharp + \mu_0(|x(0)| + |\delta|_\infty, t) + \frac{\bar{\alpha}_1\bar{\delta}_1}{p_1} \right\} \right\} \\ &\leq -\frac{2(1-\omega_0)\bar{\alpha}_1}{p_1}v(x_1(t)) \\ &\quad + \frac{2\bar{\alpha}_1^2\bar{\eta}^2}{p_1^2}(2T+\bar{\sigma})\sup_{m \in [t-4T-2\bar{\sigma}, t]} v(x_1(m)) \\ &\quad + \frac{p_1}{4\omega_0\bar{\alpha}_1}\left[\frac{\bar{\alpha}_1\bar{\eta}}{p_1}(2T+\bar{\sigma})(\xi_*^\sharp + \mu_0(|x(0)| + |\delta|_\infty, t)) \right. \\ &\quad \left. + \frac{\bar{\alpha}_1^2\bar{\eta}(2T+\bar{\sigma})\bar{\delta}_1}{p_1^2} + \xi_*^\sharp + \mu_0(|x(0)| + |\delta|_\infty, t) + \frac{\bar{\alpha}_1}{p_1}\bar{\delta}_1\right]^2 \end{aligned} \tag{41}$$

where the last inequality applied Young's inequality $ab \leq \frac{\bar{\alpha}_1\omega_0}{p_1}a^2 + \frac{p_1}{4\bar{\alpha}_1\omega_0}b^2$ to the terms in curly braces.

By (7e), we can assume that $\omega_0 \in (0, 1)$ is small enough so that

$$\frac{(1-\omega_0)\bar{\alpha}_1}{p_1} > \frac{\bar{\alpha}_1^2\bar{\eta}^2}{p_1^2}(2T+\bar{\sigma}).$$

From Lemma 4 (with $c_1 = 2(1-\omega_0)\bar{\alpha}_1/p_1$ and $c_2 = 2\bar{\alpha}_1^2\bar{\eta}^2(2T+\bar{\sigma})/p_1^2$) and the second inequality in (41), there is a $\mu_1 \in \mathcal{KL}$ and a class \mathcal{M} function $T_e^\sharp : [0, +\infty) \rightarrow [0, +\infty)$ such that for all $t \geq T_e^\sharp(|\xi(0)|)$, we have

$$\begin{aligned} v(x_1(t)) &\leq \left\{ \frac{p_1^3(1+\omega_0)}{8\bar{\alpha}_1^2\omega_0(p_1(1-\omega_0) - \bar{\alpha}_1\bar{\eta}^2(2T+\bar{\sigma}))} \right. \\ &\quad \times \left[\frac{\bar{\alpha}_1\bar{\eta}(2T+\bar{\sigma})\xi_*^\sharp}{p_1} + \frac{\bar{\alpha}_1^2\bar{\eta}(2T+\bar{\sigma})\bar{\delta}_1}{p_1^2} + \xi_*^\sharp + \frac{\bar{\alpha}_1\bar{\delta}_1}{p_1} \right]^2 \left. \right\} \\ &\quad + \mu_1(|x(0)| + |\delta|_\infty, t), \end{aligned} \tag{42}$$

by the argument that led to (31) and the linear growth of the x_1 dynamics.

3.4.3. Third step: deriving bounds on the original state variables

Using (42), it follows that with the choice $\mu_2 = \sqrt{2\mu_1}$, we get

$$|x_1(t)| \leq \gamma_a + \mu_2(|x(0)| + |\delta|_\infty, t), \tag{43}$$

where $\gamma_a = \sqrt{2B_a}$ and B_a is the quantity in curly braces in (42), by the subadditivity of the square root and the formula $v(x_1) = \frac{1}{2}x_1^2$. We next find analogous bounds for x_2 and x_3 .

From (31) and the definition $\xi_2 = x_2 - \alpha$ from (14), and also using (9b), we deduce that

$$\begin{aligned} \left| x_2(t) + \frac{k^2}{(1-e^{-kT})^2} \right. \\ \left. \times \int_{t-T}^t \int_{m-T}^m e^{k(\ell-t)} \frac{\bar{\alpha}_1}{p_1} \text{sat}_{p_1}(\eta(\ell)x_1(\sigma(\ell)) + \delta_1(\ell)) d\ell dm \right| \\ \leq \xi_*^\sharp + \mu_0(|x(0)| + |\delta|_\infty, t) \end{aligned} \tag{44}$$

and so also

$$\begin{aligned} |x_2(t)| &\leq \xi_*^\sharp + \mu_0(|x(0)| + |\delta|_\infty, t) \\ &\quad + \frac{k^2}{(1-e^{-kT})^2} \frac{\bar{\alpha}_1}{p_1} \int_{t-T}^t \int_{m-T}^m e^{k(\ell-t)} [\bar{\eta}|x_1(\sigma(\ell))| + \bar{\delta}_1] d\ell dm \end{aligned} \tag{45}$$

for all $t \geq T_d^\sharp(|\xi(0)|)$, since $|\text{sat}_{p_1}(r)| \leq r$ for all $r \geq 0$. From (45) and (43) and the first equality in (10), we deduce that for all $t \geq T_e^\sharp(|\xi(0)|) + 2T + \bar{\sigma}$, we have

$$|x_2(t)| \leq \xi_*^\sharp + \mu_0^\sharp(|x(0)| + |\delta|_\infty, t) + \frac{\bar{\alpha}_1}{p_1} [\bar{\eta}\gamma_a + \bar{\delta}_1] \tag{46}$$

where $\mu_0^\sharp = \mu_0 + (\bar{\alpha}_1/p_1)\bar{\eta}\mu_2 \in \mathcal{KL}$. Moreover, since $x_3(t) = \dot{\alpha}(t) + \beta(t) + \xi_3(t)$, we have

$$\begin{aligned} |x_3(t)| &\leq \left[\frac{k^3}{(1-e^{-kT})^2} \int_{t-T}^t \int_{m-T}^m e^{k(\ell-t)} |\phi(\ell)| d\ell dm \right. \\ &\quad + \frac{k^2}{(1-e^{-kT})^2} \int_{t-T}^t e^{k(\ell-t)} |\phi(\ell)| d\ell \\ &\quad + \frac{k^2}{(1-e^{-kT})^2} \int_{t-2T}^{t-T} e^{k(\ell-t)} |\phi(\ell)| d\ell \left. \right] \\ &\quad + \frac{k}{1-e^{-kT}} \int_{t-T}^t e^{k(\ell-t)} |\omega(\ell)| d\ell + |\xi_3(t)| \end{aligned} \tag{47}$$

for all $t \geq 2T$, by (9b), where we note (for later use in the proof) that the quantity in squared brackets in (47) is an upper bound for $|\dot{\alpha}_1(t)|$. Next observe that our choices of y_1 and y_2 from (2) give

$$|\phi(t)| \leq \frac{\bar{\alpha}_1}{p_1} |\eta(t)x_1(\sigma(t)) + \delta_1(t)|$$

and

$$|\omega(t)| \leq \frac{\bar{\beta}_1}{p_2} \left| x_2(\sigma(t)) + \delta_2(t) - \frac{k^2}{(1 - e^{-kT})^2} \int_{\sigma(t)-T}^{\sigma(t)} \int_{m-T}^m e^{k(\ell-\sigma(t))} \phi(\ell) d\ell dm \right| \quad (48)$$

for all $t \geq 2T + \bar{\sigma}$. It follows from (43) and (46) that we can find a function $\mu_3 \in \mathcal{KL}$ such that

$$|\phi(t)| \leq \phi_* + \mu_3(|x(0)| + |\delta|_\infty, t),$$

where $\phi_* = \frac{\bar{\alpha}_1}{p_1} (\bar{\eta}\gamma_a + \bar{\delta}_1)$ (49)

and

$$|\omega(t)| \leq \frac{\bar{\beta}_1}{p_2} \left[\xi_*^\sharp + \frac{\bar{\alpha}_1}{p_1} [\bar{\eta}\gamma_a + \bar{\delta}_1] \right]$$

$$+ \frac{\bar{\beta}_1}{p_2} \left(s \int_{\sigma(t)-T}^{\sigma(t)} \int_{m-T}^m e^{k(\ell-\sigma(t))} d\ell dm \phi_* + \bar{\delta}_2 + \mu_3(|x(0)| + |\delta|_\infty, t) \right) \leq \omega_* + \frac{\bar{\beta}_1}{p_2} \mu_3(|x(0)| + |\delta|_\infty, t), \quad (50)$$

by enlarging T_e^\sharp as needed without relabeling and using the first equality in (10), where $s = k^2/(1 - e^{-kT})^2$ and where

$$\omega_* = \frac{\bar{\beta}_1}{p_2} \left[\xi_*^\sharp + \frac{\bar{\alpha}_1}{p_1} (\bar{\eta}\gamma_a + \bar{\delta}_1) + \phi_* + \bar{\delta}_2 \right]. \quad (51)$$

Also, by using (10) and the upper bound on $|\dot{\alpha}_1(t)|$ that we obtained in squared brackets in (47), we have $|\dot{\alpha}(t)| \leq 2k|\phi|_{[t-2T, t]}/(1 - e^{-kT})$ for all $t \geq 2T$. Therefore, we deduce from the formula $x_3(t) = \dot{\alpha}(t) + \beta(t) + \xi_3(t)$ from (14) and from our bounds on ϕ and ω from (49) and (50) (and the asymptotic stability property of the ξ_3 subsystem) that we can find a class \mathcal{M} function $T_f : [0, +\infty) \rightarrow [0, +\infty)$ and a function $\mu_4 \in \mathcal{KL}$ such that

$$|x_3(t)| \leq \frac{2k}{1 - e^{-kT}} \phi_* + \omega_* + \mu_4(|x(0)| + |\delta|_\infty, t) \quad (52)$$

for all $t \geq T_f(|\xi(0)|)$, using the formula for β from (9b) and the second equality in (10). The theorem now follows from combining the upper bounds (43), (46), and (52); see Appendix D.

4. Application to visual landing of aircraft

To illustrate our results, we consider the lateral dynamics of an Airbus airliner in a glide phase which must align with a runway using a body fixed monocular camera [22], using imprecise, sampled, or delayed output measurements. This problem is a challenge of strong relevance in cases where the runway is unequipped or in the case of GPS loss, where the output delays and sampling arise from image processing. More precisely, the position, size and heading of the runway are unknown, so the relative position (Δ_X, Δ_Y) and heading Δ_ψ of the aircraft with respect to it are unmeasured. See Fig. 1, and [23] for valuable research on vision based aircraft control, which does not provide the input-to-state stability to uncertainty under sampling that we provide here.

As noted in [3], this research was motivated by this simplified lateral guidance model provided by Airbus:

$$\begin{cases} \dot{\Delta}_Y = V \text{sat}_{L_\psi}(\Delta_\psi) \\ \dot{\Delta}_\psi = \frac{g}{V} \text{sat}_{L_\psi}(\varphi) \\ \dot{\varphi} = \text{sat}_{L_u}(u_{\text{lat}}), \end{cases} \quad (53)$$

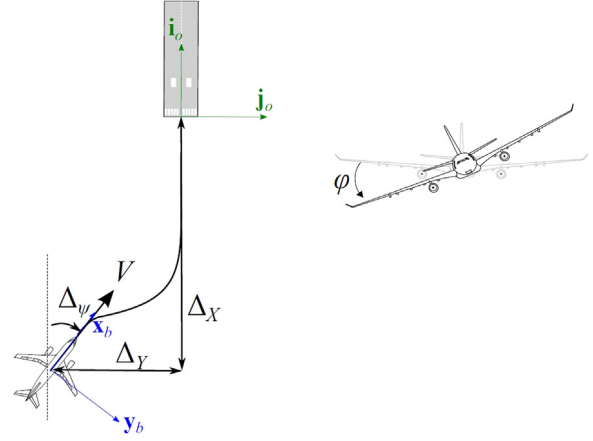


Fig. 1. Notation used in the alignment part of the glide phase.

Table 1

Maximum allowable values according to our main result for the parameter values (54).

$\bar{\sigma}$ (ms)	$\bar{\delta}_1$ (cm)	$\bar{\delta}_2$ (cm/s)
878	0	0
0	152.5	0
0	0	5.5
100	67.02	2.4

where u_{lat} is the input, $V = 72 \text{ m}\cdot\text{s}^{-1}$ is constant all along the final approach, $g = 9.81 \text{ m}\cdot\text{s}^{-2}$, and φ (resp., u_{lat}) is the aircraft roll angle (resp., the guidance/outer loop control action). Then (53) can be transformed into the system (1) by applying the changes of coordinates $x_1 = \Delta_Y$, $x_2 = V\Delta_\psi$, and $x_3 = g\varphi$ and setting $L_1 = VL_\psi$, $L_2 = gL_\varphi$, $L_3 = gL_u$, and $u = gu_{\text{lat}}$. Here, we assume that we can extract the quantities $y_1 = \eta(t)\Delta_Y(\sigma(t)) + \delta_1(t)$, $y_2 = \Delta_\psi(\sigma(t)) + \delta_2(t)$, and $y_3 = \varphi(t)$ from the images and inertial measurement unit, where $\eta(t) \in [1, 2]$ and $\delta_1(t)$ and $\delta_2(t)$ represent the measurement noise, which are mainly due to image acquisition and processing, and $\sigma(t)$ is due to the fact that the images are sampled and processed. Therefore, we choose $\bar{\eta} = 2$.

The saturation limits are $L_1 = 25 \text{ m}\cdot\text{s}^{-1}$, $L_2 = 7 \text{ m}\cdot\text{s}^{-2}$, and $L_3 = 6 \text{ m}\cdot\text{s}^{-3}$. With the preceding choices, the values

$$k = 0.1, T = 2, L_4 = 1, \bar{\alpha}_1 = 1.23, p_1 = 24, \bar{\beta}_1 = 0.2, \text{ and } p_2 = 2.5 \quad (54)$$

satisfy (7) from Theorem 1, when $\bar{\sigma}$, $\bar{\delta}_1$, and $\bar{\delta}_2$ are chosen as follows, where 878 ms in the first row of the table and 5.5 in the third row of the table corresponds to choosing $\bar{\sigma} = 0.878$ and $\bar{\delta}_1 = 0.055$ respectively in our conditions (7) on our constants (and similarly for the other rows).

In Table 1, the first line gives the maximum value of $\bar{\sigma}$, in the special case $\bar{\delta}_1 = \bar{\delta}_2 = 0$ that we discussed in Section 3.2 (corresponding to choosing $\bar{\sigma} = 0.878$ in (7) because of the scaling of the physical quantities). Then the next two lines show maximum disturbance values in the special case that we discussed in Section 3.2 where $\bar{\sigma} = 0$, which corresponds to the undelayed case where $\sigma(t) = t$ where there is no sampling in the outputs. In practice, assuming that image processing and acquisition is done within 878 ms seems reasonable (since, for instance, some image processing algorithms run at around 67 ms in [24]); indeed, once correctly initialized, the computer vision algorithm must simply track the runway (which is a trapezoid) in the image. The second (resp. third) line gives the maximum value of $\bar{\delta}_1$ (resp., $\bar{\delta}_2$) assuming $\bar{\sigma} = 0$ and $\bar{\delta}_2 = 0$ (resp., $\bar{\delta}_1 = 0$). Finally, we can determine maximal allowable values

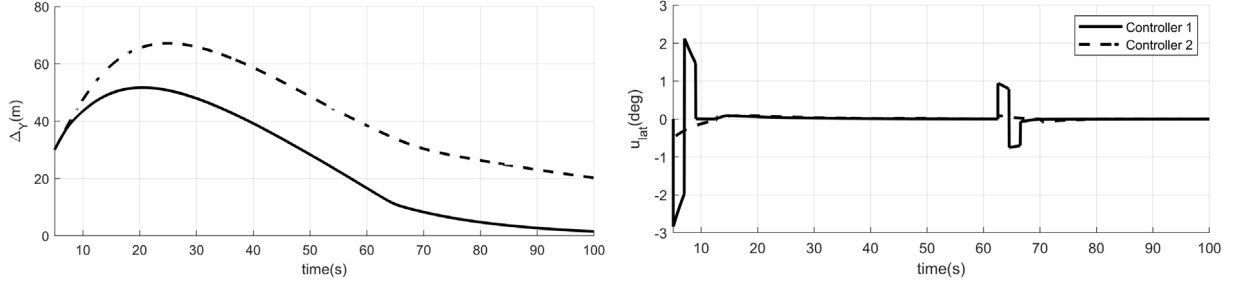


Fig. 2. State $\Delta\gamma$ and control u_{lat} using values from last line of Table 1.

when all of these values are nonzero, as follows. Assume that the image processing and acquisition are performed at 100 ms. Then, a good compromise is in the last line, in which $\bar{\delta}_1$ and $\bar{\delta}_2$ are selected such that (7) hold with $\bar{\sigma} = 100$ ms, $\bar{\delta}_1 = 1.525x$ m, and $\bar{\delta}_2 = .055x$ m/s, where the value $x = 0.4395$ was selected as the largest x such that (7) hold when $\bar{\delta}_1 = 1.525x$ m, and $\bar{\delta}_2 = .055x$ m/s. This is a compromise, because $\bar{\sigma}$ is reduced from 878 ms, to allow positive $\bar{\delta}_i$ values that agree with a suitable percent of their maximum values. Moreover, for the values $\bar{\sigma} = 0$, $\bar{\delta}_1 = \bar{\delta}_2 = 0.27$, $k = 0.1$, $T = 2$, $L_4 = 1$, $\bar{\alpha}_1 = 1.6$, $p_1 = 69$, $\bar{\beta}_1 = 0.2$, and $p_2 = 2.5$, the assumptions of Theorem 1 are again satisfied, but the assumptions of [4] would not be satisfied, because the preceding values give $L_1(1 - e^{-1})^2/(40(1 + 2e^{-1} + e^{-2})) - \bar{\delta}_2 < 0$, so Theorem 1 is less restrictive than [4].

For comparison purposes, we name our guidance solution from Theorem 1 ‘Controller 1’. For the plots above, we used the values of $\bar{\sigma}$ and $\bar{\delta}_1$ and $\bar{\delta}_2$ calculated in the last row of the table, with the choice $\sigma(t) = i\bar{\sigma}/2 - \bar{\sigma}/2$ for all $t \in [i\bar{\sigma}/2, (i+1)\bar{\sigma}/2]$ and $i \geq 0$ (to incorporate the effects of sampling and delay). One can also apply a second controller called ‘Controller 2’ to (53) based on [4], by choosing the parameters in [4] to be $q = 0.07$ (which is the parameter of [4, Remark 1]), $r = 0.13$, $\lambda = \lambda_a = 0.007$, $\bar{\sigma}_* = 0.07$, and $\epsilon = 0.01$. These choices of parameters give the value $\bar{v} = 0.63$ for the corresponding parameter in [4]. We were unable to find larger values for λ or r while respecting the assumptions of the main result of [4]; these values have a direct impact on controller performance. Fig. 2 shows how Controller 1 succeeds to lower a lateral deviation of 30 m for an initial heading deviations $\Delta\psi = 3\text{deg}$ within 42 s. Moreover, Controller 1 (in terms of radians) has the bound

$$\begin{aligned} L_4 + \bar{\alpha}_3 + \bar{\beta}_2 &= L_4 + \frac{4k^2\bar{\alpha}_1}{(1 - e^{-kT})^2} + \frac{2k\bar{\beta}_1}{1 - e^{-kT}} \\ &= 1 + \frac{4(0.1)^2(1.23)}{(1 - e^{-0.1(2)})^2} + \frac{2(0.1)(0.2)}{1 - e^{-0.1(2)}} = 2.718 \end{aligned} \quad (55)$$

that is ensured by our theorem. We start the plots at time $t = 4$ because Controller 1 from (4a) is 0 on the interval $[0, 2T] = [0, 4]$. In the right panel of Fig. 2, we see that $|u_{\text{lat}}|$ (expressed in degrees per second) stays below its required bound $(180/(\pi g)) \times 2.718 = 15.87$. It also shows that the Controller 2 is unable to reduce the lateral deviation in such a short time. This indicates that the compromise between robustness and performance is worse for Controller 2. In other words, the conditions for the main result of [4] are more conservative.

5. Conclusions

We used a recent backstepping approach to derive a useful new class of bounded controls for a chain of saturated integrators that arises in the visual landing of aircraft under image processing. This overcame the challenge of having imprecise, delayed,

or sampled output measurements by proving an input-to-state stability estimate. Our numerical simulations illustrated potential advantages of this work over previous methods. In future work, we hope to merge our results with existing methods for approximating delays to cover cases where σ may not be known, and to transition this work to practice to improve the performance of aircraft during the glide phase.

Declaration of competing interest

The authors declare that they have no known competing financial interests or personal relationships that could have appeared to influence the work reported in this paper.

Appendix A. Proof of Lemma 1

Simple calculations (based on substituting (6a)–(6b) into (5)) show that the functions v_i from (4b)–(4d) satisfy $v_1(z_t) = \dot{\alpha}(t)$, $v_2(y_t, z_t) = \ddot{\alpha}(t)$, and $v_3(y_t, z_t) = \beta(t)$ for all $t \geq 0$. This allows us to rewrite (4a) as (9a). Also, we can apply variation of parameters on the interval $[t - T, t]$ (to the system $\dot{q} = k(-q + b)$ with the choice $(q(t), b(t)) = (z_3(t), \omega(t))$, then with the choice $(q(t), b(t)) = (z_2(t), z_1(t) - e^{-kT}z_1(t - T))$, and finally with the choice $(q(t), b(t)) = (z_1(t), \phi(t))$) to prove that (9b) holds for all $t \geq 2T$. It remains to prove the bounds (9c).

To this end, we use (9b) to prove the bounds on the derivatives of α and β in (9c); the bounds on α and β in (9c) follow from the definition of the saturation and (9b) and (10). We continue to use the common notation $s = k^2/(1 - e^{-kT})^2$ and the equalities and inequalities to follow should be understood to hold for all $t \geq 2T$. We have

$$\dot{\alpha}(t) = -k\alpha(t) + s \left[\int_{t-T}^t e^{k(\ell-t)} \phi(\ell) d\ell - \int_{t-2T}^{t-T} e^{k(\ell-t)} \phi(\ell) d\ell \right], \quad (A.1)$$

and therefore also

$$\begin{aligned} |\dot{\alpha}|_\infty &\leq k\bar{\alpha}_1 + s\bar{\alpha}_1 \left[\frac{1}{k} (1 - e^{-kT}) + \frac{1}{k} (e^{-kT} - e^{-2kT}) \right] \\ &= k\bar{\alpha}_1 + s\bar{\alpha}_1 \frac{1}{k} (1 - e^{-kT}) (1 + e^{-kT}) = \bar{\alpha}_2, \end{aligned} \quad (A.2)$$

by our choice of $\bar{\alpha}_2$ in (8). Also, since

$$\begin{aligned} \ddot{\alpha}(t) &= -k\dot{\alpha}(t) \\ &+ s(-k) \left[\int_{t-T}^t e^{k(\ell-t)} \phi(\ell) d\ell - \int_{t-2T}^{t-T} e^{k(\ell-t)} \phi(\ell) d\ell \right] \\ &+ s[\phi(t) - 2e^{-kT}\phi(t - T) + e^{-2kT}\phi(t - 2T)], \end{aligned} \quad (A.3)$$

our formulas for $\bar{\alpha}_2$ and $\bar{\alpha}_3$ from (8) and the bound $\bar{\alpha}_1$ on ϕ give

$$\begin{aligned} |\ddot{\alpha}|_\infty &\leq \frac{2k^2\bar{\alpha}_1}{1 - e^{-kT}} + [s(1 - e^{-kT}) + s(e^{-kT} - e^{-2kT})] \bar{\alpha}_1 \\ &+ s(1 + 2e^{-kT} + e^{-2kT}) \bar{\alpha}_1 \leq 4\bar{\alpha}_1 s = \bar{\alpha}_3. \end{aligned} \quad (A.4)$$

Finally, since

$$\dot{\beta}(t) = -k\beta(t) + \frac{k}{1 - e^{-kT}} (\omega(t) - \omega(t - T)e^{-kT}), \quad (\text{A.5})$$

we have

$$|\dot{\beta}|_\infty \leq k\bar{\beta}_1 + \frac{k}{1 - e^{-kT}} (1 + e^{-kT}) \bar{\beta}_1 = \bar{\beta}_2, \quad (\text{A.6})$$

by our choice of $\bar{\beta}_2$ in (8) and our bound $\bar{\beta}_1$ on ω , which completes our proof of the bounds (9c).

Appendix B. Proof of Lemma 3

Consider any solution $q : [T_0, \infty) \rightarrow \mathbb{R}$ of (11). If there is a time $t_* \geq \bar{T}$ where $|q(t_*)| \leq \bar{M}$, and a time $t > t_*$ and an $\epsilon > 0$ such that $|q(t)| \geq \bar{M} + \epsilon$, then let T_{\min} be the smallest time $t > t_*$ such that $|q(t)| \geq \bar{M} + \epsilon$. Then, if $q(T_{\min}) > 0$, then $\dot{q}(T_{\min}) = -\mathcal{G}(T_{\min}, q(T_{\min})) + H(T_{\min}) \leq -g_0 + \bar{H} < 0$, which implies that there is a smaller time $t \in (t_*, T_{\min})$ at which $q(t) \geq \bar{M} + \epsilon$, which contradicts the minimality of T_{\min} . On the other hand, if $q(T_{\min}) < 0$, then $\dot{q}(T_{\min}) = -\mathcal{G}(T_{\min}, q(T_{\min})) + H(T_{\min}) \geq g_0 - \bar{H} \geq 0$, so there is a smaller time $t \in (t_*, T_{\min})$ at which $q(t) \leq -\bar{M} - \epsilon$, which again contradicts the minimality of T_{\min} .

The preceding argument implies that for each $t \geq \bar{T}$ such that $|q(t)| \leq \bar{M}$, we have $|q(s)| \leq \bar{M}$ for all $s \geq t$. It follows that if $t \geq \bar{T}$ is such that $|q(t)| > \bar{M}$, then $|q(r)| > \bar{M}$ for all $r \in [\bar{T}, t]$. Therefore, if $t \geq \bar{T}$ is a time when $q(t) > \bar{M}$, then $\dot{q}(\ell) \leq -g_0 + \bar{H}$ for all $\ell \in [\bar{T}, t]$, so applying the Fundamental Theorem of Calculus to q on the interval $[\bar{T}, t]$ gives $0 < \bar{M} \leq q(t) \leq q(\bar{T}) + (\bar{H} - g_0)(t - \bar{T}) \leq |q(T_0)| + (|\mathcal{G}|_\infty + |\mathcal{H}|_\infty)(\bar{T} - T_0) + (\bar{H} - g_0)(t - \bar{T})$, which implies that

$$t \leq \frac{|q(T_0)| + (|\mathcal{G}|_\infty + |\mathcal{H}|_\infty)(\bar{T} - T_0)}{g_0 - \bar{H}} + \bar{T}. \quad (\text{B.7})$$

Similarly, if $t \geq \bar{T}$ is a time when $q(t) < -\bar{M}$, then $\dot{q}(\ell) \geq g_0 - \bar{H}$ for all $\ell \in [\bar{T}, t]$, so we have $0 > -\bar{M} \geq q(t) \geq q(\bar{T}) - (\bar{H} - g_0)(t - \bar{T}) \geq -|q(T_0)| - (|\mathcal{G}|_\infty + |\mathcal{H}|_\infty)(\bar{T} - T_0) - (\bar{H} - g_0)(t - \bar{T})$, which again gives (B.7). Hence, by separately considering the cases $|q(\bar{T})| \leq \bar{M}$ and $|q(\bar{T})| > \bar{M}$, it follows that we can choose

$$T_*(s) = \frac{s + (|\mathcal{G}|_\infty + |\mathcal{H}|_\infty)(\bar{T} - T_0)}{g_0 - \bar{H}} + \bar{T} \quad (\text{B.8})$$

to satisfy our requirements, because $|q(t)| \leq \bar{M}$ for all $t \geq T_*(|q(T_0)|)$.

Appendix C. Proof of Lemma 4

First, observe that $\frac{\Delta_1}{c_1 - c_2}$ is well-defined because $c_1 > c_2$. Let $\tilde{v}(t) = v(t) - \frac{\Delta_1}{c_1 - c_2}$. Then

$$\dot{\tilde{v}}(t) \leq -c_1 \tilde{v}(t) + c_2 \sup_{m \in [t-h, t]} \tilde{v}(m) \quad (\text{C.9})$$

for all $t \geq 0$. Since $c_1 > c_2$, the required constant c_s exists. Also, the function $p(t) = e^{-c_s t}$ satisfies

$$\dot{p}(t) = -c_1 p(t) + c_2 \sup_{m \in [t-h, t]} p(m) \quad (\text{C.10})$$

for all $t \geq 0$, by our choice of c_s . It now suffices to prove that $l_v p(t) > \tilde{v}(t)$ for all $t \geq -h$. To this end, suppose that there is a constant $t_c > 0$ such that $l_v p(t) > \tilde{v}(t)$ for all $t \in [-h, t_c)$ and $l_v p(t_c) = \tilde{v}(t_c)$, for the sake of obtaining a contradiction. Let $w(t) = \tilde{v}(t) - l_v p(t)$. Then, using $l_v p(t_c) = \tilde{v}(t_c)$ and (C.9)–(C.10), we get

$$\dot{w}(t_c) \leq c_2 \left[\sup_{m \in [t_c-h, t_c]} \tilde{v}(m) - \sup_{m \in [t_c-h, t_c]} l_v p(m) \right] < 0, \quad (\text{C.11})$$

where the last inequality in (C.11) follows because if we choose a $t_* \in [t_c - h, t_c]$ such that $\sup_{m \in [t_c-h, t_c]} \tilde{v}(m) = \tilde{v}(t_*)$, then the quantity in squared brackets in (C.11) is $\tilde{v}(t_*) - l_v p(t_c - h)$, which is negative if $t_* = t_c - h$ (by our choice of t_c) and is also negative if $t_* \in (t_c - h, t_c]$ because in that case it is bounded above by $l_v(p(t_*) - p(t_c - h)) < 0$. From $\dot{w}(t_c) < 0$ and $w(t) < 0$ when $t \in [-h, t_c)$, we deduce that $w(t_c) < 0$, which is a contradiction. Hence, $w(t) < 0$ for all $t \geq -h$. Thus $\tilde{v}(t) < l_v p(t)$ for all $t \geq -h$, which gives the conclusion.

Appendix D. Completion of proof of Theorem 1

By combining the upper bounds (43), (46), and (52) for the $|x_i(t)|$'s and recalling the formulas for the components of ξ , we can construct functions $\beta_0 \in \mathcal{KL}$ and $\gamma_0 \in \mathcal{K}_\infty$ and a class \mathcal{M} function $T_g : [0, +\infty) \rightarrow [0, +\infty)$ such that

$$|x(t)| \leq \beta_0(|x(0)|, t) + \gamma_0(|\delta|_\infty) \quad (\text{D.12})$$

for all $t \geq T_g(|x(0)|)$, where the construction of T_g used the fact that our formulas (14) imply that there is a class \mathcal{M} function $\Theta : [0, +\infty) \rightarrow [0, +\infty)$ such that $|\xi(0)| \leq \Theta(|x(0)|)$ holds for all initial states $\xi(0)$ and $x(0)$, so we can choose $T_g(s) = T_f(\Theta(s))$. Also, the linear growth of the x dynamics provides a constant $\bar{L} > 0$ and a function $\alpha_* \in \mathcal{K}_\infty$ such that

$$|x(t)| \leq \bar{L} e^{\bar{L} T_g(|x(0)|) - t} \alpha_*(|x(0)|) + \bar{L} \alpha_*(|\delta|_\infty) \quad (\text{D.13})$$

for all $t \in [0, T_g(|x(0)|)]$.

In fact, (5)–(6b) provide a constant $\bar{c} > 0$ such that $|\dot{z}(t)| \leq \bar{c}(|z|_{[t-T-\bar{\sigma}, t]} + |x|_{[t-\bar{\sigma}, t]} + |\delta|_\infty)$ and therefore also

$$|z|_{[t-T-\bar{\sigma}, t]} \leq \bar{c} \int_0^t (|z|_{[l-T-\bar{\sigma}, l]} + |x|_{[l-\bar{\sigma}, l]}) dl + \bar{c} t |\delta|_\infty, \quad (\text{D.14})$$

for all $t \geq 0$ (since we assumed that the initial functions for the z dynamics are 0). Therefore, we can apply Gronwall's inequality to the function $\mathcal{F}(t) = |z|_{[t-T-\bar{\sigma}, t]}$ to find a constant $\bar{c}^\sharp > 0$ such that

$$|z(t)| \leq \bar{c}^\sharp e^{\bar{c}^\sharp T_g(|x(0)|)} (|x|_{[0, t]} + |\delta|_\infty) \quad (\text{D.15})$$

for all $t \in [0, T_g(|x(0)|)]$, which we can use to find positive constants $\bar{c} > 0$ and \bar{c}_* and a constant $\alpha_a > 0$ so that the right side of (1) is bounded by $\bar{c}(e^{\bar{c}_* T_g(|x(0)|)} \alpha_a |x|_{[0, t]} + |\delta|_\infty)$ for all $t \in [0, T_g(|x(0)|)]$, and then we can apply Gronwall's inequality to the x system (as we did for the z system) to get the required constant $\bar{L} > 0$. The final input-to-state stability estimate now follows by adding the bounds for (D.12)–(D.13) for $|x(t)|$ to find a bound that holds for all $t \geq 0$.

References

- [1] F. Mazenc, M. Malisoff, New control design for bounded backstepping under input delay, *Automatica* 66 (2016) 48–55.
- [2] F. Mazenc, M. Malisoff, L. Burlion, J. Weston, Bounded backstepping control and robustness analysis for time-varying systems under converging-input-converging-state conditions, *Eur. J. Control* 42 (2018) 15–24.
- [3] F. Mazenc, L. Burlion, V. Gibert, Stabilization with imprecise measurements: application to a vision based landing problem, in: *Proceedings of the 2018 American Control Conference*, pp. 2978–2983.
- [4] F. Mazenc, L. Burlion, M. Malisoff, Stabilization and robustness analysis for a chain of saturating integrators with imprecise measurements, *IEEE Control Syst. Lett.* 3 (2) (2019) 428–433.
- [5] Y. Zhu, M. Krstic, H. Su, C. Xu, Linear backstepping output feedback control for uncertain linear systems, *Internat. J. Adapt. Control Signal Process.* 30 (8–10) (2016) 1080–1098.
- [6] J. Gomes da Silva Jr., I. Queinnec, S. Tarbouriech, Regional stability analysis of discrete-time dynamic output feedback under aperiodic sampling and input saturation, *IEEE Trans. Automat. Control* 61 (12) (2016) 4176–4182.

- [7] S. Tarbouriech, G. Garcia, J. Gomes da Silva Jr., I. Queinnec, *Stability and Stabilization of Linear Systems with Saturating Actuators*, Springer-Verlag, Berlin, Germany, 2011.
- [8] G. Chesi, R. Middleton, LMI-Based fixed order output feedback synthesis for two-dimensional mixed continuous-discrete-time systems, *IEEE Trans. Automat. Control* 63 (4) (2018) 960–972.
- [9] S. Tarbouriech, J. Gomes da Silva Jr., Synthesis of controllers for continuous-time delay systems with saturating controls via LMIs, *IEEE Trans. Automat. Control* 45 (1) (2000) 105–111.
- [10] F. Mazenc, A. Iggidr, Backstepping with bounded feedbacks, *Systems Control Lett.* 51 (3–4) (2004) 235–245.
- [11] F. Mazenc, L. Praly, Adding an integration and global asymptotic stabilization of feedforward systems, *IEEE Trans. Automat. Control* 41 (11) (1996) 1559–1578.
- [12] R. Sepulchre, M. Jankovic, P. Kokotovic, *Constructive Nonlinear Control*, Springer-Verlag, Berlin, Germany, 1996.
- [13] F. Mazenc, M. Malisoff, Stabilization of nonlinear time-varying systems through a new prediction based approach, *IEEE Trans. Automat. Control* 62 (6) (2017) 2908–2915.
- [14] D. Karagiannis, A. Astolfi, A new solution to the problem of range identification in perspective vision systems, *IEEE Trans. Automat. Control* 50 (12) (2005) 2074–2077.
- [15] F. Mazenc, S. Mondié, S.I. Niculescu, Global asymptotic stabilization for chains of integrators with a delay in the input, *IEEE Trans. Automat. Control* 48 (1) (2003) 57–63.
- [16] L. Burlion, M. Malisoff, F. Mazenc, Stabilization and robustness analysis for a chain of saturating integrators arising in the visual landing of aircraft, in: *Proceedings of the 58th IEEE Conference on Decision and Control*, Nice, France, 11–13 December 2019 (in press).
- [17] F. Mazenc, M. Malisoff, T. Dinh, Robustness of nonlinear systems with respect to delay and sampling of the controls, *Automatica* 49 (6) (2013) 1925–1931.
- [18] A. Palmeira, S. Tarbouriech, I. Ghiggi, Sampled-data control under magnitude and rate saturating actuators, *Internat. J. Robust Nonlinear Control* 26 (15) (2016) 3232–3252.
- [19] A. Seuret, J. Gomes da Silva Jr, Taking into account period variations and actuator saturation in sampled-data systems, *Systems Control Lett.* 61 (12) (2012) 1286–1293.
- [20] H. Khalil, *Nonlinear Systems*, third ed., Prentice Hall, Englewood Cliffs, NJ, 2002.
- [21] E. Fridman, *Introduction to Time-Delay Systems: Analysis and Control*, Springer, New York, NY, 2014.
- [22] L. Burlion, H. de Plinval, Vision based anti-windup design with application to the landing of an airliner, *IFAC-PapersOnLine* 50 (1) (2017) 10482–10487.
- [23] F. Le Bras, T. Hamel, R. Mahony, C. Barat, J. Thadasack, Approach maneuvers for autonomous landing using visual servo control, *IEEE Trans. Aerosp. Electron. Syst.* 50 (2) (2014) 1051–1065.
- [24] L. Garcia Carrillo, A. Dzul Lopez, R. Lozano, C. Pegard, *Quad Rotorcraft Control, Vision-Based Hovering and Navigation*, Springer Verlag, New York, NY, 2013.

Troisième partie

Conclusions et perspectives

Conclusions & Perspectives

"Mais examinez toutes choses ; retenez ce qui est bon" (1 Th 5 :21).

La plupart des travaux que nous avons présentés dans ce manuscrit sont susceptibles de faire l'objet d'extensions, que nous même, ou d'autres, pourront réaliser. Plus spécifiquement, nous tentons à présent de donner les grandes lignes de nos travaux à venir.

8.4 Direction générale de nos travaux

Souvent guidés par les applications aéronautiques et spatiales, nos travaux de recherche au cours de ces dernières années ont donc principalement porté sur la commande et l'observation de systèmes saturés, contraints, ou appartenant à des classes particulières de systèmes non linéaires (strict-feedback notamment). Parce qu'il existe cependant des liens étroits entre ces classes de systèmes, il devient difficile de rattacher nos travaux actuels à l'une ou l'autre de ces classes ; en effet, les applications aéronautiques et spatiales sur lesquelles nous travaillons demandent bien souvent de nous intéresser à un problème où se mêlent nos différents sujets de recherche.

Notre objectif principal est de contribuer à apporter des solutions à quelques sous problèmes bien choisis du problème ambitieux et ouvert de la commande des systèmes aérospatiaux lorsque la dynamique

- est non linéaire,
- n'est pas parfaitement connue,
- et que tout l'état du système n'est pas mesuré.

A moyen terme, nos travaux porteront notamment sur la synthèse de commandes saturées ou contraintes lorsque les paramètres du système à contrôler sont incertains (constants ou temps variant), que des perturbations exté-

rieures mais bornées agissent sur le système ou que sont présentes des dynamiques supplémentaires mal connues (il peut s'agir par exemple du couplage entre les dynamiques longitudinales et latérales pour un avion, de modes souples ou du ballottement d'ergol pour un satellite d'observation etc...). Ces dynamiques offrent un degré de complexité supplémentaire car elles dépendent de l'évolution du système et n'ont pas de raison de rester bornées.

8.5 Quelques travaux en cours et à venir

Nous présentons à présent quelques perspectives plus techniques sur lesquelles nous travaillons déjà ou que nous avons l'intention d'étudier prochainement.

Vers le développement de nouvelles méthodes pour la commande sous contrainte de systèmes linéaires (ou non linéaires) à paramètres incertains

Nous avons vu comment la technique OIST pouvait étendre la synthèse anti-windup aux contraintes de sorties. Il y a encore beaucoup de travaux à effectuer sur cette nouvelle approche; notamment, il faudrait développer de nouveaux outils de synthèse et d'analyse (pour déterminer par exemple l'invariant dans lequel l'état initial doit être) lorsque :

- la sortie à contraindre est non minimum de phase,
- les contraintes de plusieurs sorties sont transformées en des saturations imbriquées portant sur une seule entrée de commande,
- les sorties sont des fonctions non linéaires de l'état du système à contrôler.

Notons que le problème de maintenir plusieurs points dans le champ de vision d'une camera illustre ces différentes problématiques [21, 44].

Enfin, le problème qui nous semble le plus intéressant est celui de contraindre les sorties des systèmes à paramètres incertains car c'est probablement là où les méthodes basées sur la prédiction de l'évolution de l'état du système deviennent conservatrices, le champ des possibles devenant alors trop important. En complément de l'approche OIST, nous avons aussi commencé à travailler sur les "Reference Governors" [64, 79, 59] lors de notre séjour au Michigan en 2017-2018. Considérant à nouveau les systèmes linéaires sous contraintes et à paramètres incertains, nous avons obtenu des résultats préliminaires en utilisant des ERGs (Explicit Reference Governors) [25]. Nous aimerions montrer que ces résultats pourraient être étendus à des classes de systèmes non linéaires comme par exemple les systèmes polynômiaux.

Vers l'amélioration des performances des commandes non linéaires

D'une manière générale, nous souhaiterions travailler de manière plus approfondie sur la performance des systèmes bouclés par des commandes non linéaires et notamment sur la recherche de conditions moins conservatives. Par exemple, le Backstepping est, comme nous l'avons rappelé, une méthode standard de stabilisation globale d'une classe particulière de systèmes non linéaires. Nous l'avons étendu afin de résoudre quelques problèmes bien particuliers comme par exemple notre problème de guidage basé vision qui revenait à utiliser des mesures imprécises, retardées et/ou échantillonnées. Nous avons en tête deux pistes de réflexion que nous aimerions suivre de plus près :

- nous proposons de paramétrer la loi de commande obtenue par la méthode du backstepping (ou une autre méthode constructive) voire même de lui ajouter des états dynamiques de manière à obtenir davantage de degrés de liberté pour la régler ; cela reviendrait en quelque sorte à adapter à ce type de commande une pratique qui se fait déjà sur les systèmes linéaires ; il s'agit de la paramétrisation de Youla de l'ensemble des correcteurs stabilisants qui permet d'obtenir des degrés de libertés supplémentaires afin d'améliorer les performances du système linéaire bouclé [84, 5, 39].
- l'utilisation d'observateurs par intervalles pourrait permettre d'améliorer la performance des commandes non linéaires. En effet, si on considère par exemple notre problème de guidage basé vision, on devrait pouvoir accélérer la convergence de la commande par Backstepping borné [88, 89, 91] si on calcule à chaque instant l'intervalle auquel appartient la grandeur imprécise (l'inverse de la profondeur) en lieu et place de l'intervalle maximal et constant qu'on a utilisé jusqu'à présent. Lorsque l'intervalle se rétrécit on devrait être capable de retrouver les performances de la commande qu'on appliquerait si on n'avait pas d'imprécision sur les sorties mesurées. La même remarque s'applique à la commande anti-windup robuste (à la méconnaissance de la profondeur) que nous avons proposée dans [27].

8.6 Nouvelles applications

Nos futurs travaux seront appliqués aux engins aérospatiaux précédemment mentionnés mais aussi à de nouveaux concepts. Citons par exemple :

- les ailes de nouvelle génération ("morphing wings") qui devraient permettre d'améliorer l'efficacité aérodynamique des appareils tout en réduisant la consommation de carburant. Sur le plan théorique, il

pourrait s'agir de contrôler des systèmes non linéaires en utilisant des commandes à hystérésis [112].

- les taxis "volants" ou véhicules à décollage vertical (voir par exemple [4, 11, 69, 105]). Ces engins sont particulièrement en vogue outre Atlantique. Boeing et Airbus ont déjà leur propre prototype et Uber souhaite tester de tels véhicules en zone urbaine dès 2020. Sécuriser la transition de la plateforme dans des conditions dégradées est aussi un challenge que nous souhaiterions relever.
- des drones hyper "agiles" utilisant entre autre des servomoteurs pour changer la direction de poussée des hélices ("tilting rotors") [77, 96, 102].

Enfin, nous avons récemment été retenu pour participer à un nouveau projet financé par le département Américain de l'énergie (DOE). Nous allons travailler au sein d'un consortium et nous nous intéresserons au co-design des paramètres du modèle et de la commande non linéaire d'une éolienne offshore.

8.7 Création d'un Laboratoire drone

Enfin, nous ne pouvons clore ce manuscrit sans mentionner notre nouveau « laboratoire drone » à l'université de Rutgers. Notre but est d'utiliser des petits drones à voilures fixes ou tournantes afin d'illustrer nos activités de recherche et de montrer leur applicabilité aux systèmes temps réel. Dans un premier temps, nous allons nous focaliser sur les expérimentations indoor. Nous disposons notamment d'une des plus grandes arènes de vol du New Jersey pour effectuer de tels tests : celle-ci s'appelle le "Buehler Aerospace Lab" et est équipée du système de capture de mouvement "VICON". Ensuite, nous irons dans un second temps réaliser des essais à l'extérieur. Nous avons bon espoir d'utiliser ces moyens expérimentaux pour renforcer la visibilité de nos résultats de recherche en automatique non linéaire.



FIGURE 8.1 – Été 2019 : "lancement" du laboratoire avec quelques étudiants.



FIGURE 8.2 – L'arène de vol du Buehler Aerospace Lab (Rutgers University) sera très utile pour le vol "indoor".

Bibliographie

- [1] A. P. Aguiar and J. P. Hespanha. Robust filtering for deterministic systems with implicit outputs. *Systems & Control Letters*, 58(4) :263 – 270, 2009.
- [2] T. Ahmed-Ali, E. Fridman, F. Giri, L. Burlion, and F. Lamnabhi-Lagarrigue. Using exponential time-varying gains for sampled-data stabilization and estimation. *Automatica*, 67 :244–251, 2016.
- [3] T. Ahmed-Ali, E. Fridman, F. Giri, M. Kahelras, F. Lamnabhi-Lagarrigue, and L. Burlion. Observer design for a class of parabolic systems with large delays and sampled measurements. *to appear in IEEE Trans. on Automatic Control*, 2020.
- [4] T.-B. Airimitoiaie, G. P. Aguilar, L. Lavigne, C. Farges, and F. Cazaurang. Convertible aircraft dynamic modelling and flatness analysis. 51(2) :25 – 30, 2018. 9th Vienna International Conference on Mathematical Modelling.
- [5] D. Alazard and P. Apkarian. Exact observer-based structures for arbitrary compensators. *International Journal of Robust and Nonlinear Control*, 9(2) :101–118, 1999.
- [6] P. Apkarian and D. Noll. Nonsmooth H_∞ synthesis. *IEEE Transactions on Automatic Control*, 51(1) :71–86, 2006.
- [7] P. Apkarian, L. Ravanbod-Hosseini, and D. Nolls. Time domain constrained H_∞ synthesis. *International Journal of Robust and Nonlinear Control*, 21(2) :197–217, 2011.
- [8] M. Arcak. Unmodeled Dynamics in Robust Nonlinear Control. PhD Thesis. University of California, Santa Barbara., 2000.
- [9] M. Arcak and D. Nesic. A framework for nonlinear sampled-data observer design via approximate discrete-time models and emulation. *Automatica*, 40(11) :1931 – 1938, 2004.
- [10] J. R. Azinheira and A. Moutinho. Hover control of an UAV with backstepping design including input saturations. *IEEE Transactions on Control Systems Technology*, 16(3) :517–526, 2008.

- [11] J. M. O. Barth, J. Condomines, M. Bronz, L. R. Lustosa, J. Moschetta, C. Join, and M. Fliess. Fixed-wing uav with transitioning flight capabilities : Model-based or model-free control approach? a preliminary study. In *2018 International Conference on Unmanned Aircraft Systems (ICUAS)*, pages 1157–1164, 2018.
- [12] S. Bertrand, N. Guénard, T. Hamel, H. Piet-Lahanier, and L. Eck. A hierarchical controller for miniature VTOL UAVs : Design and stability analysis using singular perturbation theory. *Control Engineering Practice*, 19(10) :1099 – 1108, 2011.
- [13] J-M. Biannic, L. Burlion, and S. Tarbouriech. Finite-time LPV analysis of a vision based landing system with anti-windup augmentation. *IFAC-PapersOnLine*, 51(26) :37 – 42, 2018. 2nd IFAC Workshop on Linear Parameter Varying Systems LPVS 2018.
- [14] A. Bourdelle, L. Burlion, J.-M. Biannic, H. Evain, S. Moreno, C. Pittet, A. Dalmon, S. Tanguy, and T. Ahmed-Ali. Towards new controller design oriented models of propellant sloshing in observation spacecraft. In *AIAA Scitech 2019 Forum*, 2019.
- [15] J.V. Burke, D. Henrion, A.S. Lewis, and M.L. Overton. Hifoo - a matlab package for fixed-order controller design and H_∞ optimization. 39(9) :339 – 344, 2006. 5th IFAC Symposium on Robust Control Design.
- [16] L. Burlion. *Contribution à l'analyse et à la commande des systèmes non linéaires à commande échantillonnée*. Ph.D. thesis, University of Paris Orsay, 2007.
- [17] L. Burlion. A new saturation function to convert an output constraint into an input constraint. In *2012 20th Mediterranean Conference on Control Automation (MED)*, pages 1217–1222, 2012.
- [18] L. Burlion, T. Ahmed-Ali, and F. Lamnabhi-Lagarrigue. On the stabilization of sampled-data nonlinear systems by using backstepping on the higher order approximate models. *International Journal of Control*, 79(9) :1087–1095, 2006.
- [19] L. Burlion, T. Ahmed-Ali, and N. Seube. Glider's roll control based on backstepping. In *Proc of the IFAC Conference on Control Applications in Marine Systems (CAMS 2004)*, 2004.
- [20] L. Burlion, J-M. Biannic, and T. Ahmed-Ali. Attitude tracking control of a flexible spacecraft under angular velocity constraints. *International Journal of Control*, 92(7) :1524–1540, 2019.

- [21] L. Burlion and H. de Plinval. Keeping a ground point in the camera field of view of a landing UAV. In *2013 IEEE International Conference on Robotics and Automation*, pages 5763–5768, 2013.
- [22] L. Burlion and H. de Plinval. Vision based anti-windup design with application to the landing of an airliner. In *20th IFAC World Congress*, pages 10482 – 10487, 2017.
- [23] L. Burlion, E. Duraffourg, T. Ahmed-Ali, and F. Lamnabhi-Lagarrigue. Global asymptotic stabilization for some nonlinear models of flexible aerospace vehicles. In *52nd IEEE Conference on Decision and Control*, pages 4230–4235, 2013.
- [24] L. Burlion and I. V. Kolmanovsky. Aircraft vision-based landing using robust extended command governors. In *21st IFAC World Congress*, 2020.
- [25] L. Burlion, M. M. Nicotra, and I. V. Kolmanovsky. A fast reference governor for the constrained control of linear discrete-time systems with parametric uncertainties. In *2018 IEEE Conference on Decision and Control (CDC)*, pages 6289–6294, 2018.
- [26] L. Burlion, C. Poussot-Vassal, P. Vuillemin, M. Leitner, and T. Kier. Longitudinal manoeuvre load control of a flexible large-scale aircraft. *19th IFAC World Congress*, 47(3) :3413 – 3418, 2014.
- [27] L. Burlion, L. Zaccarian, H. de Plinval, and S. Tarbouriech. Discontinuous model recovery anti-windup for image based visual servoing. *Automatica (revision 1 under review)*, 2018.
- [28] C.I. Byrnes and A. Isidori. New results and examples in nonlinear feedback stabilization. *Systems & Control Letters*, 12(5) :437 – 442, 1989.
- [29] A. Casavola, E. Mosca, and D. Angeli. Robust command governors for constrained linear systems. *IEEE Transactions on Automatic Control*, 45(11) :2071–2077, 2000.
- [30] E. Chambon. *Commande de systèmes linéaires sous contraintes fréquentielles et temporelles. Application au lanceur flexible*. PhD thesis, Ecole doctorale EDSYS, 2016.
- [31] E. Chambon, L. Burlion, and P. Apkarian. Robust output interval constraint using o/i saturation transformation with application to uncertain linear launch vehicle. In *2015 European Control Conference (ECC)*, pages 1802–1807, 2015.
- [32] E. Chambon, L. Burlion, and P. Apkarian. Overview of linear time-invariant interval observer design : towards a non-smooth optimisation-

- based approach. *IET Control Theory Applications*, 10(11) :1258–1268, 2016.
- [33] E. Chambon, L. Burlion, and P. Apkarian. Time-response shaping using output to input saturation transformation. *International Journal of Control*, 91(3) :534–553, 2018.
- [34] C. Chauffaut, F. Defaÿ, L. Burlion, and H. de Plinval. Uav obstacle avoidance scheme using an output to input saturation transformation technique. In *2016 International Conference on Unmanned Aircraft Systems (ICUAS)*, pages 227–234, 2016.
- [35] F. Chaumette and S. Hutchinson. Visual servo control. i. basic approaches. *Robotics Automation Magazine, IEEE*, 13(4) :82–90, 2006.
- [36] F. Chaumette and S. Hutchinson. Visual servo control. ii. advanced approaches [tutorial]. *Robotics Automation Magazine, IEEE*, 14(1) :109–118, 2007.
- [37] S. W. Chen, S. S. Shivakumar, S. Dcunha, J. Das, E. Okon, C. Qu, C. J. Taylor, and V. Kumar. Counting apples and oranges with deep learning : a data-driven approach. *IEEE Robotics and Automation Letters*, 2(2) :781–788, 2017.
- [38] T. Cheviron, F. Plestan, and A. Chriette. A robust guidance and control scheme of an autonomous scale helicopter in presence of wind gusts. *International Journal of Control*, 82(12) :2206–2220, 2009.
- [39] B. Clément and G. Duc. Flexible arm multiobjective control via Youla parameterization and LMI optimization. 33(14) :143 – 148, 2000. 3rd IFAC Symposium on Robust Control Design (ROCOND 2000), Prague, Czech Republic, 21-23 June 2000.
- [40] R. Cunha, C. Silvestre, J. Hespanha, and A.P. Aguiar. Vision-based control for rigid body stabilization. *Automatica*, 47(5) :1020 – 1027, 2011.
- [41] T. Cunis, L. Burlion, and J-P. Condomines. Piecewise polynomial modeling for control and analysis of aircraft dynamics beyond stall. *Journal of Guidance, Control, and Dynamics*, 42(4) :949–957, 2019.
- [42] T. Cunis, J-P. Condomines, and L. Burlion. Local stability analysis for large polynomial spline systems. *provisionally accepted to Automatica*, 2020.
- [43] O. Dahl, Y. Wang, A.F. Lynch, and A. Heyden. Observer forms for perspective systems. *Automatica*, 46(11) :1829 – 1834, 2010.
- [44] H. de Plinval and L. Burlion. Nonlinear visual servoing control for VTOL UAVs with field of view constraint. In J. Bordeneuve-Guibé,

- A. Drouin, and C. Roos, editors, *Advances in Aerospace Guidance, Navigation and Control*, pages 531–548. Springer International Publishing, 2015.
- [45] H. de Plinval, P. Morin, and P. Mouyon. Nonlinear control of underactuated vehicles with uncertain position measurements and application to visual servoing. In *American Control Conference (ACC), 2012*, pages 3253–3259, 2012.
- [46] H. de Plinval, P. Morin, and P. Mouyon. Stabilization of a class of underactuated vehicles with uncertain position measurements and application to visual servoing. *Automatica*, 77 :155–169, 2017.
- [47] K. Deguchi. Optimal motion control for image-based visual servoing by decoupling translation and rotation. In *Proceedings. 1998 IEEE/RSJ International Conference on Intelligent Robots and Systems. Innovations in Theory, Practice and Applications (Cat. No.98CH36190)*, volume 2, pages 705–711 vol.2, 1998.
- [48] G. Dolanc and S. Lumbar. Pegase – helicopter and aeronef navigation airborne system experiments. In *TransSLO workshop*, 2007.
- [49] E. Duraffourg. *Commande non linéaire en présence de modes souples. Applications aérospatiales*. Ph.D. thesis, University of Paul Sabatier, Toulouse, 2014.
- [50] E. Duraffourg, L. Burlion, and T. Ahmed-Ali. Finite-time observer-based backstepping control of a flexible launch vehicle. *Journal of Vibration and Control*, 24(8) :1535–1550, 2018.
- [51] E. Duraffourg, L. Burlion, T. Ahmed-Ali, and F. Lamnabhi-Lagarrigue. Non-linear control of the longitudinal rotational dynamics of a flexible aircraft. In *2013 European Control Conference (ECC)*, pages 335–340, 2013.
- [52] A. Dzul, T. Hamel, and R. Lozano. Helicopter’s nonlinear control via backstepping techniques. In *2001 European Control Conference (ECC)*, pages 463–468, 2001.
- [53] I. Fantoni and R. Lozano. *Non-linear Control for Underactuated Mechanical Systems*. Springer, 2002.
- [54] L. Fiorentini, A. Serrani, M.A. Bolender, and D.B. Doman. Nonlinear robust adaptive control of flexible air-breathing hypersonic vehicles. *Journal of Guidance, Control and Dynamics*, Vol. 32, No.2, pages 401–416, 2009.
- [55] M. Fliess and H. Sira-Ramírez. An algebraic framework for linear identification. *ESAIM : Control, Optimisation and Calculus of Variations*, 9 :151–168, 2003.

- [56] T. Folin, T. Ahmed-Ali, F. Giri, L. Burlion, and F. Lamnabhi-Lagarrigue. Sampled-data adaptive observer for a class of state-affine output-injection nonlinear systems. *IEEE Trans. on Automatic Control*, 61(2) :462–467, 2016.
- [57] R. Freeman and L. Praly. Integrator backstepping for rounded controls and control rates. *IEEE Transactions on Automatic Control*, 43(2) :258–262, 1998.
- [58] S. Galeani, S. Tarbouriech, M. Turner, and L. Zaccarian. A tutorial on modern anti-windup design. *European Journal of Control*, 15(3-4) :418 – 440, 2009.
- [59] E. Garone, S. Di Cairano, and I. Kolmanovsky. Reference and command governors for systems with constraints : A survey on theory and applications. *Automatica*, 75 :306 – 328, 2017.
- [60] M. Gevers. A decade of progress in iterative process control design : from theory to practice. *Journal of Process Control*, 12(4) :519 – 531, 2002.
- [61] G. Gibert, L. Burlion, A. Chriette, J. Boada, and F. Plestan. New pose estimation scheme in perspective vision system during civil aircraft landing. *IFAC-PapersOnLine*, 48(19) :238 – 243, 2015. 11th IFAC Symposium on Robot Control, SYROCO 2015, Salvador, Brazil, August 2015.
- [62] V. Gibert, L. Burlion, A. Chriette, J. Boada, and F. Plestan. Nonlinear observers in vision system : application to civil aircraft landing. In *2015 European Control Conference (ECC)*, pages 1818–1823, 2015.
- [63] V. Gibert, F. Plestan, L. Burlion, J. Boada-Bauxell, and A. Chriette. Visual estimation of deviations for the civil aircraft landing. *Control Engineering Practice*, 75 :17 – 25, 2018.
- [64] E. G. Gilbert and K. T. Tan. Linear systems with state and control constraints : the theory and application of maximal output admissible sets. *IEEE Transactions on Automatic Control*, 36(9) :1008–1020, 1991.
- [65] R. Goebel, R. G. Sanfelice, and A. R. Teel. *Hybrid Dynamical Systems : Modeling, Stability, and Robustness*. Princeton University Press, 2012.
- [66] G.C. Goodwin, J. De Dona, O.J. Rojas, and M. Perrier. A brief overview of nonlinear control. 2001.
- [67] G.C. Goodwin, M.M. Seron, and J.A. de Dona. *Constrained Control and Estimation : An Optimisation Approach*. Springer, 1st edition, 2010.

- [68] K. Graichen and M. Zeitz. Feedforward control design for finite-time transition problems of nonlinear systems with input and output constraints. *IEEE Transactions on Automatic Control*, 53(5) :1273–1278, 2008.
- [69] J. Hauser, S. Sastry, and G. Meyer. Nonlinear control design for slightly non-minimum phase systems : Application to v/stol aircraft. *Automatica*, 28(4) :665 – 679, 1992.
- [70] J. Hervas and M. Reyhanoglu. Control of a spacecraft with time-varying propellant slosh parameters. *12th International Conference on Control, Automation and Systems*, pages 1621–1626, 2012.
- [71] J. Hill and W. T. Park. Real time control of a robot with a mobile camera. In *9th ISIR*, pages 233–246, 1979.
- [72] S. Hutchinson, G. D. Hager, and P. I. Corke. A tutorial on visual servo control. *IEEE Transactions on Robotics and Automation*, 12(5) :651–670, 1996.
- [73] M. Jankovic and B. K. Ghosh. Visually guided ranging from observations of points, lines and curves via an identifier based nonlinear observer. *Systems & Control Letters*, 25(1) :63 – 73, 1995.
- [74] M. Jankovic, P.V. Kokotovic, and R. Sepulchre. *Constructive Nonlinear Control*. Springer Verlag, 1997.
- [75] R.E. Kalman and R.S. Bucy. New results in linear filtering and prediction theory. *ASME. J. Basic Eng*, 33(1) :95–108, 2001.
- [76] D. Karagiannis and A. Astolfi. A new solution to the problem of range identification in perspective vision systems. *IEEE Transactions on Automatic Control*, 50(12) :2074–2077, 2005.
- [77] F. Kendoul, I. Fantoni, and R. Lozano. Modeling and control of a small autonomous aircraft having two tilting rotors. *IEEE Transactions on Robotics*, 22(6) :1297–1302, 2006.
- [78] P. V. Kokotovic. The joy of feedback : nonlinear and adaptive. *1991 Bode Prize Lecture, IEEE Control Systems Magazine*, 12(3) :7–17, 1992.
- [79] I. Kolmanovsky, E. Garone, and S. Di Cairano. Reference and command governors : A tutorial on their theory and automotive applications. In *2014 American Control Conference*, pages 226–241, 2014.
- [80] M. Krstic and M. Bement. Nonovershooting control of strict-feedback nonlinear systems. *IEEE Transactions on Automatic Control*, 51(12) :1938–1943, 2006.

- [81] M. Krstic, I. Kanellakopoulos, and P.V. Kokotovic. Adaptive nonlinear control without overparametrization. *Systems & Control Letters*, 19(3) :177 – 185, 1992.
- [82] M. Krstic, P.V. Kokotovic, and I. Kanellakopoulos. *Nonlinear and Adaptive Control Design*. John Wiley & Sons, Inc., New York, NY, USA, 1st edition, 1995.
- [83] Z. Lin and A. Saberi. Semi-global exponential stabilization of linear discrete-time systems subject to input saturation via linear feedbacks. *Systems & Control Letters*, 24(2) :125 – 132, 1995.
- [84] J. Maciejowski. *Multivariable Feedback Design*. Addison-Wesley Longman Publishing Co., Inc., Boston, MA, USA, 1st edition, 1990.
- [85] E. Malis, F. Chaumette, and S. Boudet. 2-1/2-D visual servoing. *IEEE Transactions on Robotics and Automation*, 15(2) :238–250, 1999.
- [86] D. Q. Mayne. Model predictive control : Recent developments and future promise. *Automatica*, 50(12) :2967 – 2986, 2014.
- [87] F. Mazenc and O. Bernard. Interval observers for linear time-invariant systems with disturbances. *Automatica*, 47(1) :140 – 147, 2011.
- [88] F. Mazenc, L. Burlion, and V. Gibert. Stabilization of a nonlinear system that arises in the context of vision based landing of an airliner. In *2018 IEEE Conference on Decision and Control (CDC)*, pages 5313–5318, 2018.
- [89] F. Mazenc, L. Burlion, and V. Gibert. Stabilization with imprecise measurements : application to a vision based landing problem. In *2018 Annual American Control Conference (ACC)*, pages 2978–2983, 2018.
- [90] F. Mazenc, L. Burlion, and M. Malisoff. Backstepping design for output feedback stabilization for a class of uncertain systems. *Systems & Control Letters*, 123 :134 – 143, 2019.
- [91] F. Mazenc, L. Burlion, and M. Malisoff. Stabilization and robustness analysis for a chain of saturating integrators with imprecise measurements. *IEEE Control Systems Letters*, 3(2) :428–433, 2019.
- [92] F. Mazenc and A. Iggidr. Backstepping with bounded feedbacks. *Systems & Control Letters*, 51(3) :235 – 245, 2004.
- [93] F. Mazenc and M. Malisoff. New control design for bounded backstepping under input delays. *Automatica*, 66 :48 – 55, 2016.
- [94] F. Mazenc, M. Malisoff, L. Burlion, and J. Weston. Bounded backstepping control and robustness analysis for time-varying systems under converging-input-converging-state conditions. *European Journal of Control*, 42 :15 – 24, 2018.

- [95] F. Mazenc, M. Malisoff, and J. Weston. New bounded backstepping control designs for time-varying systems under converging-input-converging-state conditions. In *2016 IEEE 55th Conference on Decision and Control (CDC)*, pages 3167–3171, 2016.
- [96] G. Michieletto, M. Ryll, and A. Franchi. Control of statically hoverable multi-rotor aerial vehicles and application to rotor-failure robustness for hexarotors. In *2017 IEEE International Conference on Robotics and Automation (ICRA)*, pages 2747–2752, 2017.
- [97] M. Netto, A. Annaswamy, S. Mammarr, and S. Glaser. A new adaptive control algorithm for systems with multilinear parametrization. In *2006 American Control Conference*, pages 4100–4105, 2006.
- [98] R. Olfati-Saber. Nonlinear control of underactuated mechanical systems with application to robotics and aerospace vehicles. PhD Thesis. Massachusetts Institute of Technology., 2001.
- [99] B. Patin. helicoPter and aEronef naviGation Airborne System Experiments. *Rapport technique du projet pégase, Dassault Aviation*, 2011.
- [100] R. Postoyan, T. Ahmed-Ali, L. Burlion, and F. Lamnabhi-Lagarrigue. On the lyapunov-based adaptive control redesign for a class of nonlinear sampled-data systems. *Automatica*, 44(8) :2099–2107, 2008.
- [101] O.J. Rojas and G.C. Goodwin. A simple anti-windup strategy for state constrained linear control. *IFAC Proceedings Volumes*, 35(1) :109 – 114, 2002. 15th IFAC World Congress.
- [102] M. Ryll, H. H. Bühlhoff, and P. R. Giordano. A novel overactuated quadrotor unmanned aerial vehicle : Modeling, control, and experimental validation. *IEEE Transactions on Control Systems Technology*, 23(2) :540–556, 2015.
- [103] A. Seuret, C. Prieur, S. Tarbouriech, A. R. Teel, and L. Zaccarian. A nonsmooth hybrid invariance principle applied to robust event-triggered design. *IEEE Transactions on Automatic Control*, 64(5) :2061–2068, 2019.
- [104] G. Shi, X. Shi, M. O’Connell, R. Yu, K. Azizzadenesheli, A. Anandkumar, Y. Yue, and S. Chung. Neural lander : Stable drone landing control using learned dynamics. In *2019 International Conference on Robotics and Automation (ICRA)*, pages 9784–9790, 2019.
- [105] X. Shi, K. Kim, S. Rahili, and S. Chung. Nonlinear control of autonomous flying cars with wings and distributed electric propulsion. In *2018 IEEE Conference on Decision and Control (CDC)*, pages 5326–5333, 2018.

- [106] Y. Shirai and H. Inoue. Guiding a robot by visual feedback in assembling tasks. *Pattern Recognition*, 5(2) :99 – 108, 1973.
- [107] E. D. Sontag. Comments on integral variants of ISS. *Systems & Control Letters*, 34(1) :93 – 100, 1998.
- [108] S. Tarbouriech and M. Turner. Anti-windup design : an overview of some recent advances and open problems. *IET Control Theory & Applications*, 3(1) :1–19, 2009.
- [109] K. P. Tee, S. S. Ge, and E. H. Tay. Barrier lyapunov functions for the control of output-constrained nonlinear systems. *Automatica*, 45(4) :918 – 927, 2009.
- [110] J. Tsiniias. Input to state stability properties of nonlinear systems and applications to bounded feedback stabilization using saturation. *ESAIM : Control, Optimisation and Calculus of Variations*, 2 :57–87, 1997.
- [111] M.C. Turner and I. Postlethwaite. Multivariable override control for systems with output and state constraints. *International Journal of Robust and Nonlinear Control*, 14(13-14) :1105–1131, 2004.
- [112] J. Valasek. *Morphing Aerospace Vehicles and Structures*. John Wiley & Sons, LTd, 2012.

